



<https://theses.gla.ac.uk/>

Theses Digitisation:

<https://www.gla.ac.uk/myglasgow/research/enlighten/theses/digitisation/>

This is a digitised version of the original print thesis.

Copyright and moral rights for this work are retained by the author

A copy can be downloaded for personal non-commercial research or study,  
without prior permission or charge

This work cannot be reproduced or quoted extensively from without first  
obtaining permission in writing from the author

The content must not be changed in any way or sold commercially in any  
format or medium without the formal permission of the author

When referring to this work, full bibliographic details including the author,  
title, awarding institution and date of the thesis must be given

Enlighten: Theses

<https://theses.gla.ac.uk/>  
[research-enlighten@glasgow.ac.uk](mailto:research-enlighten@glasgow.ac.uk)

**GLOBAL AND LOCAL EFFECTS OF  $^{14}\text{C}$  DISCHARGES  
FROM THE NUCLEAR FUEL CYCLE**

Martin McCartney, B.Sc. (Hons)

Chemistry Department,  
University of Glasgow

A thesis submitted to the University of Glasgow in partial  
fulfilment of the requirements for the degree of  
Doctor of Philosophy.

May 1987

ProQuest Number: 10995568

All rights reserved

INFORMATION TO ALL USERS

The quality of this reproduction is dependent upon the quality of the copy submitted.

In the unlikely event that the author did not send a complete manuscript and there are missing pages, these will be noted. Also, if material had to be removed, a note will indicate the deletion.



ProQuest 10995568

Published by ProQuest LLC (2018). Copyright of the Dissertation is held by the Author.

All rights reserved.

This work is protected against unauthorized copying under Title 17, United States Code  
Microform Edition © ProQuest LLC.

ProQuest LLC.  
789 East Eisenhower Parkway  
P.O. Box 1346  
Ann Arbor, MI 48106 – 1346

## ACKNOWLEDGEMENTS

My sincere thanks goes to my supervisor, Prof. Murdoch Baxter, for his constant encouragement and guidance throughout this work. The helpful and enthusiastic participation of Dr Marian Scott is also acknowledged. Thanks must go to Dr Gordon Cook and Dr D Harkness for participating in the intercalibration study, to Mrs J Rodgers (for preparation of diagrams), to Mrs N Hawkes (for preparation of typescript) and to the other members of the Glasgow University nuclear geochemistry group (Vea, Paul, Joe, Francis, Keith, Alison, Andy and Phil) whose assistance came in too many varied forms to detail here. This study was supported by a Research Studentship from the Science and Engineering Research Council, to whom I am grateful. Finally, I wish to acknowledge the debt that I owe to my family and friends whose latent contribution to this work cannot be explained in simple words.

Martin McCartney

May 1987



	1.4.1.2	Health Effects in an Exposed Population . . . . .	55
	1.4.2	Radiation Dose to Man from $^{14}\text{C}$ . . . . .	58
1.5		THE ICRP DOSE LIMITATION SYSTEM . . . . .	62
1.6		AIMS OF RESEARCH . . . . .	64
	1.6.1	Local Effects of $^{14}\text{C}$ Discharges from the Nuclear Fuel Cycle . . . . .	65
	1.6.2	Global Effects of $^{14}\text{C}$ Discharges from the Nuclear Fuel Cycle . . . . .	66
CHAPTER 2		EXPERIMENTAL PROCEDURE . . . . .	67
	2.1	INTRODUCTION . . . . .	67
	2.2	SAMPLE PREPARATION . . . . .	69
	2.2.1	Sample Pretreatment . . . . .	70
		2.2.1.1 Grass . . . . .	70
		2.2.1.2 Seaweed . . . . .	70
		2.2.1.3 Potatoes . . . . .	71
		2.2.1.4 Berries . . . . .	71
		2.2.1.5 Wood . . . . .	71
	2.2.2	Sample Combustion . . . . .	72
	2.2.3	Acetylene Synthesis . . . . .	78
	2.2.4	Benzene Synthesis . . . . .	84
	2.2.5	Summary of Sample Preparation . . . . .	87
	2.3	MEASUREMENT OF ISOTOPIC FRACTIONATION . . . . .	89
	2.4	THE LIQUID SCINTILLATION TECHNIQUE . . . . .	90
	2.4.1	The Theory of Liquid Scintillation Counting . . . . .	90
	2.4.2	The Scintillation Medium . . . . .	91
	2.4.3	The Detection System . . . . .	93
	2.4.4	The Liquid Scintillation Counter . . . . .	95
	2.4.5	Optimisation of the Counter for Low-level $^{14}\text{C}$ Assay . . . . .	97
	2.5	MEASUREMENT OF $^{14}\text{C}$ SPECIFIC ACTIVITY . . . . .	102
	2.5.1	Preparation of the Standard Geometry Vial . . . . .	102
	2.5.2	Backgrounds . . . . .	103
	2.5.3	Modern Standard Activity . . . . .	107
	2.5.4	Quenching . . . . .	109
	2.5.5	Batch Composition . . . . .	114
	2.5.6	Calculation of Results . . . . .	114

2.6	RELIABILITY OF THE $^{14}\text{C}$ SPECIFIC ACTIVITY MEASUREMENTS . . . . .	117
2.6.1	Stability of the Counting Environment . . . . .	117
2.6.2	Replicate Analysis . . . . .	119
2.6.3	Intercalibration Study . . . . .	122
CHAPTER 3	LOCAL EFFECTS OF $^{14}\text{C}$ DICHARGES FROM THE NUCLEAR FUEL CYCLE . . . . .	128
3.1	INTRODUCTION . . . . .	128
3.2	OBSERVED $^{14}\text{C}$ LEVELS AROUND SELECTED NUCLEAR FACILITIES . . . . .	130
3.2.1	Background $^{14}\text{C}$ Levels . . . . .	130
3.2.2	Sellafield (BNF plc) . . . . .	132
3.2.2.1	The Spatial Distribution of the $^{14}\text{CO}_2$ Discharges . . . . .	137
3.2.2.2	The Temporal Distribution of the $^{14}\text{CO}_2$ Discharges . . . . .	150
3.2.3	Hunterston (SSEB) . . . . .	154
3.2.3.1	The Spatial Distribution of the $^{14}\text{CO}_2$ Discharges . . . . .	154
3.2.4	Dounreay (UKAEA) . . . . .	159
3.2.5	East Kilbride (SURRC) . . . . .	159
3.3	THE RADIOLOGICAL IMPACT OF $^{14}\text{CO}_2$ DISCHARGES ON THE LOCAL POPULATIONS . . . . .	161
3.3.1	Methodology . . . . .	163
3.3.1.1	The Spatial Distribution of the Local Population . . . . .	168
3.3.1.2	The Spatial Distribution of the $^{14}\text{CO}_2$ Discharges . . . . .	168
3.3.2	Sellafield . . . . .	172
3.3.2.1	1985 . . . . .	172
3.3.2.2	1984 . . . . .	189
3.3.2.3	1983 . . . . .	198
3.3.2.4	1952-1982 . . . . .	205
3.3.2.5	1952-1985 . . . . .	211
3.3.2.6	Atmospheric Dispersion Models . . . . .	221
3.3.3	Hunterston . . . . .	232
3.3.3.1	Local Doses . . . . .	232
3.3.3.2	Atmospheric Dispersion Models . . . . .	238

3.4	CONCLUSIONS . . . . .	246
CHAPTER 4	GLOBAL EFFECTS OF $^{14}\text{C}$ DISCHARGES FROM THE NUCLEAR FUEL CYCLE . . . . .	250
4.1	INTRODUCTION . . . . .	250
4.2	MODELLING THE GLOBAL CARBON CYCLE . . . . .	251
4.2.1	A History of Carbon Cycle Modelling . . . . .	252
4.2.1.1	The Atmosphere . . . . .	252
4.2.1.2	The Atmosphere-Terrestrial Biosphere System . . . . .	255
4.2.1.3	The Atmosphere-Ocean System . . . . .	257
4.2.2	Description and Validation of the Carbon Cycle Models . . . . .	259
4.2.2.1	The 1-Box Model . . . . .	260
4.2.2.2	The 3-Box Model . . . . .	265
4.2.2.3	The 8-Box Model . . . . .	269
4.2.2.4	The 25-Box Model . . . . .	272
4.2.3	Justification of Choice of Models . . . . .	279
4.3	RADIATION DOSE TO THE GLOBAL POPULATION FROM $^{14}\text{C}$ DISCHARGES FROM THE NUCLEAR FUEL CYCLE . . . . .	281
4.3.1	Short-term Effects of $^{14}\text{C}$ Discharges from the Nuclear Fuel Cycle . . . . .	282
4.3.1.1	Basic Scenarios . . . . .	283
4.3.1.2	Radiation Dose to the Public to 2050 . . . . .	290
4.3.1.3	The Radiological Impact on the Public to 2050 . . . . .	307
4.3.2	Long-term Effects of $^{14}\text{C}$ Discharges from the Nuclear Fuel Cycle . . . . .	309
4.3.2.1	Basic Scenarios . . . . .	309
4.3.2.2	Radiation Dose to the Public to Infinity . . . . .	313
4.3.2.3	The Radiological Impact on the Public to Infinity . . . . .	324
4.3.3	Chernobyl . . . . .	328
4.4	$^{14}\text{C}$ WASTE MANAGEMENT. . . . .	330
4.5	CONCLUSIONS . . . . .	334

CHAPTER 5 THE RADIOLOGICAL IMPACT OF <sup>14</sup>C DISCHARGES FROM THE  
NUCLEAR FUEL CYCLE: AN OVERVIEW . . . . . 336

APPENDIX 1 . . . . . 338

REFERENCES . . . . . 352

## ABSTRACT

The production of  $^{14}\text{C}$  in nuclear reactors and its subsequent release to the environment leads to an increase in atmospheric  $^{14}\text{C}$  specific activities and, hence, to an incremental addition to the radiation dose to man. The primary objectives of this research were to assess the radiological impact of  $^{14}\text{C}$  discharges from the nuclear fuel cycle and thereafter to comment on their acceptability on the basis of the recommendations of International Commission on Radiological Protection (ICRP). These basic objectives were subdivided into 2 assessment projects; firstly, to quantify the effects of  $^{14}\text{C}$  discharges on populations living in the locality of large nuclear installations and, secondly, to estimate the effects of  $^{14}\text{C}$  releases on the global population.

The local effects of  $^{14}\text{C}$  discharges were investigated by direct measurements of  $^{14}\text{C}$  activities in the environment around various nuclear installations within UK. The  $^{14}\text{C}$  specific activity in various biological samples (mainly grass) were measured by liquid scintillation counting of benzene. No increase in atmospheric  $^{14}\text{C}$  levels was observed in the vicinity of either the fast breeder reactor site at Dounreay or the SURRC research reactor at East Kilbride. On the other hand, increases in atmospheric  $^{14}\text{C}$  specific activities were detected around both the nuclear fuel reprocessing plant at Sellafield and, to a lesser extent, the thermal nuclear power station complex at Hunterston. The collective effective dose equivalent commitment to the population within 40 km of Sellafield, from its  $^{14}\text{CO}_2$  discharges between 1952 and 1985, is estimated at 8.4 man Sv, the largest annual collective dose of 1.3 man Sv being received in 1983. The discharges of  $^{14}\text{CO}_2$  from Hunterston in 1984, which can be regarded as a typical year for this nuclear installation, generated a collective effective dose equivalent commitment of  $15 \times 10^{-3}$  man Sv to the population within 15 km of the plant. The largest annual effective dose equivalents to individuals around Sellafield and Hunterston were 0.2 mSv (in 1982) and 11.8  $\mu\text{Sv}$  respectively. These levels do not exceed the limits recommended by ICRP, although this fact, in itself, cannot be used to justify these discharges. The  $^{14}\text{C}$  measurements herein also provide an ideal basis for testing of atmospheric dispersion models. Two such models were investigated, namely the Gaussian plume atmospheric dispersion model and the so-called hyperbolic model, the latter in fact being derived from the former. The results of the study show that the Gaussian dispersion model is excellent in predicting  $^{14}\text{C}$

levels around the Hunterston site but yields highly unsatisfactory results when applied to Sellafield. Further investigation suggests that the model's poor performance at Sellafield is largely caused by inaccurate input data. In particular, the validity of the  $^{14}\text{CO}_2$  discharge data supplied by BNF plc can be questioned. The results in essence suggest that the Gaussian dispersion model can be used to give reasonable estimates of atmospheric  $^{14}\text{C}$  levels if and only if the necessary input data for the model have been accurately determined. In the absence of such data, it is suggested that the simple hyperbolic model is utilised. The value of the latter is based on its ability to predict atmospheric  $^{14}\text{C}$  levels at practically any distance from the discharge location (except very close to the release point), from a single experimentally determined  $^{14}\text{C}$  level. The model's reliability is confirmed repeatedly during this study both at the Sellafield and Hunterston sites.

The global effects of past, present and future  $^{14}\text{C}$  discharges from the nuclear fuel cycle were investigated theoretically using carbon cycle models. As a precursor to estimation of the dose to man from reactor-derived  $^{14}\text{C}$ , atmospheric  $^{14}\text{C}$  levels resulting from a range of anthropogenic perturbations to the year 2050 were determined. The results indicate that future atmospheric  $^{14}\text{C}$  levels will not deviate significantly from the natural baseline and, indeed, will be significantly lower than those experienced during the recent past. The atmospheric  $^{14}\text{C}$  specific activity in the year 2050 is expected to be around  $234 \text{ Bq kg}^{-1}$  (carbon), corresponding to an individual effective dose equivalent rate of  $14.6 \mu\text{Sv year}^{-1}$ . The contribution of reactor-derived  $^{14}\text{C}$  to the individual effective dose equivalent rate increases steadily over this period, reaching  $1.8 \mu\text{Sv year}^{-1}$  in 2050, well within the ICRP limit. This level of dose, in itself, would provide insufficient justification for further reduction of  $^{14}\text{C}$  discharges. Nevertheless, in view of the large number of uncertainties implicit in these predictions (as epitomised by the Chernobyl accident), it is recommended that estimates of future individual effective dose equivalent rates should be continually updated in the light of the best possible information. These same uncertainties limit the study herein to the period to 2050 AD. The major significance of the  $^{14}\text{C}$  discharges, however, is that, because of the long half-life of  $^{14}\text{C}$ , coupled with its mobility in the environment, releases of this nuclide lead to the exposure of global populations over very long timescales. This concept is quantified by the collective effective dose equivalent commitment which has been

conservatively estimated in this research at 141 man Sv TBq<sup>-1</sup>. Normalised to production of 1 GW(e) year of energy via nuclear power, this value corresponds to 480 man Sv (GW(e) year)<sup>-1</sup>, thus suggesting that <sup>14</sup>C is one of the largest contributors to the total collective effective dose equivalent commitment to man from this energy source. It is therefore recommended that considerable effort should be directed towards development of cost-effective methods for <sup>14</sup>C dose reduction, i.e. in keeping with the ALARA principle. Various <sup>14</sup>C waste management strategies have been identified which, in theory, will result in significant reduction of dose to man. Of these, retention and subsequent immobilisation of the <sup>14</sup>C waste has greatest potential.

Finally, if the effective dose equivalent rate to the most exposed individual around nuclear facilities increases in parallel with the average global dose rate, then the former will soon exceed ICRP limits. This observation enforces the view that dose-reducing <sup>14</sup>C waste management strategies should be evaluated with urgency.

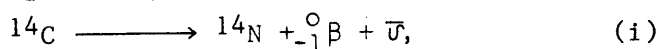
INTRODUCTION1.1 INTRODUCTION

The generation of nuclear energy routinely results in the authorised release to the environment of a wide range of radionuclides. This artificial radioactivity increases the radiation dose to which man is normally exposed from natural radioactivity and cosmic radiation. An assessment of the magnitude of this additional radiation exposure, both at the present time and in future years, is clearly of prime importance.

Considerable attention has been focussed on the radiation hazard arising from the discharge of fission and activation product nuclides ( $^{137}\text{Cs}$ ,  $^{134}\text{Cs}$ ,  $^{106}\text{Ru}$  and  $^{90}\text{Sr}$  for example) and transuranic elements, particularly plutonium. It is only relatively recently, however, that the potential significance of the  $^{14}\text{C}$  discharges from the nuclear fuel cycle has been recognised (Kelly et al., 1975; Magno et al., 1975; Hayes and MacMurdo, 1977; Killough and Till, 1978; Schwibach et al., 1978). It is expected that, despite ecological misgivings, the global installed nuclear energy capacity will continue to increase during the next century to help meet the world's growing energy demands (Hafele, 1981). Thus, it is important to determine the potential risk, if any, to the public from the resulting  $^{14}\text{C}$  discharges.

1.2 A HISTORY OF  $^{14}\text{C}$  IN NATURE

Carbon is one of the essential elements to all forms of life. It is involved in most biological and geochemical processes on the earth. Associated with the stable isotopes of carbon ( $^{12}\text{C}$  and about 1.1%  $^{13}\text{C}$ ), there is a very small inventory of  $^{14}\text{C}$  which is formed in the atmosphere and subsequently enters the natural carbon cycle. This nuclide is a pure beta-emitter (average energy 45 keV):



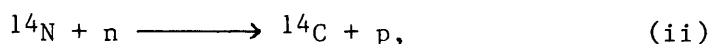
with a half-life of  $5730 \pm 40$  years (Godwin, 1962). Because of its scientific usefulness via the radiocarbon dating method, the history of  $^{14}\text{C}$  concentrations in nature has been meticulously

investigated. Such studies have brought to light the existence of both man-made and naturally produced fluctuations in the  $^{14}\text{C}$  concentration record, besides a wealth of data on the transfer of  $^{14}\text{C}$  in nature.

In assessing the effects of  $^{14}\text{C}$  discharges from the nuclear fuel cycle, it is imperative to take advantage of the techniques developed for, and the information derived from, the study of  $^{14}\text{C}$  in nature. In the following section, current knowledge of the behaviour of  $^{14}\text{C}$  in nature will be reviewed.

### 1.2.1 The Natural Production of $^{14}\text{C}$

It was Libby (1946) who first postulated the formation of radiocarbon in the upper atmosphere by the reaction of cosmic ray neutrons with atmospheric nitrogen:



and a year later the existence of naturally occurring radiocarbon was confirmed by Anderson et al. (1947). Estimates of the  $^{14}\text{C}$  production rate vary from  $1.0 \times 10^{15} \text{ Bq year}^{-1}$

(United Nations, 1977), derived from assessments of the natural  $^{14}\text{C}$  inventory, to  $1.4 \times 10^{15} \text{ Bq year}^{-1}$  (Light et al., 1973), calculated from cosmic ray flux estimates.

Considering the uncertainties involved in determining both the direct production rate and the total  $^{14}\text{C}$  inventory of the earth, these estimates are in reasonable agreement. After its production, the radiocarbon is rapidly oxidised to  $\text{CO}_2$  and becomes distributed amongst the various reservoirs of the global carbon cycle.

### 1.2.2 The Global Carbon Cycle

The global carbon cycle is an expression used to describe the movement of carbon in nature. It is useful to conceive of the carbon cycle as a series of pools of carbon interconnected by pathways of flux. The entire system ideally represents a steady state which may adjust to new steady states with changes of geological scale. The diagrammatic model of the carbon cycle in Figure 1.1 is simpler than others which are presented later in this study (c.f. Chapter 4) but the model does provide an adequate format for the presentation of data. This model description represents the natural steady state of the carbon cycle in the post-glacial period before its perturbation by man.

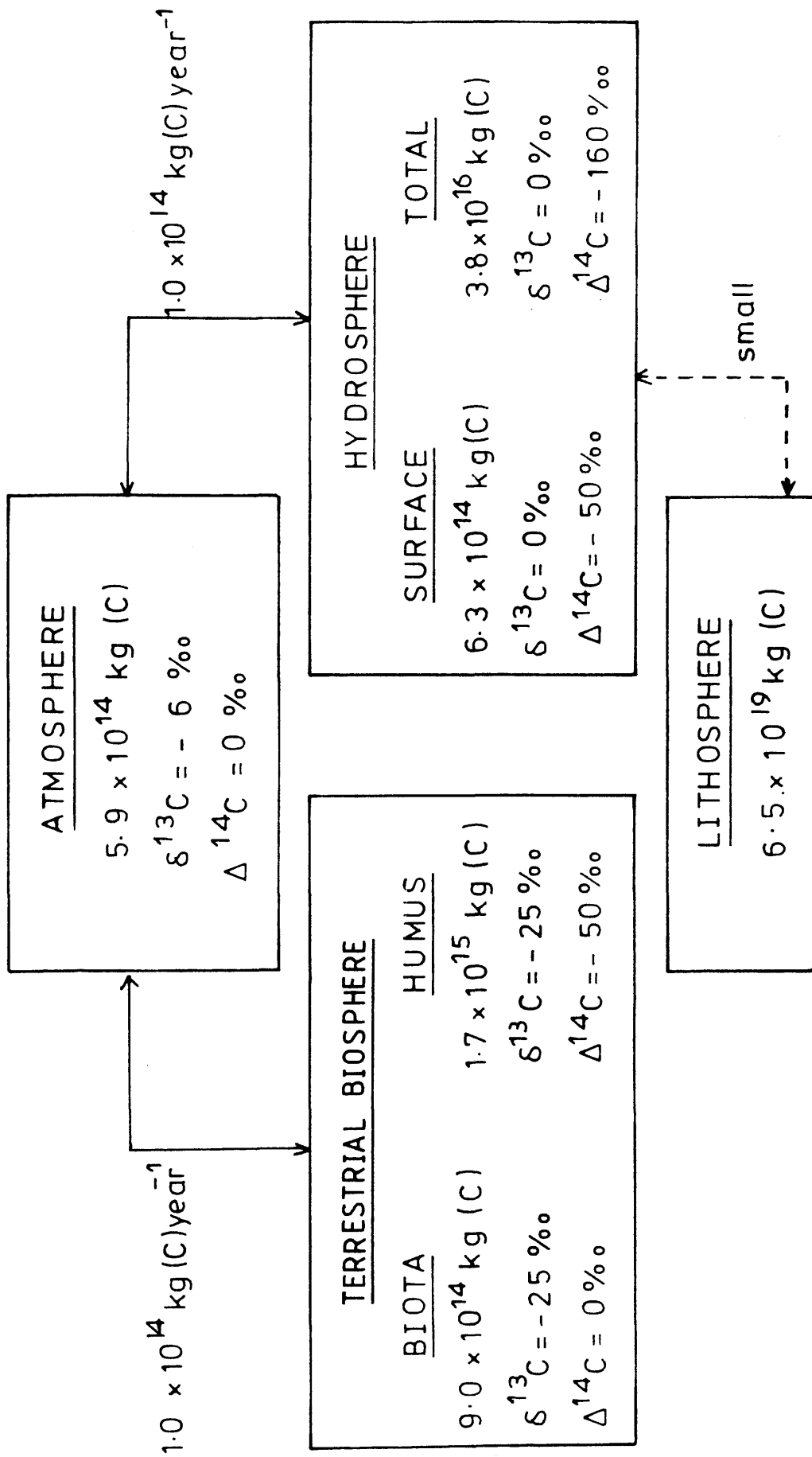


FIGURE 1-1: The global carbon cycle.

The carbon cycle (as represented in Figure 1.1) is divided into four large pools: the atmosphere, the terrestrial biosphere, the hydrosphere and the lithosphere, each of which, in turn, can be divided into constituent sub-pools. Several of these carbon cycle reservoirs are inter-connected by pathways of major carbon flux, with the more important ones being between the atmosphere and terrestrial biosphere, the atmosphere and hydrosphere and, to a lesser extent, between the hydrosphere and lithosphere. Details of the various carbon reservoirs and, where appropriate, the mechanisms of carbon transfer between them are now summarised.

#### 1.2.2.1 The Atmosphere

It is common practice to divide the atmosphere, primarily on the basis of temperature gradient, into several relatively well-defined regions, the troposphere, the stratosphere, the mesosphere, the thermosphere and the exosphere (McEwan and Phillips, 1975). The lowest region is the troposphere which contains about three quarters of the atmosphere by weight and virtually all the moisture. Above the troposphere is the stratosphere which is dry and cloudless. Almost all the carbon present in the atmosphere is contained in either the troposphere (~84%) or the stratosphere (~16%) (Baxter and Walton, 1970). Therefore, the remaining regions, the mesosphere, the thermosphere and the exosphere, are unimportant from the standpoint of the carbon cycle.

Mixing processes in the atmosphere are primarily due to eddy diffusion and convection, although the latter is largely confined to the troposphere. In general, the mixing processes in the stratosphere are slower than in the troposphere, most of the movement being due to horizontal diffusion. This fact can be clearly demonstrated by comparing the interhemispheric mixing of carbon in the two different layers of the atmosphere. For the comparatively turbulent troposphere the exchange time for the interhemispheric mixing of carbon is estimated at around 1 year (Lal and Rama, 1966; Nydal, 1967, 1968) whereas in the stratosphere it is estimated at around 5 years (Lal and Rama, 1966; Nydal, 1967, 1968). The carbon exchange time from stratosphere to troposphere is similar to the interhemispheric exchange times, i.e. around 2-4 years (Nydal, 1967, 1968; Young

Estimates of the inventory of carbon in pre-agricultural terrestrial biota range from  $7-11 \times 10^{14}$  kg (Olson, 1974, 1985; Matthews, 1983). The major uncertainties arise in calculating the size of tropical rain and subtropical forests. In general, the carbon in this reservoir has a residence time of less than 100 years (Houghton et al., 1985a; Olson et al., 1985). The smaller pools of rapidly exchanging organic carbon (residence time 1-2 years; plant leaves, small branches and roots, litter, invertebrates, decomposers), when combined, are equal to about 20% of the total living pool. Only very small fractions of total carbon in terrestrial carbon pools ( $4 \times 10^{12}$  kg) are represented by animals, including humans.

The quantity of carbon in humus,  $1.5-2.0 \times 10^{15}$  kg (Bolin et al., 1981; Olson et al., 1985), is larger than that in terrestrial biota. Uncertainties in the estimate are the result of differing predictions of the peat content of soils. Estimates of residence times of carbon in humus tend to be relatively longer, in the region of 100-1000 years (Houghton et al., 1985a; Olson et al., 1985).

#### 1.2.2.3 The Hydrosphere

The hydrosphere is made up of both freshwater (e.g. polar ice caps, lakes, rivers, etc.) and oceans. However, as far as the carbon cycle is concerned, it is sufficient to focus on the oceans alone, since the amount of carbon contained in the freshwater component of the hydrosphere and in its associated fluxes is insignificantly small by comparison to that in the oceans (Kempe, 1979a).

In assessment of  $\text{CO}_2$  exchange between atmosphere and oceans, the latter reservoir is commonly divided into functional layers. The surface layer extends on average to about 75 m; it is heated by the sun and agitated by the wind and thus is relatively well-mixed (Bolin et al., 1979, 1981). Beneath this layer is a boundary region (the thermocline) which is relatively stable because of decreasing temperature and increasing density with depth from the mixed layer to about 1000 m. The thermocline is in essence a barrier to mixing and isolates the deep ocean from surface waters. When surface waters are sufficiently cold and/or

and Fairhall, 1968; Walton et al., 1970). Because all the atmospheric exchange times are rather short, i.e. the mixing of carbon within the atmosphere is rapid, it is reasonable, for most purposes, to conceive of the atmosphere as one, well-mixed, carbon reservoir.

The natural inventory of carbon in the atmosphere is thought to be around  $5.9 \times 10^{14}$  kg, or 280 ppm (volume) (Neftel et al., 1985; Friedli et al., 1986), although estimates vary from  $5.5\text{--}6.1 \times 10^{14}$  kg (Bray, 1959; Stuiver, 1978; Barnola et al., 1983). The overwhelming bulk of the carbon is present as  $\text{CO}_2$ , with the principle naturally occurring minor constituents being CO and  $\text{CH}_4$ .

The atmosphere exchanges carbon with both the terrestrial biosphere and the hydrosphere and so the residence time of carbon in the atmosphere is rather short, about 4 years (Nydal, 1967, 1968; Young and Fairhall, 1968; Walton et al., 1970; Gammon et al., 1985).

#### 1.2.2.2 The Terrestrial Biosphere

The terrestrial biosphere is a large heterogeneous carbon reservoir and can be subdivided in many different ways. The most common approach involves its division into terrestrial biota and humus fractions. The terrestrial biota compartment comprises all living, as well as all standing dead, material; fallen and below ground dead matter constitutes the humus component.

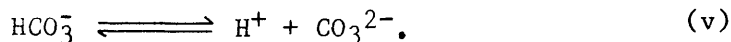
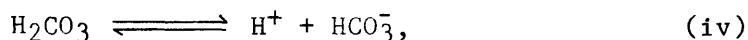
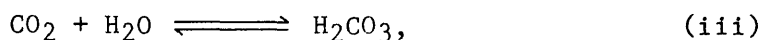
The exchange of carbon between the atmosphere and the terrestrial ecosystem is driven by the processes of photosynthesis, respiration and decomposition. Green plants assimilate  $\text{CO}_2$  from the atmosphere via photosynthesis. Part of this  $\text{CO}_2$  is used by the plant to meet its metabolic requirements and is respired through leaves and root systems. The remainder is available to heterotrophic organisms which either consume the plant matter directly or decompose the plant litter gradually. The total amount of carbon exchanged between the atmosphere and biosphere in this manner is difficult to determine but most estimates lie in the range  $6\text{--}12 \times 10^{13}$  kg year<sup>-1</sup> (Degens et al., 1984; Houghton et al., 1985a).

saline, however, the thermocline weakens and surface waters sink (or mix) to depth and spread horizontally to produce a complex worldwide circulation pattern (Solomon et al., 1985). Surface waters descend mainly in polar regions and deep waters upwell from various depths elsewhere, particularly along the eastern sides of the major ocean basins. As well as these advective fluxes, the world's oceans are continuously stirred by the process of diffusion. Diffusion is the random mixing accomplished by the hosts of eddies and backwashes which are everywhere at work in the oceans (Broecker and Peng, 1982).

Carbon is present in the oceans in many different forms. Dissolved inorganic carbon (90% bicarbonate,  $\text{HCO}_3^-$ ) is the most abundant form. The total amount of inorganic carbon in the well-mixed surface water reservoir,  $5.6-6.6 \times 10^{14}$  kg (Baes et al., 1976; Bjorkstrom, 1979; Killough and Emanuel, 1981) is close to that of the atmosphere. The total amount in the entire ocean reservoir is around  $3.5-3.9 \times 10^{16}$  kg (Bolin et al., 1979; Olson et al., 1985). Organic carbon (approximating to  $[\text{CH}_2\text{O}]_n$ ) is much less abundant (being dominated by dead organic matter), about  $10^{15}$  kg being present in the entire ocean (Mopper and Degens, 1979). Living carbon, about  $4 \times 10^{12}$  kg, is mainly represented by the photosynthesising organisms (the phytoplankton) confined to the surface region; carbon in zooplankton and larger animals is much less ( $2 \times 10^{10}$  kg). The ocean reservoir also contains carbonate solids (primarily formed by marine organisms), which are found both suspended in the water column and incorporated in sediments (Bolin et al., 1979). This material is largely calcium carbonate produced in surface waters and partially redissolved at depth. The deposits are generally confined to ocean depths less than 4 km, i.e. above the carbonate compensation depth. The top ~10 cm of these deposits are sufficiently mixed by the foraging and burrowing activities of bottom animals that it may be reasonable to include this system as a reactive part of the ocean reservoir (Solomon et al., 1985). The inventory of carbon present as calcium carbonate in these mobile deposits is about  $4 \times 10^{12}$  kg (Baes et al., 1976). The deeper sediments constitute the lithosphere.

The exchange of  $\text{CO}_2$  across the atmosphere-ocean interface

is governed by the difference between the partial pressures of  $\text{CO}_2$  ( $p\text{CO}_2$ ) in the atmosphere and surface waters. Transfer is generally assumed to be by molecular diffusion through a thin film and is controlled by temperature, wind stress and processes such as turbulent mixing. The  $p\text{CO}_2$  in the atmosphere is proportional to the ratio of the masses of  $\text{CO}_2$  and dry air, whereas the  $p\text{CO}_2$  in surface waters depends on the chemical equilibria amongst carbon compounds (Keeling, 1973), e.g. the reactions of primary concern are:



The gross annual exchange of carbon between the atmosphere and the oceans is estimated at  $1.0\text{-}1.1 \times 10^{14}$  kg (Bolin et al., 1979). For carbon in the surface ocean the residence time is around 5-8 years (Craig, 1957; Bolin et al., 1981; Baes et al., 1985) but in the deep ocean it is far longer, around 500-1000 years (Craig, 1957; Bolin et al., 1981; Baes et al., 1985).

#### 1.2.2.4 The Lithosphere

The lithosphere is the largest carbon reservoir. It contains about  $6.5 \times 10^{19}$  kg of carbon, of which 75% is bound as various inorganic carbonates and the remainder as either organic or non-carbonate carbon (Kempe, 1979b). The inorganic carbon is principally in forms of  $\text{CaCO}_3$ , such as calcite or aragonite. Fossil fuels are an economically important component of the organic carbon although they contribute perhaps less than 1% of its mass.

The lithosphere exchanges carbon directly with the hydrosphere. Carbon flux across the ocean-sediment interface can be generated by a number of processes. Sedimentation can occur by gravitational sinking of organic particles or by precipitation of dissolved carbonates. In the reverse direction, return of sedimentary carbon to the hydrosphere can be caused by diagenetic dissolution of carbonates. However, although the oceans and the underlying sediments constitute the two largest carbon reservoirs, the carbon flux between the two is extremely small (Olson et al., 1985). Subsequently, the residence time of carbon in the lithosphere is extremely large (around  $10^8$  years). For these

reasons, the lithosphere is not usually included in models of the dynamic carbon cycle.

#### 1.2.2.5 $^{14}\text{C}$ in the Global Carbon Cycle

After its formation in the upper atmosphere (predominantly in the stratosphere),  $^{14}\text{C}$  becomes distributed amongst the various reservoirs of the carbon cycle. The distribution of both stable and unstable isotopes of carbon is assumed to be governed by the same exchange processes. Nevertheless, differences in the  $^{14}\text{C}$  specific activities of the various carbon pools do exist. Such differences are brought about by two separate effects, namely by isotopic fractionation and ageing.

Isotopic fractionation induces small changes in the  $^{14}\text{C}/^{12}\text{C}$  ratios when carbon is transferred from one reservoir to another. This effect is caused by slight differences in the thermodynamic properties of the isotopes (Craig, 1953). The isotopic fractionation value,  $\delta^{13}\text{C}$ , for each reservoir is presented in Figure 1.1 (for explanation of  $\delta^{13}\text{C}$  scale see Section 2.3).

The second and by far more dominant effect is that of the decay of radiocarbon. That is, during residence of the radiocarbon in any one carbon pool, it gradually decays with a half-life of 5730 years. Therefore, the reservoirs which involve the longest residence time of carbon have, in general, the lowest  $^{14}\text{C}$  specific activities. Other factors, e.g. the  $^{14}\text{C}$  specific activity in the reservoirs with which carbon is exchanged, do also have some influence on the resulting value. Since the radiocarbon is formed in the atmosphere, which in turn has a short carbon residence time, it is this reservoir which has the highest  $^{14}\text{C}$  specific activity,  $226 \text{ Bq kg}^{-1}$  (carbon) (Karlen et al., 1964). Terrestrial biota, which are in reasonably rapid equilibrium with the atmosphere, have, on average, a similar  $^{14}\text{C}$  specific activity but the longer residence times of carbon in humus induce in it a slightly depressed activity of around  $215 \text{ Bq kg}^{-1}$  (carbon). The  $^{14}\text{C}$  specific activity in the hydrosphere basically decreases with depth. Well-mixed surface waters have an activity similar to that of humus, while the average value for the deep ocean is around  $190 \text{ Bq kg}^{-1}$

(carbon). It can be assumed that the lithosphere, which is essentially removed from the dynamic carbon cycle, contains no radiocarbon at all. The  $^{14}\text{C}$  specific activities, as presented by Bolin et al. (1981), are shown in Figure 1.1 as  $\Delta^{14}\text{C}$  values. These values represent the per mil deviation of the  $^{14}\text{C}$  specific activities from the natural atmospheric value of  $226 \text{ Bq kg}^{-1}$  (carbon), after being corrected for isotopic fractionation (see Section 2.5.6).

### 1.2.3 Radiocarbon Dating

For radiocarbon dating purposes, it is assumed that the distribution of  $^{14}\text{C}$  in the various carbon reservoirs has remained constant throughout the ~50 000 year time period covered by the method. This assumption of equilibrium implies constancy of the  $^{14}\text{C}/^{12}\text{C}$  ratio in all reservoirs of the cycle, of the  $^{14}\text{C}$  production rate and of the carbon exchange rates between the reservoirs. During the lifetime of living materials an equilibrium is established whereby assimilation of  $^{14}\text{C}$  is balanced by radioactive decay. At death, however,  $^{14}\text{C}$  uptake ceases, while decay of the  $^{14}\text{C}$  continues. On the assumption that the material remains a closed system, the  $^{14}\text{C}$  concentration decreases with time according to the half-life of  $^{14}\text{C}$ . Accurate measurement of the residual  $^{14}\text{C}$  activity allows the age of the sample to be calculated.

Investigation of the validity of the various assumptions of radiocarbon dating commenced as soon as physical and chemical techniques had developed adequately. Although the approximate validity of the assumptions were initially justified by dating known-age Egyptian dynasty samples (Libby, 1952), experimental errors were relatively large and the observed agreement was therefore no more than approximate. As more accurate radiocarbon detection methods became available, then temporal variations in the atmospheric  $^{14}\text{C}/^{12}\text{C}$  ratio came to light.

### 1.2.4 Natural Variations of $^{14}\text{C}$ Levels

In 1958, de Vries showed the existence of an increase in atmospheric  $^{14}\text{C}$  concentrations in the years around 1700 AD by about 2% relative to the 'natural' level, an anomaly subsequently called the 'de Vries effect'. Subsequent work by Willis et al.

(1960) documented similar variations.

This discovery generated the drive to construct a record of the historic fluctuations of  $^{14}\text{C}$  concentrations in the atmosphere. Such a record stretching back 8000 years was constructed by Suess (1970a) using samples of known-age tree rings as an indicator of atmospheric  $^{14}\text{C}$  levels. The samples were largely derived from the bristlecone pine tree ring chronology constructed by Ferguson and co-workers at the Laboratory of Tree-Ring Research, Arizona (Ferguson, 1968, 1969, 1970, 1972). The  $^{14}\text{C}$  record was pushed back further to 10 000 years BP, i.e. 10 000 years before 1950 (BP stands for 'Before Physics' (Flint and Deevey, 1962)), using the varve series from Lake of the Clouds, Minnesota (Stuiver, 1970). Varves are the annual layers found in clays which deposit in the beds of glacial lakes. The Swedish varve chronology of de Geer (1940) was used by Tauber (1970) to monitor  $^{14}\text{C}$  levels back to 12 500 years BP.

The variations in the atmospheric  $^{14}\text{C}$  concentrations during the past twelve millenia are illustrated in Figure 1.2 and are based on both tree ring and varve data. In general, there is excellent agreement between the data. However, before 7000 years BP, there is a discrepancy between the two sets of varve data. This is unlikely to be the result of a real difference in  $^{14}\text{C}$  levels between the two locations but could be due to errors in either or both chronologies. Two main trends are apparent from these results:

- (a) a long-term increase in  $^{14}\text{C}$  concentrations of around 10% from 2500 BP to 6000 BP
- and
- (b) short-term fluctuations of 1-2% over a period of centuries.

The large scale variation in atmospheric  $^{14}\text{C}$  levels is thought to be caused by changes in the cosmic ray flux incident on the earth's atmosphere due to changes in the earth's magnetic field (Bucha, 1970; Bruns et al., 1983). That is, as the earth's magnetic dipole moment increases, the deflection of cosmic rays increases and so the  $^{14}\text{C}$  production rate decreases (Elsasser et al., 1956). Archaeomagnetic measurements imply that the

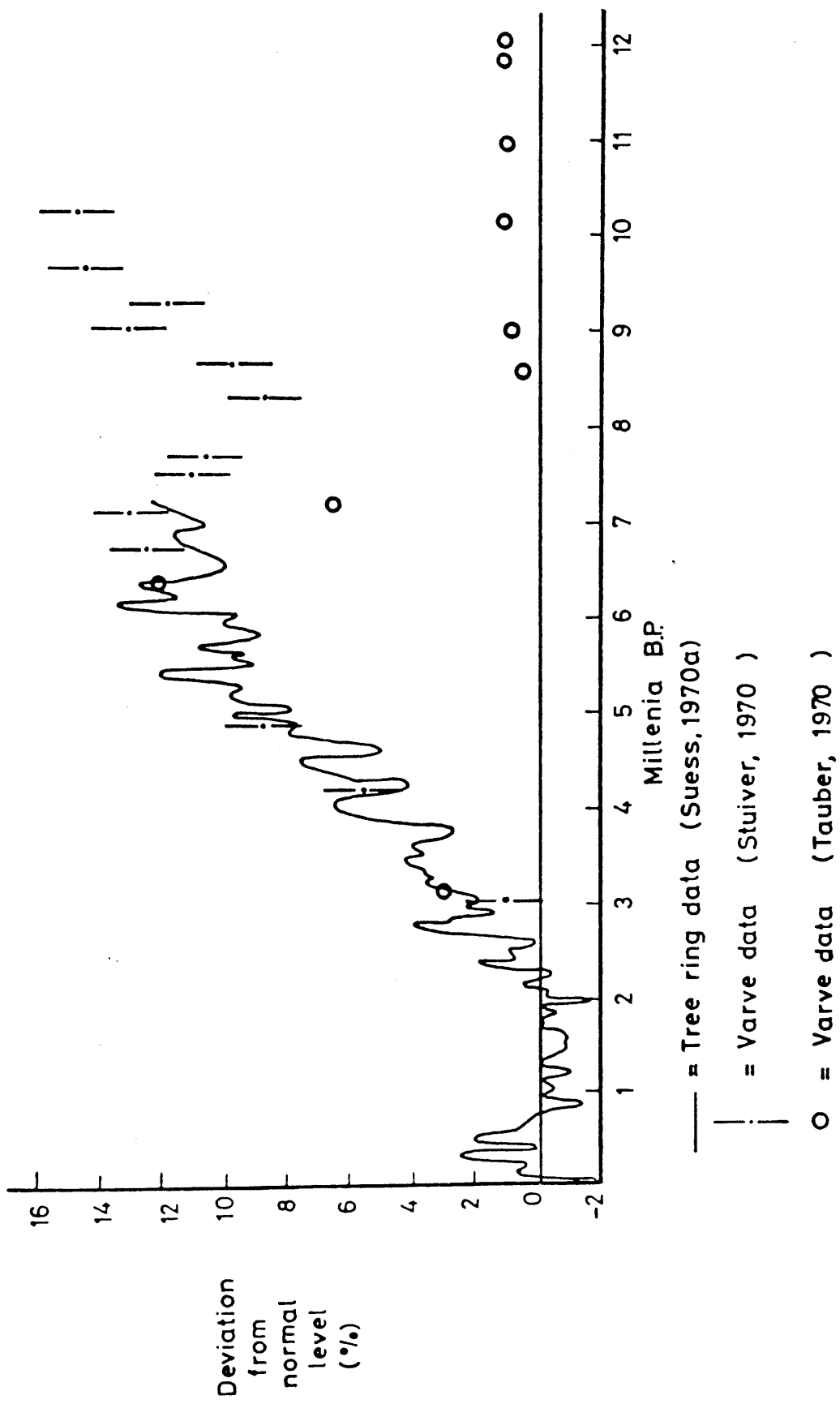


FIGURE 1-2: Atmospheric <sup>14</sup>C levels during the last 12 millennia.

earth's magnetic field has fluctuated in an approximately sinusoidal manner with a period of about 8000 years (Bucha and Neustupny, 1967).

The presence of short-term variations in the atmospheric  $^{14}\text{C}$  levels had been challenged by some (Damon et al., 1972; Ralph et al., 1973) who argued that the available data did not support the existence of such fluctuations. Later, however, several high-precision  $^{14}\text{C}$  laboratories produced results which independently confirmed the existence of short-term fluctuations (de Jong et al., 1979; Bruns et al., 1980; Stuiver, 1982). The latter are thought to be caused by changes in the solar flare (sunspot) activity (Stuiver, 1961; Suess, 1970b; Baxter and Walton, 1971). At times of high solar activity, the cosmic ray flux incident on the earth decreases and so the  $^{14}\text{C}$  production rate decreases. Variations in solar activity appear to have certain periodicities which are reflected in the  $^{14}\text{C}$  levels. Cycles from as little as 11 years up to ones of 400 years have been reported (Suess, 1970b; Houtermans, 1971; Baxter and Farmer, 1973).

It is also possible that solar activity may not only have a direct influence on  $^{14}\text{C}$  levels via production rate changes but may also induce climatic variation (Damon, 1968; Suess, 1968) which may, in turn, affect the transfer and exchange of carbon dioxide in the carbon cycle. However, work by Stuiver (1980) was unable to confirm a relationship between the climatic time series and solar activity. Nevertheless, several correlations of atmospheric  $^{14}\text{C}$  levels with general patterns of climatic change have been noted, the most remarkable of these being the correlation of the de Vries effect with the retreat of the glacier front. In addition, Lal and Venkatavaradan (1970) have suggested that the high  $^{14}\text{C}$  activity of 10 000 BP can be attributed to the last ice-age. Despite these observations, Damon (1970) and Suess (1970b) conclude independently that climatic changes in the last 8 millenia are of minor importance with respect to the previous two causes and, in fact, point out that certain climatic factors would compensate each other. For example, a decrease in global temperature could result in a decrease in the partial pressure of  $\text{CO}_2$  in the atmosphere resulting in an increase in

$^{14}\text{C}$  specific activity. On the other hand, the oceanic thermocline would be weakened, resulting in much faster oceanic mixing. The consequence would be more rapid transport of  $^{14}\text{C}$  into the oceans, that is, a decrease in atmospheric radiocarbon.

#### 1.2.5 Anthropogenic Variations of $^{14}\text{C}$ Levels

In addition to these natural variations, there have also been anthropogenic perturbations to the carbon cycle which have influenced  $^{14}\text{C}$  levels. In fact, man has been responsible for three major interferences, each of which is now discussed.

##### 1.2.5.1 The Suess Effect

The Suess effect has its origins in the Industrial Revolution and the subsequent combustion of large quantities of fossil fuels (coal, lignite, oil and gas). Since all these materials are derived from ancient sedimentary systems, they are essentially devoid of  $^{14}\text{C}$ . The carbon dioxide produced, therefore, increases the atmospheric inventory of inactive  $\text{CO}_2$  and decreases the  $^{14}\text{C}/^{12}\text{C}$  ratio. This dilution of atmospheric  $^{14}\text{C}$  levels was first detected by Suess (1955) and is thus generally known as the 'Suess effect'.

A record of  $\text{CO}_2$  emissions from fossil fuel combustion and cement production ( $\text{CO}_2$  is released during the decomposition of limestone during cement manufacture) since 1860 has been tabulated by Rotty and Masters (1985) and is shown in Figure 1.3. The data for fossil fuel combustion are taken from UN Series - World Energy Supplies and are based on fuel production rather than fuel consumption figures. The data show a nearly constant 4.3% annual rate of increase in globally emitted  $\text{CO}_2$  for more than a century, with the exception of the 2 World War periods and the depression of the early 1930s. The reduction in the rate of increase in 1973 can be attributed to the OPEC price escalation and to the subsequent reduction in production of oil.

A record of the  $^{14}\text{C}$  specific activity in the atmosphere of the northern hemisphere from 1860-1950 is shown in Figure 1.4 (obtained from various sources as compiled by Damon et al. (1973)). In sympathy with the increase in  $\text{CO}_2$  release rates the Suess effect increased in magnitude, that is the  $^{14}\text{C}$  specific

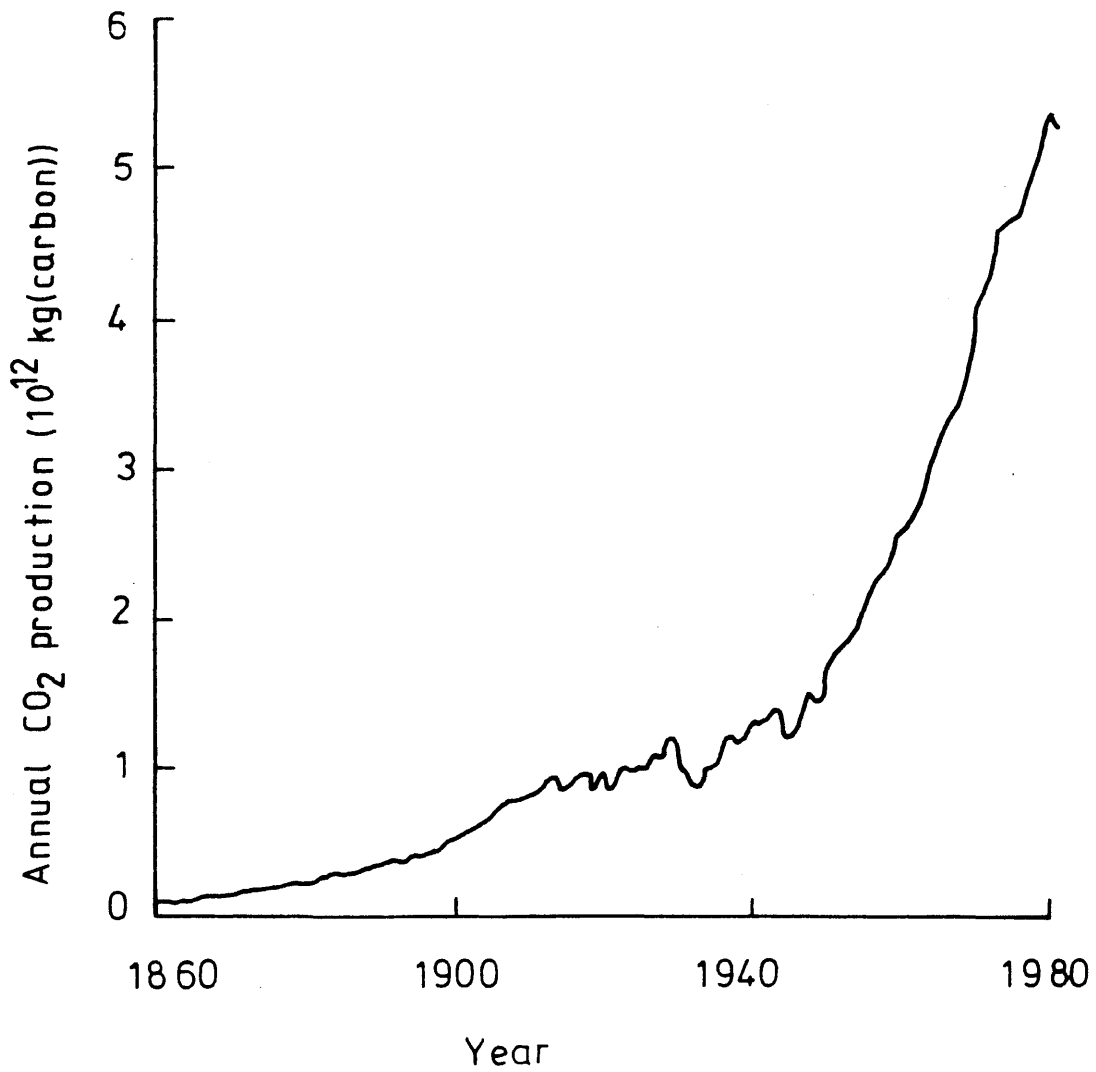


FIGURE 1-3: Production of CO<sub>2</sub> from fossil fuels and cement, 1860 - 1980.

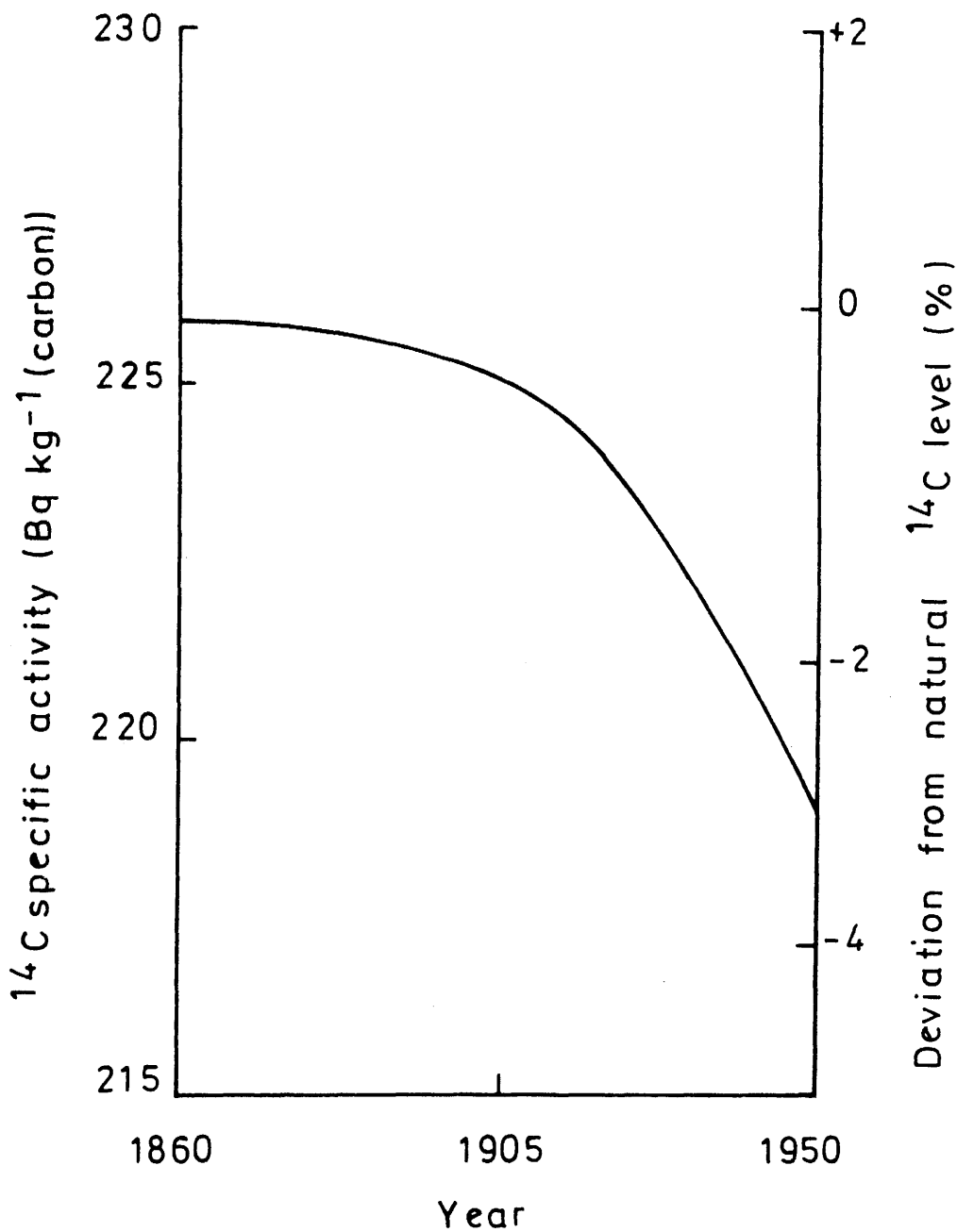


FIGURE 1:4 Atmospheric  $^{14}\text{C}$  specific activity, 1860 - 1950.

activity decreased, in fairly monotonic fashion, between 1860 and 1950 AD. By the latter date this effect amounted to approximately -2 and -3% in the southern and northern hemisphere atmospheres respectively (Suess, 1955; Fergusson, 1958; Houtermans et al., 1967). The difference between these two values is a result of (1) the finite mixing time between the two hemispheres, (2) the fact that most fossil fuel combustion took place in the more highly industrialised northern hemisphere and (3) higher atmosphere to surface ocean CO<sub>2</sub> flux in the southern hemisphere (Young and Fairhall, 1968). Further work by Stuiver and Quay (1981) confirmed that this decrease in atmospheric <sup>14</sup>C specific activities was the result, mainly, of this anthropogenic source, although a small proportion (around 0.3%) could be attributed to natural variations.

Inactive CO<sub>2</sub> emissions have been steadily increasing since 1950 and so an even more pronounced difference in the atmospheric <sup>14</sup>C specific activity would be expected. However, since the coming of the era of nuclear weapons, the Suess effect record has been totally lost, variations in environmental <sup>14</sup>C levels being dominated for the past 35 years or so by the <sup>14</sup>C increases caused by large scale atmospheric and ground-surface testing of nuclear weapons, i.e. the 'bomb effect'.

#### 1.2.5.2 The Bomb Effect

The era of nuclear weapons and their testing was ushered in on the morning of 16 July 1945 in the desert near Alamogordo, New Mexico. Over the following 40 years nuclear tests have been conducted in the atmosphere at sporadic intervals. The most significant test programmes took place during 1954-58 and particularly 1961-62 when many large yield explosions occurred (Carter and Moghissi, 1977).

Radiocarbon is produced in nuclear explosions, again via neutron activation of atmospheric nitrogen, <sup>14</sup>N(n,p)<sup>14</sup>C. It has been estimated by the United Nations (1982) that a total of  $2.2 \times 10^{17}$  Bq of <sup>14</sup>C were produced by nuclear weapon tests up to 1980. This value corresponds to an average production rate of  $4.0 \times 10^{14}$  Bq Mton<sup>-1</sup> but the latter figure is not representative of any given nuclear explosion because the

production of  $^{14}\text{C}$  depends on the type of nuclear device exploded and on whether the explosion occurs at the earth's surface or high in the atmosphere. A surface test produces approximately 50% of the  $^{14}\text{C}$  produced by the same device in an air test because about half of the escaping neutrons are captured in the soil or water rather than in the atmosphere. The estimated production of  $^{14}\text{C}$  for each year during the period 1945-1980 is shown in Figure 1.5. In fact, 1980 is the year in which the last reported nuclear explosion in the atmosphere took place (Cambray et al., 1985).

The effect of this injection of radiocarbon on atmospheric  $^{14}\text{C}$  levels is shown in Figure 1.6. The data shown are based mainly on ground-level measurements of  $^{14}\text{C}$  in atmospheric  $\text{CO}_2$  at mid and high latitudes of both hemispheres. This data set is based on the work of many people (Broecker and Walton, 1959; Munnich, 1963; Ostlund and Engstrand, 1963; Olsson and Karlen, 1965; Sternberg and Olsson, 1967; Nydal, 1968; Vogel and Lerman, 1969; Olsson and Klasson, 1970; Vogel, 1970; Walton et al., 1970; Baxter and Walton, 1971; Vogel and Marais, 1971; Baxter and Stenhouse, 1976; Tans, 1978; Nydal et al., 1979; Nydal and Lovseth, 1983; Segl et al., 1983; Harkness, pers. comm., 1986; this work, Chapter 3) but all the measurements up to 1977 have been brought together in a compilation by Tans (1981).

The majority of the nuclear weapon tests occurred in the northern hemisphere and hence  $^{14}\text{C}$  levels in the northern hemisphere were significantly higher than those in the southern hemisphere. This effect is another manifestation of the finite mixing time between the two hemispheres. The values obtained at low latitudes are, as expected, intermediate between those given for both hemispheres (Nydal, 1968; Young and Fairhall, 1968). Another point of interest is that maximum levels in the northern hemisphere were observed in 1963/64, approximately two years after the period of maximum production. The explanation of this delay is that after large atmospheric nuclear explosions most of the  $^{14}\text{C}$  is transported directly into the stratosphere which has a finite residence time of several years. Equilibrium with the troposphere therefore occurs relatively slowly.

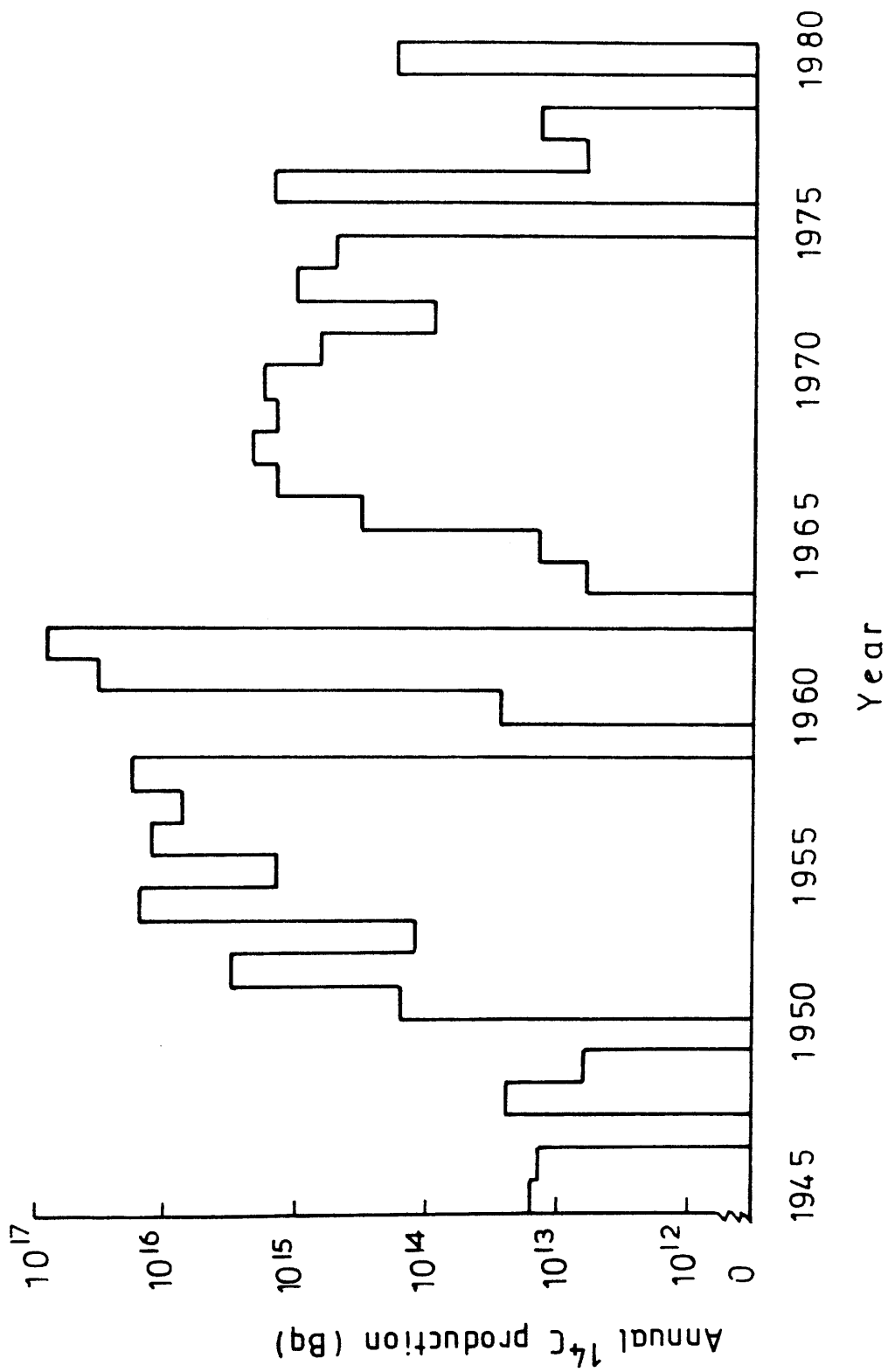


FIGURE 1-5: Production of  $^{14}\text{C}$  from nuclear weapon tests, 1945 - 1980.

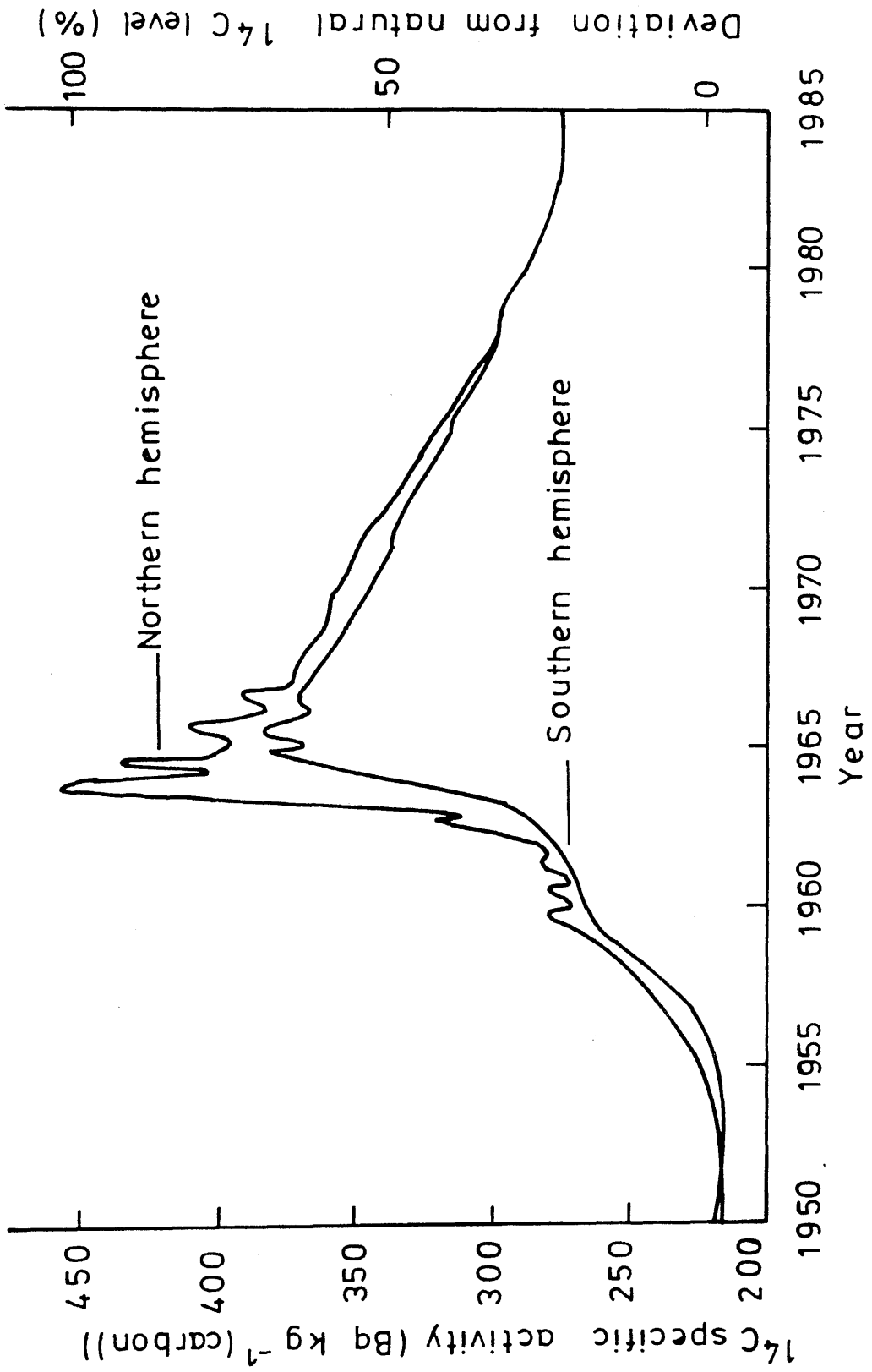


FIGURE 1-6: Atmospheric  $^{14}\text{C}$  specific activity, 1950 - 1985.

Following the maximum levels of 1963/64, the mean  $^{14}\text{C}$  specific activity in the atmosphere has since gradually decreased to its present-day level of around  $275 \text{ Bq kg}^{-1}$  (carbon) as the excess  $^{14}\text{C}$  has been taken up by the biosphere and oceans.

### 1.2.5.3 Changes in Land Usage

The final activity of man to affect the  $^{14}\text{C}$  levels is that of disturbing terrestrial ecosystems. Such changes in land usage modulates the carbon flux between the atmosphere and the biosphere. Practices which enhance the atmospheric pool of carbon are clearing of forests, industrial use of wood, use of firewood and decomposition of soil organic matter. Transfers in the opposite direction may be effected by intentional or inadvertant creation of ecosystems which accumulate high levels of phytomass.

Estimates of the net transfer of carbon between the atmosphere and the biosphere are at best reasoned guesses and their accuracy and reliability are accordingly low. However, it seems probable that at present the biosphere is a net source of carbon to the atmosphere. Based on the most recent analyses (Molofsky et al., 1984; Detwiler et al., 1985; Houghton et al., 1985b), the net flux of carbon from terrestrial ecosystems to the atmosphere, as a result of changes in land use, is estimated to lie within the range  $0-2.6 \times 10^{12} \text{ kg year}^{-1}$ . Even so, the possiblity that the biosphere is a net sink for atmospheric carbon cannot be totally discarded (Hampicke, 1979). Estimates of the total carbon release from the biosphere in the past have been obtained by two different methods. One approach is to assemble historic deforestation and agricultural expansion data and to calculate the inventory of carbon involved (Houghton et al., 1983). The other method is to reconstruct changes in the storage of carbon in the biosphere from tree ring  $^{13}\text{C}$  data (Peng et al., 1983). Recent analyses based on both techniques suggest a range of  $9-18 \times 10^{12} \text{ kg}$  for total carbon releases to the atmosphere. The reconstructed time series for terrestrial biospheric fluxes of Houghton et al. (1983) and Peng et al. (1983) are shown in Figure 1.7. The differences between the two data sets are quite striking which, once again, underlines the uncertainties inherent in these calculations.

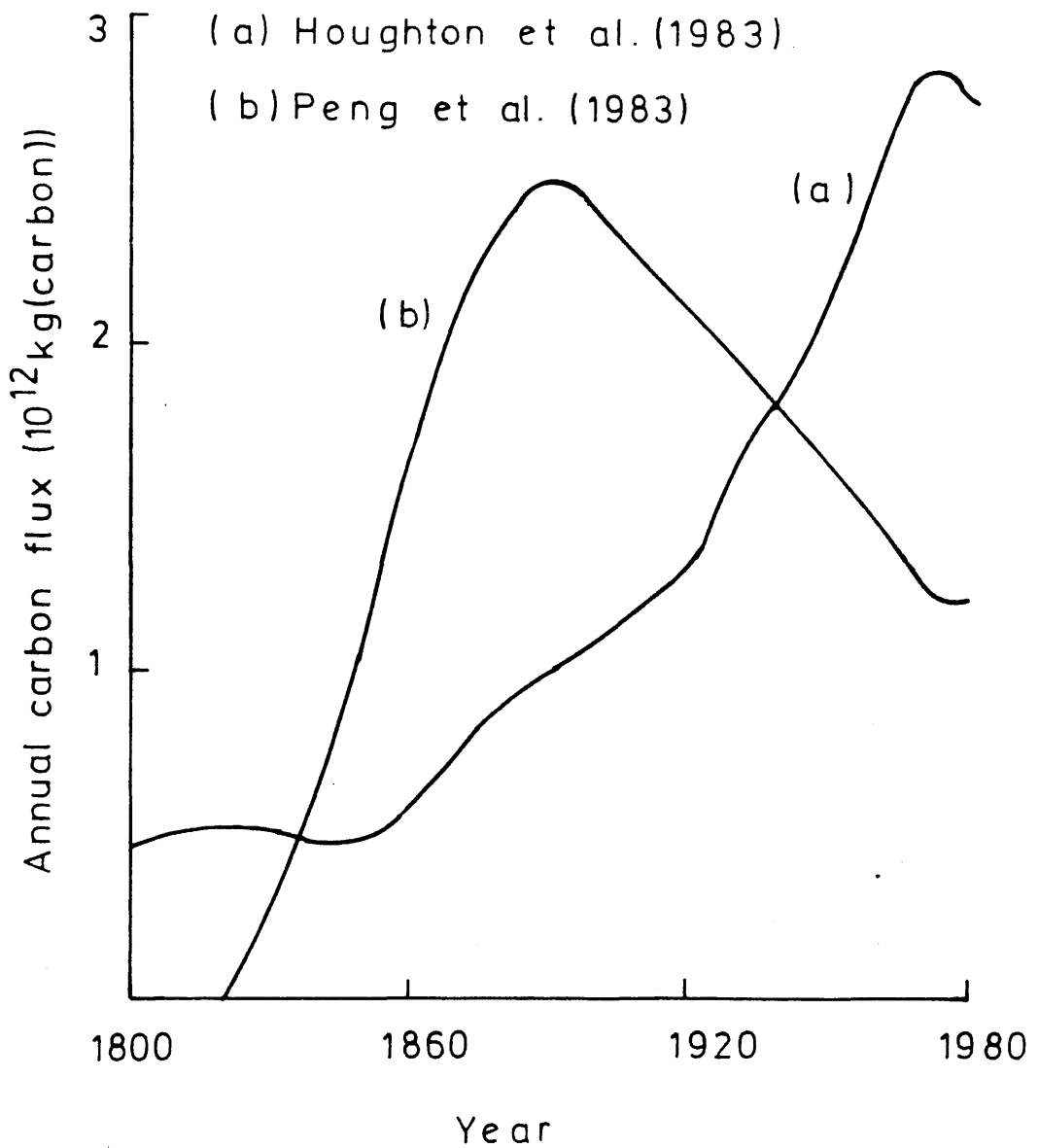


FIGURE 1.7 : Net flux of carbon to the atmosphere from terrestrial ecosystems, 1800 - 1980 .

The significance here of this carbon flux from the biosphere is that it increases the atmospheric carbon dioxide concentration and hence increases the absolute amount of  $^{14}\text{C}$  in the atmosphere. However, since this transfer of carbon involves two pools which are in reasonably rapid equilibrium with each other, i.e. the  $^{14}\text{C}$  specific activities are similar, this effect should not actually modify the  $^{14}\text{C}/^{12}\text{C}$  ratio in the atmosphere to a major extent. Nevertheless, although man's changes in land usage do not directly alter the atmospheric  $^{14}\text{C}$  specific activity, it could, in conjunction with  $\text{CO}_2$  releases from fossil fuel combustion, indirectly influence it via the greenhouse effect and  $\text{CO}_2$ -fertilisation.

It is a well-documented fact that these two activities, land use changes and fossil fuel combustion, have together caused a steady increase in atmospheric  $\text{CO}_2$  concentrations over the last 150 years. This increase has been closely monitored since 1958 at Mauna Loa (Bacastow and Keeling, 1981; Keeling et al., 1982) and is shown in Figure 1.8. Records of atmospheric  $\text{CO}_2$  concentrations before 1958 are not very reliable but it seems likely that the natural level is around 280 ppm (c.f. Section 1.2.2.1). So, in Figure 1.8, the Mauna Loa record has been interpolated back to the natural level in 1800 AD, i.e. before any significant anthropogenic perturbations occurred. Now, since  $\text{CO}_2$  is a strong absorber and black radiator of infra-red radiation, an increase in the atmospheric  $\text{CO}_2$  concentration could produce an increase in global surface temperatures. This is known as the 'greenhouse effect' and it could produce quite dramatic changes within the global carbon cycle. However, the exact nature of the feedback of climate on the global carbon cycle is, as yet, very unclear. In any case, no significant deviation from normal global temperatures has yet been observed. Another possible effect is that the increased  $\text{CO}_2$  concentrations in the atmosphere could stimulate plant growth and so increase the size of the biosphere. This effect, known as ' $\text{CO}_2$ -fertilisation', was first suggested by Bacastow and Keeling (1973). However, at this time, there is no direct evidence that net ecosystem production has responded to increasing  $\text{CO}_2$  levels in the atmosphere (Woodwell, 1983). Indeed, recent work suggests that a significant fertilisation effect does not seem likely when

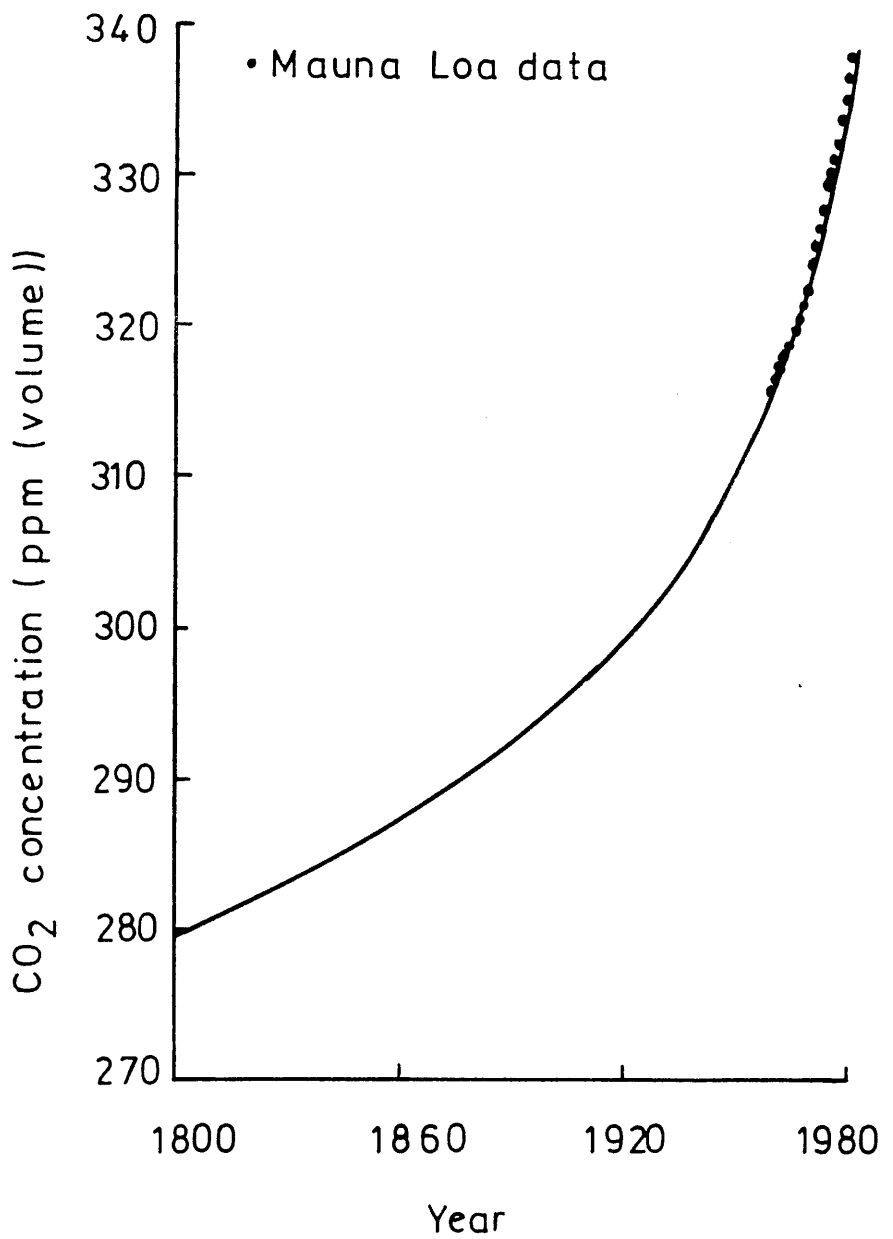


FIGURE 1.8: Atmospheric concentrations of carbon dioxide, 1800 - 1980.

other growth limiting factors (nutrients, water and light) are taken into account.

A fortuitous consequence of these anthropogenic perturbations is that they represent the almost ideal global tracer experiment by which to test the validity of carbon cycle models and, in particular, the exchange rates between different carbon reservoirs. This matter will be discussed in greater detail in Chapter 4.

### 1.3 $^{14}\text{C}$ DISCHARGES FROM THE NUCLEAR FUEL CYCLE

In recent years, a new potential source for the artificial modulation of  $^{14}\text{C}$  levels has become apparent. This new source is  $^{14}\text{C}$  produced in nuclear reactors and subsequently released to the environment. Certainly, at present, this represents a minor  $^{14}\text{C}$  input to the carbon cycle relative to the foregoing effects. However, with predicted future expansion, the nuclear industry could soon be producing very significant fluxes of  $^{14}\text{C}$ . In this section, the production and release of  $^{14}\text{C}$  from the nuclear fuel cycle will be discussed and, in addition, the history and potential future of the nuclear industry will be reviewed.

#### 1.3.1 The History of Nuclear Power

The first man-made self-sustaining nuclear chain reaction was induced by Professor Fermi and co-workers using the now famous 'pile' in the squash court of Chicago University on 2 December 1942. The development of nuclear energy was pushed initially by military programmes. The plutonium production piles at Hanford (USA), Windscale (UK) and Marcoule (France) were all primarily built to produce plutonium for nuclear weapons while the first power applications came with development of the nuclear submarine propulsion units in USA. The application for civil electricity generation followed quickly. In the UK, once-through air-cooled graphite piles of Windscale led to the closed cycle, carbon dioxide-cooled reactors of Calder Hall, the first of which came into operation in 1956. In the USA, the first civil nuclear power station, Shippingport, started up in 1957. These stations were essentially prototype systems rather than fully commercial stations and the nuclear power era is generally accepted as having

been ushered in by the order to General Electric, USA for the Oyster Creek nuclear power station and construction of the MAGNOX reactors in the UK. Oyster Creek came into operation in 1969, the MAGNOX reactors in 1962. These stations were bought by electricity companies because, for the first time, commercial tenders for nuclear power plants showed that the electricity they would generate was cheaper than that from contemporary coal or oil fired stations. The following years showed rapid expansion of nuclear power as more manufacturers and fuel supply companies entered the growing market. By 1 January 1984 there were 317 nuclear power reactors in operation, in 25 countries, with a net electrical power generating capacity of just under 191 GW(e). The growth of the world's nuclear capacity is shown graphically in Figure 1.9 and is based on data from IAEA (1984).

### 1.3.2 <sup>14</sup>C Waste Arisings in Nuclear Reactors

There are many different types of nuclear reactors but they all work on the same basic principles. Nuclear reactions in the nuclear core produce heat which is used to produce steam which, in turn, is used to drive an electrical generator. The main components of an 'average' thermal nuclear reactor are shown in Figure 1.10.

The reactor fuel contains the nuclides to be fissioned ( $^{235}\text{U}$ ,  $^{233}\text{U}$  or  $^{239}\text{Pu}$ ). With each fission, heat is released and neutrons are generated which assure a self-sustaining chain of fissions and thus a continuous source of heat. The control rods can be used to absorb neutrons and so slow down the rate of reaction. Typical control rod materials are boron and cadmium. The moderator is a material used to slow down fast neutrons to thermal neutrons, without unduly absorbing them, so that the probability of the neutrons causing fission is increased. Graphite (C), light water ( $\text{H}_2\text{O}$ ) and heavy water ( $\text{D}_2\text{O}$ ) are all commonly used as moderators. The coolant is a medium used to remove heat from the reactor core and to generate steam to drive electrical generators. Common coolants are water and carbon dioxide.

There are, at present, six general thermal reactor designs in use throughout the world, although many reactors contain their own

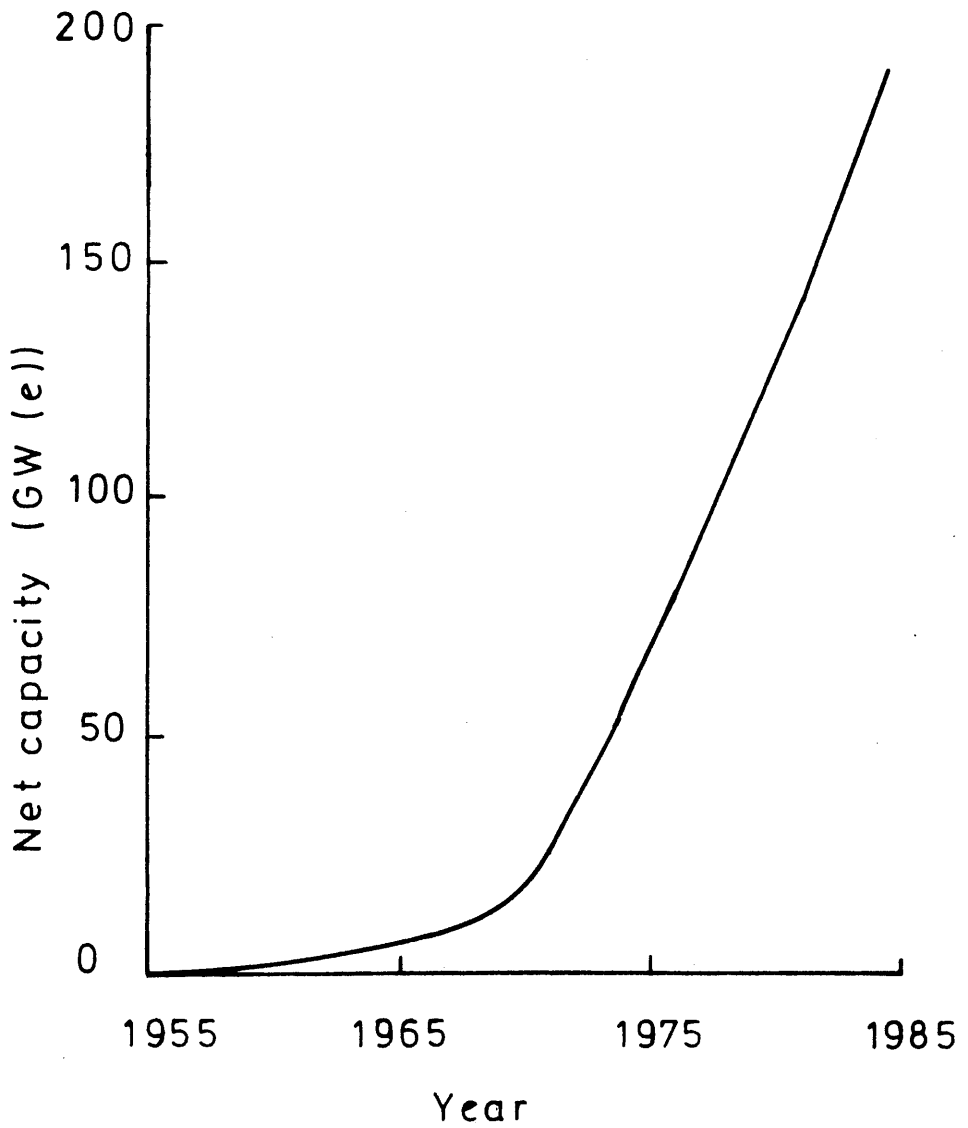


FIGURE 1-9: Nuclear electrical generating capacity, 1955 - 1984.

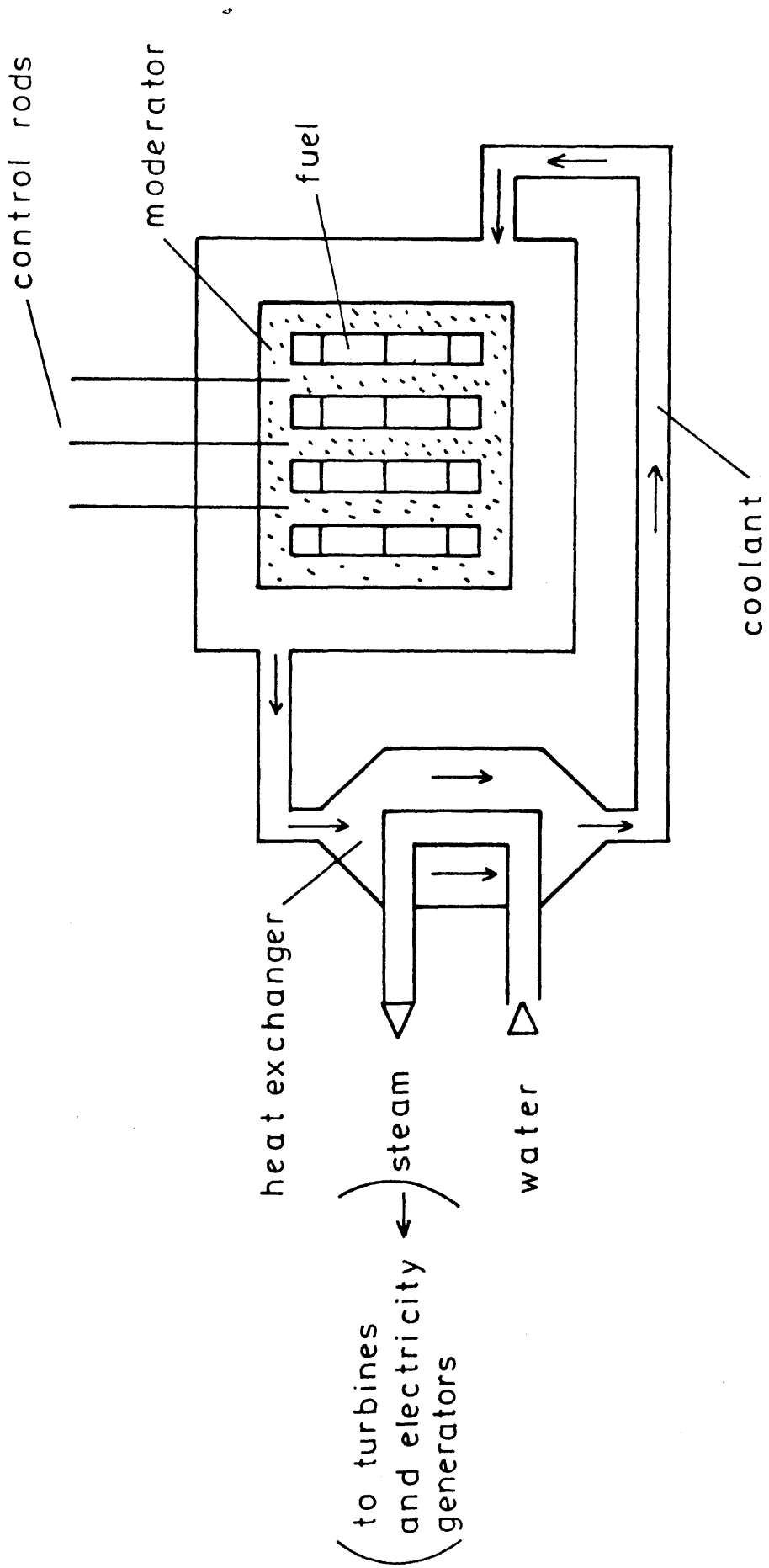


FIGURE 1·10: Schematic diagram of an 'average' thermal nuclear reactor.

specific modifications on a general design. The main reactor types are the two light water systems (the pressurised water and boiling water reactors), the heavy water reactor, the gas-cooled reactor, the advanced gas-cooled reactor and the high temperature gas-cooled reactor. These reactors are all similar to the basic design set out in Figure 1.10. Over the coming decades it is expected that the new liquid-metal-cooled fast breeder reactor will become more popular. This has a quite different design from thermal systems as it uses fast neutrons and produces more fissile material than it destroys (hence the name - fast breeder). The breeding is achieved by surrounding the fuel with a fertile material, i.e. material capable of being converted into fissile material ( $^{232}\text{Th}$  and  $^{238}\text{U}$  for example). Further in the future it is hoped to develop a fusion reactor system in which, as the name suggests, the heat is generated via fusion as opposed to fission reactions.

$^{14}\text{C}$  can be produced in reactors by a number of different nuclear reactions in the fuel, moderator, coolant and core construction materials. Figure 1.11 summarises the relevant reactions. Basically, all the  $^{14}\text{C}$  produced in nuclear reactors is formed via neutron activation reactions. The production rates for the various reactions will depend upon:

- (a) the neutron flux,
- (b) the neutron capture cross-section of the target atom at a particular neutron energy,
- (c) the amount of the target element present in the different reactor components

and

- (d) the abundance of the target isotopes in the target elements.

The target elements are carbon, oxygen and nitrogen. Carbon and oxygen are often major constituent elements of the reactor design, e.g. in the coolant ( $\text{H}_2\text{O}$ ,  $\text{CO}_2$ ), moderator (graphite,  $\text{H}_2\text{O}$ ) or in the fuel ( $\text{UO}_2$ ). Nitrogen, on the other hand, is present mainly as an impurity in the fuel or in the structural material. Nevertheless, the  $^{14}\text{N}$  activation reaction is usually the most important contributor to  $^{14}\text{C}$  production because of its high neutron capture cross-section and high isotopic abundance in natural nitrogen, as shown in Table 1.1 (the main exception is the graphite-moderated reactor in which the  $^{13}\text{C}(\text{n}, \gamma)^{14}\text{C}$

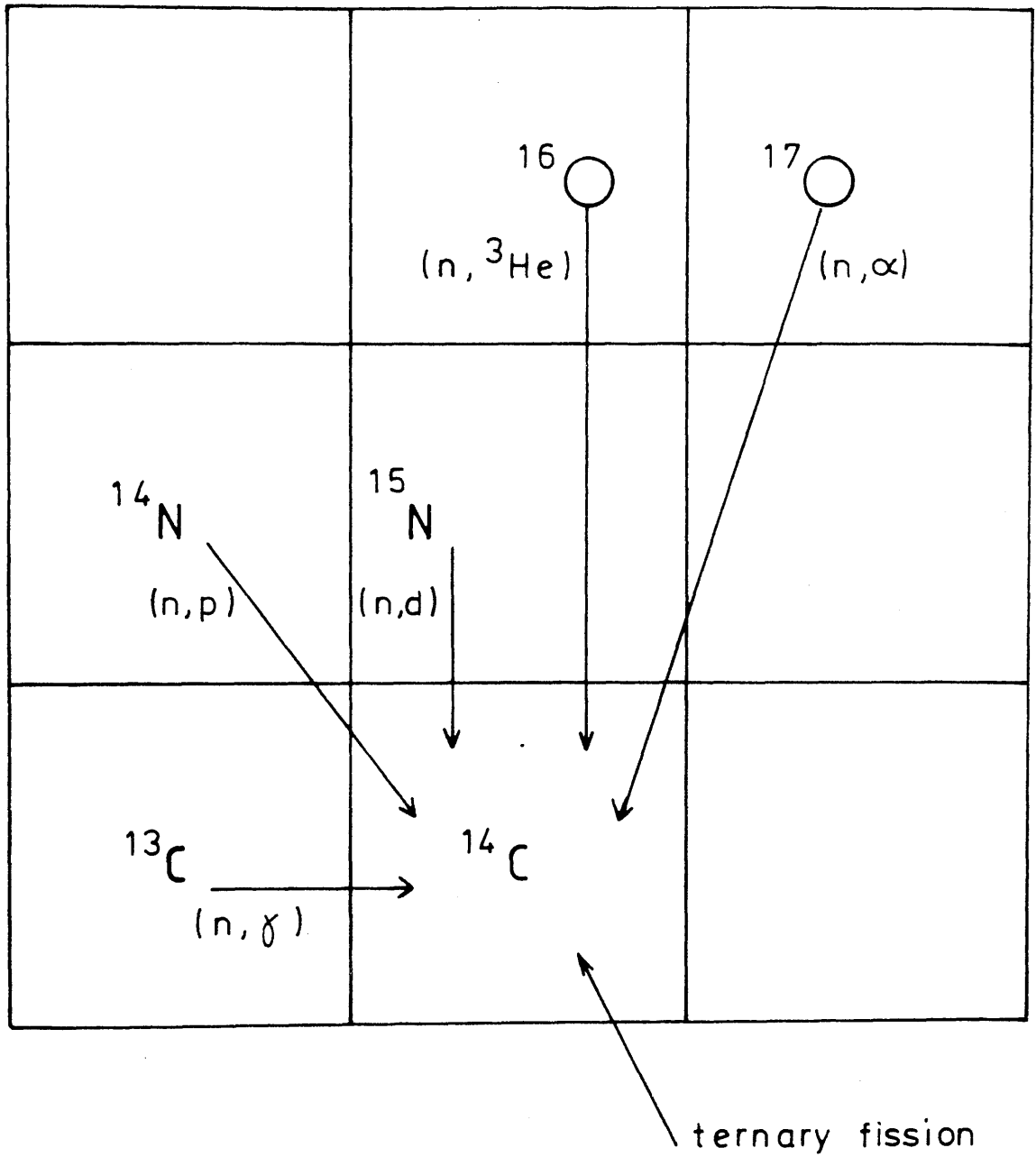


FIGURE 1-11: Nuclear reactions which contribute to the formation of  $^{14}\text{C}$ .

Table 1.1: Activation reactions producing  $^{14}\text{C}$

Reaction	Natural isotopic abundance of target elements (%)	Neutron capture cross-section (barns)	
		Thermal neutrons	Fast neutrons
$^{13}\text{C}(n,\gamma)^{14}\text{C}$	1.108	$1.0 \times 10^{-3}$	$5.0 \times 10^{-7}$
$^{14}\text{N}(n,p)^{14}\text{C}$	99.635	1.8	$1.3 \times 10^{-2}$
$^{15}\text{N}(n,d)^{14}\text{C}$	0.365	small	$1.0 \times 10^{-3}$
$^{16}\text{O}(n,^3\text{He})^{14}\text{C}$	99.759	small	$3.0 \times 10^{-8}$
$^{17}\text{O}(n,\alpha)^{14}\text{C}$	0.037	$2.4 \times 10^{-1}$	$1.2 \times 10^{-4}$

route is as important as the  $^{14}\text{N}(n,p)^{14}\text{C}$  reaction). Because the  $^{14}\text{N}$  activation reaction is so dominant in  $^{14}\text{C}$  production, the levels of nitrogen impurity in all reactor core materials are important parameters. The nitrogen levels vary widely and are sometimes not known very accurately. This fact introduces a considerable element of uncertainty into calculations of  $^{14}\text{C}$  arisings in reactors. Compared to these uncertainties,  $^{14}\text{C}$  production via ternary fission is insignificant. The ternary fission yield of  $^{14}\text{C}$  is currently estimated at around  $1.7 \times 10^{-6}$  per fission for all fissile nuclides (Hayes and MacMurdo, 1977) which corresponds to about  $0.02 \text{ TBq (GW(e) year)}^{-1}$  in light water reactor fuel. On this basis, the contribution of ternary fission to  $^{14}\text{C}$  production can largely be neglected for the purposes of this study.

The place of origin of  $^{14}\text{C}$  within a nuclear reactor has a strong influence on its discharge pathway. One can basically distinguish between three locations of  $^{14}\text{C}$  generation, namely:

- (a)  $^{14}\text{C}$  in the fuel and/or its cladding and associated components,
  - (b)  $^{14}\text{C}$  in structural materials of the core (and solid moderator, if applicable)
- and
- (c)  $^{14}\text{C}$  in the reactor coolant (and liquid moderator, if applicable).

The  $^{14}\text{C}$  produced in the fuel and/or its cladding and associated components may be removed from the reactor to a nuclear fuel reprocessing plant. The  $^{14}\text{C}$  in the fuel is released to the environment during chemical dissolution of the fuel (in the case of the commonly used PUREX process, the  $^{14}\text{C}$  is released in the form of  $\text{CO}_2$  (United Nations, 1981)) and the rest of the  $^{14}\text{C}$  will constitute a separate solid waste arising. Of course, at present, not all countries reprocess their spent nuclear fuel. In these cases, the  $^{14}\text{C}$  in fuel will further add to the solid waste arisings. The  $^{14}\text{C}$  produced in the structural material of the reactor or in a solid moderator will usually remain in the reactor until decommissioning occurs. The  $^{14}\text{C}$  produced in the coolant or in a liquid moderator is usually released to the environment at the reactor itself. This

release is either from the coolant purification and treatment system or from the plant ventilation system.

The amount of  $^{14}\text{C}$  produced, its chemical speciation and its discharge pathway will all depend on the details of each individual reactor system - all of which will now be discussed. The assumption will be made throughout the following sections that the spent nuclear fuel is reprocessed. However, by re-allocating the gaseous  $^{14}\text{C}$  discharges from the reprocessing plant to a solid waste arisings pool, an estimate of the alternative situation (i.e. no reprocessing) can be obtained.

#### 1.3.2.1 The Pressurised Water Reactor (PWR)

In these reactors the fuel used is enriched  $\text{UO}_2$  and the core is cooled and moderated by light water under about 150 atmospheres pressure. Many American reactors are of this type, including that at Three Mile Island. Despite the loss of coolant incident which triggered the Three Mile Island accident, this is the most popular reactor design in use today and is expected to remain the most common type constructed in the near future. For this reason, the details of this reactor's operating conditions are as well known as those of any reactor type.

$^{14}\text{C}$  production in PWRs occurs in the fuel ( $^{14}\text{N}(\text{n},\text{p})^{14}\text{C}$  and  $^{17}\text{O}(\text{n},\alpha)^{14}\text{C}$ ), in the coolant/moderator ( $^{17}\text{O}(\text{n},\alpha)^{14}\text{C}$ ), in the fuel cladding ( $^{14}\text{N}(\text{n},\text{p})^{14}\text{C}$ ) and in the structural material of the reactor core ( $^{14}\text{N}(\text{n},\text{p})^{14}\text{C}$ ). As mentioned previously, the main uncertainty in predicting the theoretical  $^{14}\text{C}$  production rate is in estimating the concentration of nitrogen impurities in the various components of the reactor. The estimates, by various authors, of the  $^{14}\text{C}$  production rates in the different components of a PWR, shown in Table 1.2, suggests an average overall production rate of  $2.4 \text{ TBq (GW(e) year)}^{-1}$ .

The fate of this  $^{14}\text{C}$  follows the basic guidelines previously stated. The  $^{14}\text{C}$  produced in the structural material of the reactor core will remain in the reactor until decommissioning. The  $^{14}\text{C}$  in the fuel and its cladding will be transferred to a nuclear fuel reprocessing plant where the

Table 1.2:  $^{14}\text{C}$  production in a PWR

Author	$^{14}\text{C}$ production rate (TBq (GW(e) year) $^{-1}$ )			
	Fuel	Coolant/moderator	Fuel cladding	Structural material
Hayes and MacMurdo (1975)	0.4	0.1	-	-
Kelly et al. (1975)	0.5	0.2	-	-
Fowler et al. (1976)	0.8	0.1	-	-
United Nations (1977)	0.4	0.2	-	-
Davis (1979)	0.7	0.2	0.4	0.8-1.2
Bonka (1980)	0.5	0.3	0.7	-
Average	0.6	0.2	0.6	1.0

$^{14}\text{C}$  in the fuel will be released to the environment (probably as  $\text{CO}_2$ ) and the remainder of the  $^{14}\text{C}$  will constitute a solid waste arising. The  $^{14}\text{C}$  formed in the water coolant/moderator is released to the atmosphere at the reactor itself. This  $^{14}\text{C}$  tends to be in the reduced form since the primary cooling circuit water contains hydrogen in excess to recombine with the oxygen produced by radiolysis. Under such conditions simple hydrocarbon compounds will be formed.

In general, measurements of  $^{14}\text{C}$  discharges from the PWR fuel cycle are in good agreement with the theoretical estimates. Kunz et al. (1974), for example, estimated, from measurements of decay-tank gas and containment air at three PWRs, a  $^{14}\text{C}$  release rate in airborne effluents of around  $0.2 \text{ TBq (GW(e) year)}^{-1}$ . Of this  $^{14}\text{C}$  release, over 80% was found to be in a hydrocarbon form, i.e.  $\text{CH}_4$  and  $\text{C}_2\text{H}_6$ . It has been suggested, however, that it is not entirely correct to assume that all the  $^{14}\text{C}$  produced in the reactor coolant is released to the atmosphere at the reactor. Firstly, Kunz (1985) has measured  $^{14}\text{C}$  discharges in liquid effluents from PWRs but these have been so small (1% of the  $^{14}\text{C}$  produced in the coolant) that, compared to the large uncertainties in other parameters, they can be ignored. Secondly,  $^{14}\text{C}$  has been found in the ion-exchange resins used in the coolant purification system. These resins are usually disposed of in low-level radioactive waste burial sites. Martin (1986) has observed the release of  $^{14}\text{C}$  at low-level radioactive waste burial sites, from these resins. Therefore, although this process may slightly delay the release of  $^{14}\text{C}$ , it does not prevent it. So, in light of present knowledge, it is reasonable to assume that all the  $^{14}\text{C}$  formed in the coolant/moderator is discharged to the atmosphere. Although a small amount of this  $^{14}\text{C}$  release will not occur at the reactor, it is, for the sake of simplicity, included in the gaseous discharges from the reactor. Finally, measurements of  $^{14}\text{C}$  emissions from PWR fuel at nuclear fuel reprocessing plants also back up the theoretical calculations. A  $^{14}\text{C}$  release rate of  $0.5 \text{ TBq (GW(e) year)}^{-1}$  was observed at the Karlsruhe reprocessing plant in Germany and the chemical form was, as expected, found to be predominantly  $\text{CO}_2$  (Schwibach

et al., 1978).

#### 1.3.2.2 The Boiling Water Reactor (BWR)

This reactor is very similar to the PWR. It uses enriched  $UO_2$  as a fuel and the core is cooled and moderated by light water. The main difference is that in the BWR the primary cooling circuit is used directly to drive an electrical generator and not indirectly through a secondary cooling circuit as in the PWR.

As would be expected from the similarities in design, the  $^{14}C$  production pathways in a BWR are the same as those in a PWR. The estimates by various authors of the  $^{14}C$  production rate in BWRs are shown in Table 1.3. These values suggest an average  $^{14}C$  production rate of  $3.3 \text{ TBq (GW(e) year)}^{-1}$  for a BWR.

The fate of the  $^{14}C$  formed in the various components of the BWR follows the normal routes, as detailed for the PWR case. Once again, measurements of  $^{14}C$  discharges from the BWR fuel cycle tend to support these theoretical calculations. Detailed measurements at the Oyster Creek BWR in the United States by Blanchard et al. (1976) suggest a  $^{14}C$  release rate of between  $0.3\text{--}0.7 \text{ TBq (GW(e) year)}^{-1}$ . In contrast to the PWR, the  $^{14}C$  released at the reactor tends to be in the oxidised form. Of the  $^{14}C$  in the BWR off-gas sample measured by Kunz et al. (1975), 95% was in the form of  $CO_2$ , 2.5%  $CO$  and 2.5% hydrocarbons. The assumption that all the  $^{14}C$  produced in the coolant/moderator is released to the atmosphere at the reactor is subject to the same provisos as in the PWR case. Measurements of  $^{14}C$  emissions from BWR fuel at the Karlsruhe reprocessing plant gave values of around  $0.6 \text{ TBq (GW(e) year)}^{-1}$ , in good agreement with the estimated value, the predominant chemical form being  $CO_2$  (Schwibach et al., 1978).

#### 1.3.2.3 The Heavy Water Reactor (HWR)

In this reactor type, the core is cooled and moderated by heavy water. The low neutron absorption of the heavy water allows the use of natural  $UO_2$  fuel.

The production of  $^{14}C$  in HWRs occurs via the same routes

Table 1.3:  $^{14}\text{C}$  production in a BWR

Author	$^{14}\text{C}$ production rate (TBq (GW(e) year) $^{-1}$ )			
	Fuel	Coolant/moderator	Fuel cladding	Structural material
Hayes and MacMurdo (1975)	1.2	0.4	-	-
Kelly et al. (1975)	0.5	0.6	-	-
Fowler et al. (1976)	0.8	0.3	-	-
United Nations (1977)	0.6	0.3	-	-
Davis (1979)	0.8	0.2	0.6	1.3-2.0
Bonka (1980)	0.4	0.2	0.6	-
Average	0.7	0.3	0.6	1.7

as that in LWRs. However, due mainly to the large moderator mass, the production rate is expected to be considerably larger than in LWRs. The estimates by various authors in Table 1.4 suggest an overall  $^{14}\text{C}$  production rate of  $18.2 \text{ TBq (GW(e) year)}^{-1}$ .

Most of the  $^{14}\text{C}$  in the coolant/moderator is released to the atmosphere at the reactor (Beninson and Gonzalez, 1981). The remainder, as in LWRs, is probably extracted by the ion-exchange resins from whence it will eventually be released. Similar quantities of the  $^{14}\text{C}$  in the gaseous effluents have been found in both reduced (e.g. deuteromethane) and oxidised (e.g. carbon dioxide) forms (Beninson, 1984). The  $^{14}\text{C}$  in the other reactor components follows the usual 'discharge' pathways.

#### 1.3.2.4 The Gas-cooled Reactor (GCR or MAGNOX)

The first GCR utilised natural uranium metal canned in a magnesium alloy (MAGNOX) and came to be known by this acronym. The reactor core is moderated by graphite and cooled by carbon dioxide. This reactor type was the initial basis of the UK nuclear energy programme.

$^{14}\text{C}$  is produced in MAGNOX reactors by neutron activation reactions on  $^{13}\text{C}$  present in the moderator and coolant, on  $^{17}\text{O}$  present in the coolant and on  $^{14}\text{N}$  present as an impurity in the moderator, coolant and fuel plus cladding. Estimates of the  $^{14}\text{C}$  production rate are presented in Table 1.5 which show that the moderator is the largest single source in the reactor. The total production rate for  $^{14}\text{C}$  in a MAGNOX reactor is calculated to be  $14.6 \text{ TBq (GW(e) year)}^{-1}$ .

The  $^{14}\text{C}$  discharges at the reactor result from leakage of  $^{14}\text{CO}_2$  from the cooling circuit. The amount of  $^{14}\text{C}$  released in this manner, however, is greater than the amount produced in the coolant. This is because some of the  $^{14}\text{C}$  formed in the moderator is released to the coolant through corrosion of the graphite. The amount of  $^{14}\text{C}$  transferred in this manner was estimated by Bush et al. (1983) to be around  $0.7 \text{ TBq (GW(e) year)}^{-1}$ , with the remainder of the  $^{14}\text{C}$  expected to stay in the moderator until decommissioning. The  $^{14}\text{C}$  in the fuel and its cladding pass to the reprocessing

Table 1.4:  $^{14}\text{C}$  production in a HWR

Author	$^{14}\text{C}$ production rate (TBq (GW(e) year) $^{-1}$ )			
	Fuel	Coolant/moderator	Fuel cladding	Structural material
United Nations (1977)	1.7	15.3	-	-
Kabat (1979)	0.7	20.6	-	-
Bonka (1980)	1.5	7.4	1.3	-
Beninson and Gonzalez (1981)	1.0	14.4	-	-
Average	1.2	14.4	1.3	1.3*

\* No calculations have been reported but, in this study, the value of this parameter is assumed to be similar to what it is for LWRs (as suggested by Bush et al. (1983)).

Table 1.5:  $^{14}\text{C}$  production in a MAGNOX reactor

Author	$^{14}\text{C}$ production rate (TBq (GW(e) year) $^{-1}$ )			
	Fuel	Coolant	Fuel cladding	Moderator
Kelly et al. (1975)	3.7	0.1	-	9.1
Bonka (1981)	4.8	0.3	1.3	11.0
United Nations (1982)	3.2	0.1	-	9.3
Bush et al. (1983)	3.7	0.4	0.3	9.5
Average	3.9	0.2	0.8	9.7

plant as usual.

#### 1.3.2.5 The Advanced Gas-cooled Reactor (AGR)

The AGR is very similar to the MAGNOX reactor except that it uses enriched  $\text{UO}_2$  fuel and higher operating temperatures to increase the reactor's thermal efficiency.

The  $^{14}\text{C}$  production mechanisms in an AGR are thus identical to the MAGNOX reactor but, as Table 1.6 shows, the absolute amounts of  $^{14}\text{C}$  produced are smaller. The average  $^{14}\text{C}$  production rate in an AGR is  $8.4 \text{ TBq (GW(e) year)}^{-1}$ .

Once again, the gaseous discharges at the reactor, via leakage of the primary cooling circuit, are augmented by  $^{14}\text{C}$  produced in the moderator and transferred to the coolant through graphite corrosion (by about  $0.4 \text{ TBq (GW(e) year)}^{-1}$ ). The remainder of the  $^{14}\text{C}$  waste arisings occur as expected, except that a small amount of the moderator, namely the graphite sleeves containing about  $0.4 \text{ TBq (GW(e) year)}^{-1}$  of the  $^{14}\text{C}$  (Bush et al., 1983), is transferred to the reprocessing plant where it is added to the solid wastes.

#### 1.3.2.6 The High Temperature Gas-cooled Reactor (HTGR)

The HTGR operates at a higher temperature than the AGR. The fuel is highly enriched uranium-carbide-coated particles which can sustain the high temperatures. The fuel is embedded in a graphite matrix which acts as a moderator, and the reactor core is cooled with helium.

Most of the  $^{14}\text{C}$  is produced by neutron activation of  $^{13}\text{C}$  and  $^{14}\text{N}$  in the fuel and moderator of the reactor, although a very small amount is formed in the coolant. The production pathways, summarised in Table 1.7, suggest an overall production rate of  $6.4 \text{ TBq (GW(e) year)}^{-1}$ .

The  $^{14}\text{C}$  produced in the coolant is discharged at the reactor, but because of the structure of the fuel elements, much, or all, of the graphite moderator has to be removed as the first step in fuel reprocessing. Most of the  $^{14}\text{C}$  in the moderator will be released at the reprocessing plant in the form of  $\text{CO}_2$

Table 1.6:  $^{14}\text{C}$  production in an AGR

Author	$^{14}\text{C}$ production rate (TBq (GW(e) year) $^{-1}$ )			
	Fuel	Coolant	Fuel cladding	Moderator
Kelly et al. (1975)	0.7	0.3	-	9.0
Bonka (1981)	0.6	0.3	1.2	3.5
Bush et al. (1983)	0.3	0.2	1.8	5.7
Average	0.5	0.3	1.5	6.1

Table 1.7:  $^{14}\text{C}$  production in a HTGR

Author	$^{14}\text{C}$ production rate (TBq (GW(e) year) $^{-1}$ )		
	Fuel assembly/moderator	Coolant	Structural materials
Magno et al. (1975)	9.3	-	-
Davis (1979)	7.4	-	-
Bonka (1981)	3.4	small	-
Bush et al. (1983)	5.6	small	small
Average	6.4	small	small

when the graphite moderator is combusted. The fate of the  $^{14}\text{C}$  in other components of the reactor is the same as described previously.

#### 1.3.2.7 The Liquid Metal Fast Breeder Reactor (LMFBR)

Fast breeder reactors are, at present, only in their infancy but it is important to consider their  $^{14}\text{C}$  production rates since they are expected to become the mainstay of the nuclear power production industry in the next century. The main fuel type used in a LMFBR consists of mixed uranium and plutonium oxides; the core is cooled with liquid sodium and contains no moderator.

The production of  $^{14}\text{C}$  in a LMFBR originates in the neutron activation of  $^{17}\text{O}$  in the fuel and  $^{14}\text{N}$  impurities in the fuel and cladding. In addition, insignificant quantities of  $^{14}\text{C}$  are expected to be formed in the coolant. The production estimates listed in Table 1.8 imply a  $^{14}\text{C}$  production rate of  $0.7 \text{ TBq (GW(e) year)}^{-1}$ , which is considerably lower than for most thermal reactors. The main reason for this reduction is that neutron capture cross-sections of target isotopes decrease rapidly as neutron energy increases (see Table 1.1). Since the neutrons produced in a LMFBR are of high energy, the neutron capture cross-sections of the target isotopes are low and thus  $^{14}\text{C}$  production rates are low.

All the  $^{14}\text{C}$  produced in a LMFBR passes to the reprocessing plant where, as always, the  $^{14}\text{C}$  in the fuel is released to the atmosphere and that in the claddings remains as a solid waste.

It is possible that, in future, carbide and nitride fuels could also be used in LMFBRs because of their greater fissile densities, improved breeding ratios and high thermal conductivities. Such fuels, particularly nitrides, would give rise to very large  $^{14}\text{C}$  production rates (carbide fuel -  $11.1 \text{ TBq (GW(e) year)}^{-1}$ , nitride fuel -  $5900 \text{ TBq (GW(e) year)}^{-1}$  (Till et al., 1976)). However, it is unlikely that these fuel types will be used on a commercial scale for some considerable time and thus they will not be discussed further in this work.

Table 1.8:  $^{14}\text{C}$  production in a LMFBR

Author	$^{14}\text{C}$ production rate (TBq (GW(e) year) $^{-1}$ )			
	Fuel	Coolant	Fuel cladding	Structural materials
Davis (1979)	0.2	-	0.5	-
Bonka (1981)	0.2	-	0.3	-
Bush et al. (1983)	0.2	small	0.7	small
Average	0.2	small	0.5	small

#### 1.3.2.8 The Fusion Reactor

It is thought likely that, sometime in the future, nuclear fusion reactors will become a major energy source. When this will happen is very uncertain and, although too little is known about the design and operation of possible future fusion reactors to consider in any detail the  $^{14}\text{C}$  waste arisings from them, they are mentioned here, merely for the sake of completeness.

Scheele and Burger (1976) have estimated  $^{14}\text{C}$  production rates for the UWMAK-II reference reactor, a 5000 MW(th) design based on magnetic confinement. A relatively high production rate of  $0.3 \text{ TBq day}^{-1}$  was indicated. The eventual fate of this  $^{14}\text{C}$  is very unclear but a small amount ( $4 \times 10^{-3} \text{ TBq day}^{-1}$ ) is expected to be released to the atmosphere at the reactor.

#### 1.3.2.9 Summary

A summary of the  $^{14}\text{C}$  waste arisings at the different reactor types (excluding fusion reactors) is shown in Table 1.9. It has to be stressed that these estimates are all based on theoretical calculations which are heavily dependent on certain ill-defined parameters, e.g. the concentration of nitrogen impurities in the various reactor components. Indeed, only a small number of these calculations have actually been independently verified from actual field measurements. Fortunately, the  $^{14}\text{C}$  production and release rates from LWRs have received comparatively major attention. Since LWRs are by far the most common type, having accurate data for these reactors is of great importance when assessing global  $^{14}\text{C}$  discharges to the environment. So, although the available data for some less popular reactors, e.g. MAGNOX, may not, for this very reason, be particularly accurate, for the dominant reactor designs, e.g. LWRs, the data are reasonably accurate. Finally, these values, as they stand, only apply to 'average' reactors. Great care would have to be taken in applying these values to any individual reactor, as there can be so many differing designs within any given reactor type.

#### 1.3.3 $^{14}\text{C}$ Discharges to the Environment: Past, Present and Future

At the beginning of 1984 there were 317 nuclear power

Table 1.9: Summary of  $^{14}\text{C}$  waste arisings

Reactor type	Total production (TBq (GW(e) year) <sup>-1</sup> )	Gaseous waste (TBq (GW(e) year) <sup>-1</sup> )		Solid waste (TBq (GW(e) year) <sup>-1</sup> )	
		Reactor	Reprocessing plant	Reactor	Reprocessing plant
PWR	2.4	0.2	0.6	1.0	0.6
BWR	3.3	0.3	0.7	1.7	0.6
HWR	18.2	14.4	1.2	1.3	1.3
MAGNOX	14.6	0.9	3.9	9.0	0.8
AGR	8.4	0.7	0.5	5.3	1.9
HTGR	6.4	small	6.4	small	small
LMFBR	0.7	small	0.2	small	0.5

stations in operation throughout the world with a net electrical power generating capacity of just under 191 GW(e). The distribution of the various reactor types is shown in Table 1.10. Most of these 317 reactors can easily be ascribed to one of the seven categories, although some, like the Russian light-water-cooled graphite-moderated reactors, are difficult to categorise. An estimate of the amount of  $^{14}\text{C}$  released to the atmosphere from nuclear power production in 1983 can be obtained using the  $^{14}\text{C}$  discharge data of Table 1.9. Assuming a load factor of 70% for each reactor, i.e. each reactor operates at 70% of its electrical power generating capacity, a total release of  $2.4 \times 10^{14}$  Bq of  $^{14}\text{C}$  over the year is obtained (for the worst possible case in which all fuel is reprocessed). This value corresponds to just under 25% of the natural  $^{14}\text{C}$  production rate.

Using the record of the growth of the world nuclear energy capacity, shown in Figure 1.9, it is possible to calculate the total amount of  $^{14}\text{C}$  released to the environment from the nuclear fuel cycle up to 1984. In this calculation it is assumed that the reactor type distribution in the past has been the same as the present day distribution. Although this assumption is obviously wrong in detail, the errors caused by using it will be small. However, it is possible that the  $^{14}\text{C}$  production rate in some reactor types may have been greater in the past than they are at present. For example, many water-cooled reactors originally used nitrogen containing compounds to control the pH of the coolant but this practice, which leads to an increase in  $^{14}\text{C}$  production, has ceased in recent years. Another example of this is the use of nitrogen gas in the Canadian version of the HWR (the CANDU) but again this practice has been curtailed. Using the simplifying assumption that the  $^{14}\text{C}$  production and release rates for reactor types in the past have been the same as they are at present is unlikely to increase significantly the errors on the final estimate. On this basis, the total amount of  $^{14}\text{C}$  released from the nuclear fuel cycle up to 1984 was  $1.8 \times 10^{15}$  Bq (again for the worst possible case in which all fuel is reprocessed). Comparing this value with the natural  $^{14}\text{C}$  production rate of around  $1.0 \times 10^{15}$  Bq year<sup>-1</sup> gives an indication of how small this anthropogenic perturbation to the

Table 1.10: Nuclear power reactors in the world (1 January 1984)

Reactor type	Number	Electrical power generating capacity	
		(GW(e))	Fraction of total (%)
PWR	148	107.9	56.5
BWR	67	45.9	24.1
HWR	26	11.0	5.8
MAGNOX	35	6.9	3.6
AGR	33	17.6	9.2
HTGR	2	0.3	0.2
LMFBR	6	1.2	0.6
<b>Total</b>	<b>317</b>	<b>190.8</b>	<b>100.0</b>

global carbon cycle has been in the past. Consequently, this artificial production of  $^{14}\text{C}$  has not caused any notable change in atmospheric  $^{14}\text{C}$  levels, which have been falling steadily since the peak of the nuclear weapons testing era in the early 1960s (see Figure 1.6).

So far, only the total amount of  $^{14}\text{C}$  released to the environment has been discussed. It must be remembered that far greater quantities of  $^{14}\text{C}$  are produced in nuclear reactors than are immediately released. The remainder of this  $^{14}\text{C}$  constitutes the solid waste arisings at the reactors and reprocessing plants. Of particular significance in this context are the graphite moderators of AGRs and MAGNOX reactors which will contain large quantities of  $^{14}\text{C}$ . The eventual fate of this  $^{14}\text{C}$  is unclear because of uncertainties over the procedures likely to be adopted during and after reactor decommissioning. The fate of other solid waste containing  $^{14}\text{C}$  is equally uncertain and is likely to be determined by considerations of radionuclides, other than  $^{14}\text{C}$ , in the waste. It should be kept in mind, therefore, that all the  $^{14}\text{C}$  produced in nuclear reactors could eventually find its way into the global carbon cycle. The total amount of  $^{14}\text{C}$  produced in nuclear reactors up to 1984 is around  $4.5 \times 10^{15}$  Bq. Compared to other man-made perturbations to the global carbon cycle, e.g. the production of  $2.2 \times 10^{17}$  Bq of  $^{14}\text{C}$  from nuclear weapon tests, however, this value still seems rather insignificant.

To the present-day, therefore, the production of  $^{14}\text{C}$  in the nuclear industry has, on a global scale, been rather unimportant. It is, however, an industry still in its infancy with a major potential for expansion. The actual future growth of the nuclear industry is very difficult to predict as it will depend not only on future trends in population growth, standards of living, etc. but also on such fickle matters as public opinion. Indeed, there have been many different predictions made for the future growth of the world's nuclear energy capacity. Figure 1.12 is an example of one such prediction and is based on the work of Edmonds and Reilly (1983a, 1983b, 1983c). Now, if the nuclear industry was to expand at such a rate and, as at present, no attempt was made to retain the  $^{14}\text{C}$  waste, then the amount of

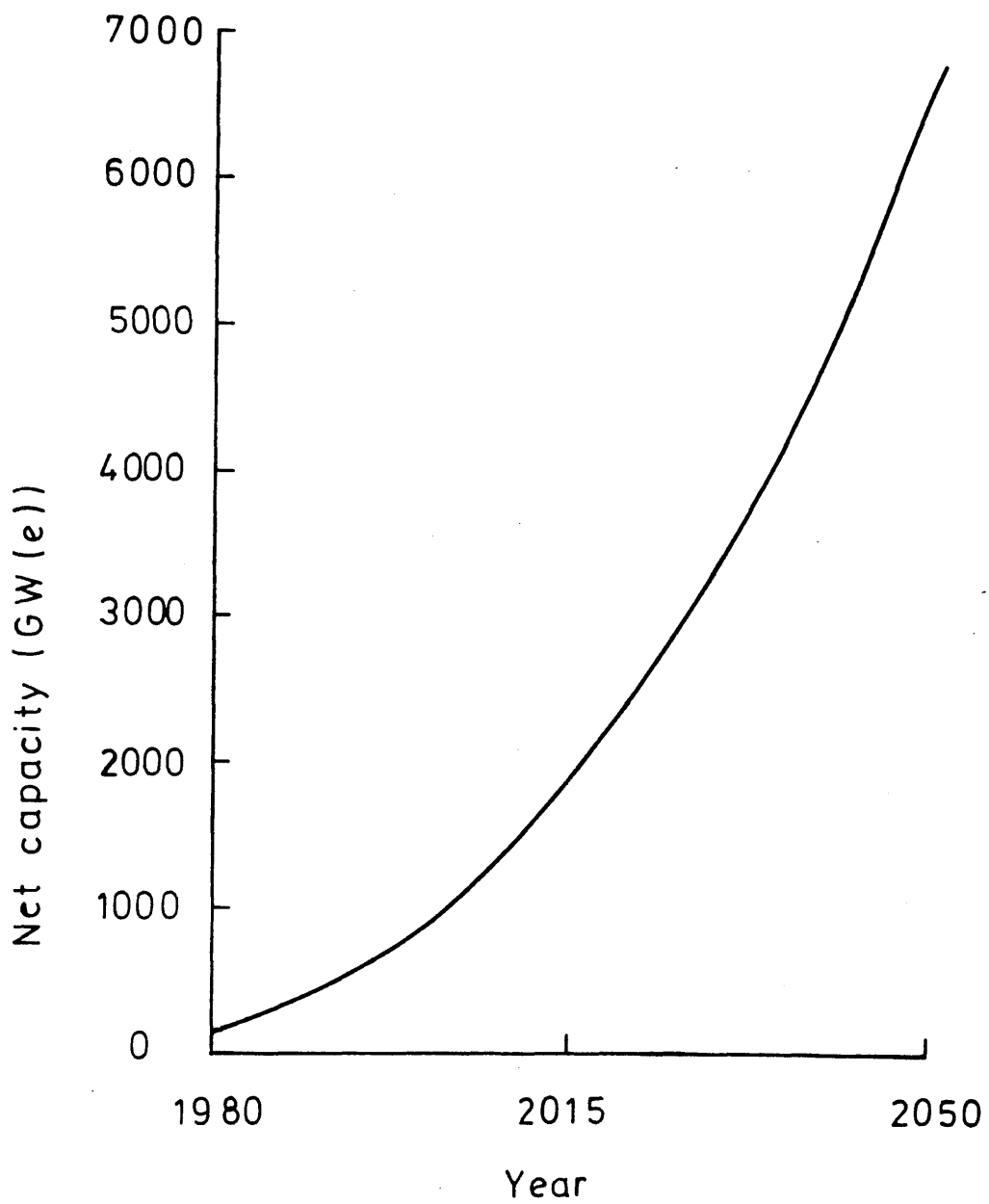


FIGURE 1-12: Predicted nuclear electrical generating capacity, 1980- 2050.

$^{14}\text{C}$  being released to the environment would increase very markedly. This, in turn, would cause an increase in atmospheric  $^{14}\text{C}$  levels and, hence, an increase in the radiation dose to man from  $^{14}\text{C}$ . A variety of future energy growth scenarios will be considered in detail later in this study and further discussion is deferred until Chapter 4.

#### 1.4 THE RADIOLOGICAL IMPACT OF $^{14}\text{C}$ ON MAN

In this section the method used to calculate the dose to man from his exposure to  $^{14}\text{C}$  will be discussed, as well as a means of estimating the subsequent occurrence of various health effects. However, it is pertinent initially to mention some of the underlying radiological concepts and to define the more important quantities used in this work.

##### 1.4.1 Radiological Concepts and Quantities

Exposure of a population to radiation may lead to the incidence of stochastic and non-stochastic health effects in the exposed populations (somatic effects) and stochastic effects in its descendants (hereditary effects). Non-stochastic effects occur only if particular threshold levels of dose are exceeded and the severity of the effect varies with dose. An example of a non-stochastic effect is the occurrence of cataracts in the eye lense. The probability of occurrence of stochastic effects is assumed proportional to dose, without threshold. The important stochastic effects are carcinogenesis (fatal and non-fatal) in the exposed population and hereditary effects in its descendants. At the levels of individual dose typically encountered from releases of radionuclides during the normal operation of nuclear installations, the potential health impact will be limited to the incidence of stochastic health effects.

##### 1.4.1.1 Dose to Man from Ionising Radiation

The biological damage associated with any radioisotope is dependent on the ionisation produced by the radiation and is thought to arise from the chemical reactions which ionised atoms subsequently undergo. The 'absorbed dose' is a measure of the energy deposited in matter by ionising radiation. The absorbed dose,  $D_T$ , in a particular tissue, T, is given by:

$$D_T = dE / dM_T , \quad (1.1)$$

where  $dE$  is the energy imparted by the ionising radiation to the matter in tissue  $T$  and  $dM_T$  is the mass of matter in tissue  $T$ .

The SI unit of absorbed dose is the 'gray' (Gy) and:

$$1 \text{ Gy} = 100 \text{ rad (old unit)} = 1 \text{ J kg}^{-1}.$$

The 'dose equivalent',  $H_T$ , in the tissue  $T$ , is a quantity which correlates better with the deleterious effects of exposure to ionising radiation and is given by:

$$H_T = D_T Q N, \quad (1.2)$$

where  $D_T$  is the absorbed dose in the particular tissue,  $Q$  is the quality factor which allows for the different biological effectiveness of various types of radiation and  $N$  is the product of all other modifying factors. A value of unity has been assigned to  $N$  by the International Commission on Radiological Protection (ICRP, 1977) but  $Q$  ranges from 1 for x-rays,  $\gamma$ -rays and  $\beta$ -particles up to 20 for  $\alpha$ -particles and other multiply-charged particles of unknown energy. The SI unit of dose equivalent is the 'sievert' (Sv) and:

$$1 \text{ Sv} = 100 \text{ rem (old unit)} = 1 \text{ J kg}^{-1}.$$

The quantity 'effective dose equivalent' is a measure of the stochastic risk assumed to result from any irradiation of the body, whether uniform or non-uniform. The effective dose equivalent,  $H_E$ , is defined as:

$$H_E = \sum_T W_T H_T, \quad (1.3)$$

where  $H_T$  is the dose equivalent in tissue  $T$  and  $W_T$  is a weighting factor representing the proportion of the stochastic risk resulting from irradiation of tissue  $T$  to the total risk when the body is irradiated uniformly. The values recommended for  $W_T$  are tabulated in ICRP (1977).

The sum of the individual effective dose equivalents in an exposed population is known as the 'collective effective dose equivalent',  $S_E$ , and is given by:

$$S_E = \int_0^{\infty} H_E N(H_E) dH_E, \quad (1.4)$$

where  $H_E$  is the effective dose equivalent and  $N(H_E)$  is the number of individuals receiving an effective dose equivalent in the range  $H_E$  to  $H_E + dH_E$ . The collective dose equivalent in an organ is obtained by substituting the dose equivalent in

that organ for the effective dose equivalent.

The integral of the collective effective dose equivalent rate over all time is known as the 'collective effective dose equivalent commitment',  $S_E^C$ , and is given by:

$$S_E^C = \int_0^{\infty} \dot{S}_E(t) dt, \quad (1.5)$$

where  $\dot{S}_E$  is the collective effective dose equivalent rate. When this integral is limited in time and the integral has not converged, the quantity is referred to as the truncated, or incomplete, collective effective dose equivalent commitment. Once again, the collective dose equivalent commitment in an organ can be obtained by substituting the dose equivalent in that organ for the effective dose equivalent.

In evaluating the collective effective dose equivalent commitment (and other similar quantities), it is convenient to distinguish between external and internal irradiation of the body. For external radiation the integration of equations (1.4) and (1.5) is relatively straightforward. For internal irradiation from radionuclides incorporated in the body, the integration is more complex; detailed knowledge is required, which is not readily available, of the time variation after intake of the dose equivalent rates in the respective tissues. The integration is more conveniently and readily performed using an alternative representation for  $S_E^C$  for internal irradiation:

$$S_E^C = \bar{H}_E \int_0^{\infty} I(t) dt, \quad (1.6)$$

where  $\bar{H}_E$  is the population-averaged effective dose equivalent received from unit intake of the nuclide by inhalation or ingestion, taking into account the age distribution and life expectancy of the population. The quantity  $I$  is the collective intake rate by inhalation or ingestion of a nuclide by the population. It is common practice to replace the quantity  $\bar{H}_E$  by the committed effective dose equivalent,  $H_{50E}$ , which is defined as the time integral of the effective dose equivalent rate,  $\dot{H}_E(t)$ , over a 50 year period following intake, i.e.:

$$H_{50E} = \int_0^{50} \dot{H}_E(t) dt. \quad (1.7)$$

The quantity, committed effective dose equivalent, was introduced in the context of occupational radiation protection, fifty years being typical of the working life time. Committed effective dose equivalents per unit intake (as well as the committed dose equivalents in various organs) have been estimated by ICRP (1981)

for a wide range of radionuclides for intakes via inhalation and ingestion. For radionuclides whose retention in the body is relatively short (e.g. the order of a year), the committed and population-averaged effective dose equivalents will be numerically comparable, i.e.  $\bar{H}_E \approx H_{50E}$ . However, for radionuclides with long retention times in the body the use of the committed dose equivalent is likely to overestimate the actual dose equivalent received by the population.

In summary, collective effective dose equivalent commitments to an exposed population are generally evaluated as:

$$S_E^C = \left( \int_0^\infty \dot{S}_E^{\text{ext}}(t) dt \right) + (H_{50E} \int_0^\infty I(t) dt), \quad (1.8)$$

where  $\dot{S}_E^{\text{ext}}(t)$  is the collective effective dose equivalent rate at time  $t$  associated with external irradiation and the other terms have previously been defined. The collective dose equivalent commitments for particular organs or tissues can be estimated by substitution of the appropriate organ or tissue dose equivalent for the effective dose equivalent in (1.8).

#### 1.4.1.2 Health Effects in an Exposed Population

Risk coefficients have been evaluated by ICRP (1977) to relate the dose equivalents in an exposed population to the incidence of specific health effects. In their derivation of these coefficients, a linear relationship between dose equivalent and effect was assumed. The ICRP has stated that the risk coefficients are intended to be realistic estimates of the effects of irradiation at low annual dose equivalents. Notwithstanding this, there remains a considerable body of scientific opinion which regards these risk coefficients as overestimates of the true risk at the levels of annual dose equivalent received by the general public. On the other hand, however, it has also been suggested that these risk coefficients are underestimates. This aspect is the subject of continuing debate and is unlikely to be resolved quickly; for the purposes of this study, linearity between dose equivalent and effect at all levels of dose equivalent is assumed, while recognising the uncertainties inherent in this approach.

No single dosimetric quantity is sufficient to enable estimation of the three categories of health effects previously

listed, i.e. fatal and non-fatal cancers in the exposed population plus hereditary effects in subsequent generations. Recourse has therefore to be made to the use of several quantities, the number of which has been kept to a minimum.

The most useful individual quantity here is the effective dose equivalent. In their derivation of the weighting factors, used to calculate the effective dose equivalent, ICRP chose to consider the risk of fatal cancer in all body organs and tissues, apart from in skin, plus the hereditary effects in the first two generations. The effective dose equivalent may be used, therefore, to give a measure of the incidence of these particular health effects; the incidence of the remaining effects must be evaluated from other quantities.

The incidence of fatal cancers in skin and of hereditary effects in subsequent generations can be evaluated from a knowledge of the dose equivalents in skin and gonads,  $H_S$  and  $H_G$  respectively. The incidence of radiation-induced non-fatal cancers is most important in the skin and thyroid. The incidence may be calculated from the dose equivalents in these organs,  $H_S$  and  $H_{TH}$  respectively.

Evaluation of the incidence of the total health effect in an exposed population therefore requires estimation of the collective effective dose equivalent commitment and of the collective dose equivalent commitments in gonads, skin the thyroid,  $S_E$ ,  $S_G$ ,  $S_S$  and  $S_{TH}$  respectively. A measure of the incidence of health effects can then be derived using the risk coefficients recommended by ICRP. A list of these risk coefficients and the quantities to which they should be applied is presented in Table 1.11. These coefficients were derived in the context of occupational exposures but they are assumed to be equally applicable to exposure of the general public. The ICRP has not proposed any risk coefficients for the incidence of non-fatal cancers arising from irradiation of the skin or thyroid and so no comment can be made about the absolute number of such effects. One further point which should be considered when dealing with health effects is that the appearance of stochastic effects following irradiation is not immediate but extends over a

Table 1.11: Application of risk coefficients in evaluating health effects

Health effect	Number of effects
All fatal cancers (except in skin) plus hereditary effects in the first two generations	$(1.65 \times 10^{-2}) S_E$
Fatal cancers in skin	$(1.65 \times 10^{-4}) S_S$
Hereditary effects in the first two generations	$(4 \times 10^{-3}) S_G$
All hereditary effects	$(8 \times 10^{-3}) S_G$
All fatal cancers	$((1.65 \times 10^{-2}) S_E) + ((1.65 \times 10^{-4}) S_S) - ((4 \times 10^{-3}) S_G)$

considerable period which may be as long as several tens of years. Age at exposure therefore exerts a considerable influence on the probability that a particular dose equivalent will induce a given health effect; the probability will decrease when life expectancy at the time of irradiation becomes comparable with or smaller than the median time required for appearance of the effect. In the approach adopted here, no account is taken of the age distribution of the population and thus the health effects will be overestimated.

#### 1.4.2 Radiation Dose to Man from $^{14}\text{C}$

Human exposure to  $^{14}\text{C}$  can occur by three principal means; external irradiation from  $^{14}\text{C}$  in the atmosphere, internal irradiation after inhalation of  $^{14}\text{C}$  in the atmosphere and internal irradiation after ingestion of  $^{14}\text{C}$  in food.

Since  $^{14}\text{C}$  is a weak beta-emitter, consideration of the external irradiation of man by  $^{14}\text{C}$  can be limited to irradiation of skin. According to the Commission of the European Communities (CEC, 1979), the dose equivalent rate in skin from the external irradiation of man by  $^{14}\text{C}$  is  $2.16 \times 10^{-8} \text{ Sv year}^{-1} (\text{Bq m}^{-3})^{-1}$ . Assuming a carbon concentration in the atmosphere of 340 ppm (volume), then the dose equivalent rate in skin,  $\dot{H}_S^{\text{ext}}(t)$ , in year  $t$ , measured in  $\text{Sv year}^{-1}$ , is given by:

$$\dot{H}_S^{\text{ext}}(t) = (3.9 \times 10^{-12}) A(t), \quad (1.9)$$

where  $A(t)$  is the atmospheric  $^{14}\text{C}$  specific activity in year  $t$  (measured in  $\text{Bq kg}^{-1}$  (carbon)). Therefore, the radiation dose to man from the external irradiation by  $^{14}\text{C}$  can be calculated directly from knowledge of the atmospheric  $^{14}\text{C}$  specific activity.

The internal irradiation of man by  $^{14}\text{C}$  is caused by the intake of  $^{14}\text{C}$  via inhalation and ingestion. For Reference Man, as defined by ICRP (1975), ingestion intake is of the order of  $0.3 \text{ kg day}^{-1}$ , with nearly complete absorption, whereas inhalation intake is about  $3 \times 10^{-3} \text{ kg day}^{-1}$ , with only 1% retained in the body. The total carbon content of the body is 16 kg, which, together with the daily intake rate, suggest a mean residence time of carbon in the body of 53 days. However, the

residence time of carbon in the individual components of the body can vary significantly from this average value. For example, Stenhouse and Baxter (1977b) suggested a value of 5-7 years for the mean residence time of carbon in the major organs of the body and the residence time of carbon in the bones is even longer. This carbon forms the structural base of all the organic matter in man and participates in almost all biological and biochemical processes. It comprises about 23% of the total body weight and is a major constituent of proteins and genetically significant structures such as DNA and RNA. It has been suggested that the radiological significance of  $^{14}\text{C}$  may be enhanced by the transmutation effect, particularly from a genetic viewpoint when the  $^{14}\text{C}$  is incorporated into genetic structures. The transmutation effect with regard to  $^{14}\text{C}$  is normally associated with 3 properties of the decay process:

- (a) nuclear recoil,
  - (b) the modified valence state
- and
- (c) the excited electronic state of the daughter nucleus  $^{14}\text{N}$ .

The limited data available, however, suggest that, compared with the absorbed energy from ionisation processes, the transmutation effect represents only a minor contribution to the radiological significance of  $^{14}\text{C}$ . Indeed, ICRP (1979) states that there is no justification for modifying existing recommendations in radiological protection on the basis of effects from transmutation.

Since the residence time of carbon in the human body is relatively short, it is justifiable to assume that the committed dose equivalents per unit intake of  $^{14}\text{C}$ , as evaluated by ICRP (1981), are numerically comparable to the dose equivalents per unit intake of  $^{14}\text{C}$  (with the dose equivalent being delivered entirely within a year of intake). According to ICRP the committed dose equivalents (committed dose equivalents in all organs as well as the committed effective dose equivalent) per unit intake of  $^{14}\text{C}$  via the inhalation of  $\text{CO}_2$  are  $6.4 \times 10^{-12}$  Sv  $\text{Bq}^{-1}$ . Therefore it can be assumed that all the dose equivalents are also  $6.4 \times 10^{-12}$  Sv  $\text{Bq}^{-1}$ . At an intake rate of  $3 \times 10^{-3}$  kg  $\text{day}^{-1}$ , the dose equivalent rates,  $H_X^{\text{inh}}(t)$ , in year  $t$ , measured in Sv  $\text{year}^{-1}$ , from the

inhalation of  $^{14}\text{CO}_2$  are given by:

$$\dot{H}_X^{\text{inh}}(t) = (7 \times 10^{-12}) A(t), \quad (1.10)$$

where  $A(t)$  is the atmospheric  $^{14}\text{C}$  specific activity in year  $t$  (measured in  $\text{Bq kg}^{-1}$  (carbon)). The corresponding values deriving from the inhalation of  $^{14}\text{C}$  in other common chemical forms, e.g.  $\text{CH}_4$  and  $\text{CO}$ , are of the same order of magnitude.

For the intake of  $^{14}\text{C}$  via the ingestion of food, ICRP (1981) has calculated all the committed dose equivalents to be  $5.7 \times 10^{-10} \text{ Sv Bq}^{-1}$ . Therefore it can be assumed that all the dose equivalents are also  $5.7 \times 10^{-10} \text{ Sv Bq}^{-1}$ . This value is independent of the carbon's chemical form. At an intake rate of  $0.3 \text{ kg day}^{-1}$ , all the dose equivalent rates,  $\dot{H}_X^{\text{ing}}(t)$ , in year  $t$ , measured in  $\text{Sv year}^{-1}$ , from the ingestion of food are given by:

$$\dot{H}_X^{\text{ing}}(t) = (6.3 \times 10^{-8}) A(t), \quad (1.11)$$

where  $A(t)$  is the food's  $^{14}\text{C}$  specific activity in year  $t$  (measured in  $\text{Bq kg}^{-1}$  (carbon)). To determine the  $^{14}\text{C}$  specific activity of the food, a simplified approach, referred to as the specific activity model, is often used. This model assumes, firstly, that all food is derived at the location of the individual and, secondly, that the  $^{14}\text{C}$  specific activity in the ingested material is equal to that in the atmosphere at the point of intake (assuming that the  $^{14}\text{C}$  is in a photosynthetically available form, i.e.  $^{14}\text{CO}_2$ ). Although conservative in nature, this approach is not expected to significantly overestimate the radiation dose to man, except for a few isolated cases. Therefore, in equation (1.11),  $A$  can be taken to represent the atmospheric  $^{14}\text{C}$  specific activity.

It has been shown that the radiation dose to man from  $^{14}\text{C}$  via all three exposure pathways is directly proportional to the atmospheric  $^{14}\text{C}$  specific activity. The relative importance of the various exposure pathways can be evaluated by considering the dose equivalent rates received by an individual from naturally produced  $^{14}\text{C}$  (i.e. when  $A(t) = 226 \text{ Bq kg}^{-1}$  (carbon)). The contributions from the various exposure pathways to the effective dose equivalent rate and the dose equivalent rates in some radiologically important organs (gonads, skin and thyroid) are shown in Table 1.12. From these results it is obvious that when calculating the radiation dose to man from

Table 1.12: Contribution from the various exposure patchways to an individual's dose equivalent rates from naturally produced  $^{14}\text{C}$

Exposure pathway	Dose equivalent rate (Sv year <sup>-1</sup> )			
	Effective	Gonads	Skin	Thyroid
External	0	0	$9.0 \times 10^{-10}$	0
Internal (inhalation)	$1.6 \times 10^{-9}$	$1.6 \times 10^{-9}$	$1.6 \times 10^{-9}$	$1.6 \times 10^{-9}$
Internal (ingestion)	$1.4 \times 10^{-5}$	$1.4 \times 10^{-5}$	$1.4 \times 10^{-5}$	$1.4 \times 10^{-5}$
Total	$1.4 \times 10^{-5}$	$1.4 \times 10^{-5}$	$1.4 \times 10^{-5}$	$1.4 \times 10^{-5}$

$^{14}\text{C}$ , the only exposure pathway worth considering is the internal irradiation of man via the ingestion of  $^{14}\text{C}$  in food. The other two exposure pathways are insignificantly small by comparison.

The dose equivalent rates of Table 1.12 can be combined with the risk coefficients recommended by ICRP to estimate the incidence of particular health effects arising from the exposure of an assumed population (comprising  $10^{10}$  people) to naturally produced  $^{14}\text{C}$  for one year. The results in Table 1.13 show that the number of health effects determined from the collective effective dose equivalent rate alone, does not significantly underestimate the total number of health effects (excluding non-fatal cancers). This, therefore, serves as a good example of the usefulness of the collective effective dose equivalent term in evaluating the radiological impact of  $^{14}\text{C}$  on man. Of course, it should be remembered that, although these results give some idea of the relative importance of the various radiological quantities, the absolute numbers of the various health effects calculated in this fashion should be treated with a shade of scepticism.

So, to summarise, in evaluating the radiation dose to man from  $^{14}\text{C}$ , two main points should be considered. Firstly, the only significant exposure pathway is the internal irradiation of man via the ingestion of  $^{14}\text{C}$  in food, the subsequent radiation dose being directly proportional to the atmospheric  $^{14}\text{C}$  specific activity. Secondly, a fair estimate of the radiological impact of  $^{14}\text{C}$  on man is indicated by the collective effective dose equivalent commitment alone but in more rigorous investigations the collective dose equivalent commitments in particular organs (namely, gonads, skin and thyroid) must also be included. However, due to the number of approximations in the derivation of the risk coefficients, the value of converting dose equivalents to the number of health effects is questionable and figures derived in such a manner should be treated with caution.

## 1.5

### THE ICRP DOSE LIMITATION SYSTEM

The system of dose limitation recommended by ICRP (1977) is commonly used as a basis for establishing limits for the release

Table 1.13: Health effects induced by the annual dose to man from naturally produced  $^{14}\text{C}$  (assuming  $10^{10}$  population)

Health effect	Number of effects
All fatal cancers (except in skin) plus hereditary effects in the first two generations	2310
Fatal cancers in skin	23
Hereditary effects in the first two generations	560
All hereditary effects	1120
All fatal cancers	1773

of radioactive materials to the environment. The fundamental requirements of the system are:

- (a) that the practice giving rise to the exposure should produce a net benefit (i.e. all exposures should be justified),
- (b) that all exposures should be 'as low as reasonably achievable', economic and social factors being taken into account (the so-called ALARA or optimisation principle) and
- (c) that the exposure of individuals should not exceed specified limits.

Justification is rarely of concern in establishing release limits and consideration can be limited to optimisation of exposure and ensuring compliance with dose limits.

Optimisation of exposures requires the calculation of the radiation dose received by the entire population from any given practice. The ICRP has recommended the use of cost-benefit analysis to help decide what levels of exposure are 'as low as reasonably achievable'. This technique allows the costs of measures to reduce doses to be balanced against the benefits from the dose reductions achieved.

The overriding constraint in establishing limits for the discharge of radioactive materials is that the doses to individuals must not exceed the prescribed limits. For individual members of the public the annual effective dose equivalent limit recommended is 5 mSv. It is also suggested on the basis of risk considerations that continued exposure over a lifetime should be limited to correspond to an annual individual effective dose equivalent of 1 mSv.

It is on the basis of these recommendations, therefore, that the acceptability of the  $^{14}\text{C}$  discharges to the environment from the nuclear fuel cycle should be judged.

## 1.6

### AIMS OF RESEARCH

The production of  $^{14}\text{C}$  in nuclear reactors and its subsequent release to the environment leads to an increase in atmospheric  $^{14}\text{C}$  specific activity and, hence, to an increase in the radiation dose to man. The object of the work (which is

performed within the framework of an IAEA coordinated research programme on  $^{14}\text{C}$  from nuclear installations) is to assess the radiological impact of  $^{14}\text{C}$  discharges from the nuclear fuel cycle on man and so to comment on their acceptability on the basis of the recommendations of ICRP. This basic objective can then be subdivided into two categories; to assess the effect of  $^{14}\text{C}$  discharges on populations in the vicinity of large nuclear installations and to estimate the effect of the  $^{14}\text{C}$  discharges on the global population. The main objectives within each category will now be briefly discussed.

#### 1.6.1 Local Effects of $^{14}\text{C}$ Discharges from the Nuclear Fuel Cycle

The exposures to  $^{14}\text{C}$  of populations living in the vicinity of large nuclear installations will be greater than those of the general public.  $^{14}\text{C}$  discharged into the atmosphere is carried along by the wind and dispersed by the action of turbulent diffusion until, eventually, it is effectively homogeneously mixed into the atmosphere. Therefore,  $^{14}\text{C}$  levels around a nuclear installation will be higher than the average global levels and so the radiation dose to the local population will be higher.

The primary aim of this section of the study is to quantify the exposures to  $^{14}\text{C}$  of populations in the vicinity of several nuclear installations within the UK. The installations investigated are:

- (a) the nuclear fuel reprocessing plant Sellafield, in Cumbria,
  - (b) the thermal nuclear power station at Hunterston, on the Ayrshire coast,
  - (c) the prototype fast breeder reactor at Dounreay, in the north of Scotland
- and
- (d) the Scottish Universities research reactor at East Kilbride, near Glasgow.

The assessment of the exposures is based on the direct measurement of  $^{14}\text{C}$  levels in the environment around these nuclear installations.

These same  $^{14}\text{C}$  measurements also provide the ideal basis for the testing of atmospheric dispersion models. So, in this study, it is intended to check the veracity of some of these

models. In particular, the validity of the Gaussian plume model, which is commonly employed in calculating the atmospheric dispersion of radionuclides, will be evaluated.

#### 1.6.2 Global Effects of $^{14}\text{C}$ Discharges from the Nuclear Fuel Cycle

Because of its long half-life and direct incorporation into the carbon cycle,  $^{14}\text{C}$  discharges from the nuclear fuel cycle will also lead to the irradiation of the entire global population. The primary objective of this section of the work is to quantify this effect, however, this assessment must be carried out in two distinct subsections.

In the first part an attempt will be made to estimate the actual doses to man from the past, present and future  $^{14}\text{C}$  discharges from the nuclear fuel cycle. Predictions of future changes in the atmospheric  $^{14}\text{C}$  level due to the various anthropogenic perturbations will also be included. However, due to uncertainties in the necessary input data, this section is limited to determining the short-term effects of the  $^{14}\text{C}$  discharges.

In the second part of this study, the object is to determine the long-term effects of the  $^{14}\text{C}$  discharges. This assessment will consider the effect of a notional release of  $^{14}\text{C}$  from the nuclear fuel cycle. The total detriment to man, the temporal distribution of the dose and the effect of various waste disposal options will all be investigated.

EXPERIMENTAL PROCEDURE2.1 INTRODUCTION

The measurement of radiocarbon in environmental samples requires the use of sophisticated physical and chemical techniques to overcome its inherent problems. Two main factors induce these difficulties; firstly,  $^{14}\text{C}$  is a weak beta-emitter (maximum energy 156 keV, average energy 45 keV) and, secondly, its concentrations in nature are very small. Indeed, the natural atmospheric specific activity of  $226 \text{ Bq kg}^{-1}$  (carbon) (Karlen et al., 1964) corresponds to approximately 1 radiocarbon atom per  $10^{12}$  stable carbon atoms. Thus an appropriate counting system must have high detection efficiency for  $^{14}\text{C}$  and low background count rate, i.e. a high signal to noise ratio. In addition, to reduce the errors on final results, the samples should be counted for long periods of time, i.e. around 1-2 days. This means that the counting equipment must also have long-term electronic stability. To sum up, a  $^{14}\text{C}$  counting system must have the following characteristics:

- (a) a high beta detection efficiency,
  - (b) a low background count rate
- and
- (c) long-term stability of background and beta detection efficiency.

Early systems counted samples in the form of solid elemental carbon (Anderson et al., 1947; Libby, 1952). Unfortunately, the low energy beta particles from  $^{14}\text{C}$  decay suffered a high degree of self-absorption, so the overall efficiency of detection was only around 5%. Another disadvantage was that the carbon could not be easily purified and, with the advent of nuclear weapons testing, fission product contamination became troublesome. The development of gas proportional and liquid scintillation techniques soon rendered this method obsolete (Kulp, 1954).

The gas counting method was the first to overcome many of the problems of the original radiocarbon counting technique. By converting a sample to a suitable gas, self-absorption effects, so predominant in the solid sample method, were eliminated and the

gaseous compound could be easily purified from fission product contamination. Initial work used a mixture of CO<sub>2</sub> and CS<sub>2</sub> gas but further improvements in gas preparation and purification techniques promoted the use of methane (Burke and Meinschein, 1955), acetylene (Barker, 1953; Suess, 1954) and, most popular of all, carbon dioxide (de Vries and Barendsen, 1953) as individual counting gases. The gas is then counted in the proportional, rather than the Geiger, region, hence allowing only the energy range of interest to be monitored by discriminating against lower and higher energy pulses. This, together with shielding, anti-coincidence circuitry and recent advances in component design, has produced a counting system with high efficiency, low background and long-term electronic stability.

The application of liquid scintillation techniques to radiocarbon measurements was first reported by Hayes et al. (1953) but its large-scale use was delayed for two decades. Liquid scintillation samples may be easily purified from extraneous radioactive material and do not exhibit the property of radiation self-absorption. This method also utilises the technique of energy discrimination, which, together with the use of coaxial photomultiplier tubes, coincidence logic and refrigeration, helps the counting system to meet the required criteria of high efficiency, low background and electronic stability.

In general, the efficiencies of liquid scintillation systems are lower than those of gas proportional systems. On the other hand, the relatively dense liquid phase means that, in general, much larger quantities of sample carbon can be counted. In fact, both gas and liquid counting systems are at present in common use by radiocarbon laboratories and current research is concentrated on improving the precision of measurement by each method (Tans and Mook, 1978; Pearson, 1979). Other current developments include the adaptation of the accelerator for radiocarbon measuring purposes (Gove et al., 1980; Grootes et al., 1980; Hedges et al., 1980) but this technique is still at a very early stage.

The method used in this work is that of liquid scintillation counting. In general, the gas counting technique is more suited to small samples, say <2 g (carbon) and, since the sample sizes

used here are far greater than this, liquid scintillation counting would appear to be the more appropriate system. In addition, this system incorporates automatic sample-changing facilities which allow the pseudo-simultaneous monitoring of background and modern standard levels. The main practical problem inherent in this technique relates to the necessary conversion of a sample's carbon into a medium suitable for liquid scintillation counting. Because of the characteristics of this detection method only certain classes of compounds can be considered. The counting medium should be a colourless liquid which is either soluble in the scintillation counter solvent system or capable of becoming the solvent itself by dissolving small amounts of scintillator compounds. Also, a large number of common organic materials cause varying degrees of scintillation light quenching and are, therefore, not suitable. Despite these essential requirements, several successful procedures have been devised for converting sample carbon into forms suitable for liquid scintillation counting. Arnold (1954) used ethanol but in succeeding years dissolved acetylene (Audric and Long, 1954), methyl borate (Pringle et al., 1957) and dissolved carbon dioxide (Barendsen, 1957) were all used as the counting material. Attention then turned to synthesised benzene as the scintillation solvent (Tamers, 1960; Starik et al., 1961) and steady progress has since been made with this system. The advantages of benzene are that it contains 92% carbon, has excellent scintillation properties, is stable and its carbon content can be produced entirely from sample carbon. Thus, in this work,  $^{14}\text{C}$  activities of all samples were measured by liquid scintillation counting of benzene synthesised from the samples' original carbon content.

## 2.2 SAMPLE PREPARATION

Once a particular sample has been collected for radiocarbon analysis, it must be properly prepared, i.e. in this case, the sample's carbon has to be converted to benzene. There are four main practical steps in this process:

- (a) pretreatment of the sample to remove all contaminating non-contemporaneous material,
- (b) conversion of the sample's carbon to carbon dioxide,
- (c) conversion of the carbon dioxide to acetylene

and

(d) trimerisation of the acetylene to benzene liquid.

These four steps are now discussed in detail.

### 2.2.1 Sample Pretreatment

It is essential to any radiocarbon analysis that the sample contains only those carbon atoms which constituted the material at the time of its isolation from the carbon cycle. The types of contamination to which a sample may be subjected in the field can be conveniently categorised under two major headings, namely 'chemical' or 'superficial'. For example, inorganic samples such as bone and shell may be 'chemically contaminated' by percolating ground waters containing carbonates and bicarbonates which can be incorporated into the sample matrix via ion exchange. 'Superficial contamination', on the other hand, can involve impregnation of a sample by non-contemporaneous materials, e.g. rootlets, soil components and soil itself. The type of contamination and hence the appropriate pretreatment depends largely on the nature and history of the sample.

In this work grass and wood comprised the majority of samples analysed, although hawthorn berries, blackberries, potatoes and seaweeds were also assayed. For most of these samples pretreatment was carried out only a matter of days after the sample had been isolated from the carbon cycle. This short time period all but eliminated the chances of 'chemical contaminants' being present and so simplified pretreatment methods.

#### 2.2.1.1 Grass

The grass is initially inspected for any extraneous matter, e.g. insects, soil, paper, etc., which may have been accidentally picked up during sample collection. It is then thoroughly dried in an oven at 50°C for a few days.

#### 2.2.1.2 Seaweed

The seaweed is washed in distilled water and then dried in an oven as above.

#### 2.2.1.3 Potatoes

The potatoes are cleaned in distilled water, to remove any traces of soil, macerated in a blender and then dried in an oven as before.

#### 2.2.1.4 Berries

Two types of berries were incorporated in the sampling programme, the hawthorn berry and the blackberry. The pretreatment carried out is the same in either case. Firstly, the stems and leaves of the berry are removed. Then, after washing in distilled water, the fruit is boiled in 2 M hydrochloric acid for several hours to remove any inorganic carbonates. Finally, the berries are washed again in distilled water and oven-dried.

#### 2.2.1.5 Wood

The problems inherent in pretreatment of tree rings are rather unique in that the major source of contamination derives from within the tree itself. The essential requirement of the pretreatment process is to isolate the carbon atoms in a specific tree ring which were incorporated during that year of growth. The main problem lies in discriminating between these particular carbon atoms and others which were incorporated into the tree in another year and have since migrated into the ring of interest. Various authors, including Olsson (1980), have shown that the various fractions of wood within a given ring can have significantly different  $^{14}\text{C}$  levels. This observation can be explained in a number of ways. For example, it has been proved that atmospheric carbon can be incorporated in wood fractions at the time when it is converted from sapwood to heartwood (Cain and Suess, 1976). In addition, radial transfer of resin (Jansen, 1970) and holdover of food from previous years (Fairhall and Young, 1970) can induce this transport phenomenon. It is necessary, therefore, to identify and isolate a fraction of the wood which remains unaffected by the above processes. Fortunately, cellulose, which is the cellular or primary structural material in wood, is not subject to migration. The cellulose in each ring is not in dynamic equilibrium with the metabolism of the tree and so, once synthesised, remains fixed, thus fulfilling the criteria necessary for this work.

Cellulose extraction from a particular tree ring is a lengthy process. The first step is to isolate the pertinent ring from the bulk of the tree. For the tree studied here, a larch, this separation can be quite easily achieved by chiselling, as the rings are reasonably broad and well-defined. Then match-stick sized pieces of the wood are treated in boiling 2 M potassium hydroxide (KOH) solution for about 8 hours. This process removes any humic acids from the wood and solubilises the lignin. The sample is then filtered and washed in distilled water. The first alkali treatment produces an intense darkening of the KOH solution due to extensive removal of the above contaminants and so this entire procedure is repeated two or three times until the final KOH solution is light yellow in colour. The dehumified wood is then soaked in 2 M hydrochloric acid for about 1 hour, thus neutralising any residual alkali.

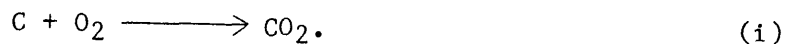
There are many different methods for extracting cellulose from dehumified wood. Some laboratories employ both organic and inorganic solvents while others consider that either an organic or inorganic solvent is sufficient. The use of organic solvents, however, can be a source of contamination as a certain amount of carbon transfer between solvent and wood can occur (Jansen, 1972). The method employed here follows a standard technique developed by wood chemists (Wise and Jahn, 1952). The sample is added to a bleaching solution comprising 80 g sodium chlorite ( $\text{NaClO}_2$ ) and 110 ml 1 M hydrochloric acid in 3 litres of distilled water. The temperature of the bleaching medium is maintained at 70-80°C for 48 hours. The sample is then filtered and washed with distilled water but if the cellulose obtained is not pure white in colour then the bleaching stage is repeated. Once obtained, the pure cellulose is dried in an oven at 80°C.

This process for extracting cellulose from wood is particularly destructive but it does guarantee a high level of decontamination and, fortunately, large amounts of sample are available in this case. Typically a wood sample of 50 g will yield about 25 g of cellulose.

### 2.2.2 Sample Combustion

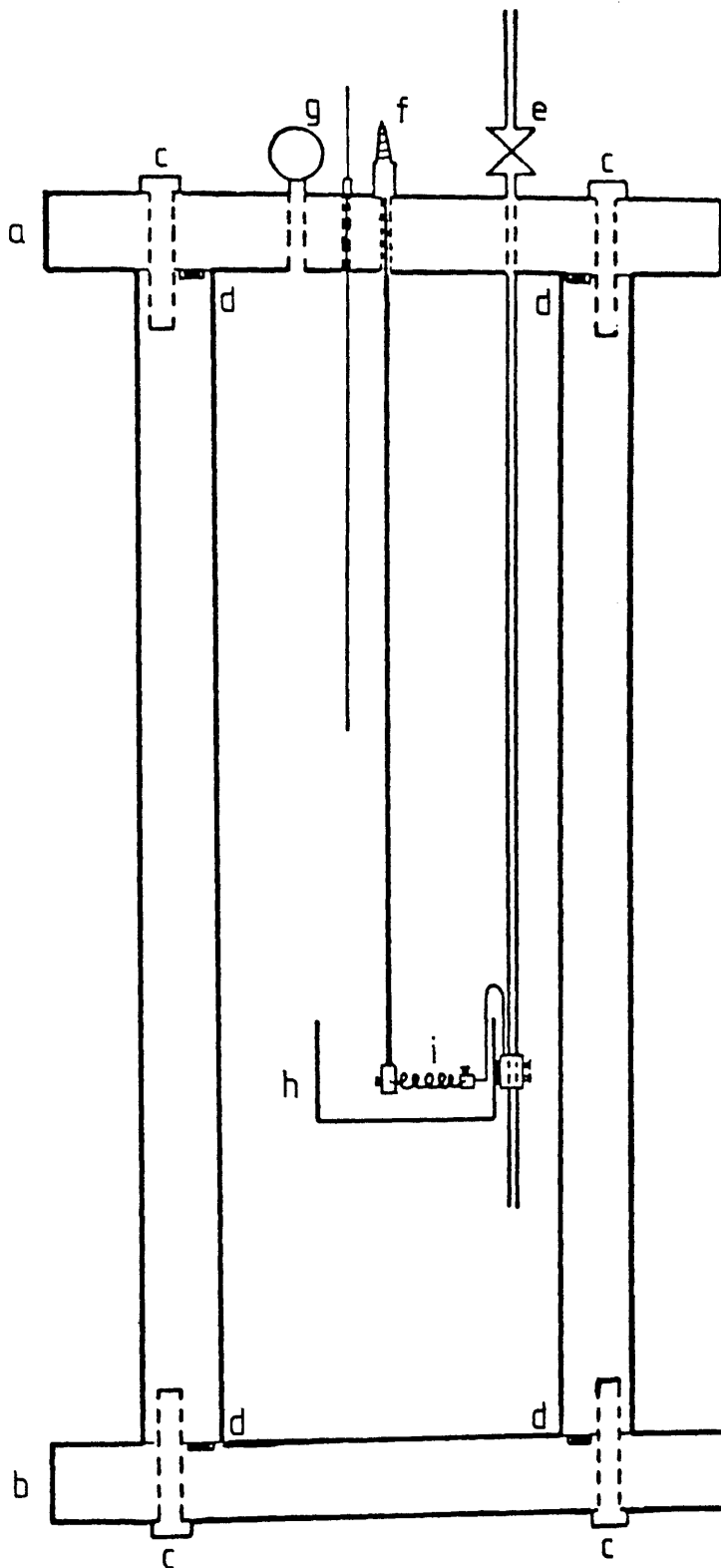
The next step in sample preparation involves conversion of the carbon in the sample to carbon dioxide. This is achieved by

combusting the sample in a pure oxygen atmosphere and the appropriate simple equation is:



The amount of sample needed is determined by the carbon content of the sample, the efficiency of the entire process and the optimal weight of benzene required for counting, in this case 7 g. The procedure initially adopted by laboratories for this combustion process followed the example set by Libby (1952) and was based on the classical technique of organic combustion analysis in which the sample is burned in a stream of oxygen in a tube furnace. However, the technique reported by Barker et al. (1969) in which the samples are oxidised in a high pressure combustion vessel affords a considerable reduction in both time and effort and forms the basis of the process used in this work.

The samples are combusted in the stainless steel reaction vessel shown in Figure 2.1. The vessel has a volume of approximately 6.4 litres and has 3 cm thick walls. The base-flange is secured by 12 high tensile bolts and the seal is completed by a neoprene 'O'-ring. The top flange, secured and sealed in the same way as the base flange, houses the filling and emptying valve, a pressure gauge and the ignition contacts. The sample is placed in a small stainless steel crucible which is mounted on the oxygen filling pipe. It is important that the lower end of the oxygen supply pipe is below the lip of the crucible to prevent dispersal of finely divided samples, with the subsequent possibility of a dust explosion. A fine resistance wire, coiled several times, is stretched across the crucible to an ignition terminal and the sample is packed closely round the wire. Before closing the vessel, the firing circuit is tested and this step further ensures that any grease on the wire, as a result of handling, is burnt off. The top flange is then securely attached to the vessel which, in turn, is connected to the CO<sub>2</sub> collection system using 0.5 cm steel tubing. The vessel is evacuated using a rotary pump and is then filled with oxygen to a pressure of 5 atmospheres, the tube connection from the oxygen cylinder to the vessel having been previously flushed with oxygen. When the bomb is pressurised, the filling valve is closed and the firing connections are made. A current of 3.5 amps is passed through the



KEY:

- a: Top flange.
- b: Basal flange.
- c: High tensile bolts.
- d: 'O-ring track and neoprene 'O-ring.
- e: O<sub>2</sub> inlet/CO<sub>2</sub> outlet valve and earth electrode.
- f: Spark plug on live electrode.
- g: Pressure gauge.
- h: Sample crucible.
- i: Ignition wire.

FIGURE 2-1: Sample combustion vessel.

resistance wire for approximately 1 minute. If the combustion is successful, then a sharp rise in temperature is felt at the base of the filling valve. The sample CO<sub>2</sub> is then left to cool in the vessel for approximately 1 hour before evacuation.

The CO<sub>2</sub> collection system is shown in Figure 2.2. It consists of a needle valve, 2 cold fingers, 3 spiral traps, a low and a high vacuum manifold. The low vacuum manifold is connected to a rotary pump and the high vacuum manifold is connected to a water-cooled mercury diffusion pump backed by a rotary pump. Traps T1 and T2 are cooled to -78°C with acetone/solid CO<sub>2</sub> slush baths and traps T3, T4 and T5 are cooled to -196°C by liquid nitrogen. The system is pumped out on low vacuum until the Bourdon gauge B1 gives a zero reading and then the CO<sub>2</sub>, in the combustion vessel, is admitted to the system via the needle valve N1. The gas flow is throttled by varying the needle valve setting to maintain a pressure of 20-30 torr on the Bourdon gauge, this pressure representing the excess oxygen being pumped away. The traps T1 and T2 freeze out any water vapour that may enter the system but allow the CO<sub>2</sub> to pass through. The CO<sub>2</sub> is then frozen out in one of the liquid nitrogen cooled traps, T3, T4 and T5. In practice, using the described flow rate, most of the CO<sub>2</sub>, that is, greater than 90%, is collected in trap T3. Emptying the combustion bomb takes about 45 minutes. Once collected, the CO<sub>2</sub> in traps T3, T4 and T5 is isolated from the rest of the system and pumped via the high vacuum manifold to a pressure of 10<sup>-3</sup> torr.

The gas is then passed into the CO<sub>2</sub> storage system, shown in Figure 2.3, where it is further purified by distillation and pumping. The storage system consists of a mass spectroscopy sampling bottle, a manometer, a cold finger and 3 storage bulbs. The liquid nitrogen traps are removed from T3 and T4 while the trap cooling T5 is replaced by an acetone/solid CO<sub>2</sub> slush bath to ensure that any water vapour which may have passed through T1 and T2 during the collection procedure does not enter the storage area. The gas sublimes into the trap T6 which is cooled to -196°C. When all the gas has been transferred, the CO<sub>2</sub> in trap T6 is again pumped via the high vacuum manifold to a pressure of less than 10<sup>-3</sup> torr. The CO<sub>2</sub> storage area consists of

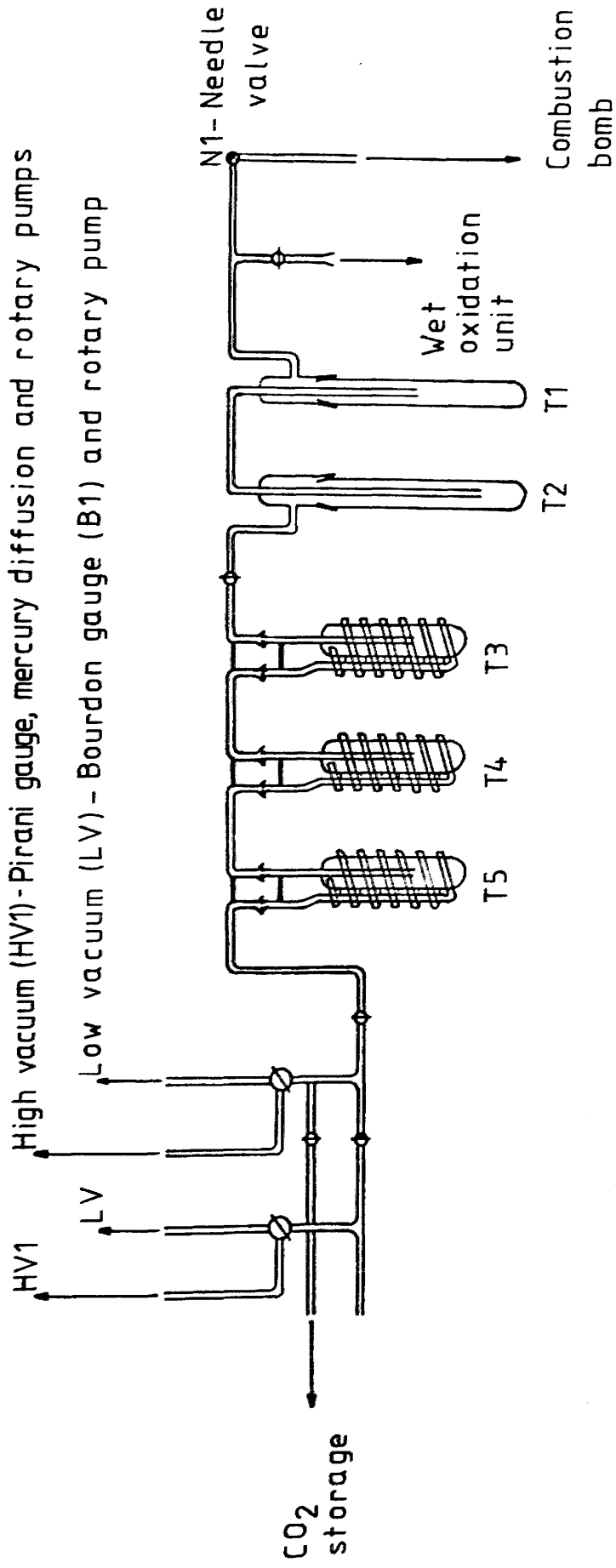


FIGURE 2-2: CO<sub>2</sub> collection system.

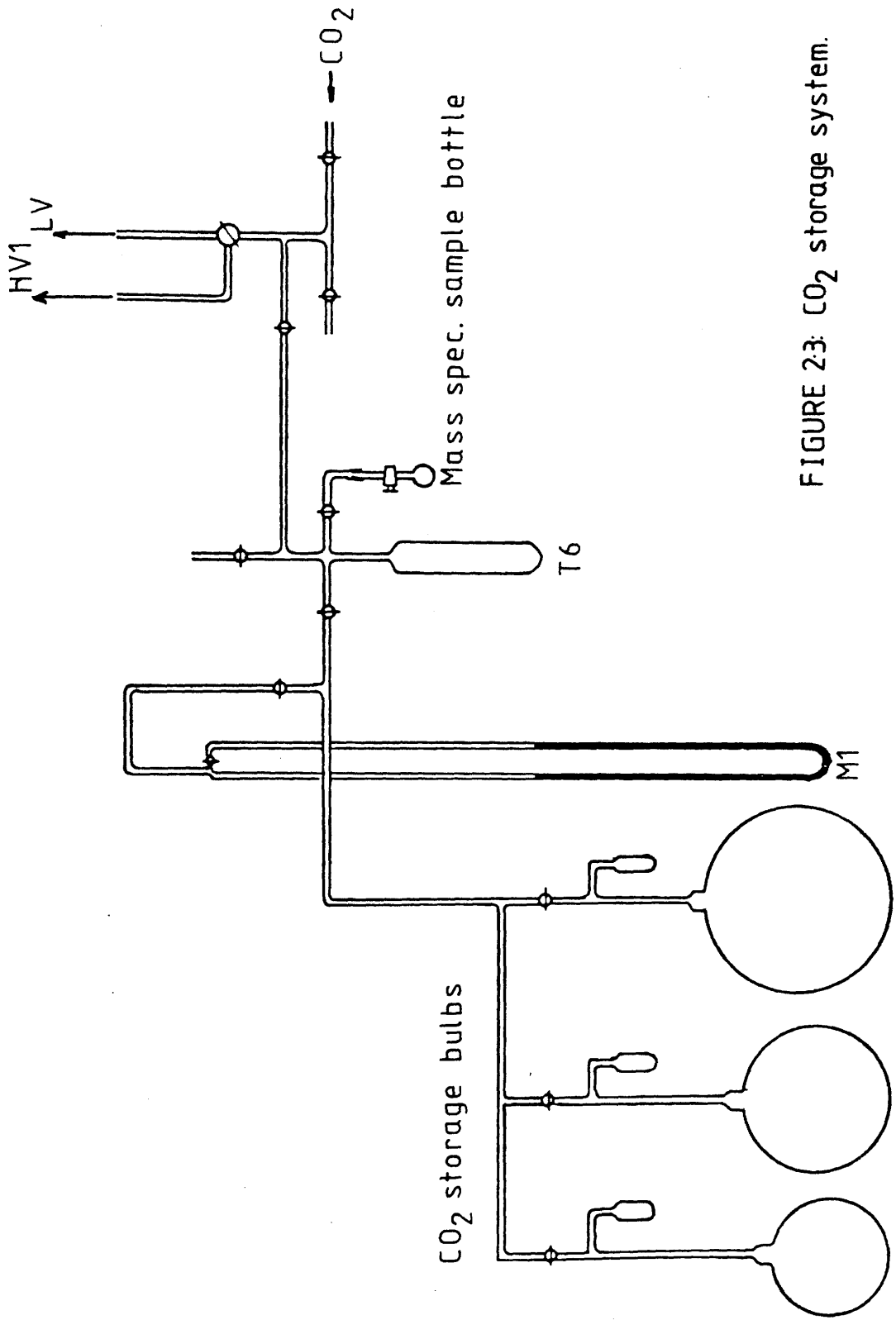
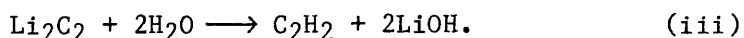
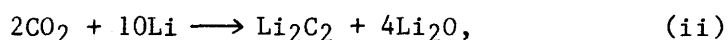


FIGURE 23: CO<sub>2</sub> storage system.

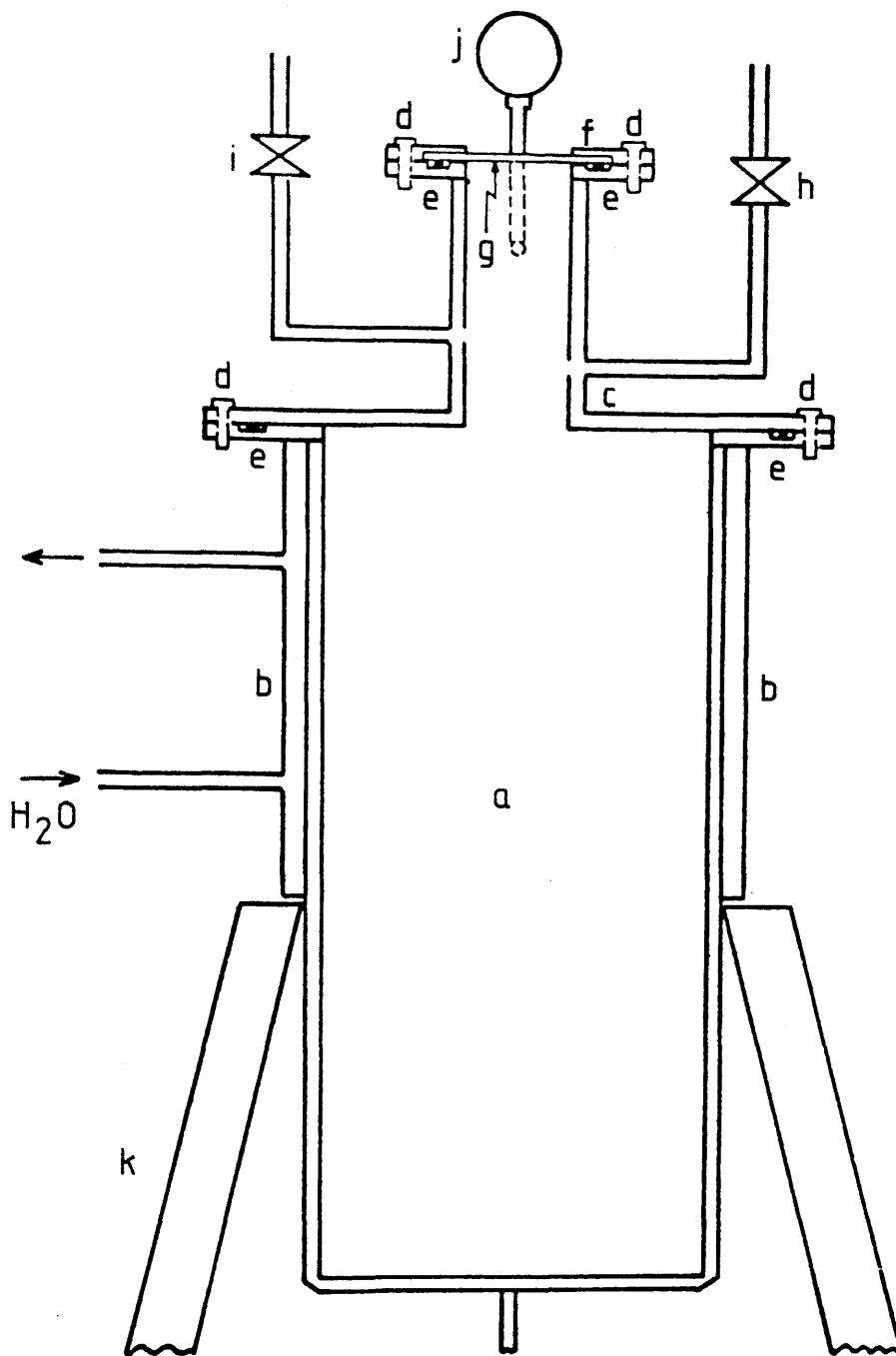
three bulbs of volumes 6, 12 and 25 litres. This arrangement facilitates the storage of a wide range of CO<sub>2</sub> quantities under conditions which reduce the problems of leakage or blow-out arising from gas pressures which are either too low or too high. Prior to collection of a CO<sub>2</sub> sample, the designated storage bulb is pumped to better than 10<sup>-3</sup> torr to eliminate possible CO<sub>2</sub> memory effects. The CO<sub>2</sub> is then transferred from T6 to the cold finger on the appropriate storage bulb. Once this has been completed, the gas is allowed to expand into the bulb and manometer system where the yield of CO<sub>2</sub> produced is measured. An aliquot of CO<sub>2</sub> is then removed for subsequent mass spectrometric analysis (discussed in Section 2.3). The efficiency of this process is very high and, on average, the percentage yield for the conversion of carbon in a sample to carbon dioxide is around 98%.

### 2.2.3 Acetylene Synthesis

The next stage in the process is to convert the carbon dioxide to acetylene. This is achieved by reacting the carbon dioxide with molten lithium followed by hydrolysis of the resulting carbide. This method was first used by Barker (1953) who had developed it from earlier work by Arrol and Glascock (1947). The reaction scheme for Barker's process is as follows:



The acetylene synthesis is performed in the stainless steel reaction vessel shown in Figure 2.4. The vessel has an approximate volume of 6.7 litres and the top half of the reaction chamber is water-cooled to prevent evaporation of molten lithium from the base of the vessel to the top, which would result in decreased yields. The top flange, housing the gas inlet/outlet valve, the water inlet valve, a Bourdon gauge and the viewport flange is secured to the main body of the vessel by 6 high tensile bolts and the seal completed by a rubber 'O'-ring. The viewport flange, consisting of a quartz window and a stainless steel surround, is secured to the vessel by 6 high tensile bolts, with an 'O'-ring again being used to complete the seal. This system is designed to facilitate quick sealing and evacuation of the vessel, as well as easy cleaning between syntheses. The whole reaction vessel is mounted on a tripod set above three 'Amal' burners.



- KEY:
- |                       |                            |
|-----------------------|----------------------------|
| a: Reaction chamber.  | b: Cooling jacket.         |
| c: Top flange.        | d: High tensile bolts.     |
| e: 'O'-ring track.    | f: Viewport flange.        |
| g: Quartz viewport.   | h: Gas inlet/outlet valve. |
| i: Water inlet valve. | j: Bourdon gauge.          |
| k: Tripod stand.      |                            |

FIGURE 2-4: Acetylene synthesis vessel.

The complete acetylene preparation and collection system is shown in Figure 2.5. It consists of the reaction vessel, a distilled water reservoir, a splash bulb, a cold finger, 2 spiral traps, a Bourdon gauge and low and high vacuum manifolds. As before, the low vacuum manifold is connected to a rotary pump but here the high vacuum pumping system consists of an air-cooled oil diffusion pump backed by a high speed rotary pump. The oil diffusion pump is used in preference to a mercury pump to safeguard against the possible formation of explosive mercury acetylides. The reaction vessel is directly connected, also, to the carbon dioxide storage system.

A quantity of lithium metal, 50% in excess of the stoichiometric quantity, is added to the reaction vessel through the viewport hole, which is quickly sealed to prevent oxidation of the lithium. The vessel is then pumped down through the low vacuum manifold, the three 'Amal' burners lit and the water for the cooling jacket turned on. After about 45 minutes heating, the carbon dioxide is admitted slowly to the reaction vessel. The silvery surface of the metal discolours to black as the carbon dioxide reacts to form the carbide (reaction (ii)) and then, as heat of reaction is evolved, the temperature of the reaction mixture increases to around 800°C. The pressure in the vessel is closely monitored and is not allowed to exceed 300 torr since, above that pressure the reaction proceeds too fast, resulting in a lowering of the acetylene yield. Towards the end of the reaction, as the carbon dioxide pressure decreases, the reaction may become rather slow. To counteract this, the remaining carbon dioxide is frozen down into the cold finger T6, the CO<sub>2</sub> storage bulb shut and the CO<sub>2</sub> allowed to expand into the reduced volume. Once all the carbon dioxide has been admitted, the reaction vessel is isolated from the rest of the system and heating is continued for a further 30 minutes. Before hydrolysis of the carbide can take place, the reaction mixture is allowed to cool for 1-2 hours and any excess pressure in the vessel is reduced by pumping.

As freshly distilled water is slowly added to the reaction vessel, the pressure on the Bourdon gauge starts to rise. The increase in pressure is due to the production of acetylene (reaction (iii)) and hydrogen (a product of the reaction of the

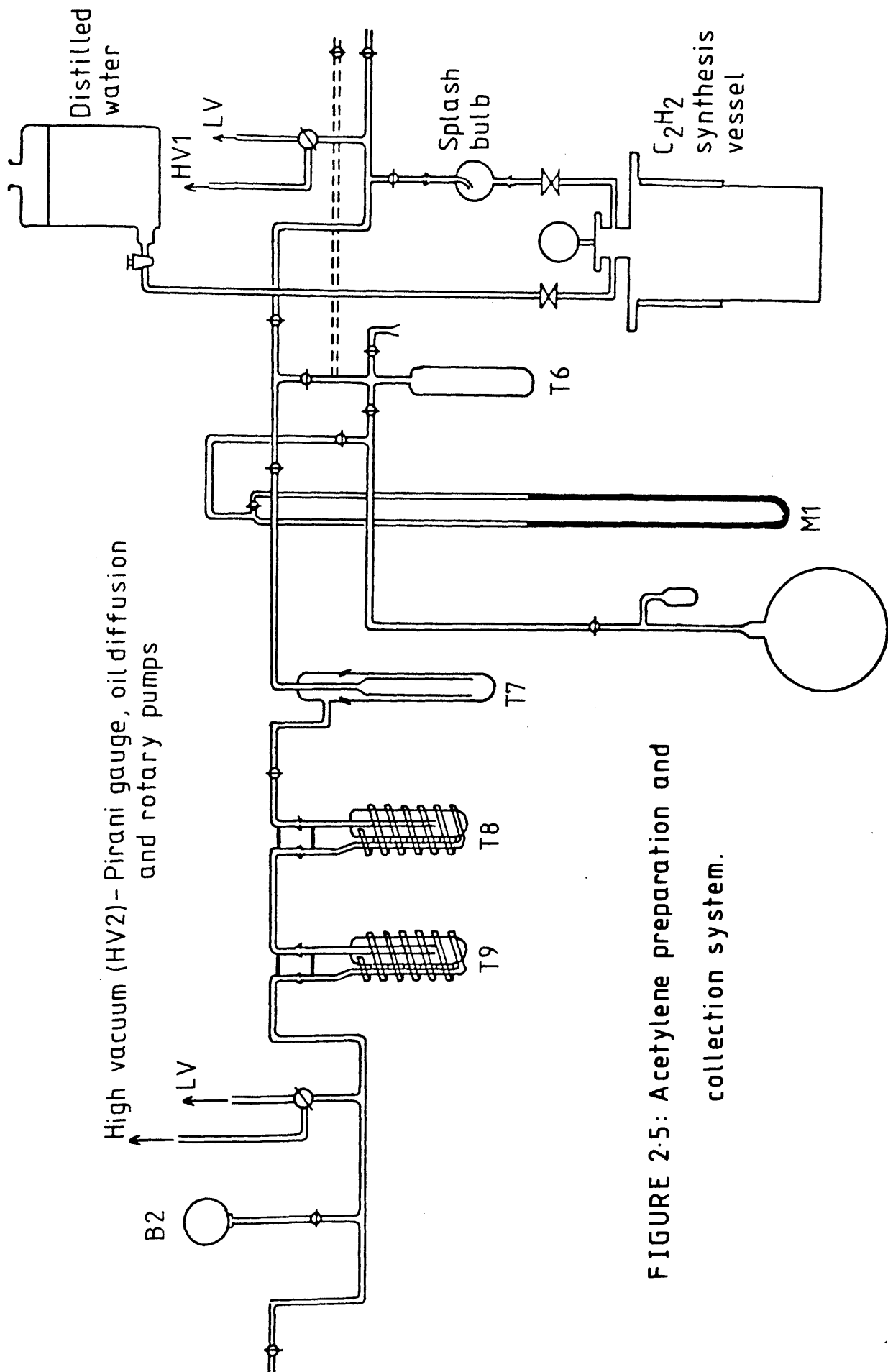


FIGURE 2.5: Acetylene preparation and collection system.

excess lithium with water). Once the pressure inside the vessel reaches about 700 torr, the supply of water is stopped and the gas outlet valve is opened to the acetylene collection system, which is being pumped out via the low vacuum manifold. The cold finger T7 is cooled to  $-78^{\circ}\text{C}$  with an acetone/solid  $\text{CO}_2$  slush bath and the spiral traps, T8 and T9, are cooled to  $-196^{\circ}\text{C}$  by liquid nitrogen. The gas flow is regulated to maintain a pressure of 20-30 torr, shown on Bourdon gauge B2, the pressure representing the hydrogen gas being pumped away. Any water vapour which enters the system is frozen out in trap T7, whereas the acetylene passes through this only to be frozen out into traps T8 or T9. At this flow rate, practically all the acetylene remains in T8. Once the pressure in the reaction vessel has dropped to about 200 torr, the gas outlet valve is shut. This process is repeated until, on the addition of more distilled water, no further gas is evolved. To collect the final traces of acetylene, the pressure in the reaction vessel is reduced to around 80 torr causing the reaction mixture to boil and, despite the presence of the splash bulb, care is necessary to prevent quantities of water distilling into the main part of the collection system. When all the product gases have been collected, traps T8 and T9 are isolated from the rest of the system and are pumped via the high vacuum manifold to better than  $10^{-3}$  torr.

Further purification of the acetylene can be achieved by passing it through two scrubbing columns containing glass beads coated with orthophosphoric acid. The acetylene purification and storage system is shown in Figure 2.6. It consists of the scrubbing columns, 2 cold fingers, a manometer, 3 storage bulbs and, as usual, a low and a high vacuum manifold. The acetylene is allowed to condense slowly from traps T8 and T9 into T11, which is cooled to  $-196^{\circ}\text{C}$ . In the process, it must pass through the scrubbing columns and trap T10, which is cooled to  $-78^{\circ}\text{C}$ . The primary function of the orthophosphoric acid is to remove ammonia from the acetylene as ammonium phosphate. The ammonia is the hydrolysis product of lithium nitride, formed from nitrogen oxide impurities in the carbon dioxide. It is necessary to replace the scrubbing columns with a fresh unit every couple of weeks as the build-up of phosphate on the beads reduces the efficiency of the cleaning procedure. Trap T10 freezes out any traces of water

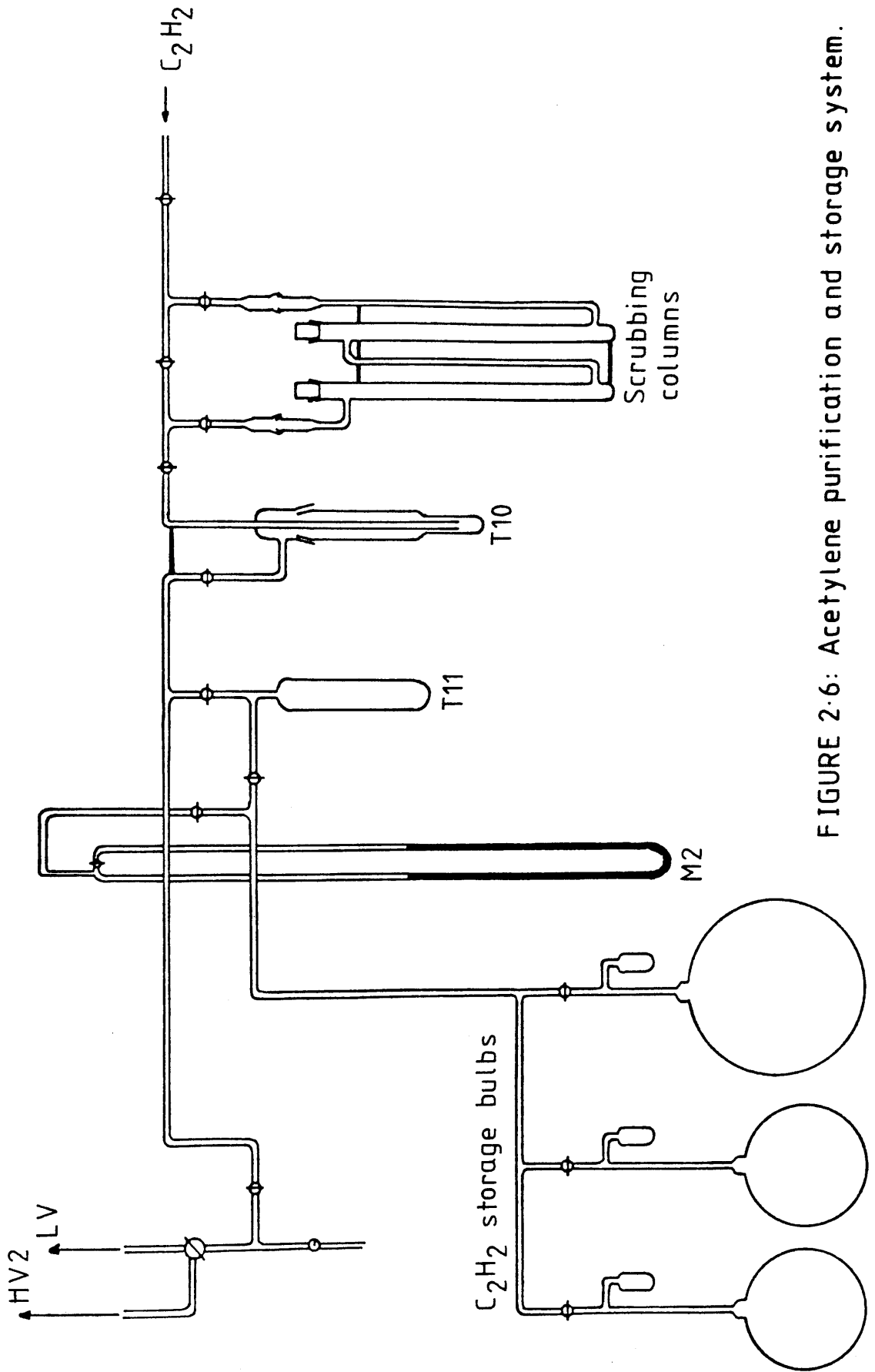
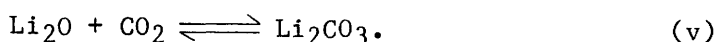
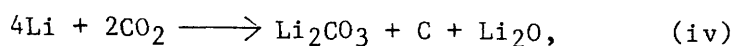


FIGURE 2-6: Acetylene purification and storage system.

vapour which may still be in the system. Once isolated in trap T11, the acetylene is again pumped to around  $10^{-4}$  torr. Finally, the acetylene is distilled into the storage system and the yield measured. The three bulbs in the storage system have volumes of 5, 6 and 15 litres to facilitate the convenient storage of a wide range of acetylene quantities. Prior to the acetylene storage, the appropriate bulb is pumped to better than  $10^{-4}$  torr, thus eliminating any memory effects.

The average yield for the conversion of carbon dioxide to acetylene was around 90%. According to Tamers (1975) the main losses of carbon are likely to occur by the following pathways:



These losses can be reduced by carrying out the reaction at a high temperature ( $>600^\circ\text{C}$ ) and by using an excess of lithium, as in this study. At temperatures above  $600^\circ\text{C}$ , lithium carbonate decomposes significantly, reversing reaction (v). At temperatures of  $900^\circ\text{C}$  the regenerated carbon dioxide is converted to lithium carbide by reaction (ii) and the carbon produced in reaction (iv) is converted to lithium carbide by reaction (vi):

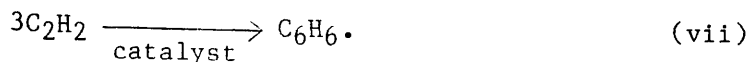


The acetylene yield in this research is less than Tamers' optimised yield of 95%, which could be explained by the slightly lower reaction temperatures employed.

#### 2.2.4 Benzene Synthesis

In the final stage of the process, the acetylene gas is converted to benzene. When benzene was initially synthesised for radiocarbon dating by Tamers (1960), the cyclotrimerisation reaction was performed by pyrolysis of acetylene at  $650^\circ\text{C}$ . This method was superseded by that of Starik et al. (1961) who introduced the use of Ziegler catalysts. Thereafter Noakes et al. (1963) introduced a diborane activated catalyst for acetylene trimerisation. By 1965, however, most laboratories using the liquid scintillation technique had switched to transition metal activated silica-alumina catalysts (Noakes et al., 1965; Tamers, 1965; Pietig and Scharpenseel, 1966). In this study, a chromium (vi) activated silica-alumina catalyst is used (KC Perlkatalysatorneu, supplied by Kali Chemie, Hannover, Germany).

The catalyst comes in pellet form, the average pellet size being 2-3 mm. Around 150 g of catalyst are used for the cyclotrimerisation of 0.5 moles of acetylene. The chemical reaction for this stage can be represented as follows:



The cyclotrimerisation reaction takes place in the catalyst tube which is essentially a cylinder 25 cm long and 5 cm in diameter. A thermocouple is embedded into the middle of the catalyst tube, which can be attached to the benzene synthesis system via a ball and socket joint. The synthesis system, shown in Figure 2.7, consists of the catalyst vessel, a demountable cold finger, a Bourdon gauge, a low and a high vacuum manifold. As in the acetylene synthesis section, the high vacuum pumping system consists of an air-cooled oil diffusion pump backed by a rotary pump. Only greaseless stopcocks and joints are used in this section to avoid the possibility of dissolving grease in the product benzene. The whole system is, of course, connected to the acetylene storage section.

Once the catalyst vessel has been charged with catalyst, it is attached to the benzene synthesis section, pumped out through the low vacuum manifold and then surrounded by a furnace and heated to 400°C. The vessel is then pumped out on high vacuum for several hours at this temperature. When a pressure of less than  $10^{-3}$  torr is reached, the vessel is allowed to cool down to around 80°C. All the acetylene is then transferred from the storage bulb to the cold finger T11 and a small aliquot of the acetylene is admitted to the catalyst vessel. The pressure of acetylene in the vessel can be monitored by the Bourdon gauge B3 and is always maintained below 600 torr. After admitting the acetylene, there is a steady drop in pressure as the gas is adsorbed by the catalyst. This pressure reduction is accompanied by a rise in temperature, as the synthesis reaction is exothermic. Once the acetylene pressure has dropped, a further aliquot is admitted to the vessel. This process is continued until the catalyst temperature approaches 150°C, at which it is allowed to cool. The cooling process is aided by distilling the product benzene from the catalyst into the demountable cold finger T12 which is cooled to -196°C. This process also helps to prevent

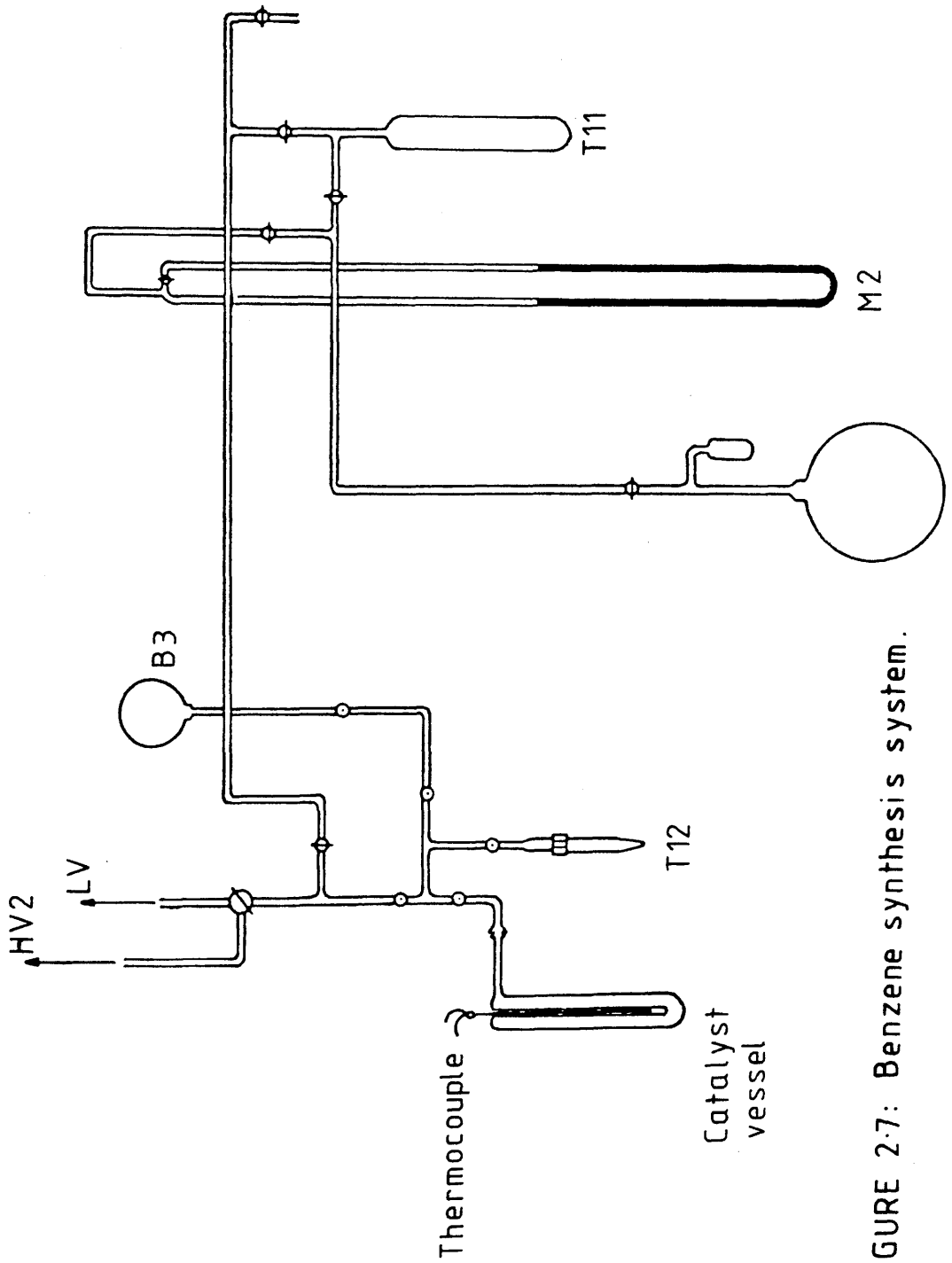


FIGURE 2.7: Benzene synthesis system.

saturation of the catalyst's active sites. Once the catalyst temperature approaches 80°C, the cold finger T12 is isolated from the system and the whole process is repeated until all the acetylene has been adsorbed onto the catalyst. Any residual traces of acetylene which are not adsorbed are condensed into the cold finger T12. The cold finger is then warmed up to release, into a reduced volume, any traces of acetylene that were condensed. This acetylene is then adsorbed onto the catalyst. Once all the acetylene has been adsorbed, the catalyst is heated up to 150°C and the product benzene collected in the cold finger T12. The benzene is then allowed to melt and the cold finger is removed from the system, labelled and sealed. It is possible to regenerate the catalyst by heating it in air to 450°C, oxidising the Cr(iv) and Cr(iii) to Cr(vi). However, because of the possibility of memory effects between syntheses, this was not done in this study and the spent catalyst was discarded after each synthesis.

The average yield for conversion of acetylene to benzene was 74%. The main carbon losses would appear to be from formation of carbonates with subsequent deactivation of the catalyst (Cr(vi)  $\longrightarrow$  Cr(iii)), as reported by Tamers (1975). These reactions are encouraged by the presence of water and by high temperatures, although both of these conditions are avoided by the experimental procedure used here. However, the design of the catalyst tube is such that, when the acetylene is adsorbed, the top half of the catalyst is used preferentially and thus a temperature gradient is likely, resulting in 'hot-spots' on the catalyst and hence lower yields. The benzene yield could easily be increased by heating the catalyst to 200°C when distilling the benzene into the cold finger. However, at this temperature, the fraction of organic impurities, e.g. toluene, also collected increases dramatically. In this work, therefore, increased purity has been favoured over increased yields.

#### 2.2.5 Summary of Sample Preparation

The sample preparation routine, including approximate times for the individual processes, is presented as a flow chart in Figure 2.8. The overall conversion yield from sample carbon to benzene is 65%. This value is rather low relative to the figures

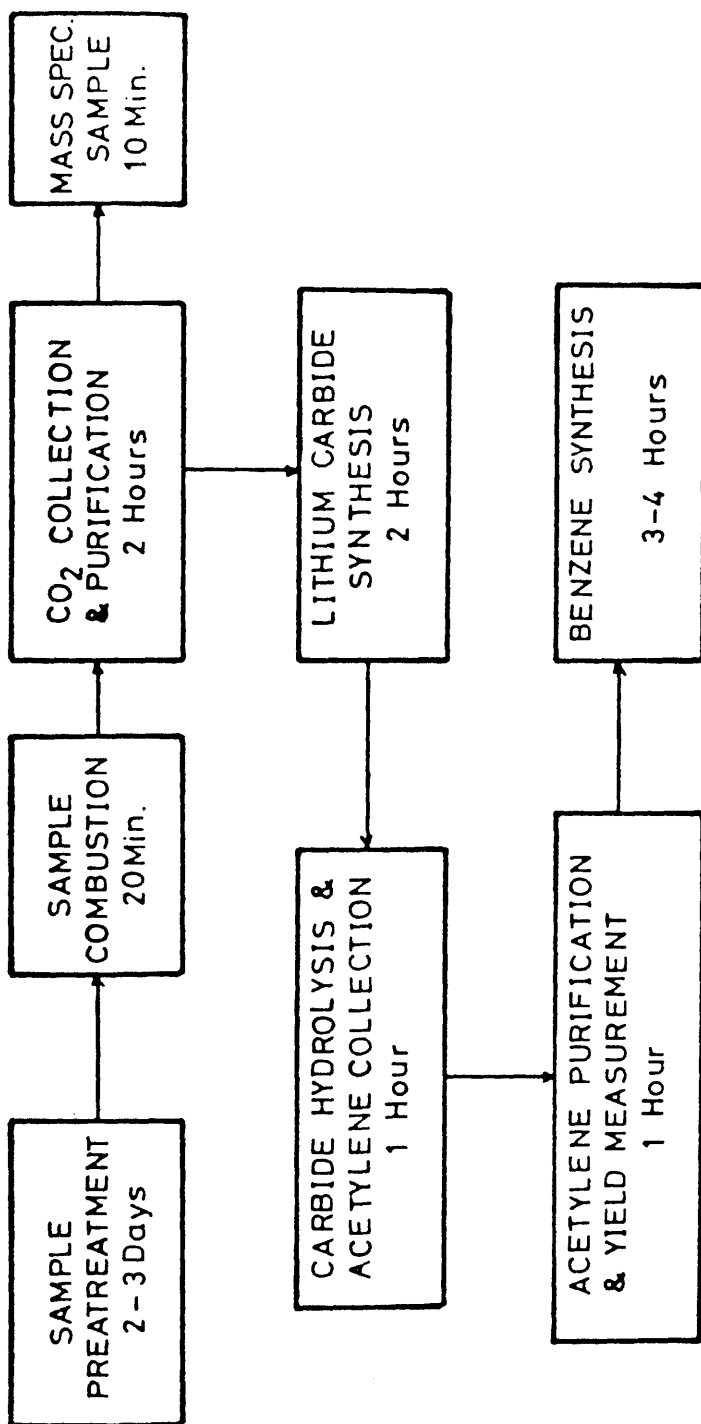


FIGURE 2.8: Sample preparation procedure.

quoted by other laboratories using similar chemical procedures (Harkness and Wilson, 1972; Tamers, 1975). However, the purity of the benzene, assessed by chromatographic analysis, has been shown to be greater than 99% with the main impurities being toluene, ethylbenzene and para-xylene.

### 2.3 MEASUREMENT OF ISOTOPIC FRACTIONATION

As a result of slight differences that exist in the thermodynamic properties of isotopes, any physical or chemical process which occurs with <100% yield may cause a change in an element's isotopic ratio. Isotopic fractionation, as this effect is known, is a significant phenomenon encountered in the transfer of carbon both in the laboratory and the environment. For example, Craig (1953) measured a 2% depletion in the  $^{13}\text{C}/^{12}\text{C}$  ratio of terrestrial organic plants relative to the  $^{13}\text{C}/^{12}\text{C}$  ratio of the atmosphere from which they assimilate  $\text{CO}_2$ . Since the  $^{14}\text{C}-^{12}\text{C}$  mass difference is double that for  $^{13}\text{C}-^{12}\text{C}$ , it can be assumed that the fractionation effect for  $^{14}\text{C}$  is twice as large as for  $^{13}\text{C}$  (Craig, 1954). So, before any comments can be made on the differing radiocarbon levels in various samples, the values must first be corrected for any isotopic fractionation which may have occurred in either the laboratory or in nature.

The extent of isotopic fractionation in a sample cannot be derived from a measure of the  $^{14}\text{C}/^{12}\text{C}$  ratio as this ratio is also perturbed by other factors, e.g. the artificial production of  $^{14}\text{C}$ . Therefore, a measurement of the  $^{13}\text{C}/^{12}\text{C}$  ratio is performed, from which a measure of the fractionation effect for  $^{14}\text{C}$  can be simply derived. The measurement of the  $^{13}\text{C}/^{12}\text{C}$  ratio is performed on an aliquot of  $\text{CO}_2$  removed from the sample after its combustion. It is assumed, with some experimental justification, that the subsequent conversion of carbon dioxide to benzene does not further modify the isotopic ratios, despite the non-quantitative yields obtained (Campbell, 1977). In this work sample  $^{13}\text{C}/^{12}\text{C}$  ratios are measured at the Scottish Universities Research and Reactor Centre using a VG Micromass 602B mass spectrometer. The Micromass 602B is a double beam collector spectrometer which allows the direct measurement of the deviation

in the sample's  $^{13}\text{C}/^{12}\text{C}$  ratio relative to a standard's  $^{13}\text{C}/^{12}\text{C}$  ratio. The observed  $^{13}\text{C}/^{12}\text{C}$  ratio in the sample is represented by an enrichment relative to the primary standard based on the general formula (Craig, 1957a):

$$\delta^{13}\text{C} = \left[ \frac{(^{13}\text{C}/^{12}\text{C})_{\text{sample}} - (^{13}\text{C}/^{12}\text{C})_{\text{standard}}}{(^{13}\text{C}/^{12}\text{C})_{\text{standard}}} \right] \times 1000\text{‰} \quad (2.1)$$

The primary standard used for carbon isotope studies is  $\text{CO}_2$  produced from PDB calcium carbonate by reaction with 100% orthophosphoric acid at  $25.2^\circ\text{C}$ . PDB is a Cretaceous belemnite, Belemnitella Americana, from the Peedee formation of South Carolina. In practice, secondary standards, previously calibrated against the primary standard, are used. The secondary standards are all supplied by the National Bureau of Standards in Washington and they are NBS(19), which is a marble sample, NBS(20) which is a limestone and NBS(21) (graphite). The enrichments of these standards with respect to the PDB standard are +1.94‰, -1.06‰ and -28.10‰ respectively, with the 1 sigma error in each case being  $\pm 0.05\text{‰}$ .

## 2.4 THE LIQUID SCINTILLATION TECHNIQUE

In this section the basic theory of liquid scintillation counting will be described. In addition, the actual system used in this work will be discussed along with details of its optimisation for low-level  $^{14}\text{C}$  counting.

### 2.4.1 The Theory of Liquid Scintillation Counting

The method of liquid scintillation counting requires the sample to be dissolved in, or placed in contact with, a scintillator medium which is itself usually a solution. The basic principles are that beta particles emitted by the samples are converted to photons of light by a 'scintillation cocktail'. A photomultiplier tube then converts the emitted photons of light into electrical pulses which are proportional to the energy of the original beta particles. Some energy is lost at each stage of the process. Energy diffusion and loss, plus quantum statistics, reduce the overall resolution of the system both during the scintillation process itself and in conversion of light energy to electrical energy in the photomultiplier.

#### 2.4.2 The Scintillation Medium

The scintillation medium usually consists of at least one type of scintillator dissolved in a solvent. The theory is that a beta particle emitted by the sample raises the solvent molecules along its path of travel to an excited state. This energy is transferred from one solvent molecule to another until it is absorbed by a scintillator molecule. The scintillator molecule then re-emits this energy, in the form of light, at its own characteristic wavelength. Very often this wavelength is too short for efficient detection and a secondary scintillator may be introduced to absorb the photons and re-emit them at longer and more detectable wavelengths. This whole process is summarised diagrammatically in Figure 2.9.

A good solvent for the scintillation medium should possess the following properties; it must:

- (a) dissolve the scintillants in sufficient concentrations,
  - (b) be a good energy transfer agent,
  - (c) have a low freezing point ( $<0^{\circ}\text{C}$ )
- and
- (d) be safe to use.

Suitable solvents are found in the aromatic hydrocarbons group and, for this work, toluene was chosen.

The prerequisites for a good scintillator are that it must:

- (a) be soluble in the solvent,
  - (b) give a good photon yield
- and
- (c) emit photons of a wavelength compatible with the response of the photomultiplier tubes.

The scintillator chosen was 'butyl-PDB' (2-(4'-tert-butylphenyl)-5-(4"-biphenylyl)-1,3,4-oxadiazole). However, the wavelength of the photon emissions by this compound is too short for optimal photomultiplier tube response, making it necessary to employ a secondary scintillator. The secondary scintillator used is 'bis-MSB' (1,4-di-(2-methylstyryl)-benzene), which emits photons with a wavelength more compatible with the photomultiplier tubes.

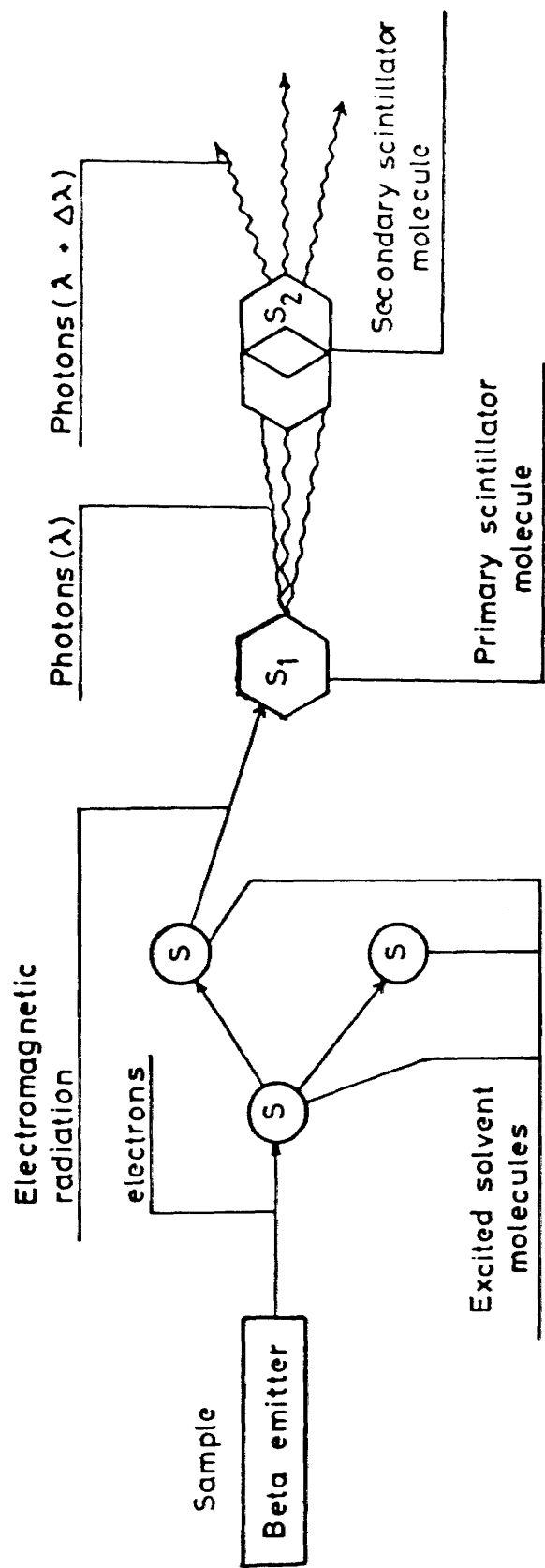


FIGURE 2.9: Energy transfer scheme in a liquid scintillator.

A batch of the 'scintillation cocktail' is produced by dissolving 3 g 'bis-MSB' and 6 g 'butyl-PDB' in 500 ml toluene.

### 2.4.3 The Detection System

The function of the detection system is to convert light into electrical energy proportional to the light output of the scintillator medium. The detection system consists of a photomultiplier tube with a glass or quartz face coated with a thin layer of CsSb. This face acts as a photocathode, for, when it is struck by light of a particular wavelength, photoelectrons are emitted. These photoelectrons are then accelerated down a chain of dynodes such that, when an electron strikes each dynode, a number of further electrons are emitted. Thus when the pulse reaches the anode (which has a large positive voltage applied to it), its amplification has been sufficient to allow it to be detected by the counter electronics. The output at the anode is proportional to the light input at the photocathode producing a pulse spectrum roughly equivalent to the energy spectrum of the isotope. A schematic diagram of this process is shown in Figure 2.10.

The main deficiency of photomultiplier tubes is their spontaneous emission of electrons at the photocathode. This phenomenon is strongly temperature dependent and the pulses at the anode are indistinguishable from those due to radioactive disintegrations in the sample. Although cooling can reduce this thermal noise (the counter assembly is maintained between 0-10°C), it still remains sufficiently high to require further counter-measures.

The most practical means of reducing thermal noise involves coincidence circuitry. Here two photomultiplier tubes are employed for light detection and the electronic logic is such that only if a pulse is received simultaneously by each tube is the event recorded as sample-derived. If a pulse is received by only one tube, it is rejected. The theory is that when photons are emitted during a radioactive decay event in the sample, a sufficient number is usually produced to cause simultaneous photoelectron emission at the photocathode of each tube; hence the pulse is recorded. However, the emission of thermal electrons

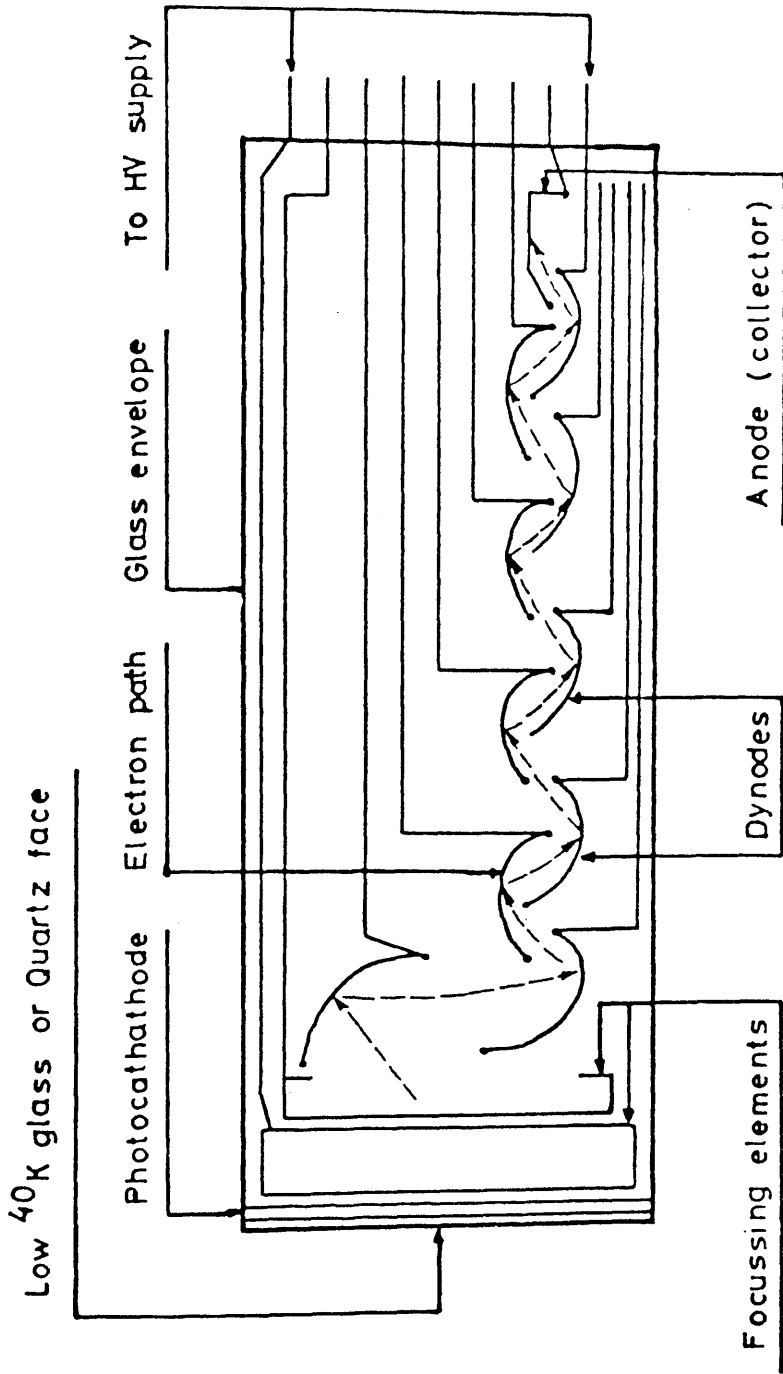


FIGURE 2-10: Schematic diagram of a photomultiplier tube.

from each photocathode is presumed to occur randomly and thus simultaneous events are unlikely. Coincidence circuitry therefore greatly reduces the thermal noise contribution to the counter background level. In addition, the use of two photomultiplier tubes allows the technique of pulse summation to be employed. This configuration adds the pulse amplitudes of both tubes before pulse height analysis, improving the counting efficiency, increasing the energy resolution and improving the signal-to-noise ratio.

#### 2.4.4 The Liquid Scintillation Counter

The counting apparatus used in this research was a Model 3330 Automatic Tri-Carb Liquid Scintillation Spectrometer constructed by the Packard Instrument Company. The basic specifications are as follows. The complete shield assembly is mounted in a 0.3 m<sup>3</sup>, temperature-controlled chest-type freezer, temperature being maintained within  $\pm 0.5^{\circ}\text{C}$  over a range of approximately  $-5$  to  $+15^{\circ}\text{C}$ . The optical chamber containing the two matched Bialkali photomultiplier tubes is screened from environmental radiation by a minimum of 5 cm of lead shielding in all directions. The 0-2400 V high voltage supply has a guaranteed stability of 0.01% per day. Output pulses from the photomultipliers are fed through high-speed coincidence and pulse-summation circuits. Three separate pulse height analysis channels are incorporated, each with a linear amplifier and a precision gain control. Three scalers record the contents of the channels. A simplified diagram of the electronics is shown in Figure 2.11. Samples are accommodated in a 300-position belt-type chamber and automatic programming enables group counting, rejection and repeat-counting modes. Complete light-tightness of the optical chamber is ensured by a 'light lock' consisting of an expanding rubber seal on the elevator and a five-leaf shutter at the chamber entrance. At the end of a count, the accumulated data are printed out on a teletype. The output lists position in sample belt, count time, counts in each channel and external standard counts. A radium-226 source of activity 0.74 MBq ( $\pm 10\%$ ) is used in the system as an external standard. When not in use the external standard is shielded by approximately 30 cm lead.

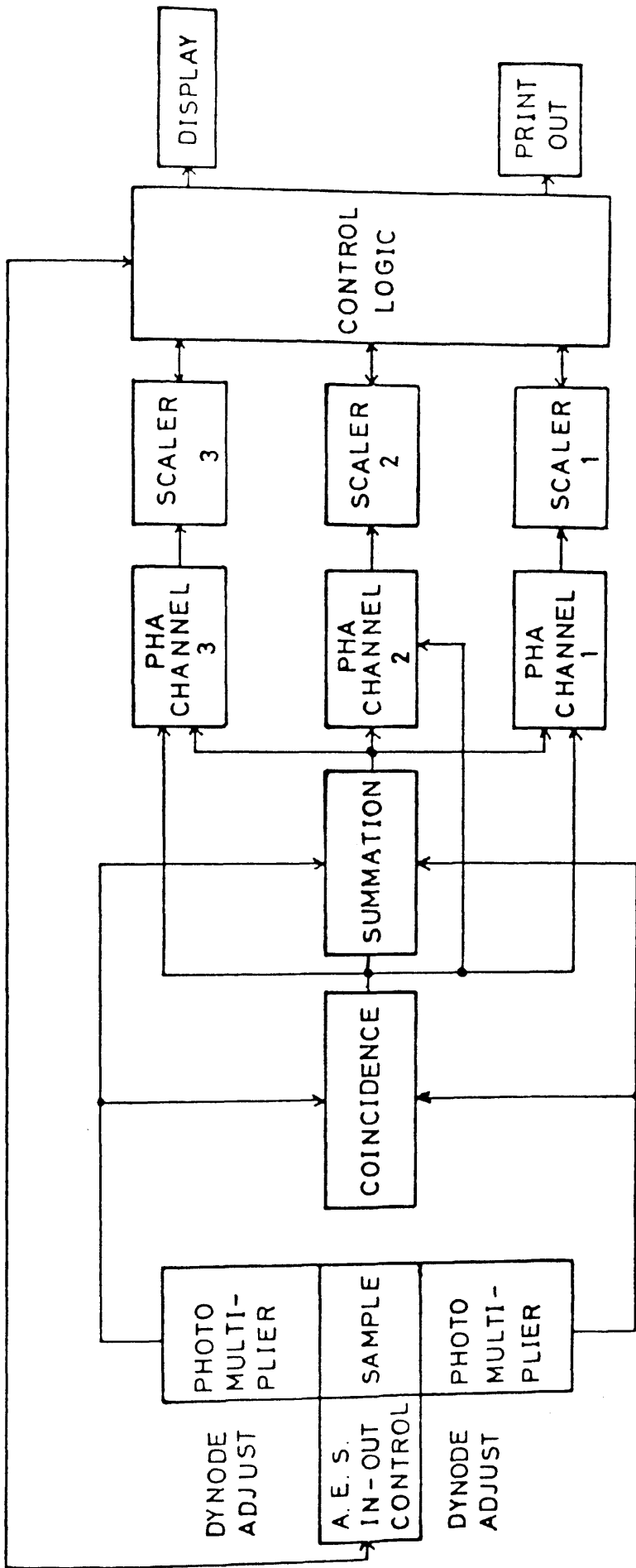


FIGURE 2-11: Schematic diagram of counting system electronics.

#### 2.4.5 Optimisation of the Counter for Low-level $^{14}\text{C}$ Assay

In general, commercially available liquid scintillation counters are designed for measurement of the several beta-emitting isotopes employed in bio-medical tracer studies. Consequently the operational parameters preset or recommended by the manufacturer do not correspond to the optimum conditions for low-level  $^{14}\text{C}$  assay. In determining the latter conditions a balance of three separate operational parameters has to be achieved, namely the high voltage supply to the photomultiplier tubes, the discriminator positions of the three independent counting channels and the amplifier gain (or attenuation) setting for each channel. The system must have a low background count rate (B) and a high counting efficiency (E), such that when the three factors have been balanced, the 'Figure of Merit' ( $E^2/B$ ) should be at a maximum. At maximum, the counter has the highest sensitivity for  $^{14}\text{C}$  detection.

One potential difficulty encountered in  $^{14}\text{C}$  detection results from the energy overlap of the  $^{14}\text{C}$  and  $^3\text{H}$  beta energy spectra. As the hydrogen content of the benzene counting medium derives from the water used in acetylene synthesis and as the water used contains naturally occurring  $^3\text{H}$ , it is important to minimise the  $^3\text{H}$  contribution to the  $^{14}\text{C}$  counting 'window'. The energy overlap between the spectra is around 12% but the mean beta energy for  $^{14}\text{C}$ , 45 keV, is higher than the maximum beta energy of  $^3\text{H}$ , 18 keV. Therefore, it should be possible to define a window for an attenuated  $^{14}\text{C}$  pulse height spectrum which, with appropriate discriminator settings, should have a very small tritium contribution. Hence, the gain settings for all three channels are set to 90%.

With these gain settings, the high voltage potentials on the photomultiplier tubes are adjusted until the efficiency of the system is at maximum. In this case, the maximum efficiency is obtained at 1364 V, as shown in Figure 2.12, which is also the point of the maximum 'Figure of Merit'.

The pulse height spectra, obtained at this gain and high voltage setting, for  $^{14}\text{C}$ ,  $^3\text{H}$  and background are shown in Figures 2.13, 2.14 and 2.15 respectively. On this basis, the

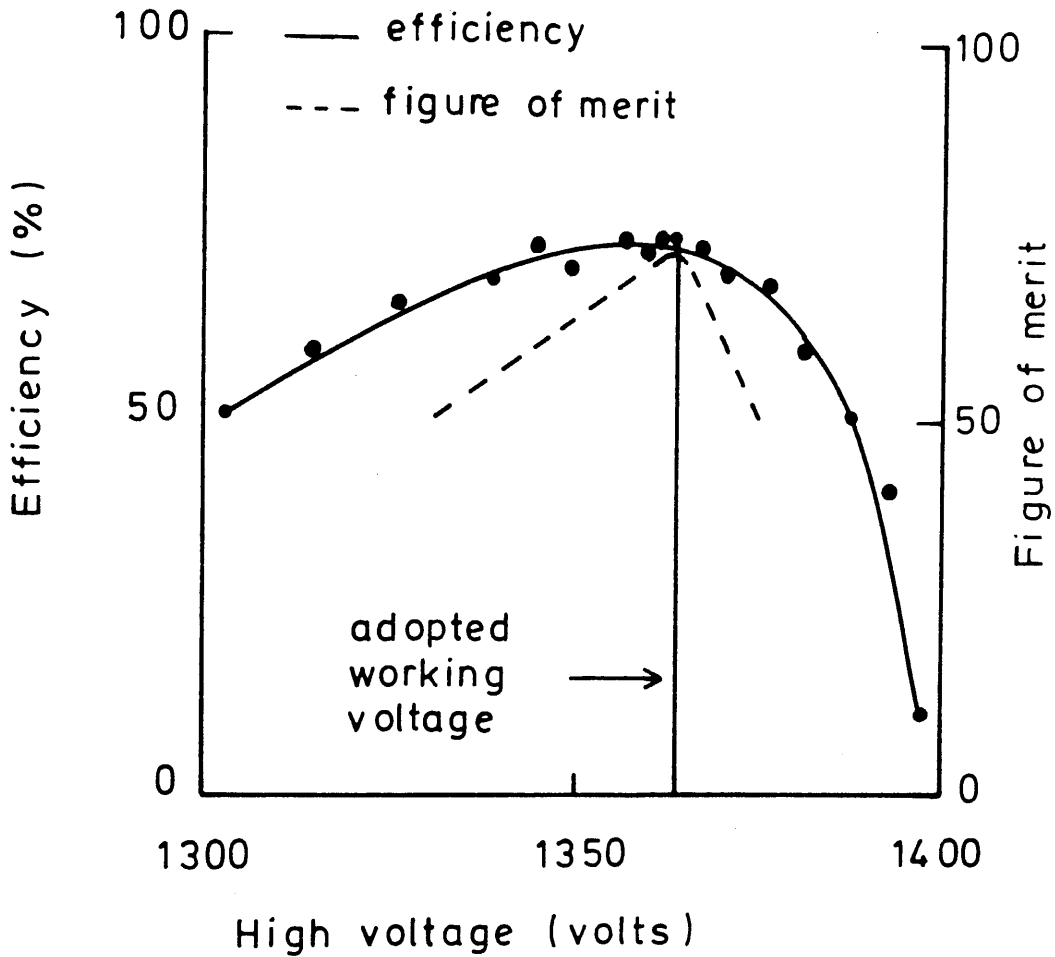


FIGURE 2-12: Variation of the  $^{14}\text{C}$  detection efficiency with high voltage.

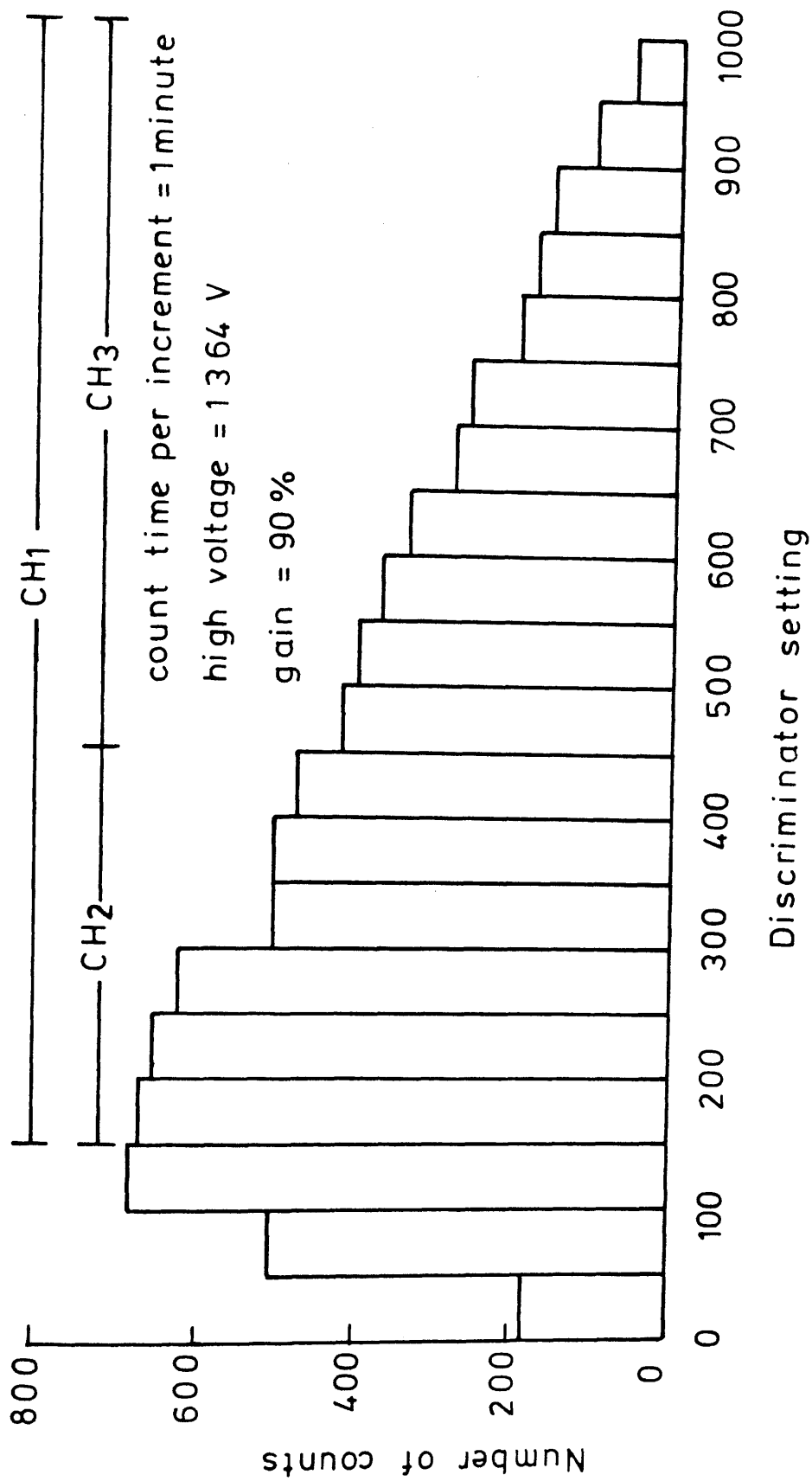


FIGURE 2.13:  $^{14}\text{C}$  pulse height spectrum.

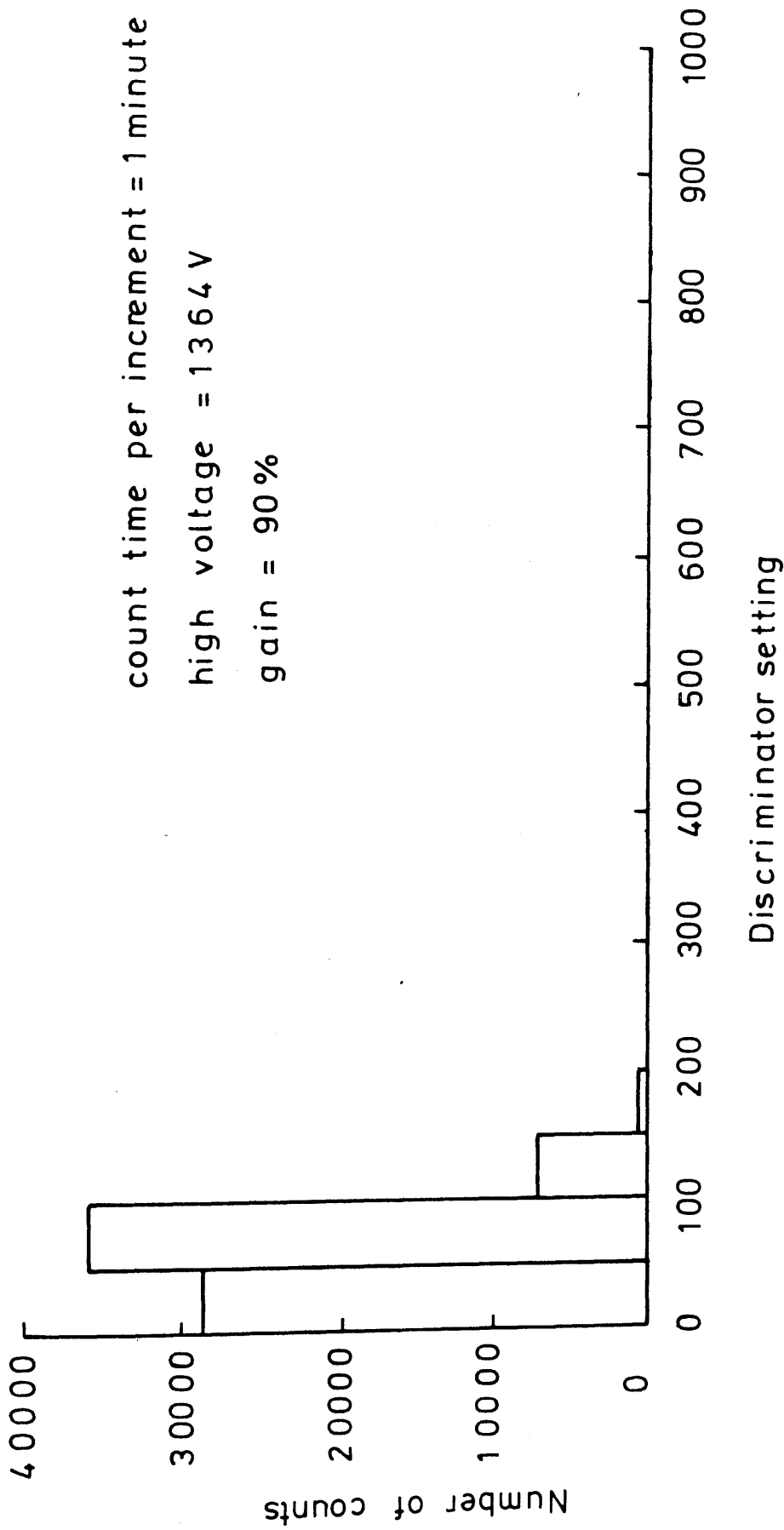


FIGURE 2.14:  $^3\text{H}$  pulse height spectrum.

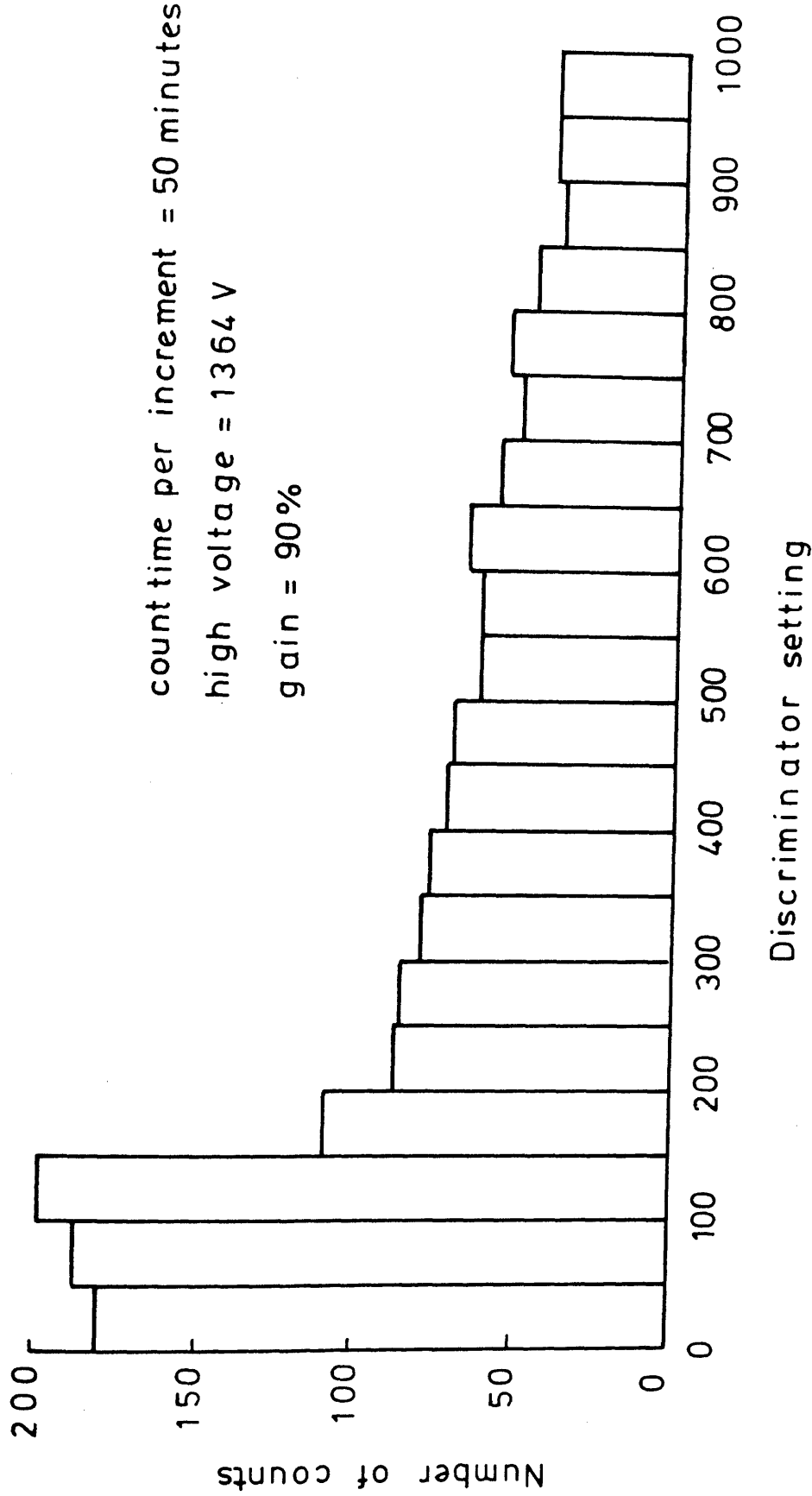


FIGURE 2-15: Background pulse height spectrum.

discriminators are set to screen off the majority of the tritium and background contributions. Channel 1, which monitors the whole  $^{14}\text{C}$  spectrum, has its lower discriminator set at 150 mV and its upper discriminator at 1000 mV. Channels 2 and 3 are set at 150-450 mV and 450-1000 mV respectively to monitor changes in the spectrum shape as a result of quenching (discussed in Section 2.5.4).

At these settings the efficiency of  $^{14}\text{C}$  detection,  $E$ , is 73% and the background count rate,  $B$ , is 7.4 counts per minute (cpm). The overall 'Figure of Merit' is therefore 715 and the efficiency for tritium is less than 0.1%. The virtual exclusion of tritium from the  $^{14}\text{C}$  window incidentally enables distilled tap water, rather than specially collected 'dead' water (i.e. no  $^3\text{H}$ ), to be used in the carbide hydrolysis reaction.

The above account summarises initial optimisation of the counting system. During the course of this research, however, and on several occasions the system had to be re-optimised after faults in the counter had developed. In each case, exactly the same procedure as above was followed, although slightly different working parameters were generated each time.

## 2.5 MEASUREMENT OF $^{14}\text{C}$ SPECIFIC ACTIVITY

Having optimised the counting system, the activity of a typical sample's carbon could now be measured. In brief, after the observed count rate has been corrected for background, dilution and quench effects, the sample's  $^{14}\text{C}$  specific activity can be calculated by comparing the corrected count rate with that of a standard. The various aspects of this process will now be discussed.

### 2.5.1 Preparation of the Standard Geometry Vial

The intercomparison of standard and sample activities required to produce a radiocarbon measurement is simplified if one is working with identical quantities of carbon. In this work a 10 ml counting geometry is adopted as the norm.

The sample container itself plays an important part in the liquid scintillation system. It must:

- (a) be resistant to attack by solvents and additives,
  - (b) be transparent at the wavelength of common scintillators,
  - (c) have reproducible geometry
- and
- (d) contain little or no residual activity.

Commercially available flame-sealable boro-silicate ampoules with a low  $^{40}\text{K}$  content and a 20 ml volume are used.

The necks of the ampoules are carefully narrowed to allow injection of sample while retaining uniformity of vial geometry. Approximately 7 g (or 8 ml) of the sample, or standard, are added to the ampoule via a Pasteur pipette. The amount of benzene added is accurately weighed. If there is not enough sample to make up the 8 ml, then the difference is made up using commercially available scintillation grade benzene which contains no radiocarbon. Finally, 2 ml of the scintillation cocktail are added to the vial which is then placed in a bed of dry ice and its neck covered with a rubber septum. Once the mixture is frozen, the rubber septum is removed and the neck sealed quickly in a hot oxy-gas flame. The ampoule is further sealed, as an additional precaution against pinhole leaks, by covering the neck with a layer of epoxy resin before being removed from the dry ice. Use of such vials, although requiring more attention to sealing, is useful as the samples can then be stored and counted repeatedly without risk of evaporative loss of volatile benzene; this is particularly important for standards and backgrounds. Not only does this process eliminate weight loss but it also avoids the problem of gradual absorption of quenching agents, such as oxygen (Williams, 1977).

### 2.5.2 Backgrounds

In measuring a sample's  $^{14}\text{C}$  specific activity it is necessary to subtract the contribution to its count rate from the background count rate, i.e. counts produced by sources other than the sample's  $^{14}\text{C}$ . Contributions to the background count rate can come from within the sample itself or from other external sources.

Contributions to the background count rate from outwith the

sample medium may come from radioactive impurities in the glass vials, radioactivity in the laboratory and counter materials, cosmic rays or from random electronic noise within the counter. These effects can be counteracted to some extent by the selection of low radioactive glass vials (Section 2.5.1), extensive shielding, refrigeration and the use of coincidence circuitry (Section 2.4.3) but they cannot be totally excluded. The extent of these effects can be monitored by preparing a background sample using the same scintillation grade benzene (SGB) as is used to dilute normal samples. Each background sample thus consists of 8 ml of SGB and 2 ml of scintillation cocktail. In theory, the sample contains no  $^{14}\text{C}$  so that each count detected must be caused by one of the aforementioned phenomena. Each time a new batch of the scintillation cocktail was prepared, a background sample containing the SGB and the new scintillation cocktail was prepared and counted to check that none of the scintillation cocktail batches had been contaminated, hence causing an increase in the background count rate. Six different background samples of this type were prepared during this research (KG/1, KG/2, KH/1, KH/2, KI/1 and KJ/1) and the average count rate for each one is shown in Table 2.1. For all samples the count rate is almost the same, around 7.3 cpm, which can be taken as the average background count rate of the  $^{14}\text{C}$  detection system. In addition, the results suggest that there is no significant contamination caused by any of the different scintillation cocktail batches.

Contributions to the background from within the sample medium could arise from impurities picked up during sample conversion to benzene. This effect can be monitored by preparing a sample of benzene from 'dead' calcium carbide. The calcium carbide is hydrolysed to acetylene in a manner analogous to the hydrolysis of the lithium carbide and the acetylene converted to benzene as before. This means that any addition to the background count rate arising from the sample preparation system will be detected. Four such samples were synthesised in the course of the research to keep a regular check on the preparation system (KGC/1, KGC/2, KGC/3 and KGC/4). By interspersing the background samples between other samples, any contamination caused by memory effects would also be detected. The average count rates for the samples are given in Table 2.2. These background count rates are much the

Table 2.1: Average background count rates for scintillation grade benzene samples

Sample	Average count rate (cpm $\pm 1\sigma$ )
KG/1	7.34 $\pm$ 0.06
KG/2	7.23 $\pm$ 0.06
KH/1	7.18 $\pm$ 0.06
KH/2	7.32 $\pm$ 0.06
KI/1	7.39 $\pm$ 0.06
KJ/1	7.35 $\pm$ 0.06

Table 2.2: Average background count rates for calcium carbide samples

Sample	Average count rate (cpm $\pm$ 1 $\sigma$ )
KGC/1	7.40 $\pm$ 0.06
KGC/2	7.23 $\pm$ 0.06
KGC/3	7.12 $\pm$ 0.06
KGC/4	7.34 $\pm$ 0.06

same as those obtained from the SGB-derived background samples. Therefore, it can be concluded that the sample preparation system does not give rise to any cross-contamination of the sample.

Both these sample types were used to monitor constantly the background contributions to the samples' count rates.

### 2.5.3 Modern Standard Activity

As a result of numerous possible sources of systematic error and of the experimental difficulty inherent in its precise assay, absolute radiocarbon measurement is exceedingly demanding and thus it is more practicable to calculate sample activities relative to that of a universally accepted standard. The primary standard for  $^{14}\text{C}$  dating is 1890 wood (Broecker and Olson, 1959), which is assumed to have the 'natural value' of the  $^{14}\text{C}$  specific activity, i.e.  $226 \text{ Bq kg}^{-1}$  (carbon). It is common practice, however, to use a secondary standard which can be directly related to the primary standard and, in this work, oxalic acid, which is distributed by the National Bureau of Standards, is used.

Like all samples, the oxalic acid is converted to benzene before being counted. This can either be done by direct combustion or by wet oxidation with acidified saturated potassium permanganate solution. The latter method is the one used in this research.

Saturated acidified potassium permanganate (30 ml of concentrated sulphuric acid per litre of solution) is slowly added to a 5 litre reaction flask containing 50 g of oxalic acid. The oxidation system is shown in Figure 2.16. Prior to addition of the oxidising solution, the reaction flask and  $\text{CO}_2$  collection system are pumped on low vacuum to better than  $10^{-1}$  torr. The reaction mixture is stirred continuously and product  $\text{CO}_2$  collected in the traps on the main  $\text{CO}_2$  collection system. One practical difference here in the collection of  $\text{CO}_2$  from that in the normal combustion method is that there is not continuous pumping as this would increase the quantity of water which distils into the collection system, resulting in blockage of the water traps. Addition of permanganate solution is continued until the reaction mixture becomes brown through precipitation of manganese

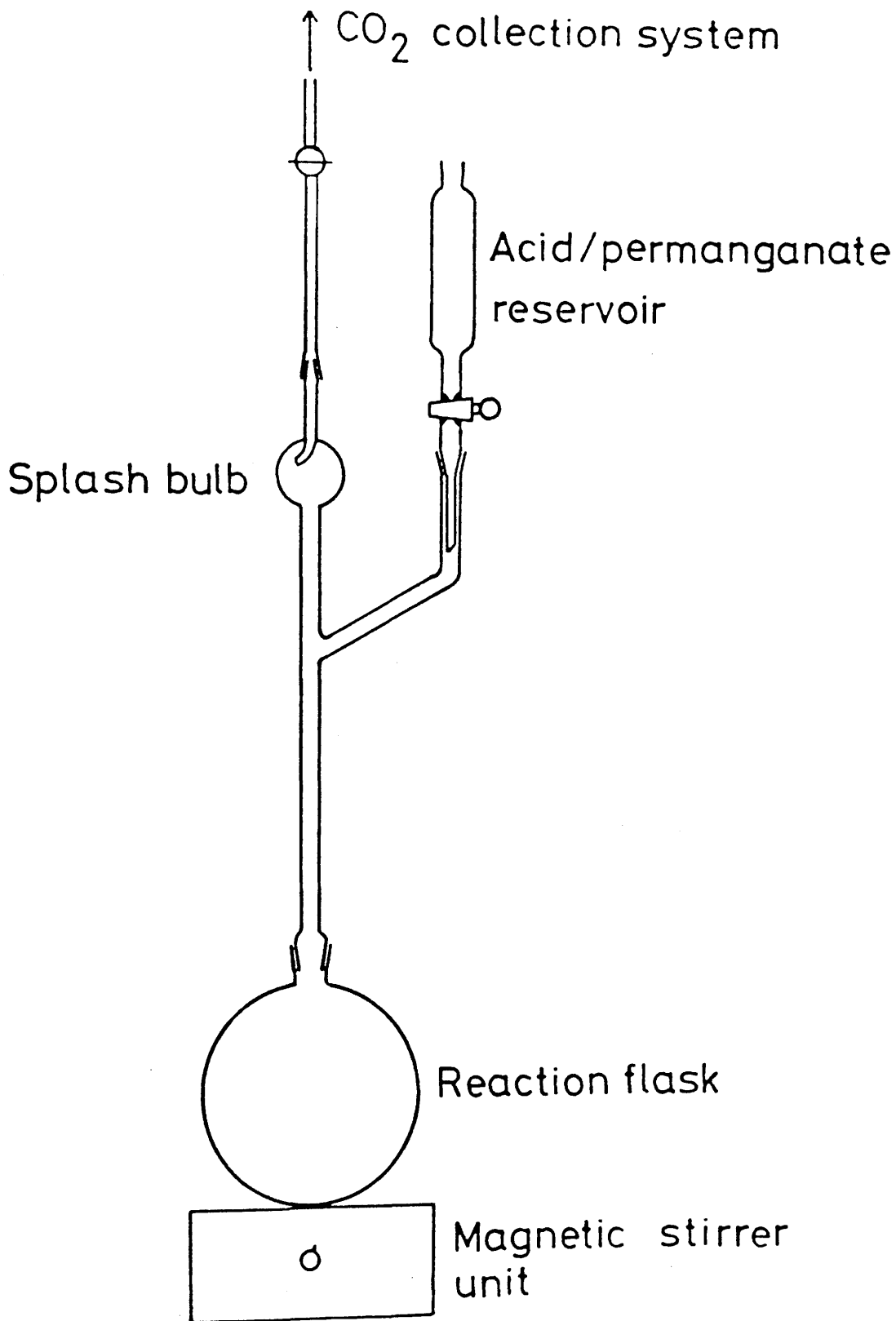


FIGURE 2-16: Wet oxidation system.

dioxide. The solution is then left for a considerable length of time to ensure completion and hence to reduce the risk of excessive fractionation (Valastro et al., 1977). The conversion of the CO<sub>2</sub> to benzene follows the procedure previously described.

Six standards were prepared at regular intervals throughout this work. The first three came from the original oxalic acid batch (SRM 4990) prepared by the National Bureau of Standards in Washington and it is assumed that 95% of the <sup>14</sup>C activity in 1950 of this oxalic acid, normalised to  $\delta^{13}\text{C} = -19\%$  with respect to PDB, is equivalent to the <sup>14</sup>C specific activity of the primary standard (Flint and Deevey, 1961; Olsson, 1970). The final three were prepared from a new batch of oxalic acid (SRM 4990-C), again provided by the National Bureau of Standards and it is assumed that 74.59% of its <sup>14</sup>C activity in 1950, normalised to  $\delta^{13}\text{C} = -25\%$  with respect to PDB, is equivalent to the <sup>14</sup>C specific activity of the primary standard (Stuiver, 1983).

#### 2.5.4 Quenching

Before various sample and standard count rates can be compared they must first be corrected for quenching. Any process which interferes with the conversion of beta-particle energy to scintillations or with light transmission reduces the amount of light which reaches the photomultiplier and is known as quenching. As a result, fewer scintillations are detected and the pulses generated are of lower voltage. Consequently, efficiency is reduced and the whole pulse voltage spectrum is shifted to a lower voltage range. Unless quenching is known to be constant or the efficiency can be estimated, the comparison of count rates derived from different samples is meaningless. Various causes of quenching are given below.

- (a) Interference with the transmission of energy from beta-particle to scintillator.

This can be caused either by chemical quenching or by dilution quenching. In chemical quenching, caused by aliphatic compounds such as ketones, amines and halogenated compounds, some of the

energy may be absorbed by an interfering substance and dissipated as heat. In dilution quenching some of the energy may be prevented from reaching excitable molecules by the dilution effect of compounds such as ethers, alcohols and esters. The overall effect is the same in either case but is far more marked for chemical quenching.

(b) Interference with the transmission of light from scintillator to photomultiplier.

The most common cause of this phenomenon is the presence of coloured impurities in the solution to be counted as these absorb part of the light emitted by the scintillator. This process is known as colour quenching but is inapplicable to the liquid scintillation counting of benzene.

(c) Self quenching.

A radioactive material may itself cause quenching if it has the properties of a quencher but, once again, this does not apply to benzene.

In liquid scintillation counting of benzene, therefore, chemical quenching, arising from impurities in the counting medium, is the main factor causing distortion of the pulse voltage spectrum, with a resulting drop in counting efficiency. The amount and type of impurities vary from sample to sample and therefore, to derive meaningful results, it is essential to determine the degree of quenching and hence the overall  $^{14}\text{C}$  detection efficiency for each sample.

This correction process could be performed using an internal standard, i.e. by adding a known aliquot of activity after counting each sample (Hayes, 1956) or via an external standard, i.e. by determining the additional counts produced by a spectrum of Compton electrons generated by an external gamma source (Horrocks, 1964). The method used in this work, however, is the channels' ratio method (Davidson and Feigelson, 1957), the theory of which is now explained.

In the counting system used here, the discriminators are set so that channel 2 monitors events from 150-450 mV and channel 3 from 450-1000 mV. In this way, any shift in the spectrum caused by quenching will be detected by a change in the channel 2 to channel 3 count rate ratio. Thus, by calibrating the system, it should be possible to determine the  $^{14}\text{C}$  detection efficiency for any sample from its channel 2 to channel 3 count rate ratio.

The calibration of the system is carried out as follows. A known amount of spiked  $^{14}\text{C}$ -toluene is added to 25 separate counting ampoules (around 70 Bq per ampoule). Next, varying amounts of a known quenching agent, acetone, are added to each vial (volumes ranges from 0-400  $\mu\text{l}$ ), the principle being that the more acetone is added the more quenching results. The total volume in each vial is then made up to 8 ml using scintillation grade benzene before adding 2 ml of scintillation cocktail. Each ampoule is then counted for 1000 minutes and, after correcting for background counts, the channel 2 to channel 3 count rate ratio and the  $^{14}\text{C}$  detection efficiency are determined. The results are shown graphically in Figure 2.17.

The calibration line adopted for the quench-efficiency correlation is a polynomial function derived using the MINITAB statistical package available on the ICL computing network. It is found that the best-fitting function is:

$$E = 71.7 - 2.59R + 0.0727R^2,$$

where E is the efficiency and R is the channel 2 to channel 3 count rate ratio.

In practice, however, the channels' ratios for most samples lie in a very narrow range of around 1-6. Therefore, a new best-fit line is determined using only those vials with channels' ratios less than 10. This data set is shown in Figure 2.18 and the equation of the best-fit line is:

$$E = 76.3 - 4.37R + 0.208R^2.$$

Using this calibrated function it is possible to relate a sample's channels' ratio to its absolute counting efficiency, hence allowing intercomparison of sample and standard count rates.

Every time the counter is re-optimised a new quench-

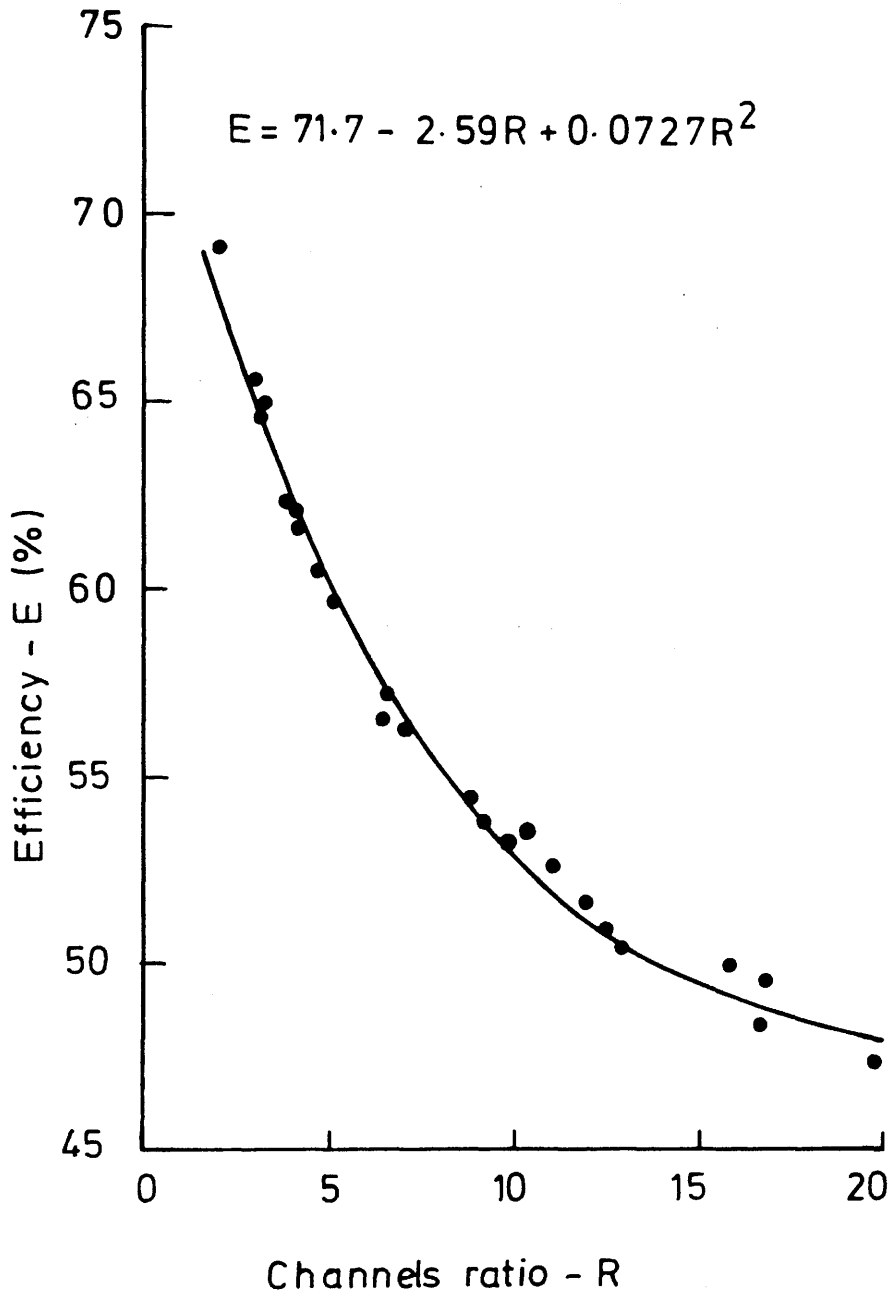


FIGURE 2-17: Quench - efficiency calibration curve.

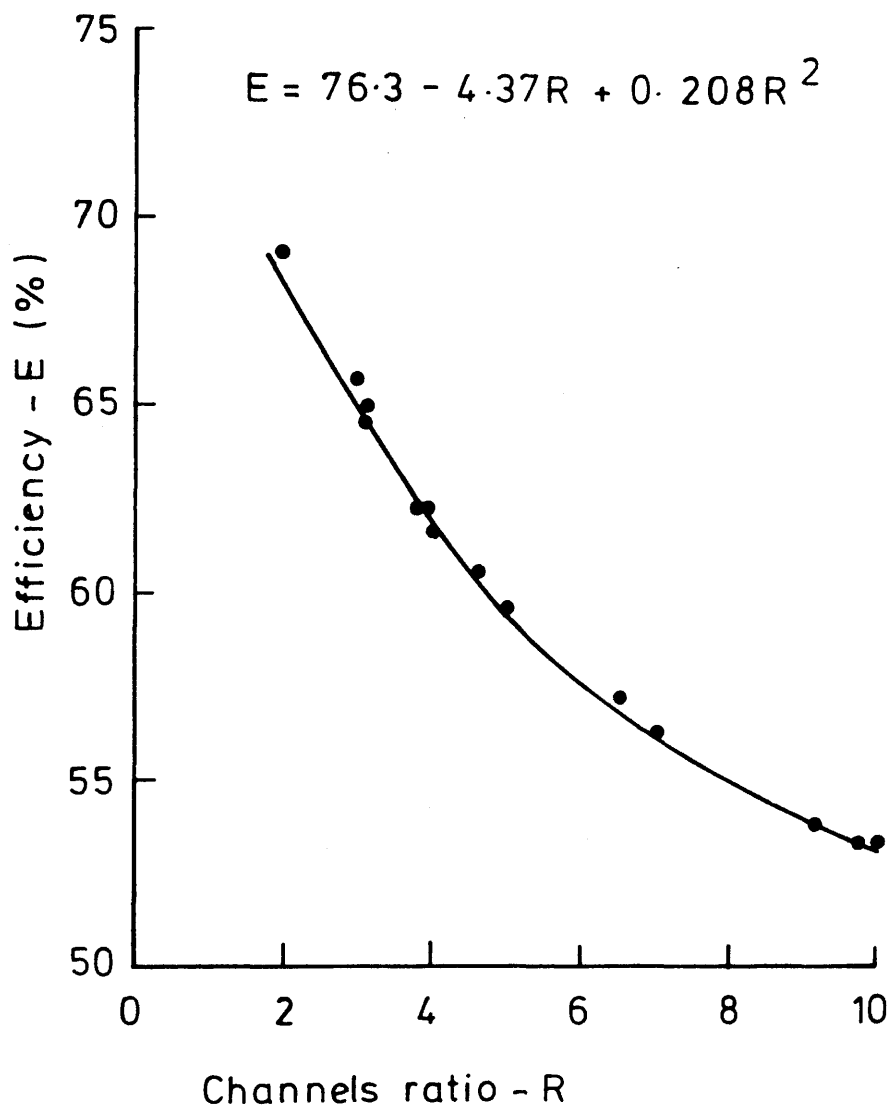


FIGURE 2-18: Quench - efficiency calibration curve (for small R).

efficiency calibration curve has to be determined. Because of the careful vial-sealing procedures previously described, the same 25 ampoules can be used, although a slightly different function is obtained each time.

#### 2.5.5 Batch Composition

One advantage of liquid scintillation counting over gas counting is the automatic sample-changing and cycling facility, as was discussed by Polach (1969). This feature allows backgrounds and standards to be monitored 'simultaneously' along with the samples. A standard batch submitted for counting normally consists of three backgrounds, three modern standards, six samples and two high-activity spikes. The two spikes are included to monitor the stability of the counting system. Each ampoule is then counted sequentially for 100 minutes, except for the spiked samples which are only counted for the length of time necessary to achieve a total of 50 000 counts (usually around 8 minutes). This cycle is repeated until each sample has been counted for a total of 20 times, i.e. for 2000 minutes.

#### 2.5.6 Calculation of Results

Count rates, representing the rates of  $^{14}\text{C}$  decay, are the basic data obtained from a liquid scintillation counter. These data can be converted into a measure of each sample's  $^{14}\text{C}$  specific activity by the method of Stuiver and Polach (1977).

It is widely recognised that all laboratories should report their results directly related to the primary standard of 1890 wood,  $A_{\text{ABS}}$ . Thus the  $^{14}\text{C}$  specific activity of a sample,  $A^*_x$ , is calculated from equation (2.2):

$$A^*_x = \frac{A_{\text{XN}}}{A_{\text{ABS}}} \times 226 \text{ Bq kg}^{-1} \text{ (carbon)}, \quad (2.2)$$

where  $A_{\text{ABS}}$  is assumed to be the  $^{14}\text{C}$  activity of 1890 wood.

$A_{\text{XN}}$  is the sample's measured  $^{14}\text{C}$  activity at its time of death (or isolation from the carbon cycle), after

correcting for isotopic fractionation. By convention the isotopic fractionation in all samples, irrespective of environment, is taken into account by normalising to -25 per mil with respect to PDB, the postulated mean value of terrestrial wood.  $A_{XN}$  is related to the sample's count rate by equation (2.3):

$$A_{XN} = A_X e^{\lambda(m-d)} \left[ 1 - \frac{2(25 + \delta^{13}C)}{1000} \right], \quad (2.3)$$

$$\text{where } \lambda = \frac{\ln 2}{t_{1/2}({}^{14}C)}. \quad (2.4)$$

$\delta^{13}C$  is measured in per mil with respect to PDB (Section 2.3),  $m$  is the year of measurement and  $d$  is the year of death of the sample. The value  $A_X$  is the sample's count rate corrected for background, quenching and dilution effects.

The measured  ${}^{14}C$  activity of the primary standard,  $A_{ABS}$ , is derived from the  ${}^{14}C$  activity of an oxalic acid secondary standard (Section 2.5.3). Two separate batches of oxalic acid were used in this work and they are related to the primary standard as follows:

$$\text{(batch SRM 4990)} \quad A_{ABS} = 0.95 A_{S1} e^{\lambda(m-1950)} \left[ 1 - \frac{2(19+\delta^{13}C)}{1000} \right], \quad (2.5)$$

$$\text{(batch SRM 4990-C)} \quad A_{ABS} = 0.7459 A_{S2} e^{\lambda(m-1950)} \left[ 1 - \frac{2(25+\delta^{13}C)}{1000} \right], \quad (2.6)$$

where again  $\delta^{13}C$  is measured in per mil relative to PDB and  $m$  is the year in which the modern count rate was measured. The values  $A_{S1}$  and  $A_{S2}$  are the count rates for the two oxalic acid batches corrected for background, quenching and dilution effects.

Many different ways of reporting  ${}^{14}C$  data exist. A sample's  ${}^{14}C$  specific activity can be quoted in  $Bq \text{ kg}^{-1}$  (carbon),  $pCi \text{ g}^{-1}$  (carbon) or even as a per mil or percentage deviation from the primary standard, designated  $\Delta^{14}C$  and PM (standing for 'percentage modern') respectively. For example, if a sample has a  ${}^{14}C$  specific activity of  $226 \text{ Bq kg}^{-1}$  (carbon), which is equivalent to  $6.11 \text{ pCi g}^{-1}$  (carbon), then

it has  $\Delta^{14}\text{C}$  and PM values of 1000‰ and 100% respectively. Occasionally, a  $^{14}\text{C}$  specific activity measurement is also quoted as a  $\delta^{14}\text{C}$  value. This gives the per mil deviation from the primary standard of a sample before it has been corrected for isotopic fractionation. In this work, however, all samples are corrected for isotopic fractionation and their  $^{14}\text{C}$  specific activities reported in  $\text{Bq kg}^{-1}$  (carbon).

All calculated sample activities are quoted to  $\pm 1\sigma$  error. There are many different sources which contribute to the overall uncertainty on each measurement and those encountered in this work are listed below.

- (a) The error on the count rate of each ampoule measured, be it a background, standard or sample. Based simply on the Poisson nature of the observed counts the estimated error on the count rate is given by equation (2.7):

$$\text{error} = \frac{(\text{total counts observed})^{\frac{1}{2}}}{\text{counting time}} \quad (2.7)$$

- (b) The error on the measured weight of sample added to an ampoule which is estimated to be  $\pm 0.0005$  g.
- (c) The error on the measured  $\delta^{13}\text{C}$  value which is estimated to be  $\pm 0.05\%$ .

- (d) The error on the efficiency estimate. The error on an efficiency predicted from the polynomial  $E = \alpha + \beta R + \gamma R^2$  for a certain R is given by equation (2.8):

$$\text{error} = S (a+(d+b)R+(g+e+c)R^2+(h+f)R^3+iR^4)^{\frac{1}{2}}, \quad (2.8)$$

where S is the standard deviation about the line and the coefficients a, b, c, d, e, f, g, h and i are derived from standard least squares analysis for linear models (Weisberg, 1980).

In compliance with the commonly accepted practice, it has been assumed that there is no error on the value of the  $^{14}\text{C}$  half-life of 5730 years. This assumption leads to a small but not significant underestimate of the overall error on the results. The overall error on the sample's  $^{14}\text{C}$  specific activity is

derived by appropriate combination of the above errors. The most important contribution to the error derives from the uncertainty in the individual count rates. This error source is an unavoidable result of the random nature of radioactive decay. It can be reduced, however, by employing long counting times and that is why each sample used in this work was counted for a total of 2000 minutes.

A FORTRAN 77 computer programme has been written to calculate sample  $^{14}\text{C}$  specific activities and their associated errors and this is presented in Appendix 1.

## 2.6 RELIABILITY OF THE $^{14}\text{C}$ SPECIFIC ACTIVITY MEASUREMENTS

One final requirement is to verify the  $^{14}\text{C}$  specific activity measurements produced by the laboratory. The integrity of the results depends on both the long-term stability of the counting system and the purity of the sample preparation procedures. Both these parameters are checked 'internally' by the laboratory itself which can detect any changes in the above conditions. Such internal standardisation, however, will not define any systematic errors in the system. These can only be discovered by 'external' standardisation involving intercalibration between laboratories. Both the internal and external monitoring of experimental procedures will now be discussed.

### 2.6.1 Stability of the Counting Environment

Once a liquid scintillation counter has been optimised for low-level assay of  $^{14}\text{C}$ , it is hoped that the counter will retain these original working conditions. In practice, however, faults do appear and thus it becomes necessary to monitor the counter closely by constant checking of the count rates of background, standard and spiked samples. Any significant changes in these values usually indicates the presence of a fault in the counting system. The liquid scintillation counter, for this work, was initially optimised in October 1984 and thereafter had to be re-optimised in April 1985 and again in December 1985.

Table 2.3 shows how the count rate of the background sample KG/1 (prepared from scintillation grade benzene) varied

Table 2.3: Variation of background count rate with time (for sample KG/1)

Date	Count rate (cpm $\pm 1\sigma$ )
26.10.84	7.48 $\pm$ 0.06
22.11.84	7.67 $\pm$ 0.06
24.12.84	7.46 $\pm$ 0.06
15.4.85	7.50 $\pm$ 0.06
19.6.85	7.61 $\pm$ 0.06
12.7.85	7.46 $\pm$ 0.06
22.10.85	7.51 $\pm$ 0.06
19.12.85	7.42 $\pm$ 0.06
28.2.86	7.26 $\pm$ 0.06

throughout the course of this study. In general, the count rate remained steady, although slight variations did occur during the periods between re-optimisation. The average count rate from October '84 - March '85 was 7.54 cpm, from March '85 - November '85 7.52 cpm and from November '85 - April '86 7.34 cpm. These fluctuations in background count rate are caused by corresponding changes in efficiency of the counter but for samples and standards are compensated for by the quench-efficiency calibration procedure.

Although the exact working conditions of the counter may be varied at each optimisation, the actual results obtained for samples and standards are not perturbed. This claim can be validated by examining, for example, the variation of the corrected count rate (corrected for background, quenching, isotopic fractionation and decay since 1950) for the modern standard, NBS/1. This count rate, shown in Table 2.4, has remained steady despite the changes in the counter's working conditions. This stability can be further demonstrated by checking the corrected count rate (corrected for background and quenching) of a spiked sample which was incorporated in every single sample batch. Table 2.5 shows how little the corrected count rate varied with time.

Data such as these suggest convincingly that the long-term stability of the Glasgow counting system is excellent.

#### 2.6.2 Replicate Analysis

The next aspect to be monitored is the reproducibility of the laboratory procedure, this depending not only on the stability of the counting system but also on the reproducibility inherent in the preparation process. As it has already been shown that the counting system is stable, the variability here primarily depends on that of sample preparation. This latter variability can be tested by counting several aliquots of benzene prepared from the same bulk sample.

All of the modern standards prepared in this work, when normalised to the value of the primary standard, should give the same  $^{14}\text{C}$  specific activity. Six different moderns were

Table 2.4: Variation of modern corrected count rate with time (for sample NBS/1)

Date	Corrected count rate (cpm $\pm 1\sigma$ )
5.11.84	186.8 $\pm$ 0.2
22.11.84	187.1 $\pm$ 0.2
10.12.84	187.0 $\pm$ 0.2
14.1.85	188.9 $\pm$ 0.2
27.2.85	190.9 $\pm$ 0.2
15.4.85	186.3 $\pm$ 0.2
3.5.85	186.9 $\pm$ 0.2
19.6.85	188.8 $\pm$ 0.2
12.7.85	188.4 $\pm$ 0.2
16.9.85	189.0 $\pm$ 0.2
3.10.85	189.1 $\pm$ 0.2
23.12.85	186.9 $\pm$ 0.2
15.1.86	185.5 $\pm$ 0.2
28.2.86	186.8 $\pm$ 0.2

Table 2.5: Variation of spike corrected count rate with time (for sample SP/2)

Date	Corrected count rate (cpm $\pm$ 1 $\sigma$ )
5.11.84	9368 $\pm$ 6
22.11.84	9330 $\pm$ 6
10.12.84	9339 $\pm$ 6
14.1.85	9386 $\pm$ 6
27.2.85	9414 $\pm$ 6
18.3.85	9423 $\pm$ 6
15.4.85	9330 $\pm$ 6
3.5.85	9292 $\pm$ 6
6.6.85	9311 $\pm$ 6
19.6.85	9339 $\pm$ 6
6.7.85	9330 $\pm$ 6
12.7.85	9301 $\pm$ 6
11.9.85	9300 $\pm$ 6
16.9.85	9348 $\pm$ 6
3.10.85	9367 $\pm$ 6
22.10.85	9358 $\pm$ 6
8.11.85	9376 $\pm$ 6
19.12.85	9320 $\pm$ 6
23.12.85	9311 $\pm$ 6
15.1.86	9245 $\pm$ 6
7.2.86	9311 $\pm$ 6
28.2.86	9301 $\pm$ 6

prepared (NBS/1, NBS/2, NBS/3, NBS/4, NBS/5 and NBS/6) and the average value for each is shown in Table 2.6. The results indicate that, as far as the NBS oxalic acid is concerned, the laboratory procedure is reproducible. However, regular assay of oxalic acid does not necessarily give a true indication of laboratory reproducibility since it requires non-routine chemical procedures (i.e. no pretreatment, wet oxidation) in converting it to benzene.

A short replicate analysis study was therefore undertaken using a bulk sample of grass, which is by far the most commonly sampled material in this work. Five different assays of this same grass sample were carried out and the results are shown in Table 2.7. The variability in the results appears to be adequately covered by the quoted errors. This suggests that the errors quoted are truly representative of the uncertainty in the sample's measured activity.

It has been noted in the past (Scott, 1983) that the errors quoted by radiocarbon laboratories tend to underestimate the true variability in results. Therefore, in order to check the initial findings of the replicate analysis, a further study was undertaken on another three grass samples. In this case, three separate aliquots of each sample were measured and the results are shown in Tables 2.8 (a), (b) and (c). Once again, for each bulk sample, all the aliquots are in good agreement with one another, with the spread of values being consistent with the quoted errors.

In conclusion, the replicate analysis suggests that the reproducibility of the laboratory procedure is very good and that the errors quoted on the final results are indeed realistic estimates of the true errors.

### 2.6.3 Intercalibration Study

It has been shown that this laboratory can reproduce consistent values for any given sample but the question still remains as to whether or not the value obtained is correct. The accuracy of the laboratory results can be checked via an intercalibration study, i.e. the  $^{14}\text{C}$  specific activity of a given sample is determined independently by at least two

Table 2.6: Average modern  $^{14}\text{C}$  specific activities for the NBS oxalic acid standards

Sample	Average $^{14}\text{C}$ specific activity ( $\text{Bq kg}^{-1}(\text{carbon}) \pm 1\sigma$ )
NBS/1	442 $\pm$ 3
NBS/2	443 $\pm$ 3
NBS/3	444 $\pm$ 3
NBS/4	446 $\pm$ 3
NBS/5	443 $\pm$ 3
NBS/6	445 $\pm$ 3

Table 2.7: Replicate analysis (1)

Sample	$^{14}\text{C}$ specific activity ( $\text{Bq kg}^{-1}$ (carbon) $\pm 1\sigma$ )
REP1/A	947 $\pm$ 4
REP1/B	940 $\pm$ 5
REP1/C	956 $\pm$ 5
REP1/D	954 $\pm$ 4
REP1/E	953 $\pm$ 4

Table 2.8: Replicate analysis (2)

(a)

Sample	$^{14}\text{C}$ specific activity ( $\text{Bq kg}^{-1}$ (carbon) $\pm 1\sigma$ )
REP2/A	276 $\pm$ 2
REP2/B	281 $\pm$ 2
REP2/C	281 $\pm$ 2

(b)

Sample	$^{14}\text{C}$ specific activity ( $\text{Bq kg}^{-1}$ (carbon) $\pm 1\sigma$ )
REP3/A	278 $\pm$ 2
REP3/B	277 $\pm$ 4
REP3/C	274 $\pm$ 2

(c)

Sample	$^{14}\text{C}$ specific activity ( $\text{Bq kg}^{-1}$ (carbon) $\pm 1\sigma$ )
REP4/A	277 $\pm$ 2
REP4/B	283 $\pm$ 2
REP4/C	283 $\pm$ 2

laboratories. Eight intercalibration samples were measured in this way; four were archaeological (INT/1 - INT/4) and four were modern materials (INT/5 - INT/8). The results from this laboratory were checked against those obtained either by the radiocarbon dating laboratory at the Scottish Universities Research and Reactor Centre (SURRC) or by a totally independent laboratory at Glasgow University (GU). The intercalibration data, shown in Table 2.9, indicate that the  $^{14}\text{C}$  measurements obtained at this laboratory are in good agreement with those from the other established radiocarbon dating facilities.

Table 2.9: Intercalibration samples

Sample	$^{14}\text{C}$ specific activity ( $\text{Bq kg}^{-1}$ (carbon) $\pm 1\sigma$ )	
	This lab.	Other lab.
INT/1 (charcoal)	194 $\pm$ 2	190 $\pm$ 1 (GU)
INT/2 (charcoal)	159 $\pm$ 1	163 $\pm$ 1 (GU)
INT/3 (charcoal)	206 $\pm$ 2	203 $\pm$ 1 (GU)
INT/4 (charcoal)	174 $\pm$ 1	169 $\pm$ 1 (GU)
INT/5 (cellulose)	279 $\pm$ 2	273 $\pm$ 1 (SURRC)
INT/6 (cellulose)	270 $\pm$ 2	271 $\pm$ 2 (SURRC)
INT/7 (grass)	950 $\pm$ 4	940 $\pm$ 3 (GU)
INT/8 (grass)	281 $\pm$ 2	275 $\pm$ 2 (GU)

(GU): Glasgow University

(SURRC): Scottish Universities Research and Reactor Centre

LOCAL EFFECTS OF  $^{14}\text{C}$  DISCHARGES FROM THE NUCLEAR FUEL CYCLE3.1 INTRODUCTION

$^{14}\text{C}$  discharges from nuclear installations have, in the past, been studied by both direct measurements of  $^{14}\text{C}$  levels in the effluents themselves (e.g. Schwibach et al., 1978; Kunz, 1985) and analyses of  $^{14}\text{C}$  levels in the local environment (e.g. Levin et al., 1980; Segl et al., 1983). However, these studies have largely concentrated on determining the  $^{14}\text{C}$  release rates from specific nuclear installations rather than assessing the effects of these  $^{14}\text{C}$  discharges on the local populations. Exposures to these near-site populations will obviously exceed those to the global average general public and thus the primary aim of the research described in this section is to quantify this local effect. A second major and related objective is to assess, develop and use mathematical models of the dispersion and distribution of discharged  $^{14}\text{C}$  in the vicinity of nuclear installations.

$^{14}\text{C}$  releases from the nuclear fuel cycle can occur in many different ways. The  $^{14}\text{C}$  can be released at various stages of the fuel cycle, it can be discharged to different phases of the environment and the chemical form of the  $^{14}\text{C}$  waste can vary depending on both its production mechanism and its discharge pathway. Within the time constraints of this research, it was not possible to investigate thoroughly all the different  $^{14}\text{C}$  discharge modes. Therefore a limited number were selected for study on the basis of both their radiological significance and practical convenience.

At present, almost all of the  $^{14}\text{C}$  discharged to the environment is released to the atmosphere, with only relatively small quantities being discharged into aquatic environments (Bush, 1984; IAEA, 1985). This bias is reflected in the study which was concentrated on atmospheric  $^{14}\text{C}$  discharges.

The chemical form in which the  $^{14}\text{C}$  is discharged to the environment tends to be either  $\text{CO}_2$ ,  $\text{CO}$  or simple gaseous hydrocarbons (mainly  $\text{CH}_4$  and  $\text{C}_2\text{H}_6$ ) (United Nations, 1981, 1982) and, in fact, the radiation dose to the exposed population is strongly dependent on the chemical form, as will now be explained. The  $^{14}\text{C}$  radiation dose to an individual is made up of three separate components:

- (a) external irradiation from  $^{14}\text{C}$  in the atmosphere,
- (b) internal irradiation from  $^{14}\text{C}$  inhaled from the atmosphere

and

- (c) internal irradiation from  $^{14}\text{C}$  ingested in foodstuffs.

The radiation dose received by an exposed population via external irradiation is of the same order of magnitude for all chemical forms of  $^{14}\text{C}$  discharge. The same can be said for internal irradiation via inhalation of atmospheric  $^{14}\text{C}$  but not for internal irradiation by ingestion of dietary  $^{14}\text{C}$ . If the chemical form of the  $^{14}\text{C}$  is other than  $\text{CO}_2$  then it is not immediately available for photosynthetic uptake by plants, will not be incorporated into foodstuffs and thus will not lead to irradiation by this route. These carbon compounds, e.g.  $\text{CO}$ ,  $\text{CH}_4$ , etc., will eventually be oxidised to  $\text{CO}_2$  in the atmosphere but this process takes several years (Kelly et al., 1975; Killough and Till, 1978), by which time they are homogeneously mixed within the atmosphere, i.e. there will be no local enhancement. On the other hand, if the  $^{14}\text{C}$  is discharged as  $\text{CO}_2$ , it will be incorporated into local foodstuffs and hence will lead to enhanced radiation exposure by ingestion. Indeed, as shown in Section 1.4.2, the radiation dose to man from  $^{14}\text{C}$  is in essence entirely derived from the ingestion of  $^{14}\text{C}$  in foodstuffs, the other two exposure pathways being insignificant by comparison. This means, therefore, that, for the atmospheric discharge of a given activity of  $^{14}\text{C}$  from a nuclear installation, the radiation dose to the local population will be far greater if it is released as  $\text{CO}_2$  than as any other chemical species. In this study, therefore, only the  $^{14}\text{C}$  discharged to the atmosphere as  $\text{CO}_2$  was considered as it is undoubtedly the most radiologically significant chemical form. In any case, the vast majority of  $^{14}\text{C}$  discharged from the nuclear fuel cycle is released as  $\text{CO}_2$ , with only the off-gas

streams at PWRs and HWRs being important sources of the reduced chemical forms (United Nations, 1972, 1977, 1981, 1982).

Most of the  $^{14}\text{C}$  discharges occur either at the nuclear reactor in which the  $^{14}\text{C}$  is produced or at a nuclear fuel reprocessing plant or, to a lesser extent, at low-level radioactive waste burial sites. Rather than attempt to cover all the various types of nuclear facilities currently in use, it was decided to concentrate on just a small number. Altogether four different nuclear facilities were investigated. They were:

- (a) the BNF plc nuclear fuel reprocessing plant at Sellafield, in Cumbria,
- (b) the SSEB thermal nuclear power station complex at Hunterston, in Ayrshire,
- (c) the UKAEA prototype fast breeder reactor at Dounreay, in Caithness

and

- (d) the SURRC research reactor at East Kilbride, near Glasgow.
- The locations of these facilities are shown in Figure 3.1 along with that of Lochcarron, which was the collection site of the control samples (i.e. those reflecting the average global atmospheric  $^{14}\text{C}$  levels) used in this work.

To summarise, this section of the study was focussed on the effects of atmospheric  $^{14}\text{CO}_2$  discharges on populations in the vicinity of the selected nuclear facilities listed above.

### 3.2 OBSERVED $^{14}\text{C}$ LEVELS AROUND SELECTED NUCLEAR FACILITIES

In this section the details of the sampling programmes carried out around the selected sites will be outlined and the results of the measurements reported. In addition, basic information on the workings of the various nuclear establishments and the reasons for their inclusion in the study will be provided. Initially, however, the results of the monitoring programme to determine the average global atmospheric  $^{14}\text{C}$  levels during the period of this research will be examined.

#### 3.2.1 Background $^{14}\text{C}$ Levels

In order to determine the local radiological impact of  $^{14}\text{CO}_2$  discharges, it is clearly necessary to quantify the enhancement of local atmospheric  $^{14}\text{C}$  levels over the average



FIGURE 3-1: Location of study areas.

global atmospheric  $^{14}\text{C}$  baseline. The average global atmospheric  $^{14}\text{C}$  level (or background  $^{14}\text{C}$  level) is not the same as the natural atmospheric  $^{14}\text{C}$  level and is constantly changing because of the various anthropogenic perturbations described in Section 1.2.5. Thus, before the local enrichment of the atmospheric  $^{14}\text{C}$  levels and, hence, the radiation dose to the exposed population can be calculated for a particular year, the background  $^{14}\text{C}$  level must first be determined for that same year.

For the years spanned by this research a measure of the average global atmospheric  $^{14}\text{C}$  levels was obtained by assay of grass samples grown in the north of Scotland. Grass was chosen as the sampling material because it had previously been shown, by correlation of bomb  $^{14}\text{C}$  levels in air and grass, that the latter material is an excellent indicator of atmospheric  $^{14}\text{C}$  specific activity levels (Tauber, 1967). The samples were collected at Lochcarron (see Figure 3.1), a remote site free from any local enhancement of  $^{14}\text{C}$  and  $^{12}\text{C}$  levels. The value for the average global atmospheric  $^{14}\text{C}$  level in a particular year is taken as the average of three separate assays of grass grown in that year. The results for 1982, 1984 and 1985, shown in Table 3.1, are  $279 \pm 2$ ,  $276 \pm 2$  and  $281 \pm 2$  Bq kg $^{-1}$  (carbon) respectively, i.e. the values are identical within error. Unfortunately, no samples were collected in 1983; hence, the value for the average global atmospheric  $^{14}\text{C}$  level in this year is assumed to be 279 Bq kg $^{-1}$  (carbon), the mean of the three year values. This data set is fully consistent with the levels predicted by the documented very gradual decrease in atmospheric  $^{14}\text{C}$  levels over the last decade (Figure 1.6). However, in the short time span measured here, this very slow rate of decrease is not evident outside the analytical error.

Values for the average global atmospheric  $^{14}\text{C}$  levels prior to 1982 are readily available in the scientific literature and have been reviewed earlier in this work (Section 1.2).

### 3.2.2 Sellafield (BNF plc)

Sellafield (which up to 1981 was known as Windscale) is the site of the only thermal nuclear fuel reprocessing plant in operation within the United Kingdom today. It is situated on the

Table 3.1: Background <sup>14</sup>C levels

Year	<sup>14</sup> C specific activity (Bq kg <sup>-1</sup> (carbon) ±1σ)	
	Measured	Average
1982	276 ± 2 281 ± 2 281 ± 2	279 ± 2
1984	278 ± 2 277 ± 4 274 ± 2	276 ± 2
1985	277 ± 2 283 ± 2 283 ± 2	281 ± 2

Cumbrian coast (see Figure 3.1) and is operated by British Nuclear Fuels plc (BNF plc). When operations began at Sellafield in 1952, its primary function was to meet the needs of the country's military programme. The plutonium and uranium in spent nuclear fuel were separated from the bulk material and recovered for use in nuclear weapons. Sellafield was then developed to serve the requirements of the UK civil nuclear energy programme, being used primarily to recover unused fissile material from spent nuclear fuel, thereby helping to extend the nuclear industry's future fuel resources. During the last 25 years, Sellafield has been used mainly to reprocess spent natural uranium fuel from Britain's MAGNOX reactors, although smaller quantities of spent uranium oxide fuel have also been reprocessed. In fact, the plant is presently being upgraded to handle far larger inventories of this oxide fuel. The quantities of fuel reprocessed at Sellafield have steadily increased during recent decades, in parallel with expansion of the nuclear industry's electrical power generating capacity.

Most of the  $^{14}\text{C}$  brought into Sellafield in spent nuclear fuel and various other waste arisings is released to the atmosphere. In 1985, for example, the estimated amount of  $^{14}\text{C}$  discharged to the atmosphere was 6.6 TBq, whereas the amount discharged to the sea was 1.3 TBq and only trivial amounts of  $^{14}\text{C}$  were disposed of as solid waste (BNF, 1986). The majority of the atmospheric  $^{14}\text{CO}_2$  discharges from Sellafield occur when the spent nuclear fuel undergoes primary chemical dissolution. This process involves dissolving the fuel in an acid solution which, in addition, converts any  $^{14}\text{C}$  present in the fuel to  $^{14}\text{CO}_2$ . Up to the present time, no attempt has been made to trap this  $^{14}\text{CO}_2$ , which is discharged directly to atmosphere via one of two particular stacks in the Sellafield plant.

According to the best estimates available at the present time, Sellafield has by far the largest  $^{14}\text{CO}_2$  discharge rate of all nuclear facilities currently in operation within Britain. It was considered appropriate, therefore, to concentrate the bulk of this study's experimental effort on this site as it would probably give rise to the largest  $^{14}\text{C}$  local radiation dose in UK.

In recent years, enhanced levels of  $^{14}\text{C}$  in the vicinity of Sellafield have been detected by several workers. The phenomenon was first observed by Otlet et al. (1983) in hawthorn berries grown in 1981 and then by Baxter and McKay (1983) who measured increased  $^{14}\text{C}$  levels in samples of grass which had grown near Sellafield in 1982. Due account of these studies was therefore taken here in the original design of the sampling programme to monitor the movement of  $^{14}\text{CO}_2$  discharged from Sellafield through the local environment.

The area covered by this study is shown in Figure 3.2, in which regions of high population have been shaded. Other details in the diagram will be explained in due course but one point which is of immediate interest is the existence of the Calder Hall nuclear power station on a site adjacent to the Sellafield works. It is possible, indeed it is likely, that the enhanced  $^{14}\text{C}$  levels which have been observed around Sellafield are not entirely due to the nuclear fuel reprocessing plant and are contributed to, to some extent, by releases from the Calder Hall nuclear power station. Before progressing further, then, it is worthwhile to comment on the magnitude of this latter effect.

The Calder Hall nuclear power station houses four MAGNOX reactors and thus discharges of  $^{14}\text{CO}_2$  from the site are expected. This facility was constructed in the 1950s on the opposite bank of the River Calder from the Sellafield works. The station was the first electrical generating nuclear power plant constructed in Britain and its capacity is subsequently rather low. The gross electrical power generating capacity of the facility is 200 MW(e). Although it was suggested earlier that it is inaccurate to apply the values of Table 1.9 to specific reactors, the data can be used here to provide a guide to the magnitude of the releases from these reactors. Assuming a load factor of 70% for the Calder Hall reactors, the average annual discharges of  $^{14}\text{CO}_2$  from the entire facility, as determined from Table 1.9, is 0.13 TBq. Although this figure is very approximate, it shows conclusively that, compared to the atmospheric  $^{14}\text{CO}_2$  discharges from Sellafield (e.g. 6.6 TBq in 1985), the discharges from Calder Hall are insignificant. Indeed, the errors on the estimate of the atmospheric  $^{14}\text{CO}_2$  discharges from Sellafield (although not quantified by BNF plc)

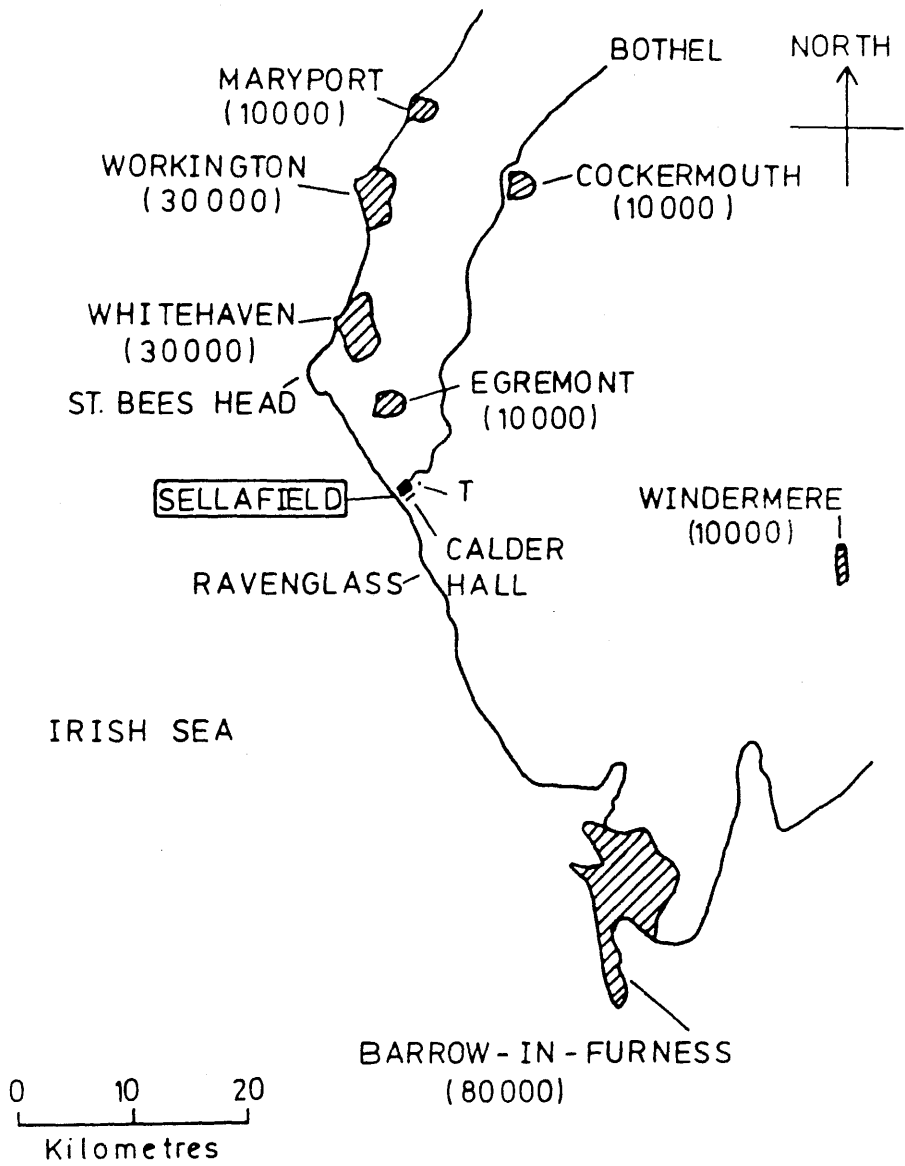


FIGURE 3.2: Sellafield study area.

are probably far greater than the discharges from Calder Hall. Basically, it is reasonable therefore to assume that any enhancement of  $^{14}\text{C}$  levels in the vicinity of Sellafield is due entirely to  $^{14}\text{CO}_2$  discharges from the nuclear fuel reprocessing plant.

The experimental programme around Sellafield was designed to monitor both the spatial and the temporal distributions of  $^{14}\text{CO}_2$  in the most relevant geographical areas and the details of both studies will now be discussed in turn.

### 3.2.2.1 The Spatial Distribution of the $^{14}\text{CO}_2$ Discharges

Each year during the period of this research (1983-1985), samples of vegetation were collected at various locations near Sellafield in an attempt to assess the spatial distribution of the  $^{14}\text{CO}_2$ . The extent of the monitoring programme was, once again, limited by the number of samples which could feasibly be analysed. Therefore, it was decided to investigate one particular transect in great detail rather than many transects in lesser detail. A transect extending in a north-easterly direction from Sellafield was the one chosen for particular study. This transect was selected because it had been shown, in a previous study by Otlet et al. (1983), to reflect the highest  $^{14}\text{C}$  levels in the Sellafield environment (although this may vary from year to year depending on both the wind rose and the  $^{14}\text{CO}_2$  release rate).

The next decision was to choose a suitable sample type. Many different plant materials have been used to monitor emissions, in the form of  $^{14}\text{CO}_2$ , from nuclear establishments. For example, Obelic et al. (1986) measured the  $^{14}\text{C}$  levels in wheat, corn, carrot, beet, lettuce, onion, parsley and hay, Povinec et al. (1986) used tree leaves, grass, nuts, grains, sugar and tree rings, Otlet et al. (1983) used hawthorn berries and Baxter and McKay (1983) used grass. An appropriate material for this study had to satisfy two main criteria:

- (a) it must be readily available throughout the area of study and
- (b) it must be truly representative of a single year's growth and of the atmospheric  $^{14}\text{C}$  level during the growing season.

Without doubt, the most readily available environmental sample type in Cumbria is grass. The wide availability of grass is such that it is possible to collect a sample within ten metres of any theoretically selected sampling location. In addition, as previously mentioned, grass has been shown to be an excellent indicator of atmospheric  $^{14}\text{C}$  specific activity levels (Tauber, 1967). Thus grass was chosen here as the primary sampling material.

The number and location of the samples collected were varied from one year to another in an attempt to improve the resolution of the dispersion profile obtained from the results. Changes were made on the basis of the data obtained in the previous year and thus the quality of the data improved from year to year. In 1983 only 14 samples were collected over a transect length of 12 km. In 1984 a 30 km transect was covered by a total of 27 samples and in 1985 35 samples were collected over 38 km. The path mapped out by the sampling points is represented in Figure 3.2 by a solid line, extending from Sellafield to Bothel.

Not all of the samples collected lay on this north-easterly transect since, at the time of their collection, the exact  $^{14}\text{C}$  discharge locations within Sellafield had not been reliably identified. Thus the origin of the transect could not be defined precisely. In addition, some environmental samples other than grass (potatoes, hawthorn berries, blackberries and seaweed) were collected to check that the uptake of  $^{14}\text{CO}_2$  in these plants was similar to that in the grass. Finally, for convenience, most of the samples were collected near to the roadside. Occasionally, however, parallel samples were also taken at a distance of a few tens of metres from the roadside to check for any polluting effect caused by road traffic.

Once collected, the samples were converted to benzene and their  $^{14}\text{C}$  specific activities measured by liquid scintillation counting as described in Chapter 2. The results for the years 1983, 1984 and 1985 are shown in Tables 3.2, 3.3 and 3.4 respectively. Unless a comment is made, the sample can be assumed to be of grass collected beside the road along the north-easterly transect. The distances are taken from the sample to a point

Table 3.2:  $^{14}\text{C}$  levels around Sellafield (1983)

Distance (km)	$^{14}\text{C}$ specific activity (Bq kg $^{-1}$ (carbon) $\pm 1\sigma$ )	Comment
0.4	946 $\pm$ 3	
0.7	388 $\pm$ 2	south-west
1.0	647 $\pm$ 2	potato
1.1	342 $\pm$ 1	south-west
1.5	543 $\pm$ 2	seaweed/west
1.9	622 $\pm$ 2	
3.7	494 $\pm$ 2	
4.9	483 $\pm$ 3	
6.4	409 $\pm$ 2	
7.9	361 $\pm$ 2	
9.0	453 $\pm$ 2	seaweed/south-east
9.5	355 $\pm$ 2	
11.2	334 $\pm$ 2	
12.0	370 $\pm$ 2	seaweed/north-west

Table 3.3:  $^{14}\text{C}$  levels around Sellafield (1984)

Distance (km)	$^{14}\text{C}$ specific activity ( $\text{Bq kg}^{-1}$ (carbon) $\pm 1\sigma$ )	Comment
0.35	700 $\pm$ 3	
0.35	729 $\pm$ 4	hawthorn Berry
0.4	1006 $\pm$ 5	
0.4	632 $\pm$ 3	west
0.5	514 $\pm$ 2	west
0.5	555 $\pm$ 3	north-west
0.7	444 $\pm$ 2	south-west
0.9	919 $\pm$ 4	
1.0	904 $\pm$ 4	potato
1.5	660 $\pm$ 3	
1.9	537 $\pm$ 2	
2.2	597 $\pm$ 3	
2.8	482 $\pm$ 2	
3.7	418 $\pm$ 2	
4.9	393 $\pm$ 2	
4.9	392 $\pm$ 2	away from road
4.9	371 $\pm$ 2	hawthorn berry
6.4	378 $\pm$ 2	
7.9	346 $\pm$ 2	
9.5	332 $\pm$ 2	
11.2	323 $\pm$ 2	
13.6	319 $\pm$ 2	
16.0	318 $\pm$ 2	
19.2	311 $\pm$ 2	
21.5	300 $\pm$ 2	
25.0	295 $\pm$ 2	
29.0	296 $\pm$ 2	

Table 3.4:  $^{14}\text{C}$  levels around Sellafield (1985)

Distance (km)	$^{14}\text{C}$ specific activity ( $\text{Bq kg}^{-1}$ (carbon) $\pm 1\sigma$ )	Comment
0.21	1076 $\pm$ 7	
0.23	928 $\pm$ 6	
0.25	889 $\pm$ 6	
0.29	897 $\pm$ 6	
0.34	1129 $\pm$ 7	
0.38	837 $\pm$ 5	
0.44	856 $\pm$ 5	
0.53	798 $\pm$ 5	
0.64	647 $\pm$ 4	
0.74	649 $\pm$ 4	
0.90	766 $\pm$ 5	
1.1	602 $\pm$ 4	
1.1	666 $\pm$ 4	hawthorn berry
1.3	545 $\pm$ 3	
1.5	496 $\pm$ 3	
1.7	473 $\pm$ 3	
1.9	492 $\pm$ 3	
2.2	490 $\pm$ 3	
2.8	429 $\pm$ 3	
3.7	372 $\pm$ 2	
4.9	326 $\pm$ 2	
4.9	296 $\pm$ 2	blackberry
6.5	324 $\pm$ 2	
7.9	312 $\pm$ 2	
9.6	307 $\pm$ 2	
11.2	300 $\pm$ 2	
13.6	294 $\pm$ 2	
13.6	320 $\pm$ 2	hawthorn Berry
16.0	293 $\pm$ 2	
19.2	293 $\pm$ 2	
21.5	307 $\pm$ 2	
25.0	289 $\pm$ 2	
29.0	299 $\pm$ 2	
32.8	311 $\pm$ 2	
37.5	297 $\pm$ 2	

midway between the two  $^{14}\text{CO}_2$  discharge locations within Sellafield and have been estimated from Ordnance Survey maps. The error associated with the distances is estimated at less than  $\pm 0.1$  km. The results for the years 1983, 1984 and 1985 will now be presented in a little more detail along with a few general comments.

### 1983

In this, the inaugural year of the study, the sampling programme was based on the results of the work carried out by Baxter and McKay (1983) who had detected enhanced  $^{14}\text{C}$  levels in grass samples within 5 km of Sellafield. In this year, then, 14 samples were collected at distances ranging from 0.4 to 12 km from Sellafield and the observed variation of the  $^{14}\text{C}$  levels with distance from the discharge site is shown graphically in Figure 3.3. In this graph the background level of 279 Bq  $\text{kg}^{-1}$  (carbon) has already been subtracted from the  $^{14}\text{C}$  specific activity values. This is therefore actually a plot of the excess  $^{14}\text{C}$  levels versus distance from Sellafield. As a visual aid, a line has been plotted through the main data set, i.e. grass samples collected beside the road along the north-easterly transect. Samples outwith the main data set have been clearly identified and the exact nature of the sample explained.

Dealing initially with the main data set, the most striking point is that a maximum excess value of 667 Bq  $\text{kg}^{-1}$  (carbon), that is around 300% above the natural level, is observed 0.4 km from the site (the closest sampling point to the discharge location). Then, as the distance from Sellafield increases, the  $^{14}\text{C}$  levels decrease, although enhanced levels are still observable at 11.2 km (the farthest sampling point from the discharge location).

Of the remaining samples, two were of grass which had grown to the south-west of the discharge location, three were seaweed samples and one was a potato sample. The grass samples were not deliberately chosen away from the north-easterly transect but were collected before the  $^{14}\text{CO}_2$  discharge locations had been identified. They do, however, help to demonstrate the fact that the distribution of  $^{14}\text{CO}_2$  around Sellafield will vary with

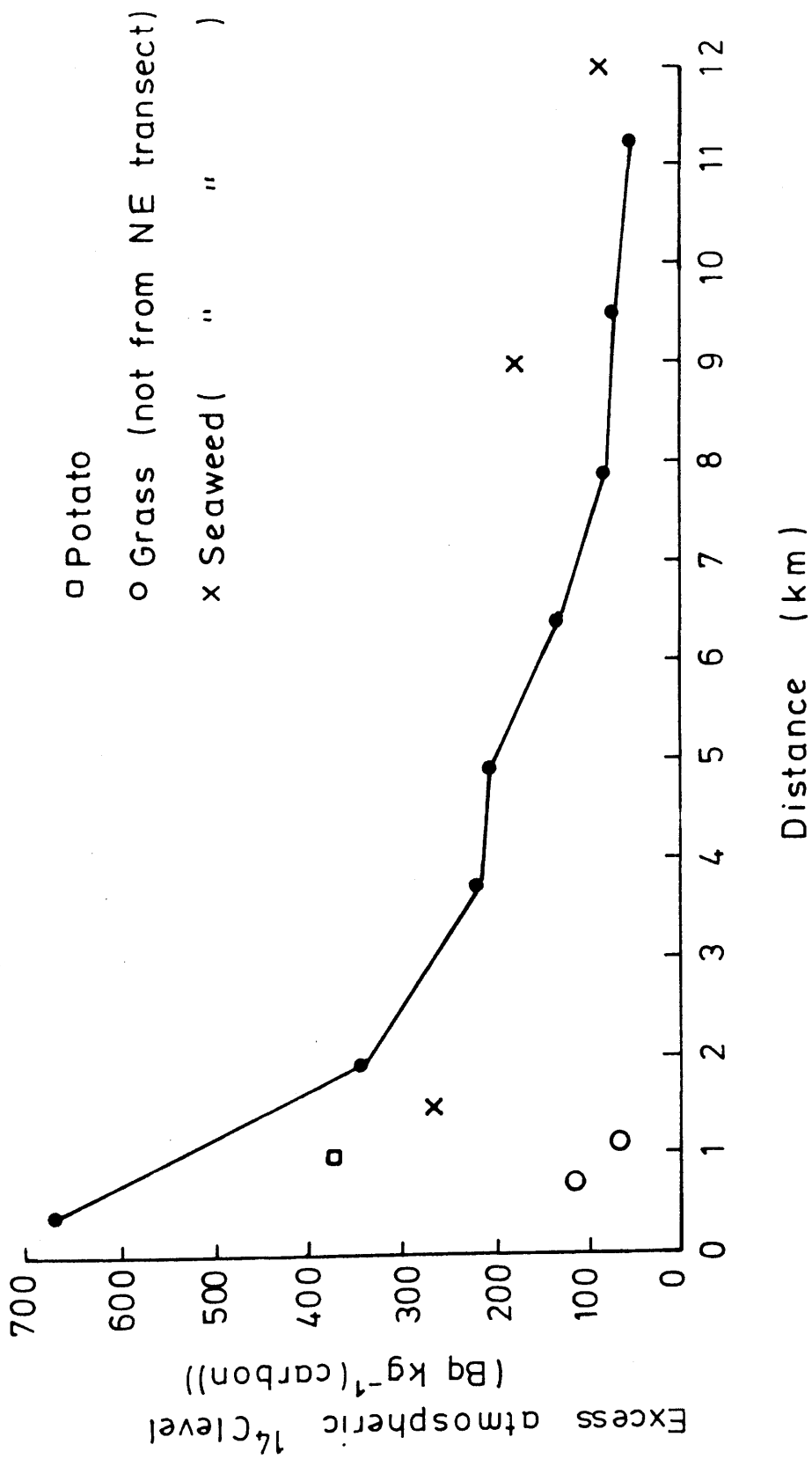


FIGURE 3.3: Excess atmospheric <sup>14</sup>C levels around Sellafield, 1983.

direction. The potato sample, collected 1 km along the north-easterly transect, appears to have a  $^{14}\text{C}$  level similar to that which would be expected from the grass data. This fact lends some credence to the assumption later that the  $^{14}\text{C}$  specific activity in grass is the same as that in foodstuffs ingested by man. The  $^{14}\text{C}$  levels measured in the seaweed samples, on the other hand, are not in particularly good agreement with the grass samples. These seaweed samples were obviously not collected along the north-easterly transect but along the Cumbrian coast (at the Sellafield pipeline from which liquid waste is discharged into the Irish Sea, at Ravenglass and at St Bees Head) and so the absolute  $^{14}\text{C}$  levels would not be expected to agree. However, although based on a small number of observations, the rate of dilution of the  $^{14}\text{C}$  as derived from the seaweed samples would appear to be slower than that derived from the grass samples. Since all the seaweed samples were collected in different directions, this observation may simply be a manifestation of the prevailing weather conditions or it may be caused by some other physical process. For example, the assimilation of carbon by seaweed is considerably more complex than for the terrestrial plant materials discussed, as its carbon is derived from both the atmosphere and the sea. The  $^{14}\text{C}$  specific activities in the seaweeds could, therefore, be dominated by the liquid  $^{14}\text{C}$  discharges from Sellafield and the dispersion of  $^{14}\text{C}$  released to the sea is very different from the atmospheric dispersion of  $^{14}\text{CO}_2$ . Analysis of the marine system lies outwith the scope of the present study. It can be suggested, however, that the limited data available could imply that dilution of  $^{14}\text{C}$  released to the Irish Sea may not be as rapid as that of  $^{14}\text{CO}_2$  discharged to atmosphere. Further research on  $^{14}\text{C}$  in marine environment could well be worthwhile.

#### 1984

Three main points, extracted from the previous year's data, could be usefully incorporated into this year's programme. Firstly, samples should be collected at distances of less than 0.4 km from the discharge location to ascertain where the maximum level occurs. Secondly, a greater number of samples should be collected over the first few kilometres over which the  $^{14}\text{C}$

levels appear to decrease rapidly. Finally, the transect should be extended beyond 11 km from Sellafield in an attempt to determine the full geographical extent of the local enhancement of  $^{14}\text{C}$  levels. Based on these considerations, a total of 27 samples were collected at distances up to 29 km from Sellafield. Figure 3.4 shows a plot of the observed variation in  $^{14}\text{C}$  specific activities (after subtraction of the background level of  $276 \text{ Bq kg}^{-1}$  (carbon)) with distance for this year and, as before, a line has been drawn through the main data set merely as a visual aid.

A maximum excess value of  $730 \text{ Bq kg}^{-1}$  (carbon) was observed 0.4 km from the plant, with enhanced levels decreasing with increasing distance from Sellafield but being still detectable to the farthest sampling point (29 km). Samples collected closer than 0.4 km from Sellafield also show a decrease in  $^{14}\text{C}$  levels relative to the observed maximum activity, suggesting that the latter is, in fact, very close to the 'true' highest level. However, because of the perimeter fence surrounding the Sellafield works, it was not possible to sample significantly closer than 0.35 km from the discharge location.

Outwith the main data set, four other grass samples which had grown away from the north-easterly transect were also collected in this year. These four samples, once again, help to illustrate how the distribution of the  $^{14}\text{CO}_2$  from Sellafield varies directionally. Of the remaining samples, one was of potatoes, two were of hawthorn berries and two were grass samples collected away from the roadside. All of these latter samples were collected along the north-easterly transect. The two grass samples collected away from the roadside showed  $^{14}\text{C}$  specific activities similar to those for samples collected beside the road at corresponding distances from the discharge location. This observation suggests that, for this study at least, there is no significant pollution effect (e.g. fossil  $\text{CO}_2$  from petrol combustion) caused by road traffic in this region. Finally, the  $^{14}\text{C}$  levels in all forms of vegetation (potatoes and hawthorn berries) appear to be in good agreement with those in grass collected from similar locations.

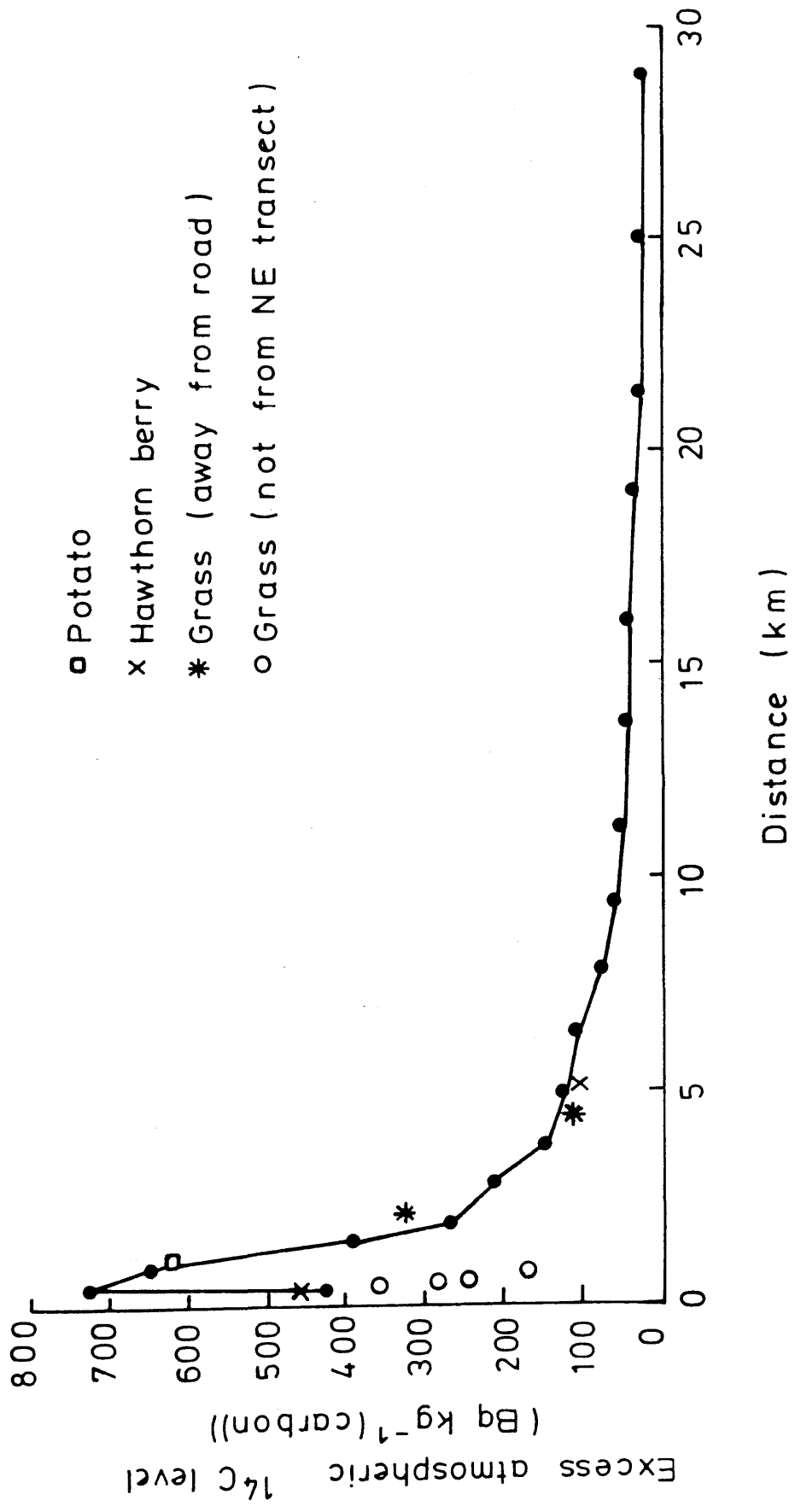


FIGURE 3-4: Excess atmospheric <sup>14</sup>C levels around Sellafield, 1984.

In this, the concluding year of the study, a major effort was made to produce a very high resolution picture of the atmospheric  $^{14}\text{C}$  dispersion profile. To this end, a total of 35 samples, all lying along the north-easterly transect, were collected. On the basis of the previous year's results, the length of the transect investigated was extended to nearly 40 km from Sellafield. Also, a very large number of samples (17) were collected over the first 2 km, of which a greater number than before were collected less than 0.4 km from the discharge location. To do this it was necessary to obtain permission from BNF plc to collect grass samples inside the Sellafield site itself. Three such samples were collected between the perimeter fence and the discharge sites, the number being restricted by the limited availability of vegetation in this area. Figure 3.5 shows the observed variation of the excess  $^{14}\text{C}$  levels with distance in 1985 and, as before, a line has been drawn through the main data set. This diagram becomes somewhat cluttered at the shorter distances because of the large number of samples collected in this area. Therefore, for clarity, the observed  $^{14}\text{C}$  levels over the first 2 km have been plotted separately in Figure 3.6.

A maximum  $^{14}\text{C}$  specific activity of  $848 \text{ Bq kg}^{-1}$  (carbon) above the background level is observed 0.34 km from the plant. A basic trend of decreasing  $^{14}\text{C}$  levels with increasing distance from this point is observed on either side of this peak. This distribution is in agreement with the observations from the previous years' data but the more detailed picture in 1985 also brings to light the existence of fairly large fluctuations around this general trend. Another noteworthy point is that, although the  $^{14}\text{C}$  levels decrease markedly between 1 and 15 km, they remain fairly constant between 15 and 40 km, showing that the rate of dilution decreases rapidly with distance.

Only three samples outwith the main data set were included in this study, all of which were collected beside the road along the north-easterly transect. The two hawthorn berry samples and the blackberry sample all had  $^{14}\text{C}$  levels similar to those in grass collected from the same locations. However, the two hawthorn berry samples do have  $^{14}\text{C}$  levels slightly higher

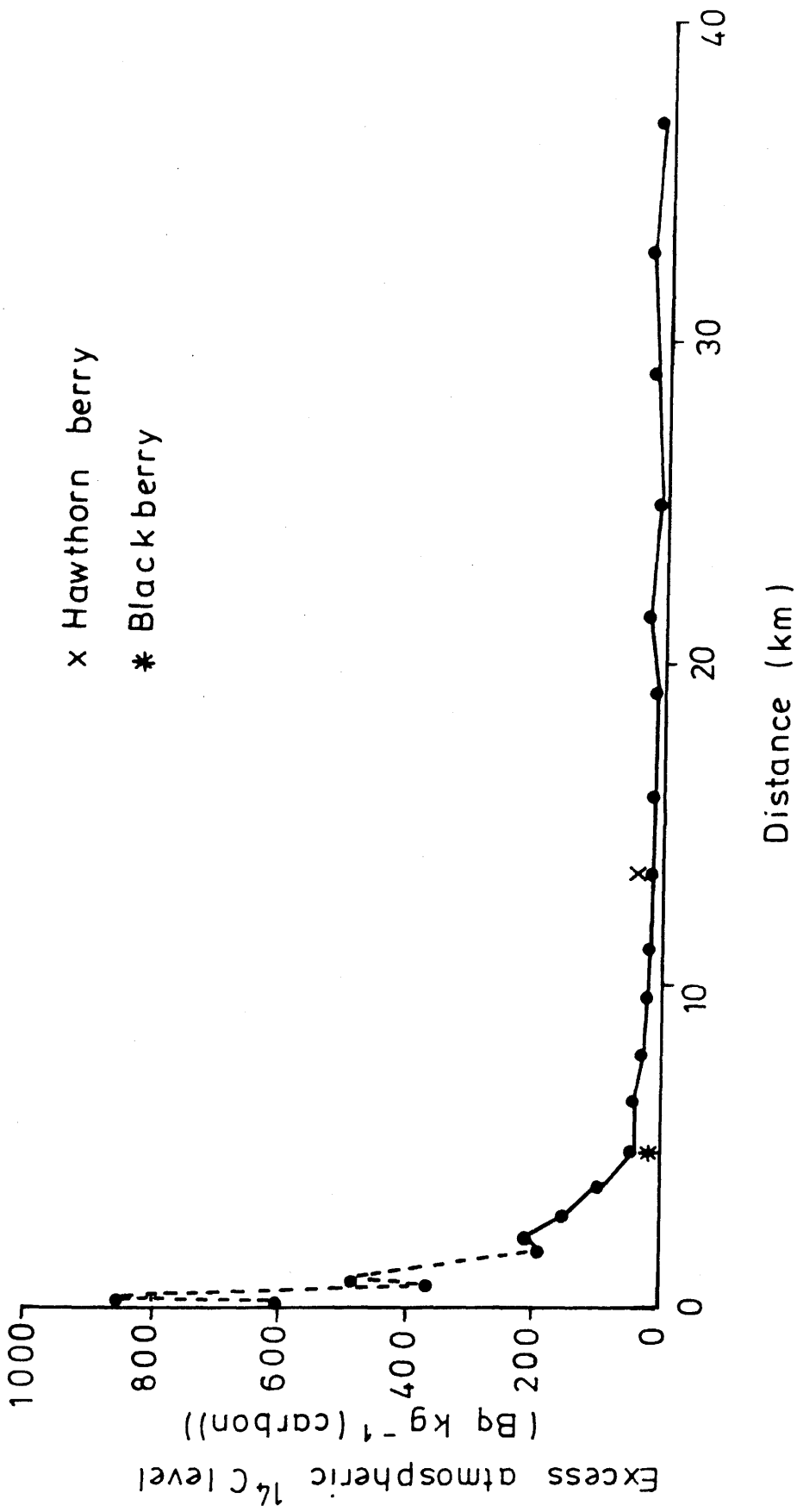


FIGURE 3.5: Excess atmospheric <sup>14</sup>C levels around Sellafield, 1985.

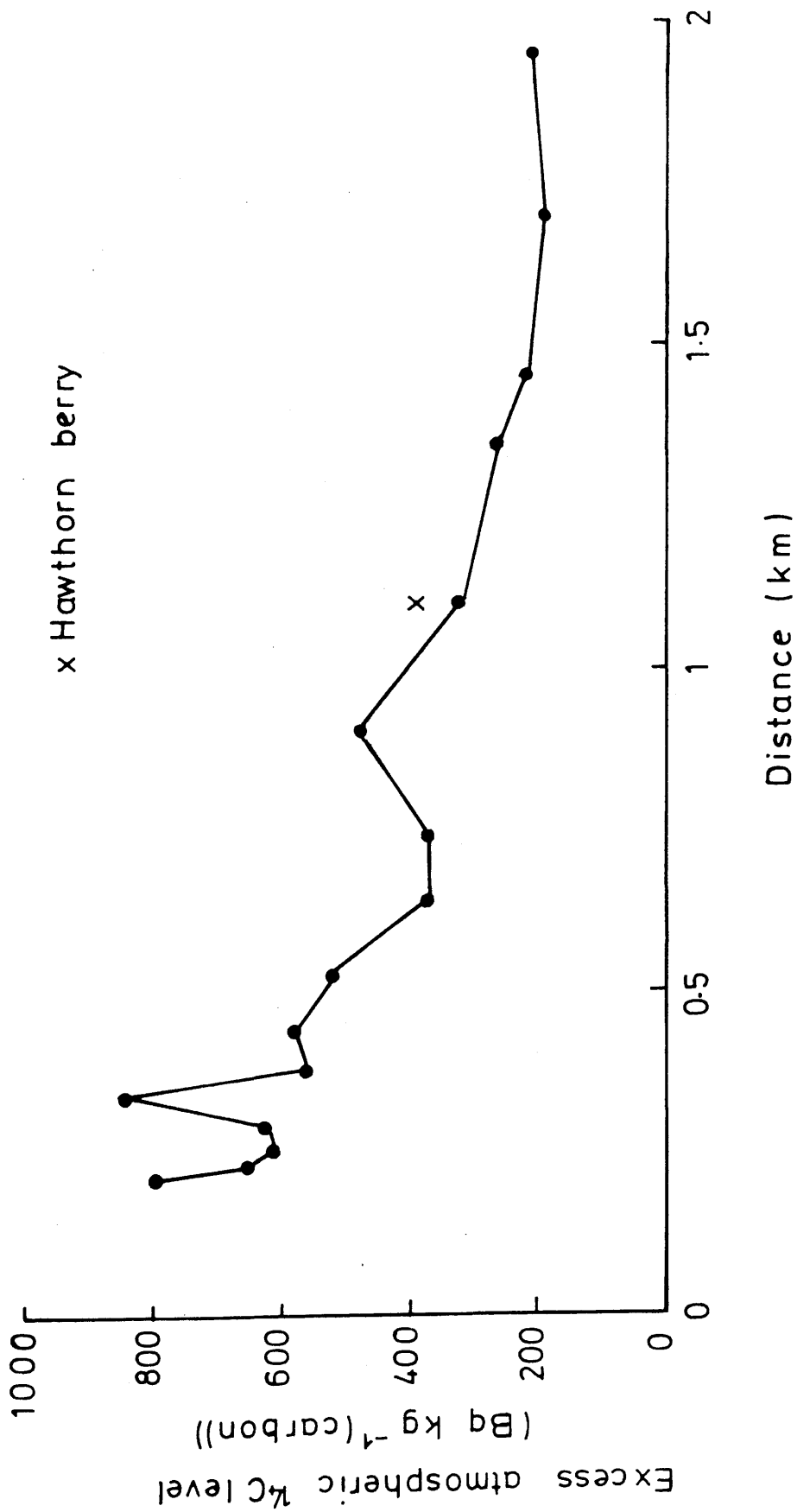


FIGURE 3.6: Excess atmospheric  $^{14}\text{C}$  levels within 2 km of Sellafield, 1985.

than the corresponding grass samples, whereas the blackberry sample has a slightly lower  $^{14}\text{C}$  level. These small differences in the  $^{14}\text{C}$  specific activities between various plant types may be caused by differences in their growing season. For example, the slightly increased  $^{14}\text{C}$  level in both hawthorn berry samples over the corresponding grass samples could reflect a high growth rate at a time of higher than average  $^{14}\text{CO}_2$  discharges from Sellafield or at a time of frequent winds blowing along the north-easterly transect. However, although differences in  $^{14}\text{C}$  levels between various plant types are distinctly possible, in general, the magnitude of this effect is small and most plants do have very similar  $^{14}\text{C}$  levels.

Finally, it is worth noting that the  $^{14}\text{C}$  specific activities detected around Sellafield are significantly higher than those measured in environmental samples around other nuclear installations (e.g. Levin et al., 1980; Segl et al., 1983; Obelic et al., 1986; Povinec et al., 1986). This observation certainly suggests that Sellafield is one of the largest sources of artificial  $^{14}\text{CO}_2$  in the world today.

### 3.2.2.2 The Temporal Distribution of the $^{14}\text{CO}_2$ Discharges

The  $^{14}\text{CO}_2$  discharges from Sellafield have been monitored during the period of this research (1983-1985) by the assay of plant materials grown in the near-site environment. However, nuclear fuel has been reprocessed at Sellafield since 1952 and thus a study was instigated to determine the  $^{14}\text{C}$  levels in the local environment for the period between the start of operations at Sellafield and the start of this research work, i.e. 1952-1982. A larch tree, planted around 1933 at a site 1.3 km to the north-east of Sellafield (marked by a 'T' in Figure 3.2) and felled in 1983, was obtained. As explained in Section 2.2.1.5, the cellulose fraction of a tree ring is an excellent indicator of ambient atmospheric  $^{14}\text{C}$  levels in the year of growth of that particular tree ring. Therefore, by measuring the  $^{14}\text{C}$  specific activities in the cellulose fractions of the individual tree rings of the larch covering the period 1952-1982, a measure of past environmental  $^{14}\text{C}$  levels can be obtained. The values obtained for the ambient atmospheric  $^{14}\text{C}$  specific

activity levels, in the vicinity of the tree, for each year during the period 1952-1982 are listed in Table 3.5. The results are also shown graphically in Figure 3.7 along with the average global  $^{14}\text{C}$  levels for the same period.

For the period up to 1978, a similar set of measurements have been generated by Otlet et al. (1983) on the rings of a sycamore tree grown near Sellafield. This tree grew at a different site from the larch used in this study and it is therefore difficult to draw comparisons between the two data sets but certainly the same basic trends are apparent. No significant deviation from global atmospheric  $^{14}\text{C}$  levels would appear to have occurred before the middle of the 1960s. During the next few years, however, atmospheric  $^{14}\text{C}$  levels around Sellafield steadily increased until they gradually levelled off towards the end of the decade. Since then, atmospheric  $^{14}\text{C}$  activities have, in general remained fairly steady but with large annual fluctuations occurring around the average level.

It is worth pointing out at this stage that there is no clear evidence from this tree data to suggest that large amounts of  $^{14}\text{CO}_2$  were discharged into the atmosphere during the 1957 Windscale fire. In that incident, which occurred in October of the year, fire destroyed the core of one of the plutonium producing reactors and it is to be expected that significant amounts of  $^{14}\text{CO}_2$  would have been released into the atmosphere. However, compared to the general trend in  $^{14}\text{C}$  levels over that period, no discernable  $^{14}\text{C}$  enrichment is observed in the 1957 tree ring. The explanation of the absence of an effect could be that, for the duration of the fire, the wind direction was not towards the tree and, more importantly, that the growth rate of the tree at that time of the year is likely to have been very low. Indeed, records show that a north, north-westerly wind was the most prevalent during the period of the fire, i.e. away from the tree. Whatever the reason, the result is that very little information on the escape of  $^{14}\text{CO}_2$  to the atmosphere during the 1957 Windscale fire can be obtained from these data.

Nevertheless, the general information derived from this tree is of considerable value (as will be seen later) in determining

Table 3.5:  $^{14}\text{C}$  levels of the larch tree

Year	$^{14}\text{C}$ specific activity ( $\text{Bq kg}^{-1}$ (carbon) $\pm 1\sigma$ )
1952	228 $\pm$ 2
1953	234 $\pm$ 2
1954	262 $\pm$ 2
1955	259 $\pm$ 2
1956	250 $\pm$ 2
1957	263 $\pm$ 2
1958	277 $\pm$ 3
1959	317 $\pm$ 2
1960	308 $\pm$ 2
1961	309 $\pm$ 2
1962	337 $\pm$ 2
1963	454 $\pm$ 4
1964	463 $\pm$ 3
1965	480 $\pm$ 3
1966	467 $\pm$ 3
1967	591 $\pm$ 5
1968	719 $\pm$ 5
1969	524 $\pm$ 4
1970	477 $\pm$ 3
1971	432 $\pm$ 3
1972	591 $\pm$ 4
1973	683 $\pm$ 5
1974	501 $\pm$ 3
1975	746 $\pm$ 3
1976	743 $\pm$ 6
1977	625 $\pm$ 5
1978	401 $\pm$ 2
1979	408 $\pm$ 2
1980	453 $\pm$ 2
1981	599 $\pm$ 3
1982	727 $\pm$ 6

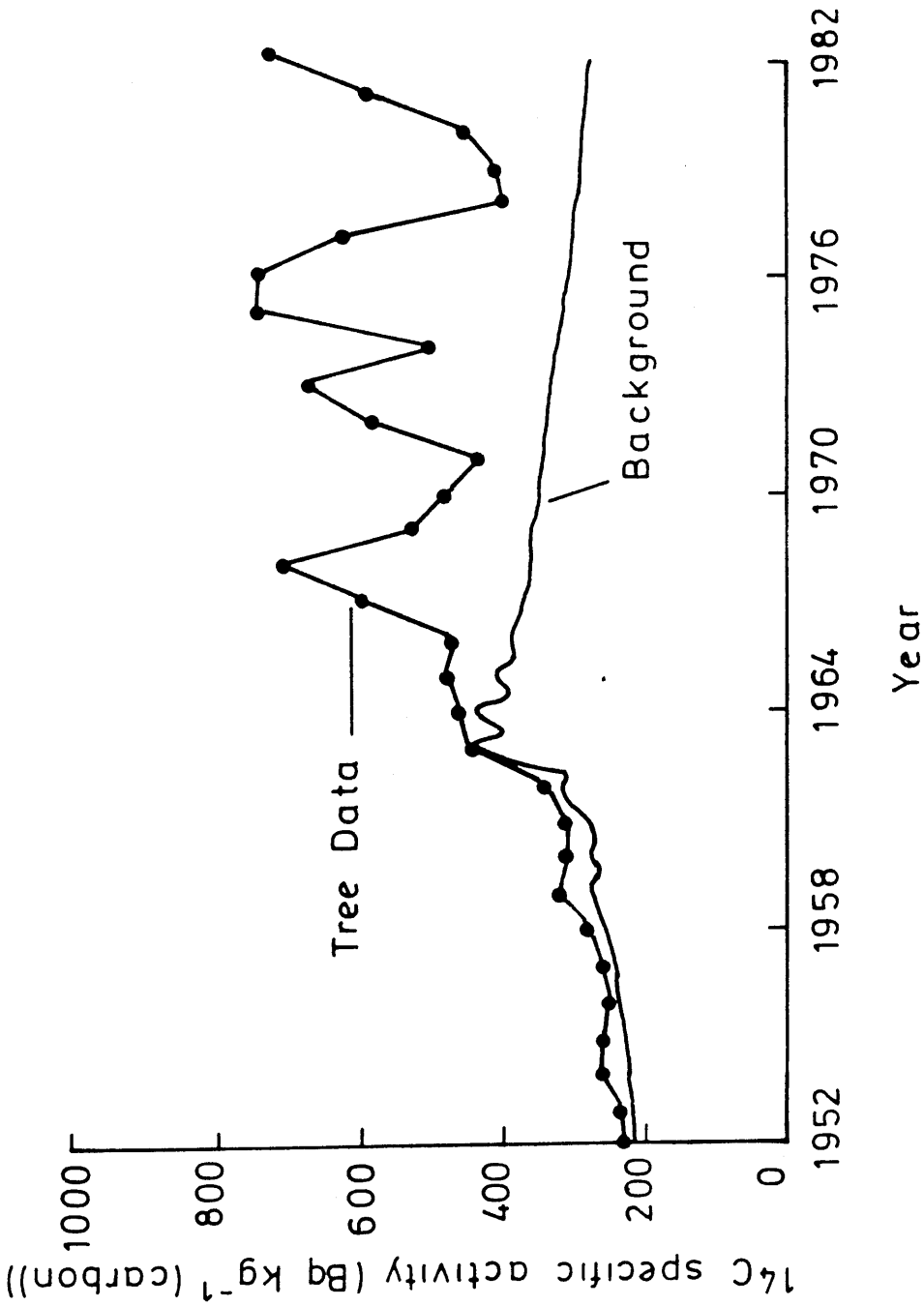


FIGURE 3.7: Atmospheric  $^{14}\text{C}$  levels around Sellafield, 1952 - 1982.

the local effects of  $^{14}\text{CO}_2$  discharges from Sellafield. For the time being, however, these results along with those from the 1983, 1984 and 1985 transects, clearly show that the local population around Sellafield has, over many years, been consistently exposed to enhanced  $^{14}\text{C}$  levels relative to the background  $^{14}\text{C}$  levels. However, exposures prior to 1983 have not been unusually high relative to those thereafter.

### 3.2.3 Hunterston (SSEB)

Hunterston is the site of two nuclear power generating stations. The original plant, Hunterston-A, which consists of two GCRs (or MAGNOX reactors), was first connected to the national grid in 1964. Shortly thereafter, construction of a second station, Hunterston-B, commenced. Hunterston-B comprises two AGRs, the first of which was connected to the national grid in 1976, the other following a year later. The net electrical power generating capacity of the Hunterston complex is 1340 MW(e), approximately 80% of the power being contributed by the new station. This makes Hunterston one of the largest generators of nuclear power in the country. It is situated on the Ayrshire coast in the west of Scotland (see Figure 3.1) and is operated by the South of Scotland Electricity Board (SSEB).

The  $^{14}\text{C}$  production and release pathways are expected to follow the general pattern for these reactor types, as described in Section 1.3.2. It is estimated by the SSEB that the total activity of  $^{14}\text{C}$  discharged from Hunterston amounts to no more than 2.25 TBq year<sup>-1</sup> (Tweedy, pers. comm., 1985), with the great majority of this  $^{14}\text{C}$  being discharged into the atmosphere as  $^{14}\text{CO}_2$ . This estimate is based almost entirely on theoretical calculations, with very little experimental justification. Certainly, before this study, there had been no reported measurements on  $^{14}\text{C}$  levels in plants from the vicinity of Hunterston.

#### 3.2.3.1 The Spatial Distribution of the $^{14}\text{CO}_2$ Discharges

The extent of this study was limited to the spatial distribution of the  $^{14}\text{CO}_2$  discharged to the atmosphere from the Hunterston complex in 1984. The design of the sampling programme was based very strongly on the experience gained during

the Sellafield study. The sampling material was chosen to be grass, as before. The samples were mainly collected beside the road in the area to the east of Hunterston (i.e. in the direction of the most prevalent wind). However, as before, samples were also collected away from the road to check for any fossil CO<sub>2</sub> polluting effect caused by road traffic. The length of the transect studied was just over 15 km and a total of 20 samples were taken over this distance. The path mapped out by the samples is shown in Figure 3.8 by a solid line extending inland from Hunterston on the coast to Lochwinnoch. The shaded regions in this diagram identify the major population areas.

Once collected, the samples were converted to benzene and their <sup>14</sup>C specific activities measured as described in Chapter 2. The results are listed in Table 3.6 and, unless a comment is made, the sample can be assumed to be of grass collected beside the road to the east of Hunterston. All distances are taken from the sample point to the middle of the <sup>14</sup>CO<sub>2</sub> discharge locations and have been estimated from Ordnance Survey maps (the associated error is probably less than ± 0.1 km). The results are also shown graphically in Figure 3.9, in which a line has been plotted through the main data set.

A few general comments can be made from initial inspection of these results. Firstly, the same basic trend as that apparent at Sellafield is noticeable. That is, a maximum value is observed within 0.5 km of the discharge sites, the values at increasing distances fluctuating around a general downward trend towards the average global levels. The maximum value of 187 Bq kg<sup>-1</sup> (carbon) above the background level is, in this case observed about 0.4 km away. However, as at Sellafield, even at relatively large distances, the <sup>14</sup>C levels do not appear actually to reach the average global <sup>14</sup>C levels (as measured in the control samples). Finally, although only one grass sample was collected at a site removed from the roadside, it gives a value in good agreement with that of grass collected at a similar distance from the plant but beside the road. Therefore, on the basis of not only this result but also those obtained at Sellafield, it can be assumed that there is no significant effect on environmental <sup>14</sup>C levels caused by road traffic at the sites studied during

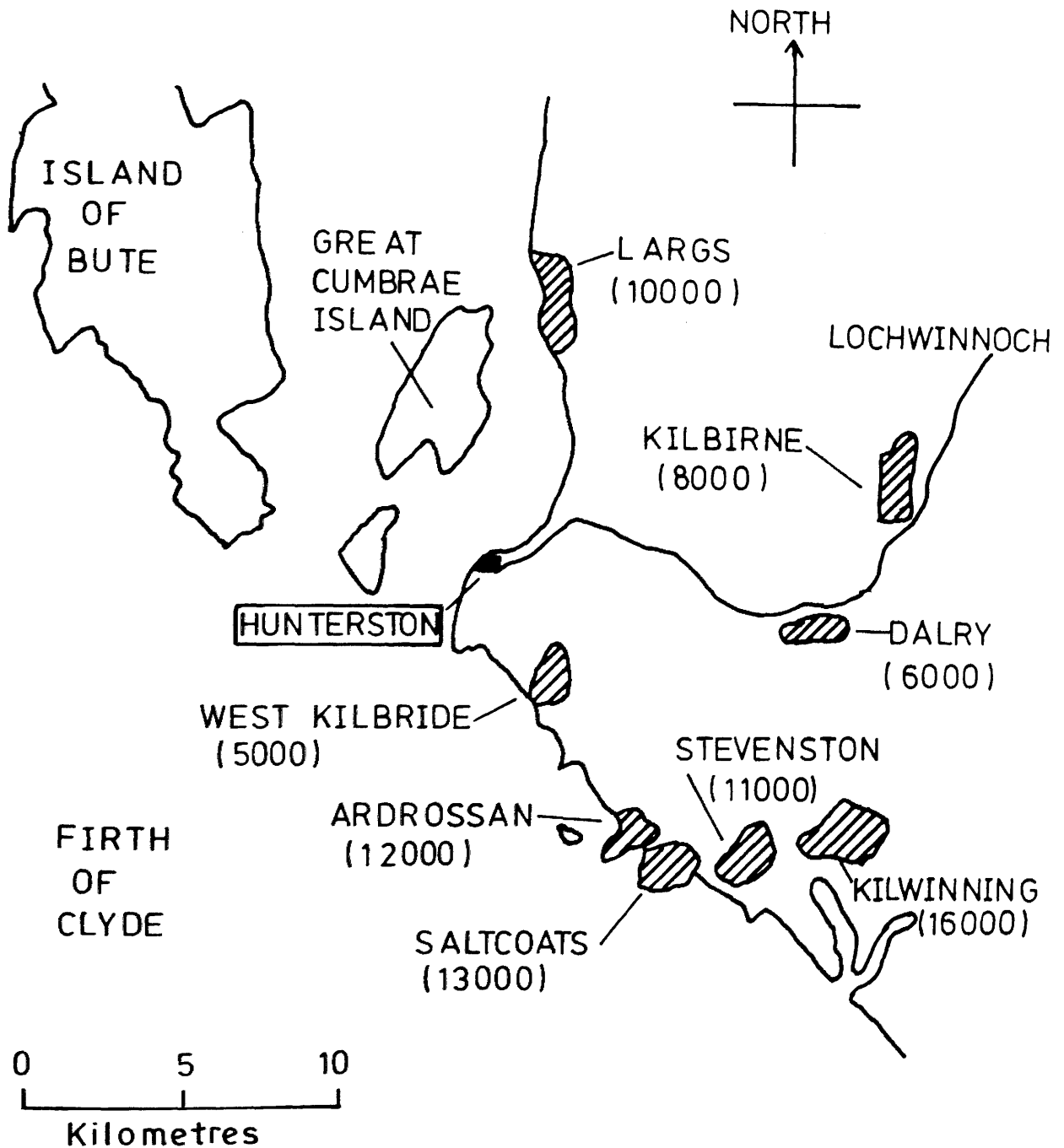


FIGURE 3-8: Hunterston study area.

Table 3.6:  $^{14}\text{C}$  levels around Hunterston (1984)

Distance (km)	$^{14}\text{C}$ specific activity (Bq kg $^{-1}$ (carbon $\pm 1\sigma$ ))	Comment
0.1	357 $\pm$ 2	
0.4	463 $\pm$ 2	
0.8	355 $\pm$ 2	
1.2	301 $\pm$ 2	
1.3	288 $\pm$ 2	
1.6	282 $\pm$ 2	
1.9	310 $\pm$ 2	
2.0	310 $\pm$ 1	
2.6	292 $\pm$ 1	
2.9	277 $\pm$ 1	
3.4	283 $\pm$ 1	
3.8	283 $\pm$ 1	
4.4	283 $\pm$ 1	
5.0	283 $\pm$ 1	
6.1	282 $\pm$ 1	
6.1	280 $\pm$ 1	away from road
6.8	279 $\pm$ 1	
9.2	284 $\pm$ 2	
12.0	281 $\pm$ 2	
16.5	285 $\pm$ 2	

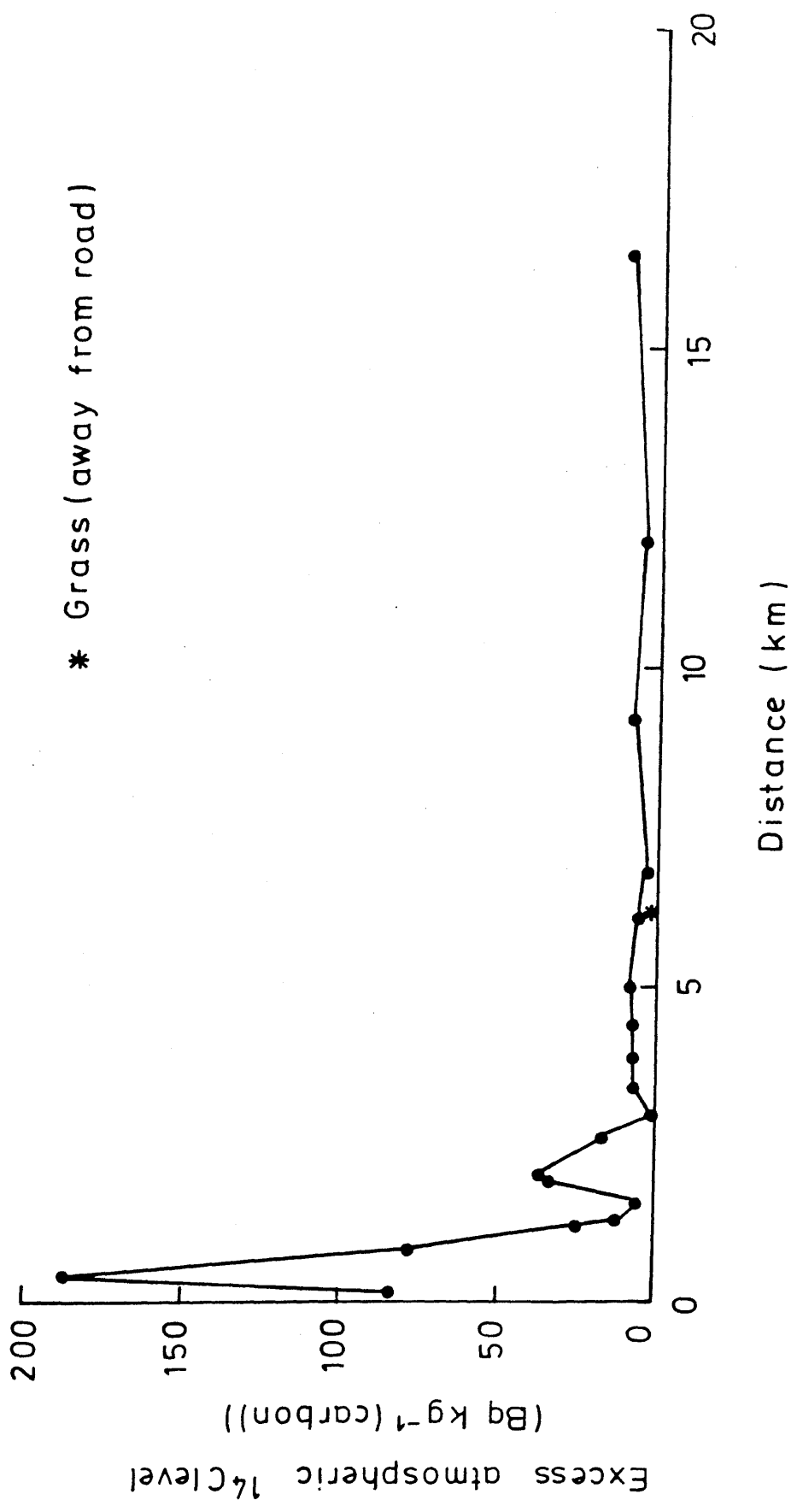


FIGURE 3.9: Excess atmospheric <sup>14</sup>C levels around Hunterston, 1984.

this work.

In conclusion, the  $^{14}\text{C}$  levels are, in general, considerably lower at Hunterston than at and around Sellafield, in agreement with the  $^{14}\text{CO}_2$  discharge estimates of the respective operators. Nevertheless, the results indicate that the local population around Hunterston are exposed to enhanced  $^{14}\text{C}$  levels relative to the average global population.

#### 3.2.4 Dounreay (UKAEA)

Dounreay which is situated on the northern coast of Scotland (see Figure 3.1), is the site of Britain's prototype fast breeder reactor. This liquid metal fast breeder reactor, which is operated by the United Kingdom Atomic Energy Authority (UKAEA), has an electrical power generating capacity of 242 MW(e) but, being a prototype, it has a rather low load factor (around 10%). According to current estimates (as discussed in Section 1.3.2.7), the  $^{14}\text{C}$  production rate in fast breeder reactors is low and the releases of  $^{14}\text{CO}_2$  to the atmosphere from the reactor are therefore expected to be minimal. However, since these estimates are based totally on theory, having no experimental evidence to back them up, it was decided to carry out a preliminary study to discover whether or not detectable amounts of  $^{14}\text{CO}_2$  were being discharged from Dounreay. In 1984 2 grass samples were collected within 2 km of this nuclear establishment.

The results which are presented in Table 3.7, certainly indicate that, relative to Sellafield and Hunterston, there is no significant  $^{14}\text{CO}_2$  discharge to the atmosphere from the fast breeder reactor. Both samples had  $^{14}\text{C}$  levels identical, within error, to the average global  $^{14}\text{C}$  levels of 276 Bq kg<sup>-1</sup> (carbon). This finding suggests that any  $^{14}\text{CO}_2$  discharges from Dounreay are so low that they do not represent a measurable radiological hazard to the local population and, in consequence, no further work was carried out in this area.

#### 3.2.5 East Kilbride (SURRC)

The final nuclear facility investigated was the Scottish Universities Research Reactor Centre (SURRC) situated at East

Table 3.7:  $^{14}\text{C}$  levels around Dounreay (1984)

Distance (km)	$^{14}\text{C}$ specific activity (Bq kg <sup>-1</sup> (carbon) $\pm 1\sigma$ )
1	276 $\pm$ 2
2	274 $\pm$ 2

Kilbride, near Glasgow (see Figure 3.1). This reactor is very different from the other nuclear facilities discussed so far as it is used primarily for research activities. The reactor uses an enriched uranium fuel and utilises water as both coolant and moderator. It has a maximum power of 300 kW(e), which is over 4000 times smaller than that of the Hunterston complex. Obviously, because of its size, the  $^{14}\text{CO}_2$  discharges from the reactor would be expected to be relatively small. However, for this same reason (i.e. its size), it is situated far closer to large populations than most nuclear facilities. East Kilbride itself has a population of over 65 000 and nearby Glasgow and its surrounds contain well over 800 000 people. Therefore, even small quantities of  $^{14}\text{CO}_2$  discharged from East Kilbride could lead to significant collective doses to the local population. As at Dounreay, a preliminary survey was carried out to determine whether or not measurable quantities of  $^{14}\text{CO}_2$  were being discharged from the site. Therefore, in October 1985, 2 grass samples were collected from the vicinity of this reactor. These samples were collected far closer to the discharge location than were the samples at most other sites because the stack from which most of the  $^{14}\text{CO}_2$  would be discharged is rather low relative to those at other sites. In fact, the sampling site (within 100 m downwind) covered the area of maximum predicted  $^{14}\text{C}$  content, as calculated by dispersion models.

The results, listed in Table 3.8, show no enhancement of the  $^{14}\text{C}$  levels. So, as at Dounreay, the preliminary study suggested that no significant quantities (or at least no detectable quantities) of  $^{14}\text{CO}_2$  are discharged at this site and hence no further work was instigated.

### 3.3

#### THE RADIOLOGICAL IMPACT OF $^{14}\text{CO}_2$ DISCHARGES ON THE LOCAL POPULATIONS

The results of the environmental sampling programme, reported in the previous section, clearly indicate that the populations around two of the sites studied, namely Sellafield and Hunterston, are exposed to enhanced levels of  $^{14}\text{C}$ . This section therefore presents an assessment of the radiological hazards to populations in the vicinity of Sellafield and Hunterston from their respective  $^{14}\text{CO}_2$  discharges. Initially, however, the

Table 3.8:  $^{14}\text{C}$  levels around SURRC, East Kilbride (1985)

Distance (km)	$^{14}\text{C}$ specific activity (Bq kg <sup>-1</sup> (carbon) $\pm 1\sigma$ )
0.05	278 $\pm 1$
0.10	279 $\pm 1$

methodology used to quantify the radiation dose to the local population will be described.

### 3.3.1 Methodology

The methodology utilised in this study is largely based on that recommended by the IAEA (1985) which is itself derived from earlier work by the CEC (1979) and is as follows. The collective dose equivalent commitment,  $S^C$ , in an exposed population, is defined as:

$$S^C = \int_0^{\infty} H^C N(H^C) dH^C, \quad (3.1)$$

where  $H^C$  is the individual dose equivalent commitment and  $N(H^C)$  is the number of people receiving a dose equivalent commitment between  $H^C$  and  $H^C + dH^C$ . Equation (3.1) can be transformed to the following form which facilitates the numerical evaluation of the collective dose equivalent commitment:

$$S^C = \int_d \int_{\theta} \int_t N(d, \theta, t) \dot{H}(d_i, \theta_j, t) dt d\theta dd, \quad (3.2)$$

where  $N(d, \theta, t)$  is the number of people at time  $t$ , at distance  $d$  and azimuthal angle  $\theta$ , relative to the point of discharge and  $\dot{H}(d, \theta, t)$  is the individual dose equivalent rate at  $(d, \theta, t)$ .

The spatial distribution of the population and of the  $^{14}\text{CO}_2$  will, in reality, be continuously varying functions of distance,  $d$ , and azimuthal angle,  $\theta$ , relative to the discharge point. These variations can be approximated in the manner indicated in Figure 3.10. The area surrounding the discharge point is divided into a number of annuli of varying radii; these annuli are further subdivided into a number of sectors of width  $\Delta\theta$ . The selection of annular segments represents a compromise between minimising computational effort, the availability of appropriate site-specific data and ensuring that any error introduced into the dose estimation as a result of the approximation is insignificant relative to the other uncertainties in the overall assessment.

Assuming that the resolution of the annuli is adequate, then the collective dose equivalent commitment in any segment,

$$(d_i, \theta_j), \text{ can be evaluated as:} \\ S^C(d_i, \theta_j) = \int_t N(d_i, \theta_j, t) \dot{H}(d_i, \theta_j, t) dt, \quad (3.3)$$

where  $N(d_i, \theta_j, t)$  is the population and  $\dot{H}(d_i, \theta_j, t)$  is the mean dose equivalent rate in the  $i$ th distance band and  $j$ th annular

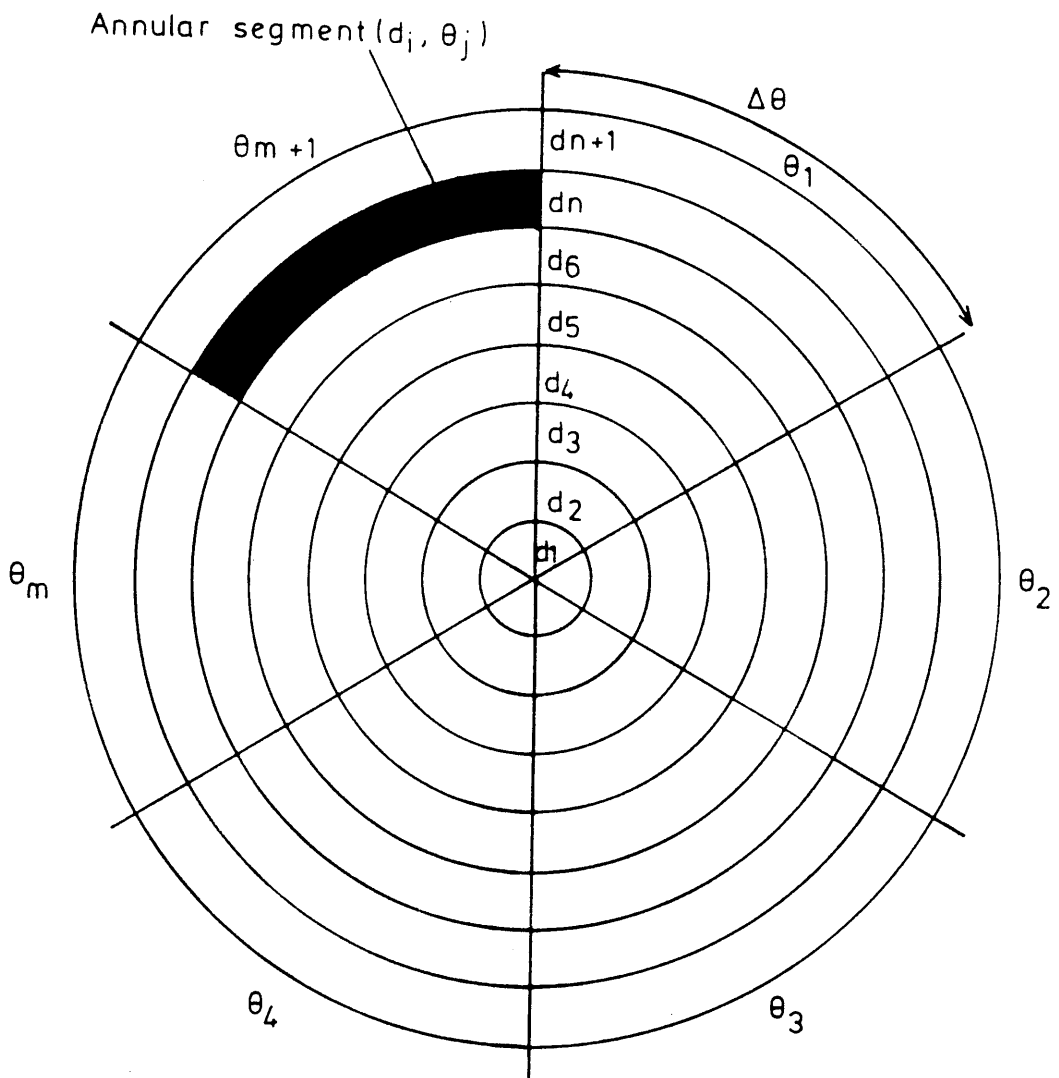


FIGURE 3-10: Scheme of annular segments adopted to represent the spatial distribution of the population and activity in various parts of the environment.

segment. The spatial component of the integration of total collective dose equivalent commitment specified in equation (3.2) can thus be reduced to a summation over the various annular segments. The collective dose equivalent commitment becomes:

$$S^C = \sum_i \sum_j \int_t N(d_i, \theta_j, t) \dot{H}(d_i, \theta_j, t) dt. \quad (3.4)$$

If the magnitude of the population in each segment is assumed to remain constant over all time, equation (3.4) reduces to:

$$S^C = \sum_i \sum_j N(d_i, \theta_j) \int_t \dot{H}(d_i, \theta_j, t) dt. \quad (3.5)$$

A method is now needed to determine the individual dose equivalent rate from the  $^{14}\text{CO}_2$  released to the atmosphere. The only significant contribution to the radiation dose to man from  $^{14}\text{CO}_2$  comes from the ingestion of  $^{14}\text{C}$  in foodstuffs. Hence, the problem can be reduced to one of producing a method to determine the individual dose equivalent rate from the ingestion of  $^{14}\text{C}$  which has been incorporated into food from  $^{14}\text{CO}_2$  discharged into the atmosphere. In the absence of a model at this time which accurately describes in detail the temporal behaviour of  $^{14}\text{CO}_2$  once injected into the terrestrial environment, a simplified approach, often referred to as the specific activity model, is used.

The basic assumptions of the specific activity model are, firstly, that all food ingested by a person is derived at the location of the individual and, secondly, that the  $^{14}\text{C}$  specific activity of the ingested material is equal to that in the atmosphere at the point of intake (the validity of these assumptions will be discussed later). Hence, the dose equivalent rate,  $\dot{H}$ , is directly proportional to the atmospheric  $^{14}\text{C}$  specific activity, C:

$$\dot{H} = C \times \text{constant}. \quad (3.6)$$

The time integral of the dose equivalent rate (in other words, the dose equivalent commitment) at location  $(d_i, \theta_j)$  following the continuous release of  $^{14}\text{CO}_2$  for a year is given by:

$$\int_t \dot{H}(d_i, \theta_j, t) dt = K \int_t C(d_i, \theta_j, t) dt, \quad (3.7)$$

where  $C(d_i, \theta_j, t)$  is the average annual ground level

$^{14}\text{CO}_2$  specific activity in air at location  $(d_i, \theta_j)$ , in the year  $t$ , measured in  $\text{Bq kg}^{-1}$  (carbon) and  $K$  is the annual dose equivalent for unit concentration of  $^{14}\text{CO}_2$  in air. This constant,  $K$ , is numerically equivalent to  $6.3 \times 10^{-8}$   $\text{Sv year}^{-1} (\text{Bq kg}^{-1} (\text{carbon}))^{-1}$ , as explained in Section 1.4.2.

It is implicit in the specific activity model that the dose to the local population is only delivered when the enhanced  $^{14}\text{C}$  specific activity in air and thus the discharges are maintained. Therefore, the dose to the local population from the discharge of  $^{14}\text{CO}_2$  throughout a given year,  $t_k$ , will be delivered totally within the year  $t_k$ , the dose in all other following years being zero. Thus the dose equivalent commitment to an individual at location  $(d_i, \theta_j)$ , following the continuous release of  $^{14}\text{CO}_2$  in the year  $t_k$ , can be rewritten as:

$$\int_t \dot{H}(d_i, \theta_j, t) dt = (6.3 \times 10^{-8}) C(d_i, \theta_j, t_k), \quad (3.8)$$

where  $C(d_i, \theta_j, t_k)$  is the average annual ground level  $^{14}\text{CO}_2$  specific activity in air at location  $(d_i, \theta_j)$  in the year of the  $^{14}\text{CO}_2$  discharge,  $t_k$ .

The collective dose equivalent commitment to the local population from the ingestion of  $^{14}\text{C}$  discharged into the environment in the year  $t_k$  is given by equation (3.9):

$$S^c(t_k) = (6.3 \times 10^{-8}) \sum_i \sum_j N(d_i, \theta_j) C(d_i, \theta_j, t_k) \quad (3.9)$$

The temporal component of the integration of total collective dose equivalent commitment specified in equation (3.5) can thus be reduced to a summation over the various years,  $t_k$  (where  $k = 1, 2, 3, p, p+1$ ), in which  $^{14}\text{CO}_2$  discharges occurred. The collective dose equivalent commitment becomes:

$$S^c = (6.3 \times 10^{-8}) \sum_i \sum_j N(d_i, \theta_j) \sum_k C(d_i, \theta_j, t_k). \quad (3.10)$$

It should be remembered that, for  $^{14}\text{C}$ , the effective dose equivalent and the dose equivalent in all organs are the same and therefore equation (3.10) can be used to calculate any of these quantities. For, the majority of this work, the collective effective dose equivalent commitment alone will be referred to since, for  $^{14}\text{CO}_2$ , it is the single most important radiological quantity.

It is worth pausing at this stage to discuss the validity of

the assumptions intrinsic in the  $^{14}\text{C}$  specific activity model. The assumption that all foodstuffs ingested by a person are derived at the location of the individual seems rather unrealistic when applied to present-day Britain. Certainly, in today's industrial societies, it is common practice for a high proportion of an individual's food supply to be derived not only from within and throughout the individual's country but, indeed, from all over the world. Therefore, the adoption of this assumption is likely to lead to overestimation of the dose to the local population but as it could be valid for critical group members (self-sufficiency, etc.) it is not totally unreasonable. On the other hand, the remaining assumption, that the  $^{14}\text{C}$  specific activity of the ingested material is equal to that in the atmosphere at the point of intake, is essentially justifiable. In fact, the validity of this assumption has been demonstrated for many different plants, e.g. barley, wheat, rye, oats and grass (Tauber, 1967), which have been shown to be in rapid equilibrium with the atmosphere. In the specific activity model, however, the equilibrium is assumed to be instantaneous, which is obviously not correct. Use of this assumption will not lead to an error in the estimation of the magnitude of the dose but may rather distort the time period over which the dose is delivered. The model predicts that doses are only delivered while the specific activity of carbon in air is maintained, i.e. only during the release. In reality, doses during the period of release are likely to be lower than those estimated but with gradually decreasing doses being delivered at times after the release has ceased. This phenomenon is observed, to some extent, in the work carried out by Stenhouse and Baxter (1977a, 1977b, 1979). This showed both a lag and dilution in the  $^{14}\text{C}$  levels of human tissues relative to the bomb enhanced atmospheric  $^{14}\text{C}$  levels. To sum up, then, adoption of the specific activity model must be qualified in two respects. The first, and perhaps most important, is that the doses evaluated will be overestimated. The second is that the temporal distribution of the dose will be distorted by the model.

This model has, in fact, been widely recommended for use in the assessment of doses from  $^{14}\text{C}$  discharges (CEC, 1979; United Nations, 1982; IAEA, 1985). Therefore, throughout the course of this work, the  $^{14}\text{C}$  specific activity model has been

used, although the conservative nature of this approach is recognised.

In this study, then, the collective effective dose equivalent commitment to the local population from  $^{14}\text{CO}_2$  discharged to the atmosphere has been calculated using equation (3.10). The data needed to solve this equation are the spatial distributions of both the population and the excess  $^{14}\text{CO}_2$  in the years of interest. The manner in which these data are determined will now be described.

#### 3.3.1.1 The Spatial Distribution of the Local Population

For all but the most sensitive studies, the spatial distribution of the population can be obtained from information held by the appropriate local authorities. For most regions, certainly within the United Kingdom, data are readily available on the population in the various electoral wards contained within a specified area. These data do not give the exact location of each individual but localise the population into groups of various sizes. Determining the spatial distribution of the population merely involves noting the annular segment into which each particular group falls. The size of these groupings varies with population density. In densely populated areas, the groups may consist of a few thousand people, whereas in sparsely populated areas the groups may only comprise a few hundred people. Thus, although this centralisation of individuals must lead to a loss of definition in the population distribution picture, it is structured in such a way that any errors introduced by this approach are likely to be acceptably small except, as previously stated, for the most sensitive studies.

#### 3.3.1.2 The Spatial Distribution of the $^{14}\text{CO}_2$ Discharges

The spatial distribution of  $^{14}\text{CO}_2$  discharged from a specific site can be determined either experimentally or theoretically. An experimental determination is, on the whole, more reliable and hence more desirable although, in the absence of experimental data, a theoretical determination must suffice. Both methods will now be briefly described.

### Experimental Method

The experimental determination of the spatial distribution of  $^{14}\text{CO}_2$  discharges relies on the actual measurement of the  $^{14}\text{C}$  specific activity in the atmosphere at various distances and directions from the discharge location. This can be done either directly by the measurement of the  $^{14}\text{C}$  specific activity in air or indirectly by the measurement of the  $^{14}\text{C}$  specific activity in vegetation (which is then assumed to equal the  $^{14}\text{C}$  specific activity in air). In most experimental determinations of the spatial distribution of the  $^{14}\text{CO}_2$ , it is not possible to obtain measurements at all distances and directions within a specified area around the discharge location. Therefore, the  $^{14}\text{C}$  specific activities at certain places have to be interpolated from the measured points. Thus, even in the most detailed experimental determinations, a limited degree of theoretical estimation is normally necessary.

### Theoretical Method

The theoretical determination of the spatial distribution of  $^{14}\text{CO}_2$  discharges relies on the ability of mathematical models to mirror the processes of atmospheric dispersion.

The problem of predicting the distribution of airborne material released from a source is commonly approached by solving the diffusion transport equation. A number of models have been developed to solve the equation, depending upon the simplifying assumptions made and the boundary conditions imposed. The dispersion model which has found most frequent application, for the purposes of estimating regional collective doses, is the Gaussian dispersion model. Clearly, other models exist which provide a better representation of the physical processes occurring in the atmosphere (e.g. eddy diffusivity models); however, such models are, in general, more complex, require considerably greater computation time to obtain results and it would be fair to comment that they have not yet been developed to a state where they can be readily applied. The major advantages of the Gaussian dispersion model are its relative simplicity, ease of use and the availability of meteorological data expressed in terms of a diffusion typing scheme directly applicable to this model. It is considered that, for most applications, the accuracy

of the Gaussian dispersion model's predictions is adequate within the framework of collective dose assessments, particularly in the context of the inherent uncertainties in other parts of the overall assessment. Certainly, for estimating the doses to local populations from the discharge of  $^{14}\text{CO}_2$  from a given source, this model has been both widely recommended for use (CEC, 1979; Miller, 1984; IAEA, 1985) and, indeed, widely used (Killough and Rohwer, 1978; Bush et al., 1983). It should be noted that one major objective of this study is to test the validity of the Gaussian dispersion model, with particular reference to its suitability for prediction of the nuclide distribution resulting from a continuous gaseous release. This matter will be discussed in more detail at a later stage.

Detailed descriptions of the Gaussian dispersion model can be found elsewhere (Turner, 1970; Pasquill, 1974) and only the basic features are summarised here. The fundamental assumptions of the model are that the vertical dispersion of activity may be described by a Gaussian distribution, while the horizontal dispersion is Gaussian for a short release and uniform across a sector of angle  $\alpha$  for a continuous release. This study is basically concerned with  $^{14}\text{CO}_2$  released to the atmosphere during the normal operations of a nuclear facility. These discharges tend to be essentially continuous all year round and hence there is no need at present to consider further the behaviour of short-term releases.

For the continuous release of a nuclide, the ground level activity concentration in air,  $C_{ij}(r)$ , measured in  $\text{Bq m}^{-3}$  (air), at a distance  $r$  from the source within a specified sector,  $i$ , for each set of meteorological conditions,  $j$ , (i.e. for each stability category,  $j$ ) is given by:

$$C_{ij}(r) = (Q / ((2\pi)^{1/2} r \alpha U_{sj} \sigma_{zj})) F_j(h, A_j), \quad (3.11)$$

where  $Q$  is the release rate ( $\text{Bq s}^{-1}$ ),

$r$  is the horizontal distance from the source (m),

$\alpha$  is the angular width of the sector (radians),

$U_{sj}$  is the wind speed at the source height for stability category  $j$  ( $\text{ms}^{-1}$ ),

$\sigma_{zj}$  is the standard deviation of the vertical Gaussian distribution for stability category  $j$  (m),

$h$  is the release height (m),

$A_j$  is the depth of the mixing layer (the distance between the ground and the mixing height, i.e. the boundary between two different atmospheric stability regimes) for

$$F_j(h, A_j) = 2 \left( \exp\left(-\left[\frac{h}{2\sigma_{zj}}\right]^2\right) + \exp\left(-\left[\frac{2A_j - h}{2\sigma_{zj}}\right]^2\right) + \exp\left(-\left[\frac{2A_j + h}{2\sigma_{zj}}\right]^2\right) \right). \quad (3.12)$$

The formulation in equation (3.12) allows adequate inclusion of the effects of reflections from both the ground and the top of the mixing layer for small values of the vertical dispersion coefficient,  $\sigma_{zj}$ , (ie. when  $\sigma_{zj} < A_j$ ). As the vertical dispersion coefficient becomes large (i.e. when  $\sigma_{zj} \geq A_j$ ), the vertical concentration distribution becomes uniform throughout the mixing layer and the concentration is given by:

$$C_{ij}(r) = \frac{Q}{r \propto U_{sj} A_j}. \quad (3.13)$$

In all cases, it is assumed that there is no activity within the mixing layer from a source outside it and that no activity released into the mixing layer escapes from it.

The average activity concentration in air at ground level in the  $i$ th sector may then be obtained by summing the concentration obtained for each set of meteorological conditions weighted by the fractional occurrence of these conditions:

$$C_{ij}(r) = \sum_j f_{ij} C_{ij}(r), \quad (3.14)$$

where  $f_{ij}$  is the frequency of meteorological condition  $j$  within the  $i$ th sector. For  $^{14}\text{C}$ , the activity concentration, measured in  $\text{Bq m}^{-3}$  (air), can be converted to the atmospheric  $^{14}\text{C}$  specific activity, measured in  $\text{Bq kg}^{-1}$  (carbon), by multiplying  $C_{ij}(r)$  by the conversion factor  $5490 \text{ m}^3$  (air)  $\text{kg}^{-1}$  (carbon).

For nuclides, such as  $^{14}\text{C}$ , which do not deposit on the ground, this method, as recommended by Clarke (1979), is suffice for predicting their ground-level activity concentrations in air at distances up to a few tens of kilometres from the source. The model is, however, only recommended for use in areas of reasonably constant topography and with discharges from sources which are not in a position significantly affected by turbulence from nearby buildings. So, assuming that a particular discharge site can

satisfy these conditions and that all the necessary site-specific data are available, the Gaussian dispersion model, as described here, can be used to evaluate the  $^{14}\text{C}$  specific activity in each annular segment.

### 3.3.2 Sellafield

The local radiological impact of  $^{14}\text{CO}_2$  discharges from Sellafield has been assessed for the period 1952-1985, i.e. from the start of operations at Sellafield up to the present-day. This assessment is based on data obtained from the four separate sampling programmes described in Section 3.2.2. The results derived from each individual sampling programme are now presented, followed by a discussion of the general conclusions.

#### 3.3.2.1 1985

The first step in the assessment process is to choose appropriate values for the widths and radii of the annular segments. This choice is made on the basis of the resolution of the available data, i.e. the spatial distribution of both the population and the  $^{14}\text{CO}_2$  discharges.

The distribution of the population around Sellafield is obtained from listings of the number of people in each electoral ward and was provided by the Northern Regional Health Authority. The  $^{14}\text{C}$  levels in all directions are derived from the samples measured along the north-easterly (NE) transect. To be more exact, these measured samples transgressed an area lying between  $15^\circ$  and  $45^\circ$  due north. It is assumed in this work that these measured  $^{14}\text{C}$  levels are representative of the average levels in the area lying between  $0^\circ$  and  $60^\circ$  due north and so the area around Sellafield is split into 6 sectors, each with an angular width of  $60^\circ$ . It could be argued that a smaller angular width should be selected. However, in deriving the  $^{14}\text{C}$  levels in other directions, the measured  $^{14}\text{C}$  levels have to be combined with meteorological data. These data are collected at Squires Gate meteorological station near Blackpool (70 km south of Sellafield) and are partitioned into  $10^\circ$  sectors. Thus, the use of these data in deriving the  $^{14}\text{C}$  levels, in directions other than NE, introduces a further element of uncertainty to the results. On this basis, therefore, it would not appear

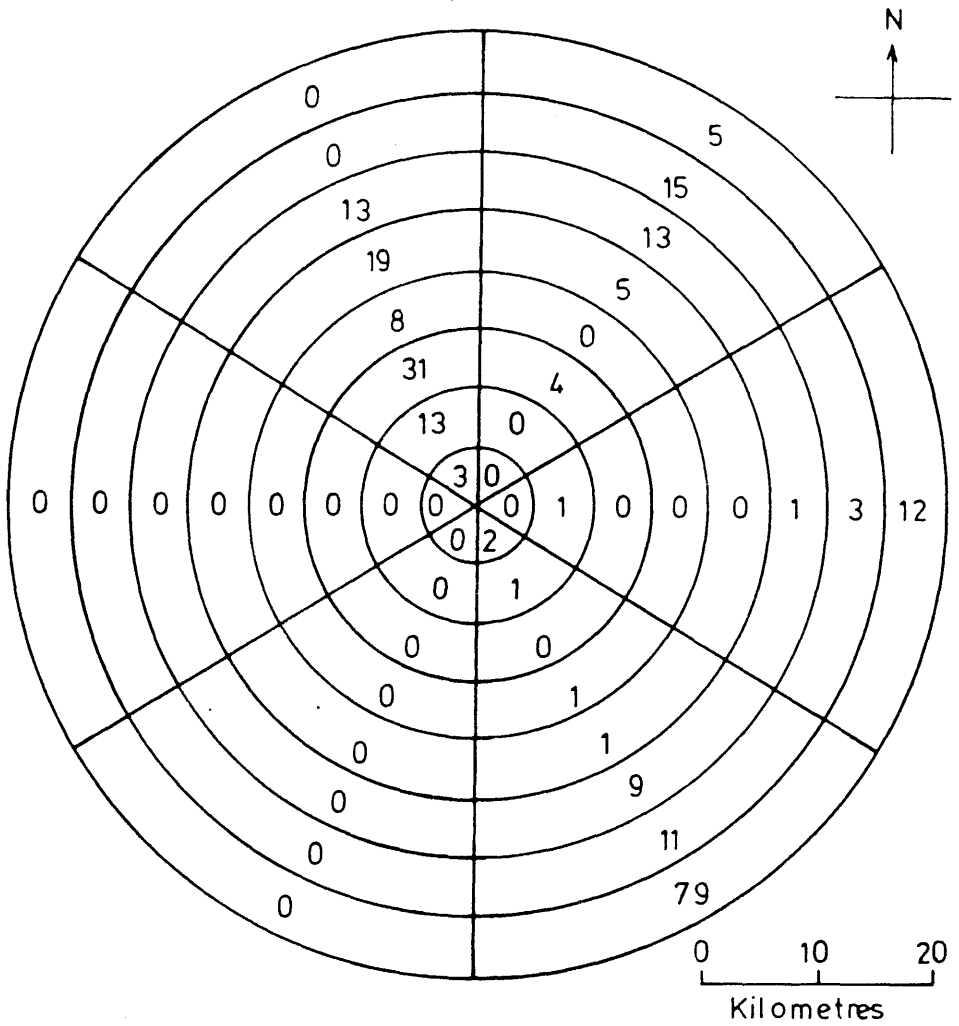
justifiable to decrease the angular width of sectors. Distance bands are chosen in such a way that a good estimation of the average atmospheric  $^{14}\text{C}$  level in each annular segment can be made. Inspection of the variation of the  $^{14}\text{C}$  levels with distance, shown in Figure 3.5, suggests that 5 km distance bands would be adequate for all but the initial 5 km region around Sellafield. However, taking into account the sparsity of the population in this region, there is little to be gained by using smaller distance bands. In fact, it was found that an adequate and meaningful resolution was obtained using 5 km distance bands throughout the study area. In other words, the radius of the smallest annulus is taken to be 5 km, with the radius of each subsequent annulus increasing by a further 5 km.

Values for the width and radii of the annular segments having been determined, the next step is to define the limit of the local population. For radionuclides which ultimately become globally dispersed, it is not always a clear cut matter to determine where the limit of the 'local dose' occurs, i.e. the point at which the enhanced levels around the discharge point have decreased to the average global levels. This is certainly the case for  $^{14}\text{C}$  as can be demonstrated via the 1985 results shown in Figure 3.5. Over the last 15 km or so of the transect, the  $^{14}\text{C}$  levels remain fairly steady just above the average global activity. Although the differences between the  $^{14}\text{C}$  specific activities of the control samples and those of the Sellafield samples at these larger distances are small (e.g.  $16 \text{ Bq kg}^{-1}$  (carbon) at 37.5 km), they do appear to be statistically significant, due largely to the accuracy of the analytical technique, i.e. the associated error on both these measurements is  $\pm 2 \text{ Bq kg}^{-1}$  (carbon) ( $1\sigma$ ). Therefore, this deviation at distance may be an accurate reflection of the normal dispersion pattern or, on the other hand, it may be caused by small differences in the global  $^{14}\text{C}$  levels between the Sellafield environment and the control point in the north-west of Scotland. Although this is only a small effect, it could be radiologically significant if it encompasses an area of high population. The method invoked here is to assume that any differences between  $^{14}\text{C}$  levels in near-site and control samples are due entirely to local  $^{14}\text{CO}_2$  discharges. However, the area over which the local

dose is assessed is limited to that within which measurements were actually taken, i.e. they will not be extrapolated beyond the farthest sampling point. The most remote sampling point at which an enhanced  $^{14}\text{C}$  level was observed was at nearly 40 km and therefore this is taken as the limit for the local dose calculation. This assumption does not imply that there is no component of local dose delivered at distances beyond this upper limit but rather than the errors involved in estimating such doses beyond this point would be so large as to make the assessment meaningless.

To calculate the dose to the population within 40 km of Sellafield, it is necessary to determine both the population and the average atmospheric  $^{14}\text{C}$  levels in each of the annular segments. As previously mentioned, the spatial distribution of the population was obtained from information held by the Northern Regional Health Authority and is shown in Figure 3.11. The largest populations in the area are found on the coastline which runs through the NW and SE sectors. The population inland from Sellafield is very sparse and the area predominantly to the west is covered by the Irish Sea and thus is uninhabited. The spatial distribution of the  $^{14}\text{CO}_2$ , however, is not as easily determined.

The  $^{14}\text{C}$  levels at various distances along the NE transect have been provided by the experimental data. The  $^{14}\text{C}$  levels at distances between sampling points are simply assumed to lie on a straight line between the data for the sampling points. The use of any other method would involve unjustifiable assumptions concerning the atmospheric dispersion of  $^{14}\text{CO}_2$ . The average  $^{14}\text{C}$  level in each 5 km segment is then calculated from the area under the line defined by the experimental data in the corresponding segment. The  $^{14}\text{C}$  levels along the NE transect are thus provided by the results of the experimental study but, of course, it is necessary to determine also the  $^{14}\text{C}$  levels in the other 5 directions. The direction in which the  $^{14}\text{CO}_2$  is dispersed is determined by the wind direction. Thus, by comparing the time during which the wind direction is towards a particular sector with that for which it is within the NE sector, it is possible to predict the  $^{14}\text{C}$



(Figures refer to the number of thousands of people in each annular segment.)

FIGURE 3-11: Spatial distribution of the population around Sellafield.

levels in the other 5 sectors. This, of course, assumes that the dispersion of  $^{14}\text{CO}_2$  is identical in all directions and is dependent only on wind direction. This approach is perhaps contrary to present understanding of the subject, which considers other conditions, e.g. temperature, ground roughness and atmospheric stability, to have important roles to play in atmospheric dispersion. However, thus far, no mathematical model has been developed and proven to have the ability to represent atmospheric dispersion accurately based on these many variables. The approximation has been invoked here, therefore, that the atmospheric dispersion characteristics of  $^{14}\text{CO}_2$  are identical in all directions and are dependent only on wind direction.

This approach can, in fact, be convincingly supported by experimental evidence collected by other workers. Stewart and Wilkins (1985) showed that the dispersion of  $^{129}\text{I}$  around Sellafield is dependent only on the distance from the discharge location and the wind rose. That is, if the  $^{129}\text{I}$  activities were normalised to a uniform wind rose, then they would be the same, for a given distance, in any direction. Also, in work carried out by Otlet et al. (1983), it was demonstrated that for  $^{14}\text{CO}_2$  discharges from Sellafield, the rate of dispersion along all transects investigated was very similar. In addition, the differences in the absolute  $^{14}\text{C}$  levels measured were reconcilable with the wind rose data. The measured  $^{14}\text{C}$  levels along the E, N and NE transects were all similar and were all higher than those along the SE transect which were, in turn, higher than those along the NW transect (i.e. E, N, NE > SE > NW). The trend in the appropriate wind rose data for the same year was E > SE, NE, N > NW, i.e. very similar to that suggested by the measured data. These experimental studies suggest that, certainly to a first approximation, it is reasonable to assume that the relative dilution of  $^{14}\text{CO}_2$  along all sectors is identical, with the absolute levels depending only on wind rose. The exact details of this technique, as applied to  $^{14}\text{CO}_2$  discharges from Sellafield, will now be explained.

From the meteorological data collected at Blackpool, the period of time during which the wind was blowing into a particular

sector is determined. Since the radiation dose to man from  $^{14}\text{CO}_2$  arises mainly from the photosynthetic uptake of carbon by plants, the time-span investigated is limited to that during which photosynthesis occurs, as recommended by Killough and Rohwer (1978). This time period was approximated to the hours 8:00-20:00 for the months April to September inclusive. The  $^{14}\text{C}$  level at a distance  $r$  from the discharge point, in a sector  $X$ ,  $C(r,X)$ , is given by:

$$C(r,X) = \frac{T_X}{T_{NE}} (C(r,NE)), \quad (3.15)$$

where  $C(r,NE)$  is the  $^{14}\text{C}$  level at a distance  $r$  in the NE sector and  $T_X$  and  $T_{NE}$  are measures of the time during the growing season in which the wind was blowing into the  $X$  and NE sectors respectively. The wind rose for the time period of interest is shown in Figure 3.12(a) and the distribution of the  $^{14}\text{C}$  levels around Sellafield is plotted in Figure 3.12(b). The highest  $^{14}\text{C}$  levels are found to the east of Sellafield, as a direct result of the large easterly component in the appropriate wind rose.

There is one further problem associated with this technique of determining the spatial distribution of the  $^{14}\text{CO}_2$  discharges. That is, it is assumed that the  $^{14}\text{CO}_2$  release rate from Sellafield is constant throughout the year and that the growth rate of grass is constant throughout the growing season. If either of these conditions is not satisfied, then the method will produce a distorted picture of the  $^{14}\text{C}$  spatial distribution. It is likely that neither of these conditions will be fully met in any particular year but, relative to the other uncertainties in the assessment, the resulting errors are likely to be small and, in evaluations spanning several years, could well be self-cancelling.

Having now estimated the spatial distribution of both the population and the  $^{14}\text{CO}_2$  discharges, the dose to the local population can be calculated in the manner previously described. The results of this assessment are presented in Figure 3.13. The collective effective dose equivalent commitments to the local population at various distances from Sellafield are presented in tabular and diagrammatic form in parts (a) and (b) respectively of

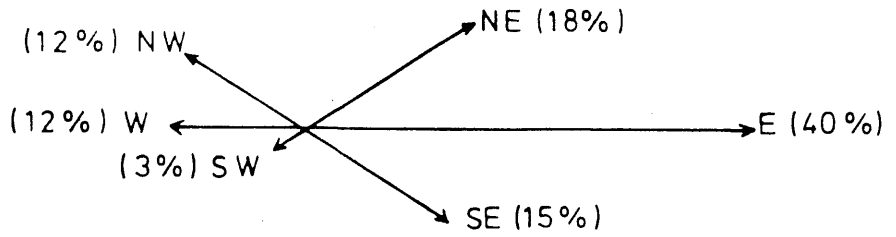


FIGURE 3-12(a): Wind rose for 'growing period' (Sellafield, 1985).

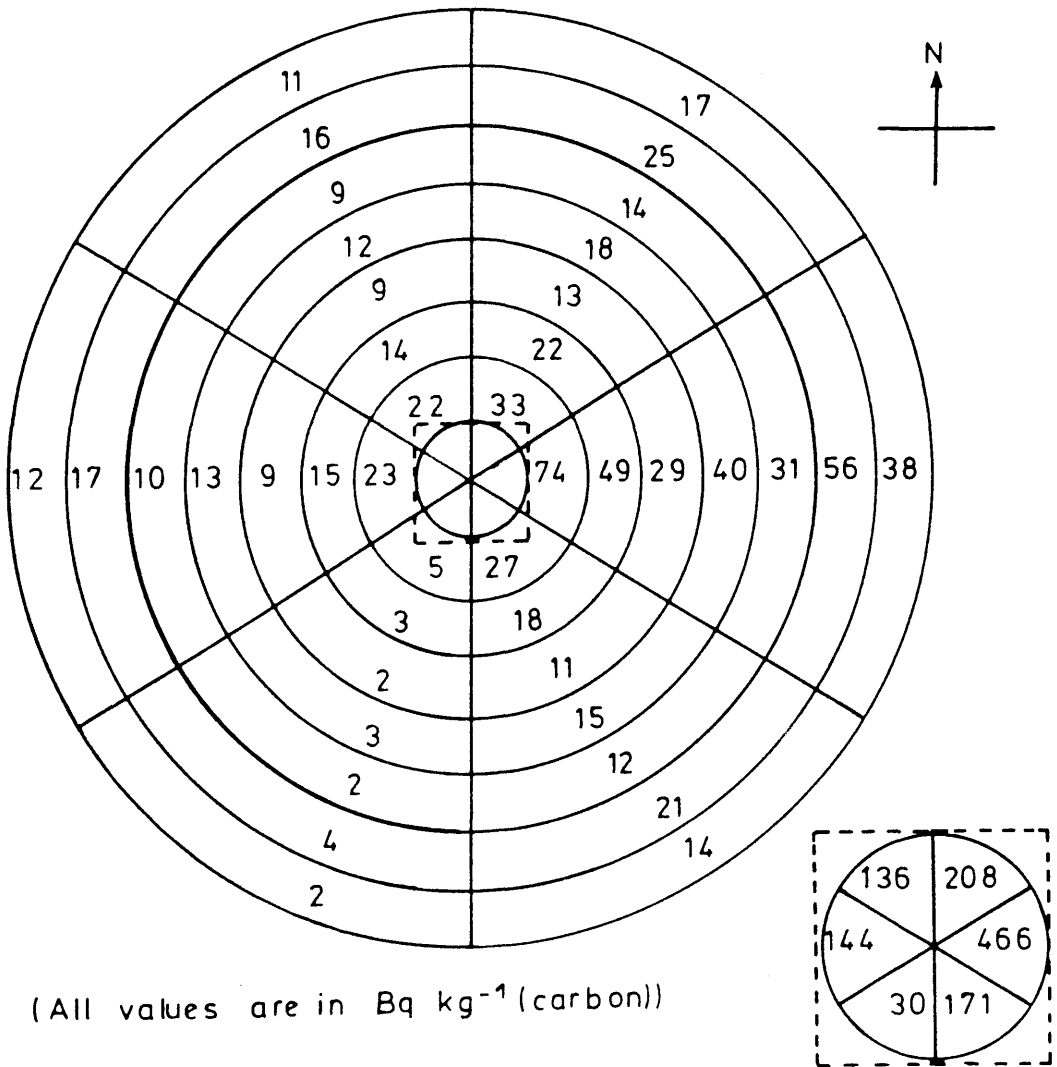
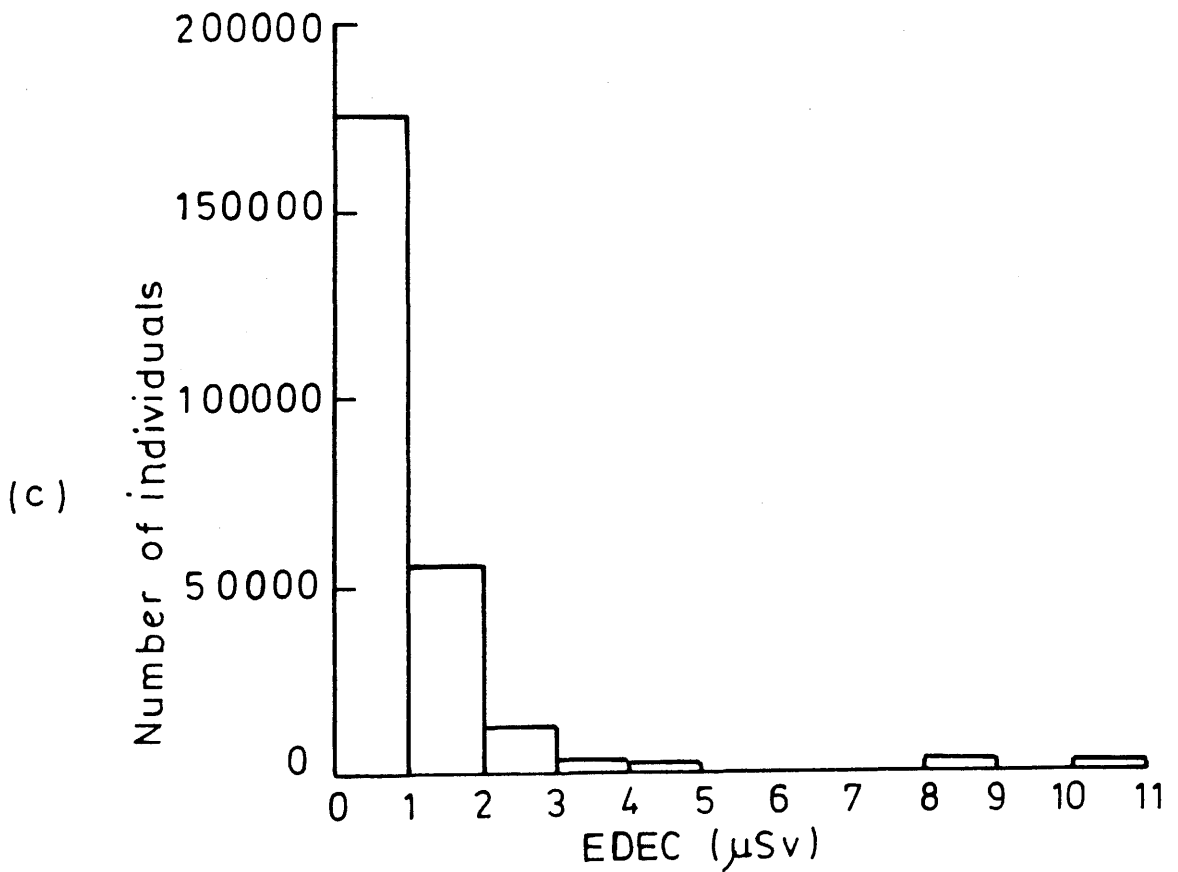
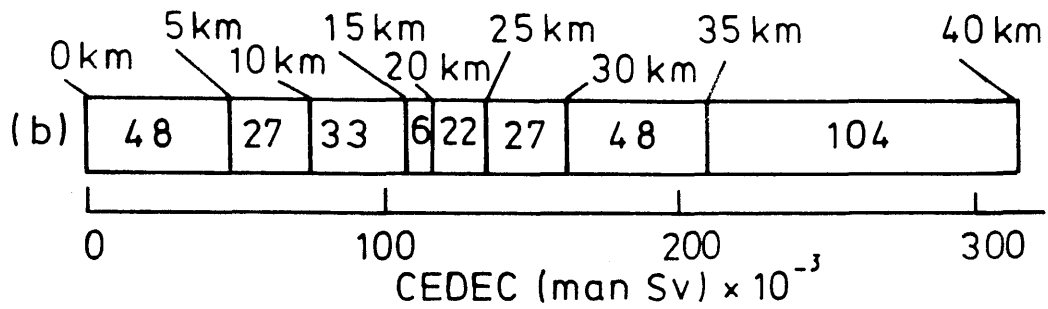


FIGURE 3-12(b): Spatial distribution of  $^{14}C$  around Sellafield, 1985.

(a)

Radius (km)	0-5	0-10	0-15	0-20	0-25	0-30	0-35	0-40
CEDEC (man Sv) $\times 10^{-3}$	48	75	108	114	136	163	211	315



(d) Maximum individual EDEC = 0.12 mSv.

[ EDEC : Effective Dose Equivalent Commitment.  
 CEDEC; Collective EDEC. ]

FIGURE 3.13 : Doses to the population around Sellafield, from  $^{14}\text{CO}_2$  discharges in 1985.

Figure 3.13. The collective effective dose equivalent commitment received by the population within a 40 km radius of Sellafield was 0.315 man Sv. It is noticeable that the collective dose in each 5 km segment does not decrease in a regular manner as distance from source increases. In fact, a large percentage of the dose (around 30%) is derived from the outermost region (35-40 km). This effect is caused by counteraction of the decreasing  $^{14}\text{C}$  levels with distance by a general increase in population density as distance from Sellafield increases. Hence, this collective dose is the integral of a wide range of individual doses. For example, at one extreme, a large percentage of the collective dose is delivered to a large number of people receiving relatively small doses (notably the inhabitants of Barrow-in-Furness, located in the outermost region of the south-easterly sector). At the other end of the scale, a similar percentage of the collective dose is delivered to a small number of people receiving relatively large doses, e.g. the population within 5 km of Sellafield. It is therefore interesting to divide the collective effective dose equivalent commitment into ranges of individual effective dose equivalent commitments. This has been illustrated in part (c) of Figure 3.13 and demonstrates that the majority of the collective dose is accumulated at levels well below the maximum dose resulting from the discharge. In actual fact, the number of individuals receiving a dose in the range 0-1  $\mu\text{Sv}$  is almost 100 times greater than the number of individuals receiving doses of greater than 10  $\mu\text{Sv}$ .

The maximum individual dose received by a member of the exposed population, presented in part (d) of Figure 3.13, falls outwith the ranges quoted in part (c). This effect is a result of the fact that segmentation of the area around Sellafield leads to a loss of resolution in the range of predicted individual doses. This loss of resolution is insignificant except to determinations of the maximum individual dose. To estimate the latter parameter, another approach, which will now be explained, must be adopted.

The highest measured  $^{14}\text{C}$  level in 1985 is 848  $\text{Bq kg}^{-1}$  (carbon) above the average global level, which was observed in a grass sample grown in the NE sector about 0.35 km from the discharge location. It is possible that higher

levels still may have been present at a point where no sample was collected. It is unlikely, in fact, that the highest level was sampled. However, because of the large number of samples collected over the first few kilometres, it can be assumed that the highest observed  $^{14}\text{C}$  level is, in reality, reasonably close to the 'true' highest value. As seen from the wind rose in Figure 3.12(a), the  $^{14}\text{C}$  levels in the east sector are expected to have been higher than those in any other sector. Thus, using equation (3.15), it can be calculated that the maximum  $^{14}\text{C}$  level in the Sellafield environment during 1985 was  $1900 \text{ Bq kg}^{-1}$  (carbon) above the average global level and was situated at a point 0.35 km from the discharge location, lying in the east sector. The maximum dose would therefore be received by an individual who lived 0.35 km to the east of Sellafield. It can be calculated, using equation (3.8), that the effective dose equivalent commitment received by that individual would be 0.12 mSv. Now it must be remembered that it is inherent in the specific activity model that the dose to the local population from  $^{14}\text{CO}_2$  discharges in a given year is delivered entirely within that same year. This assumption means that, although all the results have been presented here as dose commitments (i.e. over all time), they are also numerically equivalent to the annual doses. Hence, the maximum value of the effective dose equivalent commitment to an individual, 0.12 mSv, is the same as the value of the maximum annual effective dose equivalent to an individual. An annual effective dose equivalent of 0.12 mSv corresponds to around 2.5% of the annual effective dose equivalent limit for members of the public. In this case, the 5 mSv limit has been utilised although it is further recommended by ICRP that exposure over a lifetime should not average more than  $1 \text{ mSv year}^{-1}$ . The ramifications of this further requirement imposed on the discharges will be discussed later.

It was previously decided that extension of the dose estimate beyond the maximum sampling point at 40 km would introduce unacceptable uncertainty to the results. There is therefore no need for a theoretical determination of the  $^{14}\text{C}$  levels in the area of interest around Sellafield as they have already been derived from an experimental study. However, the data set provided by the experimental study forms the ideal basis for

testing the validity of atmospheric dispersion models. Hence, all the data necessary for application of the Gaussian dispersion model were collected and the model then used to predict  $^{14}\text{C}$  levels along the NE transect.

The data on the average wind speeds at 10 m ( $U_{10j}$ ) and on the occurrence of the various atmospheric stability categories ( $j$ ) are derived from information provided by the Meteorological Office. The values for the ground roughness term ( $Z_0$ ), its associated coefficient ( $n$ ) and the mixing layer depths ( $A_j$ ), are all chosen on the basis of the recommendations of Clarke (1979). The information on  $^{14}\text{C}$  release rate ( $Q$ ) and stack heights ( $h$ ) was provided by BNF plc. Although there are two different stacks at Sellafield through which  $^{14}\text{CO}_2$  is known to be released, they are both of the same height and are sufficiently close together to be conveniently treated as a single source. Finally, the angular width of the sector of interest ( $\alpha$ ), the NE sector that is, has previously been defined as being  $60^\circ$  or  $\pi/3$ . Before the Gaussian dispersion model can be used, however, 2 further quantities, namely the average wind speed at the source height ( $U_{sj}$ ) and the standard deviation of the vertical Gaussian distribution ( $\sigma_{zj}$ ) for each stability category, must first be determined from the above data. The average wind speed at the source height for a particular stability category can be calculated from equation (3.16), (Clarke, 1979):

$$U_{sj} = U_{10j} \left[ \frac{h}{10} \right]^n. \quad (3.16)$$

The standard deviation of the vertical Gaussian distribution for a given stability category increases with distance from the release point ( $r$ ) and ground roughness ( $Z_0$ ). In this work, its value is generated via the analytical procedure devised by Hosker (1974), who developed a series of equations which give a mathematical description of  $\sigma_z$ 's dependence on distance, ground roughness and atmospheric stability. All these data are then fed into the Gaussian dispersion model (i.e. either equation (3.11) or (3.13)) to produce the predictions of the atmospheric  $^{14}\text{C}$  levels along the NE sector from Sellafield in 1985. The data employed are listed in Table 3.9 and the results shown in Figure 3.14, along with the observed  $^{14}\text{C}$  levels.

As Figure 3.14 demonstrates, the  $^{14}\text{C}$  levels predicted by

Table 3.9: Data for Gaussian dispersion model (Sellafield, 1985)

Stability category (j)	Frequency of occurrence ( $f_j$ )	Average wind speed at 10 m ( $U_{10j}$ ) ( $m\ s^{-1}$ )	Mixing layer depth ( $A_j$ ) (m)
A	$7.2 \times 10^{-4}$	1.5	1300
B	$1.0 \times 10^{-2}$	2.6	900
C	$5.0 \times 10^{-2}$	3.7	850
D	$1.2 \times 10^{-1}$	8.0	800
E	$9.0 \times 10^{-4}$	3.0	400
F	0	-	-
G	0	-	-

ADDITIONAL DATA:

- (1) Release rate (Q) =  $0.21\ MBq\ s^{-1}$ ,
- (2) Release height (h) = 120 m,
- (3) Ground roughness term ( $Z_0$ ) = 0.4 m,
- (4) Ground roughness coefficient (n) = 0.275,
- (5) Angular width of sector ( $\alpha$ ) =  $\pi/3$ .

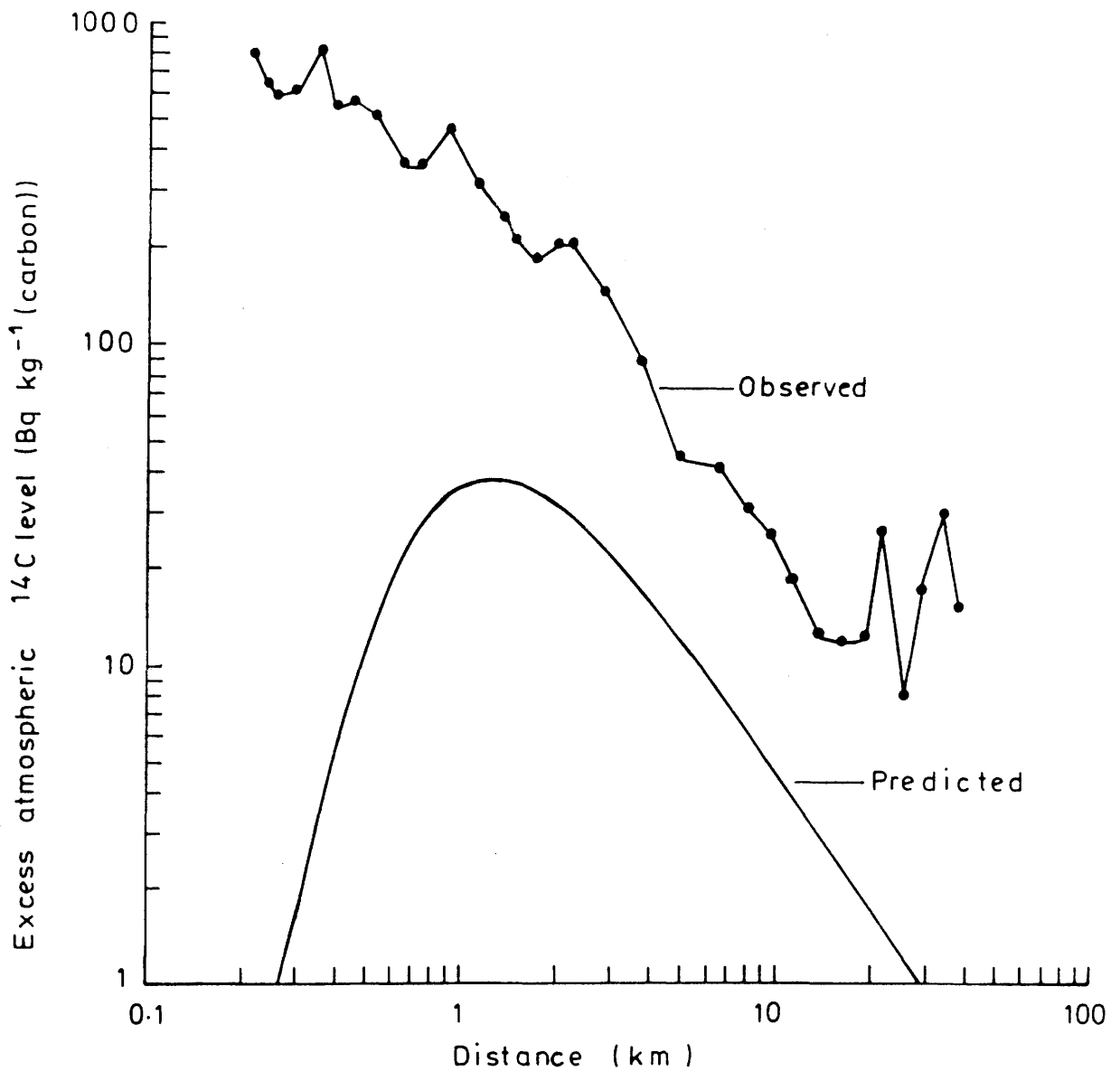


FIGURE 3.14: Atmospheric <sup>14</sup>C levels around Sellafield in 1985, as predicted by the Gaussian dispersion model.

the Gaussian dispersion model are very different from those measured directly in the practical programme. The maximum value above the average global level predicted by the model ( $40 \text{ Bq kg}^{-1}$  (carbon)) is not only around 20 times smaller than the observed maximum but is situated around 1.3 km from the source, whereas the observed maximum occurs at around 0.35 km. On closer observation, however, a certain similarity between the observed and predicted values can be noted. That is, after the initial peak close to the plant, both sets of  $^{14}\text{C}$  levels drop off in what appears to be a hyperbolic manner. Certainly, at large distances from the source, this behaviour is predicted by the Gaussian dispersion model. For, as the distance,  $r$ , increases, the standard deviation of the vertical Gaussian distribution,  $\sigma_z$ , increases and, once  $\sigma_z$  is sufficiently large, all concentrations can be calculated using equation (3.13). For the release of  $^{14}\text{CO}_2$  from a specific location into a sector with a given set of meteorological conditions, expression (3.13) can be equated to the simple hyperbolic function:

$$C = \frac{k}{r}, \quad (3.17)$$

where  $C$  is the atmospheric  $^{14}\text{C}$  specific activity,  $r$  is the distance from the discharge location and  $k$  is a constant which is dependent only on the release rate. Over the distances being considered in this work, according to the Gaussian dispersion model, this condition is approached but never actually reached. Nevertheless, the experimental data do suggest that atmospheric dispersion of the  $^{14}\text{CO}_2$  follows this trend over the majority of the area investigated (with the exception of the first kilometre). In light of the disappointing nature of the predictive results obtained from the Gaussian dispersion model, this hypothesis seemed worth investigating. Thus, in Figure 3.15, the observed  $^{14}\text{C}$  levels have been plotted against the inverse of distance from the discharge location. The samples collected within 1 km of the source are not included since the initial dispersion of the  $^{14}\text{CO}_2$  does not appear to be controlled in this manner. All the measured samples beyond 1 km lie reasonably close to the hyperbola defined by the equation  $y = 359x + 279$  where  $y$  is the  $^{14}\text{C}$  specific activity and  $x$  is the inverse of the distance from the discharge location. The best-fit line through the points was obtained by linear regression, the degree

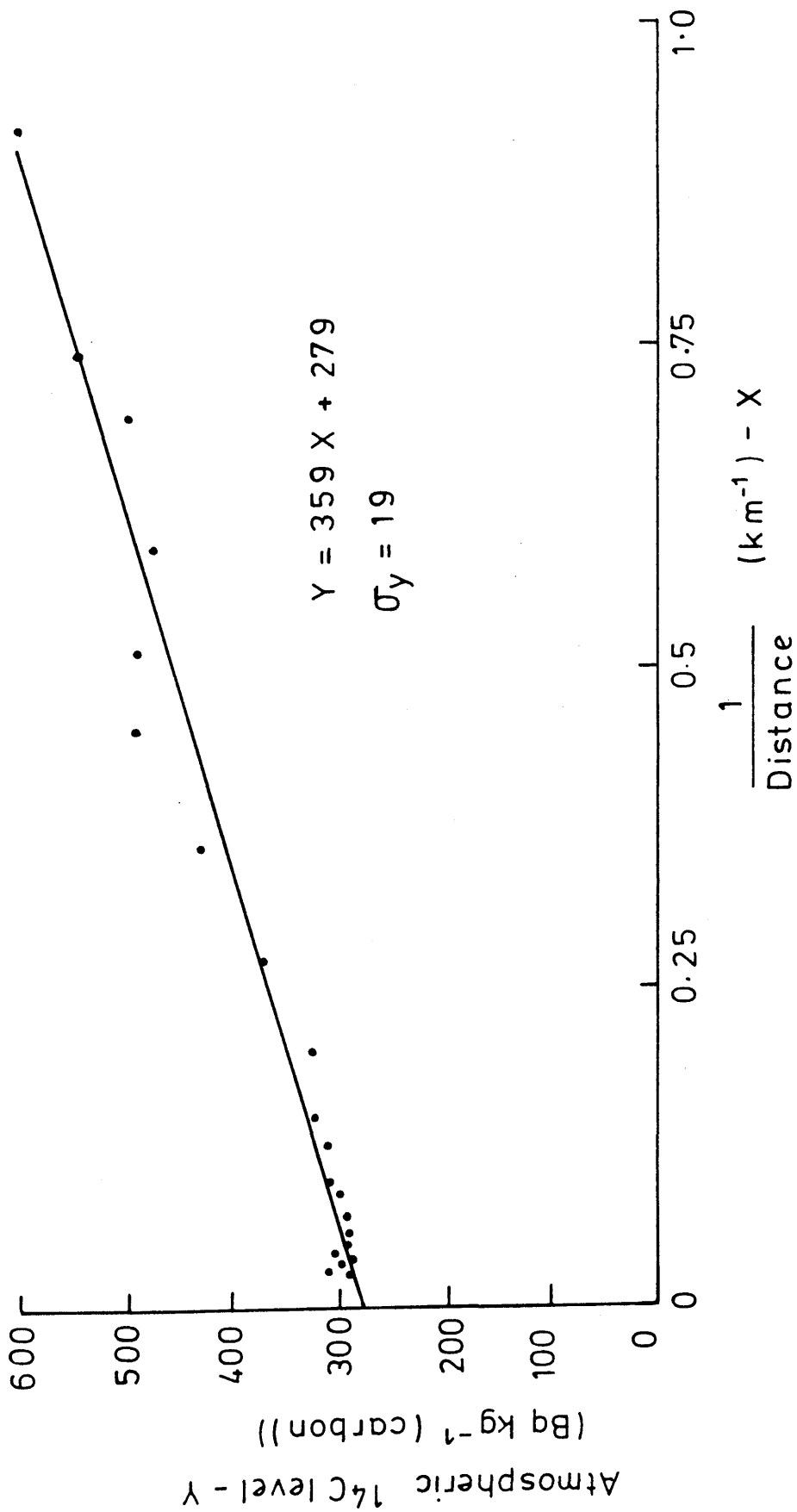


FIGURE 3-15: Atmospheric <sup>14</sup>C level versus distance<sup>-1</sup> for Sellafield, 1985.

of fit is excellent ( $R^2 = 97\%$ ) and the standard deviation about the line is  $19 \text{ Bq kg}^{-1}$  (carbon). This graph suggests that a good approximation to the atmospheric dispersion of  $^{14}\text{CO}_2$  can be made using this simple hyperbolic function. In addition, the ordinate intercept of this function ( $279 \text{ Bq kg}^{-1}$  (carbon)) gives a clear and quantitative indication of the existence and magnitude of the average global  $^{14}\text{C}$  level ( $\sim 279 \pm 2 \text{ Bq kg}^{-1}$  (carbon)). This close agreement between the observed and predicted average global  $^{14}\text{C}$  level further supports the use of this hyperbolic function to describe the atmospheric dispersion of  $^{14}\text{CO}_2$  from Sellafield in 1985.

Both these atmospheric dispersion models can be used to calculate the doses to the local population. One further assumption has to be made in the case of the hyperbolic function and that is that the  $^{14}\text{C}$  levels from 0-1 km remain constant at the value predicted by the model for 1 km. Although this is clearly not the case, it should lead to a reasonable estimate of the average  $^{14}\text{C}$  levels over this area. Since the populations so close to nuclear facilities are generally very small in number, this assumption should not cause a large error in the overall dose estimate. The average  $^{14}\text{C}$  levels in each of the annular segments around Sellafield can then be calculated from both models and the doses to the local population worked out as before. The estimates of the doses to the population within given radii of the plant, as calculated from the two models, are listed in Table 3.10 along with the estimates obtained from the experimental data. Over the 40 km, the estimates of the doses derived from the experimental data ( $0.315 \text{ man Sv}$ ) and the hyperbolic function ( $0.228 \text{ man Sv}$ ) are in good agreement. The dose calculated from the Gaussian dispersion model ( $0.035 \text{ man Sv}$ ) is, however, almost a factor of 10 less than either of these predictions. The obvious conclusion concerning the two atmospheric dispersion models is that, in this case, the Gaussian dispersion model is totally inappropriate for calculation of the doses to the local population, whereas the hyperbolic function is reasonably good. It is noticeable that the predictions derived from the experimental data and the hyperbolic function are very similar at distances up to 30 km from the plant but start to diverge at larger distances. This deviation occurs because, at these large

Table 3.10: Estimates of the collective effective dose equivalent commitment to the population around Sellafield (1985) from various techniques

Distance band (km)	CEDEC ( $10^{-3}$ man Sv)		
	Experimental data	Gaussian plume model	Hyberbolic model
0-5	48	6	43
0-10	75	12	81
0-15	108	19	124
0-20	114	20	131
0-25	136	22	147
0-30	163	26	169
0-35	211	28	184
0-40	315	35	228

(CEDEC: collective effective dose equivalent commitment)

distances, where the population density is generally high, even small differences in predicted  $^{14}\text{C}$  levels lead to large differences in the subsequent collective dose estimate. Such an observation gives further support to the decision not to extrapolate the dose estimates beyond 40 km.

### 3.3.2.2 1984

The method used to assess the doses to the local population around Sellafield in 1984 is based on the approach already described for the 1985 calculations. For example, the width and radii used for the annular segments in 1985 are also utilised here. In addition, it is assumed that the spatial distribution of the population, as shown in Figure 3.11, has remained unchanged. In this year, however, the  $^{14}\text{C}$  levels along the NE transect have been experimentally determined only over 30 km. The results of this study have already been presented in Figure 3.4. In order to extend the distance over which the  $^{14}\text{C}$  levels are known, it is necessary to utilise atmospheric dispersion models. Although the results of the 1985 study strongly suggest that a simple hyperbolic function gives a far superior prediction of  $^{14}\text{C}$  levels than the more complicated Gaussian dispersion model, both models are given due consideration.

Initially, the Gaussian plume atmospheric dispersion model is considered. All the data necessary for the execution of this model are obtained from the same sources as before. The data used are listed in Table 3.11 and the  $^{14}\text{C}$  levels predicted are shown in Figure 3.16, along with the observed  $^{14}\text{C}$  levels. In general, the magnitude and the extent of the enhanced  $^{14}\text{C}$  levels predicted by the model are far smaller than the observed  $^{14}\text{C}$  levels. In particular, the maximum level predicted is only  $27 \text{ Bq kg}^{-1}$  (carbon) above background around 1.1 km from Sellafield, whereas the maximum observed value is, in fact,  $730 \text{ Bq kg}^{-1}$  (carbon) 0.4 km from the plant. So, once again, the use of this model would appear to be undesirable.

An attempt was then made to link the downward trend of the observed  $^{14}\text{C}$  levels to a simple hyperbolic function. This has been done in Figure 3.17 which shows a plot of the observed  $^{14}\text{C}$  levels versus the inverse of the distance from the

Table 3.11: Data for Gaussian dispersion model (Sellafield, 1984)

Stability category (j)	Frequency of occurrence ( $f_j$ )	Average wind speed at 10 m ( $U_{10j}$ ) ( $m s^{-1}$ )	Mixing layer depth ( $A_j$ ) (m)
A	$6.7 \times 10^{-4}$	1.5	1300
B	$1.2 \times 10^{-2}$	3.0	900
C	$3.1 \times 10^{-2}$	3.5	850
D	$5.0 \times 10^{-2}$	6.9	800
E	$9.5 \times 10^{-4}$	2.1	400
F	0	-	-
G	0	-	-

ADDITIONAL DATA:

- (1) Release rate (Q) =  $0.22 \text{ MBq s}^{-1}$ ,
- (2) Release height (h) = 120 m,
- (3) Ground roughness term ( $Z_0$ ) = 0.4 m,
- (4) Ground roughness coefficient (n) = 0.275,
- (5) Angular width of sector ( $\alpha$ ) =  $\pi/3$ .

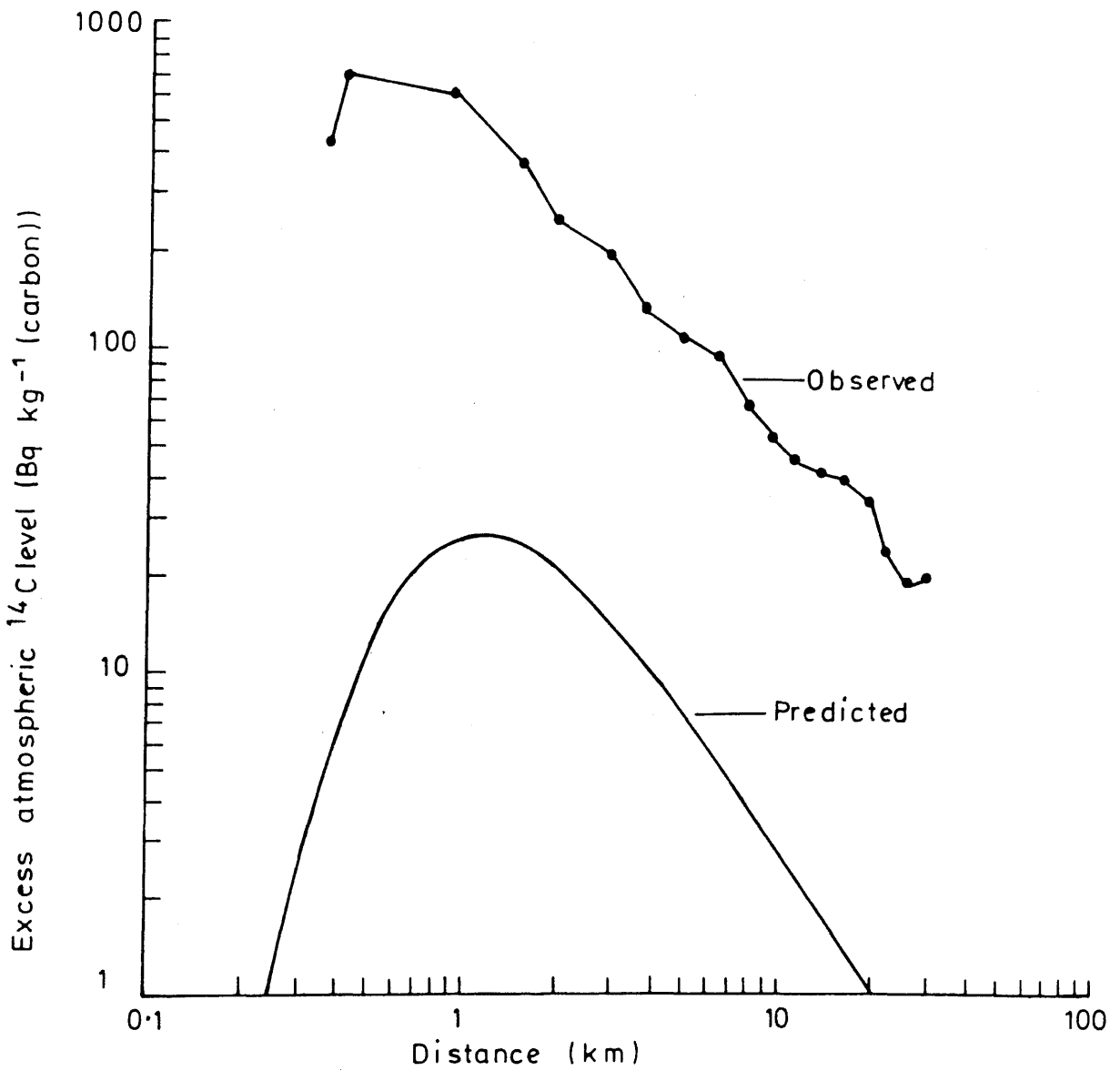


FIGURE 3-16: Atmospheric  $^{14}\text{C}$  levels around Sellafield in 1984, as predicted by the Gaussian dispersion model.

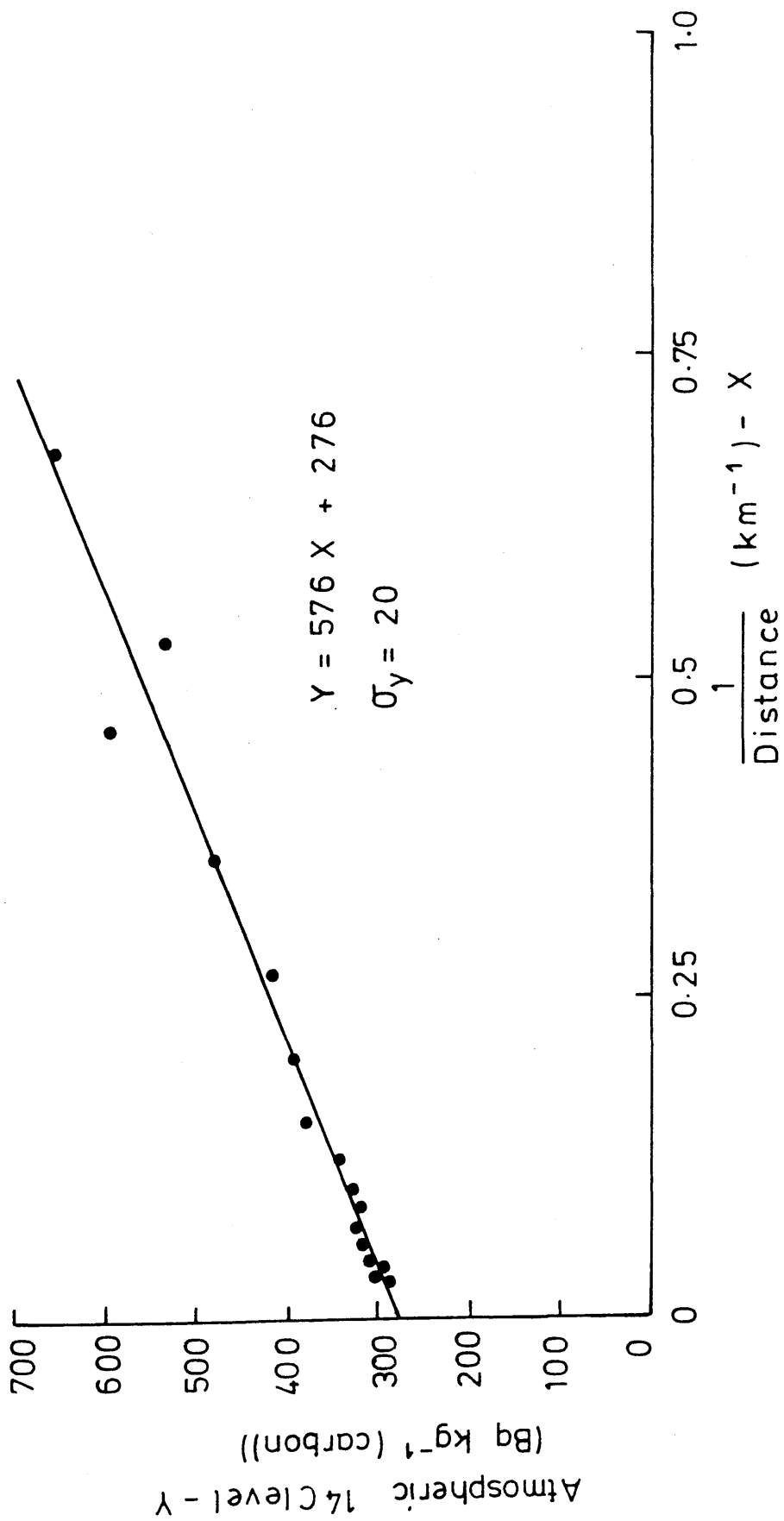


FIGURE 3-17: Atmospheric  $^{14}\text{C}$  level versus distance $^{-1}$  for Sellafield, 1984.

discharge point. The observed levels (beyond 1 km from the source) are in remarkably good agreement with the best-fit line,  $y = 576x + 276$ , the degree of fit is excellent ( $R^2 = 97\%$ ) and the standard deviation about the line is  $20 \text{ Bq kg}^{-1}$  (carbon). Also, the ordinate intercept ( $276 \text{ Bq kg}^{-1}$  (carbon)) is, within error, identical to the measured average global  $^{14}\text{C}$  level. This supporting evidence again suggests that this model can justifiably be used to predict the  $^{14}\text{C}$  levels beyond the 30 km distance. By the very nature of a hyperbolic function, estimates of the  $^{14}\text{C}$  levels can be made up to distances approaching infinity. However, there is no experimental evidence to suggest that such an enhancement does in fact exist. It was decided, therefore, for the sake of uniformity, to limit the study to the area within 40 km of Sellafield.

The average  $^{14}\text{C}$  level in each of the annular segments lying in the NE sector between 0 and 30 km from the source are calculated from the measured values and those lying between 30-40 km are calculated from the predictions of the hyperbolic function,  $y = 576x + 276$ . The average  $^{14}\text{C}$  levels in other directions are then determined from both these values and the appropriate wind rose data, using equation (3.15). The wind rose for the hours 8:00-20:00 for the months April to September inclusive, is shown in Figure 3.18(a) and the spatial distribution of the  $^{14}\text{CO}_2$  around Sellafield for 1984 is presented in Figure 3.18(b). This information is then combined with the spatial distribution of the population to give estimates of the resultant dose to the local population from the 1984  $^{14}\text{CO}_2$  discharges from Sellafield. These results are shown in Figure 3.19.

The collective effective dose equivalent commitment to the population at various distances from the discharge location are listed in part (a) of Figure 3.19 and are shown diagrammatically in part (b). The dose received by populations within given radii were consistently far higher in 1984 than in 1985, despite the fact that the reported amount of  $^{14}\text{CO}_2$  discharged by Sellafield in 1984, 7 TBq (BNF, 1985), is only slightly greater than the activity discharged in 1985, 6.6 TBq. This discrepancy is a result of the fact that, in general, the wind, during the 1984 growing season, was directed more frequently than in 1985

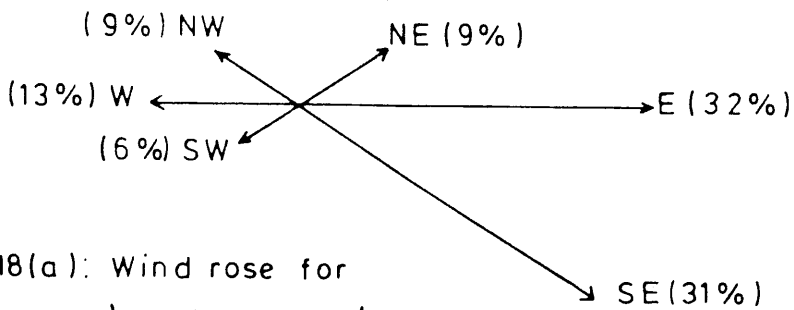


FIGURE 3.18(a): Wind rose for 'growing period' (Sellafield, 1984).

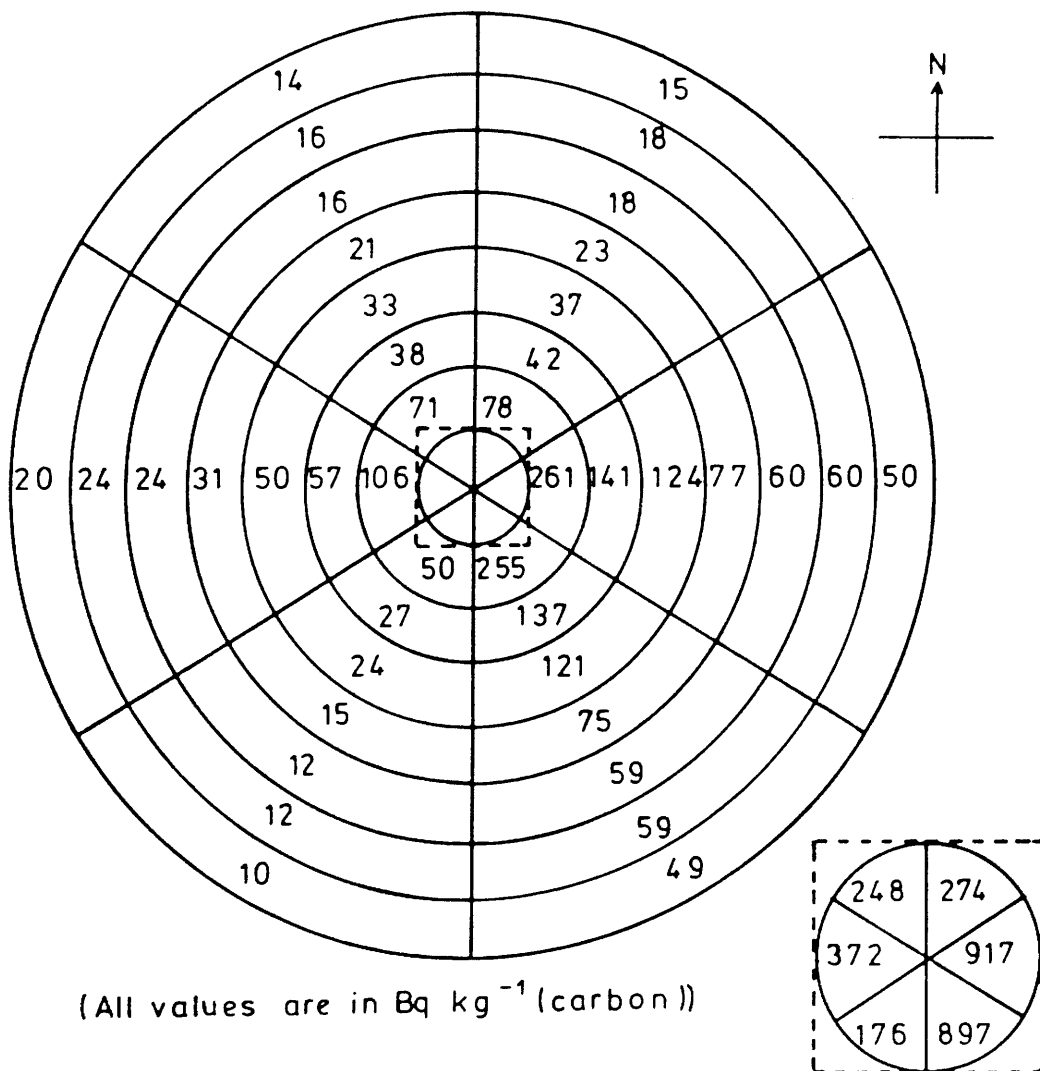
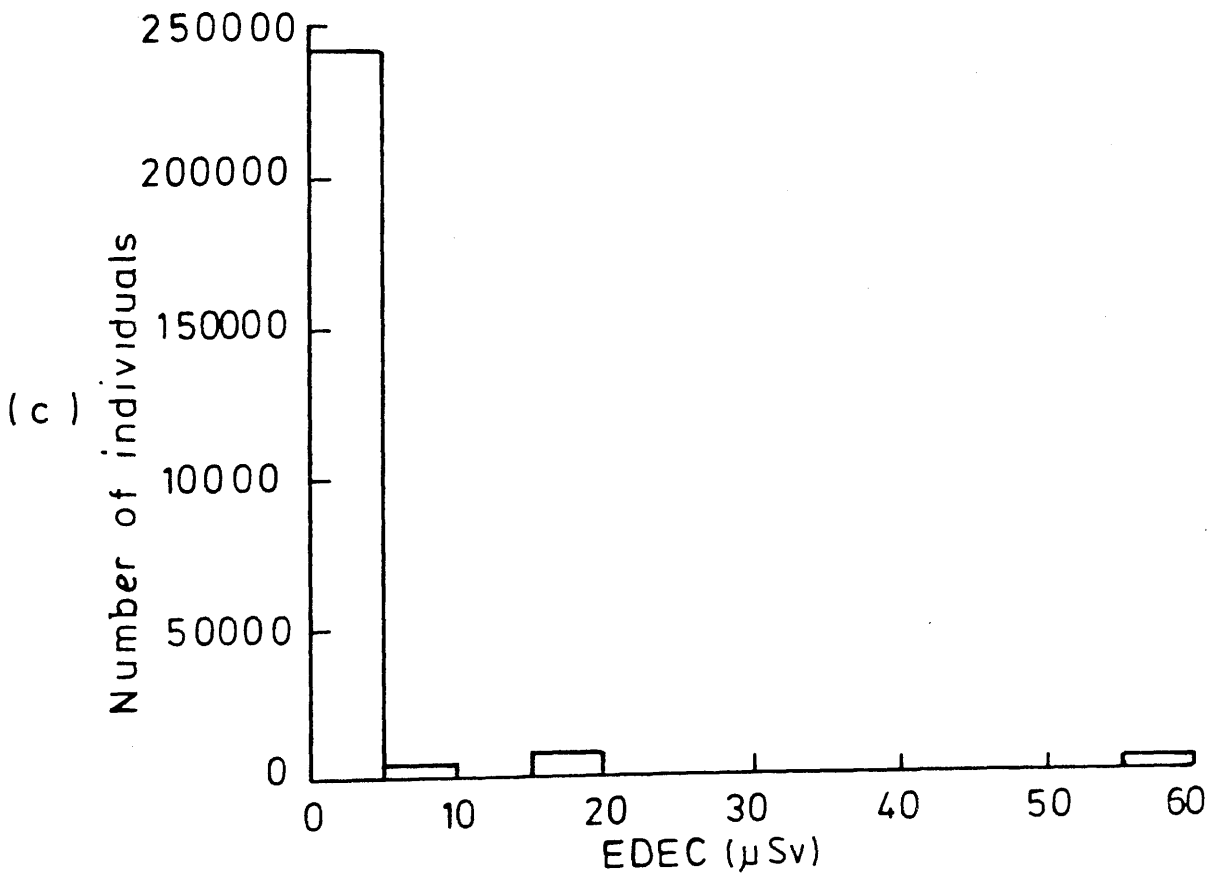
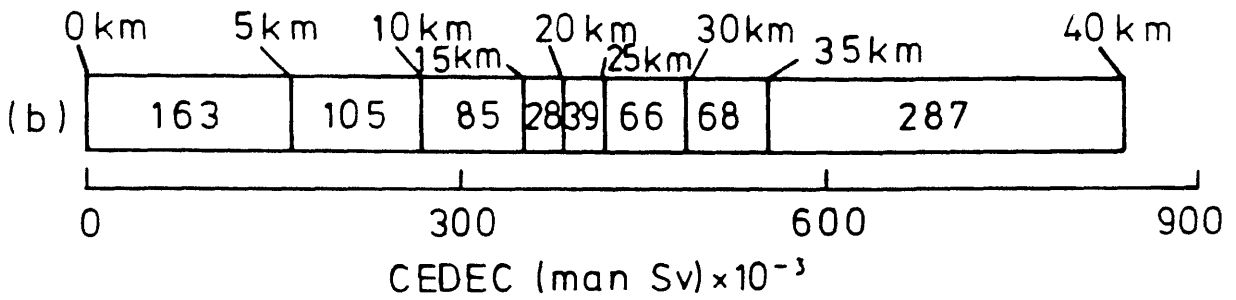


FIGURE 3.18(b): Spatial distribution of  $^{14}C$  around Sellafield, 1984.

(a)

Radius (km)	0-5	0-10	0-15	0-20	0-25	0-30	0-35	0-40
CEDEC (man Sv) $\times 10^{-3}$	163	268	353	381	420	486	554	841



(d) Maximum individual EDEC = 0.15 mSv.

FIGURE 3.19: Doses to the population around Sellafield, from  $^{14}\text{CO}_2$  discharges in 1984.

towards more densely populated areas. The 40 km collective effective dose equivalent commitment value of 0.841 man Sv derives its largest contribution from the large population areas in the 35-40 km region, although the next largest contribution comes from the sparsely populated area within 5 km of Sellafield. The latter population will obviously be receiving far larger individual doses than the former. The range of individual effective dose equivalent commitments for 1984, shown in part (c) of Figure 3.18, is also greater than in 1985 but, again, the large majority of the dose was received at relatively low levels. This, however, does not give an accurate assessment of the maximum individual dose received by a member of the exposed population.

Inspection of the wind rose (Figure 3.18(a)) and the spatial distribution of the  $^{14}\text{C}$  around Sellafield (Figure 3.18(b)) suggests that the maximum exposed individual will live in the sector to the east of Sellafield. The maximum observed  $^{14}\text{C}$  level is found 0.4 km NE of the plant, being, in this case,  $730 \text{ Bq kg}^{-1}$  (carbon) above background. According to the wind rose, this corresponds to a maximum predicted  $^{14}\text{C}$  level of  $2444 \text{ Bq kg}^{-1}$  (carbon), approximately 0.4 km to the east of the source. This value, in turn, corresponds to an annual effective dose equivalent of 0.15 mSv or, in other words, an effective dose equivalent commitment of 0.15 mSv as stated in part (d) of Figure 3.19, to the maximum exposed individual (or 3% of the annual effective dose equivalent limit of 5 mSv). Once again, it is possible that the maximum  $^{14}\text{C}$  level measured does not correspond to the actual maximum level along the NE sector but, in all likelihood, any differences between these two values will be rather small.

Finally, it is worth briefly considering how the collective dose estimates vary between methods of calculation. As before, three distinct methods were used here; the collective doses could be derived from the experimental data, from the predictions of the Gaussian dispersion model or from the predictions of the hyperbolic function previously defined. The collective effective dose equivalent commitment estimates at various distances from Sellafield, for all 3 methods, are listed in Table 3.12. Also listed are the estimates used in this work which were based on the

Table 3.12: Estimates of the collective effective dose equivalent commitment to the population around Sellafield (1984) from various techniques

Distance band (km)	CEDEC ( $10^{-3}$ man Sv)			
	Experimental data	Gaussian plume model	Hyberbolic model	This work
0-5	163	11	179	163
0-10	268	18	286	268
0-15	353	22	382	353
0-20	381	24	407	381
0-25	420	26	452	420
0-30	486	28	529	486
0-35	-	30	597	554
0-40	-	41	885	841

experimental data over the 0-30 km distance and on the data from the hyperbolic function over the 30-40 km distance. At all distances the estimates from the experimental data and the hyperbola are very similar. Those derived from the Gaussian dispersion model are consistently around 20 times smaller than the other two methods. So, as regards the two atmospheric dispersion models, the conclusions drawn from this data set agree with those from the 1985 study. In other words, once again, the results suggest that, for the calculation of the radiological impact of  $^{14}\text{CO}_2$  discharges from Sellafield, the Gaussian dispersion model is totally inappropriate, whereas the simple hyperbolic model is most suitable.

### 3.3.2.3 1983

The assessment of the dose to the local population due to the  $^{14}\text{CO}_2$  discharges from Sellafield in 1983 is based on the principles used for the years 1984 and 1985. The same values for the width and radii of the annular segments are used. The spatial distribution of the population is assumed to be the same and the assessment is again limited to the area within 40 km of the plant. The experimental programme in this year, the results of which have been presented in Figure 3.3, only covered the area within 11 km of the plant. Once again, therefore, in order to estimate the doses to the exposed population within 40 km of Sellafield, it is necessary to make use of atmospheric dispersion models.

Despite the unfavourable reports obtained for the years 1984 and 1985, the applicability of the Gaussian dispersion model is initially investigated. The data used in the calculation are listed in Table 3.13 and the model's predictions of the atmospheric  $^{14}\text{C}$  levels are plotted in Figure 3.20 along with the observed values. As before, the results indicate that the Gaussian dispersion model does not accurately represent the true situation for this year. The predicted  $^{14}\text{C}$  levels are consistently smaller than the observed levels. The maximum predicted level of  $38 \text{ Bq kg}^{-1}$  (carbon) above background, approximately 1 km from the plant, bears little resemblance to the maximum observed level of  $668 \text{ Bq kg}^{-1}$  (carbon) 0.4 km away.

The next step is to attempt to match the observed  $^{14}\text{C}$

Table 3.13: Data for Gaussian dispersion model (Sellafield, 1983)

Stability category (j)	Frequency of occurrence ( $f_j$ )	Average wind speed at 10 m ( $U_{10j}$ ) ( $m s^{-1}$ )	Mixing layer depth ( $A_j$ ) (m)
A	$2.1 \times 10^{-3}$	1.7	1300
B	$1.8 \times 10^{-2}$	2.5	900
C	$3.5 \times 10^{-2}$	3.5	850
D	$5.6 \times 10^{-2}$	8.2	800
E	0	-	-
F	$4.5 \times 10^{-4}$	2.6	100
G	0	-	-

ADDITIONAL DATA:

- (1) Release rate (Q) =  $0.22 \text{ MBq s}^{-1}$ ,
- (2) Release height (h) = 120 m,
- (3) Ground roughness term ( $Z_0$ ) = 0.4 m,
- (4) Ground roughness coefficient (n) = 0.275,
- (5) Angular width of sector ( $\alpha$ ) =  $\pi / 3$ .

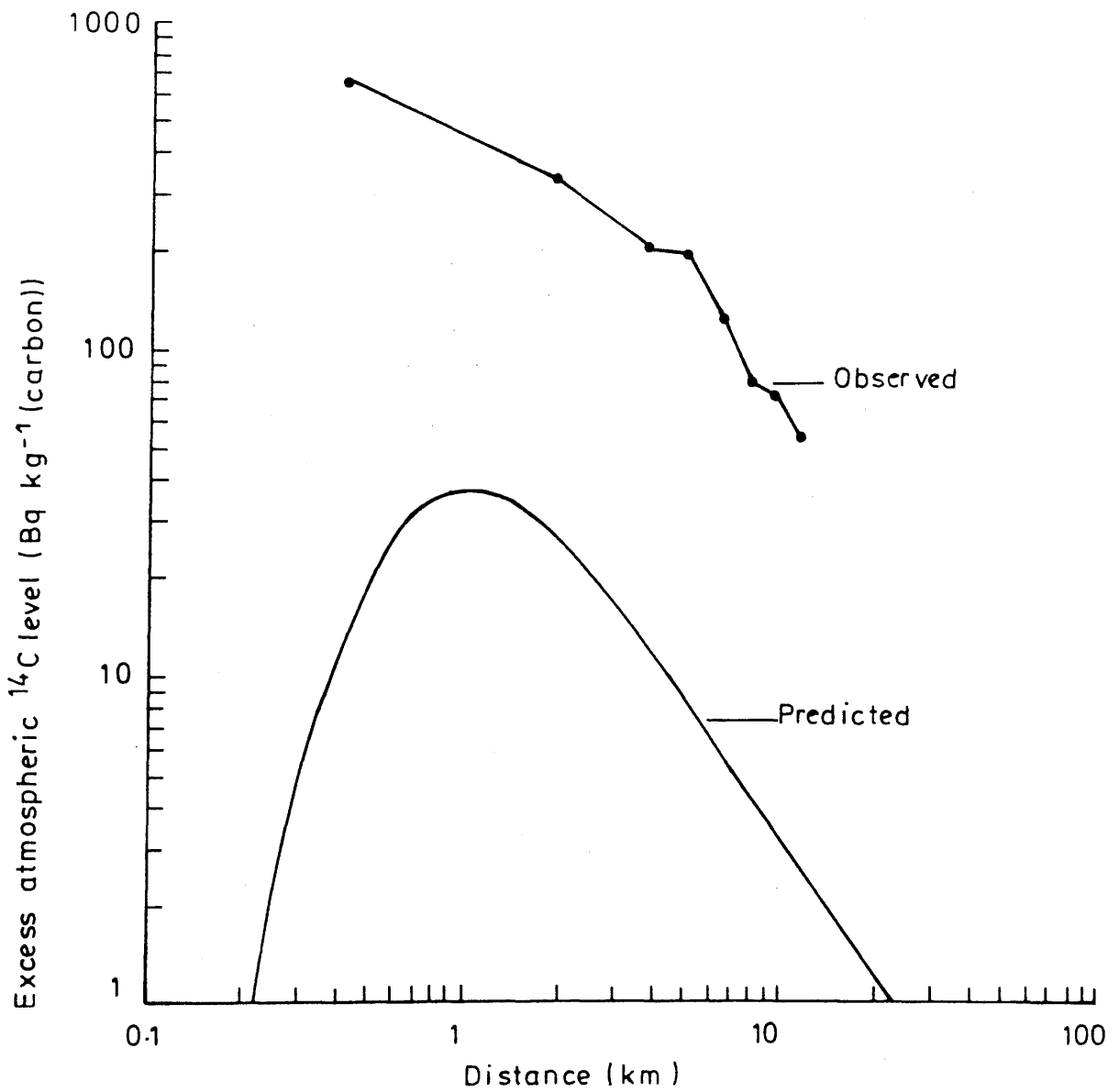


FIGURE 3-20: Atmospheric  $^{14}\text{C}$  levels around Sellafield in 1983, as predicted by the Gaussian dispersion model.

levels (for distances greater than 1 km) to a hyperbolic function. This has been done in Figure 3.21 and again the degree of fit is excellent ( $R^2 = 95\%$ ). The best fit line is  $y = 667x + 293$  with a standard deviation of  $29 \text{ Bq kg}^{-1}$  (carbon). The ordinate intercept of  $293 \text{ Bq kg}^{-1}$  (carbon) is again close to the measured  $^{14}\text{C}$  background level.

The  $^{14}\text{C}$  levels along the NE transect between 0-10 km are obtained from the experimental data and those from 10-40 km are obtained from the hyperbolic model. These data, when combined with the wind rose for that year's growing season (shown in Figure 3.22 (a)), give an estimate of the  $^{14}\text{C}$  levels around Sellafield in all directions (Figure 3.22 (b)). These  $^{14}\text{C}$  levels are used together with the population grid to estimate the radiation dose to the local population and the results are shown in Figure 3.23. It should be remembered that the accuracies of the  $^{14}\text{C}$  activities and hence of the doses are not as high as in the previous years discussed because of the fewer number of samples on which the values are based.

The collective effective dose equivalent commitment to the local population is tabulated in part (a) of Figure 3.23 and is shown diagrammatically in part (b). The amount of  $^{14}\text{CO}_2$  discharged to the atmosphere from Sellafield in 1983 was 7 TBq (BNF, 1985), the same as in 1984. Nevertheless, the dose to the population within any given radius is greater than in 1984 and far greater than in 1985. This difference is due mainly to the prevailing wind direction, although it may be partially caused by the comparatively low resolution of the available data. The collective effective dose equivalent commitment, over a 40 km radius, of 1.28 man Sv is again comprised of a wide range of individual effective dose equivalent commitments, as shown in part (c) of Figure 3.23. Most of the doses are, however, delivered at levels well below the maximum range. The maximum individual dose must, of course, be calculated more accurately than this relatively low resolution picture permits.

The wind rose of Figure 3.22(a) indicates that the maximum  $^{14}\text{C}$  level and hence the maximum individual dose is again to be found in the easterly sector. The maximum observed  $^{14}\text{C}$

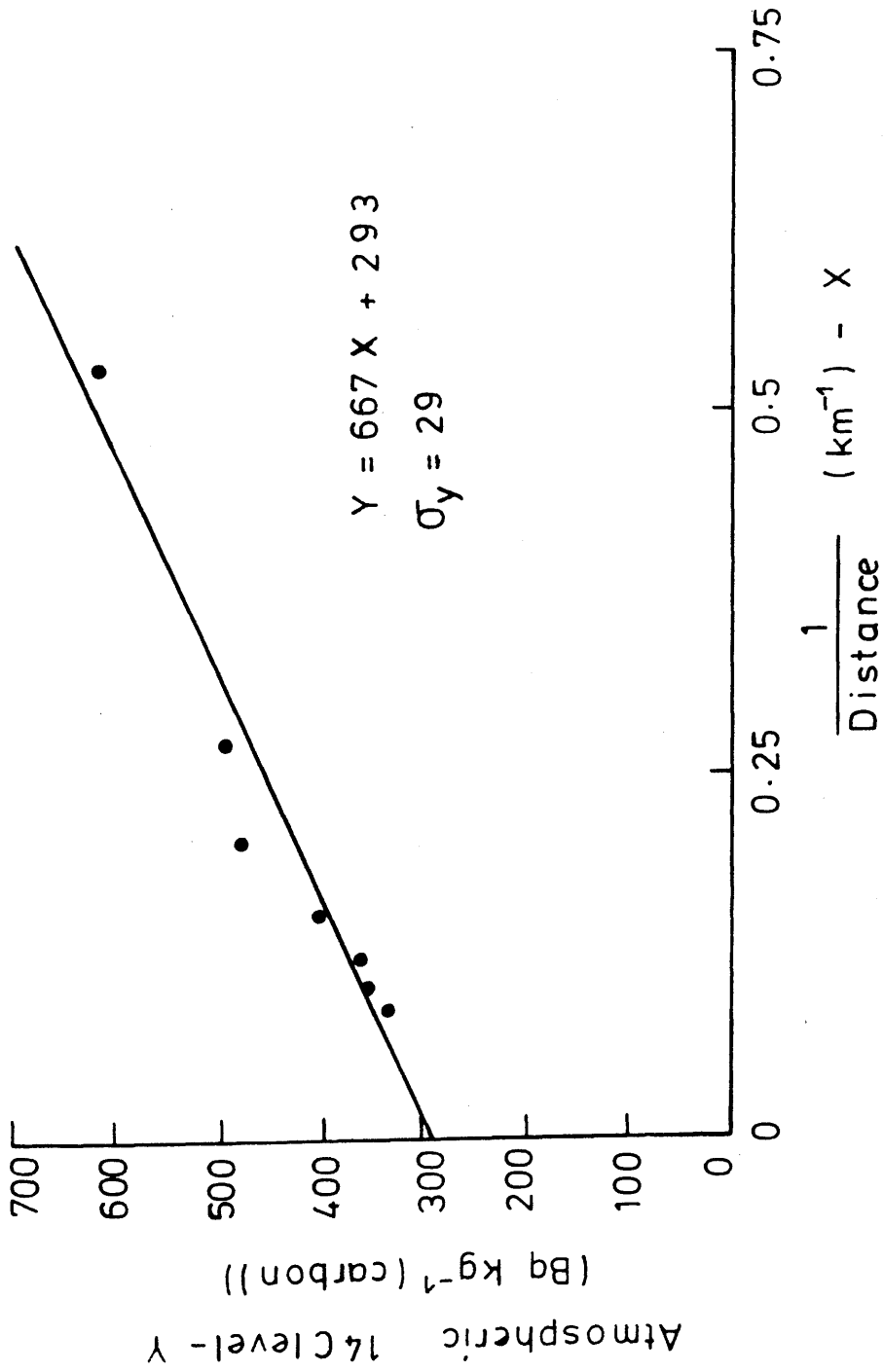


FIGURE 3.21: Atmospheric <sup>14</sup>C level versus distance<sup>-1</sup> for Sellafield, 1983 .

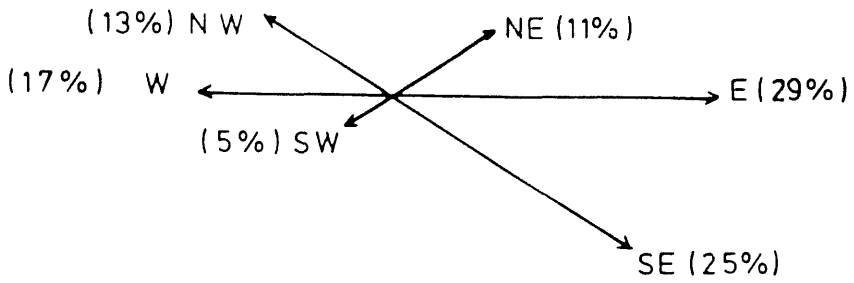


FIGURE 3.22:(a) Wind rose for 'growing period' (Sellafield, 1983).

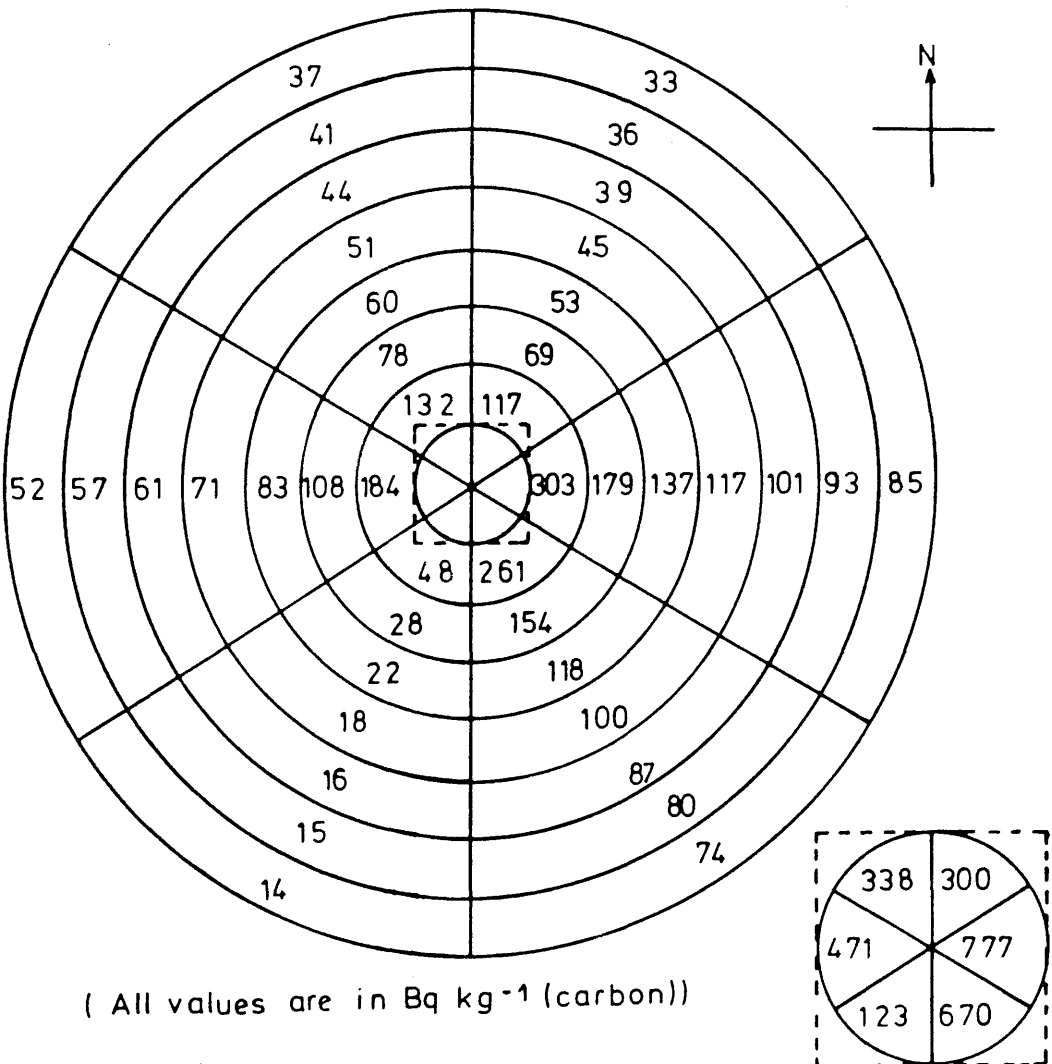
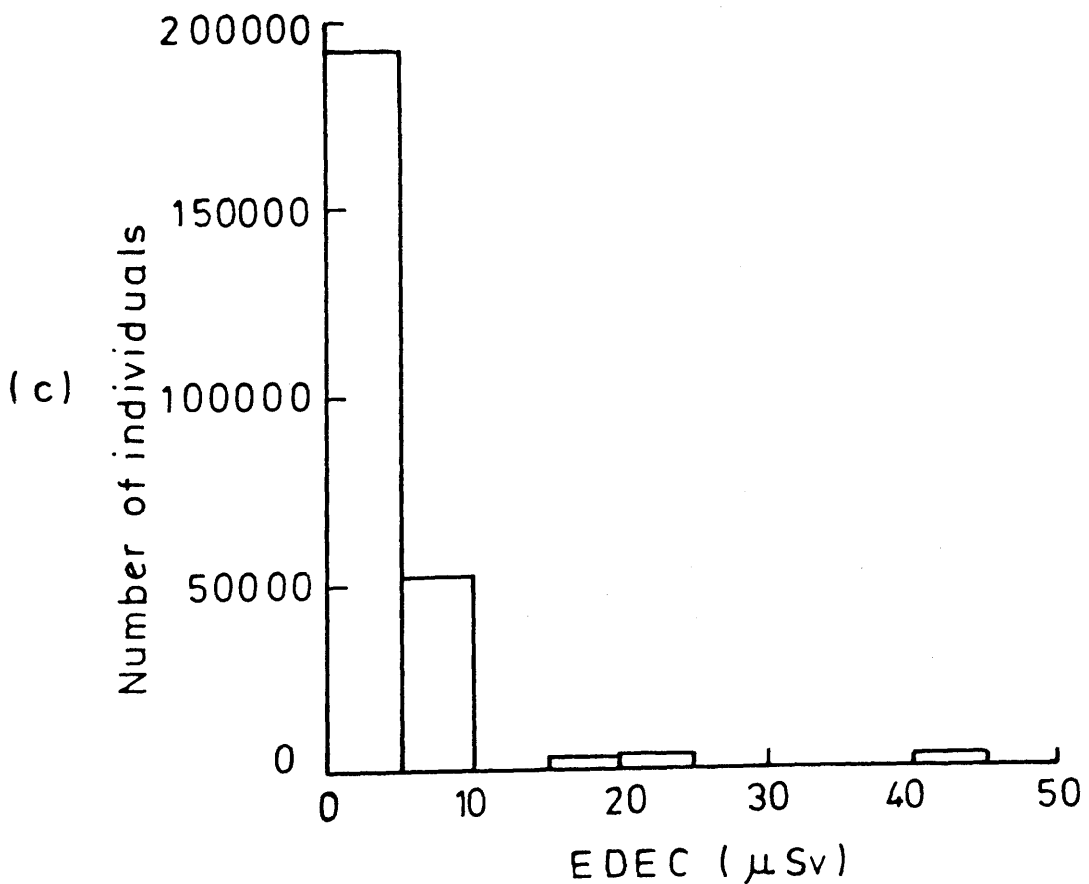
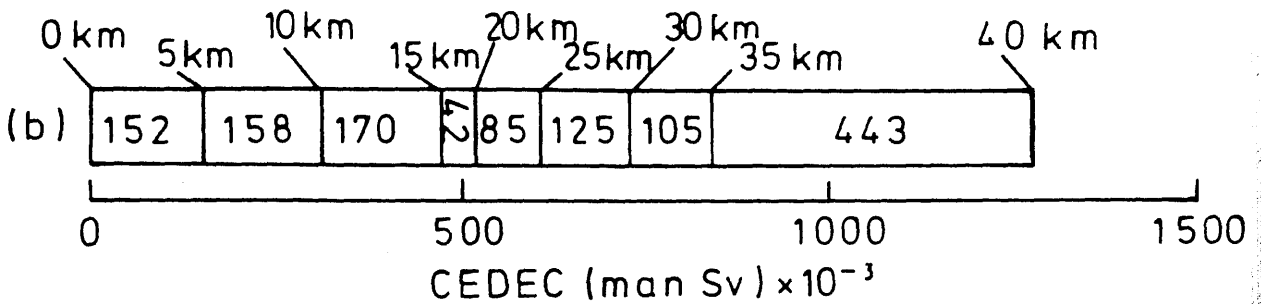


FIGURE 3.22(b): Spatial distribution of <sup>14</sup>C around Sellafield, 1983.

(a)

Radius (km)	0-5	0-10	0-15	0-20	0-25	0-30	0-35	0-40
CEDEC (man Sv) $\times 10^{-3}$	152	310	480	522	607	732	837	1280



(d) Maximum individual EDEC = 0.11 mSv.

FIGURE 3.23: Doses to the population around Sellafield, from 14  $\text{CO}_2$  discharges in 1983.

level in the NE sector is found 0.4 km from Sellafield, this time at 667 Bq kg<sup>-1</sup> (carbon) above background. The wind rose suggests that this would correspond to a maximum <sup>14</sup>C level in the Sellafield environment of 1730 Bq kg<sup>-1</sup> (carbon), 0.4 km to the east of the discharge location. This <sup>14</sup>C level delivers an effective dose equivalent commitment or an annual effective dose equivalent of 0.11 mSv to the maximum exposed individual, as stated in part (d) of Figure 3.23 (which corresponds to 2.2% of the annual effective dose equivalent limit of 5 mSv).

Finally, the three methods for calculating the atmospheric <sup>14</sup>C levels are used separately to estimate the collective effective dose equivalent commitment to the local population. The results from the three techniques are listed in Table 3.14 along with the results obtained in this study (which were derived from a hybrid of the experimental data and the hyperbolic model). The estimates of the doses calculated using the Gaussian dispersion model are consistently an order of magnitude lower than those calculated via the other two techniques, which are in good agreement with each other. This is a phenomenon which recurs throughout the three years investigated and emphasises the superiority of the hyperbolic model over the Gaussian dispersion model in predicting the <sup>14</sup>C levels around Sellafield and hence the doses to the local population.

#### 3.3.2.4 1952-1982

An assessment of the radiological impact of the <sup>14</sup>CO<sub>2</sub> discharges to the atmosphere from Sellafield prior to 1983 is based on the assay of the individual rings of a larch tree which grew in the NE sector approximately 1.3 km from the release point. The <sup>14</sup>C levels measured in the tree rings have previously been presented in Figure 3.7.

To conform with the criteria set up in the initial part of this study, the doses are only calculated up to 40 km from the plant. The same values for the width and radii of the annular segments are also used and the spatial distribution of the population is assumed to be the same as that used previously. Although this latter assumption is probably wrong, any errors

Table 3.14: Estimates of the collective effective dose equivalent commitment to the population around Sellafield (1983) from various techniques

Distance band (km)	CEDEC ( $10^{-3}$ man Sv)			
	Experimental data	Gaussian plume model	Hyberbolic model	This work
0-5	152	12	183	152
0-10	310	21	328	310
0-15	-	25	497	480
0-20	-	26	540	522
0-25	-	28	624	607
0-30	-	31	749	732
0-35	-	33	854	837
0-40	-	38	1298	1280

introduced by its use will be rather small. It is not possible to determine the radiation dose to the local population entirely from the experimental data since there is only one measured  $^{14}\text{C}$  level for each year. It is necessary, therefore, to use atmospheric dispersion models to extrapolate values for the  $^{14}\text{C}$  levels at other distances. In light of the results obtained for the years 1983, '84 and '85 it was decided to use the simple hyperbolic function method as opposed to the Gaussian dispersion model.

To define the hyperbolic function for a particular year, only two points need to be known, one of which can be obtained from the experimental data. The other point is obtained by assuming that, for each year, the  $^{14}\text{C}$  level at an infinite distance from the discharge location is equal to the background level. From these two points a hyperbola can be defined which can then be used to calculate the  $^{14}\text{C}$  levels at all distances in the NE sector greater than 1 km from the plant. The  $^{14}\text{C}$  levels at all distances in other directions can be interpolated from these values using the wind rose data as before. Due to the approximate nature of this calculation, it did not seem necessary to obtain the annual wind rose for every year of the study. Therefore, an average wind rose (derived from the years 1981-1985) is used for these calculations and is shown in Figure 3.24. This approximation may detract slightly from the accuracy of the data for a single year but will not significantly influence the accuracy of the work over the entire period. The doses to the exposed population at various distances from the plant are then determined in the manner previously described. The equation of the hyperbola obtained for each year is shown in Table 3.15 along with the doses received within various distances from Sellafield. Also listed is the maximum individual effective dose equivalent commitment received in each year by a person in the Sellafield area. As in earlier cases, the maximum individual dose is received by a person located about 0.4 km to the east of the plant. The manner in which the maximum individual dose is calculated will now be explained.

It can be assumed that the maximum  $^{14}\text{C}$  level in the NE transect will depend, basically, on the release rate and hence the

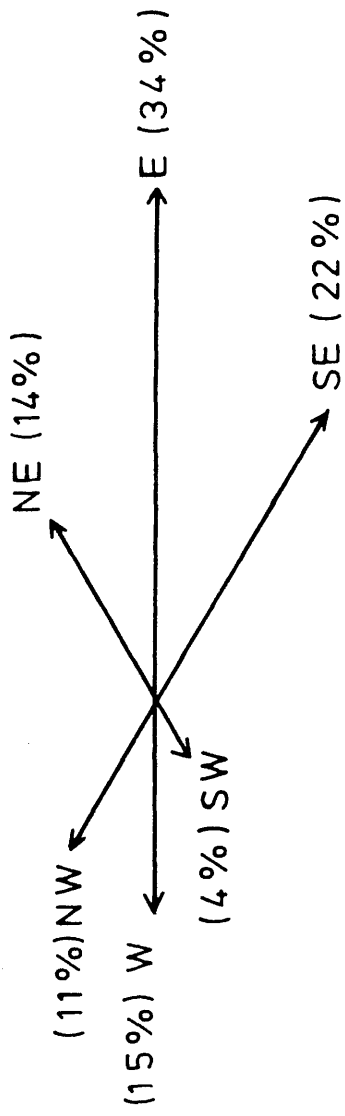


FIGURE 3.24; Average wind rose for 'growing period' (Sellafield, 1981-1985).

Table 3.15: Doses to the population around Sellafield (1952-1982) from tree data

Year	Hyperbolic function	Maximum individual EDEC ( $\mu\text{Sv}$ )	CEDEC ( $10^{-3}$ man Sv)			
			0-5 km	0-10 km	0-20 km	0-40 km
1952	$y = 10x + 220$	4	2	3	5	10
1953	$y = 16x + 221$	6	3	5	8	16
1954	$y = 46x + 226$	17	9	16	24	47
1955	$y = 38x + 229$	14	7	13	20	39
1956	$y = 17x + 237$	6	3	6	9	17
1957	$y = 22x + 246$	8	4	8	11	22
1958	$y = 22x + 260$	8	4	8	11	22
1959	$y = 51x + 278$	19	10	17	27	52
1960	$y = 39x + 278$	14	8	13	20	40
1961	$y = 35x + 283$	13	7	12	18	36
1962	$y = 24x + 319$	9	5	8	13	24
1963	$y = 0x + 454$	0	0	0	0	0
1964	$y = 38x + 434$	14	7	13	20	39
1965	$y = 91x + 409$	33	18	31	48	93
1966	$y = 101x + 389$	37	20	34	53	103
1967	$y = 286x + 371$	105	55	97	150	292
1968	$y = 464x + 362$	170	90	158	243	474
1969	$y = 214x + 359$	79	41	73	112	219
1970	$y = 163x + 351$	60	32	55	85	167
1971	$y = 111x + 347$	41	21	38	58	113
1972	$y = 329x + 338$	121	64	112	172	336
1973	$y = 457x + 331$	168	89	155	240	467
1974	$y = 229x + 324$	84	44	78	120	234
1975	$y = 559x + 316$	205	108	190	293	571
1976	$y = 564x + 308$	207	109	191	296	576
1977	$y = 419x + 302$	154	81	142	220	428
1978	$y = 134x + 298$	49	26	45	70	137
1979	$y = 151x + 292$	55	29	51	79	154
1980	$y = 215x + 287$	79	42	73	113	220
1981	$y = 411x + 283$	151	80	140	215	420
1982	$y = 581x + 279$	213	113	197	305	594

gradient of the hyperbola, although it cannot be calculated directly from this since the hyperbola only operates at distances greater than 1 km. Hence the maximum  $^{14}\text{C}$  levels have been derived by direct analogy with the 1985 observations. For 1985, the maximum observed  $^{14}\text{C}$  level along the NE transect was 2.3 times greater than the 1 km level predicted by the hyperbola and thus it is assumed that this relationship holds true for other years. The 1985 transect was chosen in preference to the 1983 or 1984 transects because a far greater number of samples were collected in this year and so the maximum observed  $^{14}\text{C}$  level is more likely to represent the actual maximum level. The wind rose (Figure 3.24) indicates that the maximum  $^{14}\text{C}$  level in the Sellafield environment will be found to the east of the plant. The maximum  $^{14}\text{C}$  level in the eastern sector for any year can then be obtained by multiplying the maximum NE value by 2.4 (the ratio of the time in which the wind direction was towards the east to that towards the north-east). The dose to the individual is calculated as before.

Earlier in this work, it was mentioned that measurements of  $^{14}\text{C}$  levels in the Sellafield environment had been made for the years 1981 and 1982 by other workers. The results of these studies can now be used to help assess the validity of the technique used to extrapolate  $^{14}\text{C}$  levels around Sellafield from the tree data. Although neither of these sampling programmes was as detailed as those here, they do provide a step up in resolution from the single tree ring measurements. It was therefore decided to compare the hyperbolic functions defined by the two separate data sets for each year. The hyperbola for 1982, based on the results of Baxter and McKay (1983), is defined by the equation  $y = 592x + 287$  (with a standard deviation about the line of  $40 \text{ Bq kg}^{-1}$  (carbon)). This hyperbola is all but identical to that obtained from the tree ring data (as listed in Table 3.15) and so lends considerable confidence to the technique used here. The hyperbola for 1981, as determined from the results of Otlet et al. (1983), is defined by the equation  $y = 1113x + 173$  (with a standard deviation about the line of  $61 \text{ Bq kg}^{-1}$  (carbon)). Now this equation differs markedly from that determined from the tree data. The gradient is almost 3 times larger than that used in this work and, perhaps more interestingly still, the

background level of  $173 \text{ Bq kg}^{-1}$  (carbon) is well below the measured level of  $283 \text{ Bq kg}^{-1}$  (carbon). Of all the years studied, this data set is unique in failing to predict the background level with a reasonable degree of accuracy. This fact casts some doubt on the suitability of this data set for the task in hand. The differences in the background and the gradient values could be simply due to the relatively large errors on these values, as demonstrated by the large standard deviation about the line. The differences in the gradients could also be caused by the different growing seasons of the sampling material (Otlet et al. (1983) used hawthorn berries). However, such large differences between plants have certainly not been observed in this work and, anyway, Baxter and McKay (1983) sampled grass and still managed to obtain a good agreement with the wood sample. In all likelihood, the differences are due to both the large errors on the hyperbolae (caused by the small number of samples on which they are based) and the differences in the growing seasons of various sampling materials. To conclude, then, these other studies help to demonstrate that the basic technique used here appears to be reliable, although the errors on the results, which are only based on two separate experimental measurements, are likely to be considerable.

Now, instead of discussing the results for this period independently, these data will be combined with those obtained earlier and the doses for the entire period investigated, 1952-1985, will be reviewed.

#### 3.3.2.5 1952-1985

In the following discussion, all figures quoted should be treated with caution. Actual errors on the figures are not given as they themselves cannot be calculated with any degree of confidence. The accuracy of the data depends largely on the number of experimental observations on which they are based and hence the general trend in errors over this period is likely to be  $1952-1982 > 1983 > 1984 > 1985$ . It is suffice to say that all values quoted merely give an estimate of the magnitude of the quantity being discussed. Nevertheless, particularly in the absence of any alternative data, these values are useful in assessing the radiological impact to the local population from the

$^{14}\text{CO}_2$  discharges from Sellafield between 1952 and 1985.

The annual collective effective dose equivalent commitment to the exposed population within selected distances from Sellafield (5, 10, 20 and 40 km) for the period of interest is shown in Figure 3.25. Within this range, the collective dose to a population within any given distance appears to be fairly uniform, independent of how remote the population is from the plant (i.e. 0-10 km or 10-20 km, etc.). This phenomenon, which was more clearly seen in the individual years 1983, '84 and '85 assessed earlier, appears to occur throughout the entire period and is caused by cancellation of the decrease in  $^{14}\text{C}$  levels as distance from Sellafield increases by the increase in population as distance increases. The main trend which becomes apparent from this graph is one of large fluctuations in doses from year to year, superimposed on a general increase in doses to the local population. In fact, the largest doses were received in 1983, with the collective effective dose equivalent commitment to the population within 40 km of the plant being almost 1.3 man Sv.

The cumulative collective effective dose equivalent commitment to the population within 40 km of Sellafield has been plotted in Figure 3.26. This shows that the collective effective dose equivalent commitment to the population within 40 km of Sellafield from its  $^{14}\text{CO}_2$  discharges for the period 1952-1985 is 8.4 man Sv, with almost half of this dose due to discharges since 1980. Using the formulation discussed in Section 1.4.1.2, this dose can be converted into a measure of health effects (remembering that for  $^{14}\text{C}$  the dose equivalent in any organ is the same as the effective dose equivalent). Thus, based on the risk coefficients recommended by ICRP, the  $^{14}\text{CO}_2$  discharges from Sellafield from 1952-1985 will cause 0.1 fatal cancers and 0.07 hereditary effects in the population within 40 km of the plant.

As adequately demonstrated for the years 1983-85, a wide range of individual doses contributes to the collective dose to the exposed population and this matter will be considered no further. However, it is of interest to examine the variation in effective dose equivalent commitment to the maximum exposed

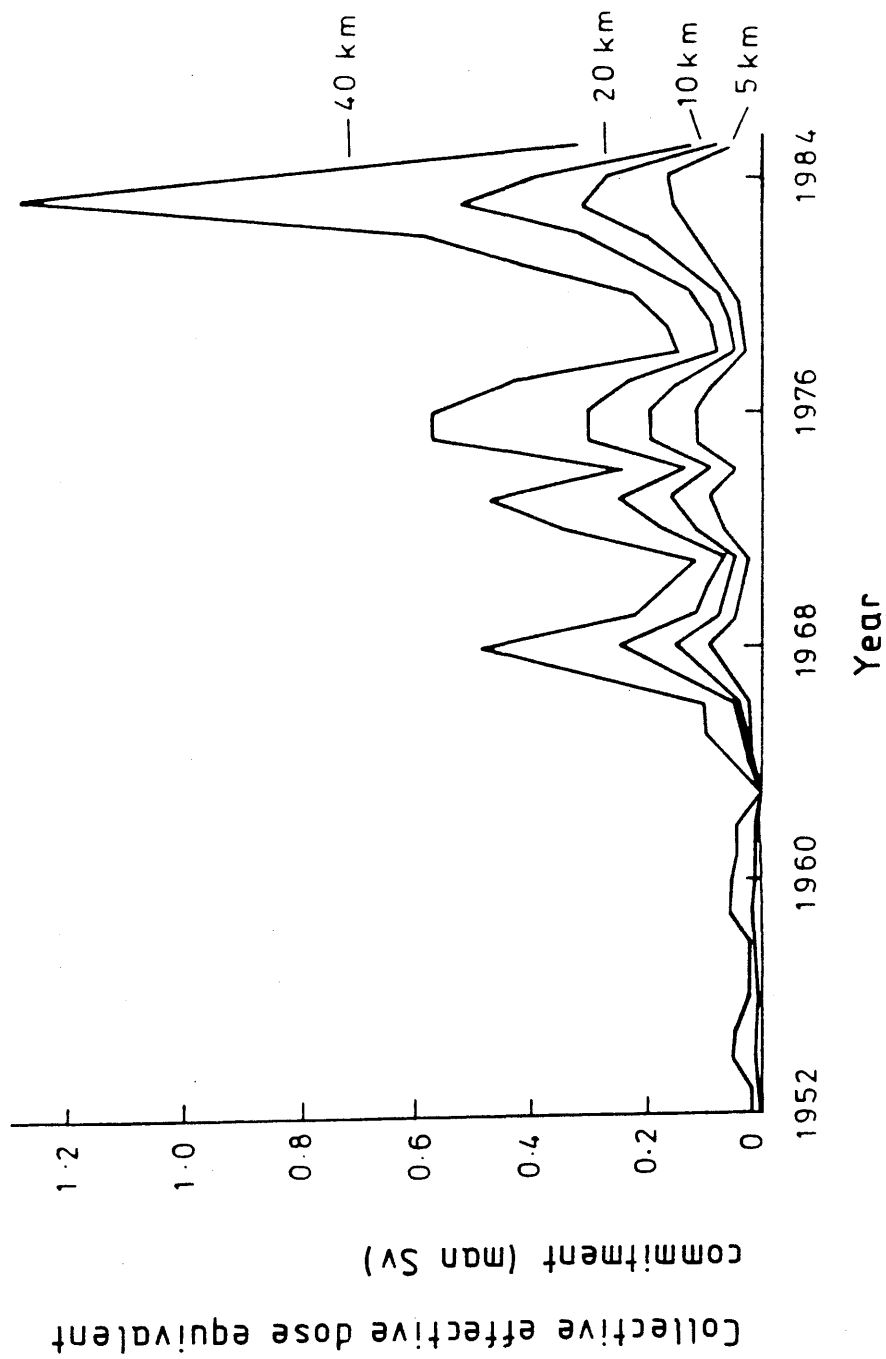


FIGURE 3-25: Annual collective effective dose equivalent commitment to populations within various distances of Sellafield, 1952-1985.

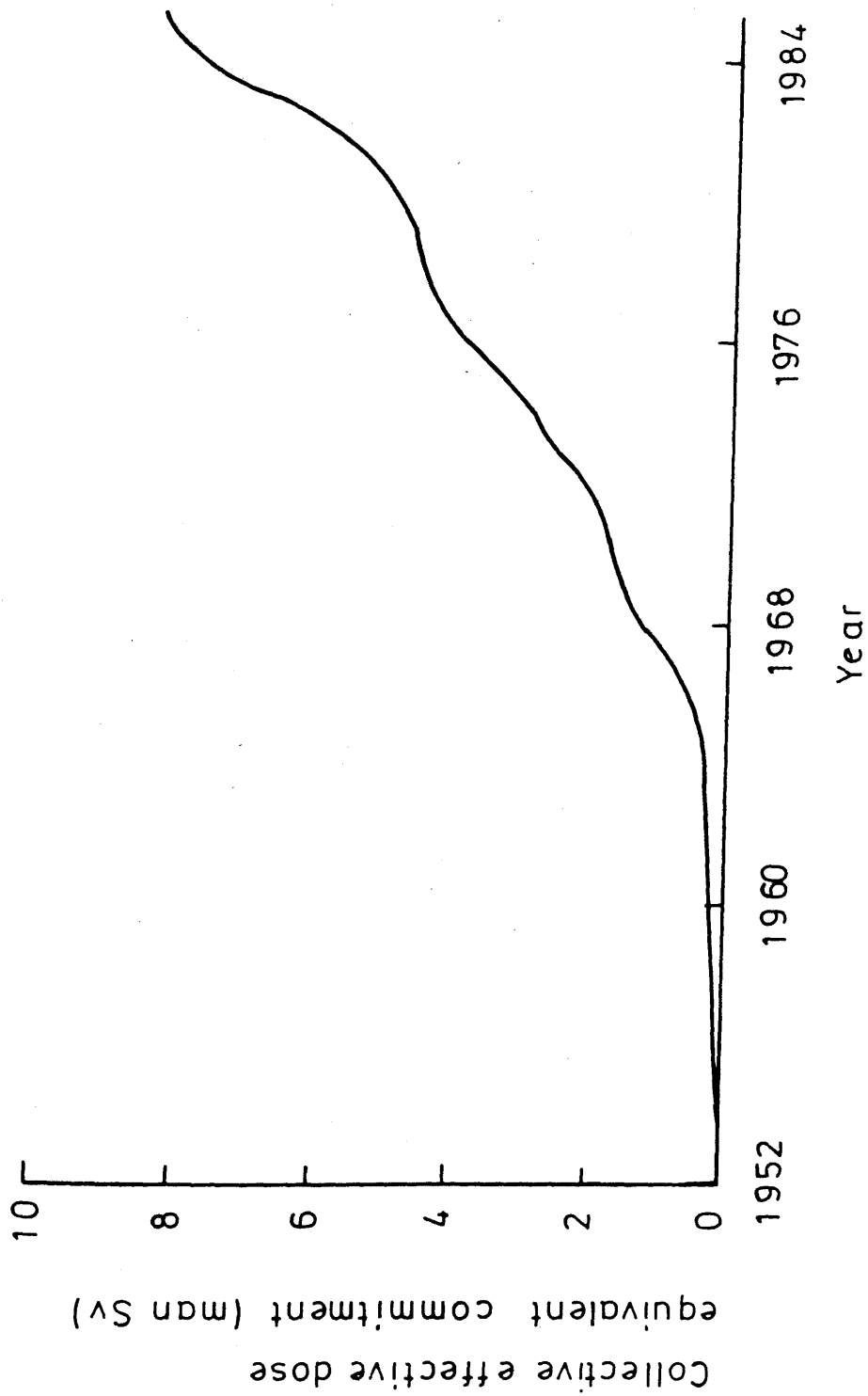


FIGURE 3-26: Cumulative collective effective dose equivalent commitment to the population within 40km of Sellafield, 1952 - 1985.

individual member of the public throughout the period of operation of Sellafield. This has been illustrated in Figure 3.27, in which both the annual variation and the cumulative total have been plotted. The highest annual individual dose was 0.2 mSv, received by a person located around 0.4 km to the east of Sellafield in 1982. This dose corresponds to 4.2% of the annual effective dose equivalent limit of 5 mSv for members of the public, as defined by ICRP. It is also stated by ICRP that the continued exposure of an individual over a lifetime should not average more than 1 mSv year<sup>-1</sup>. Now, assuming that the same person has received the maximum individual dose to members of the public for each of the 34 years during which Sellafield has been operating, then the cumulative dose, as shown in Figure 3.27, would amount to 2.5 mSv, or 7.4% of the recommended limit. Thus, even in this extreme case, the <sup>14</sup>C discharges from Sellafield have until now been well within the recommended limits. However, these limits apply to the combined exposure of the population from many nuclides and practices and they cannot be used to limit a given single practice. In fact, exposures at the limit from one single practice would leave no margin for other practices which would expose the same group. Thus, although the <sup>14</sup>CO<sub>2</sub> discharges from Sellafield do not exceed the limits recommended by ICRP, this fact in itself does not justify the discharges. Justification of such discharges is a totally different question altogether and lies outside the scope of the present study.

Throughout this discussion, reference has been made to the <sup>14</sup>CO<sub>2</sub> discharges from Sellafield during the period 1952-1985; however, these discharges have not yet been quantified. This deficiency reflects the fact that BNF plc only have a partial record of the <sup>14</sup>C discharges (from 1978 onwards) and, even then, the accuracy of these data is by no means assured. Only recently, in their 1984 annual report (BNF, 1985), it was reported that a new source of <sup>14</sup>C had been discovered within Sellafield and that all previously stated annual releases should be increased by a factor of 2. It was decided, therefore, to construct a record of the <sup>14</sup>CO<sub>2</sub> discharges from Sellafield based on the data collected in this study. The techniques used and the assumptions made will now be explained.

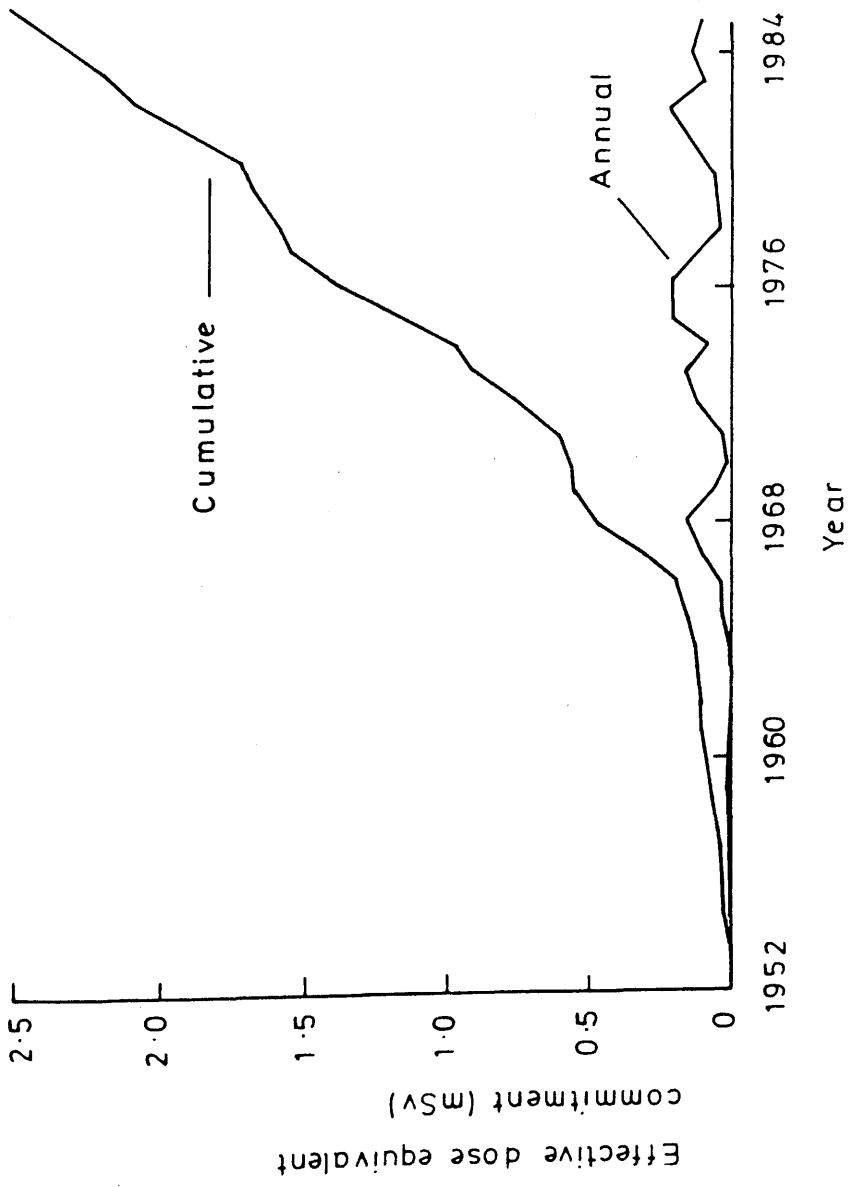


FIGURE 3-27: Effective dose equivalent commitment to the maximum exposed individual around Sellafield, 1952-1985.

As previously stated, the gradient of the hyperbola, which describes the dispersion of  $^{14}\text{CO}_2$  along the NE transect, is dependent only on the  $^{14}\text{CO}_2$  release rate into the NE sector, for a given set of meteorological conditions (frequency of stability categories, wind speed, etc.). Thus, assuming a similar set of meteorological conditions in each year, the gradients of the hyperbolae indicate the relative amount of  $^{14}\text{CO}_2$  released into the NE sector from year to year. The relative amounts of  $^{14}\text{CO}_2$  discharged from Sellafield are then obtained by adjusting the gradients for the amount of time the wind direction was towards the NE sector during the growing season in that year. The appropriate wind roses are only known exactly for the years 1981-1985, with an average wind rose being used for the 1952-1980 period. Although small errors may be introduced into the results by using an average wind rose, they are likely to be insignificant in comparison to the errors inherent in the process of correcting the gradients for the variation in wind roses from year to year. For in the correction process, it is assumed that the  $^{14}\text{CO}_2$  release rate is constant all year round. The release of  $^{14}\text{CO}_2$  is known to be continuous all year round but it is not known whether or not the rate of release is constant. The problem caused by this phenomenon can be described with the help of an example. Consider 2 separate years in which the amounts of  $^{14}\text{CO}_2$  released were identical. In year A most of the  $^{14}\text{CO}_2$  was released during the growing season when the wind was blowing towards the NE sector, whereas, in year B, most of the  $^{14}\text{CO}_2$  was released outside the growing season. In the technique used in this work, the results will suggest that far more  $^{14}\text{CO}_2$  was discharged in year A than in year B. Unfortunately, this problem cannot really be overcome and it has to be assumed in this work that the release rate is constant throughout any given year. The exact same problems are also caused by the related assumption that the growth rate of the plant material sampled is constant throughout the growing season. So, in the light of these problems, it seems reasonable to use the average wind rose for the 1952-1980 period. Thus far, only the technique for predicting the relative release rate has been described. To convert these relative values to absolute values it has to be assumed that the data reported by BNF plc are correct for at least one year. It was considered that the

most recent data, i.e. the 1985  $^{14}\text{CO}_2$  release rate, is the most likely to be correct and thus the release rates in all years were calculated relative to this value. Both the annual and the cumulative discharge data, as calculated in this study, are plotted in Figure 3.28 along with the relevant data published by BNF plc.

According to the picture presented here, the  $^{14}\text{CO}_2$  discharges from Sellafield were very small until the mid 1960s since when they have been gradually, although not steadily, increasing. The most striking fact which is evident from Figure 3.28 is the discrepancy between the discharge data calculated here and those reported by BNF plc. For example, the largest annual discharges, as calculated here, were 20 TBq in both 1983 and 1984. According to BNF plc the largest annual discharge, for the period 1978-1985 was 19 TBq in the year 1981. There are a couple of possible explanations for this observation, the simplest being that the data published by BNF plc are wrong. Another possible explanation is that the discrepancy is due entirely to the large errors inherent in this prediction technique. Certainly, when the assumptions made about both the meteorological conditions and the  $^{14}\text{CO}_2$  release rate are taken into account, not to mention the errors inherent in the hyperbolic functions, it seems likely that the results quoted for any individual year will be very approximate. Nevertheless, assuming that the BNF plc data for 1985 are correct and that both the variation in the  $^{14}\text{CO}_2$  release rate within a year and the variation in meteorological conditions between years are effectively random, as opposed to systematic, then this technique will give a reasonably accurate estimate of the total amount of  $^{14}\text{CO}_2$  released from Sellafield between 1952 and 1985. The total amount released, as shown in Figure 3.28, is predicted to have been around 190 TBq. This value suggests a collective effective dose equivalent commitment rate to the population within 40 km of Sellafield of  $4.4 \times 10^{-2}$  man Sv TBq $^{-1}$  and a maximum annual effective dose equivalent commitment rate to an individual of 13  $\mu\text{Sv}$  TBq $^{-1}$ . Of course, the value of both of these quantities in a particular year will depend not only on the  $^{14}\text{CO}_2$  release rate but also on the prevalent meteorological conditions. However, these values do allow a quick estimate of the magnitude of the respective quantities to be made.

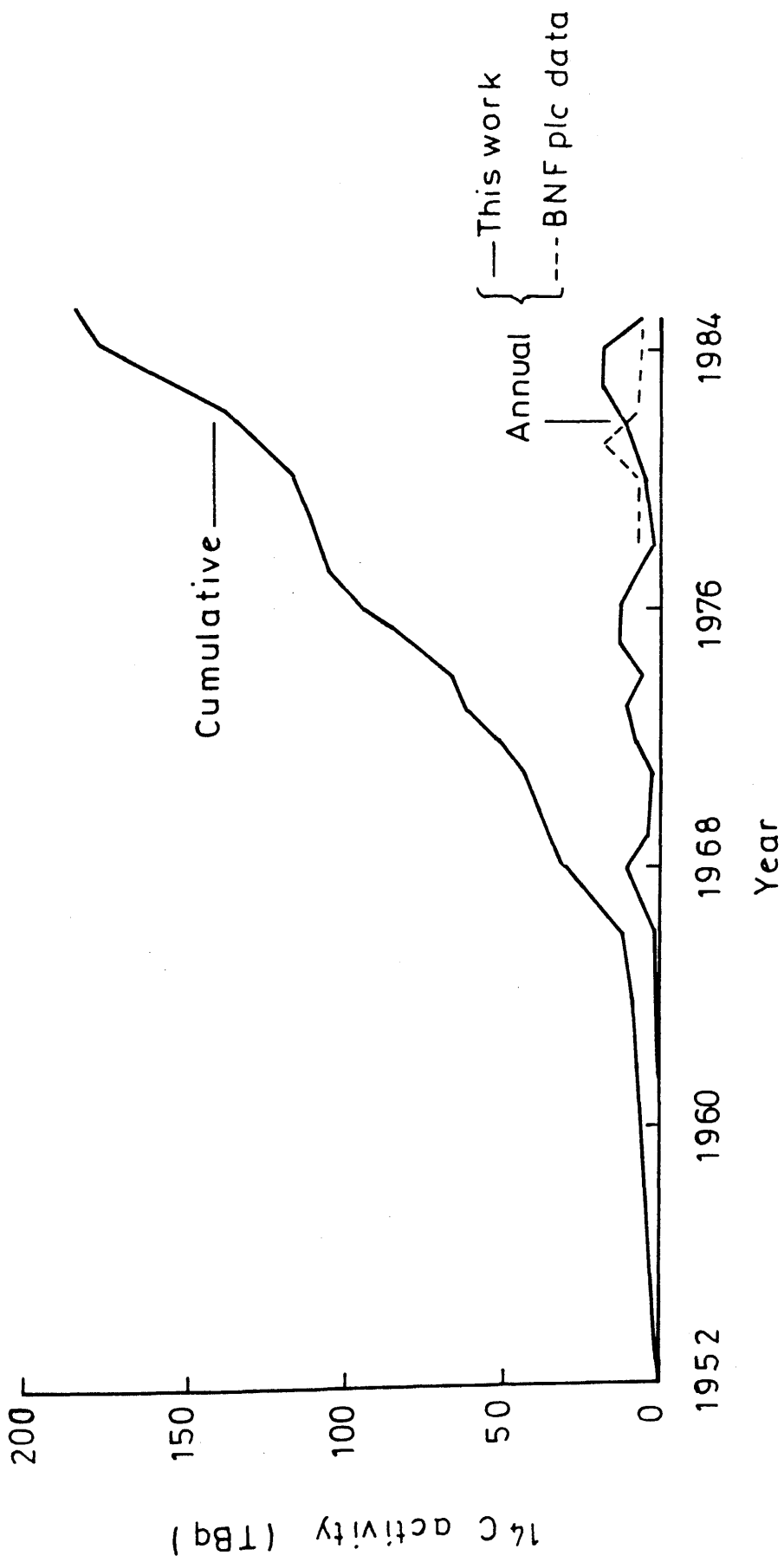


FIGURE 3.28;  $^{14}\text{C}$  discharges from Sellafield, 1952 - 1985.

To conclude then, the findings of this study will be briefly summarised. Firstly, the collective effective dose equivalent commitment to the population within 40 km of Sellafield, due to its  $^{14}\text{CO}_2$  discharges during the period 1952-1985, is 8.4 man Sv. This is not to suggest that 40 km is the limit of the extent of the local dose, rather that it is the limit of the distance over which the dose can be calculated with a reasonable degree of accuracy. Secondly, the maximum individual doses at no time during the 34 years investigated approached the recommended limits, the highest annual dose being 0.2 mSv (4% of the recommended limit of 5 mSv). Also, it should be remembered that a number of very conservative assumptions were made in the calculation of the doses. In particular, it was assumed that all the foodstuffs ingested by a person were derived at the location of the individual. In a study carried out by Wade et al. (1985), it was reported that only around 25% of the food ingested by the population around Sellafield was locally derived. This fact can be incorporated into the dose assessment process in a very simplistic manner, i.e. by assuming that 25% of an individual's foodstuff is derived from the location of the person and that the other 75% contains no excess  $^{14}\text{C}$ . Such an assumption would change the estimate of the collective effective dose equivalent commitment to the population within 40 km of Sellafield, due to its  $^{14}\text{CO}_2$  discharges during the period 1952-1985, to 2.1 man Sv. In other words, it would reduce the collective dose by a factor of 4. This suggests that individual doses would also be reduced by the same factor but it would be inappropriate to apply this criteria to the value for the maximum exposed individual as this latter quantity should represent the worst possible scenario. Indeed, this simplistic treatment of the data provided by Wade et al. (1985) still falls short of a full and complete evaluation of the doses, which would require a lengthy collation of data concerning the eating habits of this population (i.e. what do they eat, where is this food grown, when is this food grown, etc.?). Such a detailed evaluation seems inappropriate when the large errors associated with other parts of the assessment are taken into consideration. Therefore, for the sake of conservatism, it would appear to be legitimate to estimate the doses in this work on the basis of the assumption that all the foodstuffs ingested by a person were derived at the location of the individual. It is

imperative, however, that the conservative nature of this assessment is fully recognised. Despite these conservative assumptions, the atmospheric  $^{14}\text{CO}_2$  discharges from Sellafield do not contravene any of the regulations laid down by ICRP. Finally, due to the lack of published data on the historic  $^{14}\text{CO}_2$  discharges from Sellafield, an attempt was made to reconstruct the time series of  $^{14}\text{CO}_2$  discharges since 1952. This study estimated the total amount of  $^{14}\text{CO}_2$  released to the atmosphere from Sellafield during the period 1952-1985 to be around 190 TBq.

#### 3.3.2.6 Atmospheric Dispersion Models

In this section, the information obtained from the Sellafield data concerning the performance of various atmospheric dispersion models will be reviewed.

The initial model to be considered was the Gaussian plume atmospheric dispersion model. The version of the Gaussian dispersion model used here is only recommended for use in areas of reasonably constant topography and with discharges from sources which are not in a position significantly influenced by turbulence from nearby buildings. The discharge sites at Sellafield, as identified by BNF plc, are very near the NE boundary of the site, with few obstacles between themselves and the fence. Therefore, the atmospheric dispersion of the  $^{14}\text{CO}_2$  along the NE transect is not expected to be significantly affected by turbulence from nearby buildings. The topography around Sellafield is fairly typical of a British coastal area. Within a few kilometres of the coast, the area is fairly level and it is around 10-15 km inland before any sizable hills or valleys are encountered. Nevertheless, recent work by Walker et al. (1986) has indicated that topographical effects could be influencing the atmospheric dispersion of  $^{14}\text{CO}_2$  from Sellafield. Unfortunately, this hypothesis could not be verified as difficulties were encountered in attempting to resolve the separate effects of meteorology and topography. Although the possibility cannot be ruled out that local topography may have some effect on atmospheric dispersion of  $^{14}\text{CO}_2$ , any such effect is likely to be small in this case. Therefore, there is no obvious reason why the Gaussian dispersion model should not be

able to accurately predict the atmospheric  $^{14}\text{C}$  levels around Sellafield. However, as has been undisputably demonstrated for the years 1983, '84 and '85, the atmospheric  $^{14}\text{C}$  levels, predicted by the model, bear little resemblance to the observed  $^{14}\text{C}$  data (c.f. Figures 3.20, 3.16 and 3.14 respectively). Considering the accuracy of the  $^{14}\text{C}$  assay technique, it is justifiable to presume that the discrepancy must be due to errors either in the input data for the Gaussian dispersion model or inherent in the model itself.

The Gaussian dispersion model is widely used throughout the nuclear industry to predict the dispersion of radionuclides released to the atmosphere (e.g. Killough and Rohwer, 1978; CEC, 1979; Bush et al., 1983; Miller, 1984; IAEA, 1985). Subsequently, a reasonable volume of work has been carried out to test its integrity. The results of these studies suggest that, although the atmospheric concentrations predicted by the model are, in reality, only rough approximations to the true values, they do provide reasonable enough estimates for use in dose assessment studies. In general, the atmospheric concentrations predicted by the model are within a factor of 2 of the true concentrations (Weil and Jepsen, 1977; Clarke, 1979; Fields et al., 1984). So far then, two possible sources of error in the  $^{14}\text{C}$  levels predicted by the model have been identified. These are, firstly, the small errors introduced by topographical effects and, secondly, the larger errors inherent in the model itself. Taking into account these errors, the  $^{14}\text{C}$  levels predicted by the model would still be expected to be no more than a factor of 2 different from the observed levels. In this work, the  $^{14}\text{C}$  levels predicted by the model were regularly around 10-20 times smaller than the observed levels. This would suggest that an additional error is being incorporated into the model's predictions, probably via the input data for the model.

The bulk of the input data for the Gaussian dispersion model are derived from either the Meteorological Office or from BNF plc. The meteorological data are collected at a station located 70 km to the south of Sellafield and their use may introduce a slight error into the values calculated. Over such distances, however, no significant difference in meteorological conditions is

expected. This is especially true in this case where both sites are very similar in nature, i.e. they are both on the west coast of Britain. Therefore it can be assumed that all the meteorological data used are basically correct. The only problem arises when these data are combined with the  $^{14}\text{CO}_2$  release rates. As previously mentioned, in the absence of information to the contrary, it is assumed that the discharge rates are constant throughout the year. If this was not the case then the meteorological data would have to be weighted, i.e. more importance would have to be attached to the meteorological conditions during higher than average release rates. Thus the assumption that the release rate is constant may lead to discrepancies between observed and predicted  $^{14}\text{C}$  levels. However, fluctuations from a constant release rate, if present at all, would probably be fairly random so that, over an extended period, the effect of such fluctuations would be expected to cancel out to some extent. To summarise, therefore, the combination of the meteorological data and the  $^{14}\text{CO}_2$  release rate may introduce a small random error into the values predicted by the model. The results from this work, however, suggest that there is some very large systematic error causing the discrepancy between observed and predicted  $^{14}\text{C}$  levels. The evidence provided thus far indicates that this systematic error is not due to either the Gaussian dispersion model itself or the meteorological data used. This leads to the conclusion that a large systematic error is being introduced into the calculation via the input data provided by BNF plc.

The data provided by BNF plc are the  $^{14}\text{CO}_2$  annual release rates and the heights and locations of the discharge sites. Since all the predicted  $^{14}\text{C}$  levels are far smaller than the observed levels, a closer fit between the two data sets could be obtained by simply increasing the estimated  $^{14}\text{CO}_2$  annual release rate. In Figures 3.29 (a), (b) and (c),  $^{14}\text{C}$  levels predicted by the Gaussian dispersion model for each of the years 1985, '84 and '83 respectively, have again been plotted along with the observed values. This time, however, the  $^{14}\text{CO}_2$  release rates quoted by BNF plc have been increased by a factor of 10 in 1985 and by a factor of 20 in both 1984 and 1983, to be 66, 140 and 140  $\text{TBq year}^{-1}$  for the years 1985,

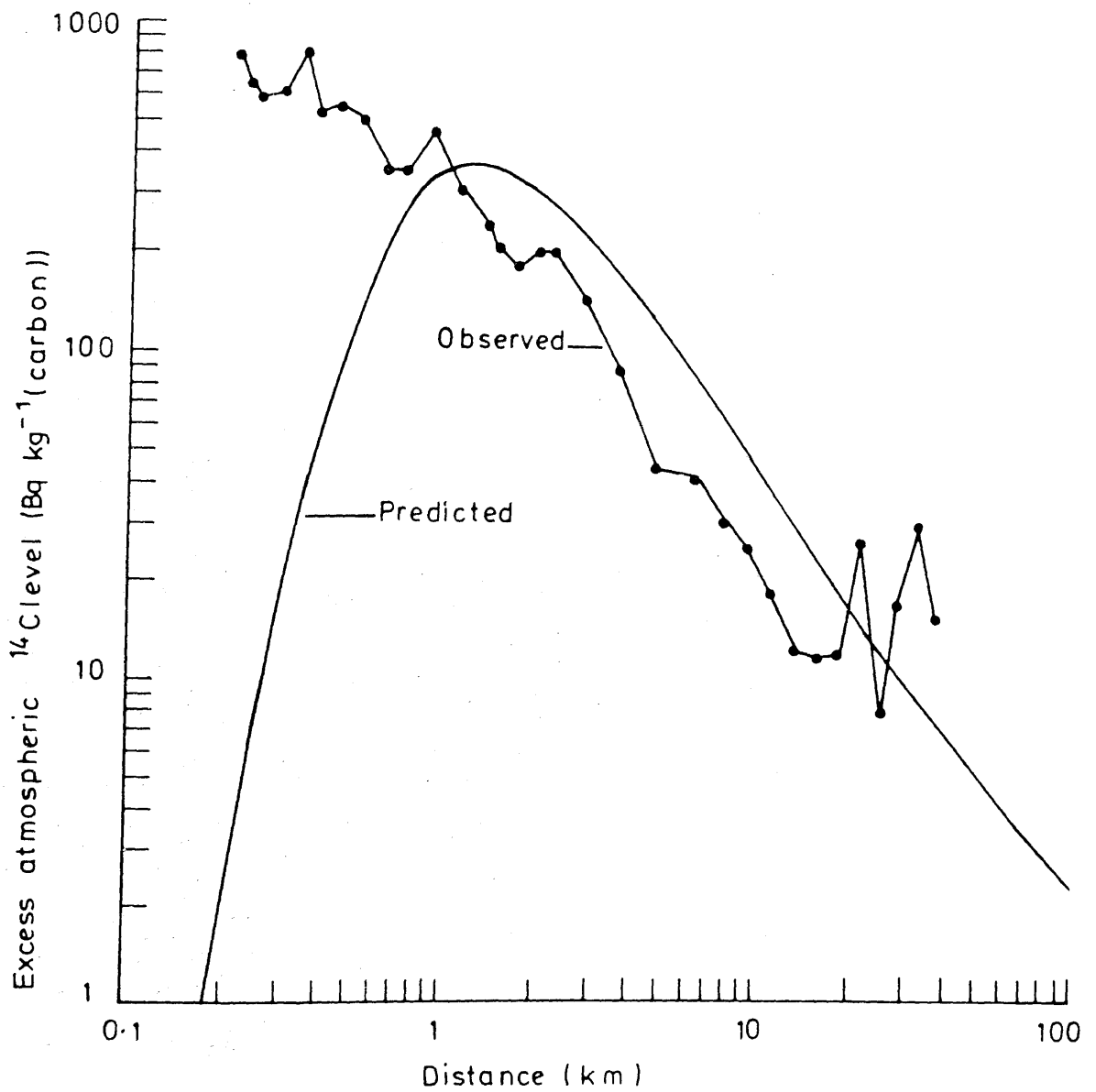


FIGURE 3.29(a): Atmospheric  $^{14}\text{C}$  levels around Sellafield in 1985, as predicted by the Gaussian dispersion model (assuming  $66 \text{ TBq year}^{-1}$  release rate),<sub>e</sub>

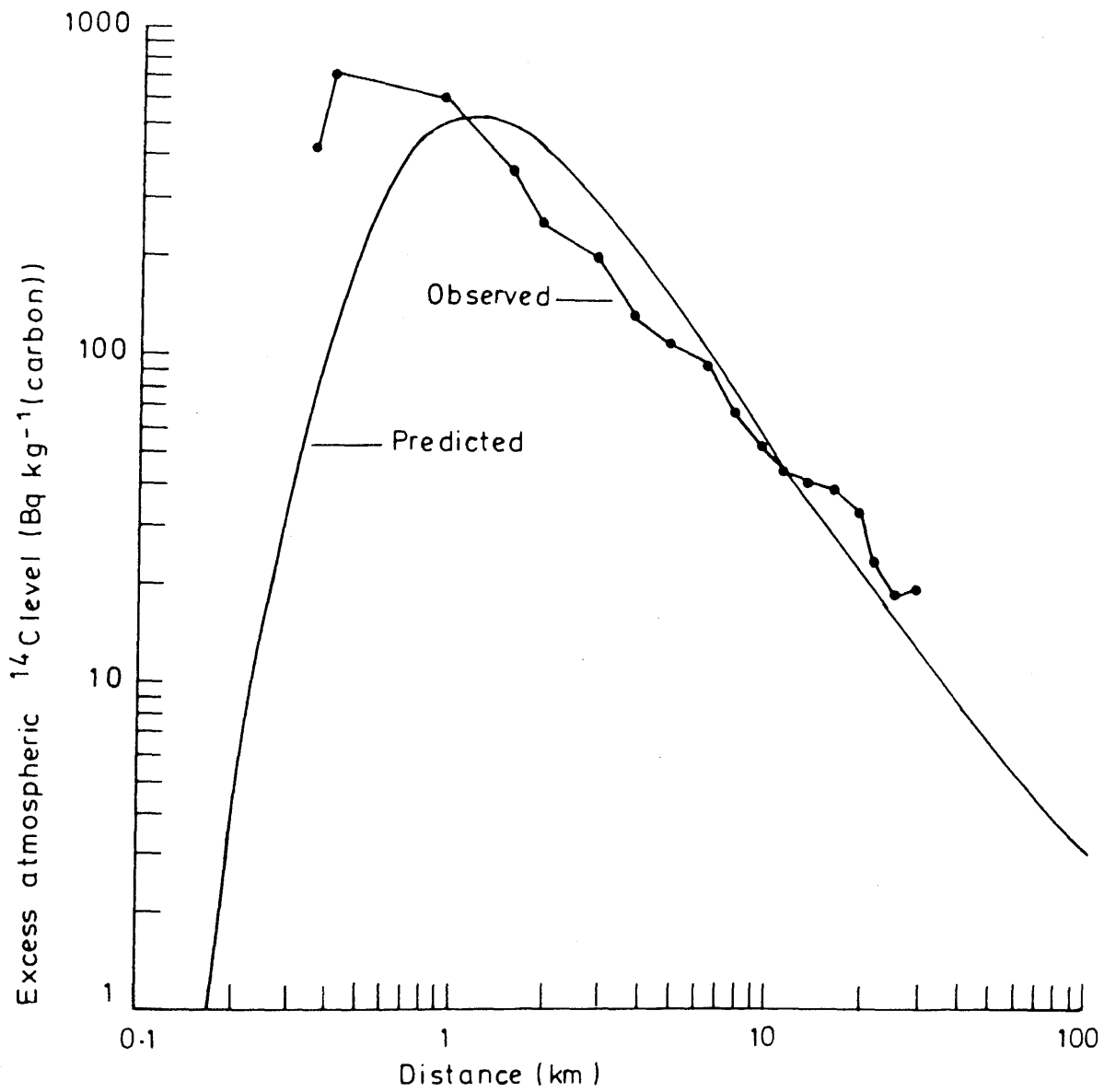


FIGURE 3-29(b); Atmospheric  $^{14}\text{C}$  levels around Sellafield in 1984, as predicted by the Gaussian dispersion model (assuming  $140 \text{ TBq year}^{-1}$  release rate)

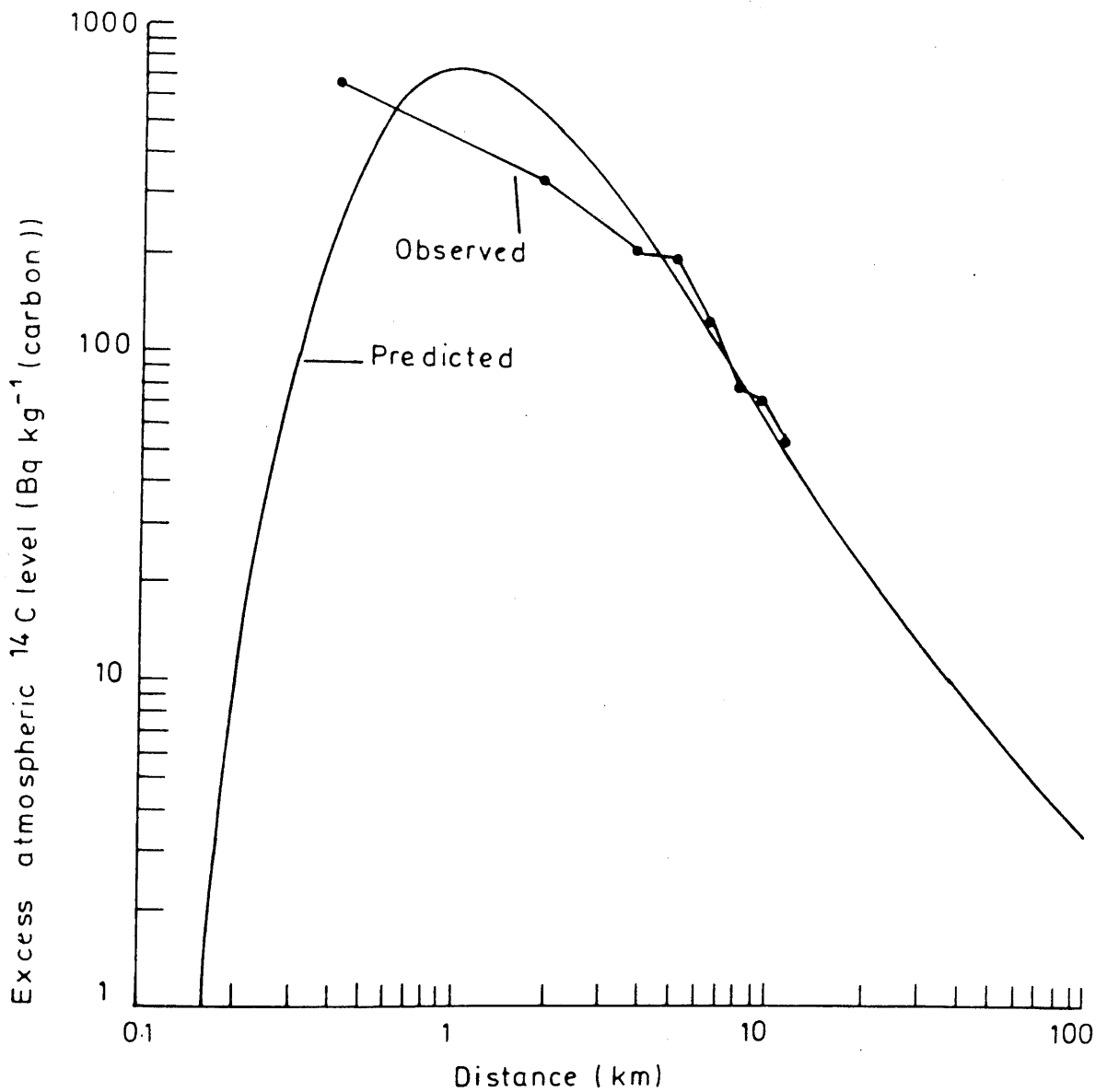


FIGURE 3.29(c) : Atmospheric <sup>14</sup>C levels around Sellafield in 1983, as predicted by the Gaussian dispersion model (assuming 140 TBq year<sup>-1</sup> release rate)

1984 and 1983 respectively. On the whole, the predictions of the model are now in reasonable agreement with the actual observations, although the basic shape of the plot is still imperfect. That is to say, the maximum level is still predicted to be further away from the discharge location than observed. In any case, even though the  $^{14}\text{C}$  discharge data published by BNF plc are relatively inaccurate (as seen by their recent revision to previously published data), it is unlikely but not impossible, that they are erroneous by as much as the factor of 10 or 20 used here. Therefore, other possible sources of error should be examined. For example, a very interesting phenomenon is observed if it is assumed that the height of the  $^{14}\text{CO}_2$  discharge location is far lower than that quoted by BNF plc. This not only increases the ground level  $^{14}\text{C}$  concentrations predicted by the model but also brings the maximum level a lot closer to the discharge location. In Figures 3.30 (a), (b) and (c), therefore, the  $^{14}\text{C}$  levels predicted by the model for the years 1985, '84 and '83 respectively, assuming the discharge height is 40 m (as opposed to the 120 m quoted by BNF plc) but using the original discharge data, have been plotted along with the observed values. As Figures 3.30 (a), (b) and (c) demonstrate, this assumption produces a far better correlation between the model predictions and the experimental observations. An even better correlation between the two data sets could be obtained by adjusting the annual discharge data. However, the point of this exercise is merely to show that the discrepancy between the predicted and observed  $^{14}\text{C}$  levels could be explained by errors in the input data and is not necessarily a manifestation of the model itself. The results obtained already clearly support this hypothesis and thus any further fine-tuning of the two data sets would be superfluous. In conclusion, it can be stated that, as it stands, the Gaussian plume atmospheric dispersion model cannot be used to give reasonable estimates of  $^{14}\text{C}$  levels in the vicinity of Sellafield. However, at present, the cause of this phenomenon cannot be unequivocally stated. It may be caused by errors in the model or, more likely, it may be due to errors inherent in the input data for the model, in particular, the data provided by BNF plc. Whatever the reason, the concept of using this model to calculate doses to the local population had to be rejected and another atmospheric dispersion model had to be investigated.

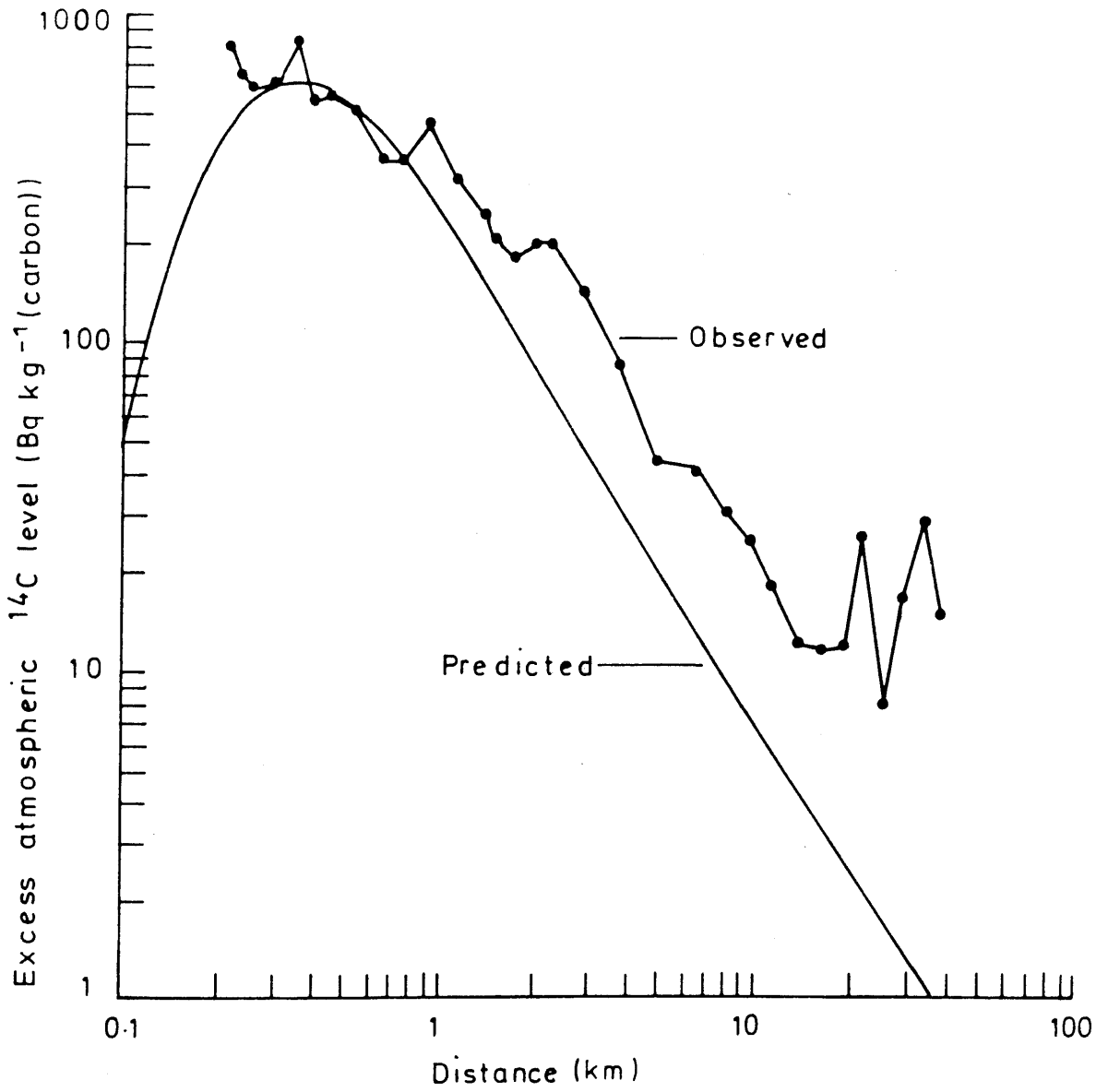


FIGURE 3-30(a) : Atmospheric <sup>14</sup>C levels around Sellafield in 1985, as predicted by the Gaussian dispersion model (assuming 40m release height).

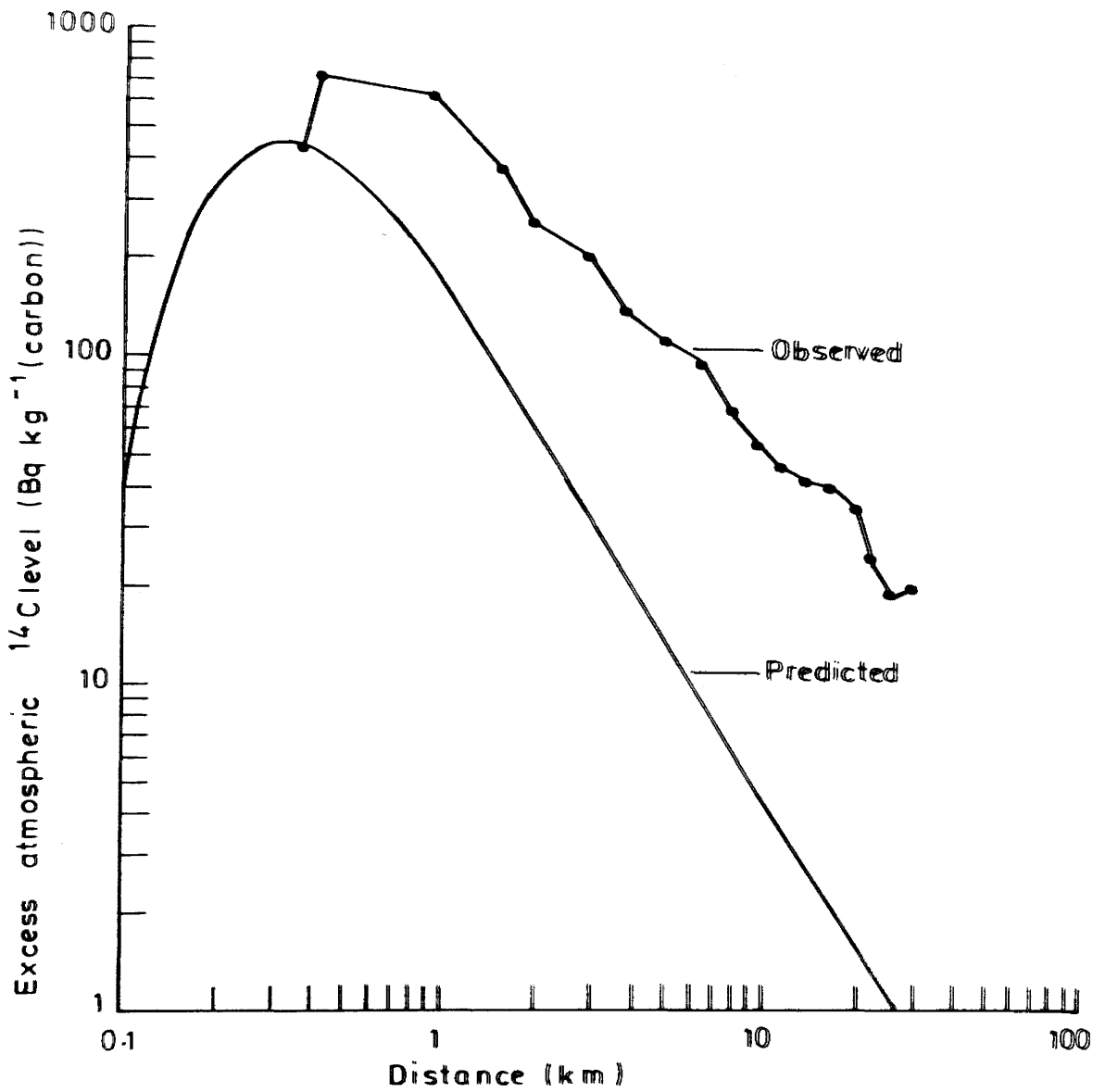


FIGURE 3-30 (b): Atmospheric  $^{14}\text{C}$  levels around Sellafield in 1984, as predicted by the Gaussian dispersion model (assuming 40m release height).

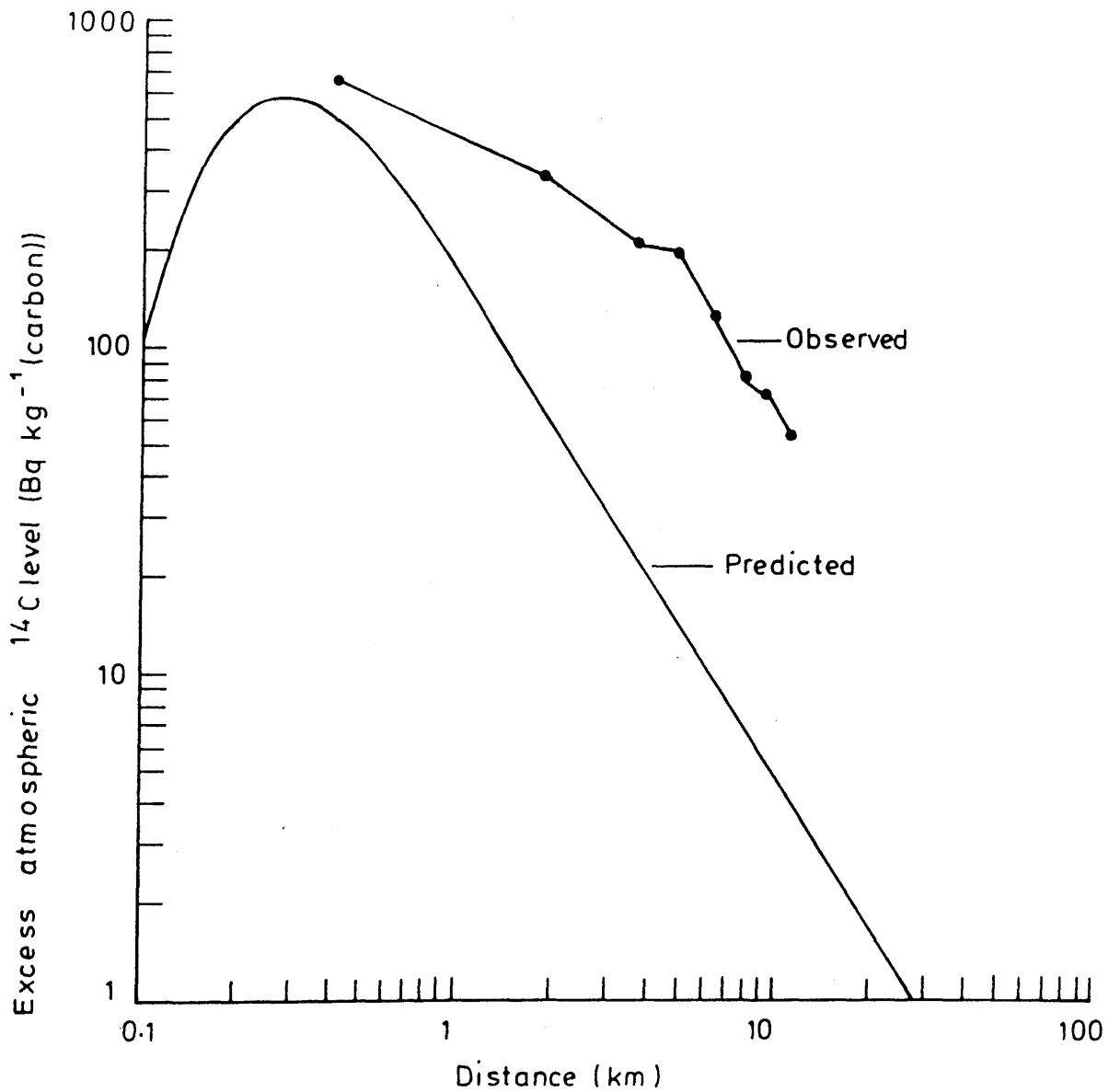


FIGURE 3.30(c): Atmospheric  $^{14}\text{C}$  levels around Sellafield in 1983, as predicted by the Gaussian dispersion model (assuming 40m release height).

The concept of the second model investigated, referred to as the hyperbolic model, is entirely different from that of the Gaussian dispersion model. The hyperbolic model does not have a very solid theoretical basis and its structure does not obviously reflect the underlying principles involved in atmospheric dispersion. It has its roots in the fact that as the distance from the discharge location increases, the governing equation of the Gaussian dispersion model tends towards a simple hyperbolic function. Nevertheless, given all the appropriate data concerning a specific release of  $^{14}\text{CO}_2$ , its dispersion could not be predicted by the hyperbolic model used here. Rather, the model depends on its ability to predict the  $^{14}\text{C}$  level at any distance relative to the level at another distance. Therefore, so long as the  $^{14}\text{C}$  level is known at any distance (other than at infinity at which the  $^{14}\text{C}$  level will reflect the background value), then the  $^{14}\text{C}$  levels at all other distances can be calculated. Obviously, the more experimentally determined points there are, then the more accurate the hyperbolic model becomes. Certainly, for the years 1983, '84 and '85, for which the validity of this model was tested (see Figures 3.21, 3.17 and 3.15 respectively) it performed excellently. The model does, however, have its limitations, the most obvious being that it cannot accurately predict  $^{14}\text{C}$  levels very close to the discharge location. This limitation is not surprising as it is implicit in the derivation of the model that its integrity increases with distance from the discharge location. In other words, the closer the discharge site, the less valid the model becomes. The results of this study suggest that the validity of the model is acceptable at all distances greater than 1 km from the discharge location. Within 1 km of the release site the hyperbolic model cannot be used to give reasonable estimates of the  $^{14}\text{C}$  levels. For the purposes of this work, this deficiency was not of critical importance and the model could still be used to provide valuable data.

The hyperbolic model therefore proved to generate excellent predictions of  $^{14}\text{C}$  levels around Sellafield at distances greater than 1 km from the plant. The only disadvantage of the model is that at least one reliable and experimentally derived  $^{14}\text{C}$  level must be previously determined.

### 3.3.3 Hunterston

The assessment of the radiological impact of  $^{14}\text{CO}_2$  discharges from Hunterston on the local population has been confined to the year 1984. However, it is considered that the results for this year will be fairly typical of those for the period since 1977, i.e. since the last reactor unit constructed at Hunterston became operational. Also, it is reasonable to assume that the  $^{14}\text{CO}_2$  discharges from Hunterston prior to this date would be considerably smaller than they are at present. The results of the dose assessment study will now be presented and the implications of the findings discussed. Finally, the conclusions reached about various atmospheric dispersion models in the previous section of this work, will be reviewed in the light of data collected in this study.

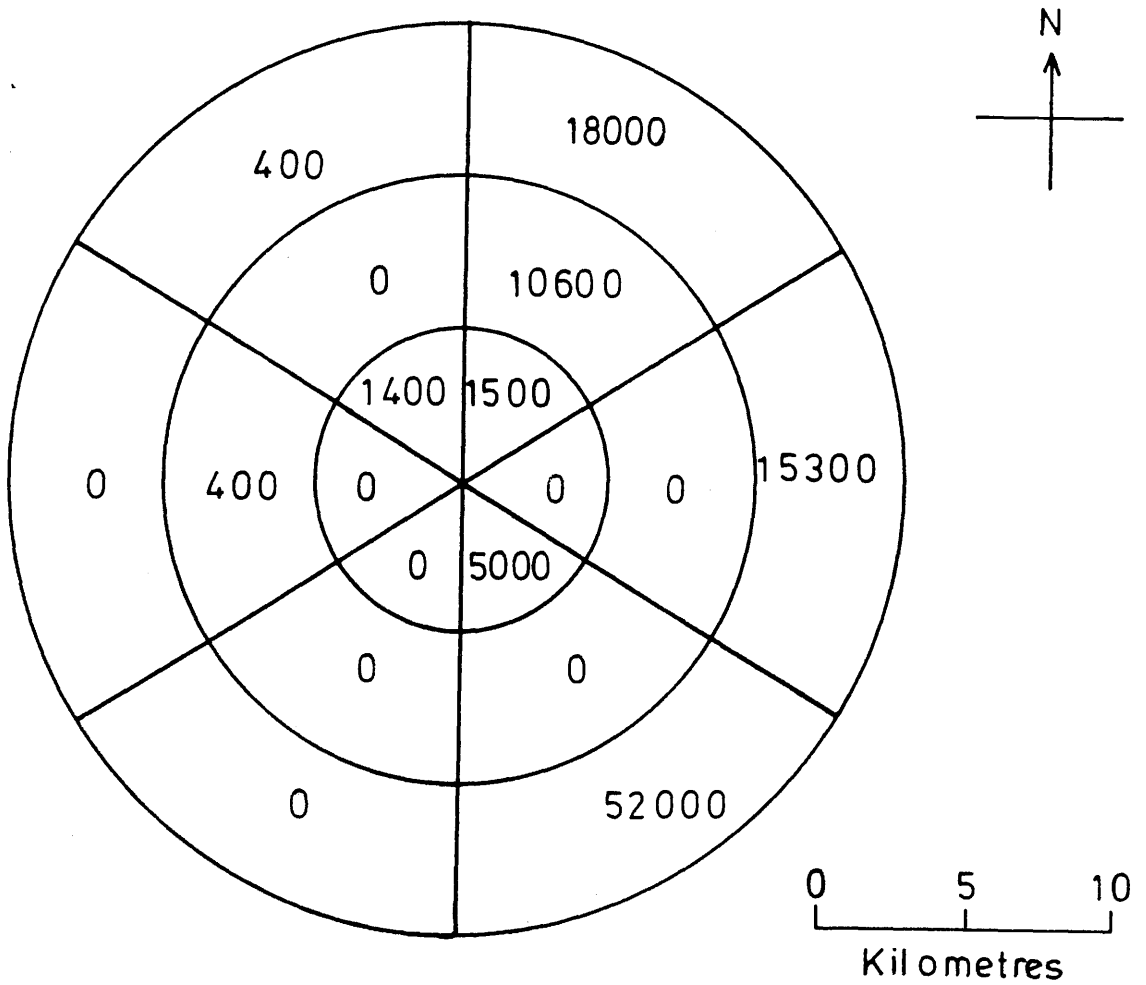
#### 3.3.3.1 Local Doses

As always, the first step in the dose assessment process is to define the physical dimensions of the annular segments to be considered. These are, of course, based on the resolution of the available data. A plot of the measured  $^{14}\text{C}$  levels against distance from the discharge location has previously been presented in Figure 3.9. All these data were obtained from samples collected on a transect that transgressed an area lying between  $60^\circ$  and  $120^\circ$  due north of Hunterston. These  $^{14}\text{C}$  levels are therefore taken to be representative of the levels throughout the entire  $60^\circ$  sector and, hence, the area around Hunterston is subsequently divided into 6 sectors, each with an angular width of  $60^\circ$ . The radii of the annuli are chosen such that the variation of activity within a given annulus is small. As in the Sellafield study, the size of the radii of the various annuli are chosen to increase in 5 km increments, i.e. 5 km, 10 km, 15 km, etc.. Certainly, for all but the initial 5 km, the variation in activity within each annulus is minimal. However, since the population within 5 km of most nuclear facilities tends to be very small, use of these radii will not lead to a significant loss of resolution for most dose assessment purposes. The final decision required is to define the extent of the local enhancement of  $^{14}\text{C}$  levels. The data in Figure 3.9 suggest that enhanced  $^{14}\text{C}$  levels are present right up to and presumably beyond the 16 km investigated. On the other hand, from about 3 km onward, very little change in

the  $^{14}\text{C}$  specific activity is noticeable, which could be taken to indicate that this value represents the true background level in this area. Such a problem was also encountered during the Sellafield study and the compromise used in that case will also be utilised here. In other words, it is assumed that all enhanced  $^{14}\text{C}$  levels measured relative to the control sample are due entirely to  $^{14}\text{CO}_2$  discharges from Hunterston but no attempt is made to extrapolate the  $^{14}\text{C}$  levels beyond the study area. This is not to say that this is the limit of the local enhancement but rather that this is the limit within which the enhancement can be reliably assessed. So, now that the dimensions of the annular segments have been defined, the next step is to determine the spatial distributions of both the population and the  $^{14}\text{CO}_2$ .

The population data are derived from information provided by Strathclyde Regional Council and are summarised in Figure 3.31. In general, populations to the west are extremely few in number, being restricted to several small island communities only. In fact, within 5 km and even 10 km of Hunterston, the population in all directions is very small. By far the largest population density is found in the outermost segment of the SE sector where several large towns, including Ardrossan, Kilwinning, Saltcoats and Stevenston, are all situated. The total population within 15 km of Hunterston is just over 75 000 which is similar, although slightly greater than, the population within 15 km of Sellafield (which is around 56 000).

The spatial distribution of the  $^{14}\text{CO}_2$  discharges is derived, as before, from a combination of the observed  $^{14}\text{C}$  levels and wind rose data. Here, the observed  $^{14}\text{C}$  levels can be used directly to obtain the average  $^{14}\text{C}$  levels in each annulus along the east sector. These results must then be combined with the appropriate wind rose data to provide the average  $^{14}\text{C}$  levels in each annulus along any other sector (c.f. equation (3.15) but, in this case, read E for NE). The wind rose data apply to the growing period of grass only, which has previously been defined to be from 8:00-20:00 hours for the months April to September inclusive. The wind rose, which is obtained from the meteorological station at Prestwick (which is approximately 30 km to the south of Hunterston), is shown in



(Figures refer to the number of people in each annular segment.)

FIGURE 3.31: Spatial distribution of the population around Hunterston.

Figure 3.32 (a) and the spatial distribution of the  $^{14}\text{C}$  is presented in Figure 3.32(b). These  $^{14}\text{C}$  levels are then used together with the population grid to estimate the radiation dose to the local population. As at Sellafield, the doses are all calculated on the assumption that all the foodstuffs ingested by an individual are derived from the same location as that individual. This assumption is no more likely to be true for Hunterston than it is for Sellafield but its use is convenient for the comparison of doses at the two sites. The results of this assessment are all presented in Figure 3.33.

The collective effective dose equivalent commitment to the local population is tabulated in part (a) of Figure 3.33 and is shown diagrammatically in part (b). The collective effective dose equivalent commitment to the population within 15 km of Hunterston is  $15 \times 10^{-3}$  man Sv. Around 70% of this dose is delivered in the outermost annulus of the grid, as a direct result of the relatively large population in this region. Therefore, it is to be expected that the majority of the collective dose will have been delivered at relatively low levels of individual doses. The distribution of the individual effective dose equivalent commitment levels is shown in part (c) of Figure 3.33 and, indeed, the huge majority of the collective dose is received at individual dose levels of less than 100 nSv. This level is around a factor of 10 lower than the maximum individual dose evaluated here of 700 nSv. However, as pointed out earlier, it is in the determination of this important radiological quantity, i.e. the maximum individual dose, that the resolution of this technique becomes unacceptable. Hence, an alternative method must be used to estimate the maximum individual dose.

A maximum observed  $^{14}\text{C}$  specific activity of 187 Bq  $\text{kg}^{-1}$  (carbon) above the background level is found 0.4 km to the east of the Hunterston complex. According to the wind rose data (Figure 3.32(a)), the highest  $^{14}\text{C}$  levels are to be found in the east sector and so this value also represents the highest  $^{14}\text{C}$  level in the Hunterston environment. A higher value still may have been observed if a greater number of samples had been collected. However, it is probable that this  $^{14}\text{C}$  value is reasonably close to the true maximum level. The maximum

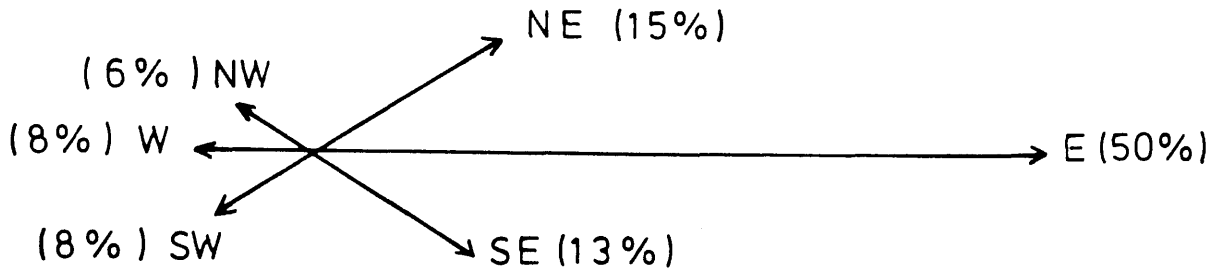
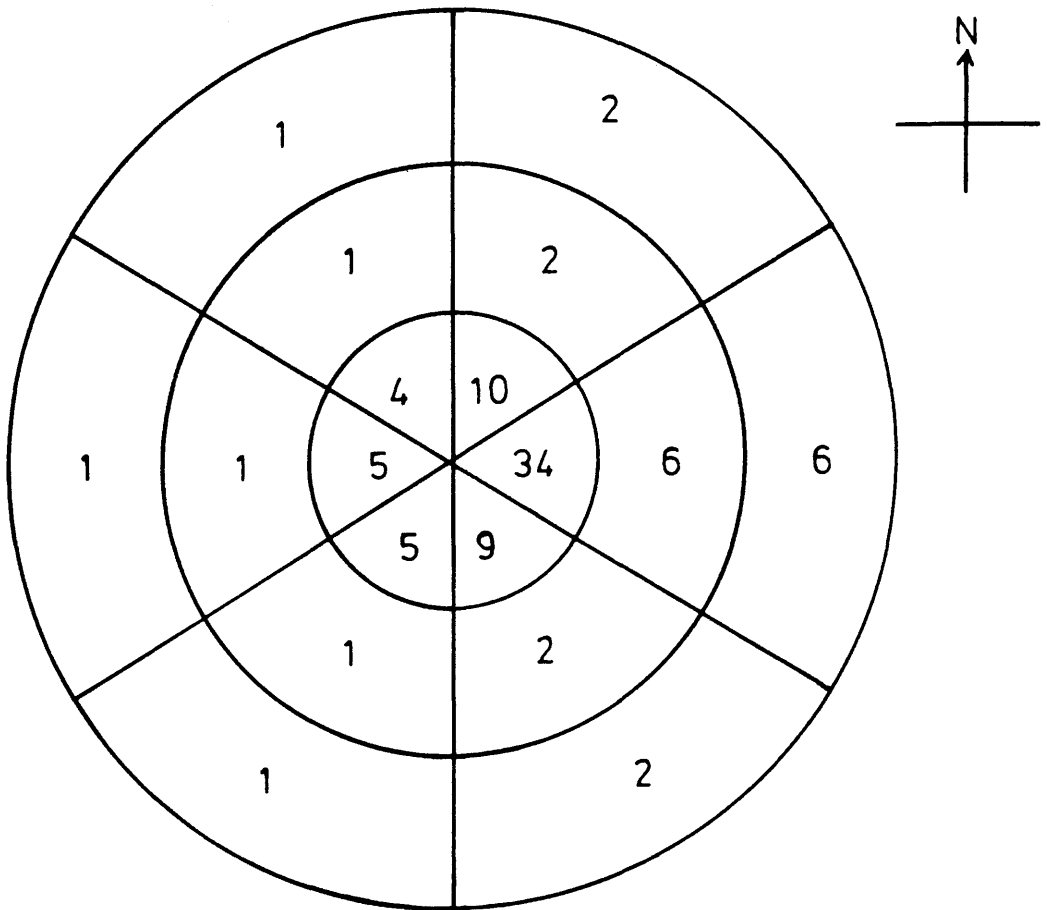


FIGURE 3.32(a): Wind rose for 'growing period' (Hunterston, 1984).

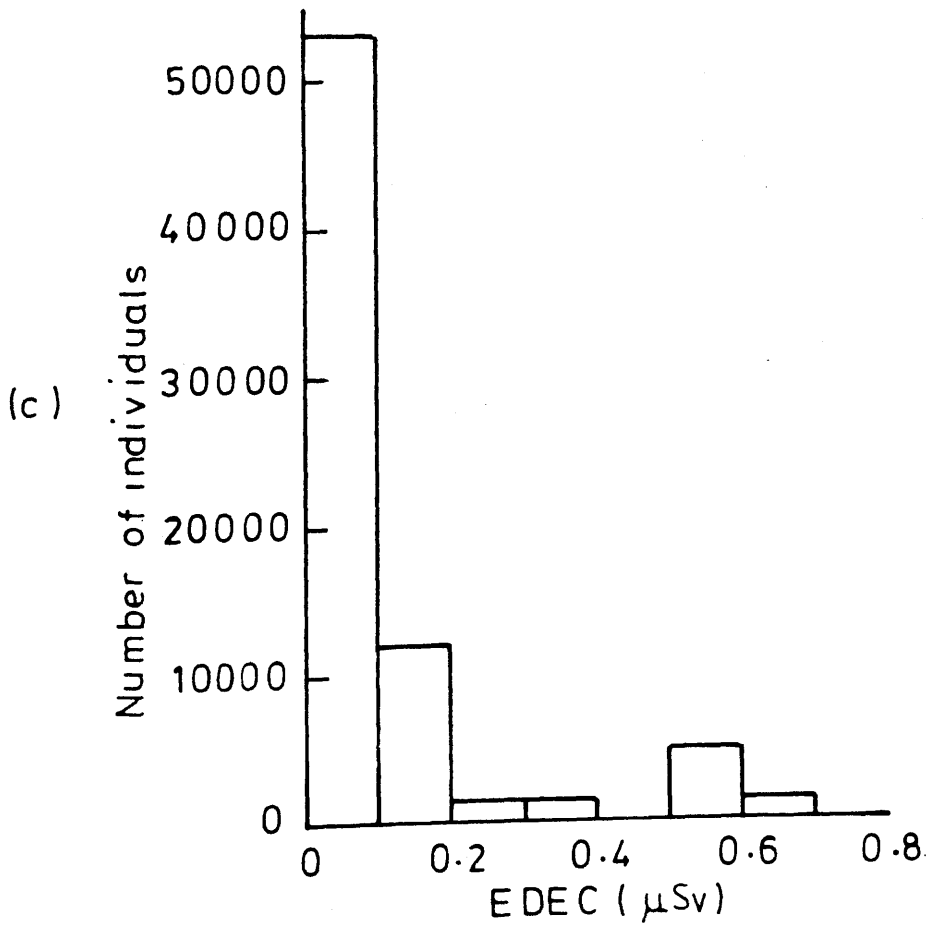
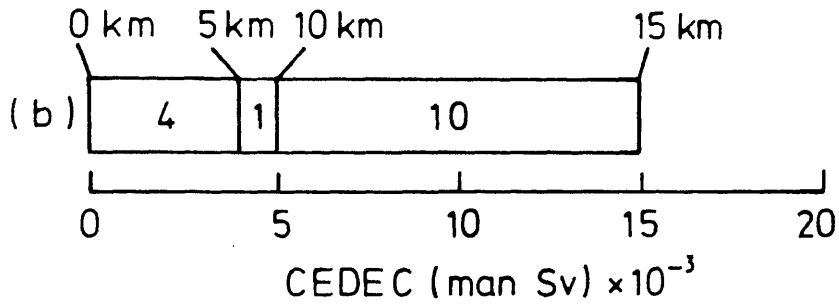


(All values are in  $\text{Bq kg}^{-1}$  (carbon))

FIGURE 3.32(b): Spatial distribution of  $^{14}\text{C}$  around Hunterston, 1984.

(a)

Radius (km)	0 - 5	0 - 10	0 - 15
CEDEC (man Sv) $\times 10^{-3}$	4	5	15



(d) Maximum individual EDEC =  $11.8 \mu\text{Sv}$

FIGURE 3-33: Doses to the population around Hunterston, from  $^{14}\text{CO}_2$  discharges in 1984.

individual dose would be received by a person who lived 0.4 km to the east of Hunterston and whose foodstuffs were all derived from this same location. Although this scenario is very unlikely, it does nevertheless represent the worst possible case. The effective dose equivalent commitment to such an individual would be  $11.8 \mu\text{Sv}$  as noted in part (d) of Figure 3.33. It is inherent in the specific activity model that this entire dose is delivered during the year of the discharge. Therefore this individual's effective dose equivalent rate for 1984 was  $11.8 \mu\text{Sv year}^{-1}$ , which corresponds to 0.2% and 1% respectively of the annual effective dose equivalent limits of 5 mSv and 1 mSv for members of the public as defined by ICRP. Thus, as at Sellafield, despite the use of very conservative assumptions, the  $^{14}\text{CO}_2$  discharges from Hunterston do not exceed the recommended limits set by ICRP.

The amount of  $^{14}\text{CO}_2$  released from Hunterston in 1984 was not directly determined by the operators (SSEB) but it is estimated to have been no more than 2.25 TBq (Tweedy, pers. comm., 1985). This value, if correct, suggests a collective effective dose equivalent commitment rate to the population within 15 km of  $7 \times 10^{-3} \text{ man Sv TBq}^{-1}$  and a maximum individual effective dose equivalent rate of  $5 \mu\text{Sv TBq}^{-1}$ . These rates are, in general, lower than at Sellafield, which averages  $2 \times 10^{-2} \text{ man Sv TBq}^{-1}$  and  $13 \mu\text{Sv TBq}^{-1}$  respectively over the period 1952-1985. Such comparisons are of little value since these estimates are all very approximate and, in any case, the values from year to year vary considerably as a function of wind rose. However, it can be stated with certainty that, firstly, the doses to the local population around Hunterston are far lower than at Sellafield and, secondly, that the discharges from Hunterston do not exceed any of the limits laid down by ICRP.

#### 3.3.3.2 Atmospheric Dispersion Models

Despite the poor performance of the Gaussian plume atmospheric dispersion model in the Sellafield study, it is re-examined here in the light of the Hunterston data and, in addition, the highly successful hyperbolic model will also be re-appraised. The acid test for these models is their ability to predict the  $^{14}\text{C}$  levels in the environment around Hunterston

and, hence, the doses to the local population. The Gaussian dispersion model is initially looked at.

The input data for the Gaussian dispersion model are presented in Table 3.16 and are largely supplied by either the Meteorological Office (from information collected at their Prestwick station) or the SSEB (the operators of Hunterston). The atmospheric  $^{14}\text{C}$  levels predicted by the model are shown in Figure 3.34, along with the observed  $^{14}\text{C}$  levels. Basically, the predicted and observed  $^{14}\text{C}$  levels are in reasonably good agreement. The predicted levels are generally higher than those observed but the basic shapes of the two data sets are very similar. For example, the model predicts a maximum  $^{14}\text{C}$  level of  $300 \text{ Bq kg}^{-1}$  (carbon) above background, 0.5 km from the discharge location and the maximum observed  $^{14}\text{C}$  level of  $187 \text{ Bq kg}^{-1}$  (carbon) is found 0.4 km from the plant. Certainly, compared with previous studies, the correlation obtained here is very good. However, before using these predictions to calculate the doses to the local population, the ability of the hyperbolic model to match the observed  $^{14}\text{C}$  levels will first be reported.

An attempt to match the observed  $^{14}\text{C}$  levels (for distances greater than 1 km) to a simple hyperbolic function has been made in Figure 3.35. A best-fit line of  $y = 24x + 279$  is obtained with a standard deviation of  $9 \text{ Bq kg}^{-1}$  (carbon). The ordinate intercept of  $279 \text{ Bq kg}^{-1}$  (carbon) is in excellent agreement with the measured background  $^{14}\text{C}$  level. However, the degree of fit ( $R^2 = 91\%$ ), although good, is not as high as that obtained at Sellafield. Therefore, the ability of this model to reproduce the observed  $^{14}\text{C}$  levels around Hunterston, although adequate, is not as excellent as in the Sellafield study. A clue to the cause of this phenomenon is to be found in the variability of the measured  $^{14}\text{C}$  levels with distance from the discharge point (see Figure 3.9). Comparison of these data with any of the spatial distribution studies carried out around Sellafield shows that significant differences between the atmospheric  $^{14}\text{CO}_2$  dispersion at the two sites exist. The most striking difference (ignoring the difference in the absolute amounts of  $^{14}\text{CO}_2$  present at the two sites) is the

Table 3.16: Data for Gaussian dispersion model (Hunterston, 1984)

Stability category (j)	Frequency of occurrence ( $f_j$ )	Average wind speed at 10 m ( $U_{10j}$ ) ( $m s^{-1}$ )	Mixing layer depth ( $A_j$ ) (m)
A	$7.0 \times 10^{-3}$	1.7	1300
B	$9.9 \times 10^{-2}$	3.1	900
C	$2.4 \times 10^{-1}$	3.7	850
D	$1.5 \times 10^{-1}$	6.3	800
E	$2.0 \times 10^{-3}$	3.2	400
F	$5.0 \times 10^{-4}$	1.5	100
G	0	-	-

ADDITIONAL DATA:

- (1) Release rate (Q) =  $0.07 \text{ MBq s}^{-1}$ ,
- (2) Release height (h) = 65 m,
- (3) Ground roughness term ( $Z_0$ ) = 0.4 m,
- (4) Ground roughness coefficient (n) = 0.275,
- (5) Angular width of sector ( $\alpha$ ) =  $\pi / 3$ .

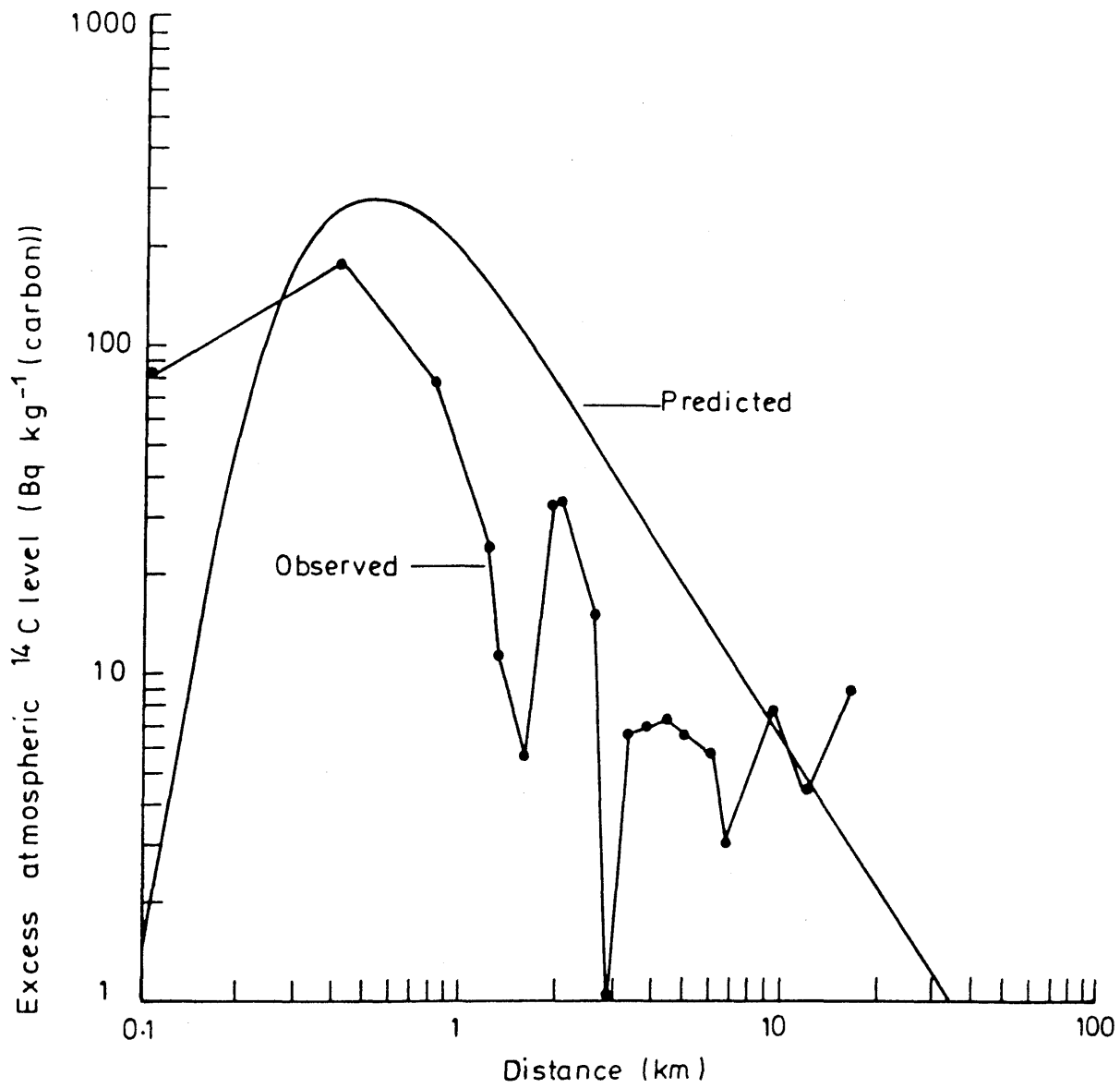


FIGURE 3-34: Atmospheric  $^{14}\text{C}$  levels around Hunterston in 1984, as predicted by the Gaussian dispersion model.

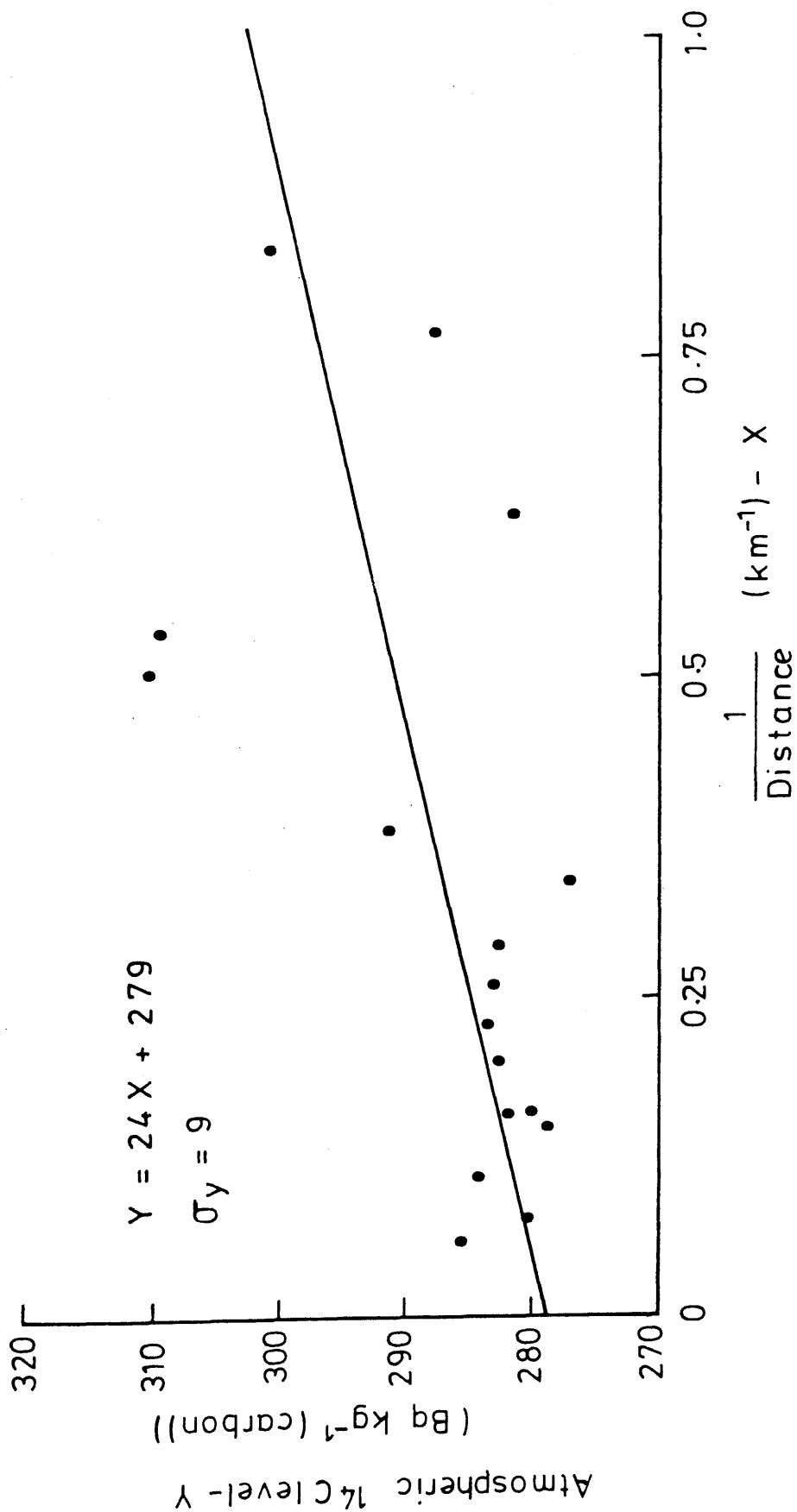


FIGURE 3-35: Atmospheric <sup>14</sup>C level versus distance<sup>-1</sup> for Hunterston, 1984.

large fluctuations superimposed upon the general downward trend of decreasing  $^{14}\text{C}$  levels around Hunterston. Such relatively large fluctuations are not as apparent in any of the Sellafield studies (c.f. Figures 3.3, 3.4 and 3.5). These fluctuations represent a move away from an ideal atmospheric dispersion profile, which is typified in the hyperbolic model and so reduces the effectiveness of the model. Thus, although the effect of these fluctuations is clear, their cause is not. One possible explanation is that they are caused by the existence of several separate  $^{14}\text{CO}_2$  release sites in Hunterston associated with the various reactors but these are all relatively close together (within a 200 m radius). Therefore, although the assumption that these several discharge locations can be treated as one single source may be slightly inaccurate, this approximation is not expected to be sufficiently significant to explain the observed large fluctuations. Another possible explanation is that they are caused by severe topographical effects in the Hunterston area. Certainly, compared to the Sellafield environment, the terrain is far more hilly. However, over the first 3 km, where some of the largest fluctuations are observed, the land is almost perfectly flat and thus this explanation also seems rather unlikely. A final possible explanation is that these fluctuations are caused by higher than average  $^{14}\text{CO}_2$  release rates, or, for that matter, higher than average  $\text{CO}_2$  uptake rates by plants during a period of extreme or atypical meteorological conditions. This explanation exploits the Achilles' heel of the monitoring technique used in this work, i.e. that it has to be presumed that the  $^{14}\text{CO}_2$  release rate from Hunterston is constant throughout the year and that the  $\text{CO}_2$  uptake rate by plants is constant throughout the growing season. The validity of this argument cannot be assessed at present, although further sampling programmes in subsequent years could ascertain whether or not these fluctuations are random or systematic. If they are random, then the above argument would be supported but if they were systematic then this explanation would appear unlikely and an alternative cause would need to be sought. Unfortunately, such an investigation proved impossible within the time constraints of this study and the cause of these fluctuations must therefore remain unknown. To sum up, the hyperbolic model's ability to match the observed  $^{14}\text{C}$  levels around Hunterston falls short

of its performance for Sellafield. This appears to be a result of the less ideal atmospheric dispersion profile obtained at Hunterston, although the cause of this is unclear. Nevertheless, the model's predictions are reasonable and thus its ability to calculate the subsequent dose to the local population is now investigated.

The  $^{14}\text{C}$  levels predicted by both the Gaussian plume atmospheric dispersion model and the hyperbolic model are used to estimate the doses to the population within 15 km of Hunterston. The results are listed in Table 3.17 along with those calculated from the observed  $^{14}\text{C}$  levels. The estimates from all methods are in reasonable agreement, with that from the hyperbolic model ( $12 \times 10^{-3}$  man Sv) being slightly closer to the  $15 \times 10^{-3}$  man Sv predicted by the observed  $^{14}\text{C}$  levels than the Gaussian dispersion model prediction ( $20 \times 10^{-3}$  man Sv). The conclusion to be drawn from these results, then, is that, for the  $^{14}\text{CO}_2$  discharges from Hunterston in 1984, both the Gaussian dispersion model and the hyperbolic model can be used to give a reasonable estimate of the atmospheric  $^{14}\text{C}$  levels and, hence, the doses to the local population.

The observation that the hyperbolic model gives a reasonable estimate of the atmospheric dispersion of  $^{14}\text{CO}_2$  is in agreement with the conclusions drawn from the Sellafield study. In contrast, the conclusion drawn concerning the accuracy of the Gaussian dispersion model in predicting atmospheric  $^{14}\text{C}$  concentrations is very much in disagreement with the initial results obtained at Sellafield. At Sellafield, the performance of the Gaussian dispersion model was very poor, although it is unclear whether this reflected faults inherent in the model or in the input data for the model. As shown in Figure 3.34, however, the Gaussian dispersion model's performance at Hunterston is certainly adequate. In fact, the correlation between the observed  $^{14}\text{C}$  levels and those predicted by the model for Hunterston, 1984, can still be improved, without the contradiction of any statements previously made. For, as stated earlier, the  $^{14}\text{CO}_2$  release rate from Hunterston in 1984 of 2.25 TBq year $^{-1}$ , as quoted by the SSEB, is only an estimate of the upper limit of the probable release rate. Thus, in reality,

Table 3.17: Estimates of the collective effective dose equivalent commitment to the population around Hunterston (1984) from various techniques

Distance band (km)	CEDEC ( $10^{-3}$ man Sv)		
	Experimental data	Gaussian plume model	Hyberbolic model
0-5	4	10	2
0-10	5	13	3
0-15	15	20	12

the actual release rate was probably smaller than this. As Figure 3.34 demonstrates, the predictions of the Gaussian dispersion model (using a release rate of  $2.25 \text{ TBq year}^{-1}$ ) are consistently higher than the observed  $^{14}\text{C}$  levels. Therefore, if a slightly lower release rate is chosen, then an even closer correlation between the two data sets could be obtained. In Figure 3.36, the  $^{14}\text{C}$  levels predicted by the Gaussian dispersion model (using a release rate of  $1 \text{ TBq year}^{-1}$ ) are plotted along with the observed  $^{14}\text{C}$  levels and, indeed, the two sets of values are in excellent agreement. It is not possible, of course, to determine whether the release rate used is in fact correct but, in the light of present knowledge, it seems likely that it will, at least, be close to the true release rate. This result, therefore, lends considerable confidence to the atmospheric  $^{14}\text{C}$  levels predicted by the Gaussian dispersion model and so has considerable ramifications on the analysis of this model's performance in the Sellafield study. For if, as this conclusion suggests, the Gaussian dispersion model does give a valid description of atmospheric dispersion processes, then the cause of the model's failure to describe accurately the dispersion of  $^{14}\text{CO}_2$  from Sellafield must lie in the input data for the model. As discussed in Section 3.3.2.6 the most likely source of error lies in the input data provided by BNF plc (e.g. discharge locations, release heights, release rates). Hence, the combined results of these studies strongly suggest that the data provided by BNF plc on the release of  $^{14}\text{CO}_2$  from Sellafield are wrong. Certainly, the Gaussian dispersion model should not be abandoned on the basis of the Sellafield data.

### 3.4

#### CONCLUSIONS

The primary aim of this section was to assess the radiological impact of  $^{14}\text{C}$  discharges from nuclear installations on the local population. While investigating this topic, valuable information was also collected concerning the performance of some atmospheric dispersion models. The conclusions reached in both areas are now summarised.

Two atmospheric dispersion models were investigated, the Gaussian plume atmospheric dispersion model and the so-called hyperbolic model, which is in fact derived from the former. The

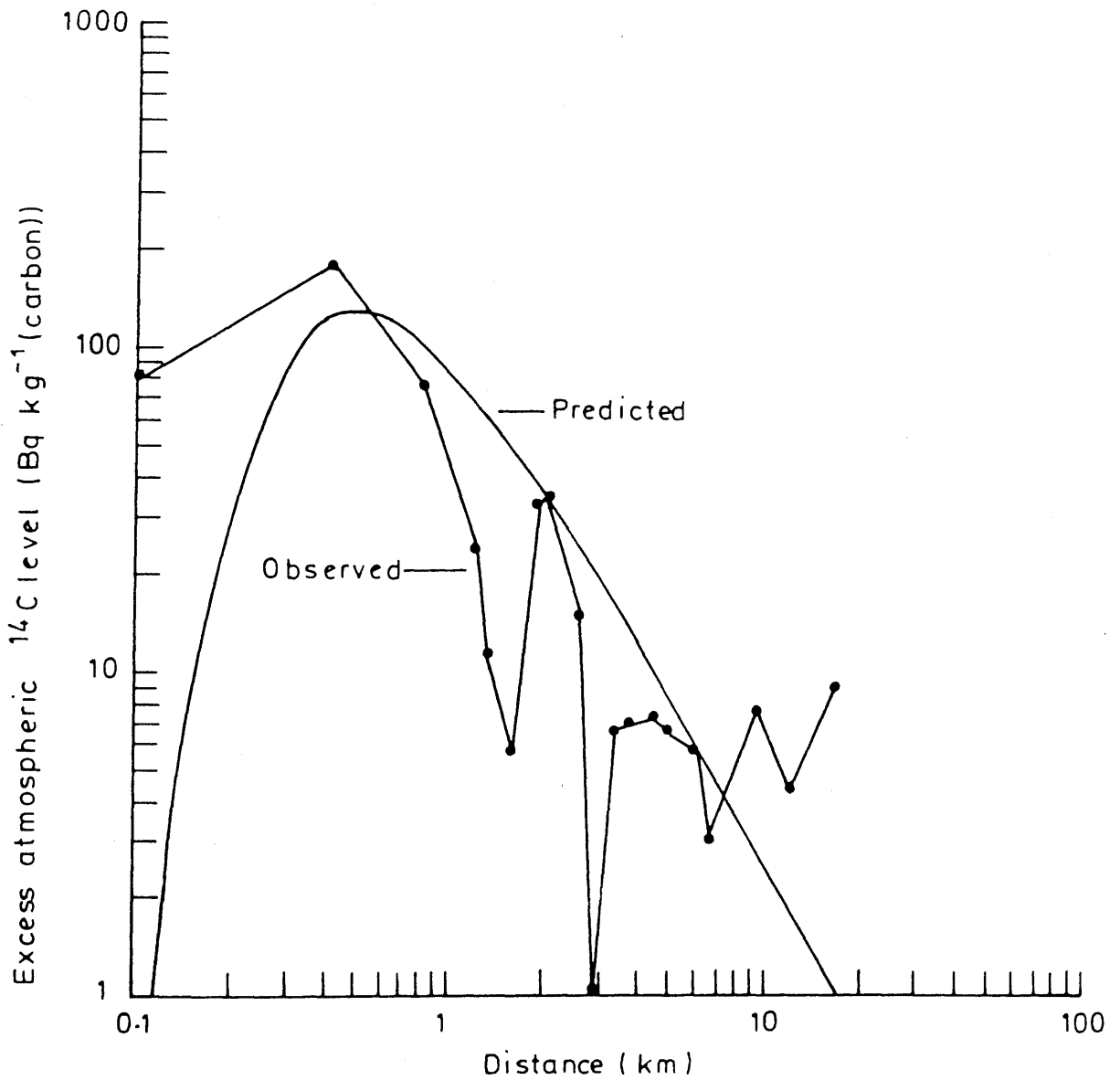


FIGURE 3.36: Atmospheric  $^{14}\text{C}$  levels around Hunterston in 1984, as predicted by the Gaussian dispersion model (assuming  $1\text{Tbq year}^{-1}$  release rate)

results of the study show that the Gaussian dispersion model is excellent in predicting  $^{14}\text{C}$  levels around Hunterston but gives highly unsatisfactory results when applied to Sellafield. Further investigation strongly suggests that the model's poor performance at Sellafield is due largely to inaccurate input data. In particular, the integrity of the data supplied by BNF plc concerning its  $^{14}\text{CO}_2$  discharges has been questioned. The results basically suggest that the Gaussian dispersion model can be used to give reasonable estimates of the atmospheric  $^{14}\text{C}$  levels if and only if the necessary input data for the model have been accurately determined. In the absence of such data, it is suggested that the simple hyperbolic model is utilised. This model relies on its ability to predict atmospheric  $^{14}\text{C}$  levels at practically any distance from the discharge location (except very close to the release point), from a single experimentally determined  $^{14}\text{C}$  level. The model's reliability has been repeatedly confirmed during this work by data collected at both Sellafield and Hunterston.

In terms of this study's radiological assessments, each nuclear installation which discharges  $^{14}\text{C}$  has its own individual characteristics and, hence, a general comment concerning the local doses at all such sites cannot be made with any degree of certainty. However, it is hoped that the range of installations investigated here covers a sufficiently wide spectrum of characteristics to be of perhaps wider relevance. Four different nuclear installations within the UK were investigated. No increase in atmospheric  $^{14}\text{C}$  levels were observed in the vicinity of either the fast breeder reactor at Dounreay or the research reactor at East Kilbride. On the other hand, increases in the atmospheric  $^{14}\text{C}$  specific activities were detected around both the nuclear fuel reprocessing plant at Sellafield and, to a lesser extent, the thermal nuclear power station complex at Hunterston. The collective effective dose equivalent commitment to the population within 40 km of Sellafield, from its  $^{14}\text{CO}_2$  discharges between 1952 and 1985, is estimated at 8.4 man Sv, with the largest annual collective dose of 1.3 man Sv being received in 1983. The discharges of  $^{14}\text{CO}_2$  from Hunterston in 1984, which can be taken as a typical year for this nuclear installation, gave rise

to a collective effective dose equivalent commitment of  $15 \times 10^{-3}$  man Sv to the population within 15 km of the plant. The largest annual effective dose equivalent to individuals around Sellafield and Hunterston were 0.2 mSv (in 1982) and 11.8  $\mu$ Sv respectively. These levels do not exceed the limits recommended by ICRP, although this fact, in itself, cannot be used to justify these discharges. Finally, it should be stressed that all these doses have been calculated on the basis of a very conservative interpretation of the specific activity model and thus, in all cases, generate the highest possible dose assessments.

GLOBAL EFFECTS OF  $^{14}\text{C}$  DISCHARGES FROM THE NUCLEAR FUEL CYCLE4.1 INTRODUCTION

Some of the waste nuclides released to the environment by the nuclear industry do not disperse beyond well-defined local boundaries because of either their short half-lives or their lack of mobility in the environment. For such nuclides, an accurate assessment of their radiological impact can be obtained from a study of their local dispersion alone. However, other nuclides, because of their long radioactive half-lives and their pattern of behaviour in the environment, become globally dispersed and act as a long-term source of irradiation of world populations.  $^{14}\text{C}$  is a prime example of such a nuclide - it has a half-life of  $5730 \pm 40$  years (Godwin, 1962), its primary atmospheric form is gaseous as  $\text{CO}_2$  and it is closely involved in many physical and biological processes notably photosynthesis and exchange within the carbon cycle. These characteristics lead to its fairly rapid and widespread dispersion, ultimately to global circulation and to incorporation into all phases of the global biosphere. Therefore, in order to execute a complete and accurate assessment of the radiological impact of  $^{14}\text{C}$  discharges from the nuclear fuel cycle, the radiation dose to both the local and global populations must be determined. The former aspect having been discussed in the previous chapter, we concentrate here on the global implications of  $^{14}\text{C}$ . Basically, the object of this section of the study is to assess the global effects of  $^{14}\text{C}$  discharges from the nuclear fuel cycle. To be more specific, the primary aim is to determine the radiation dose to the global population due to  $^{14}\text{C}$  discharges from nuclear installations.

The initial step in any process aimed at determining the radiological impact of  $^{14}\text{C}$  discharges on the world population must be to obtain a means of mimicking the movement of this excess  $^{14}\text{C}$  through the environment. In other words, mathematical representations of the dynamic carbon cycle are required. Once obtained, these models can be used, with the help of the appropriate input data, to predict the atmospheric  $^{14}\text{C}$  levels and hence the radiation dose to man, caused by  $^{14}\text{C}$  discharges

in the past, at present and in the future. The interactions of this effect with those caused by other anthropogenic perturbations to the global carbon cycle are also considered. In addition, these same carbon cycle models can be used to evaluate the effect which various waste disposal options have on the eventual dose to man.

All these results will be presented in due course but, as this brief introduction to the subject demonstrates, all the results obtained in this study depend heavily on the integrity of the carbon cycle models. Therefore, it is only fitting to start this discussion with an overview of the global carbon cycle models adopted in this work.

#### 4.2 MODELLING THE GLOBAL CARBON CYCLE

In principle, models of the global carbon cycle might be based on fundamentals of physics, chemistry and biology. In ideal circumstances, available data are used primarily for model testing and verification. In actuality, understanding of the basic processes controlling the carbon cycle is inadequate to support this approach and models are generally designed for direct calibration against data which reflect the dynamics of the cycle. Nevertheless, models of the global carbon cycle have been used for many purposes, including estimation of the future extent of the Suess effect (Revelle and Suess, 1957; Baxter and Walton, 1970), description of the uptake of bomb-derived  $^{14}\text{C}$  by the oceans and biosphere (Thommeret et al., 1983), prediction of future increases of atmospheric  $\text{CO}_2$  levels (Keeling and Bacastow, 1977; Siegenthaler and Oeschger, 1978; Niehaus and Williams, 1979; Edmonds et al., 1984) and, indeed, prediction of the radiological impact of  $^{14}\text{C}$  discharges from the nuclear fuel cycle (Kelly et al., 1975; Killough and Till, 1978; Killough, 1980; Krishnamoorthy et al., 1982; Matthies and Paretzke, 1982; Bush et al., 1983; Kocher and Killough, 1984; IAEA, 1985). In other words, carbon cycle models have a wide and varied application to many present-day scientific issues and, subsequently, there is a large and ever increasing number of such models. In the following sections, the major features of these different carbon cycle models are reviewed and, in addition, the models utilised in this study are described.

#### 4.2.1 A History of Carbon Cycle Modelling

The development of models of the carbon cycle began almost 30 years ago with simple box models (Craig, 1957b; Revelle and Suess, 1957; Bolin and Ericksson, 1959). The model proposed by Craig (1957b), shown in Figure 4.1, can be used to describe the basic assumptions common to these simple models.  $N_i$  ( $i=1-5$ ) represents the inventory of carbon in box  $i$  and  $k_{i,j}$  ( $j=1-5$ ) represents the first-order exchange rate (or transfer coefficient) from box  $i$  to box  $j$ . The carbon flux from box  $i$  to box  $j$  is taken as the product of the mass of carbon in box  $i$ ,  $N_i$ , and the appropriate transfer coefficient,  $k_{i,j}$ . The model is set up such that mass-balance is maintained, i.e. the flux of carbon leaving box  $i$  is equal to the input flux to box  $i$ . Finally, the boxes are assumed to be well-mixed and any carbon entering is assumed to be instantaneously distributed homogeneously within its boundaries.

Many alterations have since been made to this basic model of the global carbon cycle. These changes and their effects on the model's representation of the atmosphere, the biosphere and the oceans are now discussed.

##### 4.2.1.1 The Atmosphere

No particularly significant departure from Craig's simple 1-box representation of the atmosphere (Figure 4.2(a)) has been made over the years. For certain purposes, some authors have considered it beneficial to segregate the atmosphere into 2 subsections, the troposphere and the stratosphere as described in Figure 4.2(b), (Walton et al., 1970; Kelly et al., 1975; Matthies and Paretzke, 1982). In particular, this improves the model's response to the  $^{14}\text{C}$  input from nuclear weapon tests since most of the  $^{14}\text{C}$  produced in this manner was injected into the upper atmosphere (stratosphere). In addition, the atmosphere is occasionally split into a northern and a southern hemisphere (Figure 4.2(c)) as the exchange of carbon between hemispheres is slightly hindered and as exchange between the atmosphere and ocean is greater in the southern than in the northern hemisphere (Bush et al., 1983). These 3 representations of the atmosphere constitute all the basic alternatives at present, although they themselves can be combined or, indeed, further refined. For

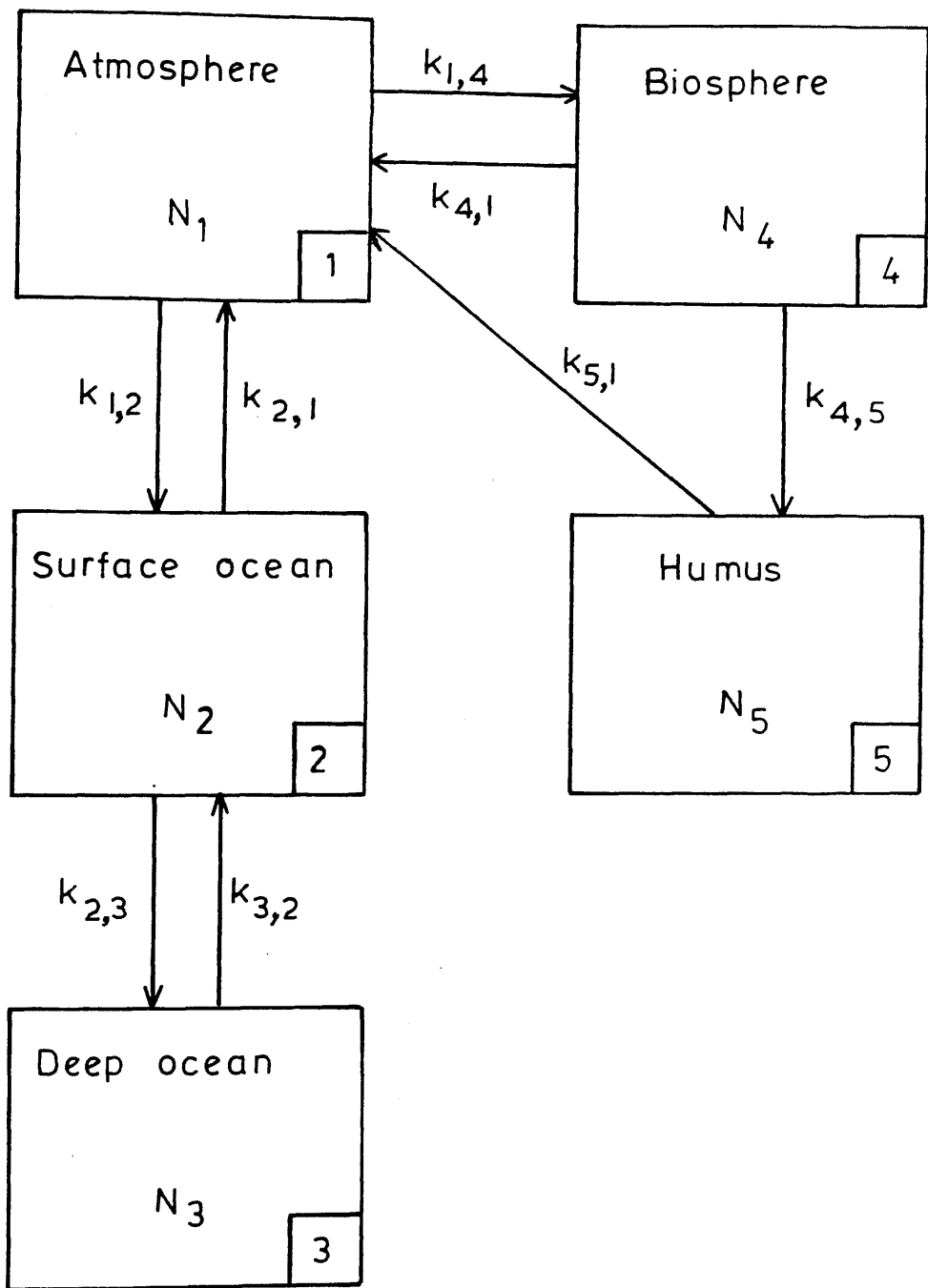


FIGURE 4.1: A simple box model of the global carbon cycle.

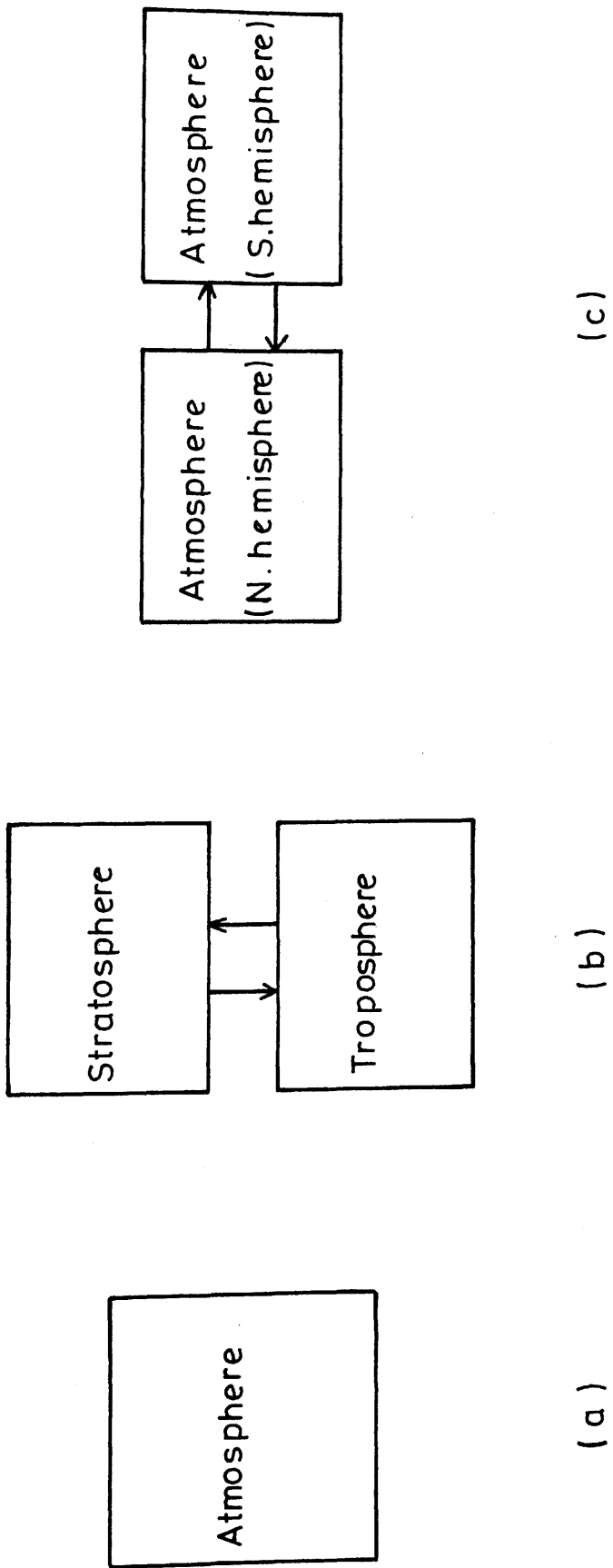


FIGURE 4.2: Alternative representations of the atmosphere.

example, a highly detailed model of the atmosphere is utilised by Bergman and McEwan (1977) who not only segregate it into a troposphere and a stratosphere but further subdivide it into four different latitude zones.

It should be stressed that these alternative representations of the atmosphere are only occasionally used and that for most long-term applications the simple 1-box representation is considered sufficient.

#### 4.2.1.2 The Atmosphere-Terrestrial Biosphere System

Considering the large variation in the time during which different carbon atoms reside in organic compounds, it seems unsatisfactory to model organic carbon as one well-mixed reservoir. Craig's approach, shown in Figure 4.3(a), was to divide the terrestrial biosphere into living and dead matter, i.e. biota and humus respectively. By assuming that the transfer from organic compounds to the atmosphere depends not only on the total amount of organic carbon but also on its distribution between living and dead matter, the dynamic properties of the organic carbon reservoir can probably be modelled better. Another common approach is to divide the biosphere into fast and slow carbon pools (Figure 4.3(b)), depending on the residence times of the carbon atoms (Machta, 1971; Keeling, 1973). For fast and slow compartments, each pool exchanges carbon with the atmosphere independently.

A further development was proposed by Bacastow and Keeling (1973) to improve the agreement between model response and CO<sub>2</sub> measurement records. They replaced the linear flux of carbon from the atmosphere to the biosphere with a non-linear flux by the introduction of a fertilisation effect. This allows the carbon flux from the atmosphere to the biosphere to increase logarithmically with increasing atmospheric CO<sub>2</sub> concentration. Although such a change does not affect the basic structure of the model, it does represent an important alternative treatment of the atmosphere-terrestrial biosphere system.

Recent emphasis on the fluxes of CO<sub>2</sub> due to forest clearing has motivated the further division of fast and slow compartments

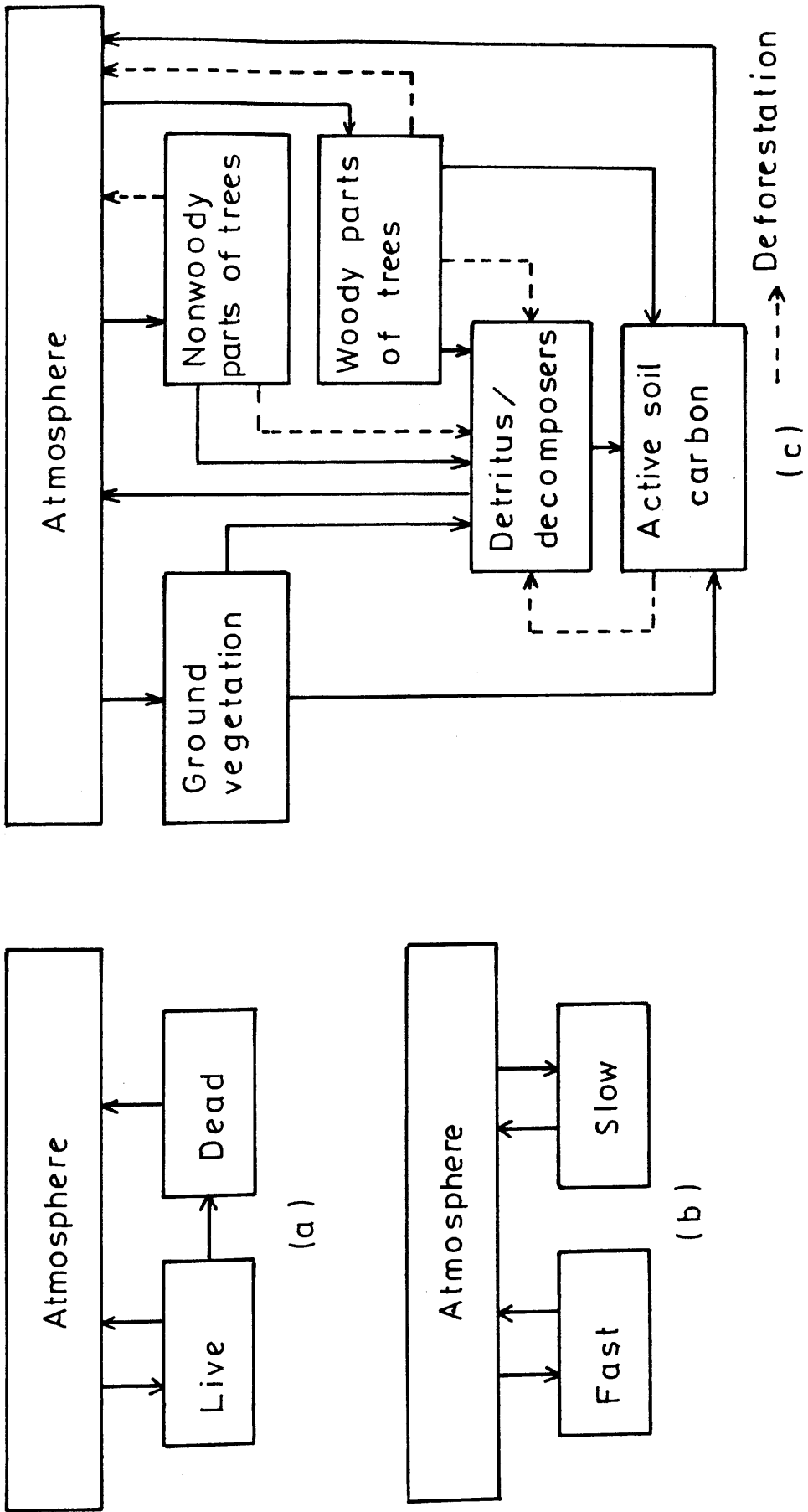


FIGURE 4·3: Alternative representations of the atmosphere - terrestrial biosphere system.

geographically into northern and southern components (Chan et al., 1979). In essence, however, this is still a 2-box treatment of the terrestrial biosphere inasmuch as the reservoirs do not correspond directly with structural components normally considered by terrestrial ecologists; this makes comparison with data difficult. The compartment diagram shown in Figure 4.3(c) is a considerable improvement in these respects. This approach, first reported by Emanuel et al. (1981), represents one of the most intricate treatments of the terrestrial biosphere. It divides the carbon in plants between 'ground vegetation' and 'trees', while carbon in dead organic matter is designated as either 'detritus/decomposers' or 'active soil carbon'.

Although not an exhaustive list, the models of the atmosphere-terrestrial biosphere system illustrated in Figure 4.3 do represent the basic choice of available structures.

#### 4.2.1.3 The Atmosphere-Ocean System

Over sufficiently long time periods, the oceans are the primary sink for excess carbon from the atmosphere (e.g. Baes et al., 1977) and, therefore, this aspect of the global carbon cycle has probably been studied in greater detail than any other. The simplest ocean model that has some physical validity is probably the 2-box model (Figure 4.4(a)), first suggested by Craig (1957b). In the original model, the surface ocean was taken to a depth of 75 m (the average depth of the actual wind-mixed layer), although, in some later models, this mixed depth was increased to 200 m (Bacastow and Keeling, 1979). A rationale for adopting this deeper surface layer is that the thermocline (from about 75 to 600 m) is a transition from surface to deep waters and the boundary in a two-compartment representation should not be at either extreme but rather somewhere near the middle of this zone. In 1973, Keeling (1973) introduced the concept of a non-linear carbon flux between the atmosphere and the surface ocean via a 'buffer factor' which represented all the physicochemical factors involved in the process (pH values, alkalinity, borate and phosphate content, etc.).

The next major development was introduced by Oeschger et al. (1975), who described a box diffusion model (Figure 4.4(b)) in

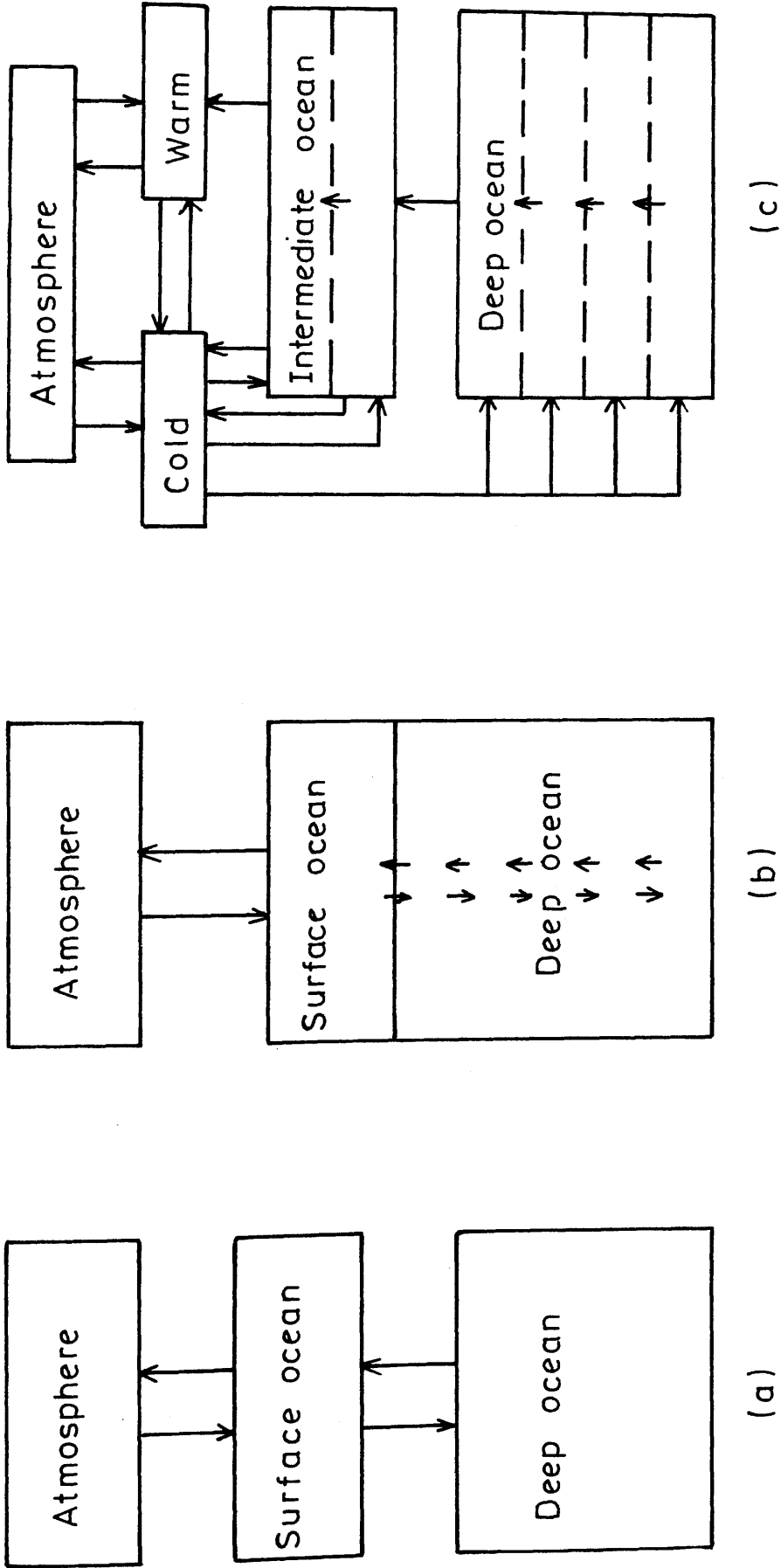


FIGURE 4.4: Alternative representations of the atmosphere-ocean system.

which the surface ocean is attributed depth of approximately 75 m corresponding to the wind-mixed layer and the deep ocean below is modelled using an eddy diffusion equation. Such a refinement considerably improves a model's resolution in representing the vertical distribution of  $^{14}\text{C}$  in the oceans.

The next phase in ocean modelling saw the proposition of a number of models whose structures are intended to be more realistic than those associated only with the simple diffusive assumption (Bjorkstrom, 1979; Broecker et al., 1980). In these advective-diffusive models (Figure 4.4(c)), water downwells directly from cold surface layers into the deep ocean. This downwelling occurs predominantly at high latitudes and is balanced by upwelling at lower latitudes, particularly near the eastern basin edges. Therefore, it is usually necessary to divide the ocean, or at least the surface ocean, into various latitude bands. Disrupting the horizontal uniformity of the oceans means that these models are often additionally referred to as multi-dimensional box models as opposed to the one-dimensional box models discussed thus far.

Many other refinements to models of the atmosphere-ocean system have been suggested. For example, Peng et al. (1983) introduced the concept of the removal of carbon from the surface ocean to the deep ocean via the sinking of particulate matter produced by the surface ocean biomass. Siegenthaler (1983) proposed a box diffusion model with a polar outcrop whereby the deep waters at high latitudes exchange carbon directly with the atmosphere. It is suffice to say, however, that practically all models of the atmosphere-ocean system are based on one of the three major types illustrated in Figure 4.4

#### 4.2.2 Description and Validation of the Carbon Cycle Models

With such a wide range of carbon cycle models readily developed and available in the scientific literature, there seemed little to gain from designing a new carbon cycle model specifically for this study. Instead, a number of existing models were considered, ranging from a simple 1-box to a 25-box model.

Before any model is incorporated into this study its ability to maintain the natural steady state condition is checked. The

next step is to validate its predictive properties against both the atmospheric  $^{14}\text{C}$  specific activity record over the last century and the Mauna Loa  $\text{CO}_2$  record (the accuracy and frequency of atmospheric  $\text{CO}_2$  measurements prior to the Mauna Loa data are, at present, not sufficiently high to warrant their inclusion). The data necessary for this validation process are the total flux of carbon into the atmosphere from the various activities of man, namely, fossil fuel combustion (and to a small extent from cement production which is incorporated into the fossil fuel data), deforestation, nuclear weapon tests and nuclear power production. All these data have already been presented in Chapter 1.

The problems associated with validating carbon cycle models in this manner have already been explained but at the present time there is, unfortunately, no feasible alternative. A description of the models considered in this work and their validation now follows.

#### 4.2.2.1 The 1-Box Model

The simplest model considered is a 1-box model of the dynamic carbon cycle. This model, whose structure is shown in Figure 4.5, was used by Thommeret et al. (1983) to describe the decrease in the atmospheric  $^{14}\text{C}$  levels of the northern hemisphere following the bomb  $^{14}\text{C}$  'spike' of the early 1960s. The nomenclature system employed to define the carbon contents of the reservoirs ( $N_i$ ) and their transfer coefficients ( $k_{i,j}$ ) is identical to that used in Figure 4.1. However, in this and all other such diagrams, the symbols  $N_i$  and  $k_{i,j}$  are omitted in the interests of clarity. The singular box is, of course, the atmosphere and the transfer coefficient represents the net flux of excess carbon from the atmosphere into the oceans and biosphere.

This model only deals directly with the excess carbon levels in the atmosphere and therefore it is automatically in the natural steady state. To obtain an optimal fit to both the Mauna Loa  $\text{CO}_2$  record and historic atmospheric  $^{14}\text{C}$  levels, the model's parameters are varied within the constraints imposed by Thommeret et al. (1983). The values chosen are listed in Table 4.1 and the model's attempts to reproduce the observed trends in atmospheric  $\text{CO}_2$  and  $^{14}\text{C}$  levels over the period 1800-1980 are shown in

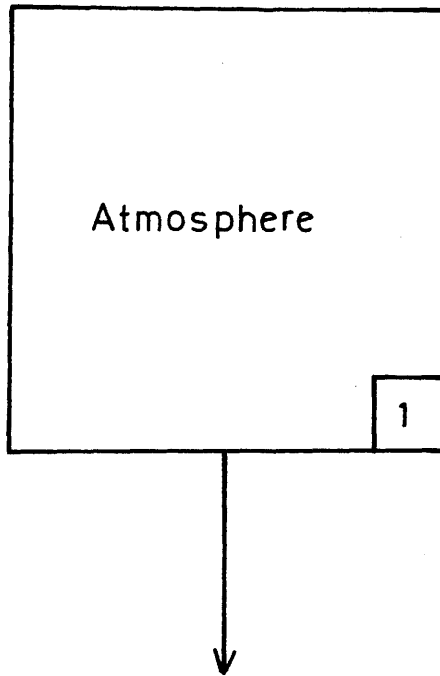


FIGURE 4·5: The 1- box model.

Table 4.1: The values of parameters used in the 1-box model

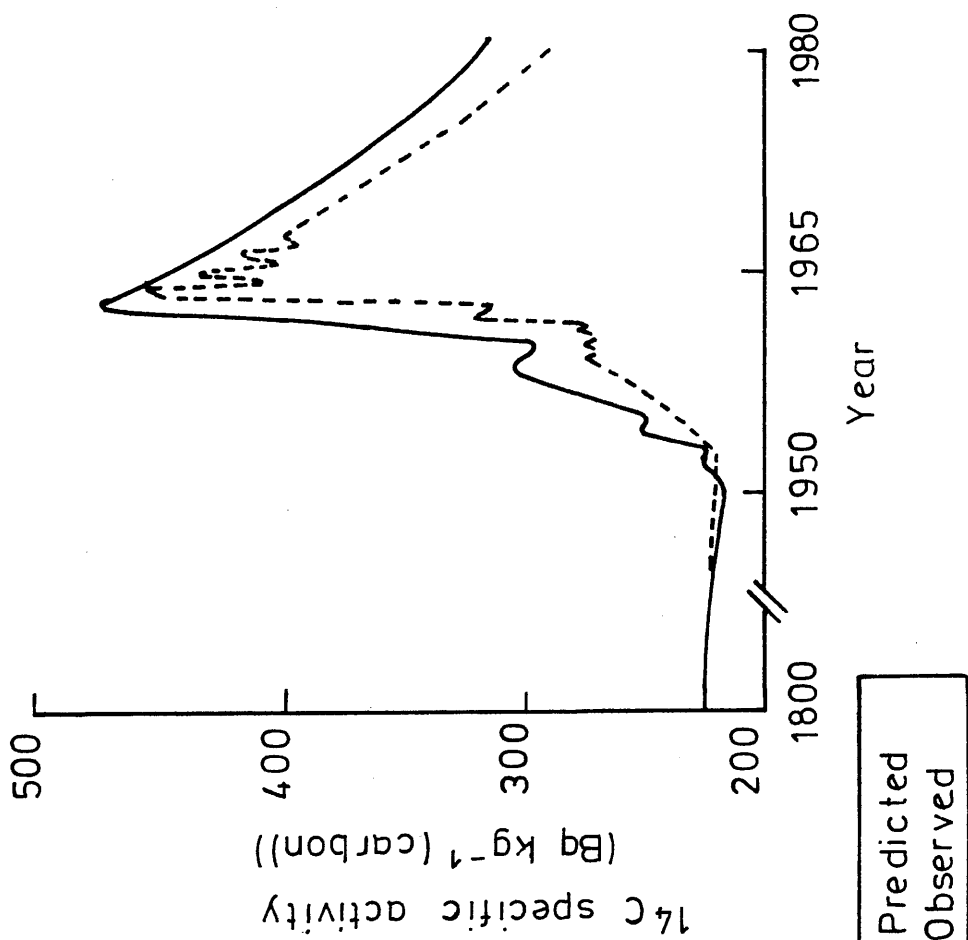
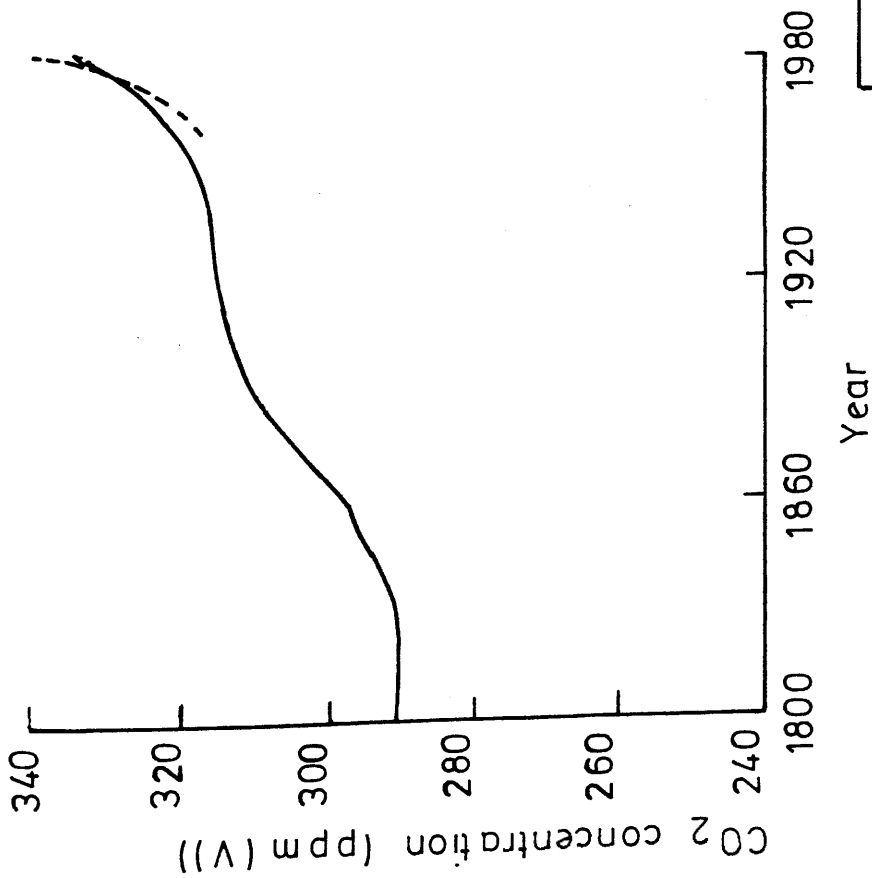
Parameter	Value
N <sub>1</sub>	6.2 x 10 <sup>14</sup> kg
k <sub>1</sub>	0.05

Figures 4.6(a) and 4.6(b) respectively.

With regard first to the predicted CO<sub>2</sub> levels shown in Figure 4.6(a), it is evident that the sharp rise in CO<sub>2</sub> levels during the last few decades, as indicated by the Mauna Loa data, is not adequately matched by the model's prediction. Nevertheless, considering the uncertainties implicit in the deforestation input data to the model, the correlation between its predictions and the Mauna Loa data is good.

In Figure 4.6(b), the model's predicted <sup>14</sup>C levels are compared against the observed values. This validation exercise is the most important as it is testing the very same aspect of the model as will be used in subsequent calculations, i.e. its ability to predict atmospheric <sup>14</sup>C levels. The first point to note is that the observed values are for the northern hemisphere only, since this model, as described by Thommeret et al. (1983), is evaluated for this hemisphere alone. In general, the agreement between the observed and predicted values is excellent. However, the maximum <sup>14</sup>C level is predicted by the model to have occurred in 1962, whereas it was actually observed in 1963. This anomaly is simply explained by the lack of a separate stratosphere box in the model. Most of the <sup>14</sup>C produced in nuclear weapon tests was injected into the upper atmosphere (stratosphere), whereas the observed <sup>14</sup>C levels correspond to values in the lower atmosphere (troposphere). Hence, the absence of a discrete stratospheric reservoir causes the model to ignore the finite mixing rate between the stratosphere and the troposphere and so causes the aforementioned effect. Another interesting point is that much of the fine structure noticeable in the observed values is not reproduced in the predictions. The fine structure is due mainly to seasonal transfer of bomb <sup>14</sup>C from the stratosphere to the troposphere. As the 1-box model does not make provisions for stratosphere to troposphere input, the model is intrinsically limited in this respect. Generally, the model does appear to exaggerate slightly the effect of all the various anthropogenic inputs to the atmosphere but, on the whole, its predictions are sufficiently accurate to justify its selection.

There are 3 main disadvantages associated with this model.



(a) Atmospheric CO<sub>2</sub> levels (b) Atmospheric <sup>14</sup>C levels

FIGURE 4.6 : Validation of the 1-box model.

Firstly, it basically applies to the northern hemisphere alone and thus errors are likely to be introduced when this model is used to represent the entire atmosphere. Secondly, it is unable to handle releases into sections of the carbon cycle other than the atmosphere. Finally, its simplicity suggests that it is probably not appropriate for use over long timescales (greater than a few hundred years).

#### 4.2.2.2 The 3-Box Model

The next model considered is a 3-box system whose structure is described in Figure 4.7. This model was constructed by Baxter and Walton (1970) with a view to studying the Suess effect. The model consists of 3 carbon reservoirs, the atmosphere, the surface ocean (incorporating the fast turnover compartment of the terrestrial biosphere) and the deep ocean, and 4 first-order exchange rates.

Once again, this model deals only with excess carbon and so, in the absence of any anthropogenic perturbation, it automatically retains the natural steady state. In calibrating the model with the CO<sub>2</sub> and <sup>14</sup>C records, its parameters are only varied within the limits defined by the original authors and the values chosen are listed in Table 4.2.

The model's attempt to reproduce the Mauna Loa CO<sub>2</sub> record is shown in Figure 4.8(a). A reasonable match is obtained, although, as for the 1-box model, the rate of increase in CO<sub>2</sub> levels observed at Mauna Loa is not attained. Again, this is as likely to reflect the failings of the input data as to be a deficiency of the model itself. The model's retrospective predictions of the atmospheric <sup>14</sup>C record are shown in Figure 4.8(b), along with the average global levels during the same period. The same basic differences between the two data sets arise here (as for the 1-box model) and for the same reasons. However, on the positive side, the general agreement between observed and predicted values is excellent. Certainly, there does seem to be a slight exaggeration of the effects of all anthropogenic inputs to the atmosphere but this does not appear to be a serious problem.

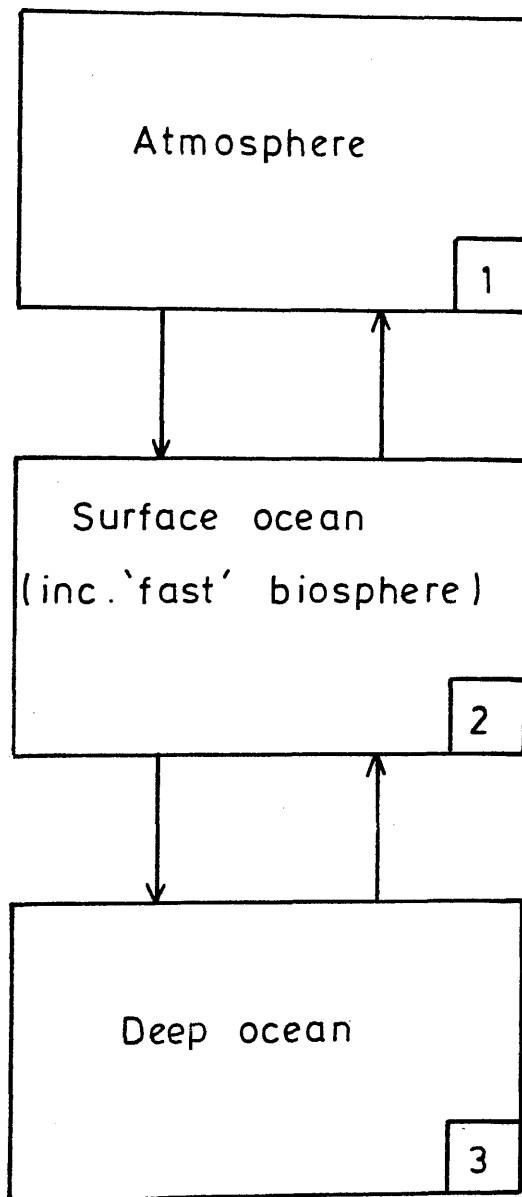
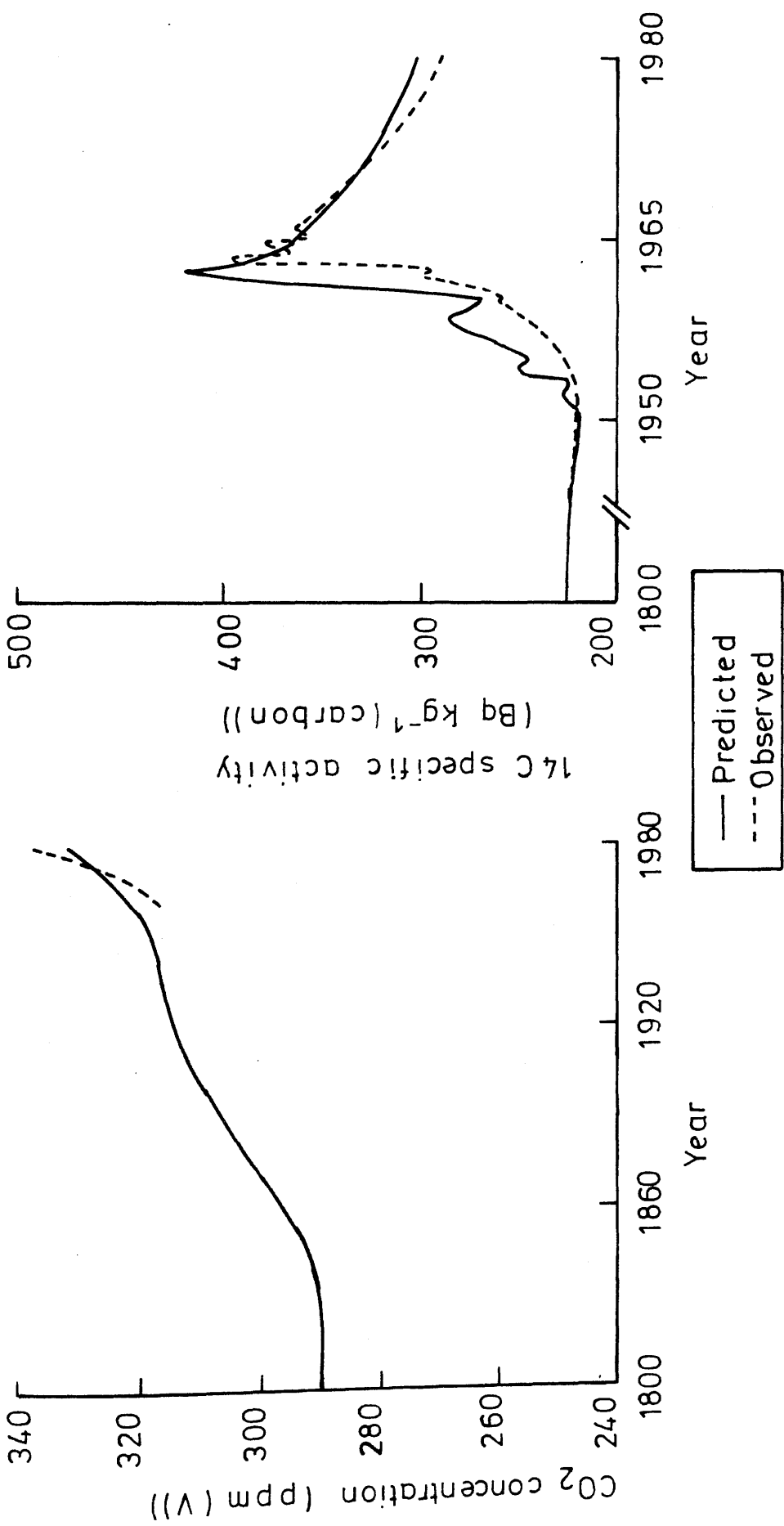


FIGURE 4.7: The 3-box model.

Table 4.2: The values of parameters used in the 3-box model

Parameter	Value
$N_1$	$6.2 \times 10^{14}$ kg
$N_2$	$1.1 \times 10^{15}$ kg
$N_3$	$3.7 \times 10^{16}$ kg
$k_{1,2}$	0.19
$k_{2,1}$	0.11
$k_{2,3}$	0.03
$k_{3,2}$	$8.5 \times 10^{-4}$



(a) Atmospheric CO<sub>2</sub> levels (b) Atmospheric <sup>14</sup>C levels

FIGURE 4.8: Validation of the 3-box model.

The major drawbacks of this model lie in its treatment of the terrestrial biosphere, i.e. it ignores the effect of the slow turnover compartment of the terrestrial biosphere and incorporates the fast turnover compartment into the surface ocean. Although this set-up appears to be satisfactory for short-term work (for which the model was originally designed), it may impair the model's performance over longer periods.

#### 4.2.2.3 The 8-Box Model

The 8-box model considered in this work is identical to that utilised by Bush et al. (1983) which is itself descended from a model described by Kelly et al. (1975). In both cases, the model was used to predict the possible effects of  $^{14}\text{C}$  discharges from the nuclear fuel cycle. Also, the model is structurally identical to the type recommended by CEC (1979). Thus, its inclusion here is reinforced by its use as the favoured model by the nuclear 'establishment' and, as such, its result provides a reference baseline against which to assess the significance of the other model's conclusions. The structure of the model, comprising 8 carbon reservoirs and 18 linear transfer coefficients, is described in Figure 4.9. The structure is essentially that of a 4-box model split into northern and southern hemispheres. The 4 main carbon reservoirs are the deep ocean, the surface ocean, the humus and a circulating carbon reservoir which incorporates not only the atmosphere but also the fast-turnover compartment of the terrestrial biosphere.

Since this model was to be used here for exactly the same purpose as that for which it was originally constructed, precisely the same working parameters as those used by the original authors were utilised. These parameters are listed in Table 4.3. Unlike the models discussed so far, the transfer coefficients do not apply to the excess carbon but to all the carbon in each reservoir. All the same, the model is constructed such that, even with this constant turnover of carbon, the model never deviates from the natural steady state starting conditions.

Before considering the models' response to the anthropogenic perturbations over the last couple of centuries, it should be pointed out that, for all such inputs to the atmosphere, it is

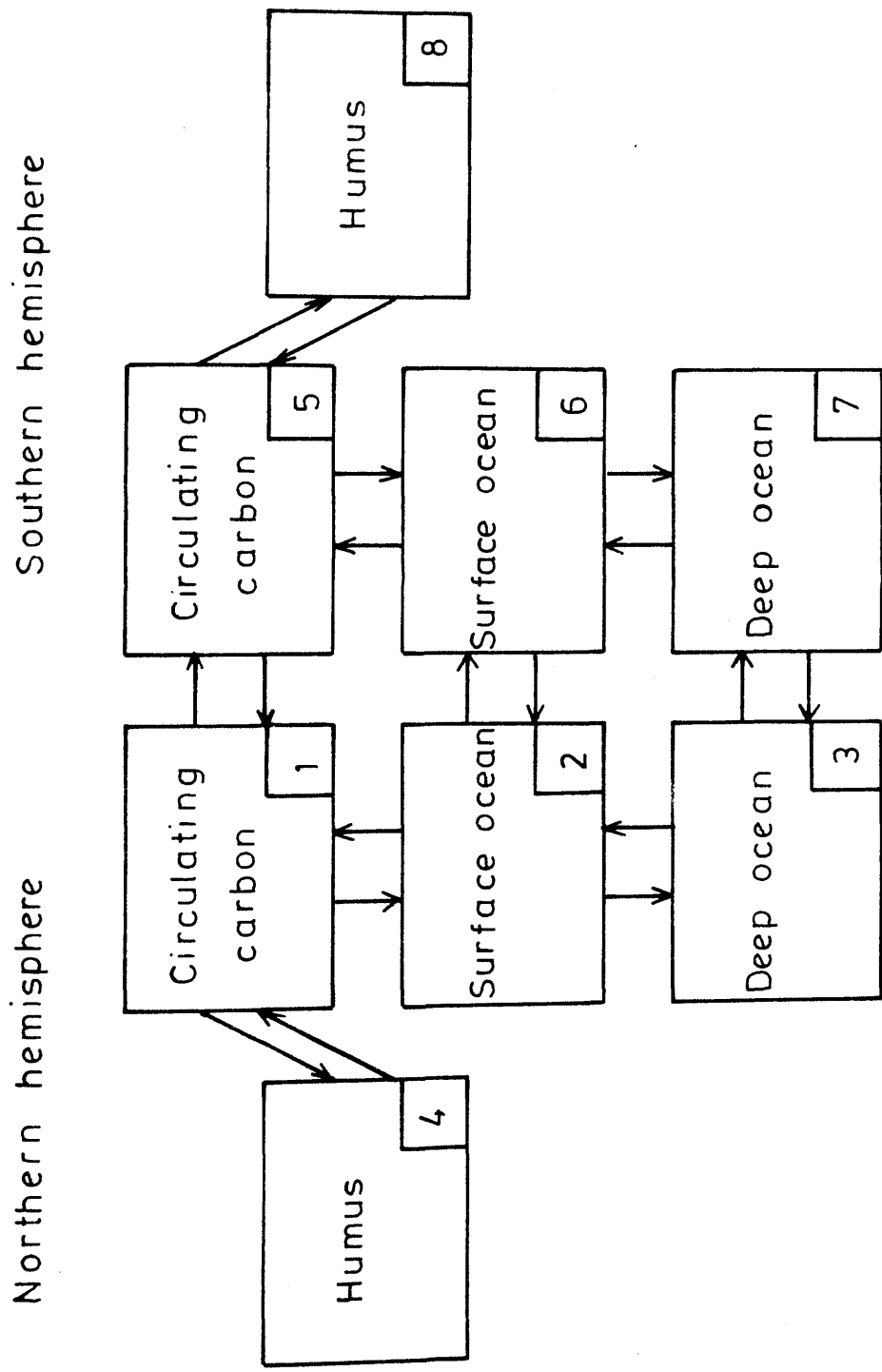


FIGURE 4-9: The 8- box model.

Table 4.3: The values of parameters used in the 8-box model

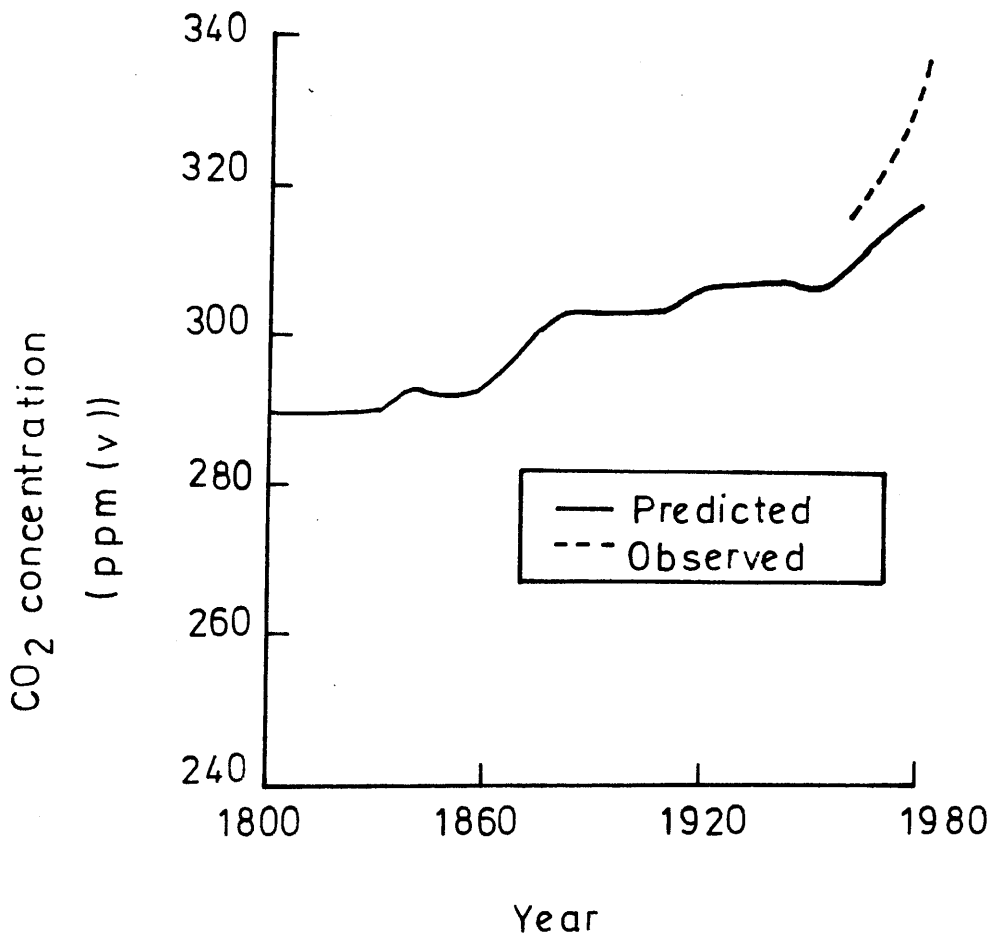
Parameter	Value
$N_1$	$3.6 \times 10^{14}$ kg
$N_2$	$5.0 \times 10^{14}$ kg
$N_3$	$1.2 \times 10^{16}$ kg
$N_4$	$1.2 \times 10^{15}$ kg
$N_5$	$3.3 \times 10^{14}$ kg
$N_6$	$7.6 \times 10^{14}$ kg
$N_7$	$2.2 \times 10^{16}$ kg
$N_8$	$4.0 \times 10^{14}$ kg
$k_{1,2}$	0.14
$k_{2,1}$	0.10
$k_{1,4}$	0.016
$k_{4,1}$	0.005
$k_{1,5}$	0.50
$k_{5,1}$	0.56
$k_{2,3}$	0.09
$k_{3,2}$	0.0032
$k_{2,6}$	0.1
$k_{6,2}$	0.066
$k_{3,7}$	0.005
$k_{7,3}$	0.0028
$k_{5,6}$	0.23
$k_{6,5}$	0.10
$k_{5,8}$	0.0061
$k_{8,5}$	0.005
$k_{6,7}$	0.09
$k_{7,6}$	0.0028

assumed that 80% entered the northern hemisphere and 20% the southern hemisphere (in accordance with the present-day population distribution (Bush et al., 1983)). This distribution is particularly apt for bomb-produced  $^{14}\text{C}$  which was generated predominantly in the northern hemisphere (United Nations, 1982). For other effects, it would also seem a reasonable approximation on the basis of the population data alone. In Figure 4.10(a) the model's reconstruction of the atmospheric  $\text{CO}_2$  record is shown along with the Mauna Loa data. In this case, the model's predictions correspond to the southern hemisphere alone since the Mauna Loa record is obtained from this hemisphere (although its values have been shown to be within 0.1% of the global mean (Keeling et al., 1982)). The model's predictions are, however, consistently around 20 ppm(V) too low (the  $\text{CO}_2$  levels predicted for the northern hemisphere are generally around 5 ppm(V) higher than those in the southern hemisphere). The atmospheric  $^{14}\text{C}$  levels since 1800, as predicted by the model, are plotted along with the observed values in Figures 4.10(b) and 4.10(c) for the northern and southern hemispheres respectively. In each case the agreement between the two data sets is excellent, with the exception of the usual two anomalies (fine structure/premature maximum). Since this ability is far more important than its reliability in predicting  $\text{CO}_2$  levels, the model clearly deserves inclusion in this study.

The main drawbacks of this model are, firstly, its treatment of the atmosphere and the fast-turnover compartment of the terrestrial biosphere as one reservoir and, secondly, the fact that its use requires a considerably greater computational effort than the models previously discussed.

#### 4.2.2.4 The 25-Box Model

The 25-box model is the most complicated representation of the carbon cycle used in this study. It was originally designed by Emanuel et al. (1984) for use in predicting the future extent of the greenhouse effect. The structure of the model, shown in Figure 4.11, comprises 25 discrete carbon reservoirs and 54 different transfer coefficients. The atmosphere-ocean system is described by a box diffusion model first proposed by Killough and



(a) Atmospheric CO<sub>2</sub> levels  
(southern hemisphere)

FIGURE 4.10: Validation of the 8-box model.

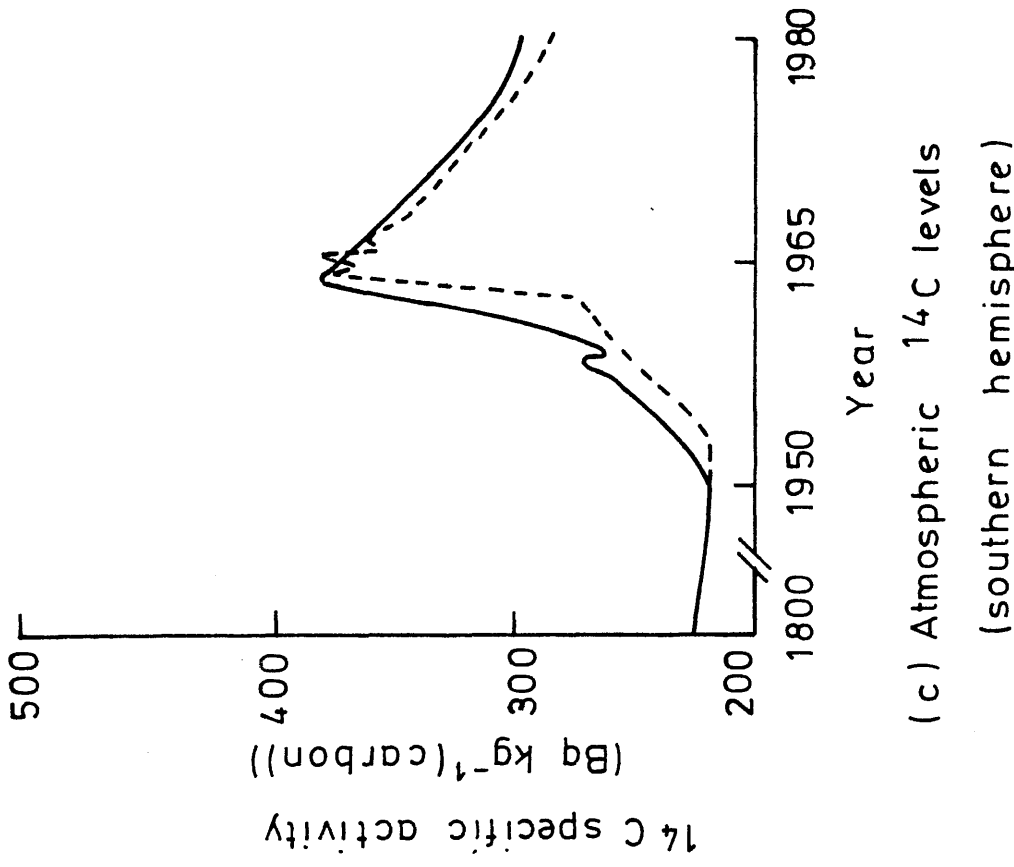
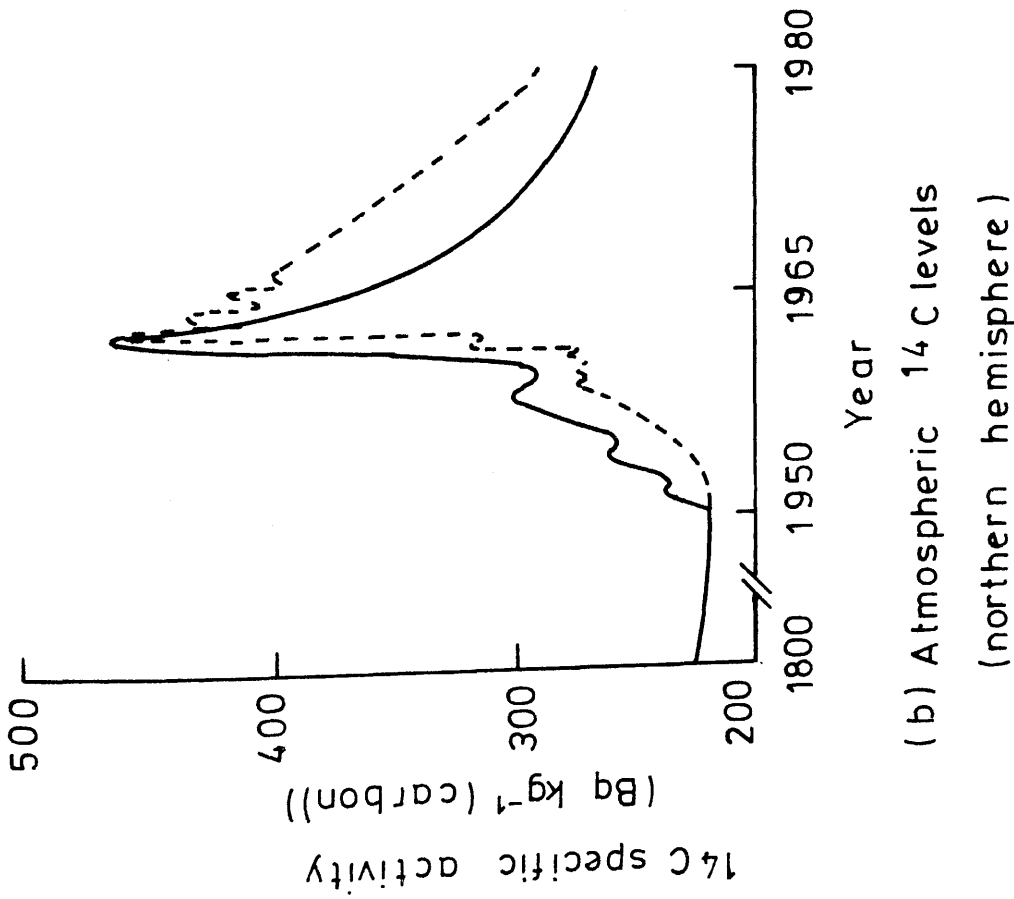


FIGURE 4.10: Validation of the 8-box model.

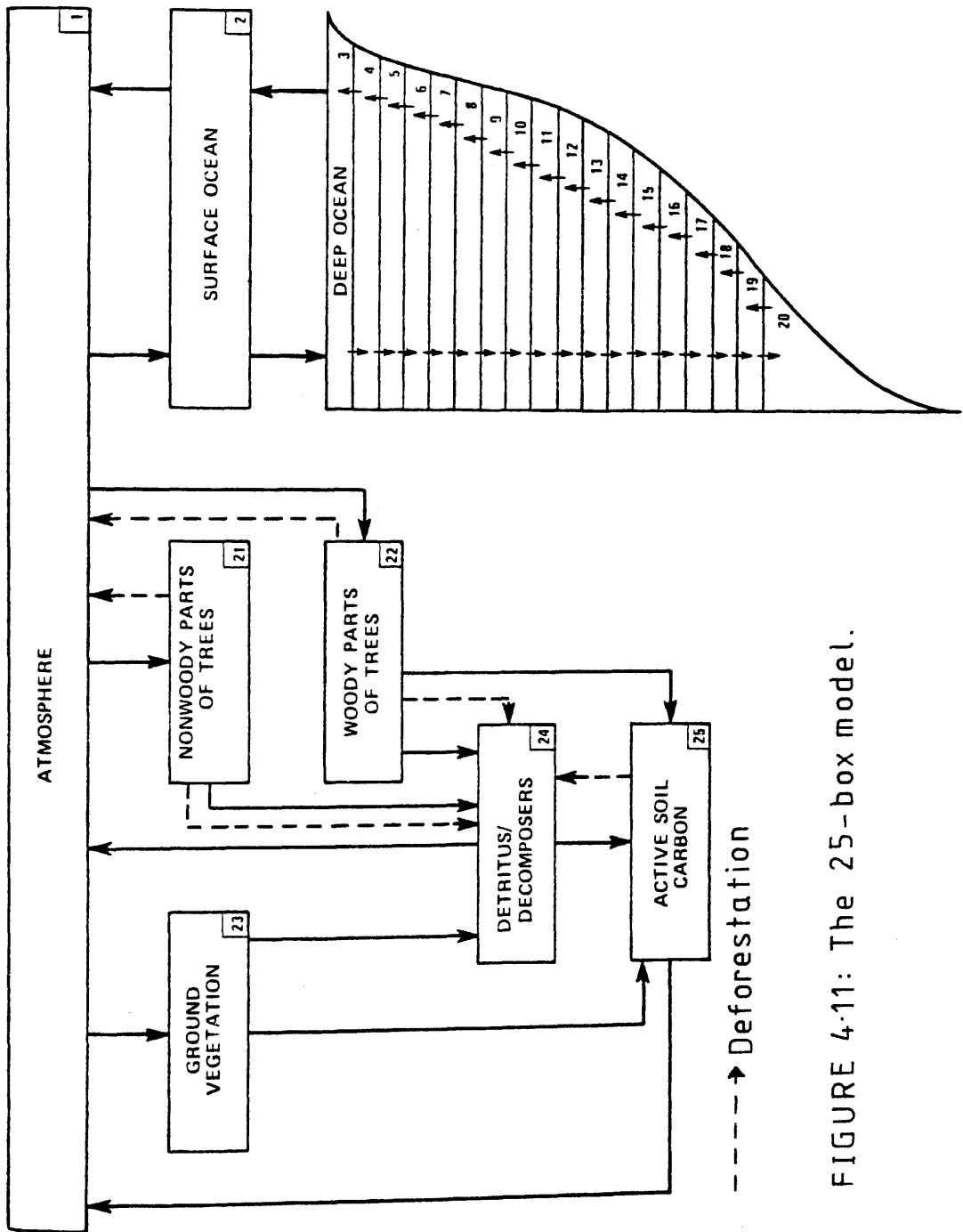


FIGURE 4-11: The 25-box model.

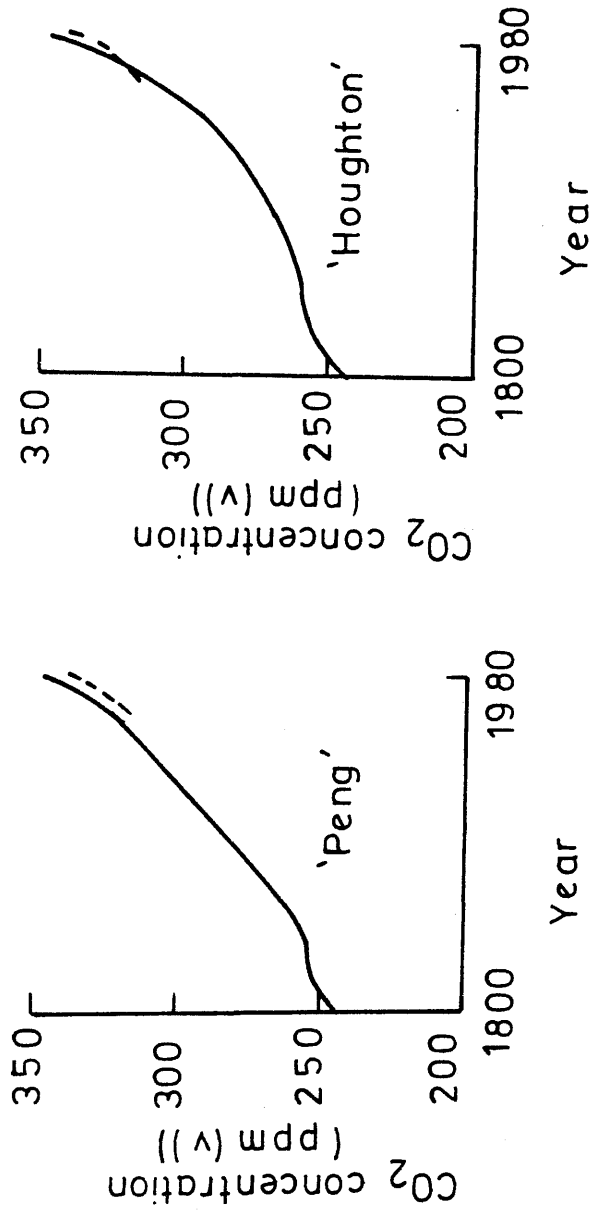
Emanuel (1981) and the terrestrial biosphere is modelled in the complex manner detailed by Emanuel et al. (1981). Non-linear exchange rates are assumed for both atmosphere-surface ocean and atmosphere-biosphere transfers.

Initially, when it was decided to utilise a carbon cycle model incorporating a diffusive treatment of the oceans, a 16-box model proposed by Killough (1980) was considered. However, problems arose while attempting to set up the model to maintain natural steady state conditions. Model parameters had to be significantly altered from those suggested by the author, thus casting some doubt on the model's integrity. While investigating the problem, this 25-box model, which also incorporates a diffusive treatment of the ocean, came to light. Since this 25-box model had, in addition, a more detailed representation of the terrestrial biosphere, it was decided to abandon the 16-box model in favour of the more refined 25-box system.

In the original work on this model by Emanuel et al. (1984), a detailed calibration procedure was outlined and thus the starting parameters suggested by the authors were adopted for this work. Selected model parameters, when set up to reproduce the natural steady state condition, are listed in Table 4.4 (a full listing is contained in Emanuel et al. (1984)). A comparison of the values in Table 4.4 to those for the other models in Table 4.1-4.3 shows that, for directly comparable parameters, the values in all models are very similar. The main difference between this model and the others is that it has more parameters, allowing it to represent the various processes in more detail. The value of  $5.2 \times 10^{14}$  kg assumed for the natural atmospheric carbon content is rather low. However, such a value is necessary to ensure reasonable agreement between the model's predicted CO<sub>2</sub> levels and the Mauna Loa data. The models' attempt to reproduce the Mauna Loa record is illustrated in Figure 4.12(a). In this case the predicted levels are all around 10 ppm(V) higher than the Mauna Loa values. Thus, even the use of a highly complex model does not produce a particularly good reproduction of the CO<sub>2</sub> record. This observation adds fuel to the argument that the fault lies in the input data. To investigate this hypothesis, the model was run again, but this time using the deforestation data

Table 4.4: The values of parameters used in the 25-box model

Parameter	Value
$N_1$	$5.2 \times 10^{14}$ kg
$N_2$	$6.6 \times 10^{14}$ kg
$(N_3 + N_4 + \dots + N_{20})$	$3.8 \times 10^{16}$ kg
$(N_{21} + N_{22} + \dots + N_{25})$	$2.0 \times 10^{15}$ kg
$k_{1,2}$	0.19
$k_{2,1}$	0.15
$k_{2,3}$	5.8
$k_{3,2}$	8.8
$k_{1,(21,22,23)}$	0.12
$k_{(24,25),1}$	0.05



(a)

(b)

FIGURE 4.12: Validation of the 25-box model using atmospheric CO<sub>2</sub> levels.

provided by Houghton et al. (1983) (all work so far has been based on the data of Peng et al. (1983)). The results, however, shown in Figure 4.12(b), are not notably different from the original values. Thus, even at this rather complex level, carbon cycle models and their predictions are not, as yet, in total harmony with reality. Turning now to the model's ability to predict atmospheric  $^{14}\text{C}$  levels since 1800, it is noticeable that much the same picture emerges as from previous models. The results, shown in Figure 4.13, suggest a good agreement between the predicted and observed levels. The maximum levels are particularly close (except for the 1 year anticipation by the model), although the model's  $^{14}\text{C}$  levels fall off rather more sharply than was actually observed.

The major drawback of this model is the fact that, due to limited knowledge of the processes involved in the carbon cycle, it is not possible to accurately quantify all of the many parameters associated with the model. Therefore, although this model, on the surface, appears to be far superior to the previous models discussed, its true effectiveness for any given purpose must still be carefully evaluated. From a practical point of view, one further disadvantage associated with this model is the large commitment of computing time necessary to run it.

#### 4.2.3 Justification of Choice of Models

It may appear peculiar that no model incorporating the advective carbon fluxes within the oceans is considered in this study. The main reason for this omission is that numerous studies have demonstrated that the behaviour of advection models is very similar to that of diffusion models (Killough and Emanuel, 1981; Edmonds et al., 1984). Both these model types are highly complicated and, hence, computationally time-consuming. In this study, therefore, only one such advanced model is considered necessary.

Another peculiarity is that, throughout the validation process and for all models, the predictions consistently failed to place accurately the temporal position of the 'bomb  $^{14}\text{C}$  peak' or to reproduce the fine structure subsequently observed in the atmospheric  $^{14}\text{C}$  levels. These failings are caused by the

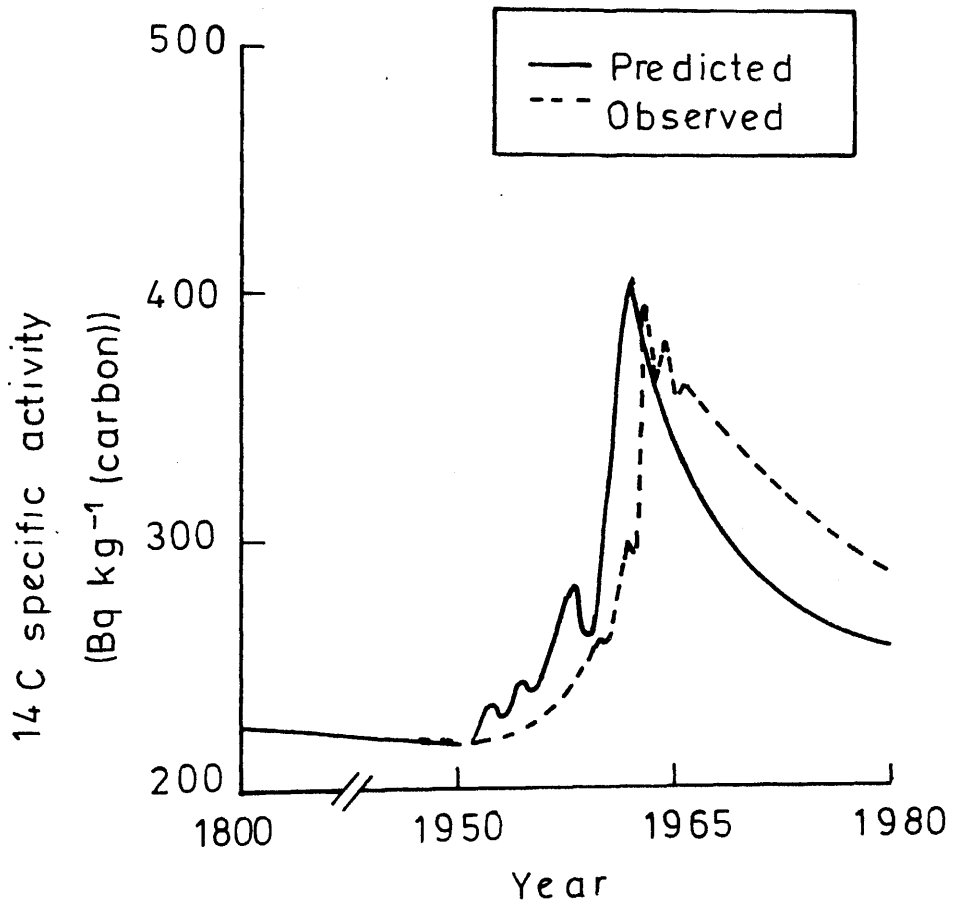


FIGURE 4-13: Validation of the 25-box model using atmospheric  $^{14}\text{C}$  levels.

lack of of a stratosphere/troposphere division in their representations of the atmosphere. It is therefore natural to question the reason for omission of such a simple addition to the models. The reason lies in the nature of the specific application for which the models are to be used here, i.e. for prediction of future atmospheric  $^{14}\text{C}$  levels. As mentioned earlier, the stratosphere/troposphere division is desirable only because of the injection of bomb-produced  $^{14}\text{C}$  into the stratosphere and the subsequent exchange of  $^{14}\text{C}$  to the troposphere. For prediction of future atmospheric  $^{14}\text{C}$  levels here it is optimistically assumed that there will be no further significant inputs of  $^{14}\text{C}$  from nuclear weapons. Furthermore, all  $^{14}\text{C}$  and  $^{12}\text{C}$  perturbations of interest in this study are low-altitude (tropospheric) processes. Thus incorporation of a stratosphere/troposphere division seems to be superfluous.

The most obvious question about the approach here is perhaps to query why four different models are being investigated. Why not concentrate on one model alone, presumably the most complex one? In fact, there are a number of advantages to be derived by considering a selection of carbon cycle models. Firstly, there is the benefit of having an inbuilt safety device allowing cross-checking of results. Secondly, it should be remembered that complex models require large amounts of computing time. Therefore, it is useful, in certain situations, to have available less complex models which allow relatively quick, although often significantly less accurate, calculations.

#### 4.3 RADIATION DOSE TO THE GLOBAL POPULATION FROM $^{14}\text{C}$ DISCHARGES FROM THE NUCLEAR FUEL CYCLE

Now that valid representations of the global carbon cycle have been obtained, it is possible, with the help of the appropriate input data, to predict the effect that  $^{14}\text{C}$  discharges from the nuclear fuel cycle will have on global atmospheric  $^{14}\text{C}$  levels and, hence, on the radiation dose to man. This investigation is, by necessity, divided into two quite distinct subsections, namely, the short and long-term effects of these  $^{14}\text{C}$  discharges. The objectives of both subsections are now explained.

In the past, the effects of  $^{14}\text{C}$  discharges from the nuclear industry have not made a notable impression on atmospheric  $^{14}\text{C}$  levels. However, it is possible that the future growth of the nuclear power industry will have a significant effect on atmospheric  $^{14}\text{C}$  levels. Thus, in this section of the study, an attempt is made to predict the future trend in atmospheric  $^{14}\text{C}$  levels, from which an estimate of the radiation dose to the world population as a result of  $^{14}\text{C}$  discharges from the nuclear fuel cycle can be made. Such work clearly requires future projection of the magnitude of the various anthropogenic perturbations on the global carbon cycle. All such projections and, in particular, the future growth of the nuclear power industry, are extremely uncertain. Therefore, it is not considered reasonable to extend these predictions beyond 2050 AD. Thus, basically, this section defines the short-term effects of these  $^{14}\text{C}$  discharges. This information on its own is, however, insufficient to quantify fully the global effects of the nuclear industry's  $^{14}\text{C}$  discharges. The relatively long half-life of  $^{14}\text{C}$ , coupled with its mobility in the environment, result in irradiation of the global population over a very long time interval. Quantification of this effect is most conveniently achieved by considering the consequence on future  $^{14}\text{C}$  levels of the release of 1 unit of  $^{14}\text{C}$ . From this information a measure of the collective effective dose equivalent commitment (or CEDEC as it will be referred to throughout this chapter) per unit release of  $^{14}\text{C}$  can be obtained. This quantity is extremely useful in evaluating the long-term radiological significance of  $^{14}\text{C}$  discharges.

Taken together, these two subsections represent as full an evaluation as is presently possible of the radiation dose to the global population from  $^{14}\text{C}$  discharges from the nuclear fuel cycle.

#### 4.3.1 Short-term Effects of $^{14}\text{C}$ Discharges from the Nuclear Fuel Cycle

Many different assumptions must be invoked to allow prediction of future atmospheric  $^{14}\text{C}$  levels and thereafter the radiation dose to the public from the nuclear industry's

$^{14}\text{C}$  discharges. Details of these assumptions will therefore be explained prior to presentation and interpretation of the results.

#### 4.3.1.1 Basic Scenarios

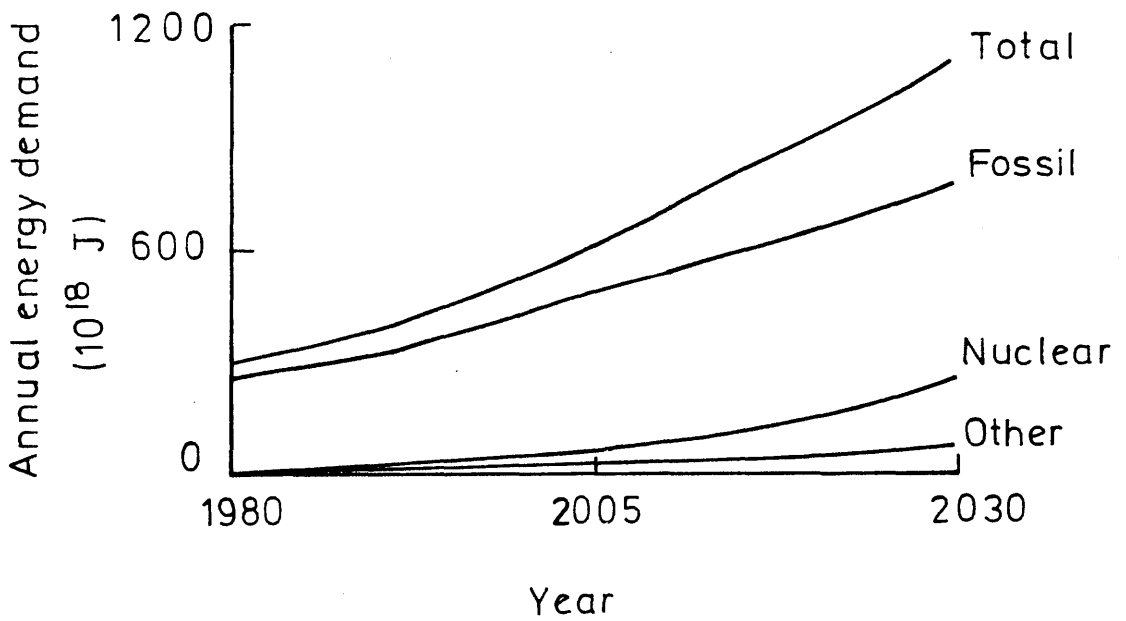
To predict future trends in atmospheric  $^{14}\text{C}$  specific activities it is necessary to quantify the future input of carbon to the global carbon cycle. The simplifying assumption is made here that the natural production rate will remain constant throughout the period to 2050. This seems a reasonable assumption since, on past evidence, any variations in the natural production rate over this period are likely to be insignificant. The problem can thus be narrowed to one of quantifying future anthropogenic perturbations on the global carbon cycle. The problem is simplified by two further assumptions. Firstly, it is assumed that there will be no future atmospheric detonations of nuclear weapons. Secondly, it is assumed that there will be no net flux of carbon from the terrestrial biosphere to the atmosphere during the period under study. Certainly, in the past, such a flux has existed but, as discussed in Section 1.2.5.3, it is far from certain whether, at the present time, the biosphere is a net sink or source of carbon. In view of this uncertainty, it seems reasonable to assume a neutral terrestrial biosphere. Finally, the problem corrupts to one of predicting both the future rate of combustion of fossil fuels and the future development of the nuclear power industry. Both of these trends are clearly highly dependent on the future electricity demand, for the major use of both resources lies in production of electricity. Future electricity demand itself depends on many factors, including population increase, economic growth and the rate of industrialisation of the Third World (Greenhalgh, 1980). Thus, in recognition of the many problems associated with future energy predictions, it seemed reasonable to limit the study to the time period to 2050.

Even with this severe limitation on the study period, there remains a wide range of feasible energy sceanrios. Thus, although a 'most probable' scenario will be defined hereafter, a broad spectrum comprising 7 scenarios is investigated. The first two predictive models are based on the findings of the International

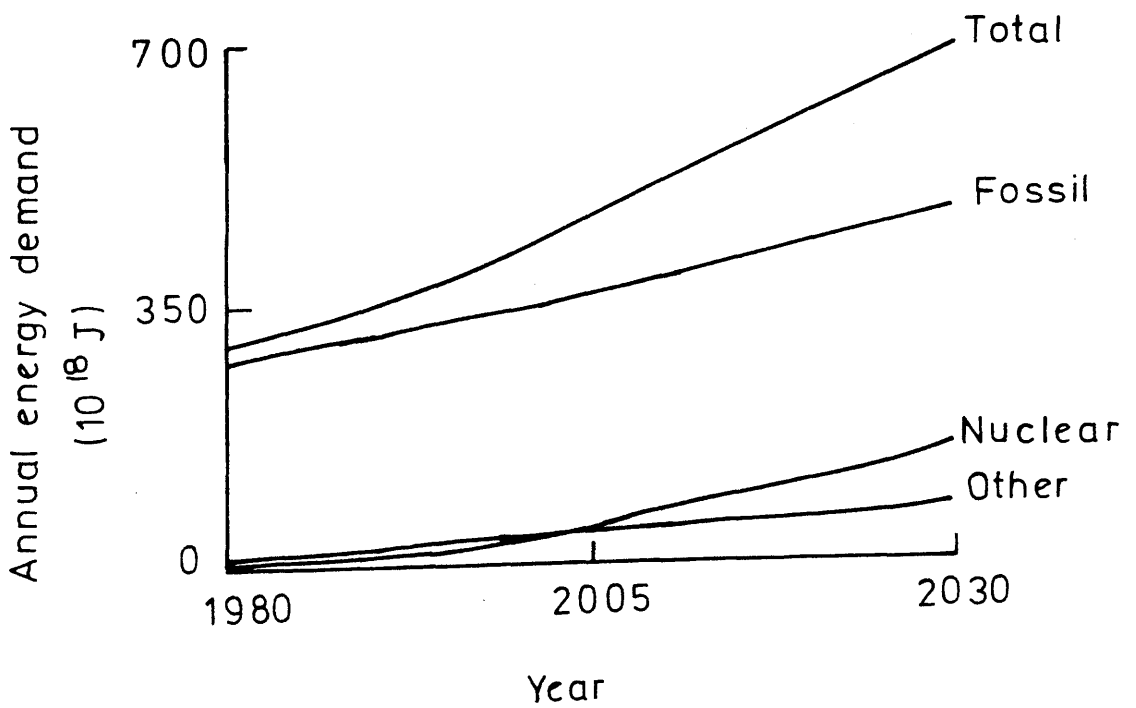
Institute of Applied Systems Analysis (IIASA) (Hafele, 1981). Figures 4.14(a) and 4.14(b) show the predicted distribution of the energy demand for the period 1980-2030 for the high and low economic growth scenarios respectively. It is perhaps worth clarifying at this stage the reasons for starting the energy projections at 1980 as opposed, for example, to 1985. The primary reason is to enable continuity of predictions. That is, complete data sets are available to allow operation of the models to 1980 but after this date some of the necessary information becomes rather uncertain. In calibrating models, therefore, it is convenient to run them to 1980 only and, hence, it is equally convenient to 'restart' the model where it terminated. Notwithstanding this factor, whenever accurate data are available, the appropriate projection is constrained to reproduce the known trend.

It is regrettable that the IIASA scenarios extend only to 2030. However, they are based on sound economic logic and, for this reason, fully merit inclusion in this study. In the remaining scenarios, the future use trends for fossil and nuclear fuels are derived from independent estimates of the possible exploitation of each fuel type. That is, for each fuel, three projections of future use are defined (a low, medium and high case). From these data, five scenarios are generated by combining the medium case for each fuel type with the three different projections for the other fuel type. Figure 4.15 shows the low (A), medium (B) and high (C) projections of future fossil fuel use, as suggested by Edmonds and Reilly (1983a, 1983b, 1983c). Also included in this diagram, for comparison, are the IIASA predictions. The projections of nuclear fuel usage are presented in Figure 4.16, in which, again, the IIASA predictions are included. The medium case (B) is based on the work of Edmonds and Reilly (1983a, 1983b, 1983c), whereas the low case (A) is based on a nuclear moratorium situation in which no increase in installed nuclear energy capacity occurs after 2000. The high case (C) follows an enhanced nuclear energy strategy defined by IIASA (Hafele, 1981) but, for this study, is extrapolated to 2050.

The projections for the future rate of combustion of fossil fuels, shown in Figure 4.15, are presented in terms of the mass of



(a) High energy demand



(b) Low energy demand.

FIGURE 4.14: Projected energy demands, 1980-2030 (IIASA).

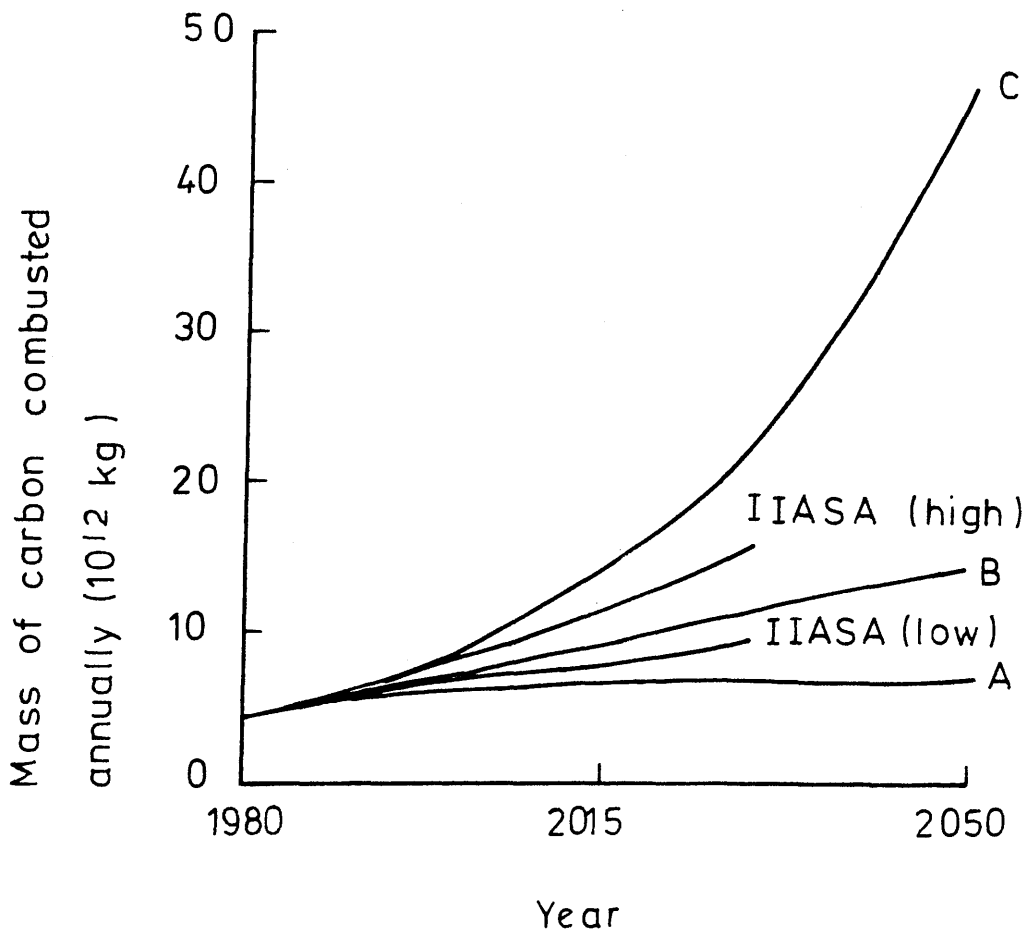


FIGURE 4-15: Projections of the future rate of combustion of fossil fuels, 1980-2050.

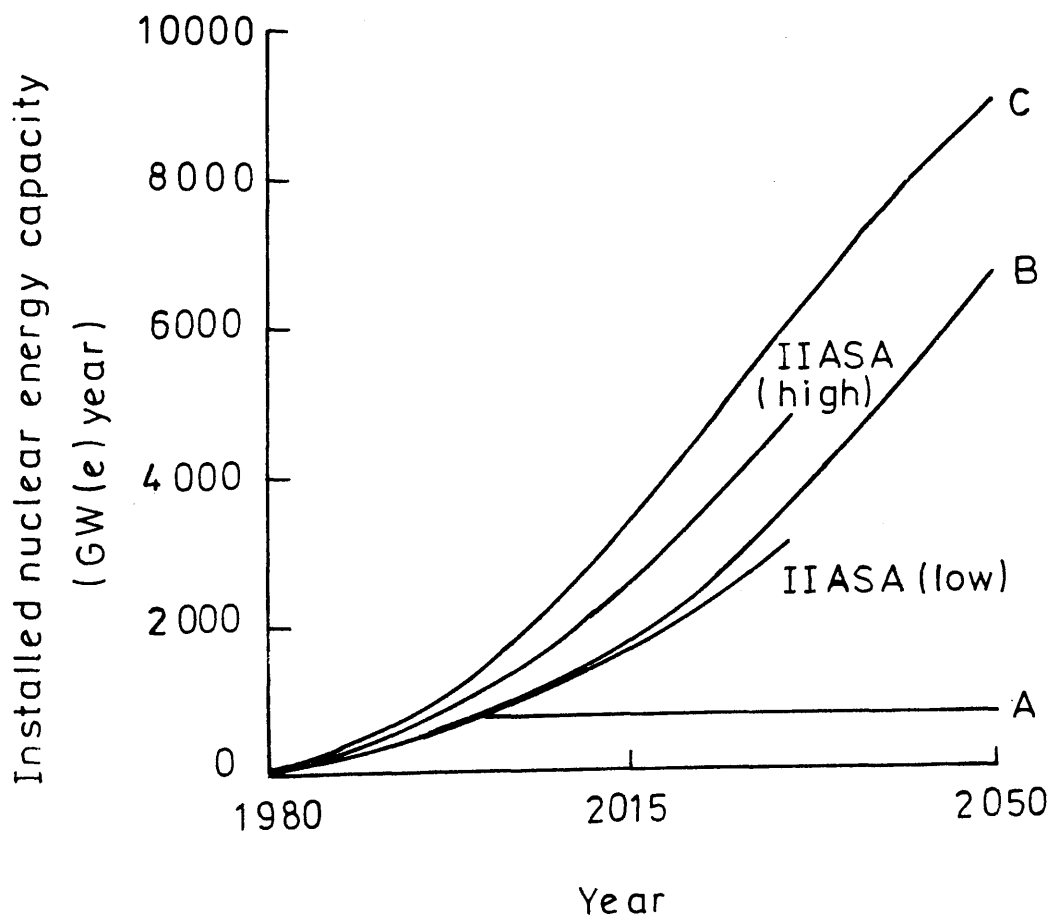


FIGURE 4.16: Projections of the future rate of growth of the nuclear industry, 1980 - 2050.

carbon combusted. In other words, these data are in the correct format for its direct incorporation into the carbon cycle models. The projected nuclear energy demands illustrated in Figure 4.16, however, are measured in terms of the installed nuclear energy capacity, whereas the models require a measure of the quantity of  $^{14}\text{C}$  discharged. A conversion factor is therefore required to transform the data for installed nuclear energy capacity into measures of  $^{14}\text{C}$  discharge. Most of the raw data from which this conversion factor is generated are listed in Table 4.5.

The reactor type distribution presented in Table 4.5 assumes that 90% of the installed nuclear energy capacity is in the form of light water reactors in the proportion of 2 PWRs to 1 BWR (Hayes and MacMurdo, 1977; Killough and Till, 1978; Matthies and Paretzke, 1982; Bush et al., 1983), with the remainder being evenly spread amongst the other reactor types. In reality, the reactor type distribution will be constantly changing over the period 1980-2050. It is, however, all but impossible to assess accurately the extent and timescale of implementation of such changes. Hence, the assumption used here, of a constant distribution, is as likely as any to reflect accurately the future trend. The  $^{14}\text{C}$  production pathways, summarised in Table 4.5, have been detailed in Section 1.3.2. Weighting these values for the adopted reactor type distribution generates a mean  $^{14}\text{C}$  production rate of  $3.40 \text{ TBq (GW(e) year)}^{-1}$ . The actual release rate is, however, only  $0.94 \text{ TBq (GW(e) year)}^{-1}$  (assuming that 50% of all spent nuclear fuel is reprocessed). Some of this  $^{14}\text{C}$  ( $0.24 \text{ TBq (GW(e) year)}^{-1}$ ) is released in a chemical form other than  $\text{CO}_2$ , e.g.  $\text{CO}$ ,  $\text{CH}_4$  and  $\text{C}_2\text{H}_2$ , and these must be treated differently as they are not available directly to the carbon cycle until they have been oxidised to  $\text{CO}_2$ . The time required for atmospheric oxidation has been estimated at around 7 years for most of these compounds (Moghissi and Carter, 1977; Killough and Till, 1978; Schwibach et al., 1978). Hence a similar delay time must be incorporated into the modelling process. The bulk of the  $^{14}\text{C}$  produced constitutes a solid waste arising, the eventual fate of which is unclear but it is unlikely to influence atmospheric  $^{14}\text{C}$  levels in the period to 2050. To obtain the  $^{14}\text{C}$  discharge rate from the nuclear fuel cycle, it is necessary now to combine the appropriate

Table 4.5:  $^{14}\text{C}$  waste arisings from the nuclear fuel cycle

Reactor type	Distribution (%)	Production rate (TBq (GW(e)year) $^{-1}$ )	Solid waste (TBq (GW(e)year) $^{-1}$ )		Gaseous waste (TBq (GW(e)year) $^{-1}$ )			
			Reactor	Reprocessing Plant	Reactor		Reprocessing plant	
					CO <sub>2</sub>	other	released	stored
PWR	60	2.4	1.0	0.6	0.04	0.16	0.3	0.3
BWR	30	3.3	1.7	0.6	0.285	0.015	0.35	0.35
HWR	2	18.2	1.3	1.3	7.2	7.2	0.6	0.6
MAGNOX	2	14.6	9.0	0.8	0.9	small	1.95	1.95
AGR	2	8.4	5.3	1.9	0.7	small	0.25	0.25
HTGR	2	6.4	small	small	small	small	0.32	0.32
LMFBR	2	0.7	small	0.5	small	small	0.1	0.1
Weighted average		3.40	1.42	0.63	0.29	0.24	0.41	0.41

data from Table 4.5 with the installed nuclear energy capacity figures and the mean load factor of 0.7 (IAEA, 1983).

For convenience, the structures of the 7 different energy scenarios are listed in Table 4.6. The IIASA projections for low and high economic growth are reflected in scenarios S1 and S2 respectively, and the remaining 5 scenarios, S3-S7, are obtained from the combination of various projections of future fossil and nuclear fuel usage. Certainly, with regard to the range of projections to 2050, scenario S4 (constructed from the medium projections of both fossil and nuclear fuel usage) appears to be the most realistic and, throughout the study, is assumed to be the 'most probable'.

Before it is possible to investigate the effects of  $^{14}\text{C}$  discharges from the nuclear fuel cycle to 2050 it is necessary to decide upon the best means of using the carbon cycle models available. The validation process for these models indicated that they are all suitable for assessing fluctuations in atmospheric  $^{14}\text{C}$  levels over short time periods. However, in Table 4.7 the deviation between the predicted and observed values of the maximum atmospheric  $^{14}\text{C}$  level after the 'bomb spike' is quantified. These results demonstrate that the more complex models produce more accurate predictions than the simpler models. So, although any of the carbon cycle models could be used in the following calculations, more accurate values will be obtained by using the more complex models.

#### 4.3.1.2 Radiation Dose to the Public to 2050

By using all the various scenarios discussed in the previous section it is obviously possible to generate a wide range of values for the radiation dose to the public to 2050 from  $^{14}\text{C}$  discharges from the nuclear fuel cycle. This aspect of the work will be considered in due course but, initially, precedence is given to determining the best estimate of the radiation dose.

The best estimate of the atmospheric  $^{14}\text{C}$  levels to 2050 is obtained by feeding the data associated with the 'most probable' energy scenario (S4) into the most complex carbon cycle model (the 25-box model). The results, presented in Figure 4.17,

Table 4.6: The structure of the seven basic energy scenarios

Scenario	Fossil fuel projection	Nuclear fuel projection
S1	IIASA (low)	IIASA (low)
S2	IIASA (high)	IIASA (high)
S3	A	B
S4	B	B
S5	C	B
S6	B	A
S7	B	C

Table 4.7: Short-term accuracy of the carbon cycle models

Model	Predicted maximum atmospheric $^{14}\text{C}$ level (Bq kg $^{-1}$ (carbon))	Deviation from observed maximum atmospheric $^{14}\text{C}$ level* (%)
1-box	474	19.7
3-box	420	6.1
8-box	405	2.3
25-box	406	2.5

\* observed maximum atmospheric  $^{14}\text{C}$  level is 396 Bq kg $^{-1}$  (carbon)

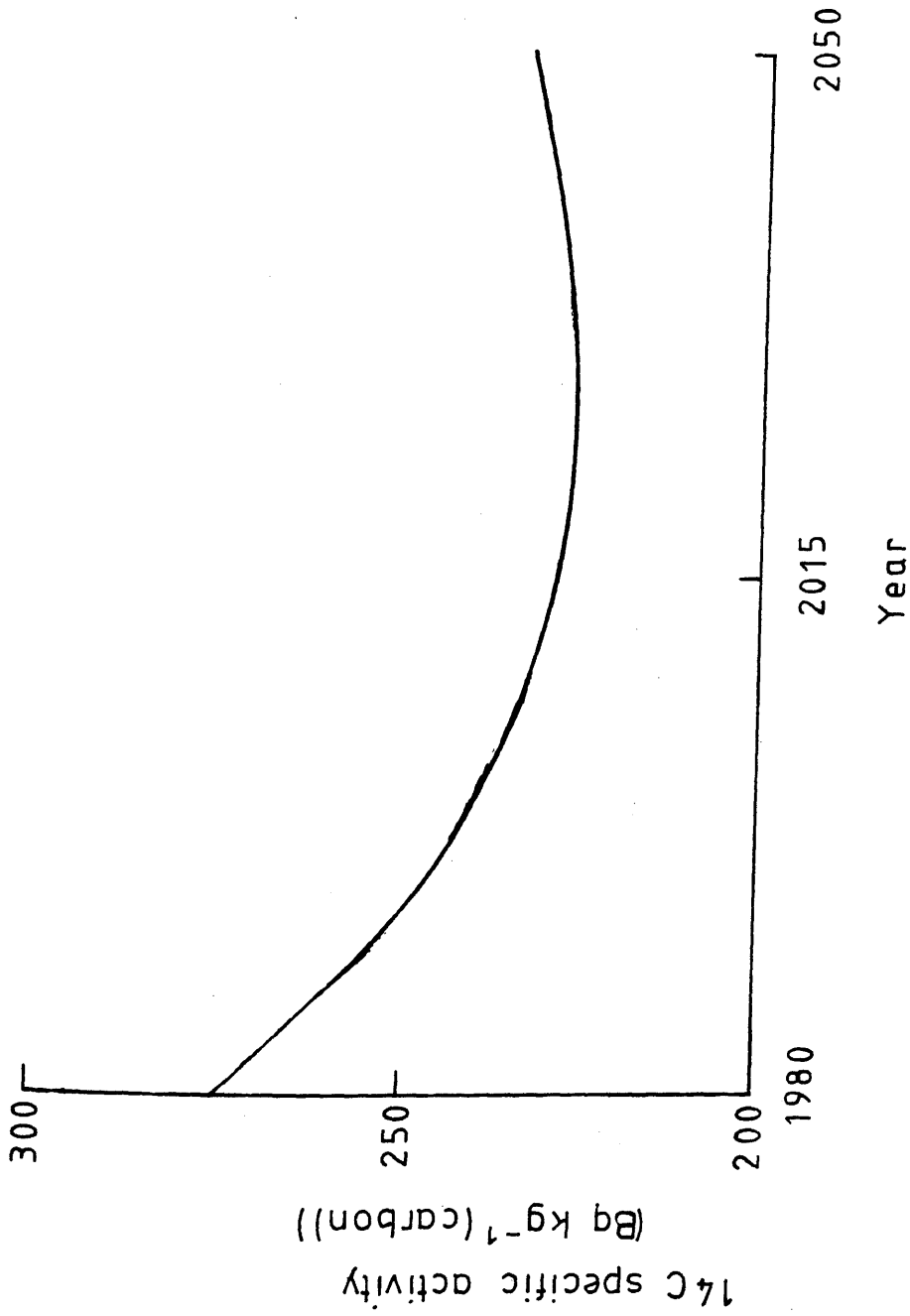


FIGURE 4.17: Future atmospheric <sup>14</sup>C levels, 1980 - 2050 (best estimate).

suggest that future values of the atmospheric  $^{14}\text{C}$  specific activity will be consistently less than the present-day level. Indeed, the value of  $234 \text{ Bq kg}^{-1}$  (carbon), predicted for 2050, is only marginally above the natural level. This effect occurs because the increase in  $^{14}\text{C}$  levels due to the nuclear industry is offset by the decrease in  $^{14}\text{C}$  activities resulting from the combustion of fossil fuels. The interaction of the various anthropogenic perturbations over the period 1800-2050 can be seen more clearly in Figure 4.18. This plot shows the effect which each individual perturbation exerts, on the assumption that it is the sole artificial influence. Deforestation barely modulates the atmospheric  $^{14}\text{C}$  levels whereas bomb-produced  $^{14}\text{C}$  has been very dominant in the past but becomes decreasingly significant with time. Thus the future situation is dominated by the constantly increasing but opposing effects of nuclear fuel-derived  $^{14}\text{C}$  and fossil fuel-derived  $^{12}\text{C}$ .

The main impetus for this study, however, is to determine the radiation dose to the public. Of course, as explained in Section 1.4, the effective dose equivalent rate to man is directly proportional to the atmospheric  $^{14}\text{C}$  specific activity (c.f. equation 1.11). This means of calculating the dose rate incorporates the specific activity model. This assumption is highlighted here because it is more valid in the assessment of global doses than of local doses. For, in this case, no errors are introduced if an individual's foodstuffs are derived from an alternative location because the atmospheric  $^{14}\text{C}$  level is assumed to be globally uniform. Stenhouse and Baxter (1977a, 1977b, 1979), however, noted that the  $^{14}\text{C}$  levels in man lagged behind and were slightly diluted relative to atmospheric activities. Therefore, although the doses calculated via the specific activity model are reasonably accurate (Wirth, 1982), any errors incurred are likely to lie on the side of conservatism. In Figure 4.19 the atmospheric  $^{14}\text{C}$  levels for the period 1800-2050 are plotted in terms of both the  $^{14}\text{C}$  specific activity and the individual effective dose equivalent rate. The horizontal line, representing the natural steady state highlights the fact that the individual effective dose equivalent rate in the future is expected to be very close to that experienced in the

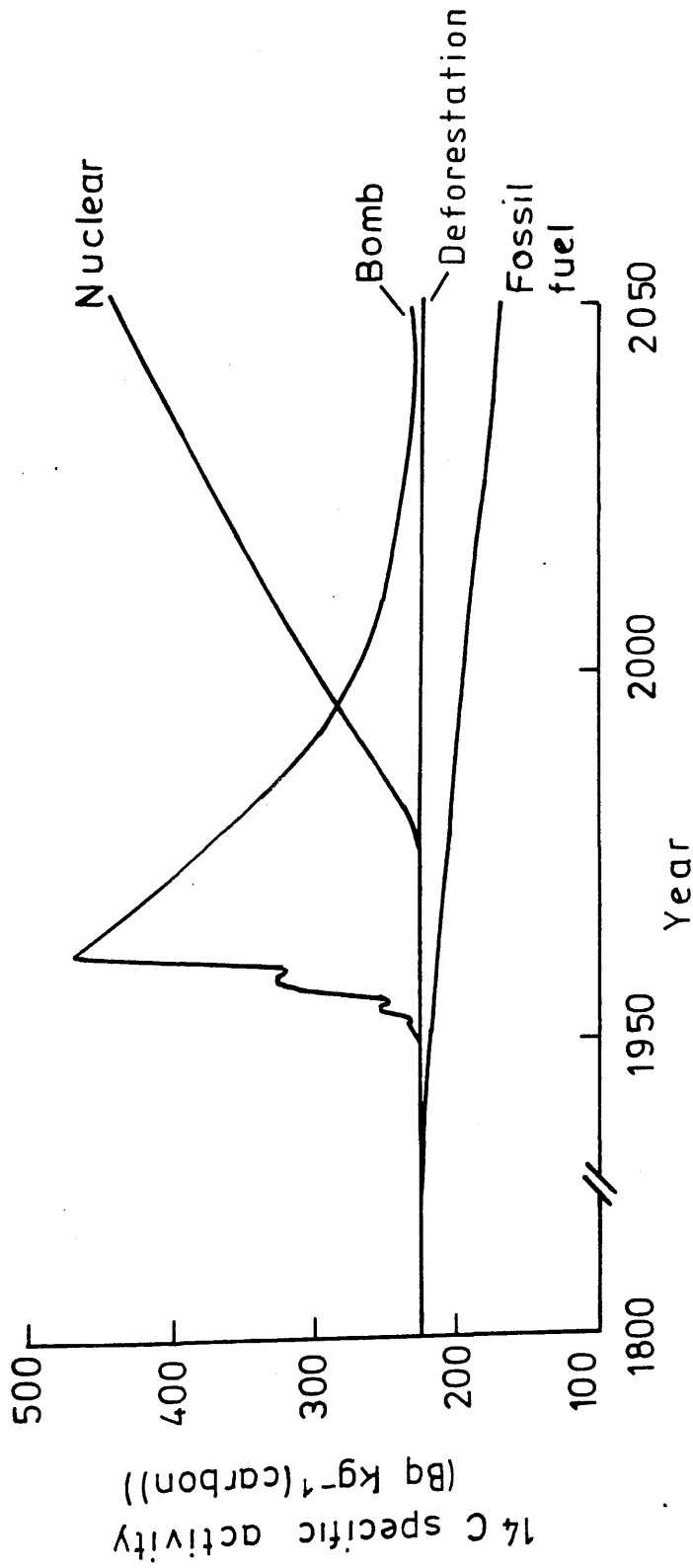


FIGURE 4.18: The effect of individual anthropogenic perturbations on the atmospheric  $^{14}\text{C}$  levels, 1800 - 2050 (best estimate).

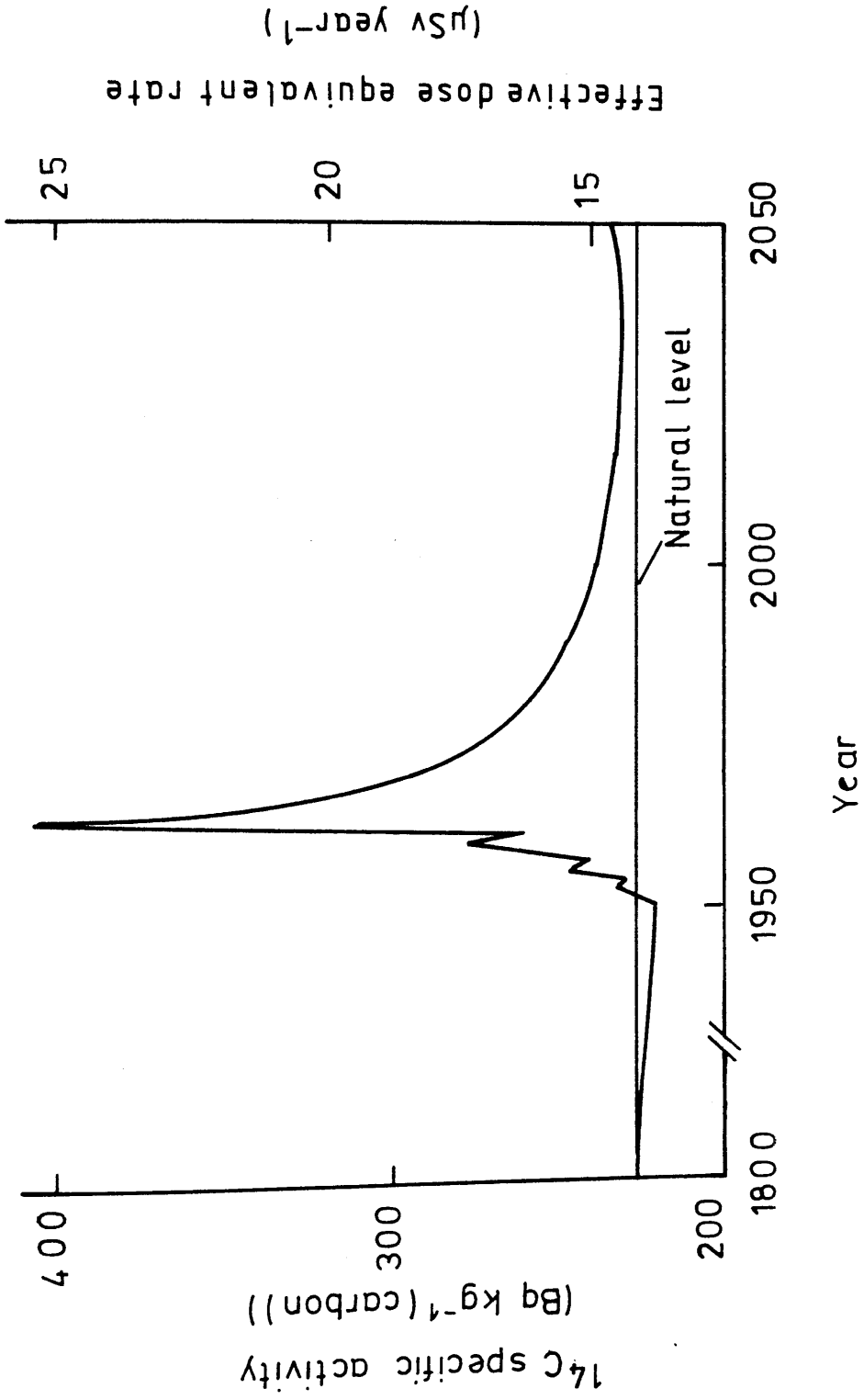


FIGURE 4.19: Atmospheric <sup>14</sup>C levels, 1800 - 2050 (best estimate).

absence of all anthropogenic perturbations. Furthermore, these predictions suggest that the future individual dose rate will be considerably lower than that experienced in the recent past.

Although future atmospheric  $^{14}\text{C}$  levels are expected to be relatively low, it must be remembered that, in the absence of a nuclear power industry, they would be lower still. The individual effective dose equivalent rate, shown in Figure 4.19, is derived from three different  $^{14}\text{C}$  sources, namely, natural, bomb and reactor-derived  $^{14}\text{C}$ , and the contribution by each of these to the total dose rate is shown in Figure 4.20. A striking feature of the results is that, although the natural  $^{14}\text{C}$  production rate is assumed constant, its contribution to the total dose rate is consistently decreasing. This phenomenon is caused by the diluting effects of both fossil fuel combustion and deforestation. A similar decrease occurs with regard to the contributions by bomb and reactor-derived  $^{14}\text{C}$  to total dose rate, although here it is a less obvious effect because of the non-uniform nature of these inputs. A qualitative assessment of Figure 4.20 shows clearly that, for the period 1800-2050, natural  $^{14}\text{C}$  is by far the dominant contributor to total dose rate. For a brief spell in the early 1960s, bomb-derived  $^{14}\text{C}$  became equally important but towards the latter part of the period of interest, this source becomes insignificant and reactor-derived  $^{14}\text{C}$  takes over as the major anthropogenic source. However, the maximum individual effective dose equivalent rate resulting from  $^{14}\text{C}$  discharges from the nuclear fuel cycle, of  $1.8 \mu\text{Sv year}^{-1}$  in 2050, is only 12% of the total dose rate of  $14.6 \mu\text{Sv year}^{-1}$  in that year (the remainder being almost entirely due to naturally produced  $^{14}\text{C}$ ).

In order to obtain some information concerning the possible range of future doses, all the scenarios discussed in the previous section are now considered. Initially, the 7 energy scenarios, as detailed in Table 4.6, were fed into the 25-box model. The future atmospheric  $^{14}\text{C}$  levels predicted by the various scenarios are shown in Figure 4.21 and the values of the maximum individual effective dose equivalent rate due to  $^{14}\text{C}$  discharges from the nuclear industry are presented in Table 4.8. For each energy scenario, the maximum dose rate occurs in the final year of the

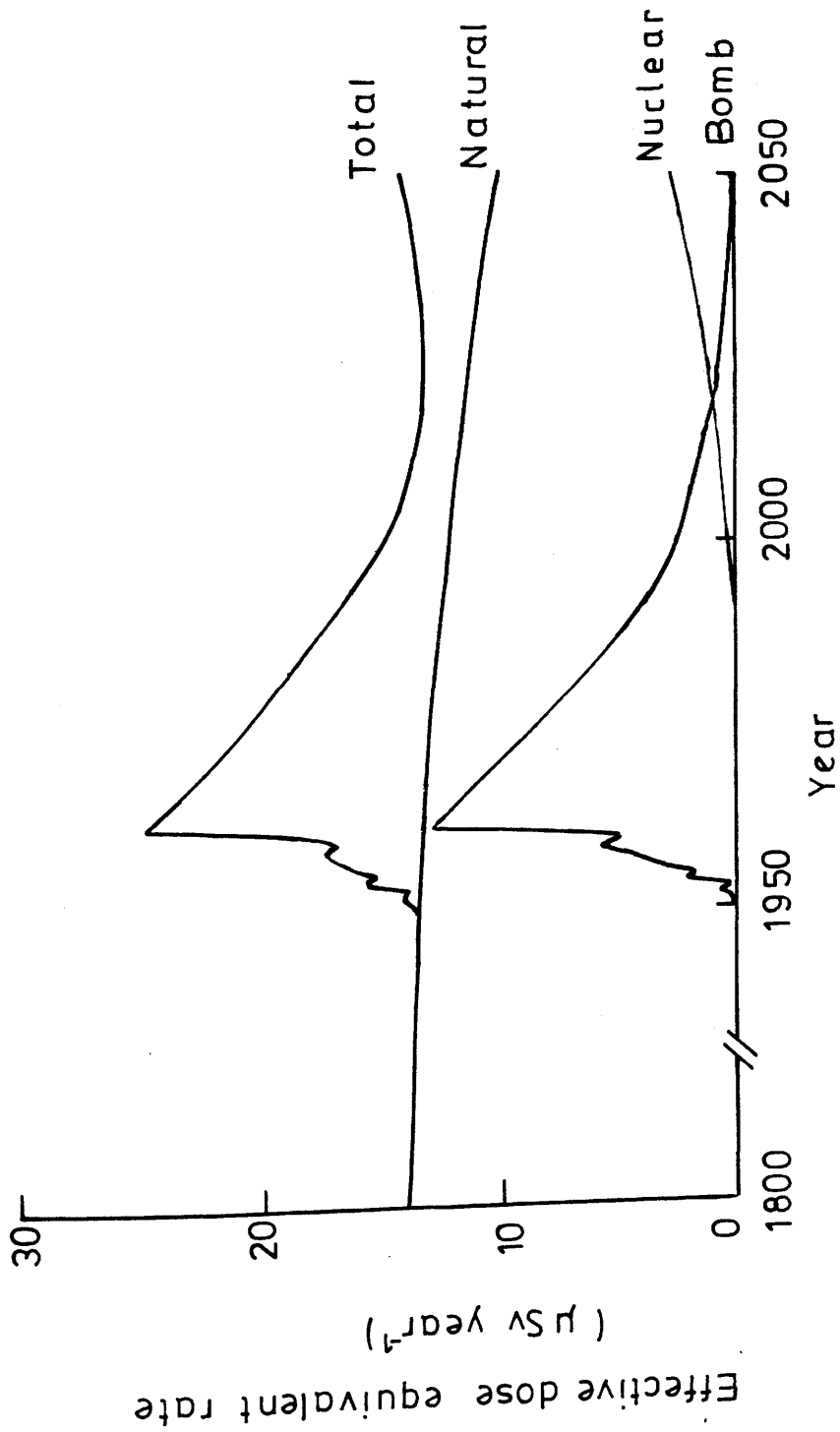


FIGURE 4.20: Contribution of the various  $^{14}\text{C}$  sources to the effective dose equivalent rate, 1800 - 2050 (best estimate).

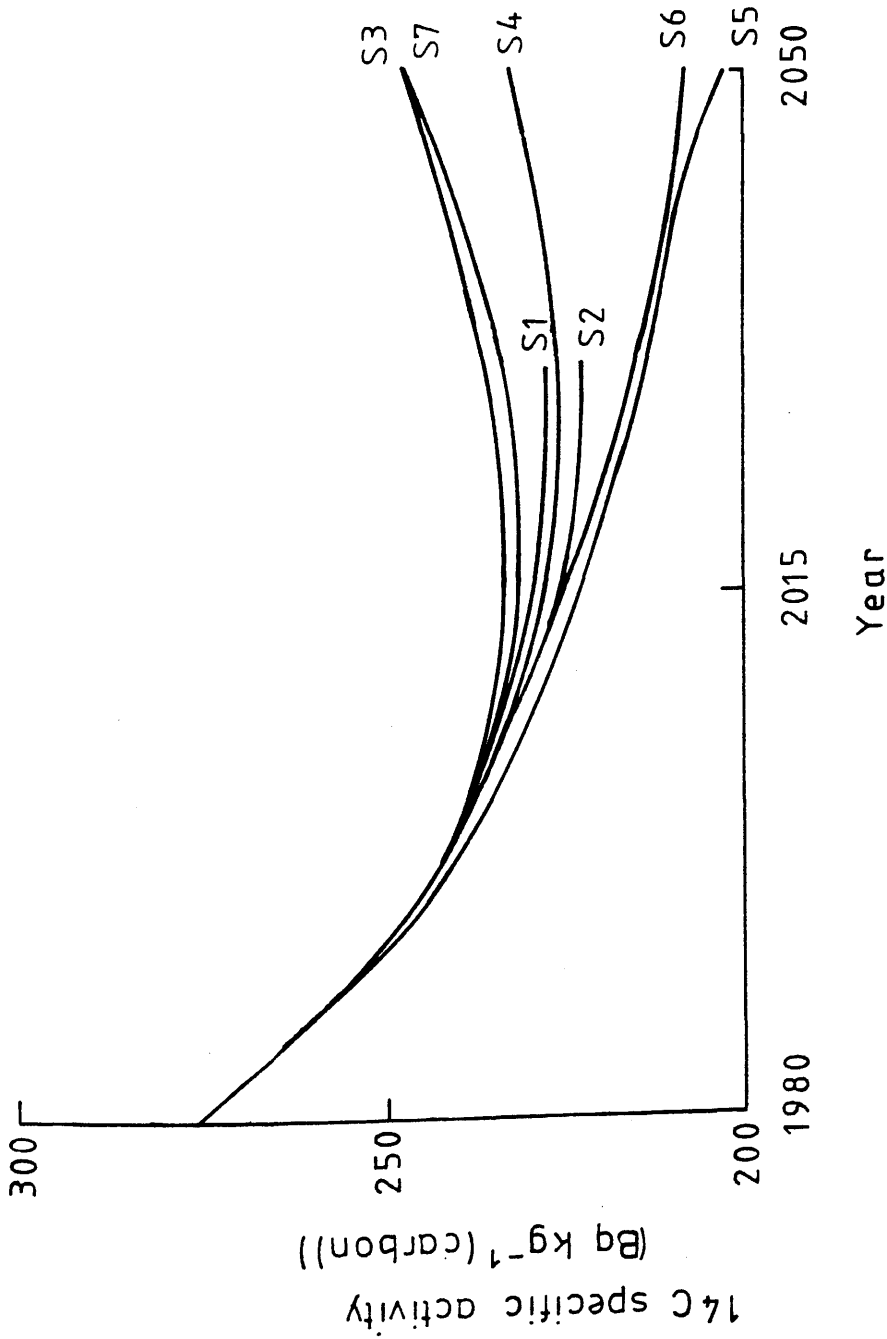


FIGURE 4.21: Future atmospheric <sup>14</sup>C levels, 1980-2050, as predicted by the 7 basic scenarios (using 25-box model).

Table 4.8: The maximum individual effective dose equivalent rate from reactor-derived  $^{14}\text{C}$ , as derived from various scenarios (using the 25-box model)

Scenario	Dose rate ( $\mu\text{Sv year}^{-1}$ )
S1	0.5
S2	0.7
S3	2.0
S4	1.8
S5	1.6
S6	0.6
S7	3.0

period covered, i.e. 2030 for S1 and S2, and 2050 for S3-S7. The values obtained for the atmospheric  $^{14}\text{C}$  specific activity in 2050, which range from 204-248  $\text{Bq kg}^{-1}$  (carbon), are largely due to the balance struck between fossil and nuclear fuel usage. The highest value is produced by S3, which combines low fossil and medium nuclear fuel use projections, whereas the lowest value is generated by S5, which combines high fossil and medium nuclear fuel use projections. On the other hand, the values obtained for the individual dose rate from  $^{14}\text{C}$  discharges from the nuclear fuel cycle depend mainly on the nuclear fuel use scenario, with the effect of fossil fuels being comparatively minor. The high value, in 2050, of  $3.0 \mu\text{Sv year}^{-1}$  is produced by S7, which contains a high nuclear fuel use projection, and the corresponding low value of  $0.6 \mu\text{Sv year}^{-1}$  is derived from S6, which has a low nuclear fuel use projection.

Thus far, all work has been performed on the 25-box model but now the effect of using the other carbon cycle models is investigated. In Table 4.9 the values predicted by the various models for the atmospheric  $^{14}\text{C}$  specific activity and the individual effective dose equivalent rate from reactor-derived  $^{14}\text{C}$ , in 2050 (assuming energy scenario S4) are listed. All the models predict very similar values for the atmospheric  $^{14}\text{C}$  specific activity (228-236  $\text{Bq kg}^{-1}$ (carbon)), whereas there is quite a large variation in the dose rates ( $1.8-3.6 \mu\text{Sv year}^{-1}$ ). A sensitivity analysis was carried out in which the dependence of the model's predictions on its initial parameter values was quantified. This demonstrated that, for short-term predictions, the models' results are very sensitive to the value adopted for the atmosphere-ocean carbon flux (a conclusion which is in agreement with the results of other such studies (Gardner and Trabalka, 1985)). Hence, it is the variation in this parameter which is largely responsible for the variation observed between the dose rates. Assuming that the 25-box model is the most accurate, this means that the simple models tend to overestimate the effect of an anthropogenic input (this hypothesis is backed up by the data contained in Table 4.7). The variation is not observed in the atmospheric  $^{14}\text{C}$  levels because all the results are very close to the natural level of  $226 \text{Bq kg}^{-1}$  (carbon), suggesting that the anthropogenic perturbations all but

4.9: The variation between models in values generated for the atmospheric  $^{14}\text{C}$  level and the individual effective dose equivalent rate from reactor-derived  $^{14}\text{C}$ , in 2050 (using S4)

Model	$^{14}\text{C}$ specific activity ( $\text{Bq kg}^{-1}(\text{carbon})$ )	Dose rate ( $\mu\text{Sv year}^{-1}$ )
1-box	228	3.6
3-box	236	2.8
8-box	231	2.4
25-box	234	1.8

cancel each other. Thus the overestimates of the simpler models tend to cancel out and all models give similar values.

To conclude this section of the work, the importance of several parameters not yet considered is discussed. Altogether, 6 further scenarios are investigated and the important assumption in each case is now highlighted.

(a) There is a deforestation effect in the future.

This scenario assumes that the rate of net transfer from the biosphere is  $2.7 \times 10^{14}$  kg year<sup>-1</sup>, i.e. equal to the 1980 value suggested by Houghton et al. (1983).

(b) All nuclear fuel is reprocessed.

(c) No nuclear fuel is reprocessed.

(d) There is a large market penetration by FBRs.

It is assumed that 50% of the installed nuclear energy capacity is in the form of FBKs (the complete reactor type distribution thus generated is listed in Table 4.10).

(e) A large quantity (20%) of <sup>14</sup>C discharges from the nuclear industry is in the form of liquid waste.

(f) <sup>14</sup>C is discharged from the pharmaceutical industry.

Following an international survey, Kunz (pers. comm., 1985)

recommended that the <sup>14</sup>C production rate for the global pharmaceutical industry in 1980 was 30 TBq year<sup>-1</sup>, increasing throughout the period of interest at 5% year<sup>-1</sup>. Of the <sup>14</sup>C produced, only 40% is released to the atmosphere

immediately, the remainder being incorporated into solid wastes which, on burial at shallow land-fill sites, are dissociated and leak to the atmosphere at a rate of 0.06% year<sup>-1</sup>. The resultant <sup>14</sup>C production and release rates are presented in Figure 4.22.

The effect of incorporating each of these parameters into scenario S4 is quantified in Table 4.11. By increasing the atmospheric carbon inventory, deforestation reduces the effect of all anthropogenic perturbations. Hence it is responsible for a very small decrease in both the atmospheric <sup>14</sup>C specific activity and the individual effective dose equivalent rate in 2050 due to <sup>14</sup>C discharges from the nuclear industry. Increasing

Table 4.10: The reactor type distribution for the high FBR utilisation scenario

Reactor type	Distribution (%)
FBR	50
PWR	30
BWR	15
HWR	1.25
MAGNOX	1.25
AGR	1.25
HTGR	1.25

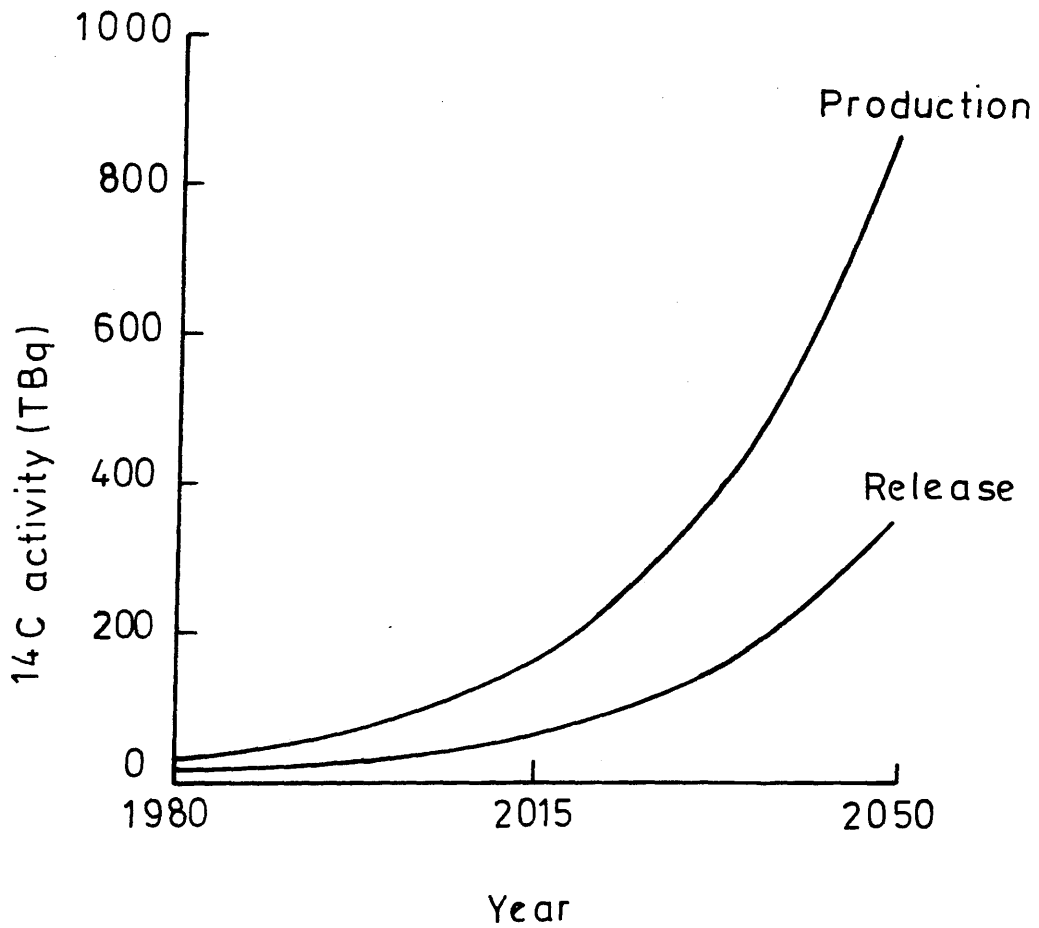


FIGURE 4-22: Future annual production and release of  $^{14}\text{C}$  used in the pharmaceutical industry, 1980-2050.

Table 4.11: The effect of various parameters on the values generated for the atmospheric  $^{14}\text{C}$  level and the individual effective dose equivalent rate from reactor-derived  $^{14}\text{C}$ , in 2050 (using S4)

Parameter	Change in value	
	$^{14}\text{C}$ specific activity ( $\text{Bq kg}^{-1}(\text{carbon})$ )	Dose rate ( $\mu\text{Sv year}^{-1}$ )
Deforestation	-1	-0.1
100% reprocessing	+27	+0.8
0% reprocessing	-27	-0.8
FBR	-23	-0.7
Liquid waste	-3	-0.1
Pharmaceuticals	+4	0

the amount of nuclear fuel that is reprocessed increases the amount of  $^{14}\text{C}$  that is released to the atmosphere and causes a comparatively large increase in both the atmospheric  $^{14}\text{C}$  level and the dose rate. Decreasing the amount of nuclear fuel that is reprocessed has an equally large effect but in the opposite direction. Increasing the FBR share of the market decreases both the atmospheric  $^{14}\text{C}$  level and the dose rate because this reactor type has a very low  $^{14}\text{C}$  production rate. A similar, although far smaller, effect is caused by increasing the fraction of  $^{14}\text{C}$  which is discharged as a liquid waste, i.e. released into the ocean as opposed to the atmosphere (thus delaying its entry into man's exposure environment). Finally, although  $^{14}\text{C}$  discharges from the pharmaceutical industry may increase atmospheric  $^{14}\text{C}$  levels, they have no effect on the individual effective dose equivalent rate from  $^{14}\text{C}$  discharges from the nuclear fuel cycle.

The scenarios discussed in this work do not cover all possible future situations and, indeed, no number of scenarios could manage this. However, it is hoped that the results presented here, provide a reasonable indication of the relative importance of various parameters.

#### 4.3.1.3 The Radiological Impact on the Public to 2050

The radiological significance of the  $^{14}\text{C}$  discharges from the nuclear fuel cycle is assessed largely on the basis of the best estimate of future atmospheric  $^{14}\text{C}$  levels. Throughout the assessment, however, it is worthwhile bearing in mind the magnitude of the uncertainties implicit in the predictions.

Estimates of future atmospheric  $^{14}\text{C}$  levels are sensitive to small changes in the future balance between the demand of fossil and nuclear fuels. Nevertheless, the results suggest that future atmospheric  $^{14}\text{C}$  specific activities and hence dose to man will not surpass historic levels. Indeed, the value of  $234 \text{ Bq kg}^{-1}(\text{carbon})$  in 2050 (corresponding to an individual effective dose equivalent rate of  $14.6 \mu\text{Sv year}^{-1}$ ) is only barely above the natural level. Although such comparisons provide a convenient means by which to place some perspective on the magnitude of this effect, they cannot be used to justify a given

discharge. The individual contribution of the reactor-derived  $^{14}\text{C}$  to the total dose must be considered. This parameter is, unsurprisingly, highly dependent on the future of the nuclear industry. In particular, the future rate of growth of installed nuclear energy capacity, besides the future policy on reprocessing spent nuclear fuel, are very significant parameters. This dependence is reflected in the results, which indicate that the dose rate accumulates with time in parallel with the increase in installed nuclear energy capacity. The maximum individual effective dose equivalent rate, observed in 2050, is  $1.8 \mu\text{Sv year}^{-1}$ , which corresponds to 0.2% of the annual dose limit of 1 mSv recommended by ICRP. Thus the  $^{14}\text{C}$  discharges from the nuclear industry up to 2050 do not, on a global scale, exceed the specified limit although they do provide a finite and ever-increasing contribution to it. Bearing in mind the large uncertainties in these estimates, it is clear that if certain paths are adopted in future by the nuclear industry, it is possible that the individual effective dose equivalent rate from the  $^{14}\text{C}$  discharges could reach significant levels relative to the annual dose limit.

One of the major potential hazards associated with the  $^{14}\text{C}$  discharges is that, because of its long half-life and high mobility in the environment, the release of this nuclide leads to exposure of the entire global population over very long timescales. To accommodate this aspect of the radionuclide's behaviour the collective dose to the exposed population should be calculated. Since this study is limited to the year 2050, it is necessary to restrict the calculation to provide a measure of the truncated CEDEC. The CEDEC is obtained by integrating the collective effective dose equivalent rate over the period of interest, as explained in Section 1.4 (c.f. equation 1.5). The collective effective dose equivalent rate,  $\dot{S}_E(t)$ , is obtained by multiplying the individual effective dose equivalent rate,  $\dot{H}_E(t)$ , by the number of people receiving that dose in year  $t$ ,  $N(t)$ , as shown in equation (4.1):

$$\dot{S}_E(t) = N(t) \dot{H}_E(t). \quad (4.1)$$

The exposed population in this case is the entire world population. An estimate of the growth in world population from 1955 (the start of the nuclear power era) to 2050, first used by

Killough (1980), is illustrated in Figure 4.23. This projection is based on the commonly held assumption that the global population will level out at around  $10^{10}$  people towards the end of the next century (United Nations, 1977; Bush et al., 1983; IAEA, 1985). The truncated CEDEC to 2050 due to  $^{14}\text{C}$  discharges from the nuclear fuel cycle is calculated by combining these data with the individual effective dose equivalent rates from the nuclear industry's  $^{14}\text{C}$  discharges shown in Figure 4.20. The results, presented in Figure 4.24, predict a dose to the public of  $3.1 \times 10^5$  man Sv. Using the risk coefficients presented in Table 1.11, this dose corresponds to approximately 4000 fatal cancers and the occurrence of 2500 hereditary effects over all generations. No specific limits on collective doses are set by the regulatory bodies other than that these should be 'as low as reasonably achievable'. For such considerations, it is necessary to calculate the total dose delivered to the public from a given  $^{14}\text{C}$  discharge. In practical terms this requires that the CEDEC, rather than the truncated CEDEC, be quantified. To complete a full assessment of the radiological significance of  $^{14}\text{C}$  discharges, therefore, the CEDEC must be determined.

#### 4.3.2 Long-term Effects of $^{14}\text{C}$ Discharges from the Nuclear Fuel Cycle

The uncertainties associated with the estimates of future utilisation of nuclear power are considerable within the period up to 2050 but, beyond that date, become indeterminately large. It is therefore impracticable to predict the actual doses to the public from this source beyond the year 2050. To determine the radiological significance of  $^{14}\text{C}$  discharges, however, it is necessary to study their environmental behaviour and levels well beyond this date. In this section of the study, therefore, the carbon cycle models are used to evaluate the CEDEC from a nominal unit release of  $^{14}\text{C}$  (taken to be 1 TBq) from the nuclear industry. However, as before, many different scenarios must be considered to obtain some idea of the wide range of future possibilities.

##### 4.3.2.1 Basic Scenarios

One important parameter, on which the future dose will depend, is the compartment of the carbon cycle into which the

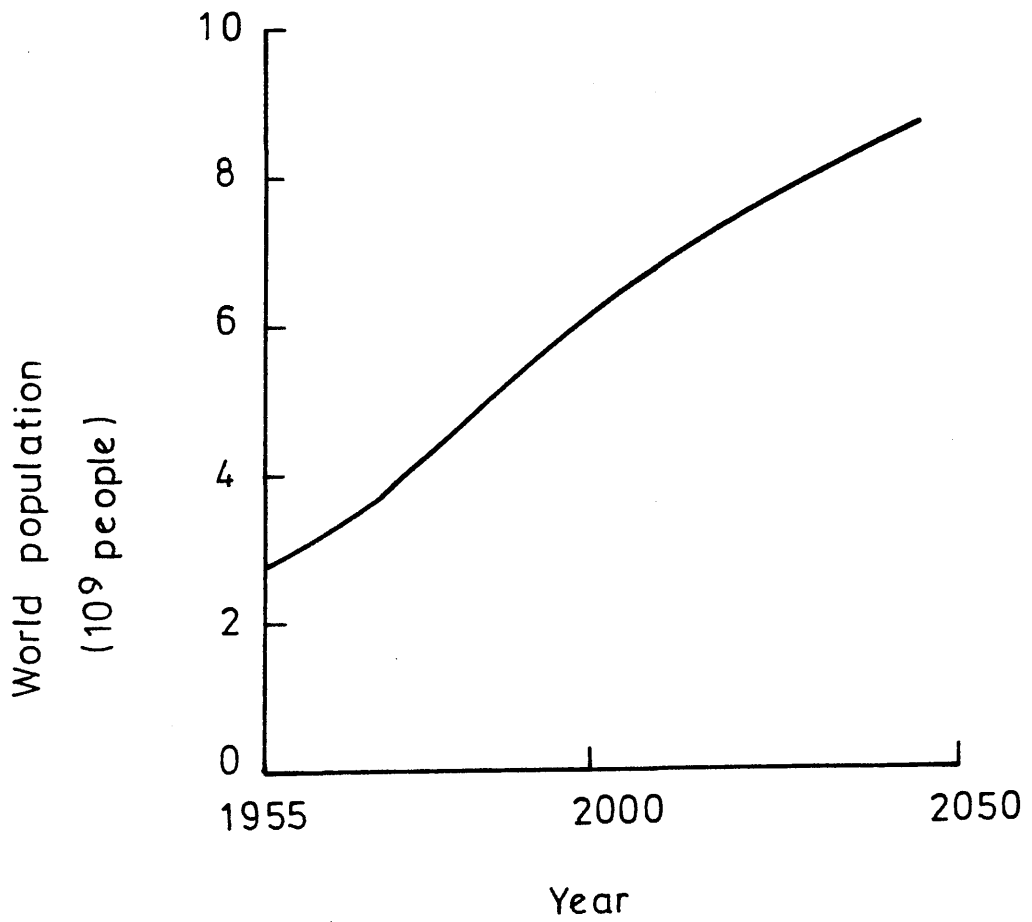


FIGURE 4.23: Projected population growth, 1955 - 2050.

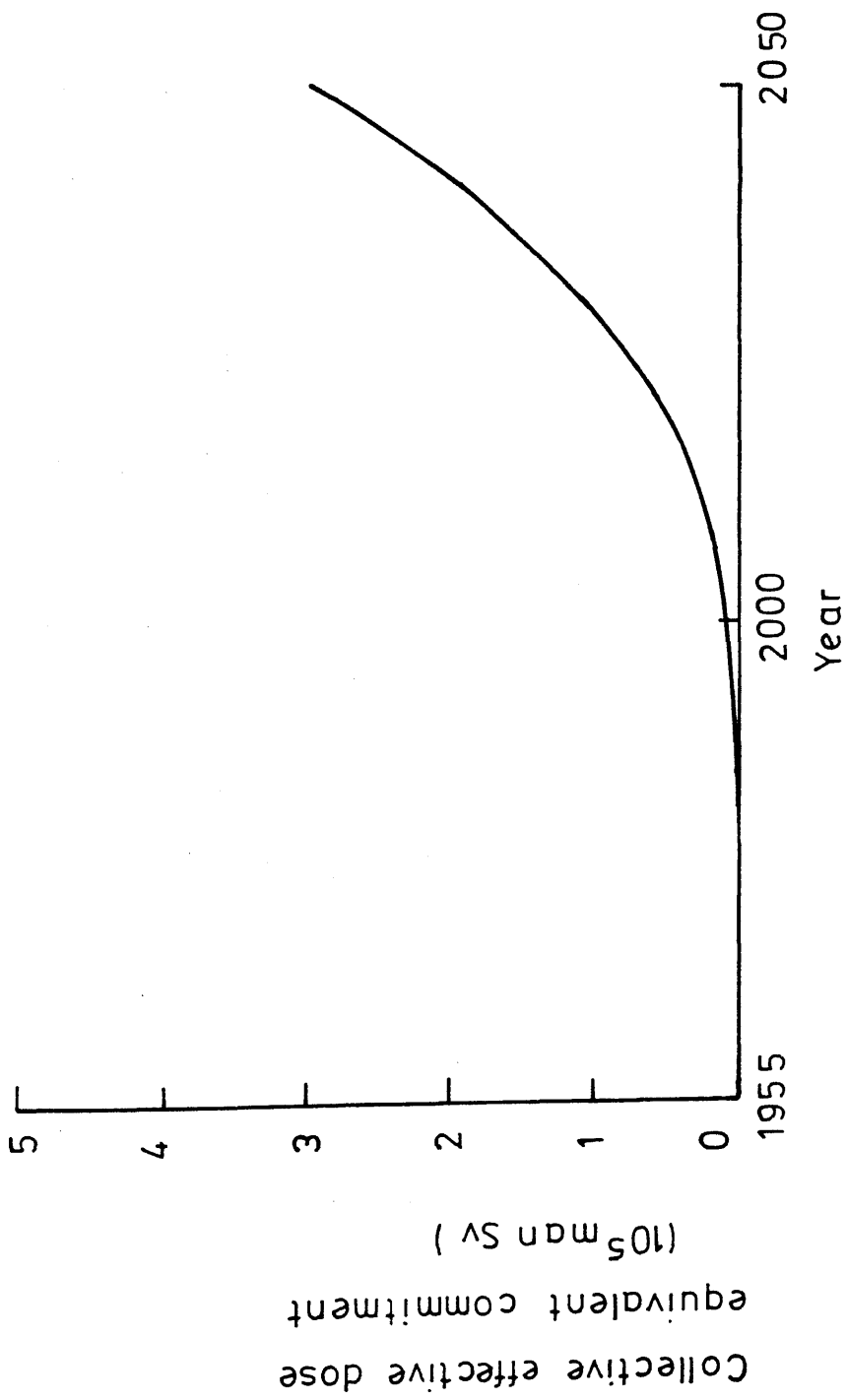


FIGURE 4.24: Truncated collective effective dose equivalent commitment, 1955-2050, due to  $^{14}\text{C}$  discharges from the nuclear fuel cycle (best estimate).

$^{14}\text{C}$  is released. Most of the  $^{14}\text{C}$  discharged by the nuclear industry is released to the atmosphere and this pathway therefore receives most attention. At present, however, small quantities of  $^{14}\text{C}$  are also released to the surface ocean and, indeed, it is possible that in future this radionuclide will also be disposed of and released in the deep ocean. These latter alternative release pathways will also be considered. The only other parameter of importance is the future rate of combustion of fossil fuels (deforestation is assumed to be negligible in this long-term context). Future production of  $\text{CO}_2$  from fossil fuel combustion is obviously uncertain. Information about potential reserves is incomplete and future demand will depend on the supply, technological development and interdependent social, economic and political patterns which have yet to emerge. Nevertheless, such estimates have often been made through adoption of a logistic growth function (Killough, 1980; Bacastow and Bjorkstrom, 1981; Matthies and Paretzke, 1982), i.e. equation (4.2):

$$\dot{P} = R P (1 - (P/P_\infty)), \quad P(t_0) = P_0. \quad (4.2)$$

This differential equation can be solved to give:

$$P(t) = P_\infty (1 + ((P_\infty/P_0) - 1) (\exp(-R(t-t_0)))), \quad (4.3)$$

where  $P(t)$  is the cumulative production of carbon to time  $t$  and  $R$  is an adjustable rate parameter. Three alternative scenarios are generated by assuming different values for  $P_\infty$ , the total recoverable reserves, which are currently estimated at around  $4-8 \times 10^{15}$  kg (Killough and Till, 1978; Rotty and Masters, 1985). The 3 alternative values chosen for  $P_\infty$  are 0, 4 and  $8 \times 10^{15}$  kg. Although the low scenario ( $P_\infty = 0$ ) is unrealistic, it is included because it gives a measure of the highest possible dose from the nuclear industry's  $^{14}\text{C}$  discharges, i.e. in the absence of any diluting effect from fossil fuel combustion. It is a real possibility that the highest scenario ( $P_\infty = 8 \times 10^{15}$  kg) may be precluded by mounting evidence of consequent climatic effects. Therefore the medium scenario ( $P_\infty = 4 \times 10^{15}$  kg) is adopted as the 'most probable' case. The simulation of future fossil fuel combustion is established such that it follows on directly from the known trends up to 1980. In other words,  $t_0$  is taken as 1980 and  $P_0$ , which is the cumulative release of carbon from 1860-1980, is set equal to  $1.7 \times 10^{14}$  kg. The adjustable rate parameter,  $R$ , is chosen to provide a smooth transition between the historical and

the projected data. All the data necessary for the production of each scenario are listed in Table 4.12 and the simulations are shown graphically in Figure 4.25. These projections indicate that the future rate of combustion of fossil fuels increases until a maximum rate is reached in 2075. Thereafter the combustion rate decreases steadily, becoming insignificant around 2300.

Finally, it is necessary to decide upon the best means of utilising the carbon cycle models available. Unfortunately, there is no data set on which the validity of the models can be assessed over long timescales (thousands of years). At a purely intuitive level, however, the 25-box model would be expected to generate the most accurate results as its complexity is more consistent with the realities of the natural system.

#### 4.3.2.2 Radiation Dose to the Public to Infinity

The best estimate of the CEDEC per unit discharge of  $^{14}\text{C}$  from the nuclear fuel cycle is obtained by using the 25-box model to calculate the increase in the atmospheric  $^{14}\text{C}$  specific activity from the release of 1 TBq of  $^{14}\text{C}$  into the atmosphere, assuming fossil fuel scenario F2. The CEDEC is then calculated, as previously explained, assuming that the population remains constant at  $10^{10}$ . Unfortunately, because of its mathematical complexity, it is impracticable to run the 25-box model for  $^{14}\text{C}$  assessment periods of much greater than  $10^4$  years, which is not sufficiently long for complete quantification of the dose to man. The integration, however, can be continued to infinity analytically, using equation (4.4), as suggested by Killough (1980):

$$S_E^C(t, \infty) = ((6.3 \times 10^{-8}) N A(t))/\lambda, \quad (4.4)$$

where  $S_E^C(t, \infty)$  is the truncated CEDEC from  $t$  to infinity,

$A(t)$  is the increase in atmospheric  $^{14}\text{C}$  specific activity in year  $t$  relative to that in the absence of the 1 TBq  $^{14}\text{C}$  input,

$N$  is the global population,

$\lambda$  is the radioactive decay constant for  $^{14}\text{C}$   
and  $6.3 \times 10^{-8} \text{ Sv (Bq kg}^{-1}(\text{carbon}))^{-1}$  is the dose rate factor for  $^{14}\text{C}$ .

The sum of this value,  $S_E^C(t, \infty)$  and the truncated CEDEC from 0 to  $t$ ,  $S_E^C(0, t)$  calculated in the normal manner, gives the value of the

Table 4.12: Data for the simulation of the fossil fuel combustion rate

Scenario	$P_{\infty}$ (kg)	$t_0$ (year)	$P_0$ (kg)	R
F1	0	-	-	-
F2	$4.0 \times 10^{15}$	1980	$1.7 \times 10^{14}$	0.326
F3	$8.0 \times 10^{15}$	1980	$1.7 \times 10^{14}$	0.319

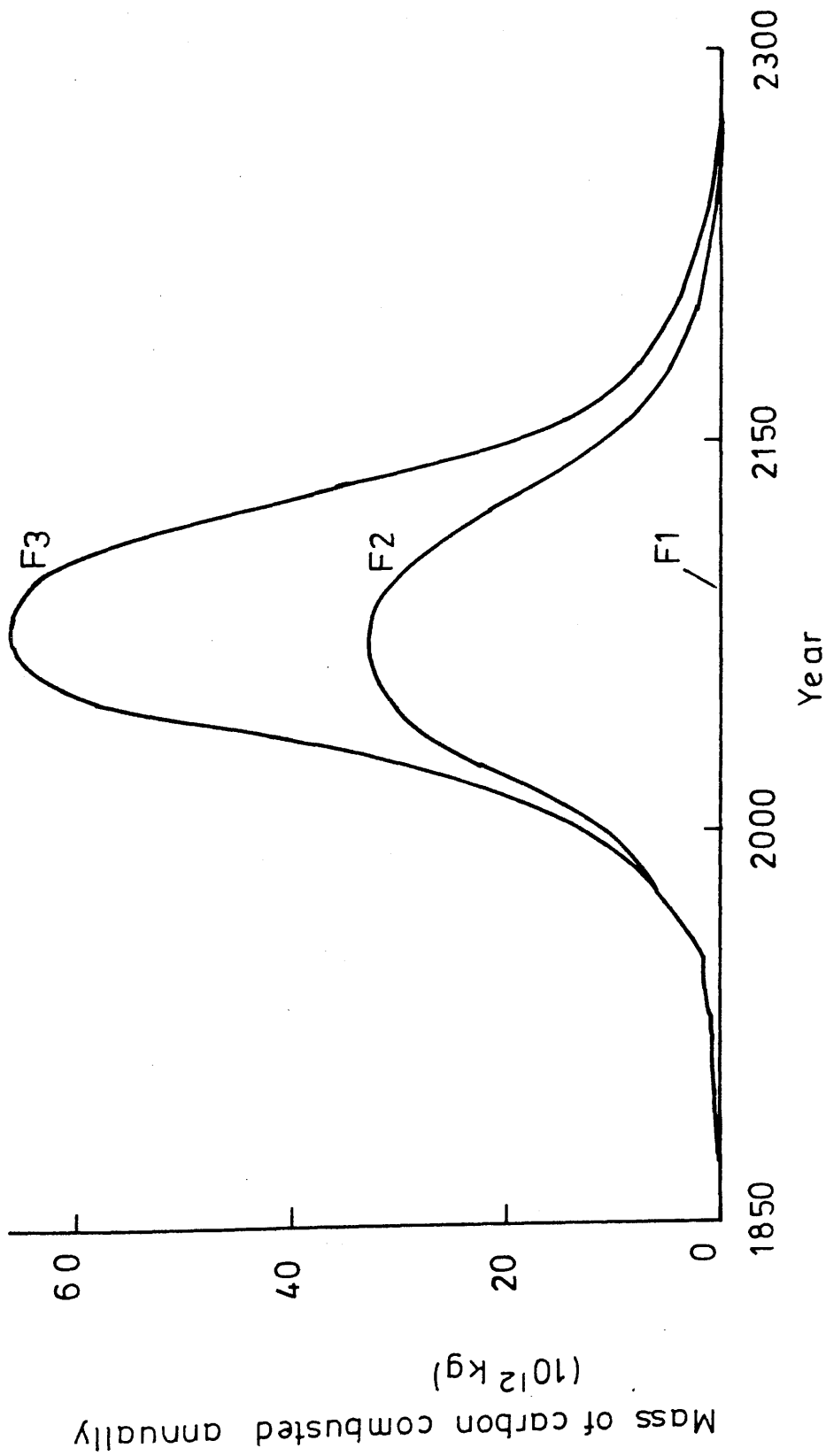


FIGURE 4.25: Projections of the rate of combustion of fossil fuels, over all time.

total dose. This treatment is possible if  $t$  is sufficiently large that the  $^{14}\text{C}$  input has become well-mixed within the global carbon cycle and thus that changes in atmospheric  $^{14}\text{C}$  levels are due only to  $^{14}\text{C}$  decay.

The build up of the CEDEC from the discharge of 1 TBq of  $^{14}\text{C}$  into the atmosphere, assuming fossil fuel scenario F2, is shown in Figure 4.26 and the variation in the individual dose rate over the same period is presented in Figure 4.27. Although the individual dose rates decrease rather sharply (by a factor of 10 in less than 100 years following discharge) the temporal development of the CEDEC is rather slow, with approximately 5, 20 and 70% of the total dose (127 man Sv) being delivered in  $10^2$ ,  $10^3$  and  $10^4$  years respectively. It should be clarified here that in this scenario it is assumed that  $^{14}\text{C}$  discharge occurs in 1980 (Figure 4.25). It is of interest to investigate the effect on the CEDEC of varying the year of  $^{14}\text{C}$  input. A selection of results is presented in Table 4.13. Basically, the lowest dose (124 man Sv) is generated when  $^{14}\text{C}$  release coincides with maximum rate of fossil fuel combustion, i.e. in the year 2075. In general, however, the variation in dose is relatively small. Many other factors can also effect the CEDEC from  $^{14}\text{C}$  discharges from the nuclear industry, some of which will now be discussed.

Three alternative fossil fuel combustion scenarios have been generated, F1, F2 (the 'most probable') and F3. The effect of these scenarios on the dose to man from release to 1 TBq  $^{14}\text{C}$  into the atmosphere are shown in Figure 4.28. Scenarios F1, F2 and F3 predict values of 141, 127 and 119 man Sv respectively for the CEDEC. The effect of fossil fuel combustion is obviously to reduce the dose to man because of the increased carbon inventory of the atmosphere. Once again, all these figures assume that the  $^{14}\text{C}$  is released in 1980.

The effect of varying the compartment of the carbon cycle into which the  $^{14}\text{C}$  is discharged is presented in Figure 4.29 (assuming F2 and  $^{14}\text{C}$  release in 1980). The largest dose (127 man Sv) is delivered following  $^{14}\text{C}$  discharge to the atmosphere. A slightly reduced dose (125 man Sv) is received when

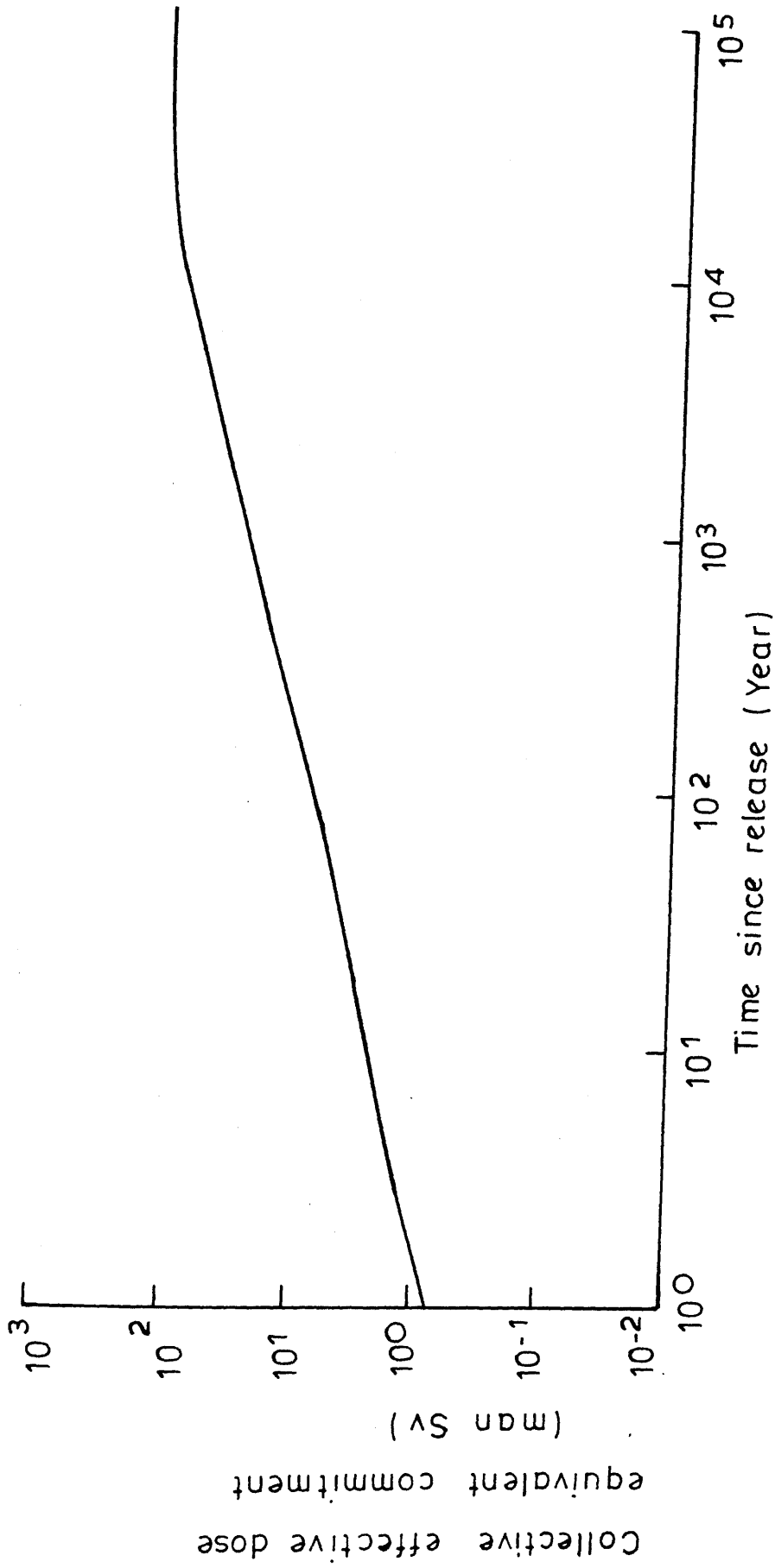


FIGURE 4-26: Collective effective dose equivalent commitment to man from the release of 1 TBq of  $^{14}\text{C}$  from the nuclear fuel cycle (best estimate).

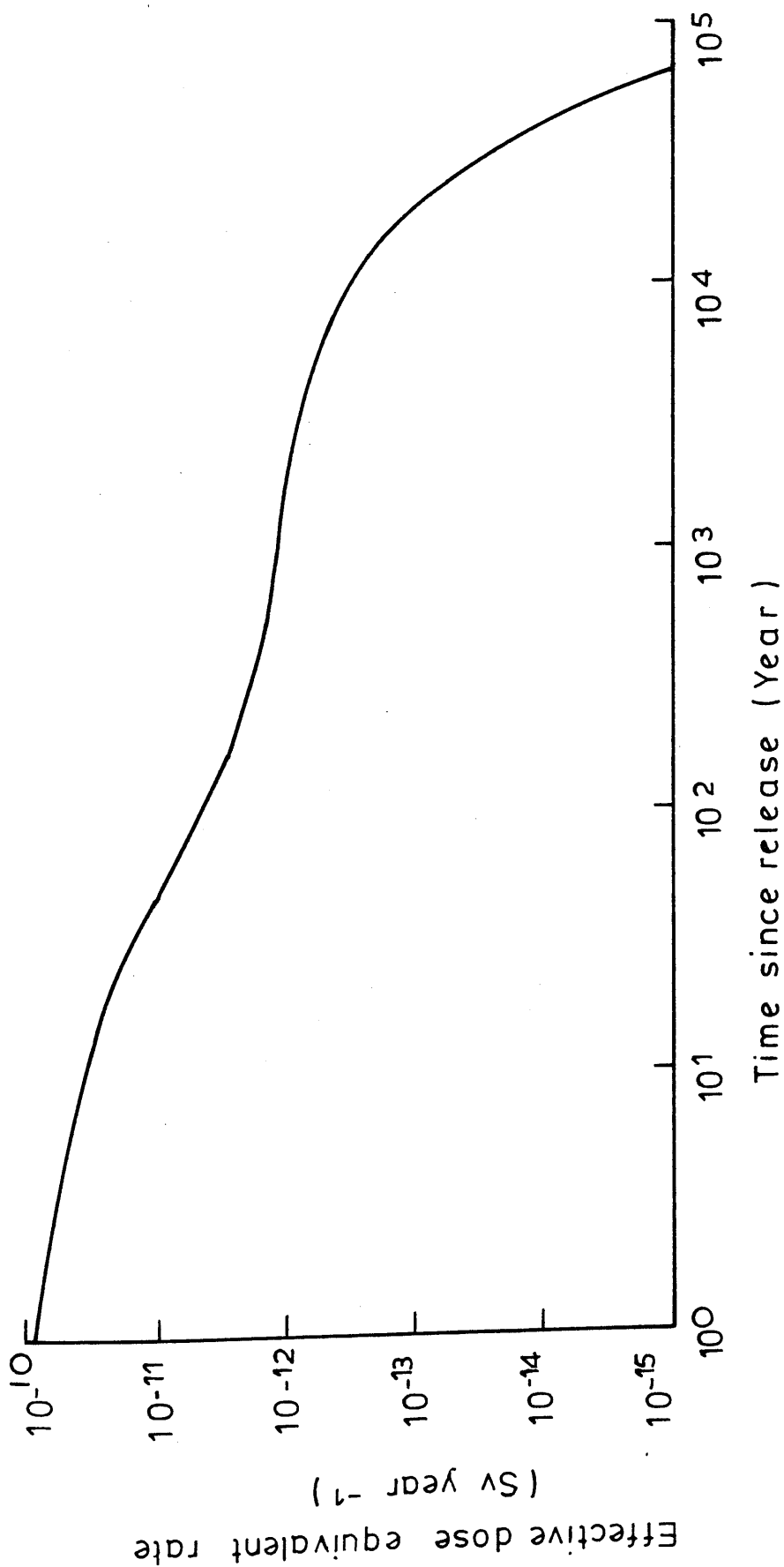


FIGURE 4-27: Variation of the individual effective dose equivalent rate with time following the release of 1TBq of <sup>14</sup>C from the nuclear fuel cycle (best estimate).

Table 4.13: The collective effective dose equivalent commitments to man from the release of 1 TBq of  $^{14}\text{C}$  into the atmosphere at various times relative to the fossil fuel combustion rate F2 (using the 25-box model)

Time of release	CEDEC (man Sv)
1955	130
1980	127
2050	125
2075	124
2100	125
3000	131

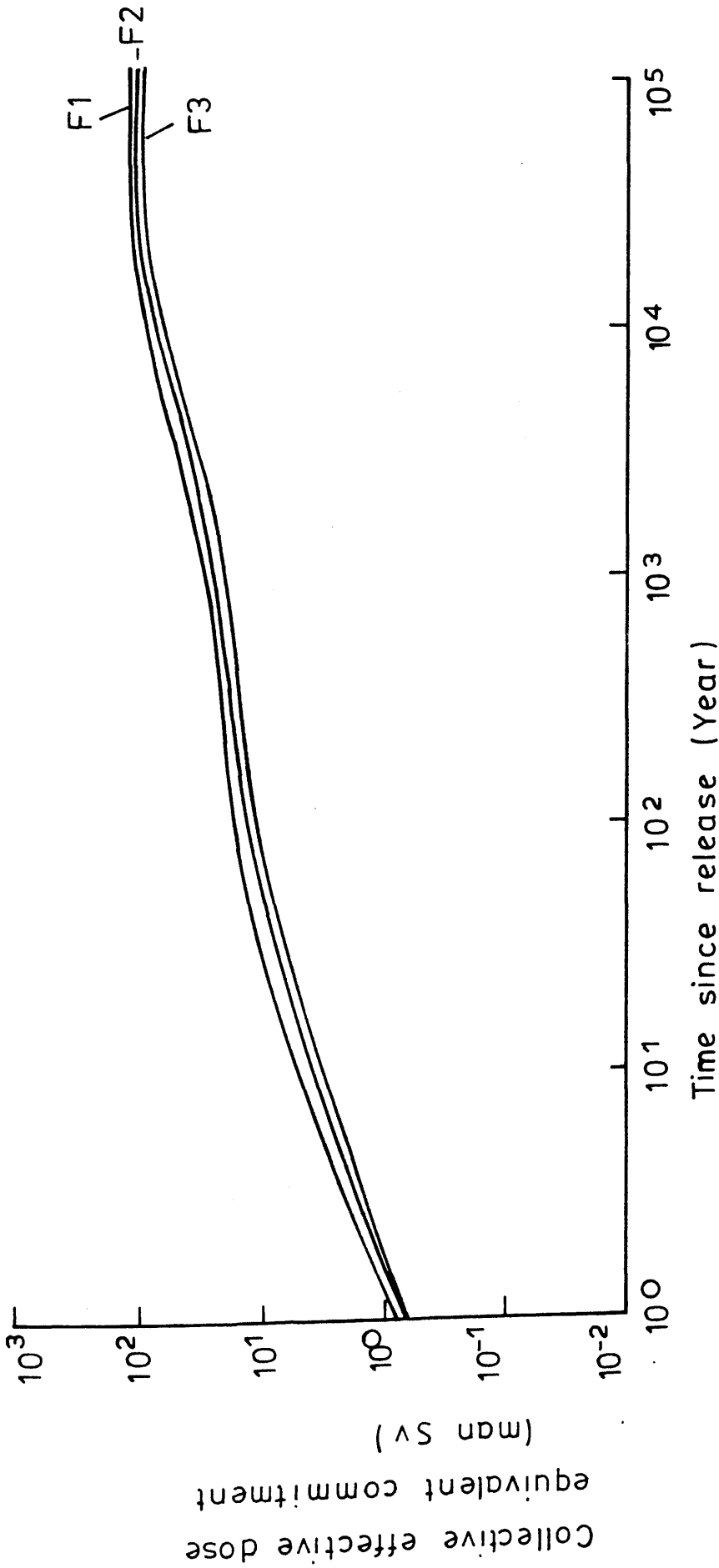


FIGURE 4-28: Collective effective dose equivalent commitment to man from the release of 1 TBq of  $^{14}\text{C}$  into the atmosphere for 3 alternative fossil fuel combustion scenarios (using 25-box model, assuming  $^{14}\text{C}$  release in 1980).

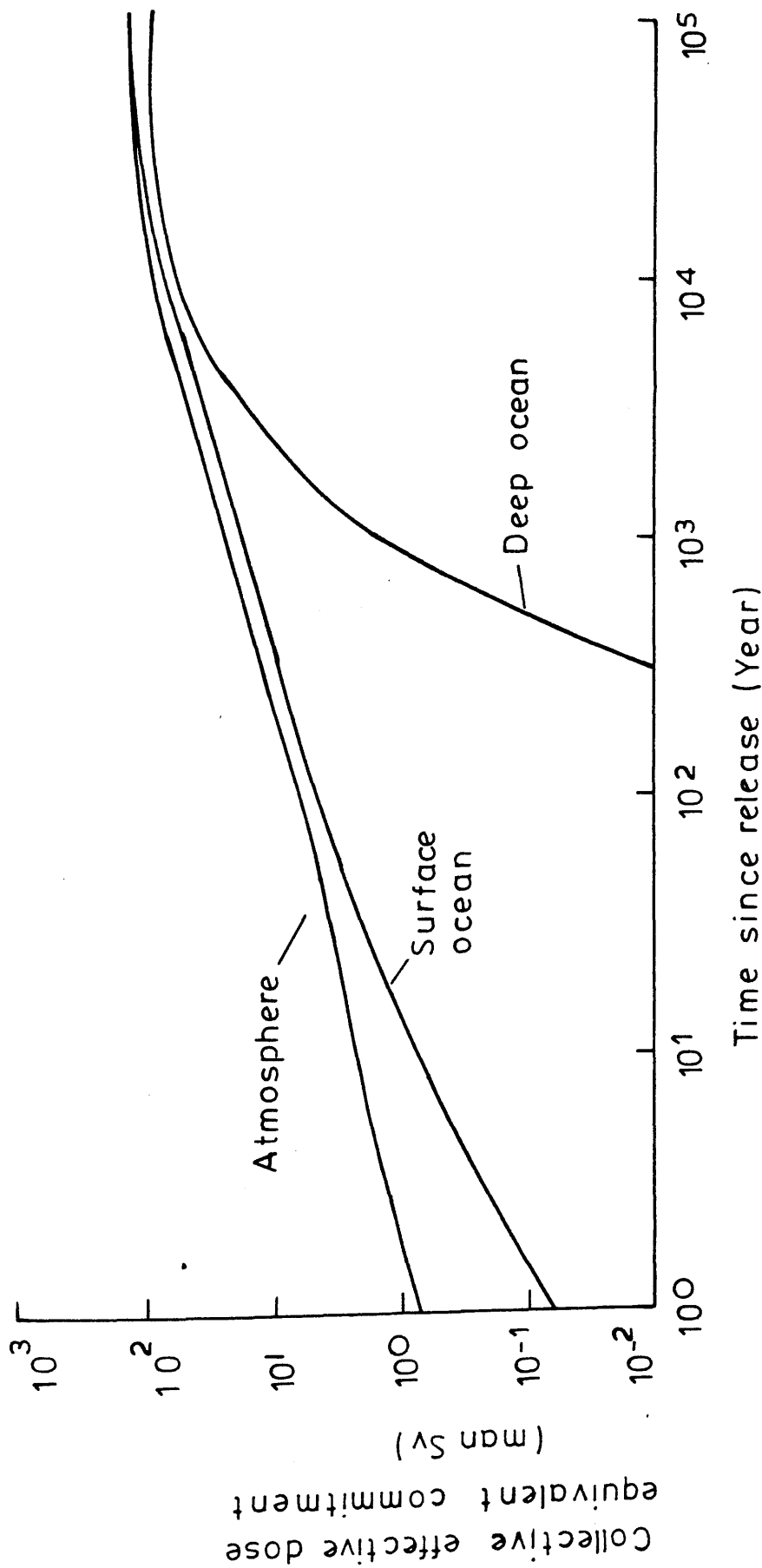


FIGURE 4-29 : Collective effective dose equivalent commitment to man from the release of 1TBq of  $^{14}\text{C}$  into various compartments of the carbon cycle (using 25-box model and F2, assuming  $^{14}\text{C}$  release in 1980).

the  $^{14}\text{C}$  is released into the surface ocean and a lower dose still (95 man Sv) results from deep ocean input. The explanation for this trend is that the deeper in the ocean the  $^{14}\text{C}$  is discharged, the longer is required for it to reach the atmosphere and terrestrial biosphere - hence the more it has decayed by the time it enters man's primary exposure environment. Since, at the present time, some  $^{14}\text{C}$  is discharged into the surface ocean, it could be argued that this parameter should be incorporated into the 'most probable' scenario. However, as the amount of  $^{14}\text{C}$  involved is very small and because the dose reduction associated with surface ocean discharge (relative to atmospheric discharge) is very small, this refinement is not considered necessary.

Thus far, all work has been based on the 25-box model, but now the predictions of the other carbon cycle models are considered. A sensitivity analysis identified the large carbon stocks and, in particular, the carbon content of the deep ocean, as being important parameters in determining the long-term distribution of  $^{14}\text{C}$  in nature. As consequence of this conclusion, the 1-box model is not included in this part of the assessment. The CEDEC predicted by the three remaining models following discharge of 1 TBq of  $^{14}\text{C}$  into the atmosphere, surface ocean and deep ocean (assuming F2 and  $^{14}\text{C}$  release in 1980) are presented in Table 4.14. For atmospheric discharge, the 25-box model predicts the largest dose (127 man Sv), the 8-box model the next largest (118 man Sv) and the 3-box model the lowest dose (114 man Sv). A similar trend is apparent in the results obtained here for the dose generated following discharge to the surface ocean. By contrast, the 25-box model predicts the lowest dose following  $^{14}\text{C}$  discharge to the deep ocean. This phenomenon reflects the highly detailed representation of the deep ocean incorporated in the 25-box model. For it divides the ocean in 19 discrete layers and, in this calculation, the  $^{14}\text{C}$  is assumed to be discharged into the deepest box. In the 3 and 8-box models, however, the deep oceans are not divided in a vertical sense and thus the  $^{14}\text{C}$ , in these cases, is assumed to be discharged uniformly throughout the deep ocean.

One further problem associated with the long-term nature of this assessment is that major fundamental change in the nature of

Table 4.14: The collective effective dose equivalent commitments to man from the release of 1 TBq of  $^{14}\text{C}$  into different compartments of the carbon cycle, as predicted by various models (assuming F2 and  $^{14}\text{C}$  release in 1980)

Model	CEDEC (man Sv)		
	Atmosphere	Surface ocean	Deep ocean
3-box	114	111	97
8-box	118	113	109
25-box	127	125	95

the carbon cycle could well occur during such long timescales, through either anthropogenic or natural processes. For example, it is possible that global warming, via the greenhouse effect, could induce large scale alterations of carbon inventories and exchange rates. Alternatively, it is feasible that within the lifetime of present-day  $^{14}\text{C}$ , the global climate could revert from interglacial to glacial conditions. It is currently impossible to predict either the likelihood or effect of any such major events and it is therefore assumed here that present-day conditions will continue to apply throughout the period of interest.

#### 4.3.2.3 The Radiological Impact on the Public to Infinity

The major parameters on which the future dose to man from  $^{14}\text{C}$  discharges from the nuclear fuel cycle depend have now been identified and their effects quantified. In addition, a best estimate of 127 man Sv TBq $^{-1}$  for the CEDEC has been determined. In reality, however, this value only applies to  $^{14}\text{C}$  discharges in 1980, with the doses derived from discharges at other times varying, according to the fossil fuel combustion rate. Consequently, this value may underestimate the radiological significance of the  $^{14}\text{C}$  discharges. Therefore, for the sake of conservatism, a dose estimate derived assuming no future fossil fuel combustion is necessary. The value of the CEDEC following the release of 1 TBq  $^{14}\text{C}$  into the atmosphere (using F1 and the 25-box model) has already been determined (Figure 4.28). The value of 141 man Sv TBq $^{-1}$  is well within the range of previously published data, 86-159 man Sv TBq $^{-1}$  (United Nations, 1972, 1977, 1981; Kelly et al., 1975; Killough and Rohwer, 1978; Schwibach et al., 1978; Bush et al., 1983; IAEA, 1985). Most of these estimates are derived from carbon cycle models although some of the studies (e.g. United Nations, 1981) derive their values by direct analogy with the natural  $^{14}\text{C}$  production rate. Thus, although the value of 127 man Sv TBq $^{-1}$  is probably closer to the mean CEDEC from  $^{14}\text{C}$  discharges from the nuclear fuel cycle, the conservative value of 141 man Sv TBq $^{-1}$  is adopted in this work for radiological assessment purposes.

Since the total long-term production of  $^{14}\text{C}$  by the

nuclear industry is unknown, the total dose to man cannot be calculated. In the short-term study, however, the future of the nuclear industry is projected to 2050 and thus the total dose to man from  $^{14}\text{C}$  produced by the nuclear industry to that date can be estimated. Here it is assumed that all the  $^{14}\text{C}$  produced by the nuclear industry is released to the environment within a short time relative to the mean effective life of  $^{14}\text{C}$ . The  $^{14}\text{C}$  production rate, according to Table 4.5, is  $3.4 \text{ TBq (GW(e) year)}^{-1}$  and, therefore, the CEDEC is  $480 \text{ man Sv (GW(e) year)}^{-1}$ . According to the most likely nuclear fuel use scenario, total energy production by the nuclear industry between 1955 and 2050 is  $1.2 \times 10^5 \text{ GW(e) year}$ . Hence the CEDEC to man from  $^{14}\text{C}$  produced by the nuclear fuel cycle between 1955 and 2050 is estimated at  $5.8 \times 10^7 \text{ man Sv}$ . Using the risk coefficients listed in Table 1.11, this dose corresponds to the incidence of  $7.5 \times 10^5$  fatal cancers and  $5 \times 10^5$  hereditary effects.

As mentioned earlier, collective doses are regulated on the basis of the ALARA principle and thus there is no specific numerical limit to be applied to this radiological quantity. To give some relative indication of the significance of the dose from reactor-derived  $^{14}\text{C}$  for the 1955-2050 period, the CEDECs from bomb-produced and naturally produced  $^{14}\text{C}$  over the same interval are calculated and shown in Table 4.15. The dose from reactor-derived  $^{14}\text{C}$  is about double that from nuclear weapon test  $^{14}\text{C}$  and is approximately four times that delivered by natural  $^{14}\text{C}$ . Although these results provide some kind of perspective, they do not necessarily resolve the question of their acceptability.

Perhaps a more informative comparison is with the doses to man from other radionuclides discharged by the nuclear industry. In a study of CEDECs from nuclear power production, the United Nations (1982) identified the long-lived nuclides which become globally dispersed, namely,  $^3\text{H}$ ,  $^{85}\text{Kr}$ ,  $^{129}\text{I}$  and  $^{14}\text{C}$ , as being particularly significant contributors to dose. The complete and incomplete CEDECs, normalised to 1 GW(e) year production, for these 4 radionuclides are detailed in Table 4.16. The values shown for  $^3\text{H}$ ,  $^{85}\text{Kr}$  and  $^{129}\text{I}$  are all derived

Table 4.15: The collective effective dose equivalent commitments to man from <sup>14</sup>C produced from various sources over the period 1955-2050

Source	CEDEC (10 <sup>7</sup> man Sv)
Nuclear	5.8
Bomb	3.1
Natural	1.3
Total	10.2

Table 4.16: The complete and incomplete collective effective dose equivalent commitments to man, over given times, from various nuclides released from the nuclear fuel cycle

Nuclide	Complete and incomplete CEDEC (man Sv (GW(e) year) <sup>-1</sup> )				
	10 <sup>1</sup> year	10 <sup>2</sup> year	10 <sup>4</sup> year	10 <sup>6</sup> year	10 <sup>8</sup> year
<sup>14</sup> C	9	24	343	480	480
<sup>129</sup> I	-	0.02	0.21	28	560
<sup>85</sup> Kr	0.9	1.9	1.9	1.9	1.9
<sup>3</sup> H	0.015	0.02	0.02	0.02	0.02

from the United Nations (1982) assessment but the  $^{14}\text{C}$  data are those produced in the present study. The dose from  $^{14}\text{C}$  is seen to dominate those from  $^3\text{H}$ ,  $^{85}\text{Kr}$  and  $^{129}\text{I}$  during the first  $10^6$  years, only the  $^{129}\text{I}$  dose exceeding that from  $^{14}\text{C}$  over all time ( $10^8$  years). Of all other waste nuclides not mentioned, only radon (2800 man Sv (GW(e) year) $^{-1}$ ) and uranium (460 man Sv (GW(e) year) $^{-1}$ ) released from mill tailings lead to comparable detriments. It is clear, therefore, that  $^{14}\text{C}$  production and discharge and their implications for collective dose delivery are relatively significant in terms of magnitude.

It should perhaps be noted that direct comparison of the data in Table 4.16 is not altogether valid. For it is inevitable that some of the assumptions used to derive the United Nations data differ from those made here in generating the  $^{14}\text{C}$  results. Nevertheless, such differences are likely to have comparatively small effects and should certainly not modify the basic conclusion significantly, i.e. that  $^{14}\text{C}$  is one of the largest contributors to CEDECs to man from nuclear power production. Hence, means of reducing the magnitude of this dose contribution should be investigated.

#### 4.3.3 Chernobyl

Towards the end of the project, an event occurred which, more than anything else, emphasises the reality of the uncertainties in all future projections. That event was the large-scale accident at the Chernobyl nuclear reactor in USSR. Throughout this work, the number and magnitude of many different uncertainties have been constantly stressed. As this event highlights, however, the list of uncertainties is far from complete. The effect of a large-scale accident at a nuclear facility was never considered, mainly because such an event was thought to be very unlikely. The accident occurred at the Chernobyl nuclear power station complex near Kiev, in the Ukraine, on 26 April 1986. The complex consisted of 6 separate nuclear reactors, two of which were still under construction but the accident itself was largely confined to reactor unit 4. These reactors, which are light-water-cooled and utilise a graphite moderator, are unique to Russia. The Russians now admit that this reactor design has deficiencies and that

these, coupled with operator errors and a deliberate flouting of safety instructions, led to the accident.

To assess the effect of this accident on atmospheric  $^{14}\text{C}$  levels it is necessary to know the inventory of  $^{14}\text{C}$  released to the environment. No reliable figures on the  $^{14}\text{C}$  production rate in this reactor design are available. Measurements from early Russian reactors of similar design suggest that their  $^{14}\text{C}$  release rates are high relative to those for other reactor types (Davis, 1979). This high production is thought to be caused by the high utilisation of nitrogen-containing compounds in various parts of the reactors. It is, however, believed that in the more modern reactor designs (including the Chernobyl reactor), these features have been discontinued. It is, in any event, not the daily  $^{14}\text{C}$  release rate which is required for this assessment but rather the  $^{14}\text{C}$  production rate. To be more precise, it is a measure of the  $^{14}\text{C}$  which, under normal circumstances, would have remained in the reactor in the absence of this accident. The main source of this  $^{14}\text{C}$  is expected to be the graphite moderator, as in AGRs and MAGNOX reactors (the 2 other reactor types which incorporate this facility). The  $^{14}\text{C}$  production rates in the moderator of AGRs and MAGNOX reactors are estimated at 5.3 and 9.0 TBq (GW(e) year)<sup>-1</sup> respectively (c.f. Section 1.3.2). For the Chernobyl reactor, a value of 10 TBq (GW(e) year)<sup>-1</sup> is assumed. This slightly higher value is chosen partially on the grounds of conservatism and partially to cater for other small additional sources of  $^{14}\text{C}$ , e.g. in the structural components of the reactor. Reactor unit 4 at Chernobyl had a capacity of 1 GW(e) year and had been in operation for almost 3 years (IAEA, 1984). Therefore, assuming a load factor of 0.7, the total amount of  $^{14}\text{C}$  produced in the moderator can be calculated to be 21 TBq. The exact extent of the damage to the reactor is, at this stage, difficult to assess but certainly the large graphite moderator was ignited and did burn freely for many days. It is therefore assumed here that the entire moderator was combusted and thus that the entire 21 TBq was released to atmosphere.

By superimposing this release onto the most likely energy scenario, S4, an estimate of its effects on future atmospheric

$^{14}\text{C}$  levels and hence on the future dose to man can be made. When this is carried out, no noticeable increase in atmospheric  $^{14}\text{C}$  levels is detected relative to the baseline previously determined. This result is not totally surprising, for, when this release is compared to that from a nuclear weapon test, its magnitude is placed in some degree of perspective. A total of  $2.2 \times 10^{17}$  Bq of  $^{14}\text{C}$  were produced by a total of 423 nuclear weapon tests (United Nations, 1982), thus averaging 520 TBq per test, i.e. 25 times greater than the Chernobyl release. These theoretical predictions have, to a certain extent, been confirmed by experimental work. Measurements of the atmospheric  $^{14}\text{C}$  levels over Britain in the period following the accident failed to produce any evidence of an increase (Harkness, pers. comm., 1986).

Obviously, this calculation was executed in a very approximate manner because of the lack of available information. Nevertheless, the results indicate that, after global dispersion of the  $^{14}\text{C}$ , no significant increase in individual dose rates should be caused by the Chernobyl accident. It is also worth noting that the accident will not cause an increase in the CEDEC to man from reactor-derived  $^{14}\text{C}$  over the period 1955-2050. This is because, in the original calculation, it was assumed that all  $^{14}\text{C}$  produced in reactors is released to atmosphere. The Chernobyl accident, according to the present understanding of it, would not have caused the production of  $^{14}\text{C}$  but merely released previously produced  $^{14}\text{C}$  to the environment sooner than planned.

#### 4.4 $^{14}\text{C}$ WASTE MANAGEMENT

The preceding discussions have implied that there is a need to investigate ways and means of reducing  $^{14}\text{C}$  doses to man. In this section, various possible strategies towards this end are identified and their effectiveness reviewed. This discussion concentrates on reduction of the CEDEC to man since it is this, from a radiological point of view, which is the most significant parameter. It should, however, be remembered that a reduction in this parameter is, in fact, dependent on a corresponding reduction of the other important radiological quantities, e.g. individual dose rates. Reduction of the dose to man from reactor-derived

$^{14}\text{C}$  must be generated primarily by decreasing the inventory of reactor-derived  $^{14}\text{C}$  in the atmosphere. For a given nuclear energy strategy, such a reduction can be achieved in three different ways:

- (a) by reducing the  $^{14}\text{C}$  production rate in nuclear reactors,
- (b) by releasing the  $^{14}\text{C}$  to a part of the carbon cycle other than the atmosphere

and

- (c) by retention and subsequent immobilisation of  $^{14}\text{C}$  wastes.

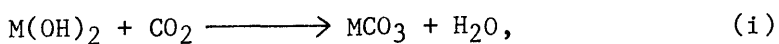
Each different method is now discussed.

The most obvious way to reduce the dose to man from reactor-derived  $^{14}\text{C}$  is to decrease  $^{14}\text{C}$  production. The fractional reduction in dose to man would be identical to that in  $^{14}\text{C}$  production. The possibilities are, however, severely limited for, in reality, the production of  $^{14}\text{C}$  is inevitable in all present reactor types. Nevertheless, there is one obvious means by which  $^{14}\text{C}$  production could be reduced, i.e. by removing the nitrogen impurities in the fuel. Very little is, however, known about the sources of nitrogen in fuel or about their possible elimination. Although, in theory, this approach could reduce subsequent doses to man, the feasibility of its implementation is difficult to assess. A study by Bush (1984) concluded that only a modest reduction in  $^{14}\text{C}$  production (by at most a factor of 5) could be achieved by this means.

The second potential means of reducing doses would require release of the  $^{14}\text{C}$  to a non-atmospheric compartment of the carbon cycle. The effects of releasing  $^{14}\text{C}$  waste into either the surface or deep ocean have already been demonstrated in Figure 4.29. The major consequence of marine release is to delay the dose delivery, the effect being more pronounced the deeper the  $^{14}\text{C}$  waste is discharged. Nevertheless, in the extreme case of  $^{14}\text{C}$  input to the deepest part of the ocean, the eventual dose to man is reduced only by a factor of 1.4. Because of this rather small potential for dose reduction, very little effort has been directed towards development of a corresponding disposal strategy.

The final approach to dose reduction is through retention and subsequent immobilisation of  $^{14}\text{C}$  wastes. Here the principle is that the  $^{14}\text{C}$  waste is isolated from the environment for a sufficient period of time to ensure that, when it enters the carbon cycle, a significant fraction of the original activity has decayed. The retention times necessary to induce various reductions in the CEDEC are listed in Table 4.17. As these data show, this strategy does in theory have the ability to reduce greatly the dose to man from reactor-derived  $^{14}\text{C}$ , although very long retention times are required. A significant research effort has been directed towards this strategy because of its large dose reduction capabilities. There are 2 basic steps needed to implement this strategy; firstly, the  $^{14}\text{C}$  waste must be retained and, secondly, the  $^{14}\text{C}$  waste must be immobilised.

The retention of  $^{14}\text{C}$  is essentially concerned with its collection from off-gas streams at reactors and reprocessing plants since, at present, this is by far the dominant discharge pathway. Various trapping processes which convert  $\text{CO}_2$  into insoluble carbonates have been identified (Bush et al., 1983). For example, in the 'direct process'  $\text{CO}_2$  reacts with an alkaline earth hydroxide to produce a stable, insoluble metal carbonate:



where M represents Ca, Sr or Ba. Although the chemical reactions involved are well known, the process-engineering aspects of their use to obtain high decontamination factors for  $\text{CO}_2$ , at high dilution and in the presence of other components, still require detailed consideration. Once the  $^{14}\text{C}$  waste has been collected, its subsequent storage and isolation from the environment must be addressed. Calcium and barium carbonates, produced in the processes discussed above, are stable chemical compounds. It is probable that they could be incorporated into a convenient matrix, such as cement or bitumen, to provide a satisfactory immobilised waste form for  $^{14}\text{C}$ , suitable for eventual disposal. The long-term stabilities of such waste forms to irradiation and to leaching have not, however, been fully studied.

Of the 3 alternative approaches discussed, that aimed at retention and subsequent immobilisation of  $^{14}\text{C}$  waste appears

Table 4.17: The waste retention times necessary to induce various reductions in the collective effective dose equivalent commitment to man from  $^{14}\text{C}$

Reduction factor	Retention time ( $10^4$ years)
5	1.3
10	1.9
50	3.2
100	3.8
500	5.1
1000	5.7

to have greatest potential. The methods discussed are, however, not mutually exclusive. The decisions on whether or not to implement any or all of these  $^{14}\text{C}$  waste management strategies are likely to rest on the ALARA principle recommended by ICRP. The application of the ALARA principle basically involves use of the technique of cost-benefit analysis. Very simply, a monetary value is attached to a given reduction in the radiation dose and, in order to warrant the implementation of a given strategy, its cost must be commensurate with the value of the resulting reduction in radiation dose. In practice, however, the ALARA principle takes into account a complex range of social and economic factors and its implementation is outwith the scope of this present study. Nevertheless, on this basis, one country (Argentina) has already implemented a  $^{14}\text{C}$  waste management programme. Their strategy involves retention of  $^{14}\text{C}$  from the off-gas streams at their HWRs and subsequent immobilisation of the waste for sufficient time to reduce the eventual dose to man by a factor of 100. In practice, this involves oxidising the  $^{14}\text{C}$  in the off-gas streams to  $\text{CO}_2$  which is then precipitated as  $\text{BaCO}_3$  which is finally immobilised in bitumen. To achieve their desired reduction in dose, the  $^{14}\text{C}$  waste must be retained for nearly 40 000 years. Only time will tell whether this objective is achieved. This example, however, shows that  $^{14}\text{C}$  waste management is recognised as worthy of action and that, given the correct set of circumstances, practical strategies can be made cost-effective.

#### 4.5

#### CONCLUSIONS

The objective of this section was to assess the radiation dose to the global population resulting from  $^{14}\text{C}$  discharges from the nuclear fuel cycle. Initially, an attempt was made to estimate the future doses to the global population due to  $^{14}\text{C}$  discharges from the nuclear industry. These estimates were limited to the period to 2050 because of uncertainties inherent in energy projections. Therefore, to obtain a measure of the entire detriment to man from  $^{14}\text{C}$  discharges, the CEDEC from a notional release of  $^{14}\text{C}$  was also calculated. The primary results obtained and conclusions reached are as follows.

As a precursor to estimating the dose to man from reactor-

derived  $^{14}\text{C}$ , the atmospheric  $^{14}\text{C}$  levels resulting from all the anthropogenic perturbations to the year 2050 were determined. The results show that future atmospheric  $^{14}\text{C}$  levels will not deviate greatly from the natural level and, indeed, will be significantly lower than those experienced in the recent past. The atmospheric  $^{14}\text{C}$  specific activity in 2050 is expected to be approximately  $234 \text{ Bq kg}^{-1}$  (carbon), corresponding to an individual effective dose equivalent rate of  $14.6 \mu\text{Sv year}^{-1}$ . The contribution of the reactor-derived  $^{14}\text{C}$  to the individual effective dose equivalent rate increases consistently over this period and reaches  $1.8 \mu\text{Sv year}^{-1}$  in 2050. This corresponds to 0.2% of the  $1 \text{ mSv year}^{-1}$  limit recommended by ICRP. Such a level of dose, in itself, provides insufficient justification for further reduction of  $^{14}\text{C}$  discharges. Because of the large number of uncertainties implicit in these predictions, however, (as epitomised by the Chernobyl accident) it is recommended that estimates of the future individual effective dose equivalent rate should be constantly updated in the light of the best possible information.

The major significance of  $^{14}\text{C}$  discharges is that, because of its long half-life, coupled with its mobility in the environment, releases of this nuclide lead to exposure of global populations over very long timescales. A conservative estimate of  $141 \text{ man Sv TBq}^{-1}$  has been derived here for the CEDEC to man from reactor-derived  $^{14}\text{C}$ . Normalised to the production of  $1 \text{ GW(e) year}$  of energy via nuclear power, this figure corresponds to a detriment of  $480 \text{ man Sv (GW(e) year)}^{-1}$ . This latter value suggests that  $^{14}\text{C}$  delivers one of the largest contributions to the dose to man from generation of nuclear power. In light of this, it is recommended that considerable effort is directed towards development of a cost-effective method for dose reduction.

Various  $^{14}\text{C}$  waste management strategies have been identified. These, in theory, will result in significant dose reduction from reactor-derived  $^{14}\text{C}$ . The most promising strategy involves the retention and subsequent immobilisation of  $^{14}\text{C}$ .

THE RADIOLOGICAL IMPACT OF  $^{14}\text{C}$  DISCHARGES FROM THE NUCLEAR FUEL CYCLE:  
AN OVERVIEW

The radiological impact of  $^{14}\text{C}$  discharges from the nuclear fuel cycle has been assessed at both local and global levels. In practice, there can of course be no global dose without a local one and vice versa and so it would be unjustifiable to imply that the two effects are separate entities. Similarly, it would be wrong, having on the one hand calculated the global doses and on the other the local doses, to sum these 2 components to quantify the total dose. In fact, the global doses calculated in Chapter 4 do represent the total dose to man resulting from  $^{14}\text{C}$  discharges from the nuclear fuel cycle. In this assessment, however, it was assumed that  $^{14}\text{C}$  released from a nuclear facility is instantaneously mixed homogeneously within the entire atmosphere and thus that the exposed global population receives the same dose. In reality, a gradient of doses is generated, these being relatively high near the release point and decreasing with increasing distance from discharge. Since these  $^{14}\text{C}$  discharge points are scattered geographically, this assumption is, in general, quite reasonable. However, the concentration factor around discharge points should be considered fully in any complete and accurate assessment of the radiological impact of  $^{14}\text{C}$  discharges from the nuclear fuel cycle. In this brief final section then, the results of the local and global studies are compared and inter-related so that perhaps a clearer overview of the situation is provided.

The assessment herein of the global effects of  $^{14}\text{C}$  discharges predicts that the individual effective dose equivalent rate will increase constantly until the limit of the study (2050) when it will average  $1.8 \mu\text{Sv year}^{-1}$ . The doses to individuals around large nuclear installations will, however, exceed these global levels. The latter increment is clearly identified in the results obtained here during the local study. The maximum annual effective dose equivalents to the most exposed individual around Sellafield and Hunterston were  $0.2 \text{ mSv}$  (in 1982) and  $11.8 \mu\text{Sv}$  (in 1984) respectively. These levels do not exceed the limits recommended by ICRP but in the Sellafield case are a significant fraction of it. However, if doses around these plants were to increase in future in a parallel manner to the global dose rate, then the limits would soon be exceeded. Hence, as regards individual dose rates, the 'dose gradient' has

considerable radiological implications. In contrast, the local enhancement of  $^{14}\text{C}$  levels is of little importance when considering collective doses. For example, the collective effective dose equivalent commitment to the population within 40 km of Sellafield, over the period 1952-1985, averaged  $2 \times 10^{-2}$  man Sv  $\text{TBq}^{-1}$ , i.e. 0.015% of the total dose (which is conservatively estimated at 141 man Sv  $\text{TBq}^{-1}$ ).

In conclusion, the basic recommendation of this study, i.e. that considerable efforts should be directed towards developing a suitable  $^{14}\text{C}$  waste management strategy, remains unchanged. It has now been demonstrated, however, that the effective dose equivalent rate to the most exposed individuals around nuclear facilities could become sufficiently large in the near future to enforce the implementation of a suitable dose reduction strategy.

A FORTRAN 77 computer programme is used in this work to calculate the  $^{14}\text{C}$  specific activities of the samples from the raw data generated by the liquid scintillation counter. An outline of the appropriate calculation procedure was included in Section 2.5.6 but, to avoid any ambiguity, a detailed account will now be given followed by a listing of the actual programme and an example of a typical input/output data set.

### Calculation Procedure

The data generated by the liquid scintillation counter consist of a list of the total counts,  $P_{xn}(C)$ , in each channel,  $C$  (where  $C = 1,2,3$ ), for each 100 minute count,  $n$ , of every vial,  $x$  (where  $x$  can be a background,  $b$ , modern standard,  $m$ , or sample,  $s$ ), included in the batch. In a few basic steps, which will now be listed, these data can, in conjunction with a few other additional pieces of information, be transformed into a measure of the  $^{14}\text{C}$  specific activities of the samples. For each step of the procedure, the parameter to be determined is identified and the equations used to quantify both the parameter and its associated error are listed. However, the reason behind the inclusion of each particular step (e.g. why the sample is corrected for isotopic fractionation) is not included since this topic has already been adequately covered in Chapter 2.

#### STEP 1:

The count rate in each channel of every vial is calculated.

The count rate,  $Q_x(C)$ , in channel  $C$  of vial  $x$  is given by:

$$Q_x(C) = \left( \sum_n P_{xn}(C) \right) / (100 \text{ nn}),$$

where  $n = 1,2, \dots, \text{nn}$  and  $\text{nn}$ , the number of times vial  $x$  has been counted for 100 minutes, is provided (i.e. the quantity  $\text{nn}$  represents a piece of additional information which must be made available).

The error on the count rate,  $EQ_x(C)$ , in channel  $C$  of vial  $x$  is given by:

$$EQ_x(C) = \left( \left( \sum_n P_{xn}(C) \right)^{\frac{1}{2}} \right) / (100 \text{ nn}).$$

#### STEP 2:

The average background count rate in each channel is calculated.

The average background count rate,  $B(C)$ , in channel  $C$  is given by:

$$B(C) = (\sum_b Q_b(C))/nb,$$

where  $b = 1, 2, \dots, nb$  and  $nb$ , the number of backgrounds in the batch, is provided.

The error on the average background count rate,  $EB(C)$ , in channel  $C$  can be determined by two different but equally acceptable methods. In this work,  $EB(C)$  is calculated using both methods but in subsequent calculations it is the higher value alone which is utilised. The two methods are, firstly:

$$EB(C) = ((\sum_b EQ_b(C)^2)^{\frac{1}{2}})/nb,$$

and secondly:

$$EB(C) = ((\sum_b (B(C) - Q_b(C))^2)^{\frac{1}{2}})/nb.$$

### STEP 3:

The count rate in each channel of all modern standards and samples is corrected for background.

The count rate (corrected for background),  $R_y(C)$ , in channel  $C$  of vial  $y$  (where  $y$  can be a modern standard or sample) is given by:

$$R_y(C) = Q_y(C) - B(C).$$

The error on the count rate (corrected for background),  $ER_y(C)$ , in channel  $C$  of vial  $y$  is given by:

$$ER_y(C) = (EQ_y(C)^2 + EB(C)^2)^{\frac{1}{2}}.$$

### STEP 4:

The count rate of all modern standards and samples is corrected for quenching. To do this, however, their efficiencies must first be calculated using the appropriate quench-efficiency calibration curve and the values of their channel 2 to channel 3 count rate ratios.

(a) The channel 2 to channel 3 count rate ratio,  $CR_y$ , of vial  $y$  is given by:

$$CR_y = R_y(2)/R_y(3).$$

The error on the channel 2 to channel 3 count rate ratio,  $ECR_y$ , of vial  $y$  is given by:

$$ECR_y = ((R_y(2)/R_y(3))^2 + ((R_y(2) ER_y(3))/R_y(3)^2)^2)^{\frac{1}{2}}.$$

(b) The efficiency,  $E_y$ , of vial  $y$  is then given by:

$$E_y = \alpha - (\beta CR) + (\gamma CR^2),$$

where the constants  $\alpha$ ,  $\beta$  and  $\gamma$ , which define the quench-efficiency calibration curve, are provided.

The error on the efficiency,  $EE_y$ , of vial  $y$  is given by:

$$EE_y = S^* (a^* + ((d^* + b^*) CR) + ((g^* + e^* + c^*) CR^2) + ((h^* + f^*) CR^3) + (i CR^4))^{\frac{1}{2}},$$

where  $S^*$ , the standard deviation about the quench-efficiency calibration curve and its coefficients,  $a^*-i^*$ , are all provided. The above equation assumes, as was the case throughout this study, that the value of  $ECR_y$  is small in comparison to  $S^*$ . Indeed, since the errors on the count rates in channels 2 and 3, and hence  $ECR_y$ , are so small by comparison to  $S^*$ , they can be ignored.

(c) The count rate (corrected for quenching),  $T_y$ , of vial  $y$  is then given by:

$$T_y = 100(R_y(1)/E_y).$$

The error on the count rate (corrected for quenching),  $ET_y$ , of vial  $y$  is given by:

$$ET_y = 100((ER_y(1)/E_y)^2 + ((R_y(1) EE_y)/E_y^2)^2)^{\frac{1}{2}}.$$

#### STEP 5:

The count rate of all modern standards and samples is corrected for dilution.

The count rate (corrected for dilution),  $U_y$ , of vial  $y$  is given by:

$$U_y = T_y/W_y,$$

where  $W_y$ , the weight of modern standard or sample-derived benzene in vial  $y$ , is provided.

The error on the count rate (corrected for dilution),  $EU_y$ , of vial  $y$  is given by:

$$EU_y = ((ET_y/W_y)^2 + ((EW_y T_y)/W_y^2)^2)^{\frac{1}{2}},$$

where  $EW_y$ , the error on the weight of modern standard or sample-derived benzene in vial  $y$ , is provided.

#### STEP 6:

The average modern count rate (normalised to the  $^{14}C$  specific

activity of the primary standard) is determined. Initially, however, the count rate of each modern standard must be normalised to the  $^{14}\text{C}$  specific activity of the primary standard.

- (a) The count rate (normalised to the  $^{14}\text{C}$  specific activity of the primary standard),  $L_m$ , of modern standard  $m$  is given by:

$$L_m = I U_m (\exp(\lambda (k - 1950))) (1 - (2(J + F_m)/1000)),$$

where  $k$ , the year in which the batch was counted,  $F_m$ , the  $\delta^{13}\text{C}$  value of the modern standard  $m$ , and  $\lambda$ , the decay constant for  $^{14}\text{C}$ , are all provided. If the modern standard  $m$  is derived from batch SRM 4990 then  $I = 0.95$  and  $J = 19$  but if it is derived from batch SRM 4990-C then  $I = 0.7459$  and  $J = 25$ .

The error on the count rate (normalised to the  $^{14}\text{C}$  specific activity of the primary standard),  $EL_m$ , of modern standard  $m$  is given by:

$$EL_m = I (\exp(\lambda (k - 1950))) (((1 - (2(J + F_m)/1000))^2 EU_m^2) + ((2 U_m EF_m)/1000)^2)^{\frac{1}{2}},$$

where  $EF_m$ , the error on the  $\delta^{13}\text{C}$  value of the modern standard  $m$ , is provided.

- (b) The average modern count rate (normalised to the  $^{14}\text{C}$  specific activity of the primary standard),  $V$ , is then given by:

$$V = (\sum_m L_m)/nm,$$

where  $m = 1, 2, \dots, nm$  and  $nm$ , the number of modern standards in the batch, is provided.

The error on the average modern count rate (normalised to the  $^{14}\text{C}$  specific activity of the primary standard),  $EV$ , can be derived in two equally applicable ways. As in STEP 2, the error is calculated by both methods but the higher value alone is used in subsequent calculations. The two methods are, firstly:

$$EV = ((\sum_m EL_m^2)^{\frac{1}{2}})/nm,$$

and secondly:

$$EV = ((\sum_m (V - L_m)^2)^{\frac{1}{2}})/nm.$$

#### STEP 7:

The count rate of each sample is corrected for isotopic fractionation and decay.

The count rate (corrected for isotopic fractionation and decay),  $Z_s$ , of sample  $s$  is given by:

$$Z_s = U_s (\exp(\lambda (k - G))) (1 - (2(25 + F_s)/1000)),$$

where  $G$ , the year in which the sample was isolated from the carbon cycle, and  $F_s$ , the  $\delta^{13}\text{C}$  value of sample  $s$ , are provided.

The error on the count rate (corrected for isotopic fractionation and decay),  $EZ_s$ , of sample  $s$  is given by:

$$EZ_s = (\exp(\lambda (k - G))) (((1 - (2(25 + F_s)/1000))^2 EU_s^2) + ((2 U_s EF_s)/1000)^2)^{\frac{1}{2}},$$

where  $EF_s$ , the error on the  $\delta^{13}\text{C}$  value of sample  $s$ , is provided.

#### STEP 8:

The  $^{14}\text{C}$  specific activity of each sample is calculated.

The  $^{14}\text{C}$  specific activity,  $A_s$ , of sample  $s$  is given by:

$$A_s = 226(Z_s/V).$$

The error on the  $^{14}\text{C}$  specific activity,  $EA_s$ , of sample  $s$  is given by:

$$EA_s = 226((EZ_s/V)^2 + ((EV Z_s)/V^2)^2)^{\frac{1}{2}}.$$

For the sake of clarity, the symbols utilised in this description do not correspond to those used in the actual programme. However, it is hoped that the concise description given will prove to be of assistance in elucidating the, unfortunately but necessarily, more cluttered description contained within the actual programme itself. A listing of the programme now follows.

Programme Listing

```
C
C   THE VARIOUS CONSTANTS ARE SET UP
C
  DIMENSION T3B(500),ERF(500),ERMF(500),ABSF(500)
  DIMENSION L(500),H1(500),H2(500),H3(500)
  CHARACTER DESC*6
  CHARACTER SAMP*6
  WRITE(6,600)
  READ(5,*)V
  WRITE(6,601)
  READ(5,*)B
  WRITE(6,603)
  READ(5,*)M
  WRITE(6,604)
  READ(5,*)MB
  WRITE(6,602)
  READ(5,*)YM
  BK1=0
  BK2=0
  BK3=0
  ERB1=0
  ERB2=0
  ERM1=0
  ERM2=0
  ABSA=0
  FER=0.05
  WER=0.0005
  V=V*20

C
C   COUNTER DATA READ IN AND VIAL COUNT RATES CALCULATED
C
  DO 100 J=1,V
  READ(4,*)L(J),H1(J),H2(J),H3(J)
100 CONTINUE
  DO 110 K=1,18
  IF(K.EQ.18) GOTO 999
  A=0
  T1=0
  T2=0
  T3=0
  DO 120 J=1,V
  IF(L(J).EQ.K) GOTO 10
120 CONTINUE
110 CONTINUE
10  A=A+1
  T1=T1+H2(J)
  T2=T2+H3(J)
  T3=T3+H1(J)
  IF(A.EQ.20) GOTO 13
  GOTO 120
13  ER=(SQRT(T3))/2000
  T1=T1/2000
  T2=T2/2000
  T3=T3/2000
  GOTO 502

C
```

C THE BACKGROUND COUNT RATES ARE NOW CALCULATED  
C

```
14 IF(K.LT.5) GOTO 15
   IF(K.EQ.MB) GOTO 16
   GOTO 17
15 IF(K.EQ.1) GOTO 510
   GOTO 511
18 BK1=BK1+T1
   BK2=BK2+T2
   BK3=BK3+T3
   WRITE(9,*)T3,ER
   GOTO 110
16 BK1=BK1/B
   BK2=BK2/B
   BK3=BK3/B
   REWIND 9
   DO 140 I=1,B
   READ(9,*)T3B(I),ERF(I)
   ERB1=(ERF(I)**2)+ERB1
   ERB2=((BK3-T3B(I))**2)+ERB2
140 CONTINUE
   ERB1=(SQRT(ERB1))/B
   ERB2=(SQRT(ERB2))/B
   IF(ERB1.GT.ERB2) GOTO 19
   GOTO 20
19 ERB=ERB1
   GOTO 512
20 ERB=ERB2
   GOTO 512
```

C  
C VIAL COUNT RATES ARE NOW CORRECTED FOR BACKGROUND, QUENCHING AND  
C DILUTION  
C

```
17 T1=T1-BK1
   T2=T2-BK2
   T3=T3-BK3
   ERX=SQRT((ER**2)+(ERB**2))
   CR=T1/T2
   IF(CR.LT.1.40) GOTO 710
   IF(CR.GT.3.55) GOTO 710
   GOTO 712
712 E=78.9-(5.69*CR)+(0.473*CR*CR)
   ERE=(0.2977)*(SQRT(13.1576+(CR*(-11.4810-11.4810))+
1((CR**2)*(2.2701+10.1895+2.2701))+((CR**3)*
2(-2.0378-2.0378))+((CR**4)*0.4118)))
   T3=(T3*100)/E
   ERX=SQRT(((ERX*(100/E))**2)+((ERE*((100*T3)/
1(E**2))))**2))
   READ(10,586)WFG,W,F,G,R,SAMP
   T3=T3/W
   ERX=SQRT(((ERX**2)/(W**2))+((WER**2)*((T3/(W**2))**2)))
```

```

C
C   THE AVERAGE MODERN COUNT RATE IS NOW CALCULATED
C
    IF(K.LT.8) GOTO 21
    IF(K.LT.11) GOTO 721
    IF(K.EQ.11) GOTO 22
    GOTO 23
21  AON=(0.95*T3)*(1-((2*(19+F))/1000))
    ERM=SQRT(((0.95*(1-((2*(19+F))/1000)))*ERX)**2)+
    1(((0.95*2*T3/1000)*(FER))**2)
    GOTO 720
721 AON=(0.7459*T3)*(1-((2*(25+F))/1000))
    ERM=SQRT(((0.7459*(1-((2*(25+F))/1000)))*ERX)**2)+
    1(((0.7459*2*T3/1000)*(FER))**2)
    GOTO 720
720 ABS=AON*(EXP(0.0001209681*(YM-1950.0)))
    ERM=SQRT(((EXP(0.0001209681*(YM-1950.0)))*ERM)**2)
    GOTO 518
24  ABSA=ABSA+ABS
    WRITE(11,*)ERM,ABS
    GOTO 110
22  AABS=ABSA/M
    REWIND 11
    DO 150 N=1,M READ(11,*)ERMF(N),ABSF(N)
    ERM1=ERM1+(ERMF(N)**2)
    ERM2=ERM2+((AABS-ABSF(N))**2)
150 CONTINUE
    ERM1=(SQRT(ERM1))/M
    ERM2=(SQRT(ERM2))/M
    IF(ERM1.GT.ERM2) GOTO 25
    GOTO 26
25  ERM=ERM1
    GOTO 519
26  ERM=ERM2
    GOTO 519
C
C   THE 14C SPECIFIC ACTIVITY OF EACH SAMPLE IS NOW CALCULATED AFTER
C   CORRECTING FOR ISOTOPIC FRACTIONATION AND DECAY
C
23  DC=T3*(EXP(0.0001209681*(YM-G)))*(1-(2*(25+F)/1000))
    ERDC=(EXP(0.0001209681*(YM-G)))*(SQRT(((1-(2*(F+25)/
    11000))**2)*(ERX**2))+(((2*T3*FER)/1000)**2))
    BQ=(DC/AABS)*226
    EBQ=226*(SQRT((ERDC/AABS)**2)+(((ERM*DC)/
    1(AABS**2))**2))
    GOTO 525
27  GOTO 110
C
C   VARIOUS READ/WRITE/FORMAT STATEMENTS ETC.
C
600 FORMAT('HOW MANY VIALS WERE COUNTED')
601 FORMAT('HOW MANY BACKGROUNDS WERE COUNTED')
602 FORMAT('IN WHAT YEAR WAS THE BATCH COUNTED')
603 FORMAT('HOW MANY MODERN STANDARDS WERE COUNTED')
604 FORMAT('ARE THE MODERNS ALL FROM SRM 4990-C (Y=8,N=5)')
586 FORMAT(1X,A2,6X,F6.4,4X,F6.2,4X,F6.1,7X,F4.1,5X,A6)

```

```

710 WRITE(6,711)
711 FORMAT('WARNING: CHANNEL RATIO OFF SCALE')
    GOTO 712
502 WRITE(6,580)K
580 FORMAT('VIAL NUMBER=',I2,' -WHAT IS IT')
    READ(5,581)DESC
581 FORMAT(A6)
    GOTO 14
510 WRITE(8,560)
560 FORMAT('BACKGROUND',5X,'CHANNEL 1',5X,'CHANNEL 2',5X,
1'CHANNEL 3',/,10('-'),3(5X,9('-')))
    GOTO 511
511 WRITE(8,561)DESC,T3,T1,T2
561 FORMAT(2X,A6,3(9X,F5.3))
    GOTO 18
512 WRITE(8,562)
562 FORMAT(52('-'))
    WRITE(8,563)BK3,BK1,BK2
563 FORMAT('AVERAGE',10X,F5.3,2(9X,F5.3))
    WRITE(8,564)ERB
564 FORMAT('ERROR',12X,F5.3)
    WRITE(8,565)
565 FORMAT(52('-'))
    WRITE(8,568)
568 FORMAT(' ',/, ' ',/, ' ')
    WRITE(8,569)
569 FORMAT('MODERN',5X,'EFFICIENCY',5X,'COUNT RATE',/,
16('-'),5X,10('-'),5X,10('-'))
    GOTO 17
518 WRITE(8,570)DESC,E,ABS
570 FORMAT(A6,8X,F4.1,10X,F6.3)
    GOTO 24
519 WRITE(8,571)
571 FORMAT(36('-'))
    WRITE(8,572)AABS
572 FORMAT('AVERAGE',21X,F6.3)
    WRITE(8,573)ERM
573 FORMAT('ERROR',24X,F5.3)
    WRITE(8,574)
574 FORMAT(36('-'))
    WRITE(8,575)
575 FORMAT(' ',/, ' ',/, ' ')
    WRITE(8,579)
579 FORMAT('SAMPLE',5X,'EFFICIENCY',5X,'14C SPECIFIC
1ACTIVITY',5X,'ERROR',/,6('-'),5X,10('-'),5X,
221('-'),5X,5('-'))
    GOTO 23
525 WRITE(8,590)DESC,E,BQ,EBQ
590 FORMAT(A6,8X,F4.1,15X,F7.1,12X,F5.1)
    WRITE(8,585)SAMP,R,G
585 FORMAT('THIS ',A6,' SAMPLE GREW ',F4.1,
1' KM FROM 14C SOURCE IN ',F6.1)
    WRITE(8,582)
582 FORMAT(' ')
    GOTO 27
999 STOP
    END

```

## Input/Output Data Set

To complete this description of the utilisation of the computer programme for determining the  $^{14}\text{C}$  specific activities of samples, an example of a typical input/output data set is presented.

Data are provided for the programme from three separate sources. Input file 4 contains the data generated by the liquid scintillation counter and files 6 and 10 contain all other necessary pieces of information. File 10 contains sample-specific data (e.g. the  $\delta^{13}\text{C}$  values) whereas file 6 contains more general data on the counting batch (e.g. when the batch was counted), the latter information being requested by the programme when required. All the data generated by the programme are directed into file 8.

Listings of these files are now presented, although, due to its comparatively large size, the listing of input file 4 is restricted to that which is necessary to allow an adequate description of the format used. The following data are all derived from a counting batch consisting of samples collected around Sellafield in 1985.

INPUT FILE 4 (excerpt):

C	VIAL	CHANNEL 1	CHANNEL 2	CHANNEL 3
C	-----	-----	-----	-----
	1	713	383	316
	5	6917	4060	2428
	11	8436	4684	3280
	12	8701	4770	3490
	2	784	430	354
	8	9098	4736	3971
	13	8975	4751	3783
	14	8559	4516	3655
	3	685	369	321
	9	9073	4888	3790
	15	8653	4589	3664
	16	9295	4823	4044
	1	704	410	286
	5	7003	4121	2445
	11	8499	4682	3353
	12	8508	4583	3521
	2	734	407	335
	8	8960	4764	3828
	13	8930	4747	3771
	14	8524	4747	3868
	3	758	370	353
	9	9032	4867	3700
	15	8707	4578	3796
	16	8934	4658	3935

INPUT FILE 6:

PROMPT:

RESPONSE:

HOW MANY VIALS WERE COUNTED	12
HOW MANY BACKGROUNDS WERE COUNTED	3
HOW MANY MODERN STANDARDS WERE COUNTED	3
ARE THE MODERNS ALL FROM SRM 4990-C (Y=8, N=5)	5
IN WHAT YEAR WAS THE BATCH COUNTED	1986.2
VIAL NUMBER=1 -WHAT IS IT	KH/2
VIAL NUMBER=2 -WHAT IS IT	KI/1
VIAL NUMBER=3 -WHAT IS IT	KGC/4
VIAL NUMBER=5 -WHAT IS IT	NBS/2
VIAL NUMBER=8 -WHAT IS IT	NBS/4
VIAL NUMBER=9 -WHAT IS IT	NBS/6
VIAL NUMBER=11 -WHAT IS IT	SL/23
VIAL NUMBER=12 -WHAT IS IT	SL/24
VIAL NUMBER=13 -WHAT IS IT	SL/25
VIAL NUMBER=14 -WHAT IS IT	SL/26
VIAL NUMBER=15 -WHAT IS IT	SL/27
VIAL NUMBER=16 -WHAT IS IT	SL/28

INPUT FILE 10:

C	VIAL	WEIGHT	D13-C	DEATH	DISTANCE	TYPE
C	----	-----	-----	-----	-----	-----
	5	7.0290	-18.80	1950.0	00.0	ACID
	8	7.0285	-17.54	1950.0	00.0	ACID
	9	7.0282	-17.47	1950.0	00.0	ACID
	11	7.0275	-29.11	1985.7	16.0	GRASS
	12	7.0293	-29.11	1985.7	19.2	GRASS
	13	7.0275	-29.56	1985.7	21.5	GRASS
	14	7.0290	-30.22	1985.7	25.0	GRASS
	15	7.0283	-30.10	1985.7	29.0	GRASS
	16	7.0265	-29.13	1985.7	32.8	GRASS

OUTPUT FILE 8:

<u>BACKGROUND</u>	<u>CHANNEL 1</u>	<u>CHANNEL 2</u>	<u>CHANNEL 3</u>
KH/2	7.274	3.973	3.201
KI/1	7.388	4.053	3.274
KGC/4	7.273	3.905	3.246
AVERAGE	7.311		
ERROR	0.035		

<u>MODERN</u>	<u>EFFICIENCY</u>	<u>COUNT RATE</u>
NBS/2	70.5	11.958
NBS/4	72.9	11.969
NBS/6	72.4	12.013
AVERAGE		11.980
ERROR		0.062

<u>SAMPLE</u>	<u>EFFICIENCY</u>	<u>14C SPECIFIC ACTIVITY</u>	<u>ERROR</u>
SL/23	71.9	293.0	1.9
THIS GRASS	SAMPLE GREW 16.0 KM FROM 14C SOURCE IN 1985.7		
SL/24	72.2	293.4	1.9
THIS GRASS	SAMPLE GREW 19.2 KM FROM 14C SOURCE IN 1985.7		
SL/25	72.6	307.3	2.0
THIS GRASS	SAMPLE GREW 21.5 KM FROM 14C SOURCE IN 1985.7		
SL/26	72.7	288.9	1.9
THIS GRASS	SAMPLE GREW 25.0 KM FROM 14C SOURCE IN 1985.7		
SL/27	72.8	298.7	1.9
THIS GRASS	SAMPLE GREW 29.0 KM FROM 14C SOURCE IN 1985.7		
SL/28	73.0	310.9	2.0
THIS GRASS	SAMPLE GREW 32.8 KM FROM 14C SOURCE IN 1985.7		

## REFERENCES

- Anderson, E.C., Libby, W.F., Weinhouse, S., Reid, A.F., Kirshenbaum, A.D. and Grosse, A.V. (1947). Natural radiocarbon from cosmic radiation. *Physical Review*, 72, 931-936.
- Arnold, J.R. (1954). Scintillation counting of natural radiocarbon: I. The counting method. *Science*, New York, 119, 155-157.
- Arrol, W.J. and Glascock, R. (1947). Conversion of carbon dioxide to acetylene on a micro scale. *Nature*, London, 159, 810.
- Audric, B.N. and Long, J.V.P. (1954). Use of dissolved acetylene in liquid scintillation counters for the measurement of carbon-14 of low specific activity. *Nature*, London, 173, 992-993.
- Bacastow, R.B. and Bjorkstrom, A. (1981). Comparison of ocean models for the carbon cycle. In: *Carbon Cycle Modelling* (B. Bolin, ed.), pp 29-79. SCOPE 16. John Wiley and Sons, New York.
- Bacastow, R.B. and Keeling, C.D. (1973). Atmospheric carbon dioxide and radiocarbon in the natural carbon cycle: II. Changes from AD 1700 to 2070 as deduced from a geochemical model. In: *Carbon and the Biosphere*, Proceedings of the 24th Brookhaven Symposium in Biology (G.M. Woodwell and E.V. Pecan, eds.), pp 86-135. US Atomic Energy Commission Report CONF-720510. NTIS, Springfield, Virginia.
- Bacastow, R.B. and Keeling, C.D. (1979). Models to predict future atmospheric CO<sub>2</sub> concentration. In: *Global Effects of Carbon Dioxide from Fossil Fuels*, Proceedings of an International Workshop (W.P. Elliott and L. Machta, eds.), pp 72-90. US Department of Energy Report CONF-770385. NTIS, Springfield, Virginia.
- Bacastow, R.B. and Keeling, C.D. (1981). Atmospheric carbon dioxide concentration and the observed airborne fraction. In: *Carbon Cycle Modelling* (B. Bolin, ed.), pp 103-112. SCOPE 16. John Wiley and Sons, New York.
- Baes, Jr, C.F., Bjorkstrom, A. and Mulholland, P.J. (1985). Uptake of carbon dioxide by the oceans. In: *Atmospheric Carbon Dioxide and the Global Carbon Cycle* (J.R. Trabalka, ed.), pp 81-112. US Department of Energy Report DOE/ER-0239. NTIS, Springfield, Virginia.
- Baes, C.F., Goeller, H.E., Olson, J.S. and Rotty, R.M. (1976). The Global Carbon Dioxide Problem. Oak Ridge National Laboratory, Oak Ridge, Tennessee, ORNL-5194.
- Baes, C.F., Goeller, H.E., Olson, J.S. and Rotty, R.M. (1977). Carbon dioxide and climate: the uncontrolled experiment. *American Scientist*, 65, 310-320.
- Barendsen, G.W. (1957). Radiocarbon dating with liquid CO<sub>2</sub> as diluent in a scintillation solution. *The Review of Scientific Instruments*, 28, 430-432.
- Barker, H. (1953). Radiocarbon dating: large-scale preparation of acetylene from organic material. *Nature*, London, 172, 631-632.

- Barker, H., Burleigh, R. and Meeks, N. (1969). New method for the combustion of samples for radiocarbon dating. *Nature*, London, 221, 49-50.
- Barnola, J.M., Raynaud, D., Neftel, A. and Oeschger, H. (1983). Comparison of CO<sub>2</sub> measurements by two laboratories on air from bubbles in polar ice. *Nature*, London, 303, 410-413.
- Baxter, M.S. and Farmer, J.G. (1973). Radiocarbon: short-term variations. *Earth and Planetary Science Letters*, 20, 295-299.
- Baxter, M.S. and McKay, K. (1983). Artificial Carbon-14 in the Terrestrial Biosphere. Report to IAEA's Coordinated Research Programme on Carbon-14 from Nuclear Facilities. IAEA, Vienna, Contract 3247/R2/CF.
- Baxter, M.S. and Stenhouse, M.J. (1976). Glasgow University radiocarbon measurements VIII. *Radiocarbon*, 18, 161-173.
- Baxter, M.S. and Walton, A. (1970). A theoretical approach to the Suess effect. *Proceedings of the Royal Society of London, Series A*, 318, 213-230.
- Baxter, M.S. and Walton, A. (1971). Fluctuations of atmospheric carbon-14 concentrations during the past century. *Proceedings of the Royal Society of London, Series A*, 321, 105-127.
- Beninson, D.J. (1984). Production, Release and Means of Control of C-14 in Heavy Water Reactors. Report to IAEA's Coordinated Research Programme on Carbon-14 from Nuclear Facilities. IAEA, Vienna, Contract 3247/R2/CF.
- Beninson, D.J. and Gonzalez, A.J. (1981). Application of the dose limitation system to the control of carbon-14 releases from heavy-water-moderated reactors. In: *The Dose Limitation System in the Nuclear Fuel Cycle and in Radiation Protection*, Proceedings of an IAEA Symposium, pp 1-19. IAEA-SM-258. IAEA, Vienna.
- Bergman, R. and McEwan, C. (1977). Dose and Dose Commitment due to Carbon-14 from the Nuclear Industry. *Aktiebolaget Atomenergi, Nykoping*, S-548.
- Bjorkstrom, A. (1979). A model of CO<sub>2</sub> interaction between atmosphere, oceans, and land biota. In: *The Global Carbon Cycle* (B. Bolin, E.T. Degens, S. Kempe and P. Ketner, eds.), pp 403-457. SCOPE 13. John Wiley and Sons, New York.
- Blanchard, R.L., Brinck, W.L., Kolde, H.E., Krieger, H.L., Montgomery, D.M., Gold, S., Martin, A. and Kahn, B. (1976). Radiological Surveillance Studies at the Oyster Creek BWR Nuclear Generating Station. US Environmental Protection Agency Report EPA-520/5-76-003. NTIS, Springfield, Virginia.
- Bolin, B., Bjorkstrom, A., Keeling, C.D., Bacastow, R. and Siegenthaler, U. (1981). Carbon cycle modelling. In: *Carbon Cycle Modelling* (B. Bolin, ed.), pp 1-28. SCOPE 16. John Wiley and Sons, New York.

- Bolin, B., Degens, E.T., Duvigneaud, P. and Kempe, S. (1979). The global biogeochemical carbon cycle. In: The Global Carbon Cycle (B. Bolin, E.T. Degens, S. Kempe and P. Ketner, eds.), pp 1-56. SCOPE 13. John Wiley and Sons, New York.
- Bolin, B. and Eriksson, E. (1959). Changes in the carbon dioxide content of the atmosphere and sea due to fossil fuel combustion. In: Atmosphere and Sea in Motion (B. Bolin, ed.), pp 130-142. The Rockefeller Institute Press, New York.
- Bonka, H. (1980). Produktion und freisetzung von tritium und kohlenstoff-14 durch kernwaffenversuche, testexplosionen und kerntechnische anlagen, einschlieBlich wiederaufarbeitungsanlagen. In: Strahlenschutzprobleme im Zusammenhang mit der Verwendung von Tritium und Kohlenstoff-14 und Ihren Verbindungen (F.E. Stieve and G. Kistner, eds.), pp 17-27. STH-Bericht 12/80. BGA, Neuherberg.
- Bray, J.R. (1959). An analysis of the possible recent change in atmospheric carbon dioxide concentration. *Tellus*, 11, 220-230.
- British Nuclear Fuels (1985). Annual Report on Radioactive Discharges and Monitoring of the Environment 1984. Health and Safety Directorate Report. BNF, Risley.
- British Nuclear Fuels (1986). Annual Report on Radioactive Discharges and Monitoring of the Environment 1985. Health and Safety Directorate Report. BNF, Risley.
- Broecker, W.S. and Olson, E.A. (1959). Lamont radiocarbon measurements VI. *American Journal of Science Radiocarbon Supplement*, 1, 111-132.
- Broecker, W.S. and Peng, T.-H. (1982). *Tracers in the Sea*. ELDIGIO Press Palisades, New York.
- Broecker, W.S., Peng, T.-H. and Engh, R. (1980). Modeling the carbon system. In: Proceedings of the 10th International Radiocarbon Conference (M. Stuiver and R. Kra, eds.). *Radiocarbon*, 22, 565-598.
- Broecker, W.S. and Walton, A. (1959). Radiocarbon from nuclear tests. *Science*, New York, 130, 309-314.
- Bruns, M., Munnich, K.O. and Becker, B. (1980). Natural radiocarbon variations from AD 200 to 800. In: Proceedings of the 10th International Radiocarbon Conference (M. Stuiver and R. Kra, eds.). *Radiocarbon*, 22, 273-277.
- Bruns, M., Rhein, M., Linick, T.W. and Suess, H.E. (1983). The atmospheric  $^{14}\text{C}$  level in the 7th millennium BC. In:  $^{14}\text{C}$  and Archaeology, Proceedings of PACT 8, Groningen, Netherlands, August 1982 (W.G. Mook and H.T. Waterbolk, eds.), pp 511-516. Council of Europe, Strasbourg.
- Bucha, V. (1970). Influence of the earth's magnetic field on radiocarbon dating. In: Radiocarbon Variations and Absolute Chronology, Proceedings of the 12th Nobel Symposium, Uppsala, Sweden, 11-15 August 1969 (I.U. Olsson, ed.), pp 501-511. John Wiley and Sons, New York.

- Bucha, V. and Neustupny, E. (1967). Changes of the earth's magnetic field and radiocarbon dating. *Nature*, London, 215, 261-263.
- Burke, Jr, W.H. and Meinschein, W.G. (1955).  $C^{14}$  dating with a methane proportional counter. *The Review of Scientific Instruments*, 26, 1137-1140.
- Bush, R.P. (1984). Carbon-14 waste management. In: *Radioactive Waste Management, Proceedings of an IAEA Conference*, pp 441-453. IAEA-CN-43. IAEA, Vienna.
- Bush, R.P., White, I.F. and Smith, G.M. (1983). Carbon-14 Waste Management. UK Atomic Energy Authority, Harwell, AERE-R10543.
- Cain, W.F. and Suess, H.E. (1976). Carbon 14 in tree rings. *Journal of Geophysical Research*, 81, 3688-3694.
- Cambray, R.S., Lewis, G.N.J. and Playford, K. (1985). Radioactive Fallout in Air and Rain: Results to the End of 1984. UK Atomic Energy Authority, Harwell, AERE-R11915.
- Campbell, J.A. (1977). Past Variations of Natural Radiocarbon as Recorded in UK Wood. Ph.D. Thesis. University of Glasgow.
- Carter, M.W. and Moghissi, A.A. (1977). Three decades of nuclear testing. *Health Physics*, 33, 55-71.
- Chan, Y.H., Olson, J.S. and Emanuel, W.R. (1979). Simulation of Land Use Patterns Affecting the Global Carbon Cycle. Oak Ridge National Laboratory, Oak Ridge, Tennessee, ORNL/TM-6651.
- Clarke, R.H. (1979). A Model for Short and Medium Range Dispersion of Radionuclides Released to the Atmosphere. National Radiological Protection Board, Chilton, NRPB-R91.
- Commission of the European Communities. (1979). Methodology for Evaluating the Radiological Consequences of Radioactive Effluents Released in Normal Operations. Joint Report by the National Radiological Protection Board and the Commissariat A L'Energie Atomique. Commission of the European Communities, Luxembourg, V/3865/1/79-EN,FR.
- Craig, H. (1953). The geochemistry of the stable carbon isotopes. *Geochimica et Cosmochimica Acta*, 3, 53-92.
- Craig, H. (1954). Carbon 13 in plants and the relationships between carbon 13 and carbon 14 variations in nature. *The Journal of Geology*, 62, 115-149.
- Craig, H. (1957a). Isotopic standards for carbon and oxygen and correction factors for mass-spectrometric analysis of carbon dioxide. *Geochimica et Cosmochimica Acta*, 12, 133-149.
- Craig, H. (1957b). The natural distribution of radiocarbon and the exchange time of carbon dioxide between atmosphere and sea. *Tellus*, 9, 1-17.

- Damon, P.E. (1968). Radiocarbon and climate. *Meteorological Monographs*, 8, 151-154.
- Damon, P.E. (1970). Climatic versus magnetic perturbations of the atmospheric  $^{14}\text{C}$  reservoir. In: *Radiocarbon Variations and Absolute Chronology, Proceedings of the 12th Nobel Symposium, Uppsala, Sweden, 11-15 August 1969* (I.U. Olsson, ed.), pp 571-593. John Wiley and Sons, New York.
- Damon, P.E., Long, A. and Wallick, E.I. (1972). Dendrochronology and calibration of the carbon-14 timescale. In: *Radiocarbon Dating, Proceedings of the 8th International Conference, Lower Hutt, New Zealand, 18-25 October 1972* (T.A. Rafter and T. Grant-Taylor, eds.), pp A28-A43. Royal Society Of New Zealand, Wellington.
- Damon, P.E., Long, A. and Wallick, E.I. (1973). On the magnitude of the 11-year radiocarbon cycle. *Earth and Planetary Science Letters*, 20, 300-306.
- Davidson, J.D. and Feigelson, P. (1957). Practical aspects of internal-sample liquid scintillation counting. *International Journal of Applied Radiation and Isotopes*, 2, 1-18.
- Davis, Jr, W. (1979). Carbon-14 production in nuclear reactors. In: *Management of Low-level Radioactive Waste* (M.W. Carter, A.A. Moghissi and B. Kahn, eds.), pp 151-191. Pergamon Press, Oxford.
- Degens, E.T., Kempe, S. and Spitzzy, A. (1984). Carbon dioxide: A biogeochemical portrait. In: *The Handbook of Environmental Chemistry* (O. Hutzinger, ed.), pp 126-261. Springer-Verlag, New York.
- Detwiler, R.P., Hall, C.A.S. and Bogdonoff, P. (1985). Land use change and carbon exchange in the tropics: II. Estimates for the entire region. *Environmental Management*, 9, 335-344.
- Edmonds, J. and Reilly, J. (1983a). A long-term global energy-economic model of carbon dioxide release from fossil fuel use. *Energy Economics*, 5(2), 74-88.
- Edmonds, J.A. and Reilly, J. (1983b). Global energy and  $\text{CO}_2$  to the year 2050. *The Energy Journal*, 4(3), 27-47.
- Edmonds, J. and Reilly, J. (1983c). Global energy production and use to the year 2050. *Energy*, 8(6), 419-432.
- Edmonds, J.A., Reilly, J., Trabalka, J.R. and Reichle, D.E. (1984). An Analysis of Possible Future Atmospheric Retention of Fossil Fuel  $\text{CO}_2$ . US Department of Energy Report DOE/OR/21400-1. NTIS, Springfield, Virginia.
- Elsasser, W., Ney, E.P. and Winckler, J.R. (1956). Cosmic-ray intensity and geomagnetism. *Nature, London*, 178, 1226-1227.
- Emanuel, W.R., Killough, G.G. and Olson, J.S. (1981). Modelling the circulation of carbon in the world's terrestrial ecosystems. In: *Carbon Cycle Modelling* (B. Bolin, ed.), pp 335-353. SCOPE 16. John Wiley and Sons, New York.

- Emanuel, W.R., Killough, G.G., Post, W.M. and Shugart, H.H. (1984). Computer Implementation of a Globally Averaged Model of the World Carbon Cycle. US Department of Energy Report DOE/NBB-0062. NTIS, Springfield, Virginia.
- Fairhall, A.W. and Young, J.A. (1970). Radiocarbon in the environment. In: Radionuclides in the Environment (R.E. Gould, ed.), pp 401-417. Advances in Chemistry Series, No. 93. American Chemical Society, Washington DC.
- Ferguson, C.W. (1968). Bristlecone pine: science and esthetics. Science, New York, 159, 839-846.
- Ferguson, C.W. (1969). A 7104-year annual-tree ring chronology for bristlecone pine, Pinus aristata from the White Mountains California. Tree-ring Bulletin, 29, 3-29.
- Ferguson, C.W. (1970). Dendrochronology of bristlecone pine, Pinus aristata establishment of a 7484 year chronology in the White Mountains of eastern-central California, USA. In: Radiocarbon Variations and Absolute Chronology, Proceedings of the 12th Nobel Symposium, Uppsala, Sweden, 11-15 August 1969 (I.U. Olsson, ed.), pp 237-259. John Wiley and Sons, New York.
- Ferguson, C.W. (1972). Dendrochronology of bristlecone pine prior to 4000 BC. In: Radiocarbon Dating, Proceedings of the 8th International Conference, Lower Hutt, New Zealand, 18-25 October 1972 (T.A. Rafter and T. Grant-Taylor, eds.), A1-A10. Royal Society of New Zealand, Wellington.
- Fergusson, G.J. (1958). Reduction of atmospheric radiocarbon concentration by fossil fuel carbon dioxide and the mean life of carbon dioxide in the atmosphere. Proceedings of the Royal Society of London, Series A, 243, 561-574.
- Fields, D.E., Miller, C.W. and Cotter, S.J. (1984). Validation of the AIRDOS-EPA computer code by simulating intermediate range transport of  $^{85}\text{Kr}$  from the Savannah river plant. Atmospheric Environment, 18, 2029-2036.
- Flint, R.F. and Deevey, E.S. (1961). Editorial statement. Radiocarbon, 3.
- Flint, R.F. and Deevey, E.S. (1962). Editorial statement. Radiocarbon, 4.
- Fowler, T.W., Clark, R.L., Gruhlke, J.M. and Russel, J.L. (1976). Public Health Considerations of Carbon-14 Discharges from the Light-water-cooled Nuclear Power Reactor Industry. US Environment Protection Agency Report ORP/TAD-76-3. NTIS, Springfield, Virginia.
- Friedli, H., Lotscher, H., Oeschger, H., Siegenthaler, U. and Stauffer, B. (1986). Ice core record of the  $^{13}\text{C}/^{12}\text{C}$  ratio of atmospheric  $\text{CO}_2$  in the past two centuries. Nature, London, 324, 237-238.
- Gammon, R.H., Sundquist, E.T. and Fraser, P.J. (1985). History of carbon dioxide in the atmosphere. In: Atmospheric Carbon Dioxide and the Global Carbon Cycle (J.R. Trabalka, ed.), pp 25-62. US Department of Energy Report DOE/ER-0239. NTIS, Springfield, Virginia.
- Gardner, R.H. and Trabalka, J.R. (1985). Methods of Uncertainty Analysis for a Global Carbon Dioxide Model. US Department of Energy Report DOE/OR/21400-4. NTIS, Springfield, Virginia.

- de Geer, G. (1940). *Geochronologica suecia principes*. Kungliga Svenska Vetenskapsakademiens Handlingar, Series A, 18.
- Godwin, H. (1962). Half-life of radiocarbon. *Nature*, London, 195, 984.
- Gove, H.E., Elmore, D., Ferraro, R.D., Beukens, R.P., Chang, K.H., Kulius, L.R., Lee, H.W., Litherland, A.E., Purser, K.H. and Rubin, M. (1980). Radiocarbon dating with tandem electrostatic accelerators. In: *Proceedings of the 10th International Radiocarbon Conference* (M. Stuiver and R. Kra, eds.). *Radiocarbon*, 22, 785-793.
- Greenhalgh, G. (1980). *The Necessity for Nuclear Power*. Graham and Trotman, London.
- Grootes, P.M., Stuiver, M., Farwell, G.W., Schaad, T.P. and Schmidt, F.H. (1980). Enrichment of  $^{14}\text{C}$  and sample preparation for beta and ion counting. In: *Proceedings of the 10th International Radiocarbon Conference* (M. Stuiver and R. Kra, eds.). *Radiocarbon*, 22, 487-500.
- Hafele, W. (1981). *Energy in a Finite World: a Global Systems Analysis*. Report of the International Institute of Applied Systems Analysis. Ballinger Publishing Co., Cambridge, Massachusetts.
- Hampicke, U. (1979). Net transfer of carbon between the land biota and the atmosphere, induced by man. In: *The Global Carbon Cycle* (B. Bolin, E.T. Degens, S. Kempe and P. Ketner, eds.), pp 219-236. SCOPE 13. John Wiley and Sons, New York.
- Harkness, D.D. and Wilson, H.W. (1972). Some applications in radiocarbon measurement at the Scottish Research Reactor Centre. In: *Radiocarbon Dating, Proceedings of the 8th International Conference, Lower Hutt, New Zealand, 18-25 October 1972* (T.A. Rafter and T. Grant-Taylor, eds.), pp B101-B115. Royal Society of New Zealand, Wellington.
- Hayes, D.W. and MacMurdo, K.W. (1977). Carbon-14 production by the nuclear industry. *Health Physics*, 32, 215-219.
- Hayes, F.N. (1956). Liquid scintillators: attributes and applications. *International Journal of Applied Radiation and Isotopes*, 1, 46-56.
- Hayes, F.N., Williams, D.L. and Rogers, B. (1953). Liquid scintillation counting of natural  $^{14}\text{C}$ . *Physical Review*, 92, 512-513.
- Hedges, R.E.M., White, N.R., Wand, J.O. and Hall, E.T. (1980). Radiocarbon dating by ion counting: proposals and progress. In: *Proceedings of the 10th International Radiocarbon Conference* (M. Stuiver and R. Kra, eds.). *Radiocarbon*, 22, 816-821.
- Horrocks, D.L. (1964). Measurement of sample quenching of liquid scintillator solutions with x-ray and gamma-ray sources. *Nature*, London, 202, 78-79.
- Hosker, R.P. (1974). Estimates of dry deposition and plume depletion over forests and grassland. In: *Physical Behaviour of Radioactive Contaminants in the Atmosphere, Proceedings of an IAEA/WHO Symposium*, pp 291-309. IAEA-SM-181. IAEA, Vienna.
- Houghton, R.A., Boone, R.D., Melillo, J.M., Palm, C.A., Woodwell, G.M., Myers, N., Moore, III, B. and Skole, D.L. (1985a). Net flux of carbon dioxide from tropical forests in 1980. *Nature*, London, 316, 617-620.

- Houghton, R.A., Hobbie, J.E., Melillo, J.M., Moore, B., Peterson, B.J., Shaver, G.R. and Woodwell, G.M. (1983). Changes in the carbon content of terrestrial biota and soils between 1860 and 1980: a net release of CO<sub>2</sub> to the atmosphere. *Ecological Monographs*, 53, 235-262.
- Houghton, R.A., Schlesinger, W.H., Brown, S. and Richards, J.F. (1985b). Carbon dioxide exchange between the atmosphere and terrestrial ecosystems. In: *Atmospheric Carbon Dioxide and the Global Carbon Cycle* (J.R. Trabalka, ed.) pp 113-140. US Department of Energy Report DOE/ER-0239. NTIS, Springfield, Virginia.
- Houtermans, J.C. (1971). Geophysical Interpretations of Bristlecone Pine Radiocarbon Measurements Using a Method of Fourier Analysis of Unequally Spaced Data. Ph.D. Thesis. University of Bern.
- Houtermans, J., Suess, H.E. and Munk, W. (1967). Effect of industrial fuel combustion on the carbon-14 level of atmospheric CO<sub>2</sub>. In: *Radioactive Dating and Methods of Low-level Counting, Proceedings of an IAEA/ICSU Symposium*, pp 57-68. UN Doc-SM-87. IAEA, Vienna.
- International Atomic Energy Agency (1983). *Energy, Electricity and Nuclear Power Estimates for the Period up to 2000*. IAEA, Vienna, IAEA-RDS-1/3.
- International Atomic Energy Agency (1984). *Nuclear Power Reactors in the World*. IAEA, Vienna, IAEA-RDS-2/4.
- International Atomic Energy Agency (1985). *The Radiological Impact of Radionuclides Dispersed on a Regional and Global Scale: Methods for Assessment and Their Application*. IAEA, Vienna, IAEA-TRS-250.
- International Commission on Radiological Protection (1975). *Report of the Task Group on Reference Man*. ICRP Publication 23. Pergamon Press, Oxford.
- International Commission on Radiological Protection (1977). *Recommendations of the International Commission on Radiological Protection*. ICRP Publication 26. Pergamon Press, Oxford.
- International Commission on Radiological Protection (1979). *Limits of Intakes of Radionuclides by Workers*. ICRP Publication 30, Part 1. Pergamon Press, Oxford.
- International Commission on Radiological Protection (1981). *Limits of Intakes of Radionuclides by Workers*. ICRP Publication 30, Part 3. Pergamon Press, Oxford.
- Jansen, H.S. (1970). Secular variations of radiocarbon in New Zealand and Australian trees. In: *Radiocarbon Variations and Absolute Chronology, Proceedings of the 12th Nobel Symposium, Uppsala, Sweden, 11-15 August 1969*. (I.U. Olsson, ed.), pp 261-274. John Wiley and Sons, New York.
- Jansen, H.S. (1972). Transfer from solvents to sample. In: *Radiocarbon Dating, Proceedings of the 8th International Conference, Lower Hutt, New Zealand, 18-25 October 1972* (T.A. Rafter and T. Grant-Taylor, eds.), pp B63-B68. Royal Society of New Zealand, Wellington.

- de Jong, A.F.M., Mook, W.G. and Becker, B. (1979). Confirmation of the Suess wiggles: 3200-3700 BC. *Nature*, London, 280, 48-49.
- Kabat, M.J. (1979). Monitoring and removal of gaseous carbon-14 species. In: *Proceedings of the 15th DOE Nuclear Air Cleaning Conference*, pp 208-230. US Department of Energy Report CONF 780819-P1. NTIS, Springfield, Virginia.
- Karlen, I., Olsson, I.U., Kallberg, P. and Kilicci, S. (1964). Absolute determination of the activity of two  $^{14}\text{C}$  dating standards. *Archiv for Geofysik*, 4, 465-471.
- Keeling, C.D. (1973). The carbon dioxide cycle: reservoir models to depict the exchange of atmospheric carbon dioxide with the oceans and land plants. In: *Chemistry of the Lower Atmosphere* (S.I. Rasool, ed.), pp 251-329. Plenum Press, New York.
- Keeling, C.D. and Bacastow, R.B. (1977). Impact of industrial gases on climate. In: *Energy and Climate*, pp 72-95. National Academy Press, Washington DC.
- Keeling, C.D., Bacastow, R.B. and Whorf, T.P. (1982). Measurements of the concentration of carbon dioxide at Mauna Loa Observatory, Hawaii. In: *Carbon Dioxide Review* (W.C. Clark, ed.), pp 377-385. Oxford University Press, New York.
- Kelly, G.N., Jones, J.A., Bryant, P.M. and Morley, F. (1975). The Predicted Radiation Exposure of the Population of the European Community Resulting from Discharges of Krypton-85, Tritium, Carbon-14 and Iodine-129 from the Nuclear Power Industry to the Year 2050. Commission of the European Communities, Luxembourg, V/2676/75.
- Kempe, S. (1979a). Carbon in the freshwater cycle. In: *The Global Carbon Cycle* (B. Bolin, E.T. Degens, S. Kempe and P. Ketner, eds.), pp 317-342. SCOPE 13. John Wiley and Sons, New York.
- Kempe, S. (1979b). Carbon in the rock cycle. In: *The Global Carbon Cycle* (B. Bolin, E.T. Degens, S. Kempe and P. Ketner, eds.), pp 343-377. SCOPE 13. John Wiley and Sons, New York.
- Killough, G.G. (1980). A dynamic model for estimating radiation dose to the world population from releases of  $^{14}\text{C}$  to the atmosphere. *Health Physics*, 38, 269-300.
- Killough, G.G. and Emanuel, W.R. (1981). A comparison of several models of carbon turnover in the ocean with respect to their distributions of transit time and age and responses to atmospheric  $\text{CO}_2$  and  $^{14}\text{C}$ . *Tellus*, 33, 274-290.
- Killough, G.G. and Rohwer, P.S. (1978). A new look at the dosimetry of  $^{14}\text{C}$  released to the atmosphere as carbon dioxide. *Health Physics*, 34, 141-159.
- Killough, G.G. and Till, J.E. (1978). Scenarios of  $^{14}\text{C}$  releases from the world nuclear power industry from 1975 to 2020 and the estimated radiological impact. *Nuclear Safety*, 19, 602-617.

- Kocher, D.C. and Killough, G.G. (1984). A review of global environmental transport models for  $^3\text{H}$ ,  $^{14}\text{C}$ ,  $^{85}\text{Kr}$  and  $^{129}\text{I}$ . In: Radioactive Waste Management, Proceedings of an IAEA Conference, pp 157-179. IAEA-CN-43. IAEA, Vienna.
- Krishnamoorthy, T.M., Sastry, V.N. and Sarma, T.P. (1982). Model calculations for the projected estimates of  $^{14}\text{C}$  burden on earth. Indian Journal of Pure and Applied Physics, 20, 119-123.
- Kulp, J.L. (1954). Advances in radiocarbon dating. Nucleonics, 12(12), 19-21.
- Kunz, C. (1985).  $^{14}\text{C}$  discharge at three light-water reactors. Health Physics, 49, 25-35.
- Kunz, C.O., Mahoney, W.E. and Miller, T.W. (1974). Carbon-14 gaseous effluent from pressurized water reactors. In: Population Exposures, Proceedings of the 8th Midyear Topical Symposium of the Health Physics Society, Knoxville, Tennessee, pp 229-234. US Atomic Energy Commission Report CONF-741018. NTIS, Springfield, Virginia.
- Kunz, C.O., Mahoney, W.E. and Miller, T.W. (1975). Carbon-14 gaseous effluents from boiling water reactors. Transactions of the American Nuclear Society, 21, 91-92.
- Lal, D. and Rama (1966). Characteristics of global tropospheric mixing based on man-made  $^{14}\text{C}$ ,  $^3\text{H}$  and  $^{90}\text{Sr}$ . Journal of Geophysical Research, 71, 2865-2874.
- Lal, D. and Venkatavaradan, V.S. (1970). Analysis of the causes of  $\text{C}^{14}$  variations in the atmosphere. In: Radiocarbon Variations and Absolute Chronology, Proceedings of the 12th Nobel Symposium, Uppsala, Sweden, 11-15 August 1969 (I.U. Olsson, ed.), pp 549-569. John Wiley and Sons, New York.
- Levin, I., Munnich, K.O. and Weiss, W. (1980). The effect of anthropogenic  $\text{CO}_2$  and  $^{14}\text{C}$  sources on the distribution of  $^{14}\text{C}$  in the atmosphere. In: Proceedings of the 10th International Radiocarbon Conference (M. Stuiver and R. Kra, eds.). Radiocarbon, 22, 379-391.
- Libby, W.F. (1946). Atmospheric helium three and radiocarbon from cosmic radiation. Physical Review, 69, 671-672.
- Libby, W.F. (1952). Radiocarbon Dating. University of Chicago Press, Chicago.
- Light, E.S., Merker, M., Verschell, H.J., Mendell, R.B. and Korff, S.A. (1973). Time dependent worldwide distribution of atmospheric neutrons and of their products. 2. Calculation. Journal of Geophysical Research, 78, 2741-2762.
- Machta, L. (1971). The role of the oceans and biosphere in the carbon dioxide cycle. In: The Changing Chemistry of the Oceans (D. Dyrssen and D. Jagner, eds.), pp 121-145. John Wiley and Sons, New York.
- Magno, P.J., Nelson, C.B. and Ellet, W.H. (1975). A consideration of the significance of C-14 discharges from the nuclear power industry. In: Proceedings of the 13th AEC Air Cleaning Conference (M.W. First, ed.), pp 1047-1055. US Atomic Energy Commission Report CONF-740807. NTIS, Springfield, Virginia.

- Martin, J.E. (1986). Carbon-14 in low-level radioactive waste from two nuclear power plants. *Health Physics*, 50, 57-64.
- Matthews, E. (1983). Global vegetation and land use: new high-resolution data bases for climate studies. *Journal of Climate and Applied Meteorology*, 22, 474-487.
- Matthies, M. and Paretzke, H.G. (1982). Assessments of long-term effects of CO<sub>2</sub> and <sup>14</sup>C: various energy scenarios. In: *Health Impacts of Different Sources of Energy, Proceedings of an IAEA Symposium*, pp 329-341. IAEA-SM-254. IAEA, Vienna.
- McEwan, M.J. and Phillips, L.F. (1975). *Chemistry of the Atmosphere*. Edward Arnold, London.
- Miller, C.W. (1984). Atmospheric dispersion and deposition. In: *Models and Parameters for Environment Radiological Assessments* (C.W. Miller, ed.), pp 11-20. US Department of Energy Report DOE/TIC-11468. NTIS, Springfield, Virginia.
- Moghissi, A.A. and Carter, M.W. (1977). Global impact of carbon-14 from nuclear reactors. In: *Proceedings of the 4th International Congress of the International Radiation Protection Association, Paris, France, 24-30 April 1977*, pp 949-951.
- Molofsky, J., Menges, E.S., Hall, C.A.S., Armentano, T.V. and Ault, K.A. (1984). The effects of land use alteration on tropical carbon exchange. In: *The Biosphere: Problems and Solutions* (T.N. Veziroglu, ed.), pp 181-194. Elsevier Science Publishing, Amsterdam.
- Mopper, K. and Degens, E.T. (1979). Organic carbon in the ocean: nature and cycling. In: *The Global Carbon Cycle* (B. Bolin, E.T. Degens, S. Kempe and P. Ketner, eds.), pp 293-316. SCOPE 13. John Wiley and Sons, New York.
- Munnich, K.O. (1963). Der kreislauf des radiokohlenstoffs in der natur. *Naturwissenschaften*, 50, 211-218.
- Neftel, A., Moore, E., Oeschger, H. and Stauffer, B. (1985). Evidence from polar ice cores for the increase in atmospheric CO<sub>2</sub> in the past two centuries. *Nature*, London, 315, 45-47.
- Niehaus, F. and Williams, J. (1979). Studies of different energy strategies in terms of their effects on the atmospheric CO<sub>2</sub> concentration. *Journal of Geophysical Research*, 84, 3123-3129.
- Noakes, J.E., Isbell, A.F., Stipp, J.J. and Hood, D.W. (1963). Benzene synthesis by low temperature catalysis for radiocarbon dating. *Geochimica et Cosmochimica Acta*, 27, 797-804.
- Noakes, J.E., Kim, S.M. and Stipp, J.J. (1965). Chemical and counting advances in liquid scintillation age dating. In: *Radiocarbon and Tritium Dating, Proceedings of the 6th International Conference*, pp 68-92. US Atomic Energy Commission Report CONF-650652. NTIS, Springfield, Virginia.

- Nydal, R. (1967). On the transfer of radiocarbon in nature. In: Radioactive Dating and Methods of Low-level Counting, Proceedings of an IAEA/ICSU Symposium, pp 119-128. UN Doc-SM-87. IAEA, Vienna.
- Nydal, R. (1968). Further investigation on the transfer of radiocarbon in nature. *Journal of Geophysical Research*, 73, 3617-3635.
- Nydal, R. and Lovseth, K. (1983). Tracing bomb  $^{14}\text{C}$  in the atmosphere 1962-1980. *Journal of Geophysical Research*, 88, 3621-3642.
- Nydal, R., Lovseth, K and Gulliksen, S. (1979). A study of radiocarbon variation in nature since the Test Ban Treaty. In: Radiocarbon Dating, Proceedings of the 9th International Conference, University of California, Los Angeles/San Diego, USA, 20-26 June 1976 (R. Berger and H.E. Suess, eds.), pp 313-323. University of California Press, Berkeley, California.
- Obelic, B., Krajcar-Bronic, I., Srdoc, D. and Horvatancic, N. (1986). Environmental  $^{14}\text{C}$  levels around the 632 MW(e) nuclear power plant Krsko in Yugoslavia. In: Proceedings of the 12th International Radiocarbon Conference (M. Stuiver and R. Kra, eds.). *Radiocarbon*, 28, 644-648.
- Oeschger, H., Siegenthaler, U., Schotterer, U. and Gugelmann, A. (1975). A box diffusion model to study the carbon dioxide exchange in nature. *Tellus*, 27, 168-192.
- Olson, J.S. (1974). Terrestrial ecosystem. In: *Encyclopaedia Britannica*, 15th edition, vol. 20, pp 144-149. H.H. Benton, Chicago.
- Olson, J.S. (1985). Cenozic fluctuations in biotic parts of the global carbon cycle. In: *The Carbon Cycle and Atmospheric CO<sub>2</sub>: Natural Variations Archean to Present* (E.T. Sundquist and W.S. Broecker, eds.), pp 377-396. American Geophysical Union, Washington DC.
- Olson, J.S., Garrels, R.M., Berner, R.A., Armentano, T.V., Dyer, M.I. and Yaalon, D.H. (1985). The natural carbon cycle. In: *Atmospheric Carbon Dioxide and the Global Carbon Cycle* (J.R. Trabalka, ed.), pp 175-214. US Department of Energy Report DOE/ER-0239. NTIS, Springfield, Virginia.
- Olsson, I.U. (1970). The use of oxalic acid as a standard. In: *Radiocarbon Variations and Absolute Chronology*, Proceedings of the 12th Nobel Symposium, Uppsala, Sweden, 11-15 August 1969 (I.U. Olsson, ed.), p 17. John Wiley and Sons, New York.
- Olsson, I.U. (1980).  $^{14}\text{C}$  in extractives from wood. In: Proceedings of the 10th International Radiocarbon Conference (M. Stuiver and R. Kra, eds.). *Radiocarbon*, 22, 515-524.
- Olsson, I.U. and Karlen, I. (1965). Uppsala radiocarbon measurements VI. *Radiocarbon*, 7, 331-335.
- Olsson, I.U. and Klasson, M. (1970). Uppsala radiocarbon measurements X. *Radiocarbon*, 12, 281-284.
- Ostlund, H.G. and Engstrand, L.G. (1963). Stockholm natural radiocarbon measurements V. *Radiocarbon*, 5, 203-227.

- Otlet, R.L., Walker, A.J. and Longley, H. (1983). The use of  $^{14}\text{C}$  in natural materials to establish the average gaseous dispersion patterns of releases from nuclear installations. In: Proceedings of the 11th International Radiocarbon Conference (M. Stuiver and R. Kra, eds.). Radiocarbon, 25, 593-602.
- Pasquill, F. (1974). Atmospheric Diffusion. Ellis Horwood, Chichester, New York.
- Pearson, G.W. (1979). Precise  $^{14}\text{C}$  measurement by liquid scintillation counting. Radiocarbon, 21, 1-21.
- Peng, T.-H., Broecker, W.S., Freyer, H.D. and Trumbore, S. (1983). A deconvolution of the tree ring based  $\delta^{13}\text{C}$  record. Journal of Geophysical Research, 88, 3609-3620.
- Pietig, F. and Scharpenseel, H.W. (1966). Determination of age by liquid scintillation spectrometry: a new catalyst for the synthesis of benzene. Atompraxis, 12, 95-97.
- Polach, H.A. (1969). Optimisation of liquid scintillation radiocarbon age determinations and reporting of ages. Atomic Energy in Australia, 12(3), 21-28.
- Povinec, P., Chudy, M. and Sivo, A. (1986). Anthropogenic radiocarbon: past, present and future. In: Proceedings of the 12th International Radiocarbon Conference (M. Stuiver and R. Kra, eds.). Radiocarbon, 28, 668-672.
- Pringle, R.W., Turchinets, W., Funt, B.L. and Danyluk, S.S. (1957). Radiocarbon age estimates obtained by an improved liquid scintillation technique. Science, New York, 125, 69-70.
- Ralph, E.K., Michael, H.N. and Han, M.C. (1973). Radiocarbon dates and reality. MASCA Newsletter, 9, 1-20.
- Revelle, R. and Suess, H. (1957). Carbon dioxide exchange between atmosphere and ocean and the question of an increase of atmospheric  $\text{CO}_2$  during the past decades. Tellus, 9, 18-27.
- Rotty, R.M. and Masters, C.D. (1985). Carbon dioxide from fossil fuel combustion: trends, resources, and technological implications. In: Atmospheric Carbon Dioxide and the Global Carbon Cycle (J.R. Trabalka, ed.), pp 63-80. US Department of Energy Report DOE/ER-0239. NTIS, Springfield, Virginia.
- Scheele, R.D. and Burger, L.L. (1976). Carbon-14 Production in Fusion Reactors. Battelle Pacific Northwest Laboratories, Richland, Washington, BNWL-2105.
- Schwibach, J., Riedel, H. and Bretschneider, J. (1978). Investigations into the Emission of Carbon-14 Compounds from Nuclear Facilities, its Measurement and the Radiation Exposure Resulting from the Emission. Commission of the European Communities, Luxembourg, V-3062/78-EN.
- Scott, E.M. (1983). An Assessment of Errors in Radiocarbon Dating. Ph.D. Thesis. University of Glasgow.

- Segl, M., Levin, I. Schoch-Fischer, H., Munnich, M., Kromer, B., Tschiersch, J. and Munnich, K.O. (1983). Anthropogenic  $^{14}\text{C}$  variations. In: Proceedings of the 11th International Radiocarbon Conference (M. Stuiver and R. Kra, eds.). Radiocarbon, 25, 583-592.
- Siegenthaler, U. (1983). Uptake of excess  $\text{CO}_2$  by an outcrop-diffusion model of the ocean. Journal of Geophysical Research, 88, 3599-3608.
- Siegenthaler, U. and Oeschger, H. (1978). Predicting future atmospheric carbon dioxide levels. Science, New York, 199, 388-395.
- Solomon, A.M., Trabalka, J.R., Reichle, D.E. and Voorhees, L.D. (1985). The global carbon cycle. In: Atmospheric Carbon Dioxide and the Global Carbon Cycle (J.R. Trabalka, ed.), pp 1-14. US Department of Energy Report DOE/ER-0239. NTIS, Springfield, Virginia.
- Starik, I. Ye., Arslanov, Kh. A. and Zharkov, A.P. (1961). Scintillation technique for counting natural radiocarbon and its use for the determination of absolute age. Radiokhimiya, 2, 67-68.
- Stenhouse, M.J. and Baxter, M.S. (1977a). Bomb  $^{14}\text{C}$  and human radiation burden. Nature, London, 267, 825-827.
- Stenhouse, M.J. and Baxter, M.S. (1977b). Bomb  $^{14}\text{C}$  as a biological tracer. Nature, London, 267, 828-832.
- Stenhouse, M.J. and Baxter, M.S. (1979). The uptake of bomb  $^{14}\text{C}$  in humans. In: Radiocarbon Dating, Proceedings of the 9th International Conference, University of California, Los Angeles/San Diego, USA, 20-26 June 1976 (R. Berger and H.E. Suess, eds.), pp 313-323. University of California Press, Berkeley, California.
- Sternberg, A. and Olsson, I.U. (1967). Uppsala radiocarbon measurements VIII. Radiocarbon, 9, 471-476.
- Stewart, S.P. and Wilkins, B.T. (1985). Areal distribution of  $^{129}\text{I}$  in west Cumbrian soils. Journal of Environmental Radioactivity, 2, 175-182.
- Stuiver, M. (1961). Variations in radiocarbon concentration and sunspot activity. Journal of Geophysical Research, 66, 273-276.
- Stuiver, M. (1970). Long term  $^{14}\text{C}$  variations. In: Radiocarbon Variations and Absolute Chronology, Proceedings of the 12th Nobel Symposium, Uppsala, Sweden, 11-15 August 1969 (I.U. Olsson, ed.), pp 197-213. John Wiley and Sons, New York.
- Stuiver, M. (1978). Atmospheric carbon dioxide and carbon reservoir changes. Science, New York, 199, 253-258.
- Stuiver, M. (1980). Solar variability and climatic change during the current millennium. Nature, 286, 868-871.
- Stuiver, M. (1982). A high-precision calibration of the AD radiocarbon time scale. Radiocarbon, 24, 1-26.

- Stuiver, M. (1983). International agreements and the use of the new oxalic acid standard. In: Proceedings of the 11th International Radiocarbon Conference (M. Stuiver and R. Kra, eds.). Radiocarbon, 25, 793-795.
- Stuiver, M. and Polach, H.A. (1977). Discussion. Reporting of  $^{14}\text{C}$  data. Radiocarbon, 19, 355-363.
- Stuiver, M. and Quay, P.D. (1981). Atmospheric  $^{14}\text{C}$  changes resulting from fossil fuel  $\text{CO}_2$  release and cosmic ray flux variability. Earth and Planetary Science Letters, 53, 349-362.
- Suess, H.E. (1954). Natural radiocarbon measurements by acetylene counting. Science, New York, 120, 5-7.
- Suess, H.E. (1955). Radiocarbon concentration in modern wood. Science, New York, 122, 415-417.
- Suess, H.E. (1968). Climatic changes, solar activity and the cosmic ray production rate of natural carbon. Meteorological Monographs, 8, 146-150.
- Suess, H.E. (1970a). Bristlecone pine calibration of the radiocarbon time-scale 5200 BC to the present. In: Radiocarbon Variations and Absolute Chronology, Proceedings of the 12th Nobel Symposium, Uppsala, Sweden, 11-15 August 1969 (I.U. Olsson, ed.), pp 303-312. John Wiley and Sons, New York.
- Suess, H.E. (1970b). Three causes of the secular  $^{14}\text{C}$  fluctuations, their amplitudes and time constants. In: Radiocarbon Variations and Absolute Chronology, Proceedings of the 12th Nobel Symposium, Uppsala, Sweden, 11-15 August 1969 (I.U. Olsson, ed.), pp 595-606. John Wiley and Sons, New York.
- Tamers, M.A. (1960). Carbon-14 dating with the liquid scintillation counter: total synthesis of the benzene solvent. Science, New York, 132, 668-669.
- Tamers, M.A. (1965). Routine carbon-14 dating using liquid scintillation techniques. In: Radiocarbon and Tritium Dating, Proceedings of the 6th International Conference, pp 53-67. US Atomic Energy Commission Report CONF-650652. NTIS, Springfield, Virginia.
- Tamers, M.A. (1975). Chemical yield optimization of the benzene synthesis for radiocarbon dating. International Journal of Applied Radiation and Isotopes, 26, 676-682.
- Tans, P. (1978). Carbon-13 and Carbon-14 in Trees and the Atmospheric  $\text{CO}_2$  Increase. Ph.D. Thesis. University of Groningen.
- Tans, P. (1981). A compilation of bomb  $^{14}\text{C}$  data for use in global carbon model calculations. In: Carbon Cycle Modelling (B. Bolin, ed.), pp 131-157. SCOPE 16. John Wiley and Sons, New York.

- Tans, P.P. and Mook, W.G. (1978). Design, construction and calibration of a high accuracy carbon-14 counting set up. Radiocarbon, 21, 22-40.
- Tauber, H. (1967). Copenhagen radiocarbon measurements VIII. Geographic variations in atmospheric  $^{14}\text{C}$  activity. Radiocarbon, 9, 246-256.
- Tauber, H. (1970). The Scandinavian varve chronology and C-14 dating. In: Radiocarbon Variations and Absolute Chronology, Proceedings of the 12th Nobel Symposium, Uppsala, Sweden, 11-15 August 1969 (I.U. Olsson, ed.), pp 173-196. John Wiley and Sons, New York.
- Thommeret, J., Thommeret, Y. and Baxter, M.S. (1983). The recent  $^{14}\text{C}$  record in the north-west Mediterranean atmosphere. Journal de Recherches Atmospheriques, 177, 45-51.
- Till, J.E., Bomar, E.S. and Bond, W.D. (1976). Potential radiation doses from  $^{14}\text{C}$  produced in advanced FBR fuels. Transactions of the American Nuclear Society, 24, 104-105.
- Turner, D.B. (1970). Workbook of Atmospheric Dispersion Estimates. US Environmental Protection Agency Report AP-26. NTIS, Springfield, Virginia.
- United Nations (1972). Ionizing Radiation: Levels and Effects. United Nations Scientific Committee on the Effects of Atomic Radiation 1972 Report to the General Assembly. United Nations, New York.
- United Nations (1977). Sources and Effects of Ionizing Radiation. United National Scientific Committee on the Effects of Atomic Radiation 1977 Report to the General Assembly. United Nations, New York.
- United Nations (1981). Environmental Behaviour and Dosimetry of Radionuclides. United Nations Scientific Committee on the Effects of Atomic Radiation 1981 Report to the General Assembly. United Nations, New York.
- United Nations (1982). Ionizing Radiation: Sources and Biological Effects. United Nations Scientific Committee on the Effects of Atomic Radiation 1982 Report to the General Assembly. United Nations, New York.
- Valastro, Jr, S., Land, L.S. and Varela, A.G. (1977). An improved procedure for wet oxidation of the  $^{14}\text{C}$  NBS oxalic acid standard. Radiocarbon, 19, 375-382.
- Vogel, J.C. (1970). Groningen radiocarbon dates IX. Radiocarbon, 12, 444-471.
- Vogel, J.C. and Lerman, J.C. (1969). Groningen radiocarbon dates VIII. Radiocarbon, 11, 351-390.
- Vogel, J.C. and Marais, M. (1971). Pretoria radiocarbon dates I. Radiocarbon, 13, 378-394.

- de Vries, Hl. (1958). Variation in concentration of radiocarbon with time and location on earth. Proceedings of the Koninkl Nederlandse Akademi Wetenschap, Series B, 61, 94-102.
- de Vries, Hl. and Barendsen, G.W. (1953). Radio-carbon dating by a proportional counter filled with carbon dioxide. Physica, 19, 987-1003.
- Wade, B.O., Eggleton, A.E.J. and Peirson, D.H. (1985). Studies of Environmental Radioactivity in Cumbria, Part 7: A Summary of Progress to December 1984. UK Atomic Energy Authority, Harwell, AERE-R11743.
- Walker, A.J., Otlet, R.L. and Longley, H. (1986). Applications of the use of hawthorn berries in monitoring carbon-14 emissions from a UK nuclear establishment over an extended period. In: Proceedings of the 12th International Radiocarbon Conference (M. Stuiver and R. Kra, eds.). Radiocarbon, 28, 681-688.
- Walton, A., Ergin, M. and Harkness, D.D. (1970). Carbon-14 concentrations in the atmosphere and carbon dioxide exchange rates. Journal of Geophysical Research, 75, 3089-3098.
- Weil, J.C. and Jepsen, A.F. (1977). Evaluation of the Gaussian plume model at the Dickerson power plant. Atmospheric Environment, 11, 901-910.
- Weisberg, S. (1980). Applied Linear Regression. John Wiley and Sons, New York.
- Williams, E.T. (1977). Brooklyn College radiocarbon dates I. Radiocarbon, 19, 1-11.
- Willis, E.H., Tauber, H. and Munnich, K.O. (1960). Variations in the atmospheric radiocarbon concentration over the past 1300 years. American Journal of Science Radiocarbon Supplement, 2, 1-4.
- Wirth, E. (1982). The applicability of the  $^{14}\text{C}$ -specific activity model. Health Physics, 43, 919-922.
- Wise, L.E. and Jahn, E.C. (1952). Wood Chemistry, Reinhold, New York.
- Woodwell, G.M. (1983). Biotic effects on the concentration of atmospheric carbon dioxide: a review and projection. In: Changing Climate, pp 216-241. National Academy Press, Washington DC.
- Young, J.A. and Fairhall, A.W. (1968). Radiocarbon from nuclear weapon tests. Journal of Geophysical Research, 73, 1185-1200.

